
SICEL
VIII Simposio Internacional sobre Calidad de la Energía Eléctrica 2015
18 - 20 de NOVIEMBRE
Temáticas :
CALIDAD DE LA ENERGÍA ELÉCTRICA
GESTIÓN ENERGÉTICA
SMART GRID
COMPATIBILIDAD ELECTROMAGNÉTICA
REGULACIÓN ENERGÉTICA
INVESTIGACIÓN SOBRE RAYOS
Patrocinadores :
SIEMENS
GRUPO PAAS-UN
UNIVERSIDAD NACIONAL DE COLOMBIA
UNIVERSIDAD TÉCNICA FEDERICO SANTA MARÍA
CENTRO BASAL AC3E
Curso adicional :
"Análisis armónico en sistemas eléctricos / Retos del análisis para frecuencias por debajo y por encima de los 2 kHz"
17 de Noviembre
Lugar :
Universidad Técnica Federico Santa María
Casa Central, Salón de Actos, Edificio T, Valparaíso
"Inscripciones Abiertas" WWW.SICEL.ORG
Información : abelardo.cuenca@usm.cl / +56 32 2654439
PATROCINAN
SIEMENS
paas un
UNIVERSIDAD NACIONAL DE COLOMBIA SEDE MANIZALES
FACULTAD DE INGENIERÍA Y ARQUITECTURA
UNIVERSIDAD TÉCNICA FEDERICO SANTA MARIA
Advanced Center for Electrical and Electronic Engineering

TABLA DE CONTENIDO

CALIDAD DE LA ENERGÍA

COMPATIBILIDAD ELECTROMAGNÉTICA

REDES INTELIGENTES

GESTIÓN ENERGÉTICA

REGULACIÓN ENERGÉTICA

INVESTIGACIÓN SOBRE RAYOS

A Novel Power Quality Index Using Discrete Wavelet Transform

Índice de Calidad de la Energía Usando Transformada Discreta de Wavelet

Victor Manuel Garrido Arévalo[1], Jorge Luis Díaz Rodríguez[2], Aldo Pardo García[3]

ABSTRACT

In this work a general index of power quality (PQ) is proposed based on the simulation of some of the phenomena that affect the power quality. Using wavelet transform and calculating the energy coefficients to obtain a characteristic pattern of each signal to calculate the PQ index, using different wavelet functions. The proposed PQ index was compared with typical measurements phenomena under study.

Keywords: Power quality, wavelet, DWT, harmonics, sags, swells

RESUMEN

En este trabajo se propone un índice general de calidad de la energía (PQ), basado en la simulación de algunos de los fenómenos que afectan la forma de onda. Usando la transformada wavelet y el cálculo de los coeficientes de energía para obtener un patrón característico de cada señal para calcular el índice PQ, utilizando diferentes funciones wavelet. El índice PQ propuesto se comparó con mediciones fenómenos típicos en estudio.

Palabras clave: Calidad de la energía, wavelet, DWT, armónicos, sags, swells.

Received: July 22th, 2015
Accepted: Sept 24th, 2015

I. INTRODUCTION

Power Quality received by the end user whether residential or industrial must be guaranteed for correct operation of the equipment and the system itself. However many phenomena, some inherent in the operation of the system, such as voltage variations due to the connection or disconnection of large loads and others produced by the same especially those with electronic components that introduce harmonics to the network, which distorts the wave. Each of these phenomena has different ways of being together making it difficult quantified comparison between one and one for identifying which affects the signal.

There have been some studies in which rates have been proposed for classifying and quantifying the effects from some phenomena that affect the power quality, for example:

In [3] a review of the application of signal processing, smart techniques and optimization techniques in the analysis of PQ is. Intelligent techniques such as fuzzy logic, neural networks and genetic algorithms and their fusion are reviewed. The authors suggest this work as a guide for deeper knowledge of the power quality.

[1] Propose an index of PQ based on discrete wavelet transform (DWT) is proposed to determine the amount of deviation of the pure desired signal. The proposed PQ index is defined as the weighted sum of percentage energy deviation of the details DWT.

[2] Propose an index that quantifies the deviation between the control voltage or current and the ideal voltage or current; this index can also be used for detection, quantification and classification of the severity of any disturbance. The index can be applied to variation in steady state and transient events. In the first case, the index is used to quantify the severity of the variation; in the latter case the index can be used for activation and event detection, but also to quantify its severity

In [4] an indicator of power quality that works using the wavelet transform, for which different functions are used bases and orders, and then determine which performs best to be compared with rates already proposed known.

[1] M.Sc., Ingeniero Electricista, Universidad de Pamplona, Colombia. E-mail: vimaga86@gmail.com

[2] M.Sc., Ingeniero Electricista, Universidad de Pamplona, Colombia. E-mail: jdiazcu@gmail.com

[3] Ph.D., Ingeniero Electricista, Universidad de Pamplona, Colombia. E-mail: apardo13@gmail.com

II. Power Quality Affectations

The study of the Power Quality is the first and most important step to identify and to solve problems of the power system. The affectation to the power systems can include damage the equipments and persons also the reduction of its performance, reliability, productivity and profitability (Saucedo & Texis, 2008)

A. *Harmonic*

Harmonics are sinusoidal voltages or currents whose frequency is an integer multiple value in which the system is designed for (fundamental frequency, typically 50 or 60 Hz) A harmonic signal can be represented by (1).

$$y(t) = Y_0 + \sum_{n=1}^{\infty} Y_n \sqrt{2}\, sen(n\omega - \varphi_n) \quad (1)$$

Where:

Y_0: The amplitude of the DC component, which is usually zero in a stable state.

Y_n: The rms value of the component of n rank.

φ_n: It is the gap of the harmonic component.

B. *Sag and Swell*

Sags and swells are similar phenomena; the first corresponds to a decrease in signal amplitude between 0.1 and 0.9 in pu, while the second goes to an increase between 1.1 and 1.8 in pu.

III. Simulation

Simulations are used for obtaining the signals for all the phenomena to be analyzed, in Fig. 1, 2, 3 and 4 are shown as an example of each of the signals used in this study.

To simulate the harmonics, use the IEC 61000-3-6 for the delineation of each component will be considered. An example of signal containing harmonics is shown in Fig. 1.

The simulated swell and sags phenomena, which set are the generation code, the duration of these at a random, more therefore variation ranges magnitude are set unit according to the above mentioned. In this way is presented in Fig. 2 and Fig. 3 sags and swells signals respectively.

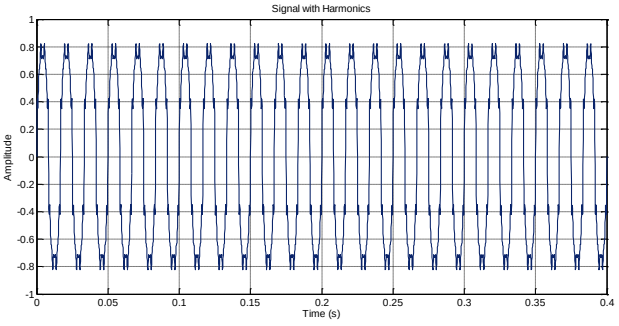

Figure 1. Signals with harmonics

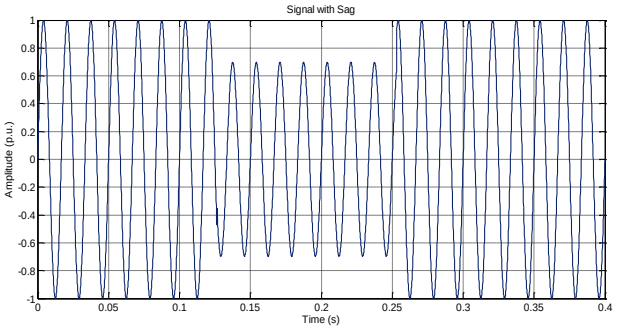

Figure 2. Signals with sags

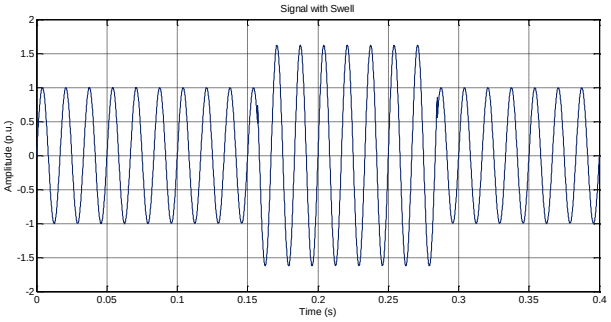

Figure 3. Signals with swell.

IV. Wavelet Transform

Is possible to analyze a signal in time and frequency using a technique called *Multiresolution Analysis*, this shows the signal at different frequencies with different resolutions [14], the main advantage of this analysis is the possibility of obtaining good time resolution but poor resolution at high frequencies and likewise, good resolution for low frequencies but poor resolution for time.

This is the benefit of wavelet transform, representing most advantage over the windowed Fourier transform, in which the entire signal is analyzed in the same selected window while the wavelet transform is discussed with variable resolution [15].

This analysis is based on obtaining the spectral components of signal amplitudes as a series of special functions, which are called *wavelets*. According Subhais Saha [16]: "*Wavelets are functions defined on finite intervals having an average value of zero*". It is necessary that the set of functions are used to form a base, which means that any signal has a unique decomposition and then reversing this decomposition can obtain the original signal [17].

The continuous wavelet transform is mathematically represented as (2):

$$C(\tau, s) = \frac{1}{\sqrt{|s|}} \int_{-\infty}^{+\infty} f(t)\, \Psi\left[\frac{t-\tau}{s}\right] dt \quad (2)$$

Where,

$$\Psi(\tau, s) = \frac{1}{\sqrt{|s|}} \Psi\left[\frac{t-\tau}{s}\right] \quad (3)$$

Thus, $C(\tau, s)$ are the coefficients of $f(t)$ in the space defined by the function $\Psi(\tau, s)$, a term which is called mother wavelet as it refers to a window function of finite length and

oscillatory nature, presenting a prototype from which a group of window functions was generated [15].

Case for the discrete wavelet transform is defined by:

$$C[j,k]=\sum_{n\in Z} f[n]\Psi_{j,k}[n] \quad (4)$$

Where the mother wavelet is

$$\Psi_{j,k}[n]=2^{-j/2}\Psi\left[2^{-j}n-k\right], \quad j,k\in Z \quad (5)$$

The parameters τ, s are defined as the dyadic scale, i.e., 2^n powers, so that $\tau=2^j k$ and $s = 2^j$ [16]

That is, the wavelet transform will be to multiply the signal of study ($f[n]$), by the wavelet at each scale j while the latter runs through the time axis. The process is repeated but with different scales until the desired number of bands or scales is obtained [14].

The analysis can be interpreted as a measure of the similarity between the bases functions ($\Psi_{j,k}[n]$) and study the signal ($f[n]$), in its frequency content, therefore, the estimated coefficients ($C[j, k]$) indicating which so next is the signal to the wavelet in a specific scale.

Figure 5 shows the process of subband coding or multiresolution using the H and G filters and a decimated by 2, the result of the high pass filter for filtering each level corresponds to a level of detail or wavelet coefficients. The result of each low pass filter is called level of approximation. Thus can be seen details of the signal in the frequency band required [17].

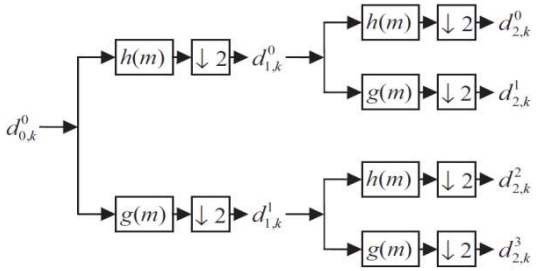

Figure 5. Two levels wavelet decomposition tree [14].

V. Methodology

One of the main advantages of using the wavelet transform is that this allows to decompose the signal into different detail coefficients which in turn allow to obtain information that can identify, classify and measure the original signal.

For the case study apply the wavelet transform to determine the first 10 coefficients detail signals with different perturbations, to subsequently calculate the energy of each level of these, this process is repeated for different wavelet mothers, so that subsequently can calculate the deviation of energy, as shown in (7):

$$Ed(j)\% = \left[\frac{En_{dist(j)}-En_{ref(j)}}{En_{ref(7)}}\right].100 \quad (7)$$

VI. Power Quality Indexes

In references [14] and [18] an analysis of different PQ indexes measuring some distortion of the waveform occurs, however these values is not only possible to establish which of these phenomena most affects the quality of the signal, and for example, while sags and swells has parameters such as the distortion duration and amplitude and for harmonics phenomena has the Total Harmonic Distortion (THD), if these values are compared is not possible to establish what signal is most affected.

A. Harmonics

The primary indicator to measure the harmonics is THD or simply THD, which can be calculated by the following equation (8): [19]

$$THD=\frac{\sqrt{\sum_{k=2}^{\infty} I_k^2}}{I_1}\cdot 100\% \quad (8)$$

Where:
I_1: Amplitude of the fundamental wave.
I_k: Amplitude of harmonic k.

B. Sags and swells

According to references [13] and [18] the sag and swell characteristic parameters are shown in Figure 10, which ΔT represents the duration of the fall or rise, while ΔU is representing its the depth.

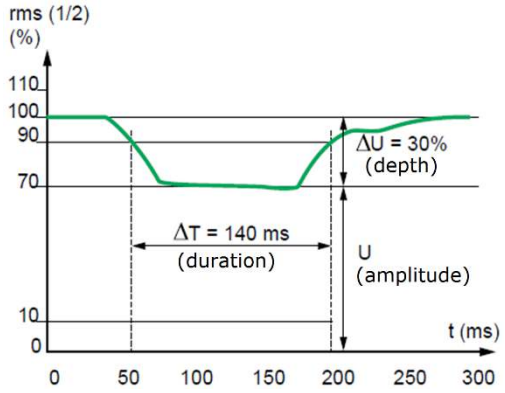

Figure 10. Sags y swells definition [20].

VII. Proposed Power Quality Index

According to the number of indexes for each of the phenomena under study, the need to present a general PQ index to evaluate and compare these distortions was observed.

Analyzing the preceding figures can easily find that every phenomenon has a singular characteristic pattern that allows easy identification, also can appreciate the differences in values for the distributions of individual energy, so, it is clear that calculating the total energy distribution of the first 10 detail coefficients of the wavelet transform can obtain a value that characterizes the magnitude of the disturbance.

The reference value to compare the effect on the signal is of course pure sine wave, which present a constant energy distribu-

tion of zero (0) for all coefficients. Using the following equation can be calculated the proposed PQ index; the sum of the absolute value of the energy distribution for each coefficient is used and normalized by dividing the result by the total number of coefficients in the study.

Thus (9) defines the PQ index.

$$PQ\_Index = \frac{\sum_{i=1}^{n} \left| E_{coef_i} \right|}{n} \quad (9)$$

Where:
$E_{coef\,i}$: Energy of the detail coefficient *i*.
n: Total number of detail coefficients.

VIII. Results

According to the provisions of the methodology, the detail coefficients and their respective energy for different wavelets are calculated as follows:

A. First case: Signal with harmonics.

Table 1 PQ_Index for Signal with Harmonics using different wavelets.

Signal	THD	PQ_Index				
		Db1	Db3	Db5	Db7	Db10
1	30,17	1543,232	134,428	45,065	50,618	26,334
2	3,05	18,393	16,190	2,119	2,915	1,598
3	2,71	17,905	12,518	0,897	4,054	2,212
4	12,97	394,895	64,240	19,121	14,633	14,894
5	8,02	127,363	41,089	7,275	11,027	8,785
6	13,70	399,652	69,980	18,074	15,881	15,230
7	9,83	194,349	50,887	9,529	11,015	8,575
8	10,78	219,615	54,317	9,053	14,780	11,872
9	6,02	85,399	30,346	7,693	6,351	5,756
10	10,45	202,511	52,971	7,997	12,377	8,950

According to Table 1 can be seen at a glance that the PQ_Index calculated with wavelet Db1 has greater difference from the THD calculated for each signal, however in Table 2 calculation error occurs

Table 2 Percentage difference for power quality indices for signal with Harmonics

Signal	% Error_Harmonics				
	Db1	Db3	Db5	Db7	Db10
1	5015,06	345,56	49,37	67,77	12,72
2	503,76	431,45	30,44	4,30	47,56
3	559,74	361,26	66,94	49,38	18,51
4	2945,29	395,40	47,46	12,85	14,86
5	1488,97	412,62	9,24	37,57	9,60
6	2818,11	410,97	31,97	15,96	11,21
7	1878,08	417,93	3,02	12,11	12,72
8	1936,46	403,67	16,05	37,06	10,08
9	1317,47	403,68	27,68	5,41	4,47
10	1838,35	407,01	23,45	18,47	14,33
Avarage	2030,13	398,95	30,56	26,09	**15,61**

As Table 2 shows that the Db10 has the lowest average error between proposed PQ_Index and THD calculated for each signal.

B. Second case: Signal with sags

In the case of signals with the particularity that sags have two reference values for measuring the magnitude of the event, in this case, duration and variation in the amplitude of the wave is observed. In this case the proposed index takes into account the combined effect of both references.

Table 3 shows the calculated values for 10 different signals affected by sags

Table 3 PQ_Index for Signal with Sags using different Wavelets.

Signal	ΔT	ΔU	PQ_Index				
			Db1	Db3	Db5	Db7	Db10
1	50	0,58	481,203	40,041	17,946	17,510	16,678
2	368	0,34	326,030	145,427	64,189	36,641	37,625
3	349	0,74	918,091	324,026	135,977	73,252	79,835
4	281	0,45	761,798	151,140	67,019	38,103	39,485
5	131	0,64	664,547	112,644	50,418	28,365	29,054
6	154	0,28	375,401	48,726	24,646	16,721	17,419
7	234	0,11	112,613	28,072	12,971	7,884	7,703
8	150	0,03	41,728	4,745	2,193	1,332	1,293
9	414	0,89	247,879	458,764	186,637	95,955	109,430
10	136	0,25	324,110	37,908	18,421	13,237	15,831

Table 4 shows the errors between the PQ_Index and reference values for sags shown, you can see that in this case the Db7 wavelet has better results, however the Db10, presents a similar error percentage.

Table 4 Percentage difference for power quality indices for signal with sags

Signal	% Error_Sag				
	Db1	Db3	Db5	Db7	Db10
1	729,66	30,96	69,06	69,81	71,25
2	858,91	327,73	88,79	7,77	10,66
3	1140,66	337,87	83,75	1,01	7,89
4	1592,88	235,87	48,93	15,33	12,25
5	938,35	76,01	21,22	55,68	54,60
6	1240,72	74,02	11,98	40,28	37,79
7	923,75	155,20	17,92	28,32	29,97
8	1290,94	58,15	26,90	55,62	56,91
9	178,52	415,46	109,70	7,81	22,96
10	1196,44	51,63	26,32	47,05	36,67
Avarage	1009,08	176,29	50,46	**32,87**	34,09

C. Third case: Signal with swell

By the similarity of the sags and swell phenomena, also applies to the reference values are the length and the variation of the wave amplitude for this case PQ_Index into account both variations to estimate the impact of this phenomenon on the waveform quality.

Table 5 PQ_Index for Signal with swells using different wavelets.

Signal	ΔT	ΔU	PQ_Index				
			Db1	Db3	Db5	Db7	Db10
1	100	21,00	276,980	30,146	14,073	8,754	8,312
2	254	57,00	323,442	116,237	55,063	35,851	32,442
3	249	46,00	248,756	95,927	45,786	29,533	27,101
4	409	75,00	120,104	213,430	107,313	72,703	63,576
5	37	7,00	59,750	2,845	1,891	1,794	0,699
6	300	66,00	483,273	142,612	75,051	54,902	49,453
7	268	13,00	253,381	34,487	16,185	10,113	9,620
8	156	63,00	1049,302	48,620	23,514	15,191	14,206
9	427	11,00	88,655	46,774	21,756	13,374	12,767
10	151	75,00	1083,512	48,004	29,040	23,442	23,337

As shown in Table 6, for the case swells, again the Wavelet Db10 presenting the best results in comparison with other stem functions.

Table 6 Percentage difference for power quality indices for signal with swells

Signal	% Error_Swell				
	Db1	Db3	Db5	Db7	Db10
1	1218,95	43,55	32,98	58,31	31,05
2	467,44	103,92	3,40	37,10	43,08
3	440,77	108,54	0,47	35,80	41,09
4	60,14	184,57	43,08	3,06	15,23
5	753,56	59,36	72,99	74,37	17,20
6	632,23	116,08	13,71	16,82	25,07
7	1849,09	165,28	24,50	22,21	26,00
8	1565,56	22,82	62,68	75,89	77,45
9	705,95	325,22	97,78	21,58	16,07
10	1344,68	36,00	61,28	68,74	68,88
Avarage	903,84	116,53	41,29	41,39	36,11

IX. Power Quality Meter

Once the PQ index is determined it is proposed to be implemented the necessary software codes and hardware to allow the PQ index calculation and the developing a device to measure the distortions which present the signal.

Likewise it is also proposed to have an intelligent classifier based on *Artificial Neural Networks* (*ANN*) to identify characteristic patterns and to determine which type of phenomenon occurs. The proposed block diagram of the meter is shown in Figure 11.

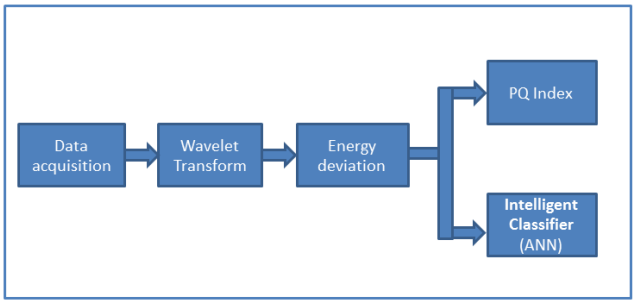

Fig. 11. Power Quality measurement and classification

X. Conclusions

In this work different phenomena that affect the power quality, later to calculate the reference values to quantify the effects they cause in the waveform simulated.

Then we proceeded to propose a general index of power quality to quantify any phenomenon and that these can be compared with each other, for this was taken into account the discrete wavelet transform since this allows to decompose the signal into different detail coefficients each with characteristics of energy.

For the calculation of the Discrete Wavelet Transform mother so that various functions used was established that is Daubechies 10 which presents better results in comparison to the index values calculated standard references.

References

[1] Chirag A, N. & Prasanta, K., 2013. Power quality index based on discrete wavelet transform. Electrical Power and Energy Systems, p. 994–1002.

[2] Ferreiraa, D. D. & Seixasb, J. M., 2015. A new power quality deviation index based on principal curves. Electric Power Systems Research, pp. 8-14.

[3] Manish, K. S. & Rajiv, K., 2012. Classification of power quality events – A review. Electrical Power and Energy Systems, pp. 11-19.

[4] Morsia, W. G. & El-Hawaryb, M. E., 2010. Novel power quality indices based on wavelet packet transform for non-stationary sinusoidal and non-sinusoidal disturbances. Electric Power Systems Research, p. 753–759.

[5] Ch. A. Naik and P. Kundu, Power quality index based on discrete wavelet transform, International Journal *of Electrical Power & Energy Systems*, Vol. 53, December 2013, pp. 994-1002.

[6] D. D. Ferreira, J. M. de Seixas and A. S. Cerqueira, "A method based on independent component analysis for single and multiple power quality disturbance classification", *Electric Power Systems Research*, Volume 119, February 2015, pp. 425-431.

[7] O. P. Mahela, A. G. Shaik and N. Gupta, "A critical review of detection and classification of power quality events",

Renewable and Sustainable Energy Reviews, Volume 41, January 2015, Pages 495-505.

[8] D. A. Tovar, "Wavelet transform and support vector machines for the arrhythmia identification". *Revista de Investigación Universidad del Quindio.* 19(10), Colombia, 2009.

[9] E. García, "Valoración de la Calidad de la Energía Eléctrica Respecto a Huecos de Tensión: Índices y Niveles de Calidad", Ph.D. dissertation, Universidad Politécnica de Valencia, España, 2008.

[10] P. A. Santafé G., "LSSVM aplicada en la estimación de la resistencia de rotor en motor de inducción Jaula de Ardilla". Master dissertation, Universidad de Pamplona, Colombia. 2012.

[11] D. Saucedo and J. Texis, "Factores que afectan la calidad de la energía y su solución", Escuela Superior de Ingeniería Mecánica y Eléctrica, Tech. Rep., México, 2008.

[12] C. Collombet, J. M. Lupin and J. Schonek, Cuaderno Técnico No. 152: Los armónicos en las redes perturbadas y su tratamiento, Schneider Electric, enero, 2001.

[13] ECAMEC. Medición de Parámetros de Calidad de Energía bajo el estándar IEC61000-4-30. Primera parte. Medición de Flicker en redes eléctricas, ECAMEC Tecnología, abril, 2009.

[14] M. Navarrete Mejía and S. Andrade Mora, Análisis y Tratamiento de la Señal Electrocardiográfica para la Detección de Parámetros de Normalidad Bajo la Plataforma Labview "Adpan-Ecg", Tech. Rep., Universidad Pontifica Bolivariana – Colciencias, Bucaramanga, 2006.

[15] P. Faundez, Procesamiento Digital de Señales Acústicas Utilizando Wavelets, Universidad Austral de Chile. Valdivia, Chile.

[16] R. V. Subhasis Saha. Adaptive wavelet filter in image coders: How important are they, Technical report, University of California, Davis, 1999.

[17] J. Martínez, Análisis de la teoría de ondículas orientadas a las aplicaciones en ingeniería eléctrica: fundamentos. Universidad Politécnica de Madrid, ETSI industriales, Departamento de ingeniería eléctrica, España, 2002.

[18] M. Romero, "Diseño de una metodología para el análisis de sags de tensión en redes de distribución", Universidad Nacional de Colombia, Bogotá, 2011.

[19] Suárez, J. A. Análisis de la distorsión armónica y los efectos de atenuación y diversidad en áreas residenciales. IEEE Latin America Tansactions. Vol. 3 No. 5. 2005.

[20] R. Calvas, Cuaderno Técnico No. 141: Las perturbaciones eléctricas en BT, Schneider Electric, Enero, 2001.

Database Modeling for Studies in Power Distribution Systems

Modelado de Base de Datos para Estudios en Sistemas de Distribución de Energía

Fábio Luís Alves Juste[1], Alberto De Conti[2]

ABSTRACT

In most power system analysis studies, databases are stored in IEEE common data format. Although convenient for data exchange between different softwares, this format is not easy to manage in studies of large systems if a user-friendly interface is not available. It also leads to difficulties in recovering data in long-term studies of system performance and power quality. In this paper, a database structure based on tables is proposed. The proposed database is written in Microsoft Office Access and managed through structured query language using MATLAB. The developed database is useful for storing the elements of a power distribution system for power flow and harmonic studies, as well as for providing data for long-term studies and reports.

Keywords: database modeling, power distribution systems, power flow studies, structured query language.

RESUMEN

En la mayoría de los estudios de análisis en sistemas de energía, las bases de datos se almacenan en el formato de datos común IEEE. Aunque conveniente para el intercambio de datos entre diferentes softwares, este formato no es fácil de manejar en estudios de grandes sistemas si un interfaz fácil de usar no está disponible. También resulta en dificultades en la recuperación de datos en estudios a largo plazo del rendimiento del sistema y de calidad de energía. En este trabajo, se propone una estructura de base de datos basada en tablas. La base de datos propuesta está escrita en Microsoft Office Access y gestionada a través del lenguaje de consulta estructurada utilizando MATLAB. La base de datos desarrollada es útil para almacenar los elementos de un sistema de distribución de energía para estudios de flujo de potencia y de armónicos, así como para proporcionar datos para estudios a largo plazo e informes.

Palabras clave: base de datos, estudios de flujo de potencia, sistemas de distribución de energía, lenguaje de consulta estructurada.

Received: July 23th 2015
Accepted: Oct 15th 2015

Introduction

Studies of power distribution systems have been developed for decades. Examples include voltage drop investigations (Kersting, 2012; Kagan, 2010) and harmonics analysis (Arrillaga, 2003). In many cases, due to the system complexity and length a significant amount of memory and storage data is required for performing a full analysis. Although professional packages are available and used worldwide (Rizy, 2002), these are neither freely-distributed nor open-source programs. They also experience difficulties when dealing with long-term studies of system performance and power quality, where data storage is necessary for comparisons between different scenarios or to demonstrate the system behavior along a period of time. In addition, data storage in IEEE common data format should present management difficulties in the development of new software, since it consists of a text file format that makes the direct access to specific information less straightforward. This context justifies the continuous development of computer programs and other types of database to support research in power distribution systems (IEEE, 2014).

In this paper, we propose a database structure that can be easily accessed for reading, writing and managing power system data. This database structure is also used for storing results of simple and advanced studies in power systems. This database is based on an open source code that can be easily changed to incorporate new features. It is now used as a support tool for studies of loadability and harmonics in power distribution systems, which are subjects currently investigated by the authors.

This paper is organized as follows. Section "Power Distribution System Models" briefly describes the modeling of the system elements, such as loads, lines and transformers. Section "Database and Structured Query Language" discusses database requirements and data management using structured query lan-

[1] Received the B.Sc. degree in electrical engineering from the Pontifical Catholic University of Minas Gerais (PUC Minas), Belo Horizonte, in 2007. He is currently master student at Federal University of Minas Gerais (UFMG), Belo Horizonte, and planning engineer at Cemig Distribution, Belo Horizonte. E-mail: fljuste@cemig.com.br

[2] Received the B.Sc., M.Sc. and Doctoral degrees in electrical engineering from the Federal University of Minas Gerais (UFMG), Belo Horizonte, in 2000, 2001, and 2006, respectively. He is currently full professor with the Department of Electrical Engineering, UFMG, and research associate with the Lightning Research Center of the same institution. E-mail: conti@cpdee.ufmg.br

How to cite: Journal Space xxxxxxxxxxxxxxxxxxxx
xxxxxxxxxxxxxxxxxxxxxxxxxxxxxxxxxxxxxxxxxxxxxxxxxxxxxxxxxxxxxxxxxxxxx

guage (SQL) in MATLAB. The interface between MATLAB and Microsoft Office Access is described in section "Database Model". Section "Application and Analysis" presents tests that were made using the 4-bus IEEE Distribution Test Feeder to investigate the behavior and functionality of the interface. Conclusions are presented in the last section.

Power Distribution System Models

Traditional radial power distribution systems have one path for power flow from source to costumers. A typical system consists of one distribution substation comprising one or more feeders. Elements of the system are the primary and secondary lines, which are typically three-phase, two-phase or single-phase, the transformers, and the three-phase, two-phase and single-phase loads.

Models of the system elements

Loads: The loads are essentially unbalanced in power distribution systems. In most cases they are modeled assuming constant power, constant current, constant impedance or any combination of these (Kersting, 2012). These models need data like in (1), where rated voltages (V_{an}, V_{bn} and V_{cn}) and apparent powers (S_a, S_b, and S_c) for each phase of the load are required. However, more data is required for models that take into account load response to voltage and frequency (IEEE, 2014) and temporal variations. A database based on tables can easily hold data for load models with these characteristics.

$$\begin{bmatrix} Z_a \\ Z_b \\ Z_c \end{bmatrix} = \left[\frac{|V_{an}|^2}{S_a{}^*} \quad \frac{|V_{bn}|^2}{S_b{}^*} \quad \frac{|V_{cn}|^2}{S_c{}^*} \right]^t \tag{1}$$

Lines: The model for overhead and underground lines in power distribution systems includes series impedances, shunt admittances and earth effects. For representing the earth return impedance, Carson's equations are used in the approximate form proposed by Kersting (2011), which is presented in (2)-(4). Additional details for obtaining the ABcd parameters of the lines are found in (Kersting, 2012). For harmonic studies, each frequency will lead to a line model that could be stored in a properly modeled database.

$$\hat{z}_{ii} = r_i + 4\omega P_{ii} G + j\left(X_i + 2\omega G \cdot ln\frac{S_{ii}}{R_i} + 4\omega Q_{ii} G\right) \tag{2}$$

$$X_i = 2\omega G \cdot \ln\frac{R_i}{GMR_i} \tag{3}$$

$$\hat{z}_{ij} = 4\omega P_{ij} G + j\left(2\omega G \cdot ln\frac{S_{ij}}{D_{ij}} + 4\omega Q_{ij} G\right) \tag{4}$$

where

$\hat{z}_{ii}$ = self-impedance of conductor i, in Ω/mi;
r_i = resistance of conductor i, in Ω/mi;
ω = system angular frequency, in rad/s;
G = $0.1609344\text{x}10^{-3}$ Ω/mi;
R_i = radius of conductor i, in ft;
GMR_i = geometric mean radius of conductor i, in ft;
$\hat{z}_{ij}$ = mutual impedance between conductors i and j, in Ω/mi;

$$P_{ij} = \frac{\pi}{8} - \frac{1}{3\sqrt{2}} k_{ij} \cos(\theta_{ij}) + \frac{{k_{ij}}^2}{16}\cos(2\theta_{ij}) \cdot \left(0.6728 + ln\frac{2}{k_{ij}}\right)$$

S_{ij} = distance between conductor i and image j, in ft;

$$Q_{ii} = -0.0386 + \frac{1}{2} ln\frac{2}{k_{ij}} + \frac{1}{3\sqrt{2}}\cos(\theta_{ij})$$

D_{ij} = distance between conductors i and j, in ft;

$$k_{ij} = 8.565 \times 10^{-4} \cdot S_{ij} \cdot \sqrt{\frac{f}{\rho}}$$

θ_{ij} = angle between a pair of lines drawn from conductor i to its own image and to the image of conductor j;
f = system frequency, in Hz;
ρ = earth resistivity, in Ωm.

Transformers: models include three-phase and single-phase transformers. In (Short, 2014) there is an extensive study about distribution transformers and their loading. Kersting (2012) shows a variety of models that can be implemented in computers for power flow studies. The widely used three-phase distribution transformer, connected delta-grounded wye step-down, is modeled through ABdc parameter matrices. In (5)-(8), these matrices are shown for a fundamental frequency application. Equation (7) was developed by the authors including the no-load current and the no-load losses, which are not considered in (Kersting, 2012).

$$[A_t] = \frac{V_{an}}{V_{AB}} \cdot \begin{bmatrix} 1 & 0 & -1 \\ -1 & 1 & 0 \\ 0 & -1 & 1 \end{bmatrix} \tag{5}$$

$$[B_t] = Z_t \cdot \begin{bmatrix} 1 & 0 & 0 \\ 0 & 1 & 0 \\ 0 & 0 & 1 \end{bmatrix} \tag{6}$$

$$[c_t] = \frac{V_{an}}{V_{AB}} \cdot \begin{bmatrix} 1 & -1 & 0 \\ 0 & 1 & -1 \\ -1 & 0 & 1 \end{bmatrix} \cdot Y_t \cdot \begin{bmatrix} 1 & 0 & 0 \\ 0 & 1 & 0 \\ 0 & 0 & 1 \end{bmatrix} \tag{7}$$

$$[d_t] = \frac{V_{an}}{V_{AB}} \cdot \begin{bmatrix} 1 & -1 & 0 \\ 0 & 1 & -1 \\ -1 & 0 & 1 \end{bmatrix} \tag{8}$$

where

V_{an} = rated phase-neutral voltage at low-voltage side, in kV;

V_{AB} = rated phase-phase voltage at high-voltage side, in kV;

Z_t = transformer short-circuit impedance referenced to the low-voltage side, in Ω;

Y_t = transformer shunt admittance referenced to the high-voltage side, in Ω;

As for loads and lines, a transformer model that includes harmonic effects should require extra data. In this case, an additional number of ABcd parameters matrices would have to be stored in the database.

Power flow method

The ABcd parameter matrices for all system elements can be combined for performing power flow studies in power distribution systems (Kersting, 2012). In this paper, the considered method is the ladder interactive technique, which makes the forward and backward calculation of the system behavior with (9) and (10) including buses between the source and the loads (Kersting, 1976). The results of power flow studies can be stored in a database for further use or for reports. This type of analysis can generate a big amount of data.

$$[V_{abc}]_m = [A] \cdot [V_{abc}]_n - [B] \cdot [I_{abc}]_m \tag{9}$$

$$[I_{abc}]_n = [c] \cdot [V_{abc}]_m + [d] \cdot [I_{abc}]_m \quad (10)$$

In the equations above, *n* refers to the backward bus, *m* refers to the forward bus, $[V_{abc}]_n$ refers to phase-neutral voltages at bus *n*, $[V_{abc}]_m$ refers to phase-neutral voltages at bus *m*, $[I_{abc}]_n$ corresponds to line currents leaving bus *n*, and $[I_{abc}]_m$ corresponds to line currents entering bus *m*.

Database and Structured Query Language

Arrillaga (2003) describes a computer implementation for harmonic studies with three base points: graphical user interface, simulation algorithm engine and database handling data structure. Some available power flow tools are able to exchange data through the IEEE common data format (Undrill, 1986), but each tool can have its own database format that generally is not open-source. In particular, the IEEE common data format is not well suited for retrieving or inserting data when a great amount of data, like data from systematic harmonic studies, has to be manipulated without a friendly interface. In addition, the IEEE common data format was proposed mostly for power flow studies in power transmission systems. Finally, most data in (IEEE, 2015) are available in MS Excel format file, i.e., table format.

Data storage in tables is visually more understandable and manageable and many softwares for storing tables that form a database are available. Some of them are the 'Microsoft Office Access', which allows up to 3 GB of database, and the 'Microsoft SQL Server Expresser 2014', freely downloadable, which allows up to 10 GB of database. Other professional softwares are SQLite and MySQL. These type of databases with the Structured Query Language (SQL) became widely used due to their simplicity and easy application (Gawlick, 2004). SQL specifies the desired result and not the way to get there. It has functions that enable users to declare what should be done with the collection of data stored in tables, like SELECT, INSERT or UPDATE. Other functions are also available.

The software MATLAB has a DataBase Toolbox that deals with external database using SQL functions. The SQL functions can be programed in .m files or used through the toolbox. Some SQL functions used in MATLAB are described as follows:

Select: the SELECT function allows retrieving data from a table for use as a variable in a computer program. Expressions (11) and (12) respectively show an SQL expression and its MATLAB representation.

$$\boldsymbol{SELECT\ Diameter\ FROM\ tbl\_OH\_CABLE\ WHERE\ Code\_Cable\ = Iris} \quad (11)$$

$$\boldsymbol{exec(connection, select\ data1\ from\ table\ where\ column = data2\ )} \quad (12)$$

Insert: the INSERT function is used by MATLAB to export data into a database. It inserts new data in a table for further use. Expressions (13) and (14) respectively show an SQL expression and its MATLAB representation.

$$\boldsymbol{INSERT\ INTO\ tbl\_CONFIGURATION\ (Frequency)\ VALUE\ (60)} \quad (13)$$

$$\boldsymbol{insert(connection, tablename, colnames, data)} \quad (14)$$

Update: the UPDATE function exports data into the database table replacing an existing one. Expressions (15) and (16) respectively show an SQL expression and its MATLAB representation.

$$\boldsymbol{UPDATE\ tbl\_PROJECT\ SET\ Node\_Order = 9\ WHERE\ Code\_Project = IEEE13} \quad (15)$$

$$\boldsymbol{update(connection, tablename, colnames, data, whereclause)} \quad (16)$$

Database Model

Othman (2012) proposed a database that stores power distribution system elements. The developed software includes a graphical user interface (GUI) developed in Microsoft.NET and C++, and a database using Microsoft SQL Server. Input data are read using forms or .txt files, which means that the user is not able to draw a system. In (Paucar, 2004), the authors developed an efficient and interactive computer program to meet the goal of being user friendly for studies of both transmission and distribution systems. They used platforms such C++, Java 3D and SQL. The distribution system program calculates the system's monetary value by using geographic information system (GIS) data. However it does not perform electric studies. Momin (2014) and Parikh (2009) integrated their GIS to their distribution system analysis software with SQL. In most other works, there is not a connection between power distribution system data and other databases managed by SQL.

In this paper, the MATLAB and Microsoft Office Access are used. MATLAB was chosen because it is widely used for simulation and new implementations in academic studies. As mentioned before, it is also convenient for its Database Toolbox that works with structured query language (SQL), which allows a relatively simple connection to external databases like the Microsoft Office Access (Gawlick, 2004). In the proposed database model, MATLAB is the front controller illustrated Fig. I, where the user can insert all data about the system and run the analysis. This is a simple GUI developed in MATLAB to allow an easy access to the .m files that manage the database. For example, to insert lines in the system one can use the menu bar "Element>Line" or the push button "Line" instead of typing the function on the MATLAB's screen. Microsoft Office Access stores the data in a background database. With those tools, the developed computational system meets the needs of storing data for power distribution systems as well as results obtained from their analysis. Those data can also be recovered for further studies.

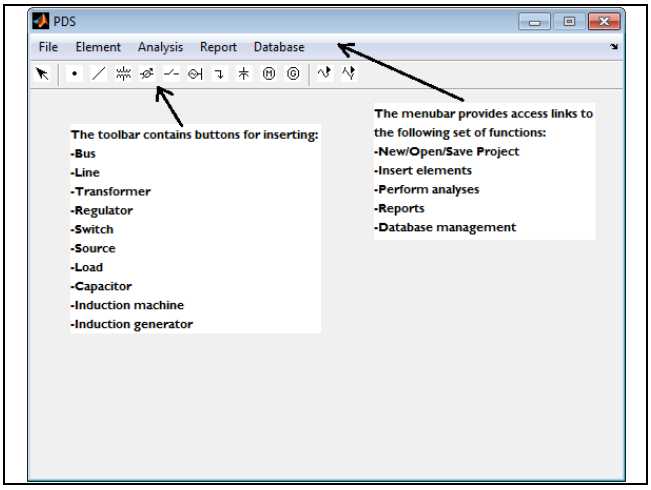

Figure 1. GUI developed at MATLAB to interface with Microsoft Office Access

Fig. 2 shows an overview of the interface between MATLAB and Microsoft Office Access. The elements of the power distribution system are modeled in .m files for MATLAB simulation and a set of analyses can be made such as power flow and loadability studies. Those .m files interact with the Microsoft Office Access database using the SQL functions discussed in the last section.

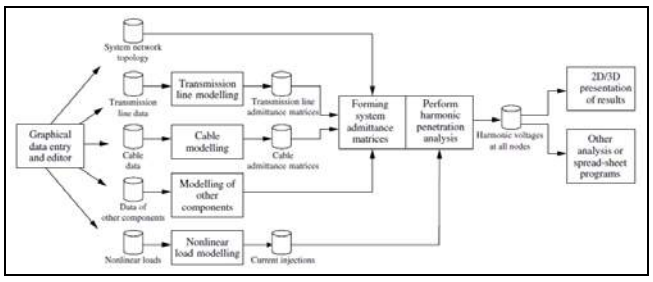

Figure 2. Interface proposed by Arrillaga (2003) for a database

The database model in Microsoft Office Access comprises a set of internal tables. There are two kinds of tables. One is for storing data, such as data for cables, structures, transformers, regulators, and capacitors. Data for overhead cables is stored in a table called *tbl_OH_CABLE*, whose columns are shown in Table I. Data from *tbl_OH_CABLE* table and from *tbl_PHASING* and *tbl_SPACING* tables are used in the procedure that calculates impedance and admittance matrices of overhead lines. The procedure was coded in .m files by using (2)-(4) and SQL functions like SELECT and INSERT. The results from the mentioned procedure are stored in a table named *tbl_CONFIGURATION*, which is illustrated in Fig. 3.

Table 1. Data for overhead cables

Column name	Data type	Description
Internal_code	Numeric integer long	Internal code [automatic increase]
Code_Cable	Char string long	Standard code cable
Size	Char string long	Cable's section size [AWG] [MCM]
Stranding	Char string long	Cable's stranding
Material	Char string long	Cable's material
Diameter	Numeric double	Cable's external diameter [in]
GMR	Numeric double	Cable's Geometric Mean Ratio [ft]
Resistance	Numeric double	Ohmic resistance at 50°C [Ω/mi]
Capacity	Numeric double	Electrical current capacity at 50°C [A]

The second kind of table stores data related to the current study, such as data for loads, buses, line parameters and results from power flow studies. For example, the 13-bus IEEE Distribution Test Feeder has 10 different lines with different configuration and length. For harmonic studies, it is needed to model 50 different impedance matrices and another 50 different admittance matrices, corresponding to the fundamental to the fiftieth harmonic order, for each line. Those data, namely ABcd parameter matrices of system elements, are stored in a table called *tbl_ABcd* that is used in power flow studies. Other tables such as *tbl_FLOW* and *tbl_RESULTS* are updated continuously until the current analysis is performed. These tables store, respectively, the power flow direction in the investigated radial power distribution system and the results of the analysis. Table 2 describes data corresponding to results of a given analysis that can be used either in a new analysis or to generate reports.

Table 2. Result data from analysis

Column name	Data type	Description
Code_Project	Char string long	Project's code
Frequency	Numeric double	System frequency or harmonic order
Voltage matrix	Numeric double	Matrix of voltage at buses [V] [pu]
Current matrix	Numeric double	Matrix of line currents [A] [pu]
Power matrix	Numeric double	Apparent power [kVA], active power [kW], reactive power [kvar]
Power factor	Numeric double	Matrix of power factor at buses
Losses	Numeric double	Matrix of lines' losses
Load	Numeric double	Matrix of loads

Application and Analysis

The interface between MATLAB and Microsoft Office Access and the storing data procedure was tested using the 4-bus IEEE Distribution Test Feeder. This feeder, shown Fig. 4, consists of an infinite bus that represents the distribution substation; two lines, one with three wires between bus 1 and 2 and the other with four wires between bus 3 and 4; a three-phase distribution transformer connected delta-grounded wye step-down; a balanced load at bus 4.

Two tests were performed. The first one was designed to investigate the use of tables that store data for future analysis. It considered the calculation of the impedance and admittance matrices from the fundamental to fiftieth harmonic order for the 4-wire overhead line shown in Fig. 5. The phase conductor is an ACSR 336.4 MCM 26/7 cable (Linnet) and the neutral conductor is an ACSR 4/0 AWG 6/1 cable (Penguin). The following information was required from the user: system fundamental frequency, earth resistivity, structure code, quantity of phases and neutrals, spacing code, phase conductor type, and neutral conductor type. The procedure ran 50 times in MATLAB, one per harmonic order, in 16.5 seconds including time for access and storage in database. In the fundamental frequency, the calculated impedance and admittance matrices are exactly as in (IEEE, 2015). All results were successfully stored in table *tbl_CONFIGURATION* and, thus, they are available for use in power flow calculations.

tbl_CONFIGURATION

Internal_code	Code_Configuration	Code_Phasing	Code_Cable_Phase	Code_Cable_Neutral	Code_Spacing	Frequency	Resistivity	Zabc	Yabc
297	601	NBAC	Dove	Penguin	500	60	100	[0.3465283977(	[0+i*6.2998079
298	602	NCAB	Penguin	Penguin	500	60	100	[0.7526283977(	[0+i*5.6989848
299	603	NCB	Raven	Raven	505	60	100	[0 0 0;0 1.3294]	[0 0 0;0 0+i*4.7
301	604	NAC	Raven	Raven	505	60	100	[1.3237932016:	[0+i*4.6658248
302	605	NC	Raven	Raven	510	60	100	[0 0 0;0 0 0;0 0	[0 0 0;0 0 0;0 0 (

Figure 3. Rows with impedance and admittance matrices for a frequency of 60 Hz, obtained from table *tbl_CONFIGURATION*, opened at Microsoft Office Access

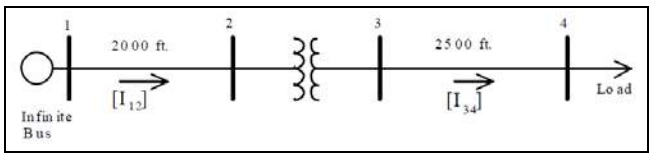

Figure 4. 4-bus IEEE Distribution Test Feeder (IEEE, 2015)

The second test was designed to calculate the 60-Hz power flow in the system of Fig. 4. It tested tables in the database related to those that are updated during the analysis. The user has to enter the following system information using the menu or the buttons illustrated in Fig. 1:

- Project number;
- Bus information: order number, rated voltage;
- Line information: send bus, receiver bus, length, structure;
- Transformer: code;
- Load: bus, type, rated voltage, frequency, powers;
- Source: bus, frequency, rated voltage.

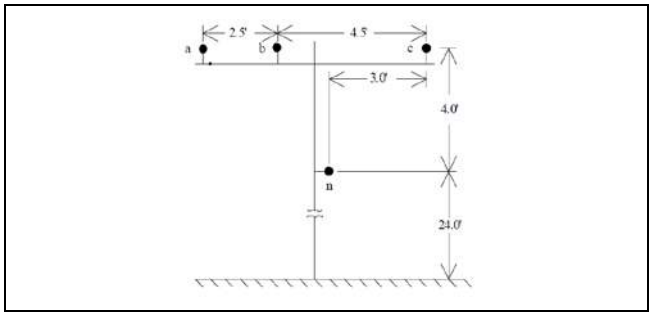

Figure 5. Structure for overhead line with 4 wires (IEEE, 2015)

The power flow routine is a procedure coded in an m. file function. During the forward and backward calculations using (9) and (10), the procedure accesses the database to get the appropriated ABcd matrices between two buses. In the.m. file function, none of variables are stored in the MATLAB workspace and thus the power flow has an additional time delay in its running time. Despite the fact that the connection between MATLAB and the database was satisfactory, the additional simulation time can be a problem in studies dealing with very large systems or in real time simulations. Table 3 shows the results obtained for the 4-bus IEEE Distribution Test Feeder, which are identical to the ones shown in (IEEE, 2015). This indicates a successful integration between MATLAB and Microsoft Office Access, since no data were lost in this task.

Conclusions

This paper demonstrates how a database model using a table format in Microsoft Access can be useful to store the elements of power distribution systems, as well as how the management of this database can be performed with MATLAB using SQL functions. The performance of the link between MATLAB and the database was tested and the results were satisfactory. Further investigations are going to focus on the connection speed between MATLAB and the Access Database, and the necessary changes in the MATLAB code to improve it.

Table 3. Results for 4-bus IEEE Distribution Test Feeder

Data from	Results from 4-bus IEEE Distribution Test Feeder	Results from MATLAB/ Access
Bus 1 [V]	$\begin{bmatrix}V_{an}\\V_{bn}\\V_{cn}\end{bmatrix}=\begin{bmatrix}7120\angle 0.0°\\7120\angle -120.0°\\7120\angle 120.0°\end{bmatrix}$	$\begin{bmatrix}V_{an}\\V_{bn}\\V_{cn}\end{bmatrix}=\begin{bmatrix}7120\angle 0.0°\\7120\angle -120.0°\\7120\angle 120.0°\end{bmatrix}$
Bus 2 [V]	$\begin{bmatrix}V_{an}\\V_{bn}\\V_{cn}\end{bmatrix}=\begin{bmatrix}7110\angle -0.3°\\7132\angle -120.4°\\7124\angle 119.6°\end{bmatrix}$	$\begin{bmatrix}V_{an}\\V_{bn}\\V_{cn}\end{bmatrix}=\begin{bmatrix}7110\angle -0.3°\\7132\angle -120.4°\\7124\angle 119.6°\end{bmatrix}$
Bus 3 [V]	$\begin{bmatrix}V_{an}\\V_{bn}\\V_{cn}\end{bmatrix}=\begin{bmatrix}2249\angle -33.7°\\2263\angle -153.4°\\2259\angle 86.4°\end{bmatrix}$	$\begin{bmatrix}V_{an}\\V_{bn}\\V_{cn}\end{bmatrix}=\begin{bmatrix}2249\angle -33.7°\\2263\angle -153.4°\\2259\angle 86.4°\end{bmatrix}$
Bus 4 [V]	$\begin{bmatrix}V_{an}\\V_{bn}\\V_{cn}\end{bmatrix}=\begin{bmatrix}1920\angle -39.1°\\2054\angle -158.3°\\1986\angle 80.9°\end{bmatrix}$	$\begin{bmatrix}V_{an}\\V_{bn}\\V_{cn}\end{bmatrix}=\begin{bmatrix}1920\angle -39.1°\\2054\angle -158.3°\\1986\angle 80.9°\end{bmatrix}$
Line 1-2 [A]	$\begin{bmatrix}I_a\\I_b\\I_c\end{bmatrix}=\begin{bmatrix}335.0\angle -35.7°\\331.8\angle -154.0°\\341.6\angle 85.6°\end{bmatrix}$	$\begin{bmatrix}I_a\\I_b\\I_c\end{bmatrix}=\begin{bmatrix}335.0\angle -35.7°\\331.8\angle -154.0°\\341.6\angle 85.6°\end{bmatrix}$
Line 3-4 [A]	$\begin{bmatrix}I_a\\I_b\\I_c\end{bmatrix}=\begin{bmatrix}1041.9\angle -64.9°\\973.7\angle 175.9°\\1007.0\angle 55.0°\end{bmatrix}$	$\begin{bmatrix}I_a\\I_b\\I_c\end{bmatrix}=\begin{bmatrix}1041.9\angle -64.9°\\973.7\angle 175.9°\\1007.0\angle 55.0°\end{bmatrix}$

References

Arrillaga, J., Watson, N., Power System Harmonics., 2nd ed., West Sussex: John Wiley & Sons, 2003.

Gawlick, D., Lenkov, D., Yalamanchi, A., Chernobrod, L., Applications for expression data in relational database systems., In: International Conference on Data Engineering, 2004, ICDE'04, IEEE, pp. 609-620.

IEEE, Distribution Test Feeders., Available at: <http://ewh.ieee.org/soc/pes/dsacom/testfeeders/index.html>. Access in: 06 Jul. 2015.

IEEE, Std 1729-2014 IEEE Recommended Practice for Electric Power Distribution System Analysis, 2014.

Kagan, N., Oliveira, C., Robba, E., Introdução aos Sistemas de Distribuição de Energia Elétrica.,2nd ed., São Paulo: Edgard Blücher, 2010.

Kersting, W., Distribution System Modeling and Analysis., 3th ed., Boca Raton: CRC Press, 2012.

Kersting, W., Green, R., The Application of Carson's Equation to the Steady-State Analysis of Distribution Feeders., In: IEEE/PES Power Systems Conference and Exposition, 2011., PSCE'11, pp. 1-6.

Kersting, W., Mendive, D., An Application of Ladder Network Theory to the Solution of Three-Phase Radial Load-Flow Problems, In: IEEE Conference Paper., Presented at the Winter Power Meeting,New York, January 1976.

Momin, A., The first interface software integrating between GIS and PDSAS in the middle east., In: Power and Energy Engineering Conference, 2014, APPEEC, IEEE PES, pp. 1-6.

Othman, B. et al., Developed software tool for distribution energy systems simulation and analysis., In: International Con-ference on Power and Energy, 2012, PECon, IEEE, pp.172-177.

Parikh, P., Nielsen, T., Transforming traditional geographic information system to support smart distribution systems., In: Power Systems Conference and Exposition, 2009., PSCE '09., IEEE/PES, pp.1-4.

Paucar, V. et al., Software development with computer graphics, distributed data base and OOP for deregulated power systems analysis., In: Large Engineering Systems Con-ference on Power Engineering, 2004., LESCOPE-04., IEEE, pp.198-202.

Rizy, D., Staunton, R., Evaluation of Distribution Analysis Software of DER Applications., US. Department of Energy, 2002, Available

at:<http://web.ornl.gov/~webworks/cppr/y2001/rpt/112228.pdf >. Access in: 04 Jun. 2014.

Short, T., Electric Power Distribution Handbook., 2nd ed., Boca Raton: CRC Press, 2014.

Undrill, J., Proposed Data Structure for Exchange of Power System Analytical Data., In: IEEE Power Engineering Review, Vol. 6 , Issue 5, 1986, pp. 26 – 31.

Characterization and relative sag source location in an electrical Distribution System

Caracterización y ubicación Relativa de fuentes de Hundimientos de voltaje en un Sistema eléctrico de distribución

L. H. Correa Salazar[1], C. C. Díaz Piñeros[2], A. L. Rivera Gómez[3] R. E. Moreno Zea[4]

ABSTRACT

This article aims to show the development and implementation of an algorithm in Matlab to characterize and determine, in an electrical distribution system, the area where the presence of sources of voltage sags. IEEE 37 Node Test Feeder and ATP software were used and faults of different nature were simulated in different parts of the system. From the raw information obtained in the simulations, the data processing is performed to proceed to implement and probe the algorithm in Matlab, which took into account factors such as system topology and comparison of measurements given by strain gauges which were placed in the distribution system and whose information is used to characterize and determine the relative sag source location. Once the algorithm is developed, its effectiveness according to the behavior of the simulated system was evaluated.

In this paper a review of relative sag source location is shown. At once, the test feeder model used for the simulation of faults is displayed, and the algorithm developed to determine the relative sags source location in the distribution system. The following are show simulated failures in the system and the results obtained by the algorithm, establishing its effectiveness and finally the conclusions and recommendations tossed the development of this project is.

Keywords: Algorithm, Distribution System, Modeling, Location, Voltage Sags.

RESUMEN

Este proyecto tiene como propósito mostrar el desarrollo e implementación de un algoritmo en Matlab para caracterizar y determinar, en un sistema de distribución, la zona donde hay presencia de fuentes de hundimientos de tensión. Para desarrollar y probar este algoritmo, se utilizó un sistema de prueba de IEEE de 37 nodos, modelado en el software ATP, y se simularon fallas de diferente naturaleza en distintos puntos del sistema. A partir de la información en bruto obtenida en las simulaciones, se realizó el tratamiento de datos para proceder a implementar el algoritmo en Matlab, el cual tuvo en cuenta elementos como la topología del sistema y la comparación de las medidas dadas por medidores de tensión que fueron ubicados en el sistema de distribución y cuya información se usó para poder determinar la ubicación relativa de fuentes de hundimientos. Una vez desarrollado el algoritmo, se evaluó la efectividad del mismo de acuerdo con el comportamiento del sistema simulado.

En este documento se muestra una reseña sobre ubicación relativa de fuentes de hundimientos de voltaje, a continuación se muestra el modelo del sistema de distribución utilizado para la simulación de fallas, y el algoritmo desarrollado para determinar la ubicación relativa de fuentes de hundimientos de tensión en el sistema de distribución, a continuación se muestran las fallas simuladas en el sistema y los resultados arrojados por el algoritmo, estableciendo así la efectividad del mismo y finalmente se muestran las conclusiones y recomendaciones que arrojó el desarrollo de este proyecto.

Palabras clave: Algoritmo, Sistema de distribución, Modelación, Ubicación, Hundimiento de voltaje.

Received: July 23th 2015
Accepted: Oct 15th 2015

I. Introduction

Power systems, divided into generation, transmission and distribution, are aimed at the demand of energy and are sufficiently known. Therefore, an important part of the power systems is the distribution system, through whom, the user, whether residential, commercial or industrial, comes to make use of the electrical energy supplied by the network operator according to energy demand, so it is necessary that there are no fault conditions present in the system, and if they occurs, it must be fixed up in the shortest possible time, keeping the system under normal operating conditions that allow the reliability, stability and a high level of power quality.

Hence, it has become essentially look for ways to identify at what point of a distribution system faults occur, so that they can be identified according to their characteristics and thus be able to maneuver and take actions that reduce the impact of these faults on the rest of the system. So far, it is not possible to accu-

[1] Correa Salazar Luis Hernando. Electrical Engineer, National University of Colombia. Specialist in Process Automation and Master in Electrical Engineering, Universidad de los Andes. Professor of Electrical Engineering Program, University of La Salle. Colombia Email: lcorrea@unisalle.edu.co.

[2] Díaz Piñeros Cristian Camilo. Electrical Engineering student. University of La Salle. Colombia. Email: cdiaz19@unisalle.edu.co.

3 Rivera Gómez Angie Lorena. Electrical Engineering student. University of La Salle. Colombia. Email: arivera33@unisalle.edu.co.

[4] Moreno Zea Raul Ernesto, Electrical Engineer, University of La Salle. Email: raul.moreno@enel.com

How to cite: Correa, L. H., Díaz, C. C., Rivera, A. L., Moreno, R. E. Characterization and relative sag source location in an electrical distribution system, Ingeniería e Investigación, Vol. xx, No. xx, xx, 2016, pp. xx

rately identify the fault location. An alternative is to place meters along the network, so that by comparison of measurements that these capture, it is possible to identify the area which occurs to minimize the impact of faults and reduce costs associated with them. And hence, a configured application is required to determine the relative sag source location and which is characterized by having high effectiveness.

II. Background

In recent years there has been a lot of work related to processing the raw information of voltage sags. This processing has been directed to the detection, classification, characterization and origin of voltage sags sources. Multiple tools have been used for the above purposes: Fourier transform, Wavelet transform, Kalman filters, and multivariable regression methods, among others.

The principles used for the detection and the origin of sags sources have also been diverse: quantification of the maximum energy and power (Kong Dong and Cheng, 2008) (Parsons, Grady, Powers and Soward, 2000); changes imped-ANCE seen by distance relay (Faisal Mohamed and Shareef, 2011), (Correa, Tumialan and Moreno, 2015); changes in the slope of the line (Li, Tayjasanant, Xu and Li, 2003), changes in the compo-nents current assets (Hamzah, Mohamed and Hussain, 2004); changes in the resistive impedance component, comparison of magnitudes of voltage dips on either side power transformer (Leborgne and Karlsson, 2008); definition of indicators and decision criteria to identify the source (Seon Dong Il and Seung, 2005), etc.

With a careful reading of the works we can conclude the following related with processing and, above all, the source of voltage sags:

The exact location of the source or origin of a voltage sag is too big a job. The technical literature reports only a precise location oriented work (Kazemi, Mohamed, Shareef and Rahi, 2014). The algorithm is called GACP-MVR, which is based on a multivariable regression model (MVR). According to the algorithm, first the optimal number and location of power quality monitors is determined and then the Mallow's Cp index is applied. Monitored busbars are considered as independent variables. Then, regression coefficients are obtained to estimate voltages at the not monitored busbars. The MVR trained models are used to determine the maximum voltage deviation and the minimum standard deviation data which sags sources are identified. The algorithm has the disadvantage that in addition to voltage measurements are required necessary training data (from simulations) where it is desirable to know what the behavior of the sags on the unmonitored buses. This training consists of a considerable number of simulations with varying impedances of failure, failure types, load increases and other parameters of interest. All aimed at understanding the behavior of unmonitored nodes.

As relative location (definition of an area, a section or group of sections which can come voltage sags) has the following:

Work (Blanco, Petit, Ordoñez and Barrera, 2013) provides the relative sag source location (meters downstream, upstream of meters, between meters) with voltage information. The algorithm considers only sags caused by faults in the network and information from at least three monitors located in the distribution network under study. Additional features of the algorithm are as follows: The descriptors are fundamental positive sequence voltages during the fault and during prefault; a number of failures is generated by ATP in a test system and the resulting information (voltage) is transferred to MATLAB with relative identification purposes (on descriptors compared with defined thresholds).

In (Barrera, Meléndez, Herraíz and Sánchez, 2009) the algorithm provides relative location (upstream or downstream of a power quality monitor). The algorithm is very simple: It is based on the calculation of the ratio of the currents of positive sequence before and during a fault in a power system.

Work (Hamzah, Mohamed and Hussain, 2009) presents an algorithm with the product of the effective current used and the power factor at the monitoring point. The basic idea, then, is to draw a graph with the evolution of this product over time. The location of the sag is determined by examining the index of the current component (ICC) at the beginning of sag. If the index is greater than before the sag occurs, then the sag occurs downstream, otherwise sag occurs upstream. In the algorithm data streams and power factors it is needed in the monitoring point.

One of the classic articles related to location of sources of voltage sags is (Leborgne and Karlsson, 2009), which only requires information of voltages. The source of the sag is located with magnitudes of sag in the primary and secondary sides of a power transformer. The main focus is the location on the edge or border point between two transmission systems. The idea is to compare the magnitude of sag, in per unit, based on the pre-fault voltage on both sides of a transformer. Two voltage drops according to a fault current and impedance transformer are defined and a comparison is made to determine whether the sag upstream or downstream of the transformer is presented.

In 2002 (Qader, Bollen and Allan, 1998), an article on the stochastic prediction of voltage sags in a transmission system was published by using two methods. The first method is the fault position which is most suitable for implementation in a software tool. This method was used to locate areas where sags are produced and for the frequency with which sags in each of the busbars presented. The other method used was that of critical distances. This method is appropriate to calculate how often sags occurring in a number of buses. Because this method is based on mathematical calculations that are made by hand and given the complexity of the calculations, the results are very limited to simple cases. One made up of 97 nodes, 400 kV, corresponding to a part of the transmission system in England and Wales system was used for this case study.

Moreover, a paper (Galijasevic and Abur, 2002) about troubleshooting using voltage measurements was published. The work consisted in taking actual measurements of voltage sags in certain nodes of a system and from these measurements, the system is modeled and areas with greater likelihood of failure were estimated and conducted the simulation with several fault resistances. After having the simulation results and using fuzzy logic, it came to check that the measurement results obtained by simulations, emulated almost precisely the values of actual measurements.

Finally, an article (Pereira, Da Silva, Kezunovic and Mantovani, 2009) on the use of an algorithm in order to locate faults was published, which generated sags in the power supplies of a distribution system. The basic principle of the algorithm is that when a fault occurs in the power sources, the propagation has different characteristics in each of the nodes which is connected a power supply and, therefore, by knowledge of these characteristics, it is possible to locate the node with faults or the area where failure of the power supply occurs. This approach ensures the efficiency

of the algorithm which provides suitable results. For the case study, a real 13,8 kV system, consisting of 134 nodes it was used.

The main contribution of this paper is validating the algorithm developed by (Blanco, Petit, Ordóñez and Barrera, 2013) and characterization (cycle to cycle) of the sags, according to Bollen Classification. With this classification it is possible to determine the type of fault that originates the sags.

III. Description of the distribution system modeling

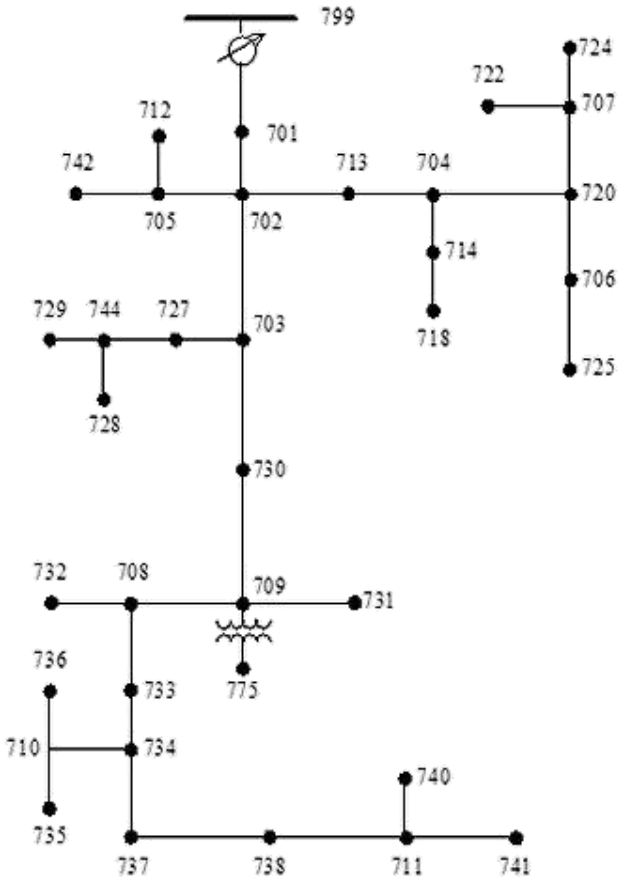

Figure 1. IEEE 37 Node Test Feeder.

For the development of this application, the IEEE 37 Node Test Feeder was used (Figure 1). This system of distribution is radial, which is quite convenient for the analysis, taking into account that the application has consistent results mostly for radial distribution systems, it means that each meter should be located on the main feeder system consecutively and not in the branches or laterals of the system or endpoints.

There is a voltage regulator in node 799, which allows the voltage supplied to the system is always the same value and has no abrupt changes in time, so that the RMS value is constant.

Modelling the system in ATP software, this is controlled by a generator, which fulfills the same function that the regulatory change that is always giving the same RMS value as a function of time.

In node 709, according to the IEEE model, the transformer is delta-delta with a capacity of 0,5 MVA and 4,8 kV transformer ratio to 0,48 kV. In the simulated system, the transformer used differs with the IEEE only in that the model is delta-Y. This is in order to be able to model ground faults and watch the behavior of the system and performance of application in this type of failure.

To verify that changes made in the system did not affect the nature of the topology and, after completing the modifications, we proceeded to perform a simulation of the system without faults that originated sags. In this case, voltages in nodes, currents by branches and reactive and active power were observed. From these data, we proceeded to compare them with results from the load flow information that appears on the test system. This observation show similar data, so that the viability of the changes was defined and that they did not have inconsistencies that could affect the development of the tests.

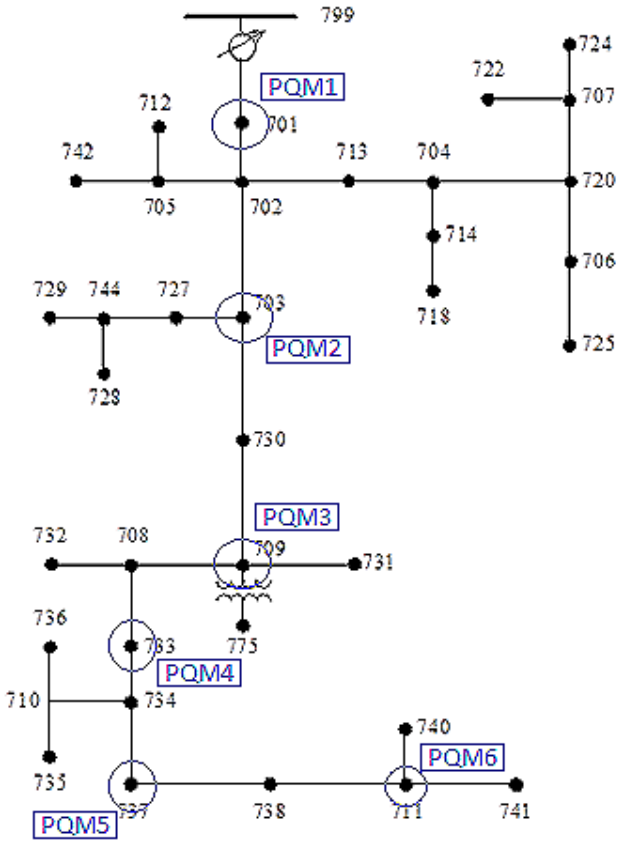

Figure 2. Distribution of voltage meters in the Test Feeder

Six meters were placed in model of the system, which store data of node voltages: the gauge number one located at node 701, the meter 2 at 703 node, meter 3 at 709 node, the meter 4 at node 733, the meter 5 at node 737 and, finally, the meter 6 is located at 711 node.

The meters are distributed along the main feeder distribution system, which is radial. This distribution is because the application does not work properly when the system is meshed, or the meters are in remote branches, or laterals, to the main feeder.

To simulate faults at first two-phase and three-phase faults were simulated, but it was not possible ground faults due to the connections of the main transformer, so it was established right put down transformer 230 kV to 4,8 kV and connecting to earth for

the purpose of generating single-phase and two-phase to ground faults. Also, changes in impedance fault, fault clearing time, fault location and type of fault which caused a large number of faults were generated.

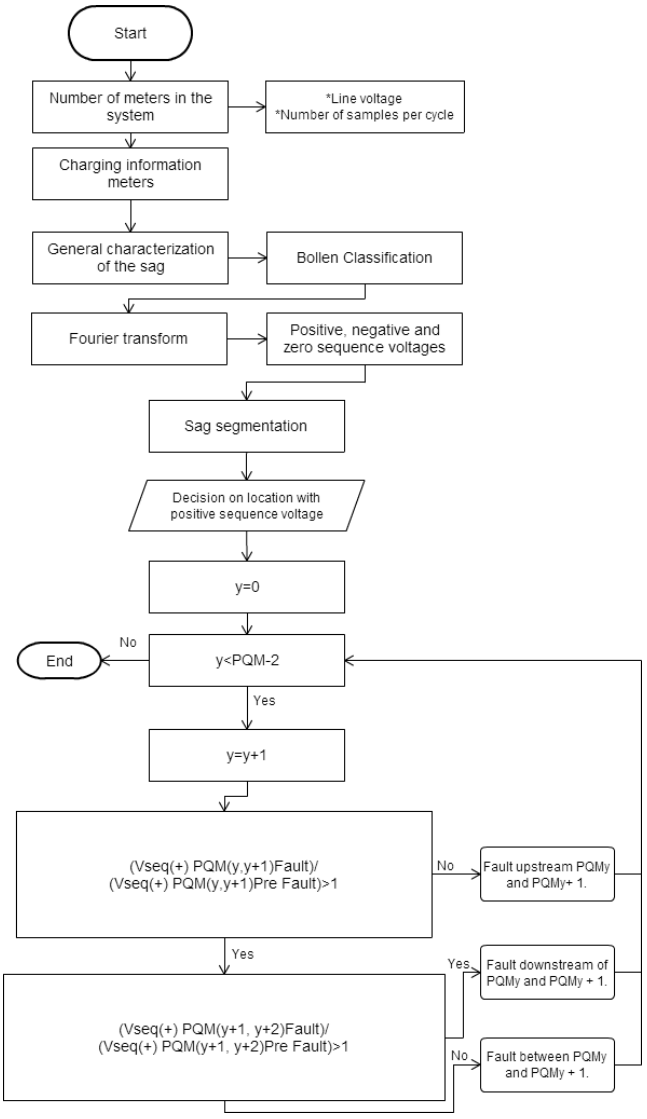

Figure 3. Description of application for characterization and voltage sag source location.

The purpose of the application is to locate the area where the sag had occurred. This application was developed from the algorithm implemented by (Blanco, Petit, Ordoñez and Barrera, 2013), since this algorithm was proposed to implement a more detailed characterization of the sag located, from the Bollen methodology.

This is done with simulated values before and during voltage sag generated by ATP software. The application, implemented in Matlab, receives raw data from ATP, and then the data obtained, shows the RMS values of the voltages, then performs the characterization of sag, ie the RMS values obtained values prefault is obtained and misses sag, considering that the sag starts when a value below of 0.9 p.u. is presented in the RMS value of the voltage wave.

After obtaining the values (duration and magnitude), the sag is classified according to Bollen methodology (Bollen, 2000), taking into account the displacement in phasors, the fall in the magnitude and type of fault. This classification throws a letter between A-G according to the sag detected by meters. One example of results for this basic characterization, for each monitor, is showed in Table I.

Table 1. Basic characterization of sags, by each monitor.

PQM	Magnitude [p.u.]	Duration [s]	Type (per cycle)
1	0,802	0,05	E-E-E
2	0,647	0,063	E-E-E
3	0,645	0,061	E-E-E
4	0,645	0,061	E-E-E
5	0,644	0,060	E-E-E
6	0,645	0,060	E-E-E

After characterization, the Fourier transform is applied to raw information of voltages (time domain). Taking into account that in ATP only magnitudes are obtained, it is necessary decompose the wave using the Fourier transform with the purpose to obtain the voltage phasor (Magnitude and angle), this procedure repeats for each phase. With this information afterwards it performs decomposition in positive, negative and zero sequence components. It should be noted that the priority will be the positive component of voltage, because this component is presented in all types of faults.

The sag's segmentation is carried out in order to have a value from the sag for later evaluation in the block of the algorithm's decision either in fault state or pre-fault state.

Finally the application use the information obtained previously (Positive sequence component and sag's segmentation) to determine the relative location where the sag occurred in the system. It is important take into account that a control index (y) is used in this step given the number of iterations.

To test the application, a total number of 120 faults were made. Table 2 shows the number and type of faults and the relative location of sags sources

Table 2. Type and number of simulated faults in the distribution system.

Faults between PQM1-PQM2	L-L	8
	L-L-L	13
	L-L-G	13
	L-G	13
	Total	**47**
Faults between PQM2-PQM3	L-L	3
	L-L-L	2
	L-L-G	2
	L-G	3
	Total	**10**
Faults between PQM3-PQM4	L-L	4
	L-L-L	4
	L-L-G	2
	L-G	5

	Total	**15**
Faults upstream PQM1-PQM2	L-L	2
	L-L-L	2
	L-L-G	1
	L-G	1
	Total	**6**
Faults downstream PQM3-PQM4	L-L	8
	L-L-L	11
	L-L-G	12
	L-G	11
	Total	**42**
Total simulated faults		**120**

IV. Results of the application.

In this work, 120 faults were simulated in ATP software for test feeder. The corresponding results were processed in the application implemented in Matlab, which showed the relative sag source location and characterization of each one. In Table 3 is listed the simulated faults in the system shown that all failures were correctly located by the algorithm. It is noteworthy that the algorithm, when it sees a failure so far the meter 4 is not strict to show if the fault is between PQM4 and PQM5 or downstream of PQM5. The application only shows directly that is downstream of the meter 4 is why even if not through about the last 2 meters, taken as true that the fault is downstream of the meter 4. Table 4 shows detailed information so that the algorithm throw in some simulated failures.

Table 3. Results obtained by the application

Relative Location	Faults (source of sags) correctly located	Faults (source of sags) incorrectly located.
Upstream PQM1-PQM2	6	0
Between PQM1-PQM2	47	0
Between PQM2-PQM3	10	0
Between PQM3-PQM4	15	0
Downstream PQM3-PQM4	42	0

According with simulations and experimental results worth analyzing they were obtained:

At least one of the monitors must detect the sag, but in this case all the information of other monitors is necessary for voltage sag source location.

Also, established the need to take samples from 10 cycles before and 10 cycles sag occur after the failure, so they reach store all the required values for the corresponding correlation analysis voltage to allow locate the region where the fault occurs.

Table 4. Some detailed results of the application.

Fault in node	Relative Sag Source Location	Fault type (Source of Sag)	Sag type
703	PQM1-PQM2	L-L-G	E
730	PQM2-PQM3	L-L	C
733	PQM3-PQM4	L-L-L	G
741	DOWNSTREAM PQM3-PQM4	L-G	B
Prim. Regulator	UPSTREAM PQM1-PQM2	L-G	B
733	PQM3-PQM4	L-L-L	G-A
724	PQM1-PQM2	L-L-L	A

Among the results, it could find that once the relative sag source location is done (location of the region where the sag occurs), the application threw a 94% effectiveness in 120 samples taken, even though the 6% remaining was not correctly located, it should not be understood as a lack of the application. Regarding the Bollen classification, it was found that 97% of the samples are classified within the classification of Bollen and 3% were not classified, this 3% belongs to some series of sags which cannot be classified by Bollen. Table 5, shows the percentage of sags that were found in each category of Bollen in the simulations. In some cases, the same sag was classified in two categories, this occurs because a phase shift caused by sag's occurrence.

Table 5. Percentage of effectiveness of sags classification.

Bollen Classification	Samples	%
A	6	80%
B	35	100%
C	24	100%
D	0	
E	21	100%
F	0	
G	20	80%
No classification	4	
With two categories	10	
Total	**120**	**100%**

V. Conclusions.

It is important to highlight the advantage of use only voltage values to determine the relative sag source location, because in the system can always find these values, but it is not always easy to obtain values of currents. This makes it more feasible and less complicated to determine the location of the sag in the distribution system, without needing to other measuring instruments that are not in the system.

The application identifies regions that may become more susceptible to failures and likewise identifies the type of sag which makes it possible to establish that a region can become more susceptible to certain types of faults, which can lead to losses in equipment and production which in the end translates into economic losses for both, the industrial sector and to network operators. This will help make the system more reliable and both, system operators and users (particularly for the industrial sector), are less affected by the consequences that generates a sag.

One of the drawbacks of the application is to reduce the region and give a more accurate location point of faults necessary to

have more meters within the system, which is not always easy, plus the algorithm is formulated in such so that the meters are along the main feeder in the distribution system, which means that if on one of the branches (laterals) of the feeder fault occurs and this branch contains many nodes, it is not possible to establish the precise location of failure within the system and other analysis and measures to more effectively determine the region where the failure occurs may be necessary.

Acknowledgements

This work was developed by CALPOSALLE and AVARC groups of Universidad de La Salle, under the project Plataforma de toma, muestreo, análisis y caracterización de datos de calidad de potencia, que permita la selección de clientes industriales potencialmente generadores de disturbios de calidad de potencia, for CODENSA S.A. E.S.P.

References

Barrera V., Meléndez J., Herraíz S., Sánchez J., A New Sag Source Relative Location Algorithm Based On The Sequence Current Magnitude, Proceedings of V Simposio Internacional Sobre Calidad de Energía Eléctrica (SICEL), Bogotá D.C., August, 2009.

Blanco J., Petit J.F., Ordóñez G., Barrera V., A New Algorithm for Relative Location of Voltage Sags Based on Voltage Measurements Only, Proceedings of VII Simposio Internacional Sobre Calidad de Energía Eléctrica (SICEL), Medellín, November, 2013.

Bollen, M.H., Understanding Power Quality Problems: Voltage Sags and Interruptions. Piscataway, IEEE Press (Ed.), New York, 2000.

Correa, L., Tumialán, J., Moreno, R., Development of application for relative sag source location through the use of S transform, Proceedings of 2nd IEEE Workshop on Power Electronics and Power Quality Applications (PEPQA), Bogotá D.C., June, 2015.

Faisal, M., Mohamed, A., Shareef, H. An effective time frequency method for voltage sag source detection, Proceedings of 21ST International Conference on Electricity Distribution (CIRED), Frankfurt, June, 2011.

Galijasevic, Z., Abur, A., Fault location using voltage measurements, IEEE Transactions on Power Delivery, Vol. 17, No. 2, Apr., 2002, pp. 441-445.

Hamzah, N., Mohamed, A., Hussain, A., A New Approach to locate the Voltage Sag Source Using Real Current Component, Elsevier Electric Power System Research, Vol. 72, Nov., 2004, pp. 113-123.

Hamzah N., Mohamed A., Hussain A., Development of New Algorithm for Voltage Sag Source Location, Proceedings of the International Multiconference of Engineers and Computer Scientists, (IMECS), Hong Kong, March, 2009.

Kazemi A., Mohamed A., Shareef H., Raihi H., Accurate voltage sag-source location technique for power systems using GACp and multivariable regression methods, Elsevier Electrical Power and Energy Systems, Vol. 56, March, 2014, pp. 97-109.

Kong, W., Dong, X., Chen, Z., Voltage Sag Source Location Based on Instantaneous Energy Detection, Elsevier Electric Power Systems Research, Vol. 78, Oct., 2008, pp. 1889-1898.

Leborgne, R., Karlsson, D., Voltage Sag Source Location Based on Voltage Measurements Only, Journal of Electrical Power Quality and Utilisation 2008, No. 1, pp. 25-30

Li, C., Tayjasanant, T., Xu, W., Liu, X., Method for Voltage Sag Source Detection by Investigating Slope of the System Trajectory", IEEE Proceedings - Generation, Transmission and Distribution, Vol.150, May., 2003, pp. 367-372.

Parsons, A.C., Grady, W.M., Powers E.J., Soward J.C., A Direction Finder for Power Quality Disturbances Based Upon Disturbance Power and Energy, IEEE Transactions on Power Delivery, Vol. 15, Jul., 2000, pp. 1081-1086.

Pereira, R.A.F., Da Silva, L.G.W., Kezunovic, M., Mantovani, J.R.S., Improved Fault Location on Distribution Feeders Based on Matching During-Fault Voltage Sags, IEEE Transactions on Power Delivery, Vol. 24, No. 2, Apr., 2009, pp. 852-862.

Qader, M.R., Bollen, M.H.J., Allan, R.N., Stochastic prediction of voltage sags in a large transmission system, IEEE Industrial and commercial power systems technical conference, May, 1998, pp. 8-18

Seon, J., Dong, J., Il, Y., Seung, I., A Method to determine the relative location of voltage sag source for power quality diagnosis, Proceedings of the 16th IFAC World Congress, Vol. 16, Jul., 2005

Strategy for improvement the performance of a fault locator based on support vector machines

Estrategia para mejorar el desempeño de un localizador de fallas basado en máquinas de soporte vectorial

D. Arredondo[1], J. Mora-Florez[2], S. Pérez-Londono[3]

ABSTRACT

This paper presents a strategy aimed to improve the performance of a fault locator based on support vector machines (SVM). The strategy is based on the definition of the best number of operative conditions for parameterization and training stages, oriented to reach the better performance in minimal time intervals. The proposed methodology is tested in three distribution power systems designed according to the national technical standards for the different voltage levels. This paper shows the dependence relation between the training and parameterization databases with the performance of the fault locator

Keywords: Electric power distribution system, fault location, support vector machine, the training and parameterization stages.

RESUMEN

En este documento se presenta una estrategia implementada para mejorar el rendimiento de un localizador de fallas basado en la máquina de soporte vectorial (SVM). La estrategia se fundamenta en la definición del mejor número de condiciones de parametrización y entrenamiento para alcanzar buenos desempeños en un mínimo tiempo posible. La metodología propuesta se valida en tres circuitos de distribución diseñados con normas técnicas colombianas con diferentes niveles de tensión. Este análisis muestra que existen relaciones de dependencia entre la base de datos de entrenamiento y parametrización con el rendimiento del localizador.

Palabras clave: Sistemas de distribución de energía eléctrica, entrenamiento y parametrización, localización de fallas, máquinas de soporte vectorial.

Received: July 23th 2015
Accepted: Oct 15th 2015

Introduction

Service continuity in power distribution systems is a very important aspect for power utilities. These have to provide a good service, but faults at the power system are difficult to avoid. Faults affect the financial balance of the utility due to the cost of compensations for low continuity indexes, non-supplied energy and maintenance team workforce, among others [Dash, et al., 2007]

The most common fault in power distribution systems is the single-phase fault [Mora, 2006]. In most of the cases, these faults are difficult to localize due the length of the feeder, the level of the power distribution automation, presence of transient faults and the constrained availability of the maintenance staff. The restoration time strongly depends on the fault location time; nowadays in most of the utilities does not have any helping tool to facilitate the automatic fault location.

To solve this problem, several methodologies have been implemented and these methods use measurements of the voltage and current at the main power substation between fault and pre-fault stages [Agudelo, et al., 2014], [Orozco, et al., 2012], [Livani & Evrenosoglu, 2014]. There are two groups of fault location algorithms, the first is called methods based on the power system model and the second one is the method based on knowledge. The first one is based on the creation of a model of the power system to estimate the distance to the fault; this methodology has the problem of multiple estimation [Thukaram, et al., 2014] [Morales, et al., 2010]. The second one is based in data mining methods and has been used to determine the faulted zone and also to solve the multiple estimation problem [Gil, et al., 2013].

Data mining are techniques to extract information from the database. The size of the database is determinant in the perfor-

[1] Debbie Johan Arredondo Arteaga. B.Sc. in Electrical Engineering from the Universidad Tecnológica de Pereira and M.Sc candidate in Electrical Engineering from the Universidad Tecnológica de Pereira, Colombia. Email: djarredondo@utp.edu.co
[2] Juan José Mora-Flórez: B.Sc. and M.Sc. in Electrical Engineering from the Universidad Industrial de Santander, Colombia. Ph.D. in Electrical Engineering from the Universitat de Girona, España. Affiliation: Associated professor at Universidad Tecnológica de Pereira, Colombia. E-mail: jjmora@utp.edu.co
[3] Sandra Pérez-Londoño: B.Sc. and M.Sc. in Electrical Engineering from the Universidad Tecnológica de Pereira, Colombia. Ph.D. in Electrical Engineering from the Universidad Nacional de Colombia. Affiliation: Associated professor at Universidad Tecnológica de Pereira, Colombia. E-mail: saperez@utp.edu.co

mance of the fault locator, one of the most critical aspect in these methods is the training time, when there are large amounts of data, the time intervals and performance will be high but Little data often will reflect in minimal time intervals, and the performance will also be low. The actual estimation to determine the optimal size of the database is not an easy problem.

In this paper is proposed a strategy to improve the performance of the fault locator based on support vector machine (SVM). The main idea is to obtain the number of operative conditions (database of faults for an operative condition of the power system) for training and parameterization stages that reach the best performance of the locator. This methodology has been implemented for three power distribution systems designed with the Colombian standards. The support vector machine based fault locator belongs to the group of knowledge-based methods and as is described in several papers, the approach presents a good performance [Gil, et al., 2013], [Agudelo, et al., 2014]. However in most of the cases, the parameters are determined in a heuristic way, then number of operative conditions used in parameterization and training stages is here analyzed to determine the best relation between the computational effort and the performance of the fault locator.

This paper is divided in five sections. The section II presents the basic theoretical aspects, while the section III explains the proposed methodology. Section IV is devoted to show and analyze the obtained results, and finally, the section V presents the main conclusions obtained on the here reported research.

Theoretical aspects

This section is devoted to present the basic concepts used in this paper; detailed information are out of the scope of this section, however it can be obtained at the provided references.

A- Support vector machine

The support vector machine (SVM), is a classification technique that has recognized advantages over other classification techniques such as robust performance, generalization capability, single parameter dependency and the use of a kernel function, among others (references).

The SVM is a binary classification technique; however, it can be generalized to be a multiclass classification technique by using a decomposition-reconstruction technique has been reported in [Mora, 2006]. The here used decomposition and reconstruction strategies are next explained.

Decomposition one vs one (OVO): This strategy is used to convert the support vector machine from a binary classification machine into a multi-class machine. In this phase, a multi class problem is decomposed in N binary classification problems [Mora, 2006].

Reconstruction by simple vote: This phase is aimed to integrate the results of the N binary problems and emulate the behavior of a single multi classification machine. This voting scheme is used in the here presented research due to its easy to implementation and the reduced quantity of ties between classes [Gutiérrez, et al., 2010], [Morales, et al., 2010].

B- Data base generation

The fault database required to develop the proposed approach, is obtained using several tools created by the research group. Some of the most relevant used tools are briefly presented.

RF simulation is an algorithm developed to generate faults in a power distribution system, which is based in techniques as Latin hypercube, sensitivity analysis, among others, to create an amount of operative conditions by variations on loads, supply voltage, power frequency, among others. In those conditions, the algorithm performs faults in every node of the analyzed power system, and voltages and currents at the main power substation are measured and stored [Mora, et al., 2006]. This tool uses an efficient combination of the Alternative transients program (ATP) and MATLAB.

Latin hypercube is the here used sampling technique, because it is independent of the analyzed model. It also reduces the number of evaluations, generating a small dataset that fully represents the total sampling space [Alzate, et al., 2014]. This technique is used here to determine the operative conditions of the analyzed power distribution system, to be simulated wit RF simulation tool in order to obtain the fault database.

Proposed methodology

The figure 1 shows the proposed methodology scheme. This scheme consists of five different stages aimed to improve the fault locator performance.

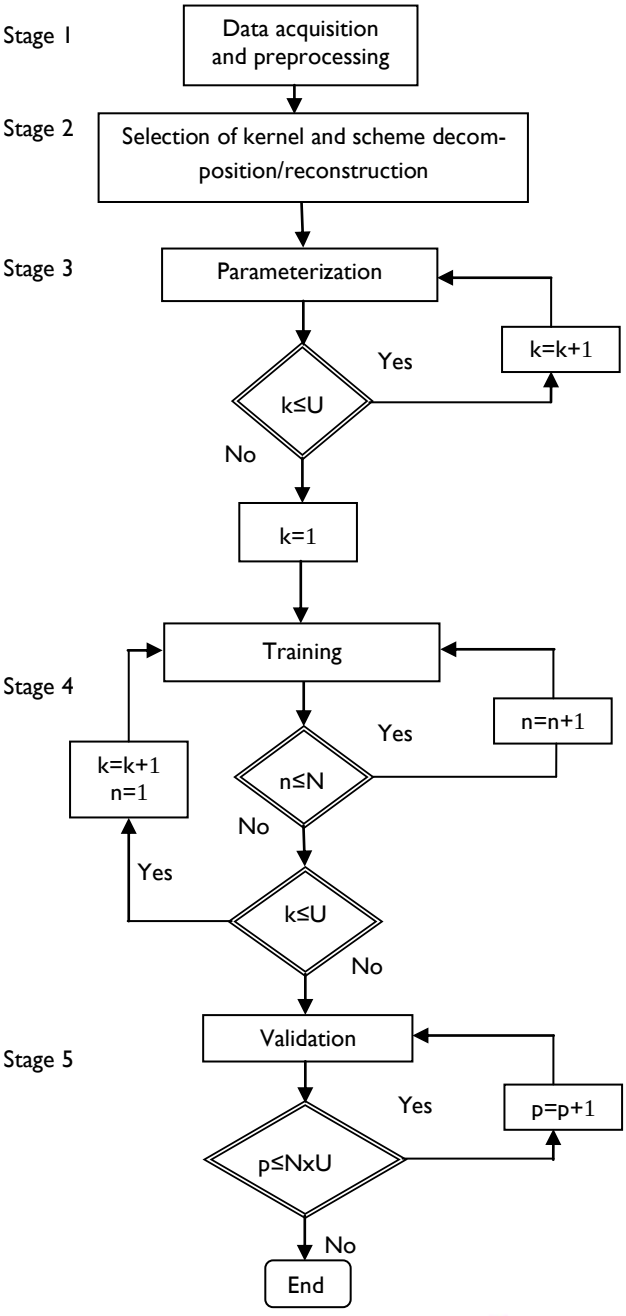

Figure 1. Methodology scheme. Source: authors

A- Stage 1: Data acquisition and preprocessing,

Data acquisition: Using the Latin hypercube technique, the variations from the rated conditions of the power distribution system are obtained. Then, by using the simulation RF tool, faults are performed in each node and using different values of fault resistance, at the analyzed power distribution system.

Data preprocessing: The data processing improves the performance of SVM while the computational effort is reduced. This process consists of feature extraction and normalization of database, which aims to eliminate unnecessary or inconsistent information for the SVM [Gil, et al., 2013]. At this stage, features as the magnitude and angles of voltages and current measured at the main power substation and during pre-fault and fault conditions, are obtained.

B- Stage 2: Selection of kernel and scheme decomposition/reconstruction

Type of kernel: Several kernels can be used, however the radial basis function (RBF) was selected due the adequate performance in all the fault location researches [Agudelo, et al., 2014], [Thukaram, et al., 2014], [Mora, 2006], [Gutiérrez, et al., 2010].

Scheme of decomposition and reconstruction: At the proposed methodology the one vs one (OVO) decomposition method has been used. In addition, single voting reconstruction method is also used. These methods transform the binary classifier in a multi-class classifier as previously explained, [Gil, et al., 2013].

C- Stage 3: Parameterization

At this stage, the optimal parameters of the classifier are determined (C and γ, where C is the penalty parameter for SVM and γ is the kernel parameter). The parameterization stage in the proposed method is an iterative phase due to the use of a determined number of operative conditions. k at figure 1, it is a counter of the number parameterizations performed; this process is repeated U times.

The Tabu metaheuristic searches the optimal parameters using as objective function the cross-validation error. Then the algorithm obtained the smallest cross-validation error, as presented in [Gil, et al., 2013].

Parameterization: This phase is the important due to the optimization algorithm (metaheuristic Tabu) because, this technique improve the separation of data. The rated operative condition is needed for this process because it is recommend using less than 1% of the all operative conditions at the database (the parameterization must to be a fast process).

The parameterization in the scheme (figure 1) must to be done with different numbers of conditions; the final idea is to determine an optimal number of parameterization conditions that improve the performance of the locator.

In this paper has been used one, three, five, seven and nine operative conditions, including the nominal condition, for the parameterization process, then U=5.

D- Stage 4: Training

At this stage, optimal parameters obtained for every parameterization are used (U parameterization). According to the previously exposed, the machine must to be trained several times (NxU).

The training process is computationally expensive; however the number of training conditions is determinant in the final performance. Therefore it is recommended use less than 10 % of the totals power system operating conditions.

The training process is performed for different numbers of conditions (N). Moreover it is important that all the training conditions have to be done for every single parameterization (k).

In training process, n and k are training counters. The numbers of training conditions chosen are 50, 100, 150, 200, 250, 300, 350, 400 and 700, then N=9. This number of conditions was choosing because the performance is good and the computational cost is not very expensive.

E- Stage 5: Validation

Using the fault database, each training process in stage 4 is evaluated for the remaining of the database not used in parameterization and training stages.

The validation phase is performed for all of the training conditions analyzed on stage 4. This process is done with more than 80 % of the total database, in this phase is determined the performace of the learning technique.

The parameter p in the scheme (figure 1), it is a counter that increments with each validation set used at the training process. The total number of training conditions is NxU, (N total number of training for each parameterization conditions, U total number of parameterization conditions).

Obtained results

At this research three distribution power systems was selected to validate the proposed strategy; these power systems are a good replica of the currently installed power distribution systems in Colombia, and probably in several regions of the world [Livani & Evrenosoglu, 2014].

The tests circuits are shown in figures 2, 3 and 4, for these circuits was obtained a large database with 5000 operative conditions.

Urban power networks, at 13.2kV rated voltage: these power distribution systems are common in the urban zones, which are mainly characterized by the presence of many single and three phase laterals and loads of relatively low power. A sample of such power systems is shown in figure 2.

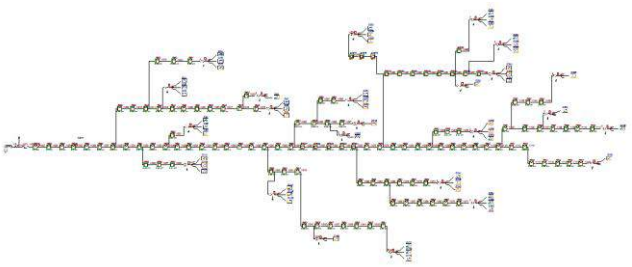

Figure 2. Urban Network at 13.2 kV rated voltage. Source: authors

Rural power networks, at 34.5 kV rated voltage: many of the power distribution systems in Colombian, have circuits, which are designed to operate at this voltage level. These are used to supply small towns and medium industries. A single line layout of this system is shown in figure 3.

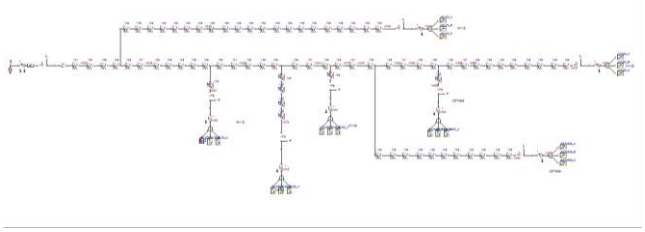

Figure 3. Rural Network at 34.5 kV rated voltage. Source: authors

Rural power network, at 44 kV rated voltage: this type of power systems can be classified as sub transmission lines [Epm, 2009]. A sample of this power feeder is shown in figure 4

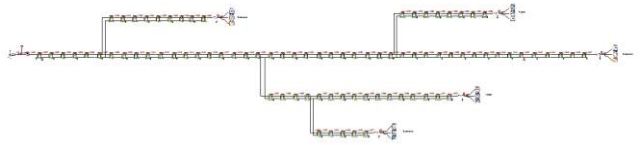

Figure 4. Rural Network at 44 kV rated voltage. Source: authors

In figures 5, 7, 9 show the performance of the fault locator related to the number of training and parameterization conditions for each analyzed power system. In addition, the training time for each circuit is illustrated in figure 6, 8 and 10. Furthermore these graphs are important because shows that better performance is computationally expensive.

Parameterization: Five different sets of operating conditions for each circuit were used in training. The different used conditions are: 1- rated condition, 2- rated condition plus two random obtained operating conditions, 3- rated condition plus four random obtained operating conditions, 4- rated condition plus six random obtained operating conditions, 5- rated condition plus eight random obtained operating conditions.

Training: At this phase, 700 operating conditions were used for each circuit. Sets of 50, 100, 150, 200, 250, 300, 350, 400 and 700 random operative conditions were considered. More operating conditions were not tested because the not affordable computational cost.

Validation: in this phase 4000 operating conditions for each circuit were used. The training models obtained at stage 4 are evaluated for each operative condition.

A- Urban power network, at 13.2kV rated voltages

The performance of the fault locator at the selected training conditions are shown in figure 5. The variable at the horizontal edge means the training conditions. The variable at the vertical edge mean, the performance of the locator. The performance is the test of the validation condition in each training model (stage 4).

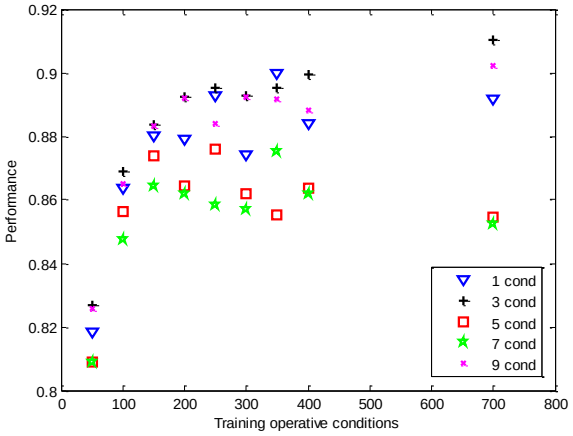

Figure 5. Performance of the fault locator versus the number of operating conditions used in training. Source: authors

As shown in figure 5, the performance increases as the number of training and parameterization conditions does. The training using more than 200 operative conditions increases the performance for some parameterization conditions, but there is not a big change. On the other hand, as is shown in figure 6, the time for training has an exponential behavior, then the use of more than 200 conditions are not recommended.

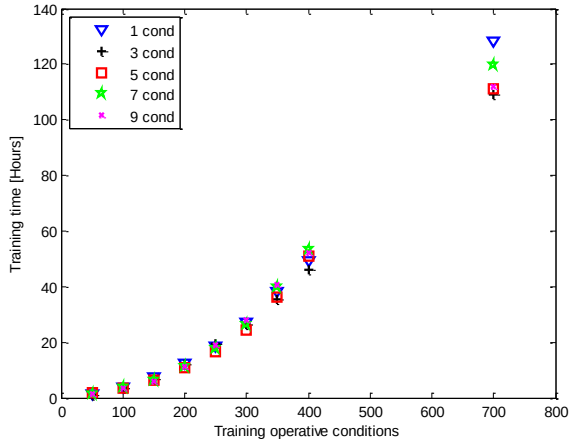

Figure 6. Time training behavior versus the number of operating conditions used in training. Source: authors

Figure 6 shows that the different sets of parameterization conditions have an insignificant increment at the training time. However the computational time is very sensible to the number of training conditions, then 200 operative conditions it is a good number to choose due to the demonstrated performance of the locator and the computational effort at the training time.

B-Rural power network, at 34.5 kV rated voltage

The performance of the locator of faults is illustrated in figure 7 for parameterization and training conditions

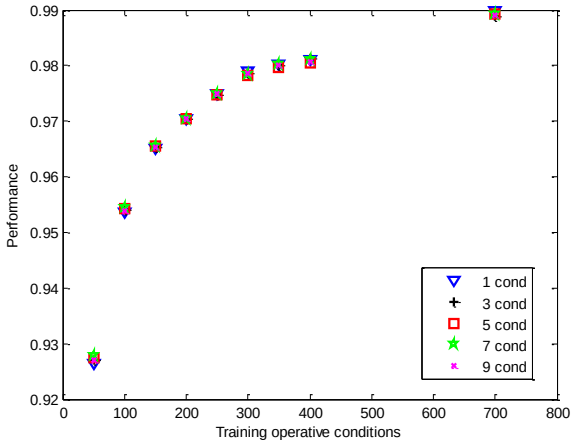

Figure 7. Performance of the fault locator versus the number of operating conditions used in training. Source: authors

Figure 7 show that the parameterization conditions do not affect the performance. Secondly, the number of training conditions has dependency with performance but 300 training conditions is a good candidate.

In figure 8 are shown the time training conditions.

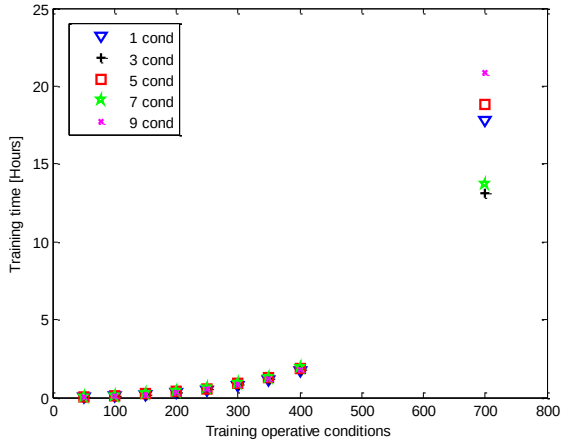

Figure 8. Time training behavior versus the number of operating conditions used in training. Source: authors

The parameterization conditions do not affect the training time however the training conditions is determinant, and it is proposed choose 300 conditions due to the low computational time cost and the performance reached with this conditions

C- Rural power network, at 44 kV rated voltage

In figure 9 are shown that the better performance is reached by 7 conditions of parameterization and 300 training operative conditions.

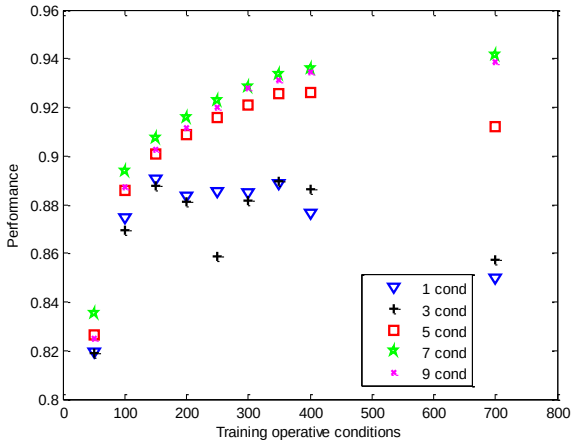

Figure 9. Performance of the fault locator versus the number of operating conditions used in training. Source: authors

The figure 9 shows that the locator is sensible to the parameterization conditions like figure 6 and the figure 10 shows the training computational efforts for 44 kV circuit.

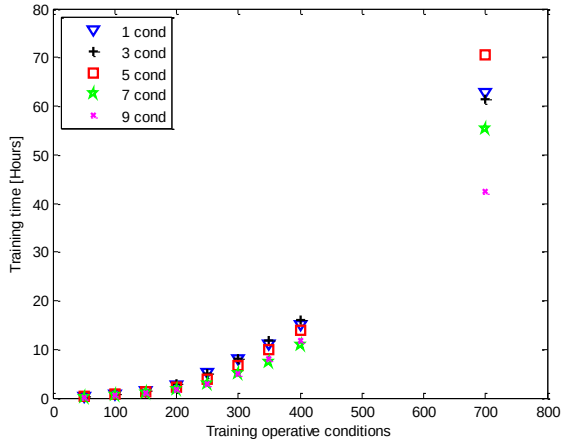

Figure 10. Time training behavior versus the number of operating conditions used in training. Source: authors

In the figure 10, it is validated the supposed in figure 9; the best performance is reached by 300 operative training conditions and seven parameterization conditions. As result, the locator of fault reached a better efficiency in an optimal training time.

In the table 1 are summarized the results for all of the analyzed power distribution systems.

Tablet 1 Summary result. Source: authors

13.2 kV	
Parameterization condition	Training condition
3	200
34.5 kV	
Parameterization condition	Training condition
1	300
44 kV	
Parameterization condition	Training condition
7	300

Conclusions

The strategy proposed allows choosing an optimal number of parameterization and training conditions, and shows the effectiveness of the fault locator based on machine learning. On the other hand, a general method for a fault location based on support vector machines is not an easy problem, due the need of selection of the adequate parameters to assure good performance.

For each analyzed power system, the method here proposed helps to obtain the operative conditions that improve the performance of the fault locator.

Finally, the setting helps to improve the performance of the SVM based fault locator, providing a useful tool to improve the power continuity at power distribution utilities.

7. Acknowledgments

This research was supported by the Universidad Tecnológica de Pereira (Colombia) and COLCIENCIAS, under the project "Desarrollo de localizadores robustos de fallas paralelas de baja impedancia para sistemas de distribución de energía eléctrica LOFADIS 2012", contract number 0977-2012. and the Master program in Electrical Engineering Universidad Tecnológica de Pereira.

References

Agudelo, C., J.; Gil, G., W.; Escobar, Z., A.; Mora F., J., Analysis of the effects of load model on a single phase fault locator based on support vector machines., Transmission & Distribution Conference and Exposition - Latin America (PES T&D-LA), 2014 IEEE PES , vol., no., 10-13 Sept. 2014, pp.1-5

Alzate, G., N.; Mora, F., J.; Perez, L., S., Methodology and software for sensitivity analysis of fault locators., Transmission & Distribution Conference and Exposition - Latin America (PES T&D-LA), 2014 IEEE PES , vol., no., 10-13 Sept. 2014, pp.1-6

Dash P. K., Samantaray S. R., Panda G., "Fault classification and section identification of an advanced series compensated transmission line using support vector machine.," IEEE Trans. Power Del., vol. 22, no. 1, Jan. 2007, pp. 67–73.

EPM. Public Enterprises of Medellín, "Standards and Technical Specifications" (Normas y especificaciones técincas), 2009. [Online]. Available:https://www.epm.com.co/site/Home/Centrodedocumentos/Proveedoresycontratistas/NormasyEspecificaciones/Normasa%C3%A9reas/Grupo2Normasde132kV.aspx. [Last access: July 2013]

Gil W., Mora J., Pérez S., Comparative analysis of metaheuristics optimization techniques to parameterize fault locators for power distribution systems., Ingeniería y Competitividad, vol. 15, no. 1, 2013, pp. 103-115.

Gutiérrez J., Mora J., Pérez S., Strategy based on genetic algorithms for an optimal adjust of a support vector machine used for locating faults in power distribution systems., Revista de la Facultad de Ingeniería, no. 53, Jun. 2010, pp. 174-187.

Livani, H., Evrenosoglu, C.Y., A Machine Learning and Wavelet-Based Fault Location Method for Hybrid Transmission Lines., Smart Grid, IEEE Transactions on , vol.5, no.1, Jan. 2014, pp.51-59.

Mora J., Localización de faltas en sistemas de distribución de energía eléctrica usando métodos basados en el modelo y métodos de clasificación basados en el conocimiento, Ph.D thesis, Universidad de Girona, España, 2006.

Mora, J.,J.; Bedoya, J.,C.; Melendez, J., Extensive Events Database Development using ATP and Matlab to Fault Location in Power Distribution Systems., Transmission & Distribution Conference and Exposition: Latin America, 2006. TDC '06. IEEE/PES , vol., no., 15-18, Aug. 2006, pp.1-6.

Morales G., Mora J., and Vargas H., Fault location method based on the determination of the minimum fault reactance for uncertainty loaded and unbalanced power distribution systems., Transmission and Distribution Conference and Exposition: Latin America (T&D-LA), 2010 IEEE/PES, Sao Paulo, Brazil, 8-10, Nov. 2010

Orozco, H.,C., Mora, F, J., Perez L, S., A robust method for single phase fault location considering distributed generation and current compensation., Transmission and Distribution: Latin America Conference and Exposition (T&D-LA), 2012 Sixth IEEE/PES, 2012, pp.1-7.

Osorio, P, J.; Mora, F, J.; Rios, P, C., Characterization of the power distribution systems as test bed for fault locators., Transmission & Distribution Conference and Exposition - Latin America (PES T&D-LA), 2014 IEEE PES , vol., no.,10-13 Sept. 2014, pp.1-6

Pérez, L., Mora, J., Pérez, S., Design of an efficient and automated fault simulation tool applied to electric power systems., Dyna, vol. 77 no. 164, Dec. 2010, pp. 178-188.

Salat, R., Osowski, S., Accurate fault location in the power transmission line using support vector machine approach, IEEE Trans. Power Syst., vol. 29, no. 2, May 2004, pp. 979–986.

Salim, R.,H., Salim, K.,C.,O., Bretas, A.,S., Further improvements on impedance-based fault location for power distribution systems, IET Generation, Transmission and Distribution, Vol. 5, 2011, pp. 467–478.

Thukaram, D., Khincha, H., Vijaynarasimha, H., Artificial Neural Network and Support Vector Machine Approach for Locating Faults in Radial Distribution Systems., IEEE Transactions on Power Delivery, vol. 20, no. 2, Apr. 2005, pp. 710-721.

Evaluation of two knowledge-based fault locators for power distribution systems

Evaluación de dos localizadores de fallas basados en el conocimiento para sistemas de distribución de energía eléctrica

N. Alzate-González[1], A. Zapata-Tapasco[2], J. Mora-Flórez [3]

ABSTRACT

This paper presents the implementation of two knowledge-based methods to locate faults on power distribution systems with distributed generation, to improve the power quality as demanded by the regulated electrical markets. Fault location methods could use additional measurements as new information to improve the results. ID3 decision tree and *k* nearest neighbor methods are implemented using measurements at substation and at the distributed generation nodes. The methods are validated using a modification of the IEEE 34-node test feeder, with two distributed generators. Several operating scenarios are considered by varying the model parameters of the power system. Additionally, a sensitivity analysis is performed to find the most critical parameters that affect the fault location methods. The results show the good performance of the fault locators and help to determine the most critical parameters of the power distribution system.

Keywords: Distributed generation, fault location, knowledge-based methods, sensitivity analysis.

RESUMEN

En este artículo se presenta la implementación de dos métodos de localización de fallas basados en el conocimiento para sistema de distribución de energía considerando generación distribuida, para mejor la calidad de la energía según lo exigido por la regulación de los mercados eléctricos. Los métodos de localización de fallas pueden utilizar las medidas adicionales como una nueva información para mejorar los resultados. Se implementa el método de árbol de decisión ID3 y los *k* vecinos más cercanos usando medidas en la subestación y en los nodos con generación distribuida. Los métodos se validaron utilizando una modificación del alimentador de prueba IEEE-34 nodos, con dos generados distribuidos. Se consideran varios estados operativos variando los parámetros de modelado del sistema de potencia. Adicionalmente, se realiza un análisis de sensibilidad para encontrar los parámetros más críticos que afectan los métodos de localización. Los resultados muestran un buen desempeño de los localizadores de fallas y ayudan a determinar los parámetros más críticos del sistema de distribución de energía.

Palabras clave: Generación distribuida, localización de fallas, métodos basados en el conocimiento, análisis de sensibilidad.

Received: July 24th 2015
Accepted: September 15th 2015

Introduction

As a consequence of the privatization of the electricity sector, the continuity of energy service is nowadays a topic of great interest for the utilities, which must pay penalties in the case of not meet the quality levels established by the regulatory agencies [Salim, et al., 2011].

Nowadays by using the new technological developments, many power distribution systems have implemented generation centers based on alternative energy sources as solar, wind, among others. Distributed generation systems (DG) introduce new problems in the control and protection of the power system due the bidirectional currents, which affects power quality [Orozco, et al., 2012].

Some fault location methods have been implemented to help in the solution of supply continuity problem, by reducing the outages duration, having a fundamental role in the fast and reliable process of service restoration [Mora, et al., 2006]. However, most of these methods were developed based on the radial nature of the power system.

On the other side, several fault location methods have been developed to determine a faulted zone based on data mining methods, and are called knowledge-based methods (KBM). Some KBM successfully implemented for fault location problem are *k* nearest neighbors (*knn*) [Mora, et al., 2009] and decision trees (ID3) [Zapata, et al., 2014].

[1] N. Alzate-González, Electrical engineer Universidad Tecnologica de Pereira, Colombia. Affiliation: Researcher at ICE3, Universidad Tecnológica de Pereira, Colombia. E-mail: naalzate@utp.edu.co.
[2] A. Zapata-Tapasco: Electrical engineer, M.Sc. Universidad Tecnologica de Pereira, Colombia. Affiliation: Researcher at ICE3, Universidad Tecnológica de Pereira, Colombia. E-mail: anfezapata@utp.edu.co.
[3] J. Mora-Florez: Electrical engineer, M.Sc Universidad Industrial de Santander, Bucaramanga, Colombia. Ph.D., Universitat de Girona, España. Affiliation: Associated professor at Universidad Tecnológica de Pereira, Pereira, Colombia. E-mail: jjmora@utp.edu.co

How to cite: Journal Space xxxxxxxxxxxxxxxxxxxx
xxxxxxxxxxxxxxxxxxxxxxxxxxxxxxxxxxxxxxxxxxxxxxxxxxxxxxxxxxxxxxxxxxxxxx

KBM are not based on the system model, since the zone under fault is determined using the measurements of voltage and current at the generation sources. Because of this, KBM can improve the results previously obtained for power distribution systems by using the measurements at the DGs. This research focuses on KBM applied to power distribution system that contains distributed generation systems.

Using the sensitivity analysis evidences the KBM dependence on the model parameters of the power distribution system. This dependence is a complex problem, because in power systems, many parameters have a considerable degree of uncertainty, especially those related to the load.

This paper presents the implementation of two knowledge-based methods applied to electric power distribution systems, which consider the presence of distributed generation. Additionally, a sensitivity analysis is performed to determine the model parameters of the power distribution system that significantly contribute on the performance of the fault locator. Therefore, this approach helps to reduce dependence on modeling parameters, which allows the development of more robust locators.

The paper is structured as follows; section 2 presents the theoretical aspects of the modern power distribution systems, knowledge-based fault locators and the sensitivity analysis. In section 3, the proposed methodology to implement the fault locator is described. The results of two KBM are discussed in section 4 and the conclusions are presented in section 5.

Theoretical Aspects

A. Modern power distribution systems

At modern power distribution systems, the distributed generation has an increasing importance due to government public policies and regulations and also due the development of many technologies, allowing large-scale implementation within the existing power electric system [Puttgen, et al., 2003]. Its implementation and integration into an existing utility can result in several benefits including line loss reduction, reduced environmental impacts, peak shaving, increased overall energy efficiency, relieved transmission and distribution congestion, voltage support, and deferred investments to upgrade existing generation, transmission, and distribution systems [Chiradeja, 2005].

However, it also implies several problems that must be take into account such the presence of harmonics due to converters, coordination of reactive power (specially with wind turbines), and the need of design and implement a more sophisticated protective relaying schemes, that considers bidirectional currents and provide safety to the personnel working on the lines [Puttgen, et al., 2003].

B. Fault locators based on knowledge-based methods KBM

KBM are based on data mining, which has become increasingly important due to the amount of data that is registered in real life processes. This dataset contains hidden information that can be seen using computational tools. One task of data mining is the classification, which aims to assign each input set of characteristics to one of a discrete set of categories or classes [Bishop, 2006]. Classification techniques belong to supervised learning, which means that each training data has a label that identifies it in one of the categories (classes) [Moguerza & Muñoz, 2006] [Burges, 1998].

Some classification techniques successfully used to solve the fault location problem are:

1. K nearest neighbor

This algorithm considers that an input vector belongs to the most frequent class, between its *k* nearest neighbors [Cover & Hart, 1967]. As advantage, this method has an easy implementation process and also has well defined statistical characteristics, which leads it as a very attractive technique to be used in any classification problem [Moreno, 2004].

2. Decision trees

A decision tree is a classification model, which divides the input space into cuboid regions, whose edges are aligned with the axes [Bishop, 2006]. Each region represents a category or class. Decision trees are based on the divide and conquer idea, developed by Hunt [Quinlan, 1993].

C. Sensitivity analysis

Sensitivity analysis studies the relation between the input and the output variable of a model. There are three kinds of methods for sensitivity analysis: selection, local and global [Tarantola, et al, 2004].

Selection methods identify a set of input variables affecting the output. These methods provide a qualitative measure and use little computational effort. Local methods identify the input variables that affect the output, but making very small changes in the input variables. Commonly, local methods vary one variable at a time while the others remain constant. Finally, global methods determine the influence of input variables in the model output. In this method, the input variables vary within different uncertainty ranges [Saltelli & Chan, 2000].

To perform sensitivity analysis is necessary to identify the problem or weakness of the model and determine the input variables that must be considered in the analysis. An uncertainty range is assigned to each input variable, according to the problem being analyzed.

Subsequently, the sensitivity analysis generates several scenarios to study the behavior of the model. A scenario is obtained assigning to each input variable a value within its uncertainty range. However, there are many combinations of values for the input variables and evaluate all of these implies a very high computational cost. Therefore, to reduce complexity, a sample of the total population is obtained through a sampling technique.

Latin hypercube sampling technique is used, which generates an *n* by *s* uncertainty matrix, where *n* represents the number of scenarios to assess and *s* represents the number of input variables to analyze. The uncertainty matrix generates values between zero and one, indicating the percentage change of each variable in each scenario [Viana & Venter, 2009] [Liefvendahl & Stocki, 2005].

Then, the model is executed repeatedly to obtain the output variable for each scenario. Finally, a statistical technique is selected for assessing the importance of each input variables with respect to the uncertainty in the output. In the literature, there are several statistical techniques to analyze the relation between the input and output variables of a model. Some of the most used techniques are: the analysis of variance (ANOVA), correlation coefficients and regression analysis.

Proposed Methodology

The proposed methodology for KBM implementation for a distributed generation system is explained below. ATP is used to model the power system and MATLAB is used for data processing.

The proposed methodology consists of four steps to find the performance of the KBM method. The last step is aiming to find the model parameters that have the bigger dependency on the performance.

A. Stage 1. Data acquisition

1. Model parameters

In this paper and due to the nature of the problem, the global sensitivity analysis was chosen. The model studied in the global sensitivity analysis is a KBM, which uses voltage and current measurements at the generation sources to calculate the faulted area. However, these measures depend on the power system model; therefore, the input variables to be analyzed are the model parameters.

To test the confidence of the proposed KBM and to simulate more accurately the distributed power system, the model parameters vary within a corresponding uncertainty range. Variation of the model parameters is performed to consider different operating states of the power system, which allows the analysis of the fault location methods in case of uncertainties at the input variables. The modeling parameters are: power factor, voltage source magnitude, voltage source unbalance, soil resistivity, system load magnitude and line length.

2. Create several operating scenarios

Using a sampling technique, *n* operating scenarios of the power system are created, each one with a different parameter variation, to study the behavior of the model in these scenarios. Latin hypercube is used, and a computational tool is implemented to vary the rated system modeled in ATP.

The computational tool automatically varies the model parameters of the power system using as input data the uncertainties matrix created by the latin hypercube and the rated system modelled in ATP. Every row of the matrix shows the percentage change in each model parameter. With these percentages determines the new value of the parameters and replaces these on the rated system, creating all operating states used to evaluate fault location methods.

3. Obtain the fault database

After being modeled all operating scenarios in ATP, a computation tool automatically simulates faults [Alzate, et al., 2014]. This tool adds a fault element to each operation state according to fault type and their fault resistance. ATP simulation provides voltage and currents signals for each generation source. These signals are converted to MATLAB for the data processing. Finally, a computation tool obtains the voltage and current phasor values, at pre-fault and fault stage in each generation source, which are the input data to evaluate the fault location method.

B. Stage 2. Zone definition and data preprocessing

The power distribution system is subdivided into zones, which are the target of the classification method. This subdivision must takes account several aspects such as the circuit topology, zone size, location of protective devices and availability of enough data in each zone to train the classification tool [Mora, et al., 2009]. In this paper, the automatic zone definition proposed in [Zapata, 2013] was used.

Data preprocessing consist in to label each fault with the respective zone. Others task as outliers detection, feature selection, noise cancelation and strategies to handle missing data are not performed.

C. Stage 3. Evaluate KBM

ID3 decision tree and *k* nearest neighbor are validated using 10-fold cross validation error. *Knn* optimal parameters are found using a fault database at rated condition. The performance index is obtained for every operating condition using the two KBM fault locators. The overall cross validation error obtained measures the confidence of the KBM based fault locators.

D. Stage 4. Evaluate a sensitivity technique

Regression analysis is used to indicate the importance of each input parameter with respect to the uncertainty in the output. Regression analysis is performed using the least squares method, which is explained in [Saltelli & Chan, 2000].

In this paper, least squares regression analysis determines the importance of the model parameters in fault location. This technique has as input data, the uncertainties matrix obtained from the latin hypercube, and the performance indices obtained by the fault location method for each operating condition. Finally, standardized Beta coefficients for each parameter are obtained. These coefficients have values between zero and one, indicating the influence of the parameters variation on the KBM fault locators.

Results and Discussion

Two knowledge-based methods were validated using the IEEE 34-node system, which is taken from the "Distribution System Analysis Subcommittee" [Radial Test Feeder]. The power systems were modified by adding two distributed generation sources at nodes 824 and 836. Figure 1 shows the power system and the zone definition.

800 operating states were generated by varying six model parameters simultaneously such as power factor, voltage source magnitude, voltage source unbalance, soil resistivity, system load magnitude and line length. The uncertainty range of each parameter is shown in Table 1. In addition, fault resistance varies from 0.05 to 40 Ω [Dagenhart, 2000].

Load magnitude has a larger variation because of the uncertainty of this parameter on the distribution system; this variation can be seen on the 'daily load profile for residential consumers'.

The variation range of the power factor, voltage source magnitude and unbalance is set according to the current regulations in Colombia. Soil resistivity variation is set according to soil characteristics, taking into account the composition, temperature and moisture of soil [Mora, et al., 2010]. And the line length variation is taken account because of possible errors in the data base of the utilities or considering variation due to temperature changes, the time and the voltage.

Single-phase A-G fault was simulated, obtaining 129600 faults at different nodes of the power system.

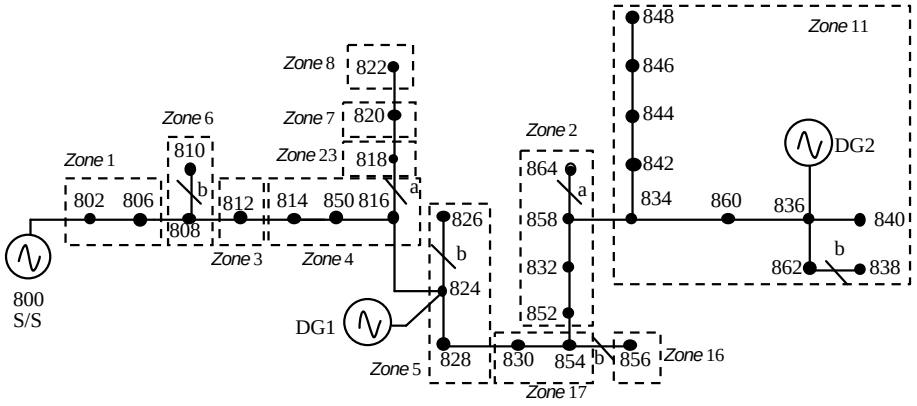

Fig 1. IEEE 34 test feeder. "Own compilation".

For *knn* method, an overall cross validation error of 8.81% was obtained for single-phase faults. For ID3 decision tree method, an error of 1.32% was obtained for single-phase faults. Both methods have a small overall cross validation error, which is attributable to the inclusion of distributed generation. Fault location methods use measures of distributed generators to improve the results and eliminate errors associated with the uncertainty in the model. The performance of *knn* method can be improved using a larger fault database or using a cross-validation with more folds.

The results of the sensitivity analysis methodology for knn and ID3 decision tree are shown in Fig. 2 and 3. Figure 2 shows the Beta coefficients obtained with *k* nearest neighbor method for single-phase A-G faults. It can be seen that the parameter that most affects the locator performance is system load magnitude.

On the other hand, a variation of power factor does not affect the fault location performance. Therefore, this parameter is insignificant for the *k* nearest neighbor method.

As shown in Fig. 3, for single-phase A-G, the parameter that most affects the ID3 fault locator performance is system load magnitude; however, in this case, beta coefficients of these parameters only reach up to 0.19, which indicates a low dependency of the parameters on the performance.

The results of both methods show that system load magnitude has the greater influence on the performance. This was expected because this is the parameter with a larger variation.

Table 1: Uncertainty ranges of the parameters. "Own compilation".

Model parameters	Uncertainty range	
	Minimum	Maximum
Power factor	-0.02	0.02
Voltage source magnitude	0.95 p.u	1.10 p.u
Voltage source unbalance	-3.4°	3.4°
Soil resistivity	80 [Ω*m]	120 [Ω*m]
System load magnitude	10%	150%
Line length	95 %	105 %

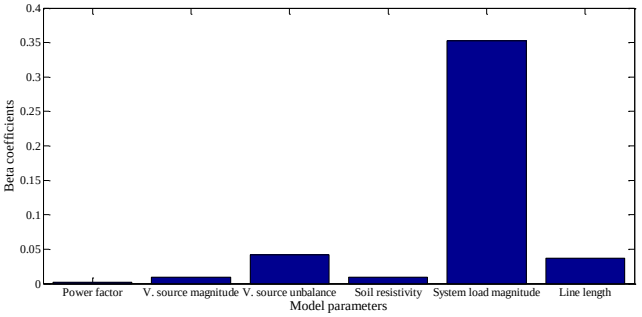

Fig. 2. Results of the sensitivity analysis with k nearest neighbor method. "Own compilation".

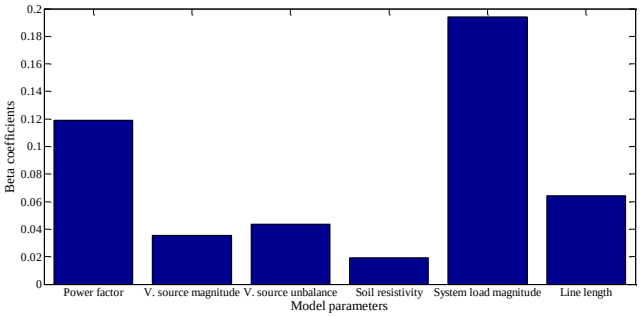

Fig. 3. Results of the sensitivity analysis with ID3 decision tree method. "Own compilation".

Concluding remarks

This paper presents an approach to locate the faulted zone on power distribution system with distributed generation using two knowledge-based methods. The 10-fold cross validation error was used to find the confidence of the methods.

ID3 decision tree and *k* nearest neighbor demonstrated a very good performance on the fault location problem at power distribution systems with GD, which is seen on the performance of ID3 with an average error of 1,32% and *knn* with an average error of 8,81%.

Finally, a sensitivity analysis for ID3 decision tree and *k* nearest neighbor was performed. The obtained Betas coefficients for both methods are small, especially for the ID3 method, which indicates that this method have a low dependence on the model parameters. A further analysis of *knn* method using a different

cross-validation has to be performed to confirm the obtained results.

Acknowledgments

This research was supported by the Universidad Tecnológica de Pereira (Colombia) and COLCIENCIAS, under the project "Desarrollo de localizadores robustos de fallas paralelas de baja impedancia para sistemas de distribución de energía eléctrica LOFADIS 2012", contract number 0977-2012; and the Master program in Electrical Engineering of Universidad Tecnológica de Pereira (Colombia).

References

Alzate, N., Mora, J., Pérez, S., Methodology and software for sensitivity analysis of fault locators, Transmission & Distribution Conference and Exposition-Latin America (PES T&D-LA), 2014 IEEE PES, Sept. 2014, pp. 1-5.

Bishop, C.M., Pattern Recognition and Machine Learning, New York, Springer-Verlag, 2006.

Burges, C., A tutorial on support vector machines for pattern recognition., Data Mining and Knowledge Discovery, 1998, pp. 121-127.

Chiradeja, P., Benefit of Distributed Generation: A Line Loss Reduction Analysis, Transmission and Distribution Conference and Exhibition: Asia and Pacific, 2005 IEEE/PES, 2005, pp. 1-5.

Cover, T., Hart, P., Nearest neighbor pattern classification, Information Theory, IEEE Transactions on, Vol. 13, No. 1, 1967, pp. 21-27.

Dagenhart, J., The 40-Ω ground-fault phenomenon, Industry Applications, IEEE Transactions, Vol. 36, No.1, Feb. 2000, pp. 30-32.

Liefvendahl, M., Stocki, R., A study on algorithms for optimization of Latin hypercubes, Journal of Statistical Planning and Inference, 2005, pp. 3231-3247.

Moguerza, J.M., Muñoz, A., Support Vector Machines with Applications. Statistical Science., 2006, pp. 322-336.

Mora, J., Melendez, J., Bedoya, J., Extensive Events Database Development using ATP and Matlab to Fault Location in Power distribution Systems, IEEE PES Transmission and Distribution Conference and Exposition: Latin America, Caracas, 2006.

Mora, J., Morales, G., Pérez, S., Learning-based strategy for reducing the multiple estimation problem of fault zone location in radial power systems, Generation, Transmission & Distribution, IET, Vol. 3, No. 4, April 2009, pp. 346-356.

Mora, J., García, G., Pérez, S., Fault resistance impedance based methods for locating faults. A comparative analysis, Dyna, Universidad Nacional de Colombia, 2010.

Moreno, F., Clasificadores eficaces basados en algoritmos rápidos de búsqueda del vecino más cercano, Ph.D. dissertation, Universidad de Alicante, Departamento de lenguajes y sistemas informáticos, España, 2004.

Orozco, C., Mora, J., Pérez, S., A robust method for single phase fault location considering distributed generation and current compensation, Transmission & Distribution Latin America Conference, Montevideo-Uruguay, Sept. 2012.

Puttgen, H.B., MacGregor, P.R., Lambert, F.C., Distributed generation: Semantic hype or the dawn of a new era?, Power and Energy Magazine, IEEE, Vol.1, No.1, Feb. 2003, pp. 22-29.

Quinlan, J., Programs for Machine Learning, Morgan Kaufmann Publishers, San Mateo California, 1993.

Radial Test Feeder, IEEE Distribution System Analysis Subcommittee. Available: http://ewh.ieee.org/soc/pes/dsacom/testfeeders/index.html.

Salim, R.H., Salim, K.C., Bretas, A.S., Further improvements on impedance-based fault location for power distribution systems, IET Generation, Transmission and Distribution, Vol. 5, 2011, pp. 467–478.

Saltelli, A., Chan, K., Sensitivity Analysis, John Wiley & Sons Ltd, United Kingdom, 2000, pp. 101-152.

Tarantola, S., Saltelli, A., Campolongo, F., Ratto, M., Sensitivity Analysis in Practice: A Guide to Assessing Scientific Models, John Wiley & Sons Ltd, United Kingdom, 2004.

Viana, F., Venter, G., An algorithm for fast optimal Latin hypercube design of experiments, International journal for numerical methods in engineering, United States, 2009.

Zapata, A., Implementación y comparación de técnicas de localización de fallas en sistemas de distribución basadas en minería de datos, Tesis de Maestría, Departamento de Ingeniería Eléctrica, Universidad Tecnológica de Pereira, 2013.

Zapata, A., Mora, J., Cortes, M., Fault location in power distribution systems using a learning approach based on decision trees, Transmission & Distribution Conference and Exposition - Latin America (PES T&D-LA), 2014 IEEE PES, Sep. 2014, pp. 1-6.

Extended formulation for elimination of multiple estimation for fault location in power distribution systems considering the load current

Formulación extendida para la eliminación de la estimación múltiple para localización de fallas en sistemas de distribución de energía considerando la corriente de carga

J. Ramírez-Ramírez[1], J. Arrieta-Giraldo[2], J. Mora-Flórez[3]

ABSTRACT

In this paper, an extension in the methodology for elimination of multiple estimation for fault location in power distribution systems considering the load current is presented. This paper presents a modification to increase the robustness of the methodology used to eliminate the multiple estimation problem, of fault location methods based on the impedance estimation for two-phase and three-phase faults. The approach here proposed uses the power distribution system parameters and the available measurements at the main power substation. Tests were performed on two power distribution systems simulated in ATP, analyzing the effect of fault resistance and load variations. The obtained results show that it is possible determine a unique fault location, eliminating the multiple estimation problem. This method also helps to improve the power continuity indexes in power distribution systems by the determination of the faulted node.

Keywords: Fault location, multiple estimation, radial power distribution systems, service continuity indexes, load current.

RESUMEN

En este artículo, se presenta una extensión de la metodología para la eliminación de la estimación múltiple para localización de fallas en sistemas de distribución de energía, teniendo en cuenta la corriente de carga. Este artículo presenta una modificación para aumentar la robustez de la metodología utilizada para eliminar el problema de la múltiple estimación de los métodos de localización de fallas basados en la estimación de impedancia para fallas bifásicas y trifásicas. El enfoque aquí propuesto utiliza los parámetros del sistema de distribución de energía y las medidas disponibles en la subestación principal. Las pruebas se realizaron en dos sistemas de distribución de energía simulados en ATP, analizando el efecto de la resistencia de falla y las variaciones de carga. Los resultados obtenidos muestran que es posible determinar una única ubicación de la falla, eliminando el problema de la múltiple estimación. Este método también ayuda a mejorar los índices de continuidad de la energía en los sistemas de distribución de energía por la determinación del nodo bajo falla.

Palabras clave: Localización de fallas, múltiple estimación, sistema de distribución de energía radial, índices de continuidad del servicio, corriente de carga.

Received: July 24th 2015
Accepted: September 15th 2015

Introduction

Service continuity in transmission and distribution systems is considered as an important aspect, especially when electricity markets are included in a competitive environment. The most common indexes of service continuity are the System Average Interruption Frequency Index (SAIFI) and System Average Interruption Duration Index (SAIDI) and faults cause supply interruptions that are responsible for low rates of these service continuity [Short,2007] [Crozier & Wisdom,1999].

In distribution systems, the presence of tapped loads, laterals, not homogeneous conductors, unbalances and large load fluctuations make that fault location as an unsolved problem. Additionally, the presence of several laterals at the power distribution system, difficulties the location of a single faulted node [Das, et al., 2000].

One of the problems in impedance based methods is the multiple estimation of the faulted node. An alternative to solve this problem is using the methodology proposed in [Morales, et al., 2009], which is based on the determination of differences between the laterals, such as the topology, tapped loads and impedance lines, to locate the fault distance, eliminating the multiple estimation

[1] Author Description: Electrical engineer, Universidad Tecnológica de Pereira, Colombia. Affiliation: Researcher at ICE3, Universidad Tecnológica de Pereira, Colombia. E-mail: daviramirez@utp.edu.co
[2] Author Description: Electrical engineer, Universidad Tecnológica de Pereira, Colombia. Affiliation: Researcher at ICE3, Universidad Tecnológica de Pereira, Colombia. E-mail: jsarrieta@utp.edu.co
[3] Author Description: Electrical engineer, Universidad Industrial de Santander, Colombia. Ph.D in engineering, Universitat de Girona, España. Affiliation: Professor at Universidad Tecnológica de Pereira, Colombia. E-mail: jjmora@utp.edu.co

problem. In [Ramírez, et al., 2014] a method in which the load current is included in the circuital analysis for single-phase faults, in the method of elimination of multiple estimation proposed in [Morales, et al., 2009], obtaining better results. Though in distribution systems, single-phase faults are the most common, the number of two and three phase faults that occurred is also considerable [Choi, et al., 2004].

According to the previously exposed, in this paper an extension of the methodology proposed in [Ramírez, et al., 2014] for analysis to two and three-phase faults in the methodology of elimination of multiple estimation considering the load current is proposed.

This paper is presented in five sections. In section II, the theoretical aspects are given. Next, in section III the extension approach is detailed described. In section IV the tests and the result analysis are presented. Finally, section V is aimed to conclude and summarize the main contributions of this research.

Theoretical aspects

Some impedance based methods eliminates the multiple estimation of the fault location, using only network parameters and voltage and current measurements at the distribution substation [Morales, et al., 2009]. The method here proposed for eliminating the multiple estimation problem is based on the classical reactance approach described in [Sachdev, et al., 1999], but considering the load current at the faulted phases, which increases its robustness.

The approach proposed in [Morales, et al., 2009] to eliminate the multiple estimation assumes that the fault has zero impedance and therefore no current flows downstream the faulted node. The estimation of the load current in the here proposed methodology is performed by an iterative process, by using an additional fault location method [Salim, et al., 2009].

Estimation of multiple faulted node.

The multiple estimation problem of the faulted node is explained by considering the power distribution system of Fig.1, where four different places with the same value of electrical reactance to locate the fault F1 are obtained (*Xd1=Xd2=Xd3=Xd4*).

By identifying only one faulted node, the approach provides accurate information to the maintenance team, in order to find and restore the fault as soon as possible [Aggarwal, et al., 1997].Considering that it is not common to find identical laterals in power distribution systems, the here proposed methodology is based on the determination of differences between the laterals, such as the topology, tapped loads and impedance lines, to locate the fault distance, eliminating the problem of multiple estimation, using a MBM as the method based on the estimation of reactance [Das, et al., 2000] [Sachdev, et al., 1999].

Estimation of the load current

The load current and the current through the fault are included in this proposal, as a contribution to the methodology initially proposed at [Salim, et al., 2009]. The current through the fault is estimated by an iterative process, which considers three variables, the voltage at the faulted node, the fault resistance and the fault distance from the initial node of the analyzed section.

Initially, it is assumed that the load current and the pre-fault current are the same. Then, the current flowing through the fault is calculated. With this approximate value of *IFn*, the circuit parameters and the available measurements, the distance to the

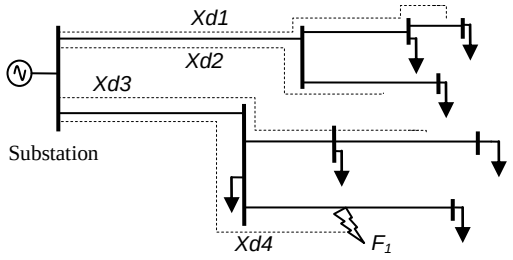

Figure 1. Multiple estimation problem of impedance based fault location methods. “Own compilation”.

fault is estimated as presented in [Salim, et al., 2011]. Subsequently, using the estimated fault distance and the Fig. 2, the load current is recalculated. An iterative process is performed to improve the estimation of the *IFn*, until the error in the fault distance from one iteration respect to the previous one, become lower than a defined tolerance [Salim, et al., 2011].

Elimination of multiple estimation method

In [Morales, et al., 2009] is presented a methodology to eliminate multiple estimation of the faulted node, also considering the mutual effect at the line impedance. Additionally, a more robust approach is also proposed, by considering the effect of the load current [Ramírez, et al., 2014].

Using the proposed approach, it is possible to estimate an error for each lateral. Having estimated multiple distances, the lateral with the lowest error corresponds to faulted lateral, because the behavior of the three-phase measurements is unique for each lateral. This is possible due to differences in line impedance, parameters and loads on each lateral [Morales, et al., 2009], [Ramírez, et al., 2014].

The implemented algorithm considers an iterative procedure, which is performed section by section, on each lateral of the power distribution system under analysis. In general, this allows the estimation of a set of distances, where the error is obtained as is presented in (1).

$$Error_i = \frac{1}{n}\frac{\sum_{j=1}^{n}|m - m_j|}{m} \quad (1)$$

The proposed method considers that at the lateral which has the lowest error (weighted differences of the distances), is where the fault is found. Thus, the faulted lateral is selected.

The line impedance from node *N* to *N+1*, and the load impedance accumulated from the end of the line, are given by (2) and (3) respectively.

$$Z_{line} = \begin{bmatrix} Z_{aa} & Z_{ab} & Z_{ac} \\ Z_{ba} & Z_{bb} & Z_{bc} \\ Z_{ca} & Z_{cb} & Z_{cc} \end{bmatrix} \quad (2)$$

$$Z_{Load} = \begin{bmatrix} Z_{La} & Z_{Lab} & Z_{Lac} \\ Z_{Lba} & Z_{Lb} & Z_{Lbc} \\ Z_{Lca} & Z_{Lcb} & Z_{Lc} \end{bmatrix} \quad (3)$$

Z_{Load} is calculated as the ratio between the pre-fault voltage and pre-fault current in the main power substation, assuming that load is Y-connected.

Proposed Extension

Two-phase to ground fault

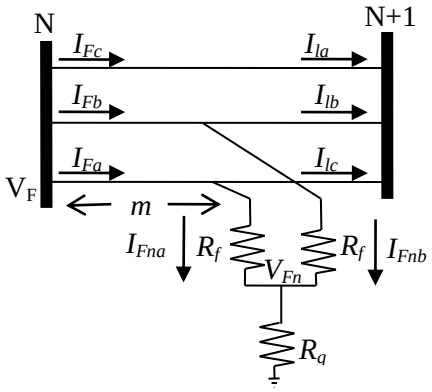

Figure 2. Three phase equivalent for a two-phase to ground fault (ab-g). "Own compilation".

In the case of two-phase to ground faults, from the analysis of the circuit shown in Figure 2, the equation (4) is obtained. For the line section between the nodes N and N+1, as shown in the test system proposed in Fig. 2, it is possible to obtain an equation of the voltage drop caused by the fault, as is shown in (4) [Morales, et al., 2009].

$$\begin{bmatrix} V_{Fa}-V_{Fn} \\ V_{Fb}-V_{Fn} \\ V_{Fc} \end{bmatrix} = \begin{bmatrix} mZ_{aa} & mZ_{ab} & mZ_{ac} \\ mZ_{ba} & mZ_{bb} & mZ_{bc} \\ mZ_{ca} & mZ_{cb} & Z_{cc}+Z_{Lc} \end{bmatrix} \begin{bmatrix} I_{Fa} \\ I_{Fb} \\ I_{Fc} \end{bmatrix} + \begin{bmatrix} R_f & 0 & 0 \\ 0 & R_f & 0 \\ 0 & 0 & 0 \end{bmatrix} \begin{bmatrix} I_{Fn_a} \\ I_{Fn_b} \\ I_{Fn_c} \end{bmatrix} \quad (4)$$

$$m = \frac{imag\left(\frac{V_{Fa}-V_{Fb}}{I_{Fn_a}-I_{Fn_b}}\right)}{imag\left(\frac{DI_{Fa}+EI_{Fb}+FI_{Fc}}{I_{Fn_a}-I_{Fn_b}}\right)} \quad (5)$$

$$m1 = \frac{imag\left(\frac{V_{Fa}-V_{Fb}-V_{Fc}+(Z_{cc}+Z_{Lc})I_{Fc}}{I_{Fn_a}-I_{Fn_b}}\right)}{imag\left(\frac{(D-Z_{ca})I_{Fa}+(E-Z_{cb})I_{Fb}+FI_{Fc}}{I_{Fn_a}-I_{Fn_b}}\right)} \quad (6)$$

Where D, E and F are given by (7).

$$\begin{aligned} D &= Z_{aa}-Z_{ba} \\ E &= Z_{ab}-Z_{bb} \\ F &= Z_{ac}-Z_{bc} \end{aligned} \quad (7)$$

Furthermore, it is possible to obtain other linearly independent equation of the complex equation presented in (4). The possible additional solution, consider only the imaginary component of the fault reactance, because this is relatively constant under variations of Rf. These equations are presented in (6).

According to the information presented above, the most appropriate equation to estimate the fault distance is presented in (5). Equation 6 is additional estimation of the distance obtained in (5), taking into account all the parameters of the analyzed lateral.

Using the proposed equations, the faulted lateral can be determined, since the behavior of three-phase measurements for each lateral is only due to differences at line impedance parameters or load on each lateral. Therefore, it is possible to obtain a fault distance using the phase measurements during fault steady state, as presented in (5). Further, by using the additional distance, the error presented in I can be estimated. Variable n represents the number of possible additional distances (in case of two-phase fault, this number is 1)[Morales, et al., 2009].

Using (1) the error is estimated to determine the faulted node using information of the faulted phase. The fault is in the lateral with the lowest error, calculated using the estimations of (5), (6) and (7).

The multiple estimation error on the unfaulted laterals is greater than the error calculated on the faulted lateral. This is due to electromagnetic coupling occurring on the faulted lateral, at the time of occurrence of the fault.

Finally, the sweep to the distribution system takes into account all the power system parameters, including the shunt admittance of the line and load couplings.

Two-phase fault

When considering the equivalent circuit under two-phase fault, the resulting equations are the same as those presented in the case of two-phase to ground fault (these are not influenced by *Rg*). As a result, (5) and (6) are also used for the case of two-phase faults [Morales, et al., 2009].

Importantly, the estimate of the fault current varied for a two-phase or two-phase to ground fault as proposed in the method described in [Morales, et al., 2009]. It is therefore important to identify the fault type to adequately estimate the load current in the section analyzed.

Three-phase to ground fault

In the case of three-phase faults, from the analysis of the circuit shown in Figure 3, the equation (8) is obtained.

$$\begin{bmatrix} V_{Fa}-V_{Fn} \\ V_{Fb}-V_{Fn} \\ V_{Fc}-V_{Fn} \end{bmatrix} = \begin{bmatrix} mZ_{aa} & mZ_{ab} & mZ_{ac} \\ mZ_{ba} & mZ_{bb} & mZ_{bc} \\ mZ_{ca} & mZ_{cb} & mZ_{cc} \end{bmatrix} \begin{bmatrix} I_{Fa} \\ I_{Fb} \\ I_{Fc} \end{bmatrix} + \begin{bmatrix} R_f & 0 & 0 \\ 0 & R_f & 0 \\ 0 & 0 & R_f \end{bmatrix} \begin{bmatrix} I_{Fn_a} \\ I_{Fn_b} \\ I_{Fn_c} \end{bmatrix} \quad (8)$$

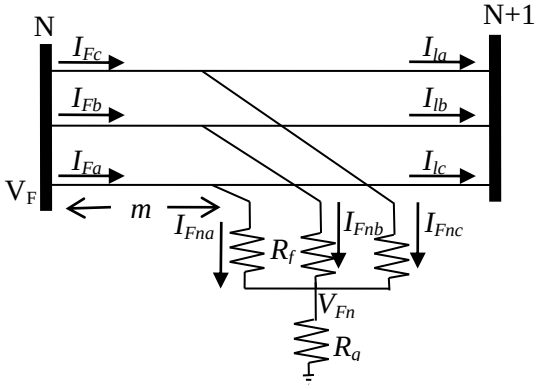

Figure 3. Three phase equivalent for a three-phase to ground fault (abc-g). "Own compilation".

From (8), three linearly independent equations for calculating m are obtained, which take into account the load current before the fault, as shown in (9), (10) and (11).

$$m1 = \frac{imag\left(\frac{V_{F_a}-V_{F_b}}{I_{Fn_a}-I_{Fn_b}}\right)}{imag\left(\frac{DI_{F_a}+EI_{F_b}+FI_{F_c}}{I_{Fn_a}-I_{Fn_b}}\right)} \quad (9)$$

$$m2 = \frac{imag\left(\frac{V_{F_b}-V_{F_c}}{I_{Fn_b}-I_{Fn_c}}\right)}{imag\left(\frac{GI_{F_a}+HI_{F_b}+JI_{F_c}}{I_{Fn_b}-I_{Fn_c}}\right)} \quad (10)$$

$$m3 = \frac{imag\left(\frac{V_{F_c}-V_{F_a}}{I_{Fn_c}-I_{Fn_a}}\right)}{imag\left(\frac{KI_{F_a}+LI_{F_b}+MI_{F_c}}{I_{Fn_c}-I_{Fn_a}}\right)} \quad (11)$$

Where G, H, J, K, L y M are given by (12)

$$\begin{aligned} G &= Z_{ba} - Z_{ca} \\ H &= Z_{bb} - Z_{cb} \\ J &= Z_{bc} - Z_{cc} \\ K &= Z_{ca} - Z_{aa} \\ L &= Z_{cb} - Z_{ab} \\ M &= Z_{cc} - Z_{ac} \end{aligned} \quad (12)$$

Because the methodology uses information from the phases not failed to calculate multiple estimates of the distance to the fault, and in this case all phases are in failure, *m* is obtained as the average of the three estimates, as shown in (13).

$$m = \frac{1}{3}(m1 + m2 + m3) \quad (13)$$

To determine the lateral under fault as proposed previously, the error is calculated using (1); In this case *n=3*.

Three-phase fault

When considering the equivalent circuit under three-phase fault, the resulting equations are the same as those presented in the case of three-phase to ground fault (these are not influenced by *Rg*). As a result, (14), (15) and (16) are also used for the case of three-phase faults [Morales, et al., 2009].

Testing and analysis

All of the proposed power systems used in tests were modeled and simulated in ATP. Two additional tools as Atpxchange and SimulacionRF were also used [Mora, et al., 2006], [Bedoya, et al., 2012]. The proposed method was implemented in Matlab.

Test power systems

The first system selected for the validation of the proposal is presented in Fig. 4, and was implemented using section lines and loads from the IEEE 34 nodes, 24.9 kV system [IEEE]. This is used to consider the elimination of the multiple estimation problem in a power system with similar laterals.

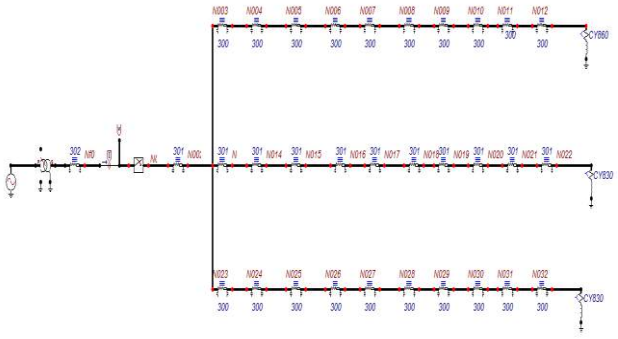

Figure 4. Power system with similar laterals. “Own compilation”.

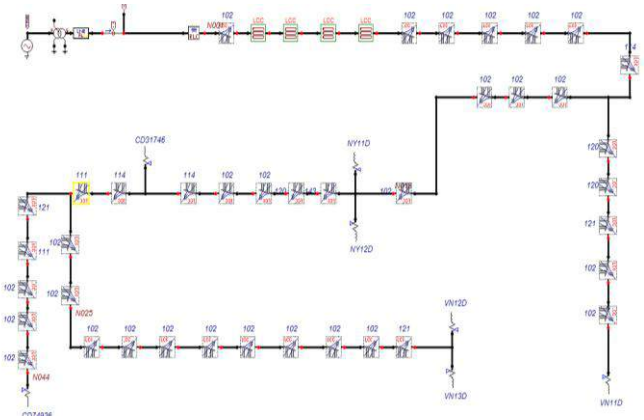

Figure 5. Real power distribution system. “Own compilation”.

The power distribution system of Fig. 4 has the same line parameters in the laterals 1 and 3, and the same impedance load in the lateral 2 and 3.Sections of line of the laterals 1 and 3 correspond to the configuration 300 of the IEEE 34 nodes system. Additionally, the load in the lateral 1 is the same as the node 860. The impedance of each section of the lateral 2 corresponds to the configuration 301 and the lateral load at the end of 2 is the same as the load on the node 830 [Morales, et al., 2009].

The second proposed test system is shown in Fig. 5, and corresponds to a real power distribution system located at Cundinamarca, Colombia. It has unbalanced loads, laterals and different line configurations, considering underground and overhead lines.

Test proposed scenarios

Two-phase, two-phase to ground, three-phase and three-phase to ground faults on a fault resistance range from 0Ω to 40Ω were simulated in all nodes for both power distribution systems [Dagenhart, 2000]. Considering the size of the power system, the analyzed faults (ab, ab-g, abc and abc-g), the fault resistances (0, 20 and 40 ohms) and the load scenarios (rated load, 1.5 rated load and 0.6 rated load), the number of analyzed faults are 324 in the case of the power system in figure 3, while 516 in the case of the power system of figure 4.

Tables I and II show the comparative behavior of the proposed approach for two-phase and three-phase faults, considering 3 different fault resistances and for different load variations.

Efficiency is calculated as the ratio of the faults adequate located and the total fault number of considered faults, under the same condition, as is given by (9). It should be noted that it is considered as a correctly localized fault, the one located at the corresponding lateral an also near to the faulted node (In a range of two nodes from the faulted one).

$$Efficiency = 100\frac{number\ of\ faults\ adecuate\ located}{total\ number\ of\ faults} \quad (14)$$

Result analysis at the power system with similar laterals: For the power system on Fig. 4, 27 faults were simulated, using three different fault resistances and also considering load variations respect to the nominal value. The results are presented in table II.

In the case of the results reported in table I, in case of a 0Ω fault resistance, fault type ab, and the system operating at nominal load, the obtained efficiency with and without consider the approach here proposed, is the same. It indicates that 14 faults (51.8519%) are identified at the corresponding lateral and at the right distance. The average reported in the last row of each table correspond to the efficiencies the performance of the methodology with and without the proposal, for each load variation stage.

The efficiency in localization of the methodology with and without the proposed, unsurprisingly, presents a very similar behavior to solid faults, regardless of variation in the load. When the fault impedance increases, is where the proposed approach makes its contribution, because as it considers the effect of the load current.

Despite the similarity in the laterals at the power system, it is noticed that in most cases the proposal improves the efficiency of the method.

Result analysis at the real power system: For the power system on Fig. 5, 43 faults were simulated, using three different fault resistances and also considering load variations respect to the nominal value. The results are presented in table II.

Although this is a real power system, which is heavily loaded and is not balanced, it shows that the proposed approach helps to obtain good results.

It can be clearly seen that in most of the cases, the efficiency of the proposed methodology is similar to the obtained in the original methodology. An acceptable overall efficiency of the strategy here proposed is observed, then the approach improves the location and elimination of multiple estimation when the fault resistance is different of zero.

TABLE I. TESTS PERFORMED IN THE CIRCUIT OF FIGURE 4. "Own compilation".

		Efficiency with original method			Efficiency with the proposed method		
Rf	**Fault type**	**Zload**	**Zload 150%**	**Zload 60%**	**Zload**	**Zload 150%**	**Zload 60%**
0	**ab**	51,8519	51,8519	37,037	51,8519	51,8519	37,037
	ab-g	85,1852	51,8519	81,4815	85,1852	51,8519	81,4815
	abc	55,5556	48,1481	48,1481	55,5556	48,1481	48,1481
	abc-g	55,5556	48,1481	48,1481	55,5556	48,1481	48,1481
20	**ab**	55,5556	51,8519	33,3333	62,963	22,2222	33,3333
	ab-g	81,4815	55,5556	29,6296	66,6667	22,2222	44,4444
	abc	44,4444	3,7037	40,7407	77,7778	70,3704	48,1481
	abc-g	44,4444	3,7037	40,7407	77,7778	70,3704	48,1481
40	**ab**	55,5556	3,7037	33,3333	55,5556	18,5185	33,3333
	ab-g	55,5556	3,7037	29,6296	55,5556	18,5185	48,1481
	abc	40,7407	18,5185	33,3333	48,1481	48,1481	48,1481
	abc-g	40,7407	18,5185	33,3333	48,1481	48,1481	48,1481
Average Efficiency		**55,5555**	**29,9383**	**40,7407**	**61,7284**	**43,2099**	**47,2222**

TABLE II. TESTS PERFORMED IN THE CIRCUIT OF FIGURE 5. "Own compilation".

		Efficiency with original method			Efficiency with the proposed method		
Rf	**Fault type**	**Zload**	**Zload 150%**	**Zload 60%**	**Zload**	**Zload 150%**	**Zload 60%**
0	**ab**	90,6977	88,3721	83,7209	90,6977	88,3721	83,7209
	ab-g	93,0233	90,6977	86,0465	93,0233	90,6977	86,0465
	abc	100	100	93,0233	100	100	93,0233
	abc-g	100	100	93,0233	100	100	93,0233
20	**ab**	65,1163	30,2326	44,186	81,3953	76,7442	65,1163
	ab-g	65,1163	34,8837	44,186	88,3721	83,7209	81,3953
	abc	4,6512	4,6512	4,6512	100	88,3721	67,4419
	abc-g	4,6512	4,6512	4,6512	100	88,3721	67,4419
40	**ab**	27,907	0	6,9767	81,3953	62,7907	72,093
	ab-g	27,907	0	6,9767	88,3721	79,0698	65,1163
	abc	4,6512	4,6512	4,6512	100	65,1163	65,1163
	abc-g	4,6512	4,6512	4,6512	100	65,1163	65,1163
Average Efficiency		**49,0310**	**38,5659**	**39,7287**	**93,6047**	**82,3644**	**75,3876**

Conclusions and future works

The methodology was successfully implemented including the load current for the two and three-phase faults, improving the efficiency in the case fault resistance values different of zero, as it was demonstrated by the obtained results in the tables I and II.

This method helps to determine the faulted lateral, even in case of similar line and load characteristics at the power distribution system. By the determination of the faulted lateral, the multiple estimation problems could be avoided, speeding up the restoration process.

As future work, considering the automation of power distribution systems is proposed as a further work the use of additional information to those obtained at the substation. According to the expected, by using information such as additional measurements and recloser and fusible operating, performance of this methodology is improved.

Finally, this approach contributes to improve the continuity indexes in real power distribution systems.

Acknowledgment

This research was supported by the Universidad Tecnológica de Pereira (Colombia) and COLCIENCIAS, under the project "Desarrollo de localizadores robustos de fallas paralelas de baja impedancia para sistemas de distribución de energía eléctrica LOFADIS 2012", contract number 0977-2012.

References

A. Bedoya, J. Mora and, S. Perez, "Estrategia de reducción para la aplicación generalizada de localizadores de fallas en sistemas de distribución de energía eléctrica". Revista EIA, ISSN 1794-1237 Número 17, p. 21-37. Julio 2012.

C. Crozier and W. Wisdom, "A power quality and reliability indexbased on customer interruption costs," IEEE Power Eng. Rev., vol. 19,no. 4, pp. 59–61, Apr. 1999.

G. Morales, J. Mora and H. Vargas. "Elimination of Multiple Estimation for Fault Location in Radial Power Systems by Using Fun mental Single-End Measurements". IEEE Transactions on power delivery, Vol. 24, No. 3, 2009.

IEEE. Distribution System Analysis Subcommittee. Radial Test Feeders. Available: http://www.ewh.ieee.org/soc/pes/sacom/testfeeders.html.

J. Dagenhart, "The 40-Ω ground-fault phenomenon". Industry Applications, IEEE Transactions on, vol.36, no.1, pp.30-32, Feb 2000.

J. Mora, J. Melendez and J. Bedoya, "Extensive Events Database Development using ATP and Matlab to Fault Location in Power distribution Systems," IEEE PES Transmission and Distribution Conference and Exposition: Latin America, Caracas, 2006.

J. Ramírez-Ramírez, J. Arrieta-Giraldo, and J. Mora-Florez, "Elimination of multiple estimation for single phase fault location in power distribution systems considering the load current," IEEE PES Transmission & Distribution Conference and Exposition, Medellin, Colombia, 2014.

M. Choi, S. Lee, D. Leeand, B. Jin "A new fault location algorithm using direct circuit analysis for distribution systems". 2004, pp. 35-41. IEEE Transactions on Power Systems.

M. Sachdev, R. Das, and T. Sidhu, "Distribution line shunt fault locations from digital relay measurements," Can. J. Elect. Comput. Eng., vol. 24, no. 1, pp. 41–47, Jan. 1999.

R. Aggarwal, Y. Aslan and A. Johns "An interactive approach to fault location on overhead distribution lines with load taps".IEEE Developments in Power System Protection Conference Publication No. 434. 1997, pp184-187.

R. Das, M. Sachdev, and T. Sidhu, "A fault locator for radial subtransmission and distribution lines," in Proc. Power Engineering Society Summer Meeting, 2000, vol. 1, pp. 443–448.

R. Salim, K. Salim, A. Bretas, "Further improvements on impedance-based fault location for power distribution systems". Generation, Transmission & Distribution, IET (Volume: 5, Issue: 4). 2011 pp. 467-678.

R. Salim, M. Resener, A.D. Filomena, K.R. Caino de Oliveira and A. S. Bretas: 'Extended fault-location formulation for power distribution systems', IEEE Trans. Power Deliv., 2009, 24, (2), pp. 508–516.

T. A. Short, Electric Power Distribution Handbook, 1st ed. London U.K.: Taylor & Francis, Apr. 2007.

Impact of the Dynamic Network Reconfiguration on Optimal Placement of Monitors for Harmonic State Estimation

Impacto de la Reconfiguración Dinámica de Red en la Localización Óptima de Monitores para la Estimación de Estado Armónico

J. Blanco[1], J.F. Petit[2], G. Ordóñez[3]

ABSTRACT

This paper addresses the impact of the dynamic network reconfiguration (DNR) on the observability of harmonic voltages and currents in smart distribution systems. Optimal placement of power quality monitors (PQMs) is generally applied without taking into account the DNR. Two indexes are proposed to assess the impact of the dynamic reconfiguration on harmonic observability and a test case is implemented. The results show the need for new formulations for optimal placement of PQMs, where a configuration of the PQMs is selected while the impact of the DNR is as low as possible.

Keywords: Dynamic network reconfiguration, harmonic observability, harmonic state estimation, optimal placement monitor, power quality, smart distribution system.

RESUMEN

Este trabajo tiene como objetivo evaluar el impacto de la reconfiguración dinámica de red sobre la observabilidad de tensiones y corrientes armónicas en redes inteligentes de distribución de energía eléctrica. Generalmente la localización óptima de los monitores de la calidad de la potencia eléctrica se aplica sin tener en cuenta la reconfiguración de la red. En el artículo se proponen dos índices para para medir el impacto de la reconfiguración dinámica sobre la observabilidad armónica y un caso de prueba es implementado. Los resultados muestran una necesidad por nuevas formulaciones del problema de localización óptima de monitores, donde la localización óptima se seleccione garantizando que el impacto de la reconfiguración dinámica sea el mínimo posible.

Palabras clave: Calidad de potencia, estimación de estado armónico, localización óptima de monitores, observabilidad armónica, reconfiguración dinámica de red, redes inteligentes de distribución.

Introduction

The concept of smart grid aims a high efficiency in the electrical systems and incorporates some characteristics as the use of digital control and real time technologies, distributed generation, dynamic optimization, distributed automation, and smart metering (Brown et al., 2010 and Haughton et al., 2010).

The dynamic network reconfiguration (DNR) in real time systems is part of these smart characteristics. DNR applied to smart distribution systems promotes advanced solutions due to the integrated technologies and procedures, for planning and operation of electrical distribution systems (Bernardon et al., 2012). DNR is an important tool to minimize the power losses as well as improve the reliability of the smart distribution networks.

The power quality plays an important role in the context of smart distribution networks with DNR. Due to the expected increase of nonlinear loads, the amount of harmonic currents injected into smart distribution networks is also increasing. At the same time, these harmonic voltages and currents cause different operational problems such as overheating and failure of equipment, false tripping of sensitive loads, misoperation of protective relays, among others (Kumar et al., 2005).

Currently, the power quality monitoring is essential to diagnose the power quality problems, for example, the harmonic components. However, installing power quality monitors (PQMs) in every component of the network is not feasible due to the financial constraints of the PQMs, voltage and current transformers, communication channels, besides the dimension of the distribution systems. Therefore, there is an increasing interest in efficient tools to know and assess the power quality of the network with a limited number of distributed PQMs. This problem can be stated as follows: how to find the optimal number and locations of PQMs while a set of observability constraints are satisfied? (Yuxin Wan et al., 2014), (Muscas et al, 2007), (Shafiee Rad et al., 2012).

The constraints in the optimal placement problem (OPP) of PQMs are usually related to the maximum system observability. In the case of harmonic components, the observability of all harmonics voltage and current must be guaranteed with the solution of OPP. Measurements obtained from a partial monitoring system are necessary to estimate the power quality state of

[1] J. Blanco is pursuing Phd studies in electrical engineering at Universidad Industrial de Santander, Bucaramanga, Colombia. E-mail: jairo.blanco@correo.uis.edu.co
[2] J.F. Petit is a Professor at the Universidad Industrial de Santander, Bucaramanga, Colombia. E-mail: jfpetit@uis.edu.co
[3] G. Ordóñez is a Professor at the Universidad Industrial de Santander, Bucaramanga, Colombia. E-mail: gaby@uis.edu.co

the whole network. Thus, the estimation of the power quality levels is performed on nodes with a partial monitoring system through of the harmonic state estimation (HSE). HSE is a technique for identifying the distribution of the harmonic components in electrical systems with limited measurements.

Various methods have been presented in the literature for placement of PQMs for harmonic state estimation. (Madtharad et al., 2005) present a new technique for optimal measurement placement based on the minimum condition number of the measurement matrix with the sequential elimination to solve the problem. The main disadvantage is that the method can guarantee only near-optimal solutions.

In (Kumar et al., 2005), a method based on genetic algorithms is proposed to solve the OPP using the approach of the minimum variance. The aim is to select the measurements (from the set of all possible measurement locations) that minimize the expected value of the differences between estimated and actual state variables. When the number of PQMs or the system size increases, a method based on genetic algorithms works better than the sequential technique.

In (Muscas et al., 2007), an optimization algorithm is proposed to choose the optimal number and position of PQMs. The optimization procedure is based on the dynamic programming and takes into account the measurement uncertainty and tolerance at line parameters. (Shafiee Rad et al., 2013) proposed an algorithm that uses minimum variance criterion and a sequential method for optimal meter placement. Singular value decomposition (SVD) method is used for observability analysis and finally a weighted least square (WLS) method for harmonic estimation is applied. The minimum trace of the covariance matrix is used to find the optimal measurement location.

The mentioned works have a particular issue: The optimal placement of PQMs is performed using error of the estimated state variables as a minimization criterion. Therefore, to find a solution to the optimal placement problem of PQMs is required a previous solution of the HSE. Other works present a new approach to guarantee the harmonic observability based on the topological connections and circuital laws. This approach is more simplified because to find the optimal placement of PQMs, a solution of HSE is not required.

This is the case of (Almeida et al., 2013), which describes a methodology based on evolutionary algorithms to find a monitoring partial system in order to guarantee the full harmonic observability of the network. Harmonic observability is verified through rules based on Kirchhoff's laws; a branch and bound algorithm and a modified genetic algorithm are used to solve the optimization problem. A most efficient configuration of the monitoring system is found with this method, compared with similar methodologies. Similarly, (Yuxin Wan et al., 2014) proposes a novel model for the optimal placement of the PQMs, considering network observability and fault location constraints. The OPP is formulated as a linear integer problem by applying Ohm's law and Kirchhoff's laws to obtain relationships between voltages and currents. This method shows higher speed and high accuracy.

The methods proposed in the previous works have a common factor that is remarkable: the solution of the OPP depends on the network topology (the interconnecting of the electrical nodes). The network topology defines the harmonic observability and once a reconfiguration is applied to the power system, a new topology appears and the harmonic observability must be evaluated again.

Thus, this paper aims to study the impact of the DNR on the optimal placement of PQMs by taking into account the constraints needed for HSE in smart distribution networks. Nevertheless, the scope of this work is the impact on the observability of the harmonic state variables, but not the impact on the harmonic state estimation. It is considered also that dynamic reconfiguration is applied to minimize the power losses, i.e. the number of the supplied customers is always the same with only changes on the network topology.

The paper is organized as follows. Optimal monitor placement for harmonic state estimation is presented in section 2. The impact of the dynamic reconfiguration on harmonic observability is analyzed in 3. Section 4 shows the numerical results using the IEEE 33-node test system. Conclusions are provided in the final section.

Formulation of the Optimal Placement of PQMs to Harmonic State Estimation.

A monitoring system is optimal when the power system observability is guaranteed and its cost is minimized (Almeida et al., 2013). Therefore, the optimal placement of PQMs for harmonic state estimation must be allowed that all harmonic voltages and currents can be measured or calculated in a distribution network. This method incorporates the cost of installing a monitor in a specific location and also determines how the transducers should be connected. This method is taken as reference for assessing the impact of the dynamic network reconfiguration on the optimal placement of PQMs.

Some definitions to understand the OPP are given in (Almeida et al., 2013):

Allocation Vector (AV): this row vector defines the configuration of the monitoring system and it has a size equal to the summation of the number of sections connected at each bus i. Thus, the possible installations of the current transformers in a set of lines connected at a same bus are incorporated. AV is defined according with (1). A PQM with six channels (measurements of three-phase voltages and currents) is considered in the problem formulation.

$$av\left(\left(v_i, i_{ij}\right)\right) = \begin{cases} 1, & \text{if a PQM is installed at bus } \boldsymbol{i} \\ & \text{and the line section } \boldsymbol{ij} \\ 0, & \text{if a PQM is NOT installed at bus } \boldsymbol{i} \\ & \text{and the line section } \boldsymbol{ij} \end{cases} \quad (1)$$

Cost Vector: It is a row vector taking into account the cost of installing a PQM at a specific node y line section. The sizes of CV and *AV* are the same. So, the total cost for a specific configuration can be calculated as shown in (2).

$$Total\ cost\ (TC) = AV * CV^t \quad (2)$$

Optimization problem: this problem is presented in (3).

$$Minimize\ \ TC = AV * CV^t$$
$$s.t.:\ ov_i \geq 1, \quad i = 1, 2, 3, \ldots, N_n, N_n + 1, \ldots, (N_n + N_b) \quad (3)$$

where N_b is the number of branches and N_n is the number of nodes of the power system. The constraints are reduced to an observability vector (*OV*), which will be explained below.

Problem's constraints: Constraints are detailed in (Almeida et al., 2013). Nevertheless, a new method to derive these constraints is proposed in this work and it is explained below. The observability vector (*OV*) is constructed from other vectors defined in (Almeida et al., 2013). To formulate a systematic approach using the problem´s structure, we propose a method to derive the constraints using only the definition of the topological incidence matrix of a distribution system.

The proposed method in this work is described below.

- Incidence matrix (*Ain*): it is constructed using the rule shown in (4). The number of rows is the number of branches (electrical lines) and the columns is the number of nodes.

$$Ain_{ij} = \begin{cases} 1 & \text{if branch } \boldsymbol{i} \text{ starts at node } \boldsymbol{j} \\ -1 & \text{if branch } \boldsymbol{i} \text{ ends at node } \boldsymbol{j} \\ 0 & \text{otherwise} \end{cases} \quad (4)$$

where $i = 1,2,\dots,N_b$ and $j = 1,2,\dots,N_n$.

- Possible locations of PQMs: L is defined as the total locations to install the PQMs and found from the incidence matrix, as shown in (5). A vector $\mathcal{L}$ of length $1 \times L$ also is defined and each element corresponds to measure the voltage i and the current of the branch j (end of the line connected at node i).

$$L = \sum |Ain_{ij}|, \quad \forall\, i,j$$
$$\mathcal{L}_k = |Ain_{ij}|,\ \forall\, |Ain_{ij}| > 0, k = 1,\dots,L \quad (5)$$
$$\mathcal{L}_k = \begin{cases} \text{voltages measured at node } \boldsymbol{i} \\ \text{currents measured at branch } \boldsymbol{j} \end{cases}$$

- Connectivity matrix (*CnM*): it is based on Kirchhoff's voltage law. Each row corresponds to a voltage or current and each column to a $\mathcal{L}_k$ (possible location of a *PQM*). Connectivity matrix is constructed as shown in (6). Two submatrices are constructed: one is CnM_V that is created from the transposed rows of Ain; the second, CnM_I is created from the values of Ain.

$$CnM = \left[\frac{[CnM_V]_{N_n \times L}}{[CnM_I]_{N_b \times L}}\right]$$
$$CnM_{V_{colum}} = \left|Ain_{i,\forall j}{}^t\right|;\ \forall i \in \mathcal{L}_k \quad (6)$$
$$CnM_{I_{ik}} = \begin{cases} 1 & \forall i \in \mathcal{L}_k \\ 0 & otherwise \end{cases}; k = 1,\dots,L$$

- Connectivity vector (*CnV*): In the optimization problem, allocation vector *AV* represents the set of possible locations of PQMs. Thus, *CnV* is obtained from (7).

$$AV = [x_1\ x_2 \dots x_L]$$
$$CnV = CnM \times AV^t \quad (7)$$

- Redundancy-From-Vector (*RFV*) and Redundancy-To-Vector (RTV): two redundancy matrices (RFM and RTM) are formulated to calculate two redundancy vectors, as shown in (8) and (9). These vectors are used to identify when the state variables of voltage at the end nodes from a branch would be simultaneously calculated. A unique redundancy vector (RV) is calculated, as shown in (10).

$$RFM = \left[\frac{[0]_{N_n \times L}}{[RFM_I]_{N_b \times L}}\right] \quad RTM = \left[\frac{[0]_{N_n \times L}}{[RTM_I]_{N_b \times L}}\right]$$
$$RFM_{I_{row-i}} = CnM_{V_{row-i}},\ \forall i,j:\ Ain_{ij} = 1 \quad (8)$$
$$RTM_{I_{row-i}} = CnM_{V_{row-j}},\ \forall i,j:\ Ain_{ij} = -1$$

$$RFV = RFM \times AV^t$$
$$RTV = RTM \times AV^t \quad (9)$$

$$RV_{m,1} = RFV_{m,1} \times RTV_{m,1},\ \ m = 1, \dots, (N_n + N_b) \quad (10)$$

- Co-connectivity vector (*CcV*): it allows determining which voltages may be calculated using the voltage values already measured or calculated. *CcV* is calculated as shown in (11).

$$CcV = \left[\frac{[CV]_{N_n \times 1}}{[0]_{N_b \times 1}}\right]$$
$$CV_j = \prod CnV_k,\ \ \forall\, m \neq j: |Ain_{im}| = |Ain_{ij}| = 1 \quad (11)$$

- Pre-Observability vector (*POV*): this vector determines if a state variable will be observable and it is calculated as shown in (12).

$$POV = CnV + RV + CcV \quad (12)$$

- Observability vector (*OV*): due to the dependence between *CcV* and *CnV*, *OV* is constructed as shown in (13). *OV* incorporates the possibility to calculate the line current of a branch when the voltages in its terminals are known.

$$OV = \left[\frac{[POV]_{N_n \times 1}}{[POV_M]_{N_b \times 1}}\right]$$
$$POV_{M\,k,1} = \prod POV_{j,1},\ \ \forall j: |Ain_{kj}| = 1 \quad (13)$$

Finally, *OV* is used as the set of constraints for the optimization problem in (3). This method to determine the constraints is applied to a test case in this work.

Impact of the Network Reconfiguration on Optimal placement of Power Quality Monitors.

Smart Grid concepts in electrical distribution systems allow notable advantages regarding to the efficient operation of the networks. Automatic network reconfiguration is one of these smart concepts and it is essential for the operation in smart distribution systems. DNR usually must be resolved taking into account the network modeling, changes in the network topology, load flow calculations and the constraints (radial network, current and voltage limits, among others). All this information must be taken into account in the optimization problem to find the best network configuration according to these constraints. This paper considers that dynamic reconfiguration is applied to minimize the power losses, while the number of the supplied customers is always the same, with only changes in the network topology.

When the DNR problem is solved, the results are applied and the network topology is changed. It is clear that *OV*, in equation (13), changes when the network topology is modified, this due to that incidence matrix changes too. Therefore, the problem of optimal placement of PQMs must be formulated and solved again. Thus, the optimal monitoring system found in a specific case cannot be optimal for different network topologies which are obtained from the DNR.

This work aims to estimate the impact of the dynamic network reconfiguration on the harmonic observability. The authors propose two indexes for quantifying the observability of the harmonic state variables from a partial monitoring system. It is important to highlight that the scope of this work is only to estimate the impact on the observability of the harmonic state variables, but not the impact on the harmonic state estimation.

The first percentage index is called Harmonic Observability Rate (*HOR*) and it is presented in (14). A value of HOR near to 100% is better because indicates a full harmonic observability.

$$HOR_{nt_i} = \left(\frac{(\#rows\ OV_j \geq 1)|_{AV^*_{nt_b}}}{(N_n + N_b)} \right) \times 100\% \qquad (14)$$

HOR_{nt_i} is calculated for each network topology nt_i and evaluates the harmonic observability in an optimal configuration of PQMs $AV^*_{nt_b}$,which was calculated previously.

In addition, the hours of operation for each nt_i can be taken into account. This allows weighting the set of observability values for each network reconfiguration and a unique index to evaluate the harmonic observability can be obtained according (5). HOR_T weighs the harmonic observability from an optimal location of PQMs $AV^*_{nt_b}$, according to the hours of operation with a particular network topology.

$$HOR_T = \frac{\sum_{i=1}^{NT_t} \left(HOR_{nt_i} \times Noh_{nt_i} \right)}{Noh_t} \qquad (15)$$

where NT_t is the total number of all network topologies generated from the DNR. A value of HOR_T near to 100% means that the harmonic observability is very good in the different network topologies generated from the dynamic reconfiguration.

Figure 1 shows the proposed method to construct the optimization problem and the procedure to evaluate the two proposed indexes.

Numerical examples and discussion

The 33-node test system is used to test the proposed indexes performance. In (Abdelsalam et al., 2014), the 33-node test system was used for optimally locating the PMUs with different network configurations and some renewable sources: Photovoltaic (PV) and Wind Power (WP). In this work, IEEE 33-node test system is analyzed in five network configurations.

Table 1 presents the network configuration cases that were taken into account in this work. In each case, there are five line sections opened to ensure the radial topology operation while the same number of customers is supplied. The operation hours in each case are determinate by the renewable sources and formulated based on a total 24 hours of the day.

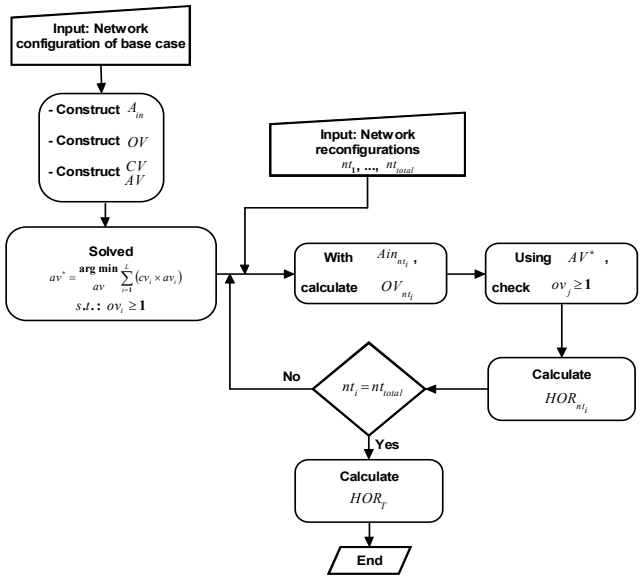

Figure 1. Proposed method to evaluate the impact of the DNR on optimal placement of PQMs

Table 1. Topologies studied and their characteristics

Network configuration	Open line sections	Distributed generation	Operation hours
Base case	13 22 26 29 37	Without PV and WP	---
RC.1	14 22 25 33 36	Low PV and high WP	5
RC.2	13 18 23 25 33	High PV and low WP	7
RC.3	10 22 25 33 37	Low PV and high WP	7
RC.4	14 18 23 25 33	Only WP	5

The OPP of PQMs is applied to case base shown in Figure 2.a and described in Table 1. The dotted lines represent the tie switches. Optimal placement of PQMs to guarantee the full harmonic observability is found using the proposed method and the results are presented in Table 2. For the solution of the OPP, the cost vector CV contains ones in all positions, i.e. the cost of installing a PQM is the same in any node of the distribution system.

Table 2. Results of the optimal placement of the PQMs for the base case

PQM	Measurements		PQM	Measurements	
	Voltage (node)	Current (branch)		Voltage (node)	Current (branch)
1	0	1	10	17	36
2	2	3	11	18	20
3	4	5	12	21	28
4	5	8	13	24	12
5	7	23	14	26	10
6	8	25	15	28	14
7	10	30	16	30	16
8	12	32	17	31	18
9	14	34			

Figure 2.b shows the placement of the PQMs and highlights the locations of the voltage and current transductors.

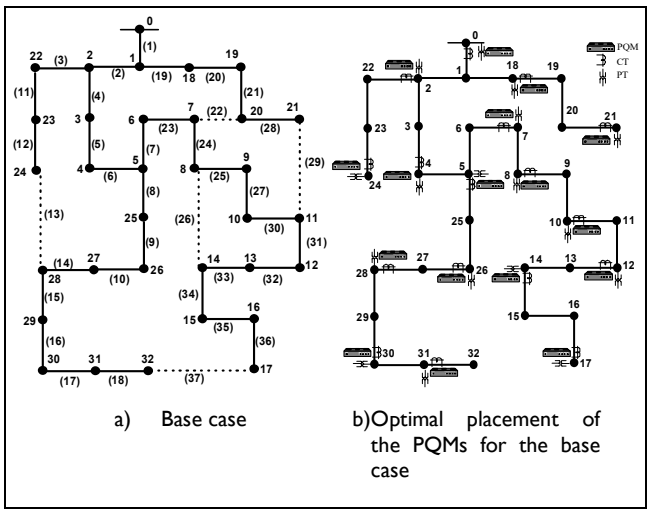

a) Base case b)Optimal placement of the PQMs for the base case

Figure 2. Base case of operation of the IEEE 33 Node test feeder and the optimal placement of the PQMs

Indexes calculation: indexes to evaluate the impact of the DNR on harmonic observability are calculated according with the proposed method presented in Figure 1. The placement of the PMQs has already been defined in Figure 2.b and the next step is to evaluate the harmonic observability for all reconfiguration cases. The results are shown in Table 3.

Table 3. Results of the indexes to evaluate the harmonic observability with optimal placement of PQMs for the base case

Network Reconfiguration cases	HOR %	HOR_T %
RC.1	100	96.15
RC.2	92.3	
RC.3	100	
RC.4	92.3	

The results show that for RC.2 and RC.4 network reconfigurations, the harmonic observability is impacted due to a 7.7 % of the system is not observable. During the operation time in this reconfiguration case is not possible to estimate all harmonic voltages and currents. However, the index HOR_T shows that when the harmonic observability is weighted in all operation time, the observability loss is less than in the worst cases. This index can be used by electrical utilities to assess the efficiency of the monitoring system installed. In addition, the electricity market regulators would require minimum standards of harmonic observability based on the proposed indexes to monitoring the harmonic components in the distribution systems.

Proposed solution to get the full harmonic observability: A modification of the objective function used in the OPP may guarantee the full harmonic observability.

The results of the OPP in the previous section were obtained using the *CV* with ones in all its positions. This means that the possible locations of PQMs are not penalized in the optimization problem. The proposal is to penalize the locations where a current measurement is on a line section that can be open in a reconfiguration case. Thus, it is required to know all reconfiguration cases and which line sections could be opened. The locations of PQMs in these line sections are penalized to avoid the observability loss due to PQMs without current measurements when a network reconfiguration is presented in the distribution system.

Table 4 shows the line sections identified and which must be penalized in the optimization problem.

Table 4. Penalty of the line sections

Line section	10	14	18	25	33	36
Cost vector value	100	100	100	100	100	100

The results of the OPP are shown in Table 5 and the new results of the indexes are shown in Table 6 using this optimal placement of the PQMs. The new optimal placement of the PQMs guarantees the full harmonic observability in the different network reconfiguration cases. It is highlighted that one additional monitor is necessary, compared to the base case without penalization, to guarantee the full harmonic observability.

Table 5. New results of the optimal placement of the PQMs for the base case

PQM	Measurements		PQM	Measurements	
	Voltage (node)	Current (branch)		Voltage (node)	Current (branch)
1	1	0	10	17	36
2	2	3	11	19	20
3	3	5	12	21	28
4	6	7	13	22	11
5	8	24	14	23	12
6	10	27	15	25	9
7	11	31	16	27	14
8	12	32	17	29	16
9	14	34	18	31	18

Table 6. Results of the Indexes to evaluate the harmonic components observability

Reconfiguration cases	HOR %	HOR_T %
RC.1	100	100
RC.2	100	
RC.3	100	
RC.4	100	

Conclusions

Optimal placement of PQMs becomes an important method to be applied in smart electric networks. However, conventional methods do not take into account the dynamic network reconfiguration in the solution of the optimal placement problem. This work presents a method to estimate the impact of the dynamic reconfiguration on harmonic observability and the results shows its good performance. When the information of the reconfigura-

tion cases was incorporated in the optimization problem, it is possible to guarantee the full harmonic observability.

In addition, the authors suggest new perspectives to solve in future works related with optimal monitor placement, such as: incorporation of the observability indexes into the optimization problem; a proposal for a multi-objective optimization problem including all network reconfiguration cases or proposals for the optimal monitoring systems based on the detection of different kinds of power quality disturbances.

References

Abdelsalam, H.A.; Abdelaziz, A.Y.; Osama, R.A.; Salem, R.H., "Impact of distribution system reconfiguration on optimal placement of phasor measurement units," Power Systems Conference (PSC), 2014 Clemson University, pp.1,6, 11-14 March,2014.

Almeida, C.F.M.; Kagan, N., "Harmonic state estimation through optimal monitoring systems," Smart Grid, IEEE Transactions on, vol.4, no.1, pp.467,478, March 2013.

Bernardon, D.P.; Pfitscher, L.L.; Canha, L.N.; Abaide, A.R.; Garcia, V.J.; Montagner, V.F.; Comassetto, L.; Ramos, M., "Automatic reconfiguration of distribution networks using Smart Grid concepts," Industry Applications (INDUSCON), 2012 10th IEEE/IAS International Conference on, pp.1,6, 5-7 Nov. 2012.

Brown, H.; Haughton, D.A.; Heydt, G.T.; Suryanarayanan, S., "Some elements of design and operation of a smart distribution system," Transmission and Distribution Conference and Exposition, 2010 IEEE PES, vol., no., pp.1,8, 19-22 April 2010.

Haughton, D.; Heydt, G.T., "Smart distribution system design: Automatic reconfiguration for improved reliability," Power and Energy Society General Meeting, 2010 IEEE , vol., no., pp.1,8, 25-29 July 2010.

Kumar, A.; Das, B.; Sharma, Jaydev, Genetic algorithm-based meter placement for static estimation of harmonic sources., Power Delivery, IEEE Transactions on, Vol. 20, No. 2, April 2005, pp. 1088-1096.

Muscas, C.; Pilo, F.; Pisano, G.; Sulis, S., "Optimal measurement devices allocation for harmonic state estimation considering parameters uncertainty in distribution networks," Electrical Power Quality and Utilisation, 2007. EPQU 2007. 9th International Conference on, vol., no., pp.1,6, 9-11 Oct. 2007

Madtharad, C.; Premrudeepreechacharn, S.; Watson, N.R.; Ratchai Saeng-Udom, "An optimal measurement placement method for power system harmonic state estimation," Power Delivery, IEEE Transactions on, vol.20, no.2, pp.1514,1521, April 2005.

Rad, M.S.; Mokhtari, H.; Karimi, H., "An optimal measurement placement method for power system harmonic state estimation," Electrical and Power Engineering (EPE), 2012 International Conference and Exposition on, pp.271,275, 25-27 Oct. 2012.

Shafiee Rad, M.; Mokhtari, H.; Karimi, H., "A new algorithm for optimal measurement placement, observability analysis and Harmonic State Estimation in power systems," Power Electronics, Drive Systems and Technologies Conference (PEDSTC), 2013 4th, pp.518,523, 13-14 Feb. 2013.

Yuxin Wan; Junwei Cao; Huaying Zhang; Zhengguo Zhu; Senjing Yao, "Optimization of the power quality monitor number in Smart Grid," Smart Grid Communications (SmartGridComm), 2014 IEEE International Conference on , vol., no., pp.230,235, 3-6 Nov. 2014.

Monitoring and control of the performance indexes in electrical power system by business intelligence

Control y monitoreo de los indicadores de desempeño en sistemas eléctricos de potencia mediante el sistema de inteligencia de negocios

L. Sayas Poma[1] and E. Jané La Torre[2]

ABSTRACT

The following article refers to the monitoring and control of power systems with integration of individual and systemic indexes that measure the true performance of the system because of their complementarity from the point of view of the evaluation of performance, this online monitoring through business intelligence to improve decision making with better support information.

Keywords: Performance, systemic indexes, individual indexes, business intelligence.

RESUMEN

El siguiente artículo hace referencia al monitoreo y control de sistemas eléctricos de potencia con la integración de indicadores individuales y sistémicos que miden el verdadero comportamiento del sistema debido a su complementariedad desde el punto de vista de la evaluación del performance, este monitoreo en línea a través del sistema de inteligencia de negocios mejora la toma de decisiones con un mejor soporte de información.

Palabras clave: Desempeño, indicadores sistémicos, indicadores individuales, sistema de inteligencia de negocios.

Introduction

In general, regulatory agencies are focused on the aspects of continuity of electric service, wave quality and customer service; Table I shows the benchmarking in countries based on the electrical power system quality (Abbad, 2007).

Table 1. Benchmarking of regulatory aspects about electricity quality service

Country	Aspects of regulatory quality	Incentives/ penalties	Quality indexes	Control of quality
Argentina	Continuity, quality of customer and wave	Penalties: Reduced rates to customers affected	System and individual indexes	Selective measurements contingency databases
Chile	Continuity, quality of customer and wave	Penalties	System and individual index	Specific customer surveys
England and Wales	Customer care	Penalties, compensation to affected customers	Individual guaranteed	Surveys, reports distributors
Norway	Voltage, frequency	Penalties	Individual indexes for continuity	Surveys, reports distributors

Since October 1997, the electrical power system quality has been based in the standard: *Norma técnica de calidad de los servicios eléctricos* (NTCSE, 1997) .The peruvian laws set by Osinergmin the obligation to monitoring and supervise the accomplishment with safety and quality standards of electrical companies. Fig.1 shows the historical and predictive calculations (Abbad, 2007) of the electrical power system quality indexes in Peru considering the NTCSE and Osinergmin process.

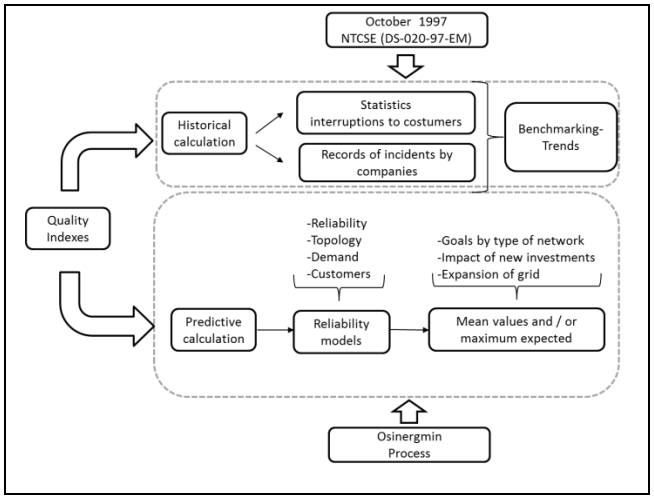

Figure 1. Historical and predictive calculations of the electrical power system quality indexes

The *Gerencia de Fiscallización Eléctrica (GFE)* in 2012 through a process of transforming data to information, it has been used techniques for support to make strategic decisions: Business Intelligence (BI).

[1] Leonidas Sayas Poma: Electrical engineer, Universidad del Centro del Perú, Perú. Master of science in power systems, Universidad Nacional de Ingeniería, Perú. Member IEEE, member AEP.
E-mail: lsayas@osinergmin.gob.pe
[2] Eduardo Jané La Torre: Mechanical and electrical engineer, Universidad Nacional de Ingeniería, Perú.
E-mail: ejane@osinergmin.gob.pe

Electrical Power System Quality

Perceived electrical power system quality

It is related to the occurrence of interruptions in the electrical system, both duration and times. Fig.2 shows a diagram of the perception of the electrical power system quality in the customers also shows in average percent of interruptions in the distributions system.

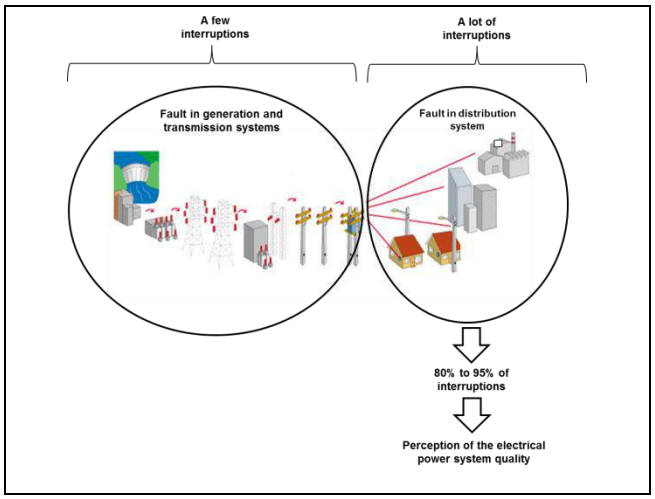

Figure 2. Perception of the electrical power system quality

Indicators of electrical power system quality

An important aspect of the electrical power system quality, how should it is measured and indexes are used. Fig. 3 shows the scopes of the systematic indexes refer to Osinergmin process in transmission and distribution system (RS-OS N° 074).

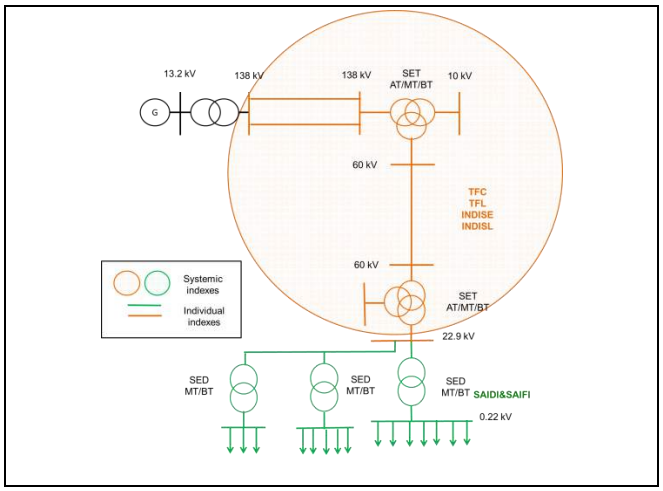

Figure 3. Evaluation of individual and systemic indexes of electrical power system quality.

Individual indexes: They reflect the level of electrical power system quality experienced by particular customer to service provided by the electric company. The NTCSE measures the individual electrical power system quality provided by the electric company to customers and sets limits for voltage level, indexes of interruptions per customer number (N) and total duration (D) of interruptions per customer (NTCSE,1997).

Systemic or global indexes: Show the average behavior or percentages of service electrical power system quality in the system, defined as: grid, service area, region, etc; where electric power is supplied. Also they are classified into client indexes: SAIFI (Interruptions / year), SAIDI (hours / year), TIEB (min / year), IIS (%) CAIFI (interruptions / year) and CAIDI (hours / year); potential indexes: NIEPI (hours), TIEPI (hours), ISS (ratio), TIEPED (minutes), energy indexes: ENS (kWh), ASCI (kWh / customers) ACCI (kWh / customers), indexes for predictability analysis: IKR (int /100 km) (Abbad, 2007).

Advantages and disadvantages of the system and individuals electrical power system quality indexes.

Continuity indexes attempt to measure the reliability of electricity supply, the number of times that interrupted the electricity supply and duration of interruption. Fig. 4 shows the approach to the electrical power system quality, the scope is: interruptions, power connected and customers supplied and effected. (Abbad, 2007)

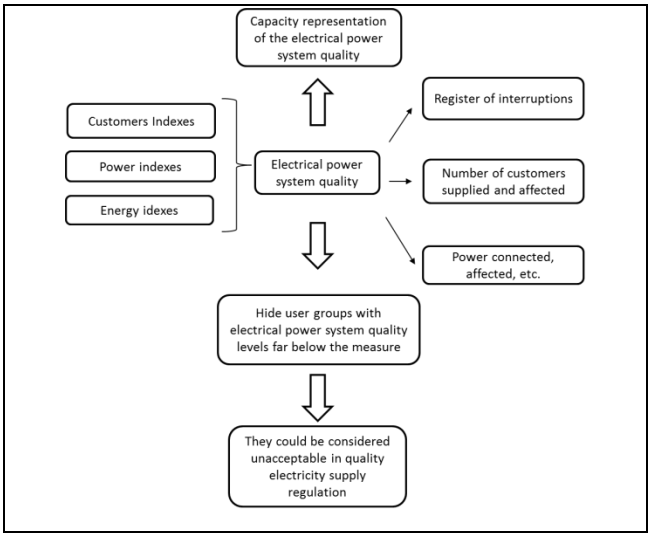

Figure 4. Electrical power system quality (systemic approach)

Fig. 5 shows the advantage of systemic index, evaluates behavior supplier in general and as this influence in the overall electrical power system quality, the disadvantage is that users who are inside are considered average, and those outside the average will not be taken into consideration.

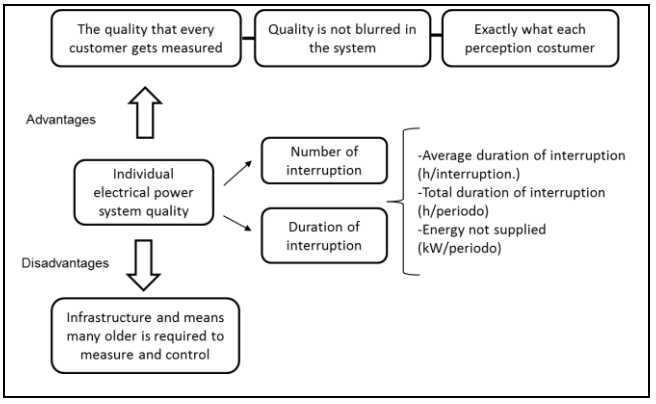

Figure 5. Electrical power system quality (particular approach)

The advantage of the individual index, it evaluate individual behavior of each client in the grid, the disadvantage is that users are not a measure of overall electricity quality and requires additional means to control and monitoring (Abbad, 2007).

In any case the pay for systematic and individual indexes is considered in both cases. In the case of Perú first there are evaluations referred to individual indexes then systemic indexes (SAIDI and SAIFI).

Complementarity of systemic and individual indexes

The quality electricity indexes approach allows the system to adjust the remuneration of distribution investments, controlling the electrical power system quality of system offered by encouraging distributor companies to invest until the optimum level of electrical power system quality; the electrical power system quality indexes approach allows a minimum level of electrical power system quality for all customers and be compensated customers who do not get the level of electrical power system quality. A better understanding of the complementarity viewed from the standpoint that the electrical power system quality provided to each customer is a stochastic phenomenon defined by a probability distribution. Because the individual indexes refer a particular customer and a compensation when the indexes is exceed the tolerance, the systemic indexes refer an average in the system and a penalty when the indexes is up the tolerance, both measure the true performance of the system because of their complementarity from the point of view of the evaluation of performance (Abbad, 2007). Fig. 6 shows the complementarity about indexes through probability distribution.

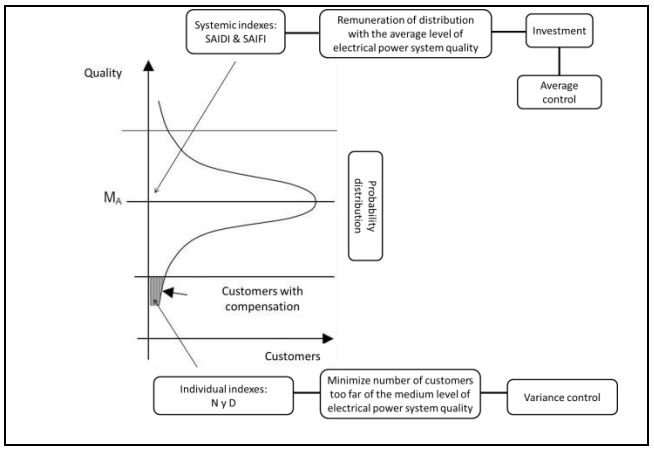

Figure 6. Complementarity of systemic and individual indexes

Optimal level of electrical power system quality

Any regulation should concern the minimization of the Net Social Cost (NSC) associated with the presentation of the electricity service, it is referred to the incurred cost by society in the presentation of considerate electricity service, is necessary to know the cost of supply the product or service, and its utility function for recipients of the product or service. Fig. 7 shows the lack of the knowledge about the cost of investments to improve de electrical power system quality, in other hand the actual customer cost when there are interruptions, so the NSC must focus to quality improvement for example through installation of signaling switching, alternative connections, etc (Abbad, 2007).

Fig. 8 shows the calculation of optimum electrical power system quality, the behavior of electrical companies (when the quality and cost increases) and customers (when the quality increases and the cost decreases)

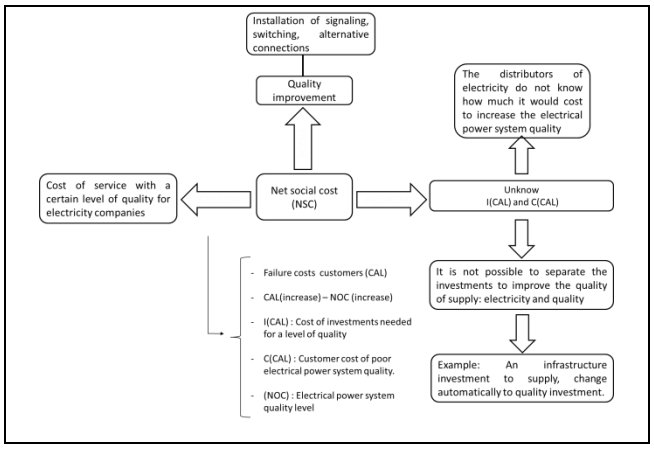

Figure 7.Approach of net social cost (NSC)

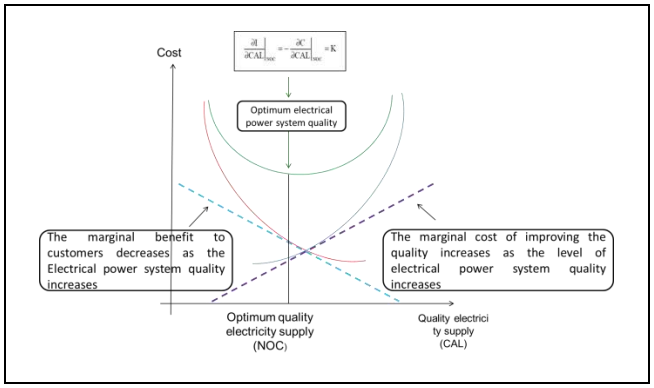

Figure 8.Diagram of optimum electrical power system quality

Economic function valuation of continuity

Fig. 9 shows each quality aspect is associated with a cost, so that different rates costs can add through economic function valuation of continuity (VEC) function (Abbad, 2007).

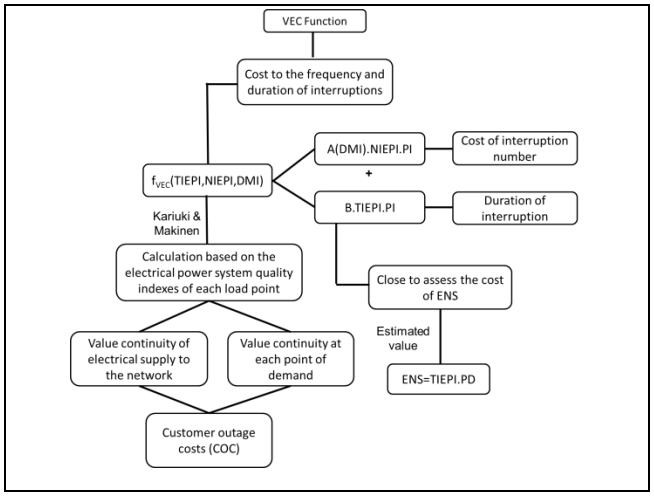

Figure 9. VEC Function

Incentives/Penalties

Through a mechanism of incentives/penalties based in system and individual indexes, to check that the remuneration of the distributor company is adequate considering the electrical power system quality offered by individual indexes to ensure the minimum level of electrical power system quality to all customers. Fig. 10 shows the regulatory aspect through incentives/penalties and the relation with individual and system electrical power system quality indexes.

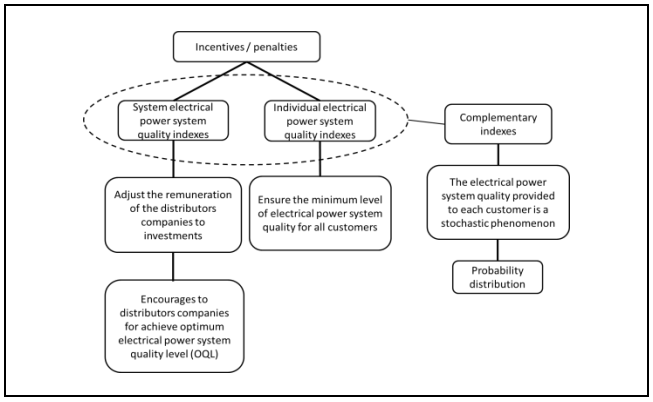

Figure 10.Approach of incentives/penalties

Global indexes that measure the performance of the system

Performance indexes for the operation of electrical distribution systems

The performance of the electrical systems of distribution is monitoring by Osinergmin through indexes showed in Table 2, SAIFI (System Average Interruption Frequency Index) and SAIDI (System Average Interruption Duration Index) (IEEE 1366-2012), tolerances are reference and set depending on the voltage level, sectors called: "Typical Distribution Sectors". (RS-OS N° 074)

Table 2. Performance indexes for the operation of electrical distribution system

Description	Index
System Average Interruption Frequency Index	**SAIFI=** $\frac{\sum_{i=1}^{n} ui}{N}$
System Average Interruption Duration Index	**SAIDI=** $\frac{\sum_{i=1}^{n} ti \times ui}{N}$

Where:
ui: Number of customers affected by each interruption
ti: Duration of each interruption (hours)
n: Number of interruptions in a time period
N: Number of customers in the grid ending the period

Critical electrical systems: The Osinergmin is monitoring the electrical systems that are being affected by sustained power interruption, which exceeded twice the tolerance or more; these systems are called "critical electrical systems", in which perceived discomfort to customers claims the authorities and representatives of customers. Through the 074 process, monitoring of interruptions by measuring the results of the calculation of certain indexes based on reports from electricity companies across an online system (Extranet), as in the case of major interruptions that are reported by the of electricity companies to Osinergmin within the next twelve (12) hours of the event occurred. Fig. 11 shows the schematic form of supervision in transmission, electric systems and critical electric system, the proactive approaches like a: monitoring transformer overload, isolated generation reserve margin and other monitoring reports.

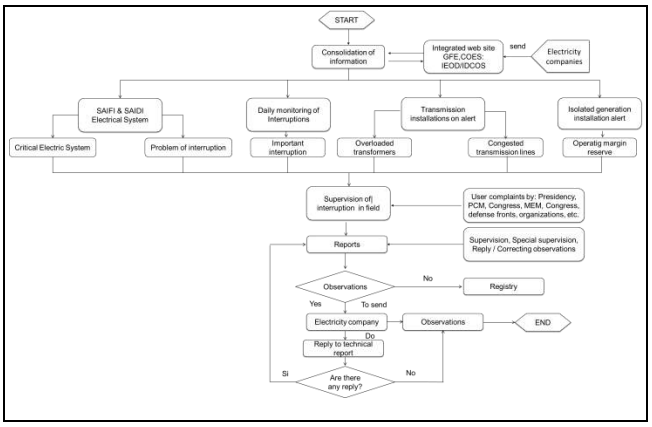

Figure 11. Monitoring scheme through process and performance indexes.

Performance indexes for the operation of electric transmission systems

The frequency and duration of disconnections that alter the electrical power system quality by the process N° 091-2006-OS / CD Osinergmin, regulating tolerances to international standards, resulting in operators concern for reducing disruptions through investments to rehabilitate the systems operating with deficiencies or overload. Table 3 shows the indexes about the process (RS-OS N° 091).

Table 3. Performance indexes for the operation of electrical transmission system

Description	Index
Failure rate of substation equipment	**TFC = N° Failure**
Failure rate of each transmission line	**TFL=** $\frac{\text{N°Failure}}{\text{Ext. LT}}$ **X100**
Unavailability of substation equipment	**INDISE = ∑HIND**
Unavailability of equipment each transmission line	**INDISL = ∑HIND**

Electrical performance indexes of isolated generation systems

The performance of power systems with isolated generation is monitoring by Osinergmin (RS-OS N° 220). Table 4 shows the indexes in the process to evaluate isolated electrical system according GART.

Table 4. Performance indexes of isolated generation system

Description	Index
Operating reserve margin generating	**MR=(PE/MD)-1**
Rate of forced outputs	**TSF=NSF/TES**
Forced unavailability index	**IIF=HIF/TES**

Control and monitoring of indexes through business intelligence

Business Intelligence

The business intelligence (BI) includes a web environment for display indexes of monitoring procedures of GFE, also has a georeferenced map. Fig. 12 shows a view of BI to monitoring with de Osinergmin process in electric system, using BI is most easily to take decisions.

Figure 12. BI Portal home

Datawarehouse: The BI has developed a database in Oracle, SQlL Server, Access and Excel files of users for ad-hoc reports, all this makes it possible to conduct consultations "on line", through the Office cognos go producing automatic reports of indexes, alert reports via email and analyzing information which are displayed via LCD screens and mobile devices, the reports of the concession made by affidavit verified by Osinergmin up the database referred. The advantages are: Minimize the time of issuance of reports, generate automatic reports, avoid printing physical reports, connection with Georeferenced GIS systems, and improved control through indexes automatic alert and making more objective decisions optimizing resources audit. Fig. 13 shows the datawerhouse's components with analysis models to analyze reports, alerts and the interaction with boss, coordinators and users.

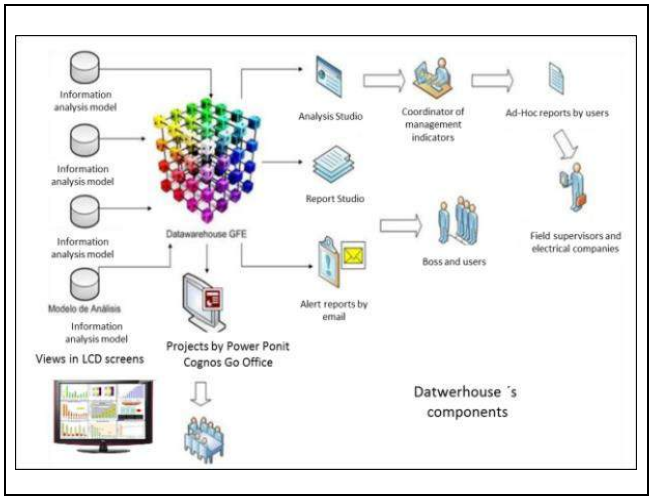

Figure 13.Integration through BI report

Results

General results

Monitoring compliance with the compensation for poor electrical power system quality (interruptions) was achieved in the period from 2004 to the First Half of 2015*, ten companies managed by FONAFE, returned to its users, through receipts, amounting to 115 million. Fig. 14 shows total compensation for poor power quality by electricity company since 2004 – 2015. The companies with the highest compensations are: Electro Oriente S.A. and Hidrandina S.A.

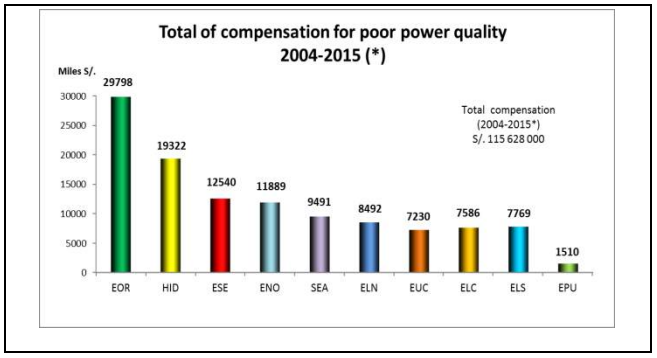

Figure 14. Total compensation 2004 – 2015

Results at the institutional level

- Control interruptions through the extranet system with information from the companies.
- Identification of electric critical systems.
- Reduced time of the monitoring process.
- Determination of systemic indexes.
- Almost immediate effectuation of disciplinary procedures.
- Automatic issuance of reports and statistical tables.

Results per process

Results of the performance monitoring of the operation of medium voltage electrical systems: This control has consolidated a safe, efficient and reliable supply, by recording specific information that is accurate and truthful provided by the actors themselves, and it is used to develop strategies for supervision and monitoring as well as to identify the location (source) and the causes of interruptions, so restore the electricity supply in reasonable time. Fig. 15 shows the monitoring of SADI in the last three years, in general the index is decreasing, the mayor percent of interruptions was in distributions system.

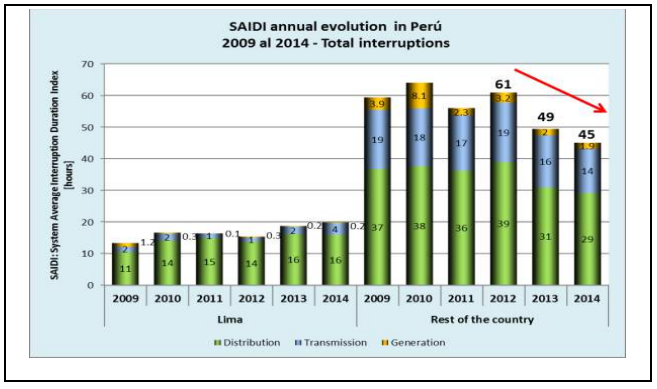

Figure 15. Monitoring of SAIDI during 2009–2014

Fig. 16 shows the monitoring of SAIDI y SAIFI in distribution system, in 2013 Electro Norte S.A. was the highest SAIDI and Electro Nor Oeste S.A. was the highest SAIFI.

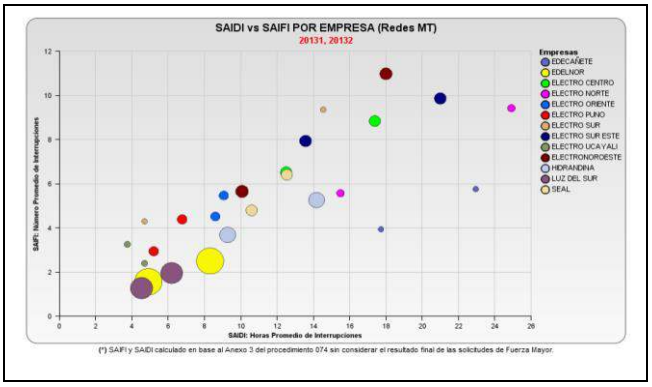

Figure 16. Monitoring of SAIDI & SAIFI during 2013

Results of Monitoring performance transmission system: This control has identified overloaded transformers and congested transmission lines to engage members of the transmission system to improve the electrical power system quality, improving facilities and / or replacing equipment and implementing contingency plans. Fig.17 shows monitoring transmission lines during 2013-2014

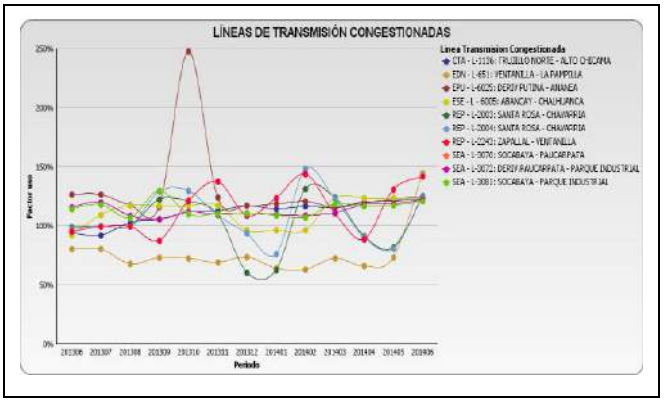

Figure 17. Monitoring of congested transmission 2013–2014

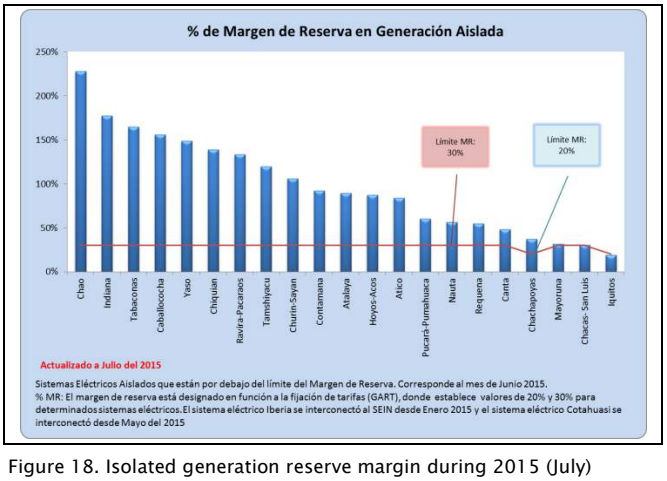

Figure 18. Isolated generation reserve margin during 2015 (July)

Results Performance Monitoring electrical systems with isolated generation: This control has identified the isolated electrical systems that violate the operating margin reserve according GART. Fig.18 shows monitoring of reserve margin during 2015(April), some electric systems like: Moyoruna and Chacas-San Luis do not have necessary reserve margin.

Conclusions

Osinergmin monitoring generation, transmission and distribution system by performance indexes.

Osinergmin use the individual (N&D) and global (SAIDI&SAIFI) indexes to monitoring the Electrical Power System Quality because they are complementary.

The monitoring process is improved by generating reports on line by BI.

The generation, transmission and distribution companies report information across the Extranet is used to generate a reliable and consistent basis for the functioning of BI.

In general, companies have improved the quality indexes of service to their customers.

Control and monitoring of performance indicators of electrical systems, has been replicated by electricity companies in Peru and other regulatory institutions like: OSIPTEL and SUNASS.

References

Abbad, J. R., Calidad del servicio, regulación y optimización de inversiones, Vol. 36, No. 1, 2007, pp.13-14, 27-46,52-66,83-84.

NTCSE, Norma Técnica de calidad de los servicios eléctricos, Vol.1, 1997 y modificaciones.pp.31-42.

RS-OS N° 074 Osinergmin - Procedimiento para la Supervisión de la Operación de los Sistemas Eléctricos (OS N° 074-2004-OS/CD). Abril. 2004. pp. 6-10.

RS-OS N° 091 Osinergmin - Procedimiento para supervisión y fiscalización del performance de los Sistemas de Transmisión (OS N° 091-2006-OS/CD). Mar. 2006, pp. 3-5.

RS-OS N° 220 Osinergmin - Procedimiento para la Supervisión de la Operatividad de la Generación en Sistemas Eléctricos Aislados (OS N° 220-2010-OS/CD), Agosto, 2010, pp. 5-9.

IEEE 1366-2012, Guide for Electric Power Distribution Reliability Indices.

Performance of True-48-Pulse DSTATCOM for Voltage Sag Mitigation

Desempeño de un DSTATCOM de 48-pulsos para la mitigación de hundimientos de tensión

O. F. Orjuela[1], H. E. Rojas[2], D. A. Gutierrez[3]

ABSTRACT

This paper presents the implementation and performance of three-phase Distribution Static Compensator (DSTATCOM) used for voltage sag mitigation. The DSTATCOM is based on a voltage source SPWM inverter with a true-48-pulse circuit-level. For simulations, IEEE-34 bus test feeder is chosen due to its topological features and wide variety of components. Simulations using ATP/EMTP software describe the DSTATCOM design process and provide experimental results. In addition, the performance of DSTATCOM in several cases is analyzed, showing that this device is a good alternative for power quality improvement in distribution systems.

Keywords: 48-pulse inverter, ATP/EMTP, DSTATCOM, IEEE-34 bus-test-feeder, sags mitigation, SPWM modulation

RESUMEN

Este artículo presenta la implementación y desempeño de un compensador estático de distribución trifásico (DSTATCOM) usado para la mitigación de hundimientos de tensión (sags). El DSTATCOM se basa en un inversor trifásico con modulacion por ancho de pulso senoidal (SPWM) con un circuito multinivel de 48 pulsos. Para las simulaciones se seleccionó el sistema de distribución IEEE-34 debido a sus características topológicas y una amplia variedad de componentes. Simulaciones usando el software ATP/EMTP describen el proceso de diselo del DSTATCOM y proporcionan resultados experimentales. Adicionalmente, el desempeño del DSTATCOM es analizado en varios casos mostrando que este dispositivo es una buena alternativa para mejorar la calidad de potencia en sistemas de distribución.

Palabras clave: ATP/EMTP, DSTATCOM, inversor de 48 pulsos, mitigación de sags, modulación SPWM, sistema IEEE-34

Received: July 22th, 2015
Accepted: Sept 24th, 2015

Introduction

A power distribution network can be affected by current and voltage-related power quality (PQ) problems such as distorted current sources and voltage disturbances (Bollen, 1999). Voltage sag is a short-duration reduction in RMS voltage between 10% and 90% of the nominal value with duration from half-cycle to a few seconds. These disturbance produce mal-operation or interruption on sensitive equipment, many times leads to complete interruptions of the industrial process and affect the proper operation of power and distribution systems.

[1] Oscar Felipe Orjuela-Sastoque. Electrical Engineering Student, Universidad Distrital Francisco José de Caldas, Colombia. Electromagnetic Compatibility and Interference Group GCEM, Colombia. E-mail: oscaror-9@hotmail.com

[2] Herbert Enrique Rojas-Cubides. Electrical Engineer, M.Sc. in Electrical Engineering and candidate to Ph.D. from Universidad Nacional de Colombia, Colombia. Assistant Professor in Electrical Engineering Department, Universidad Distrital Francisco José de Caldas Colombia. Electromagnetic Compatibility and Interference Group GCEM. E-mail: herojasc@udistrital.edu.co

[3] David Alberto Gutierrez-Casas. Electrical Engineering Student, Universidad Distrital Francisco José de Caldas, Colombia. Electromagnetic Compatibility and Interference Group GCEM, Colombia. E-mail: ozzy_loureiro@hotmail.com

Voltage sags are caused by faults and short-circuit generally associated to bad weather conditions (i.e. lightning strokes, storms, wind, etc.), energizing of larger loads and transformers, motor starting, overloads and other load variations (Bollen, 1999). Although voltage sags are less harmful than interruptions, they are more frequent, besides their effects on sensitive devices and equipment can be as important as those produced by an interruption. For these reasons, voltage sags are among the most frequent and one of the main PQ problems (McGranaghan, Mueller, & Samotyj, 1991).

The distribution static compensator (DSTATCOM) is a shunt-connected device used to mitigate PQ problems and can operate in voltage-control mode (VCM) or in current-control mode (CCM) (Kumar & Mishra, 2014). Additionally, DSTATCOM has the capability to sustain reactive current at low voltage, reduced land use and can be developed as a voltage and frequency support by replacing capacitors with batteries as energy storage (Masdi, Mariun, Mahmud, Mohamed, & Yusuf, 2004).

This paper presents the design process and implementation of a true-48-pulse DSTATCOM for voltage sag mitigation. The suitability of DSTATCOM (operation and control scheme) is verified by simulation using Alternative Transient Program (ATP/EMTP). In order to understand the DSTATCOM performance, several case studies are presented using the IEEE-34 bus test feeder. In

addition, analysis between reactive power injected by DSTATCOM and voltage sag depth is considered.

The rest of this paper is organized as follows. The configuration, operation and modeling of DSTATCOM using ATP/EMTP are summarized in Section 2 and Section 3, respectively. Section 4 describes the DSTATCOM control methodology. In section 5, the features of IEEE-34 bus test feeder and the case studies are presented. In section 6, simulations and analysis of DSTATCOM impact on test system, under voltage sag conditions, is performed. Finally, some conclusions are presented in section 7.

Configuration and Operation of DSTATCOM

Basic structure of DSTATCOM

Static compensator DSTATCOM is a three-phase electronic power device. It is connected in shunt at distribution systems near to the load (Masdi et al., 2004). The basic structure of DSTATCOM consists of a DC energy storage device (DC source or DC capacitor), a three-phase inverter module (based on IGBT, thyristor, etc.), a control stage, an AC filter, and a step-up coupling transformer (Rojas, Cruz, & Rojas, 2015). Figure 1 shows the block diagram of DSTATCOM and its connection scheme.

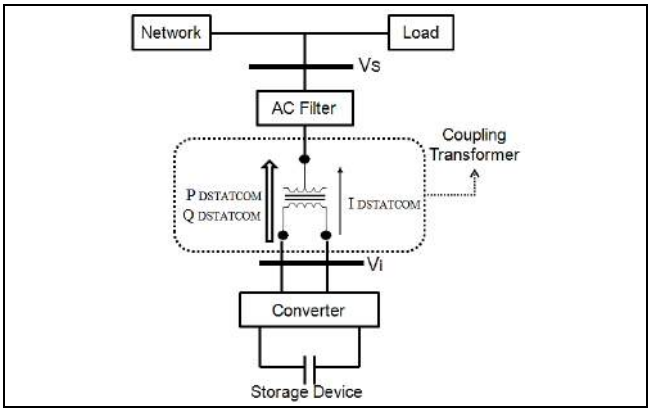

Figure 1. Block diagram of DSTATCOM
Source: Authors

Operation of the DSTATCOM

The DSTATCOM is a solid-state device with the ability to control the voltage magnitude and the phase angle, for this reason can be treated as a voltage controlled source but can also be seen as a controlled current source. The controller regulates the reactive current that flows between the compensator and the distribution system in such a way that the phase angle between the inverter voltage (Vi) and the system voltage (Vs) is dynamically adjusted so that the DSTATCOM absorbs or generates the desire reactive power at a specific point common coupling (PCC). The active power (P_{DST}) and reactive power (Q_{DST}) that flow through an impedance can be calculated using the following equations:

$$P_{DST} = [(|Vs||Vi|)/X_{Trx}] * sen(\delta) \quad (1)$$

$$Q_{DST} = [\{(|Vs||Vi|)/X_{Trx}\} * cos(\delta)] - [|Vs|^2/X_{Trx}] \quad (2)$$

where, Vi is the output voltage of the DSTATCOM, Vs is the power system voltage, X_{Trx} is the reactance of the coupling transformer and δ is the phase angle between Vi and Vs. Equations (1) and (2) show that the basic operation of DSTATCOM varies depending upon Vi.

DSTATCOM modelling and simulation

DC energy storage device

DC voltage storage device is modeling as DC source connected in parallel with a capacitor C_{DC}. The sizing of this capacitor is referred to the fault current in the system, which is defined as the different between the current before and after the fault (Masdi & Mariun, 2009). To determine the size of C_{DC} in a three-phase system the following equation is used (Hsu & Wu, 1996).

$$C_{DC} = 3 \cdot [(V_{DSTAT} * \Delta I_L * T)/(V_{C\,máx}{}^2 - V_{DC}^2)] \quad (3)$$

where, V_{DC} is the voltage across C_{DC} per phase, V_{DSTAT} is the peak voltage per phase, ΔI_L is the difference between the current before and after in the load, T is the period of one cycle of voltage and current and $V_{C\,máx}$ is the upper limit of the energy storage in C_{DC} per phase. For voltage sag conditions, the value of ΔI_L can be determine by measuring the load current before and during the disturbance (Hsu & Wu, 1996). The value of V_{DC} is determined from ATP/EMTP simulation for each case study. The value of $V_{C\,máx}$ is the upper limit of C_{DC} voltage and this can be two or three times of V_{DC}.

Power electronic stage

Usually, the DSTATCOM configuration consists of a conventional six-pulse or twelve-pulse inverter arrangement (Rojas et al., 2015). Configurations that are more sophisticated use multi-pulse or multi-level configurations. In this paper, a true-48-pulse inverter configuration is used. This configuration uses eight 6-pulse inverters connected in parallel with the same DC-source. For each six-pulse inverter, six bidirectional semiconductors are used. Figure 2 shows the configuration in ATP/EMTP for one branch that conform a six-pulse inverter.

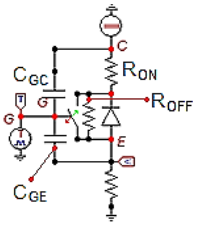

Parameters IGBT model	
R_{ON}	0,0057 Ω
R_{OFF}	240000 Ω
C_{GC}	5,49 nF
C_{GE}	9,31 nF

Figure 2. Configuration and values of a six-pulse inverter branch
Source: Authors

For the DSTATCOM model proposed in this paper, Insulated Gate Bipolar Transistors (IGBT) are used. Followed to this element is connected a resistance in series (R_{ON}) that represents the inverter losses when the IGBT is turned-on and a resistance connected in parallel (R_{OFF}) that represents the losses when the valve is turned-off. It is important to emphasize that the inverter model includes a gate-collector capacitor (C_{GC}) and a gate-emissor capacitor (C_{GE}) that represent the parasite capacitances. Finally, to complete the IGBT basic model an ideal type-13 switch controlled by TACS is used as commutation element.

In general terms, the DSTATCOM voltage source is controlled with hysteresis or ramp comparison type current regulated PWM inverter (Muni, Rao, & Vithal, 2006). The Sinusoidal Pulse Width Modulation (SPWM) technique is widely employed in order to adjust the inverter output voltage (amplitude) and the

frequency to the desired value. In this technique, the power converter switches (implemented with IGBTs) are set to the ON or OFF state according to the result of the comparison between a high-frequency constant-amplitude triangular wave (carrier) with a low-frequency (e.g., 60 Hz) reference sine wave of adjustable amplitude and/or frequency (Lakka, Koutroulis, & Dollas, 2014).

In this study, an SPWM modulation scheme is developed. For the construction of this circuit a triangular wave generator, a sine wave signal and a comparator is required. Due to ATP/EMTP does not provide a model of triangular wave generator, a triangular signal is constructed integrating a square wave. The SPWM modulation circuit in ATPDraw is presented in Figure 3. The SPWM provides an output signal with a switching frequency of 8 KHz. In addition, Figure 4 presents a six-pulse unit inverter using in the DSTATCOM model.

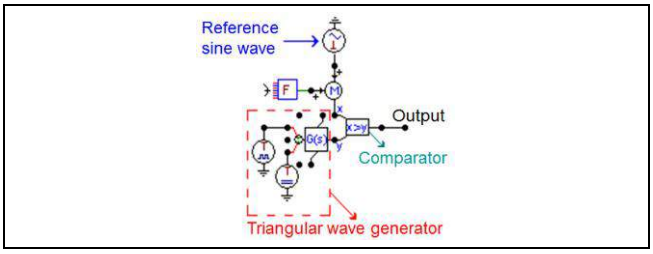

Figure 3. SPWM modulation circuit in ATPDraw
Source: Authors

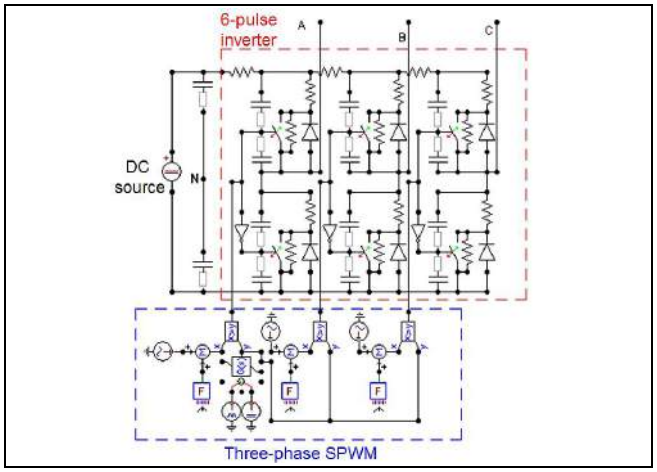

Figure 4. Six-pulse three phase unit inverter
Source: Authors

The true-48-pulses circuit for the DSTATCOM inverter uses eight intermediate transformers with a Y-Δ connection. Each 6-pulse unit has a transformer delayed 7.5° with respect to the next 6-pulse stage. The wye-connected windings of these transformers are connected in series and the windings connected in delta remove the third-harmonic components from the inverter output voltages. Figure 5 shows the connection scheme of the true-48-pulse inverter.

Figure 6 shows the line-to-line output voltage of the true-48-pulses inverter when the output of DC energy storage device is adjust to $V_{DC} = 722\,V$. In this case, the peak value of single-phase output voltage signal is 2983 V, while line-to-line output voltages reach maximum values of 5779 V. With respect to the amplitude of DC voltage, the single-phase and the line-to-line output voltages present an increase of four and eight times, respectively. In this case, the SPMW variables were placed in 1 for the amplitude modulation with a switching frequency of 8 KHz.

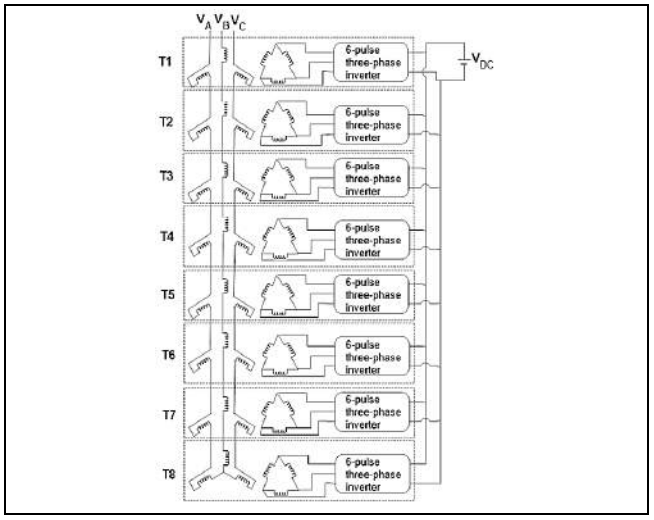

Figure 5. True-48-pulse inverter scheme
Source: Authors

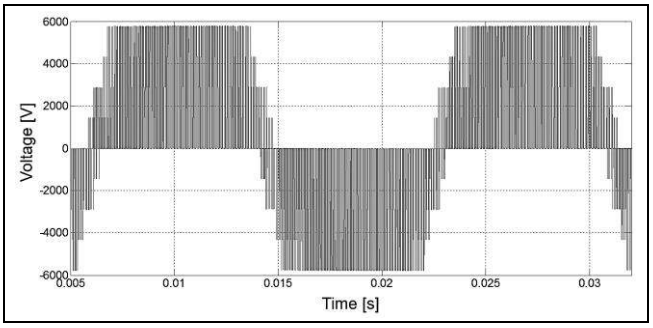

Figure 6. Line-to-line output voltage of true-48-pulse inverter
Source: Authors

The harmonic components of the single-phase output voltage of the DSTATCOM are shown in Figure 7. The analysis shows that single-phase output voltages have harmonic components between 110th and 170th order (i.e. between 6 kHz and 11 kHz). The maximum harmonic is founded in 7.98 KHz with a value of 1465 V. This output voltage presents a THDv of 80.2%.

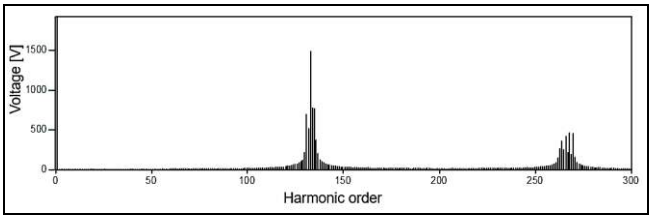

Figure 7. Harmonic components of single-phase output voltage of the true-48-pulse inverter
Source: Authors

Harmonic filter connection

Due to true-48-pulse DSTATCOM output voltages are signals composed by high-frequency harmonics, a LC low-pass filter to reduce the harmonic distortion was implemented. The values of the inductance and the capacitance of filter are 1 mH and 51 μF, respectively. The cut-off frequency of LC filter was 700 Hz and its Bode diagram is shown in Figure 8. The THDv of the filtered

output voltages is 1.24%. The peak value of single-phase output voltage is 3587 V. An example of the filtered output voltage for true-48-pulse inverter is illustrated in Figure 9.

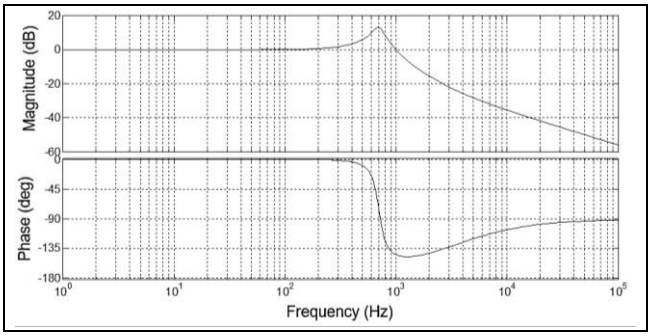

Figure 8. Bode diagram for the LC filter
Source: Authors

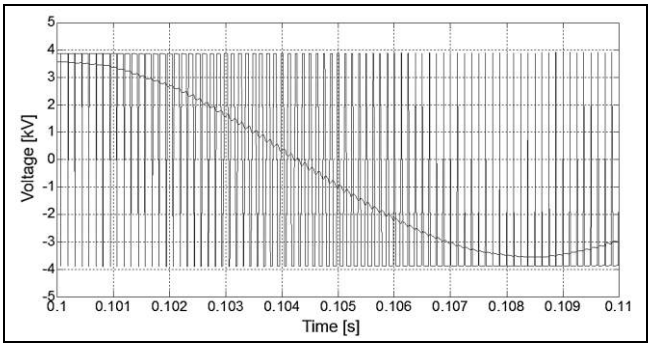

Figure 9. Single-phase output voltage of the true-48-pulse inverter. Inverter output signal (square wave), filtered signal (sine wave).
Source: Authors

Coupling transformer configuration

This device is a Y-Y transformer that allows the energy exchange between the AC system and DSTATCOM. In applications that include electronic devices the coupling transformer is used to adapt the circuit impedances, change the values of inverter output voltages and connect to the next stage. The technical features of coupling transformer are defined in section 5.

DSTATCOM control structure

The controller of DSTATCOM monitors the system behavior and governs the magnitude and phase of the output voltage signals of the inverter. The designed control scheme of DSTATCOM for voltage sag mitigation is shown in Figure 10. The phase synchronization block is composed for three single-phase PLL, which provide the synchronization angles of the DSTATCOM output signals. The reference values for the amplitude modulation process are obtained from the amplitude control. The sine wave generator takes the reference values to produce the modulation signals that feed the SPWM module.

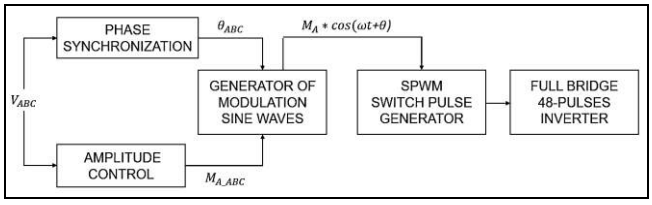

Figure 10. Block diagram of the control scheme for sag mitigation
Source: Authors

Figure 11 shows the complete circuit of the DSTATCOM for voltage sag mitigation in ATPDraw. This circuit includes the single-phase PLLs and two RMS-value meters that measure the voltages and currents of the distribution system to obtain the input signals of the model control scheme. Also, it is observed the electronic power stage (described in section 3), the LC filter and the coupling transformer.

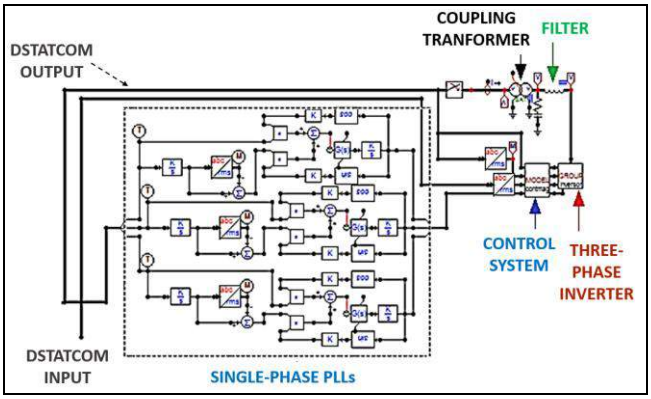

Figure 11. Control circuit for voltage sag mitigation in ATPDraw
Source: Authors

Distribution test system and case studies

IEEE-34 bus test feeder

The distribution system used in this study is based on the IEEE-34 bus test feeder. This system is chosen because of its topological features and wide variety of components. This distribution network has two voltage regulators, two capacitor banks and one low voltage lateral at 4.16 kV. The substation is rated at 2500 kVA, with a 69kV/24.9 kV transformer. Loads are modelled as three-phase (balanced or unbalanced), single-phase spot or distributed loads (IEEE Distribution System Analysis Subcommittee, 2000).

Due to IEEE-34 system is a distribution network with a radial configuration, any fault produced near to the substation transformer (node 800) significantly affects all voltage profiles of the system. To avoid this condition, the IEEE-34 system was modified connecting other substation unit, with the same characteristics of the original one, at node 846 where no loads are connected. Figure 12 shows the scheme of IEEE-34 modified system (IEEE-34M). The use of the new distributed generation (GD) unit guarantees that critical nodes are located in different points of the system reducing the relevance of nodes 800 to 814.

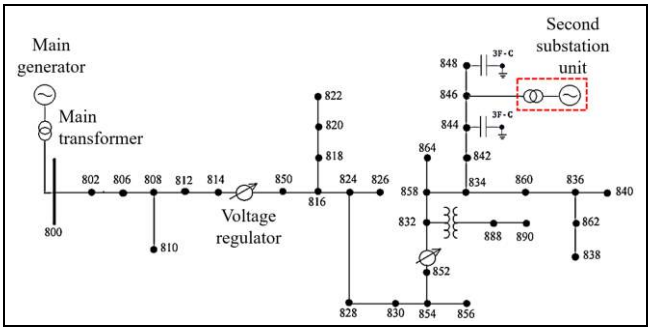

Figure 12. Scheme of IEEE-34M distribution system
Source: Authors

Case studies under PQ problems

The voltage sag conditions used in this paper were chosen using a method of stochastic generation of disturbances and assuming that voltage sags were originated only by faults. The application of this method requires the generation of random values with a probability density that are used to obtain the location of disturbance, the type of fault and the fault resistance. Applying this stochastic method, the test system has been simulated in 760 voltage sag scenarios.

The characteristics of the faults have been randomly generated with a MATLAB ® routine. In each simulation scenario, the results of fault configurations were used to estimate a local function LF. This function allows to analyze how much IEEE-34M system is affected by the occurrence of a fault condition A in a specific node k. The local function is given by:

$$LF_{Ak} = \sum_{i=1}^{13}\sum_{j=1}^{3}(V_{Ref-ij} - V_{Fault-ij})^2 \qquad (5)$$

Where, i is each node in the system, j is the phase (A, B or C), V_{Ref-ij} is the pre-fault voltage in p.u. and $V_{Fault-ij}$ is the voltage in p.u. during the voltage sag condition. Table I presents the worst cases under balanced and unbalanced voltage sags.

Table 1. Case studies for DSTATCOM implementation

Case	Node	Fault Type	Resistance Value [Ω]	Local Function	Voltage sag deep [p.u.]
1	N834	3L – 10	4	40.848	0.155
2	N842	2LG – 7	4	28.489	0.1514

Source: Authors

These are the case studies where DSTATCOM will be evaluated for voltage sags mitigation. Taking into account that the presence of voltage sags has a random nature and the most critical conditions are produced by three-line faults, the case study 1 is a valid example of the IEEE-34M system response.

Voltage sags mitigation using DSTATCOM

To analyze the response of the IEEE-34M system for each case study and to evaluate the performance of the DSTATCOM under voltage sag conditions, the following methodology is applied:

- The DSTATCOM is connected at node in which the voltage sag occurs (node with the deeper voltage)
- Evaluate the DSTATCOM response
- Analyze the DSTATCOM output voltage signals and the operation of the control scheme
- Calculate the reactive power injected by the DSTATCOM that improves the voltage profile of the IEEE-34M system and mitigates the voltage sag condition.

According to the voltage levels of the IEEE-34M system, the technical features of the coupling transformer connected to the DSTATCOM are: voltage 24.9kV/4.16kV, power 2.5 MVA, connection Y-Y and impedance 5.86%.

Case Study 1: voltage sag at node 834

In this case, a three-line fault (type 10) at node 834 with a fault resistance of 4Ω was analyzed. This scenario is the most critical of the simulated cases, producing an average voltage sag per phase of 0.155 in p.u. This voltage sag condition begins at 52.5 ms and ends at 350 ms. Figure 13, Figure 14 and Figure 15 show the voltage profile at each phase of node 834 before voltage sag (dashed line), during sag without DSTATCOM (grey line) and during sag condition with DSTATCOM (black line). It is possible to observe that DSTATCOM takes an average time of 45 ms before to starting the reactive injection.

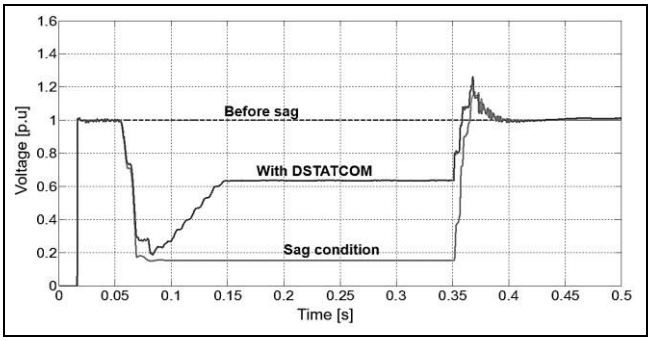

Figure 13. RMS Voltage of phase–A for case 1 (sag at node 834)
Source: Authors

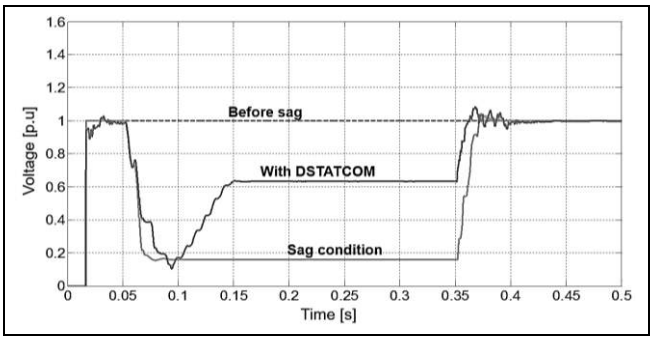

Figure 14. RMS Voltage of phase–B for case 1 (sag at node 834)
Source: Authors

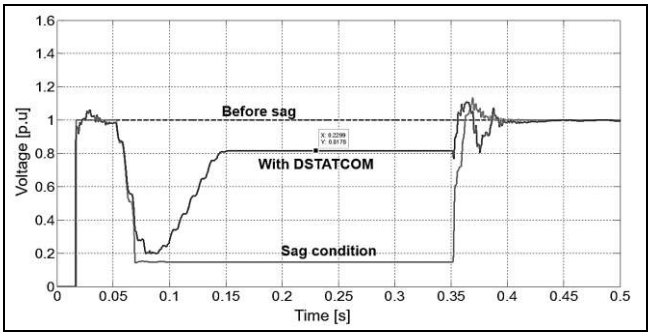

Figure 15. RMS Voltage of phase–C for case 1 (sag at node 834)
Source: Authors

In this case, the local function was reduced from 40.85 to 11.71 applying a DC voltage of 3.6 kV. In addition, the compensator improves the voltage of the node 834 reaching an average value of 0.714 p.u. per phase. With these changes, all voltages of IEEE-34M system are also improved achieving a minimum value of 0.63 p.u. at node 834 and a maximum value of 0.88 p.u. at node 890. Table 2 presents the RMS voltages per phase at the node 834 before and after the connection of DSTATCOM during the voltage sag.

Table 2. Voltage comparison at node 834 for case 1

DSTATCOM Condition	Phase A [p.u]	Phase B [p.u]	Phase C [p.u]
Without DSTATCOM	0.153	0.160	0.149
With DSTATCOM	0.664	0.631	0.817

Source: Authors

Finally, the C_{DC} value using the Eq. 3 is 148.3 μF. Finally, the reactive power of the DSTATCOM is calculated as follows:

$$Q = \omega * C_{DC} * V_{L-L}^2 \quad (4)$$

Where, $\omega = 377\ [\mathrm{rad/s}]$ and V_{L-L} is the nominal line-to-line voltage of the system at the PCC. For IEEE-34M system $V_{L-L} = 24.9\ kV$. Using the Eq. 4 the rating reactive power injected by DSTATCOM is 3462 kVAR.

Case Study 2: voltage sag at node 842

The voltage sag occurred at node 842 is due to a double-line-to-ground fault (type 7) with a resistance of 4Ω. This condition produces an average voltage sag per phase of 0.151 p.u. This voltage sag condition begins at 41.5 ms and ends at 350 ms. Figure 16, Figure 17 and Figure 18 show the voltage per phase of node 834 before voltage sag (dashed line), during sag without DSTATCOM (grey line) and during sag with DSTATCOM (black line). For this case, the DSTATCOM takes an average of 2.9 cycles (48 ms) before to inject reactive power.

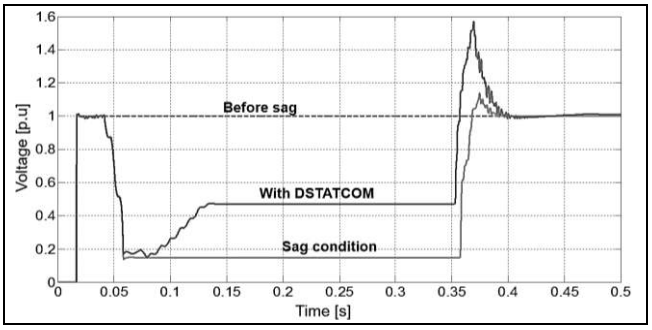

Figure 16. RMS Voltage of phase–A for case 2 (sag at node 842)
Source: Authors

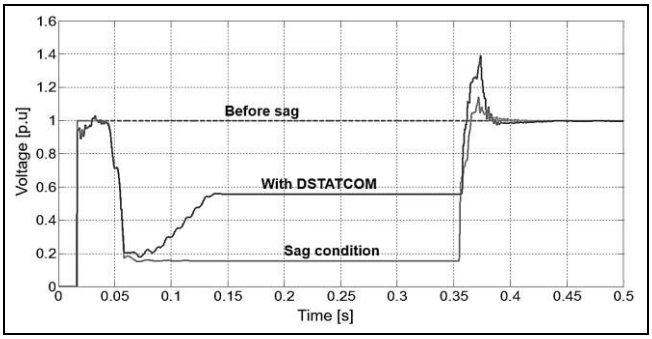

Figure 17. RMS Voltage of phase–B for case 2 (sag at node 842)
Source: Authors

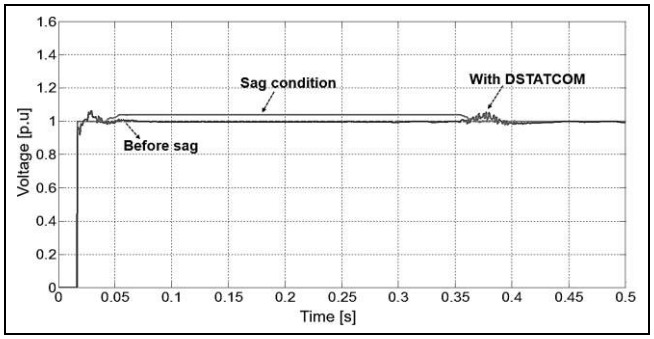

Figure 18. RMS Voltage of phase–C for case 2 (sag at node 842)
Source: Authors

In this case, the DC voltage is varied from 800 V to 3.6 kV and the local function was reduced from 28.49 to 11.71. The RMS voltages per phase at node 842 during the voltage sag condition with and without DSTATCOM are presented in Table 3. Voltages of node 842 are improved with the compensator obtaining an increase of 0.472 p.u. and 0.558 p.u. at phase A and B, respectively. In addition, all voltages of the IEEE-34M system are also improved with values above 0.5 p.u., obtaining a minimum value of 0.512 p.u. at node 830 and a maximum value of 0.778 p.u. at node 802. From these results, the C_{DC} value is 87.3 μF and the injected reactive power of DSTATCOM is 1285 kVAR.

Table 3. Voltage comparison at node 842 for case 2

DSTATCOM Condition	Phase A [p.u]	Phase B [p.u]	Phase C [p.u]
Without DSTATCOM	0.147	0.155	0.998
With DSTATCOM	0.472	0.558	0.999

Source: Authors

Conclusions

In this paper, it was observed that the presence of the DSTATCOM improve the voltage profiles not only in the affected node but also in all voltages of the distribution system. For the cases studies, it was observed that the presence of compensator has a positive effect on the system, contributes to reduce the voltage sags impact and regulates the voltage profiles in all system.

Simulation results show that the DSTATCOM should be installed directly at the bus affected by voltage sag. However, due to the depth of voltage sag conditions analyzed, which were the worst cases in all IEEE-34M test system (average sag of 0.2 p.u.), it is not possible compensate completely the voltage sag.

In addition, a true-48-pulse DSTATCOM model is presented and applied it to the study of power quality problems. The developed features and the graphic advantages available in ATP/EMTP were used to conduct all aspects of the DSTATCOM implementation, the IEEE-34M system modeling and to carry out extensive simulation results.

References

Bollen, M. (1999). *Understanding Power Quality Problems: Voltage Sags and Interruptions* (1st Ed). New York: Wiley-IEEE Press.

Hsu, C. ., & Wu, H. . (1996). A new single-phase active power filter with reduced energy-storage capacity, *143*(I), 1–6.

IEEE Distribution System Analysis Subcommittee. (2000). *IEEE 34 Node Test Feeder*.

Kumar, C., & Mishra, M. K. (2014). A voltage-controlled DSTATCOM for power-quality improvement. *IEEE Transactions on Power Delivery*, *29*(3), 1499–1507.

Lakka, M., Koutroulis, E., & Dollas, A. (2014). Development of an FPGA-based SPWM generator for high switching frequency DC/AC inverters. *IEEE Transactions on Power Electronics*, *29*(1), 356–365.

Masdi, H., & Mariun, N. (2009). Construction of a Prototype D-Statcom for Voltage Sag Mitigation. *European Journal of Scientific Research*, *30*(1), 112–127.

Masdi, H., Mariun, N., Mahmud, S., Mohamed, A., & Yusuf, S. (2004). Design of a prototype D-STATCOM for voltage sag mitigation. In *Power and Energy Conference, 2004. PECon 2004. Proceedings. National* (pp. 61–66).

McGranaghan, M., Mueller, D., & Samotyj, M. (1991). Voltage sags in industrial systems. In *Conference Record Industrial and Commercial Power Systems Technical Conference 1991* (Vol. 29, pp. 397–403).

Muni, B., Rao, S., & Vithal, J. (2006). SVPWM Switched DSTATCOM for Power Factor and Voltage Sag Compensation. In *2006 International Conference on Power Electronics, Drives and Energy Systems, PEDES '06* (pp. 1–6). New Delhi, India.

Rojas, H. E., Cruz, A. S., & Rojas, H. D. (2015). Analysis of voltage sag compensation in distribution systems using a multilevel DSTATCOM in ATP/EMTP. *DYNA*, *82*(192), 26–36.

Sensitivity analysis of fault locators in power distribution systems considering distributed generation

Analisis de sensibilidad de localizadores de fallas para sistemas de dsitribución considerando generación distribuida

N. Alzate-González[1], S. Pérez-Londoño[2] , J. Mora-Flórez [3]

ABSTRACT

This paper presents the methodology to perform the sensitivity analysis for impedance-based fault location methods, considering power distribution systems and the presence of distributed generation. The proposed methodology helps to determine the power distribution system model parameters, which significantly affect the fault locator performance. Having identified such parameters, the next step is to perform improvement strategies and compensations of the fault locators aimed to develop more robust locating tools. As result of the proposed methodology, a set of critical parameters of the power system model is here identified.

Keywords: Sensitivity analysis, fault location, power systems, distributed generation.

RESUMEN

En este artículo se presenta una metodología para realizar el análisis de sensibilidad para métodos de localización de fallas basados en la estimación de la impedancia, considerando sistemas de distribución de energía eléctrica con presencia de generación distribuida. La metodología propuesta permite determinar los parámetros del modelo del sistema de distribución de energía eléctrica, que afectan significativamente el desempeño del localizador. Luego de determinar estos parámetros, el siguiente paso consiste en desarrollar estrategias de mejoramiento y compensación de los localizadores de fallas para herramientas más robustos. Como resultado de la metodología propuesta, un conjunto de parámetros críticos del sistema de potencia son identificados

Palabras clave: Análisis de sensibilidad, localización de fallas, sistemas de potencia, generación distribuida.

Received: July 24th 2015
Accepted: September 15th 2015

Introduction

Quality power electrical is an important aspect in power system operation, due the requirements normally associated to the continuity indexes. One of the current applied strategies aimed to maintain the continuity indexes, are associated to fault location [Salim, et al., 2011] [Zhu, et al., 1997]. By an opportune fault location, actions as maintenance, restoration and reconfiguration of the affected power system are significantly improved.

In the case of power distribution systems, the fault location methods are normally classified in impedance-based and knowledge-based methods [Aggarwal, et al., 1997] [Das, 1998] [Mora, et al., 2008]. This research focuses on the impedance-based applied to power distribution systems with distributed generation. These methods are used to determine the distance from the substation to the faulted node using the measurements of voltage and current at the generation sources. As these methods use the power system model parameters, are highly dependent on errors normally presented in real systems due the uncertainty associated to define the values of load, conductor resistance and system capacitance and impedance at the fault time instant.

The validation of fault location methods has been performed using different methodologies. Initially, the methods consist on a simulation of several scenarios that varies the fault location and the fault resistance, however aspects associates to the power system parameters were not considered [Das, 1998]. Several approaches perform the same evaluation of the fault locator as previously presented [Salim, et al., 2011] [Zhu, et al., 1997] [Aggarwal, et al., 1997].

One of the alternatives to consider these parameters is the development of an extensive simulation tool to create a fault database in a power system by considering variations on load size, and values of fault resistance, fault location, conductor resistance, system admittance and capacitance, line arrangement, among others [Mora, et al., 2006].

[1] N. Alzate-González, Electrical engineer Universidad Tecnologica de Pereira, Colombia. Affiliation: Researcher at ICE3, Universidad Tecnológica de Pereira, Colombia. E-mail: naalzate@utp.edu.co.
[2] S. Pérez-Londoño: Electrical engineer, M.Sc. Universidad Tecnologica de Pereira, Colombia. Ph.D., Universidad Nacional de Colombia. Affiliation: Associated professor at Universidad Tecnológica de Pereira, Pereira, Colombia. E-mail: saperez@utp.edu.co.
[3] J. Mora-Florez: Electrical engineer, M.Sc Universidad Industrial de Santander, Bucaramanga, Colombia. Ph.D., Universitat de Girona, España. Affiliation: Associated professor at Universidad Tecnológica de Pereira, Pereira, Colombia. E-mail: jjmora@utp.edu.co

By using the extensive data simulation, a methodology to perform a sensitivity analysis for impedance based fault location methods applied to radial and also non-radial power distribution systems, under of hundreds of different operating conditions, is here proposed. The non-radial power systems are those which consider the presence of distributed generation.

The sensitivity analysis determines which of the modelling parameters that most affect the performance of the locator. These have to be deeply analysed to determine the best way to improve the locator. This strategy allows developing more robust fault location methods.

Finally, as contents, this paper is divided into the following sections; section two presents the theoretical aspects; section three presents the proposed sensitivity analysis methodology; section four is devoted to show the obtained results and finally, at the last section the main conclusions of this research are highlighted.

Theoretical Background

This section is devoted to present the basic aspects of the theoretical foundation, used to develop the sensitivity analysis methodology here proposed. A deep analysis or explanation are out of the scope of this paper, but can be obtained at the provided references.

A. Sensitivity analysis

The sensitivity analysis helps to determine the input parameters that most influence the output variability, by the evaluation of different scenarios that may occur in the daily operation of the power distribution system. This analysis is performed to represent real-life circumstances such as erroneous measurements, lack of information or uncertainty of some modelling parameters.

Sensitivity analysis determines:

a. If a model represent adequately the system under study. If the sensitivity analysis shows a strong dependence on parameters that supposedly are not important, then a revision of the model must be done.

b. The factors that mostly contribute to the output variability and that require additional research. Sensitivity analysis allows to strengthen the model under study, minimizing the impact of erroneous measurements.

c. The model parameters that are insignificant and can be removed of the used model, which reduces the complexity of the model.

d. If a parameter group interacts with others. Often important effects occur when two parameters vary simultaneously, this is important because these effects cannot be seen if the parameters are analyzed individually.

Sensitivity analysis has three main stages: the definition of the sampling technique, the model evaluation, and performing of technical sensitivity. These steps allow identifying the variables that most affect the fault location methods [Saltelli & Chan, 2000].

B. Latin Hypercube sampling

The defined sampling technique is the Latin hypercube. This technique generates a small set of data that completely represents the total data search space, reducing the computational cost. The most important characteristic of this sampling technique is related to the not dependence of the model being analysed [Viana & Venter, 2009].

The input data of the sampling technique consist of a number of variables *s* to be changed and *n* is the number of points to be evaluated. This technique generates an *n* by *s* matrix with values between 0 and 1, where each row represents a point to be evaluated and the columns represent the coordinates of that point [Liefvendahl & Stocki, 2005] [Glover & Kochenberger, 2002].

C. Tabu search

Tabu is a metaheuristic used here to improve the sampling process performed by Latin hypercube. This technique uses the concept of adaptive memory, so the movements are defined as "Tabu movements" to avoid the returning movements into areas that had already been visited, allowing it to escape from local optima [Glover & Kochenberger, 2002].

D. Regression analysis

Regression analysis is a statistical process which is used to determine the input variables that most affect the outputs. Through this analysis, the set of numbers called Beta coefficients are obtained. As high is the Beta coefficient, most important is the associated parameter (input) on the behaviour of the fault locator (output). The Beta coefficients are calculated using (1), where the absolute value of this coefficient indicates the importance of the variable [Saltelli & Chan, 2000].

$$\beta_j = \frac{b_j \, Sx_j}{Sy} \tag{1}$$

To calculate the variables in (1), the Equations (2), (3) and (4) are required. Where, *x* is the uncertainty matrix obtained from Latin hypercube, *y* is the vector of results and *n* is the number of evaluated points.

$$b_j = (x^T \, x)^{-1} \, x^T \, y \tag{2}$$

$$Sx_j = \sqrt{\sum_{k=1}^{n} \frac{\left(x_{kj} - \bar{x_j}\right)^2}{n-1}} \tag{3}$$

$$Sy = \sqrt{\sum_{k=1}^{n} \frac{(y_k - \bar{y})^2}{n-1}} \tag{4}$$

Methodology

The general scheme of the proposed methodology used in sensitivity analysis of impedance-based fault locator for power distribution systems considering distributed generation, is shown in Figure 1.

Sensitivity analysis is performed by a cooperative strategy between ATP and MATLAB. ATP is used as modelling and simulation software and MATLAB is used as software for handling the information.

A. Sampling using Latin Hypercube

The first step of the proposed methodology consists in sampling the total space using Latin hypercube. This technique has as input data, the variables *n* and *s*. In the specific case of the sensitivity analysis, *n* represents the number of operating states in which the power system is analysed and *s* represents the considered power system modelling parameters. The parameters considered in this paper are the magnitude and unbalance of the voltage at the generation sources, the magnitude of the load, the power factor, the line length and the system frequency. Each parameter is varied within a certain range to represent changes or different operational states of a real distribution system.

Latin hypercube generates an uncertainty matrix, *n* by *s*, where each row indicates an operating state of system and each column indicates the percentage change of each parameter.

To complement this sampling technique is used a Tabu, as previously described, to maximize the distance between samples and then ensure the uniform distribution of the sampled space.

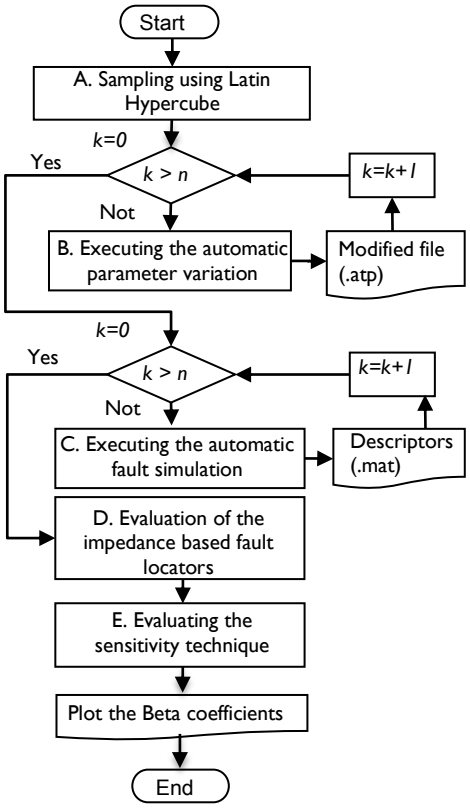

Fig. 1. Sensitivity analysis methodology. "Own compilation".

B. Executing the automatic parameter variation

Having defined the operating conditions, the automatic parameter variation is performed, by using the base ATP card that describes the nominal power system and the uncertainty matrix [Viana & Venter, 2009]. As result of this step, *n* modified ATP cards are obtained and each card represents a case that may occur in the daily operation of the distribution power system.

C. Executing the automatic fault simulation

The modified cards are the input to the automatic fault simulation tool. Each card or power system operating condition is simulated considering faults at different fault location and also different fault resistances, to obtain the values of voltage and current, during the pre-fault and fault steady states at the generation sources [Mora, et al., 2006].

D. Evaluation of the impedance based fault locators

Subsequently, the fault database of measurements of voltage and current is used to perform an extensive evaluation of the impedance based fault location method, which considers the presence of distributed generation. After evaluating the method, the error of locator is obtained by comparing the real distance of the fault and the distance obtained by the impedance based fault locator [Mora, et al., 2008].

E. Evaluating the sensitivity technique

Finally, the proposed methodology generates the Beta coefficients through the regression analysis technique. This statistical process uses the uncertainty matrix and the errors obtained by the impedance based fault locator, to calculate Beta coefficients. Each coefficient indicates the importance of the modelling parameters on the fault locator. The coefficients are presented using graphs for an easy analysis.

Test power systems and result analysis

The methodology above presented is applied to a modification of the IEEE 34-node system with distributed generation, which is obtained from the "Distribution System Analysis Subcommittee" of the "Institute of Electrical and Electronics Engineers" [IEEE distribution system]. The power system was simulated in ATP and as is shown in Figure 2 and contains a distributed source at the end of the analysed feeder. The sensitivity analysis tool is validated using one extension to consider three phase faults of the impedance-based method presented in [Orozco, et al., 2012]. Faults were located at the longest radial feeder, which is indicated in figure 2 by the dashed lines. The tests were performed considering fault resistances of 0 Ω to 40 Ω [Dagenhart, 2000].

Sensitivity analysis is performed for 200 operating conditions and varying the six parameters in the range shown in Table 1. Considering the operator experience and national normative, the range variation was defined.

Table 1: Uncertainty ranges of the parameters. "Own compilation".

Modelling parameters	Variation range	
	Minimum	Maximum
Voltage source magnitude	0.95 p.u	1.10 p.u
Voltage source unbalance	-3.4 °	3.4°
Magnitude system load	10%	150%
Power factor	-0.02	0.02
Line length	95%	105%
Frequency	59.8 Hz	60.2 Hz

Additionally, the sensitivity analysis tool, whose simplified interface is presented in figure 3, has spaces to include the working folder, the ATP card of the analysed power system and the number of operating states to be analysed, among others. In addition, the parameters to be modified and their respective ranges are also defined.

The results of the sensitivity analysis are shown on a graph, where the vertical axis represents the value of the Beta coefficients and the horizontal axis represents the nodes where faults are analysed.

A total of 32000 single-phase faults and three-phase faults were used to perform the sensitivity analysis.

A. Single-phase faults

In figure 4, the results of the average Beta coefficients for single faults are presented. The result shows how the magnitude of the load is one of the parameters that most affects the fault locator. As a consequence, a good estimation strategy of the load magnitude has to be developed as a first strategy aimed to improve the fault locator performance.

An additional parameter analysed is the line length. This parameter has a major influence in the most distant nodes from the main power substation, because the modelled admittance and impedance parameters are not accurate, therefore the resulting error is accumulated along the radial. The real systems sometimes have additional measures to the main power substation. These measures can be used to decrease the error.

The frequency is the other parameter that has a significant influence. This parameter is varied to represent measurement errors that appear in the databases of the utilities. In this case, the results show a random behaviour.

Finally, the figure shows that the unbalance of the phases of the generation sources and the load power factor are the parameters that have the lowest affect in the fault locator performance.

B. Three-phase faults

An additional result is presented in figure 5, in the case of three phase faults at the same distribution feeder.

As it is presented, the results are similar to those obtained in the case of single-phase faults. The load is the most influential parameter of the performance of the analysed fault location method. As in the previous case, variations in the power frequency and the line length are also parameters which affect the fault locator.

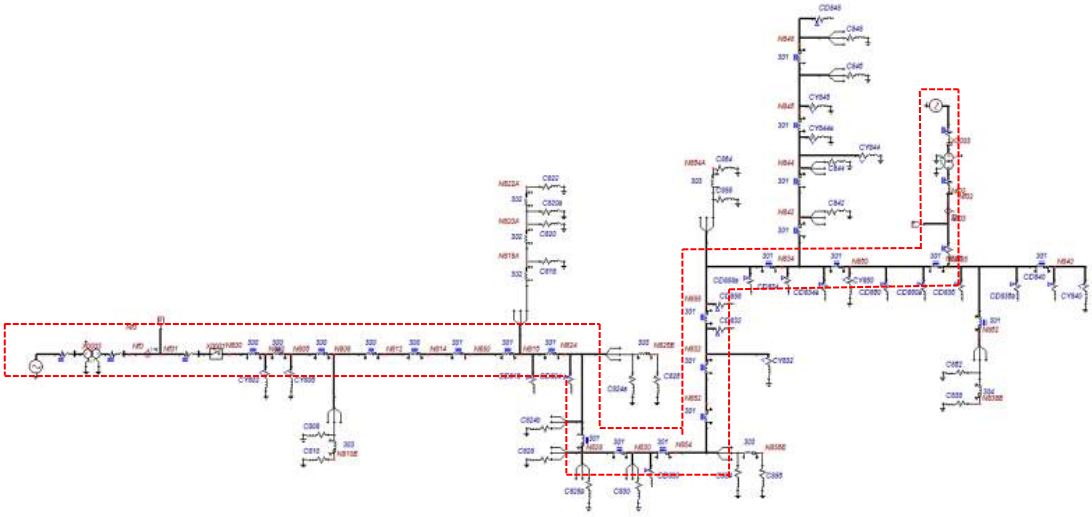

Fig. 2. IEEE 34-node power distribution system. “Own compilation”.

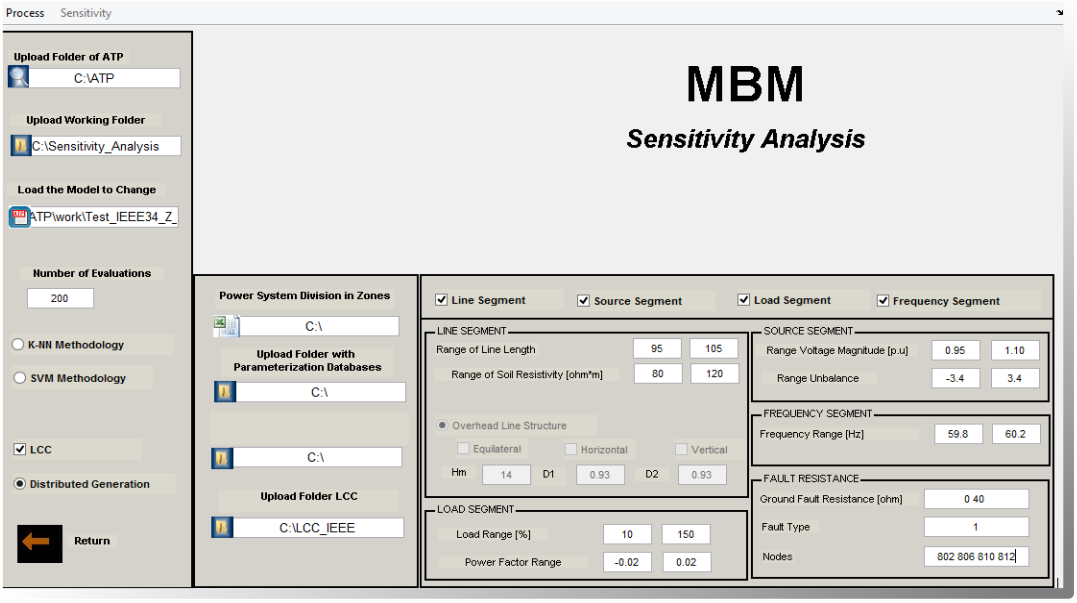

Fig. 3. Main working interface of the sensitivity analysis tool. “Own compilation”.

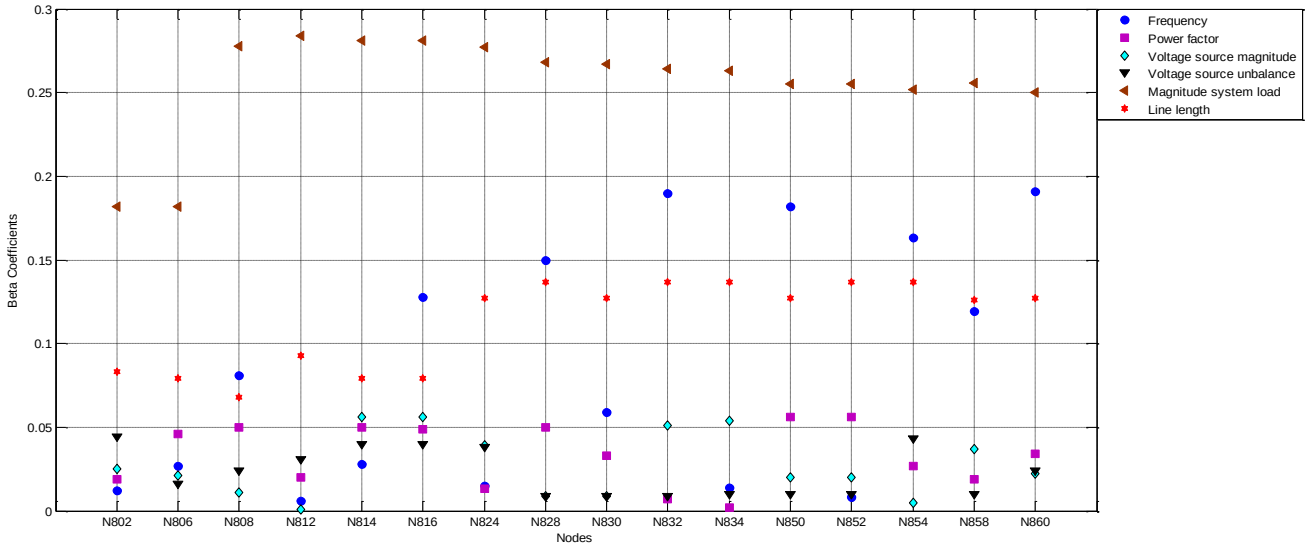

Fig. 4. Results of the sensitivity analysis for single phase fault (A-g). "Own compilation".

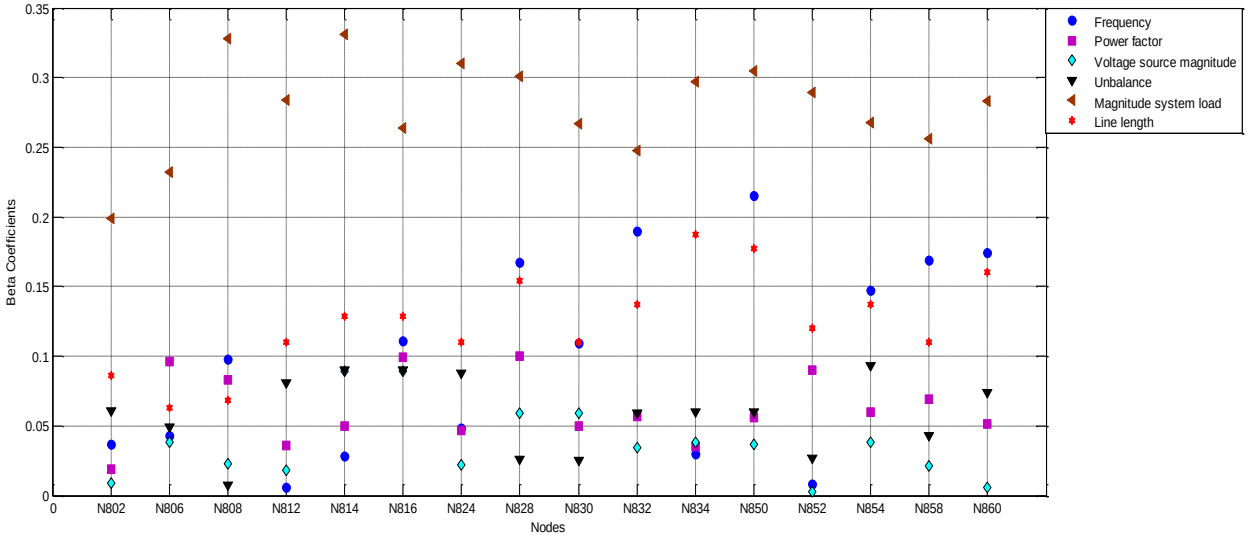

Fig. 5. Results of the sensitivity analysis for three phase faults (A-B-C-g). "Own compilation".

Conclusions

The sensitivity analysis methodology helps to identify such modelling parameters of the power distribution system, which have a significant effect on the fault locator performance. According to the obtained results for a single-phase and three phase faults, considering fault resistances form 0 and 40 Ω, the most influential parameter is the load size. Parameters as the line length and frequency also influence the fault locator performance. Then, the next step in the improving process aimed to obtain a really robust fault locator, is to develop strategies for the adequate estimation of the load size at any time, and also adequately verify the line length along the analysed feeder.

As it was demonstrated, the proposed sensitivity analysis methodology is really helpful in the fault locator improving process, by the identification of those influential parameters.

Finally, robust fault locators allow fast restoration of the power system, ensuring high levels of the power supply continuity indexes.

Acknowledgments

This research was supported by the Universidad Tecnológica de Pereira (Colombia) and COLCIENCIAS, under the project "Desarrollo de localizadores robustos de fallas paralelas de baja impedancia para sistemas de distribución de energía eléctrica LOFADIS 2012", contract number 0977-2012; and the Master program in Electrical Engineering of Universidad Tecnológica de Pereira (Colombia).

References

Aggarwal, R., Aslan, Y., Johns, A.T., An interactive approach to fault location on overhead distribution lines with load taps., IEEE Development in Power System Protection Conference, No. 434, 1997.

Dagenhart, J., The 40-Ω ground-fault phenomenon., Industry Applications, IEEE Transactions, Vol. 36, No. 1, February 2000, pp. 30-32.

Das, R., Determining the locations of faults in distribution systems., Doctoral Thesis, University of Saskatchewan, Canada, 1998.

Glover, F., Kochenberger, G., Handbook of Metaheuristics., Kluwer Academic Publishers, United States, 2002.

IEEE Distribution System Analysis Subcommittee, Radial Test Feeders., 2000.

Liefvendahl, M., Stocki, R., A study on algorithms for optimization of Latin hypercubes., Journal of Statistical Planning and Inference, 2005, pp. 3231-3247.

Mora-Florez, J., Melendez, J., Carrillo, G., Comparison of impedance based fault location methods for power distribution systems., Electric Power Systems Research, Vol. 78, Issue 4, April 2008, pp. 657–666.

Mora-Florez, J., Melendez, J., Bedoya, J., Extensive Events Database Development using ATP and Matlab to Fault Location in Power distribution Systems., IEEE PES Transmission and Distribution Conference and Exposition: Latin America, Caracas, 2006.

Orozco-Henao, C., Mora-Florez, J., Perez-Londono, S., A robust method for single phase fault location considering distributed generation and current compensation., Transmission and Distribution: Latin America Conference and Exposition (T&D-LA), 2012.

Salim, R.H., Salim, K.C., Bretas, A.S., Further improvements on impedance-based fault location for power distribution systems., IET Generation, Transmission and Distribution, Vol. 5, 2011, pp. 467–478.

Saltelli, A., Chan, K., Sensitivity Analysis., John Wiley & Sons Ltd, United Kingdom, 2000, pp. 101-152.

Viana, F., Venter, G., An algorithm for fast optimal Latin hypercube design of experiments., International journal for numerical methods in engineering, United States, 2009.

Zhu, J., Lubkeman, D., Girgis, A., Automated fault location and diagnosis on electric power distribution feeders., IEEE Transactions on Power Delivery, Vol. 12, April 1997.

Sustainable Practice in Lighting: Remanufacturing of Compact Fluorescent Lamps

Práctica Sustentable en Iluminación: Remanufactura de Lámparas de Bajo Consumo

José L. Frund[1], Diego M. N. Balducci[2], Agustín Chort[3], Carlos E. Freyre[4], Fabio M. Vincitorio[5]

ABSTRACT

Today the established paradigm in energy efficiency seems to have been symbolized by the so-called energy-saving lamps. However it is not possible to find scientific or technical publications which strongly support their use. On the contrary, it is not simple to find publications that refer to the problems that could be generated by their use.

These devices consist of two fundamental technological cores: the lamp and electronic ballast. Both have a high degree of incidence in the origin of discarding, when the user believes that the lamp has stopped working. However, a failure in the ballast may cause the discarding of an operating lamp.

In this paper, the results of faults survey that entail premature discard are shown and some practices for the remanufacturing of defective ballasts are proposed.

As a result it is concluded that up to 40% of discarded lamps can be repaired prolonging their useful life over a period of between six months and two years. In a country like Argentina, this would imply a reduction of up to 600kg of mercury per year in the dump to the environment.

Keywords: Energy-saving lamps, remanufacturing, sustainable practices, protocol.

RESUMEN

En la actualidad el paradigma establecido en eficiencia energética parece haber sido simbolizado con las llamadas lámparas de bajo consumo. Sin embargo no es posible encontrar publicaciones científicas o técnicas que avalen fuertemente su utilización. Por el contrario tampoco es simple encontrar publicaciones que hagan referencia sobre los problemas que podrían generarse por su uso.

Estos dispositivos están compuestos por dos núcleos tecnológicos fundamentales: la lámpara y el balasto electrónico. Ambos presentan un alto grado de incidencia en el origen del descarte, cuando el usuario considera que la lámpara ha dejado de funcionar. Sin embargo, un fallo en el balasto puede originar el descarte de una lámpara operativa.

En este trabajo se muestran los resultados obtenidos del relevamiento de las fallas que dan origen al descarte prematuro y se proponen prácticas para la remanufactura de los balastos defectuosos.

Como resultado se concluye que hasta un 40% de las lámparas descartadas pueden ser reparadas prologando su vida útil en un período de entre 6 meses y dos años. En un país como Argentina, esto implicaría una reducción en el volcado al medio ambiente de hasta 600kg de mercurio al año.

Palabras clave: Lámparas de bajo consumo, remanufactura, práctica sustentable, protocolo.

Received: July 21th 2015
Accepted: Oct 15th 2015

Introduction

Since the last two decades, globally speaking, there have been discussions about energy efficiency as a sustainable practice and fundamental pillar of ecology. Consumers are looking to maximize the use of energy consumed, whether to reduce costs or put into sustainable practices that will help improve the environment.

Since 2007, Argentina has a National Program for the Rational and Efficient Use of Energy (PRONUREE) [1] in which the rational and efficient use of energy has been declared as national priority interest. Among the actions implemented, a replacement

[1] José Luis Frund: Electronic Engineer, Universidad Tecnológica Nacional - Facultad Regional Paraná, Argentina. E-mail: fisicaelectronica@frp.utn.edu.ar

[2] Diego M. N. Balducci: Electromechanical Engineer, Universidad Tecnológica Nacional - Facultad Regional Paraná, Argentina. E-mail: fisicaelectronica@frp.utn.edu.ar

[3] Agustín Chort: Electronic Engineer, Universidad Tecnológica Nacional - Facultad Regional Paraná, Argentina. E-mail: fisicaelectronica@frp.utn.edu.ar

[4] Carlos E. Freyre: Electrical Engineer, Universidad Tecnológica Nacional - Facultad Regional Paraná, Argentina. E-mail: fisicaelectronica@frp.utn.edu.ar

[5] Fabio M. Vincitorio: Electronic Engineer, Universidad Tecnológica Nacional - Facultad Regional Paraná, Argentina. PhD in Industrial Engineering, Universidad de la Coruña, España. E-mail: fisicaelectronica@frp.utn.edu.ar

of incandescent lamps with compact fluorescent lamps, or CFLs was organized. Under the program, the government replaced more than 29.5 million incandescent bulbs with CFLs, in more than 8.2 million Argentine households [2].

Figure 1. CFL functional parts. On the left, the electronic ballast and on the right the compact fluorescent lamp. (Lux America 2010).

A CFL can be divided into two functional parts: the compact fluorescent lamp and the electronic ballast or auxiliary equipment (Figure 1). The compact fluorescent lamp is a miniature version of the traditional fluorescent tubes. In its composition, there is mercury in an estimated 5 to 2.5 mg [3] concentration. The auxiliary equipment is an electronic circuit, mostly based on an uncontrolled rectifier and an autoresonant inverter[4].

Since the LFC is a unique lamp-ballast, the failure of one of the two parts causes that the user must replace it with a new one. From this we can say that the expected discard of a CFL is when the fluorescent tube is dead, while the ballast is still functional, and a premature discard is when the equipment is discarded but the fluorescent tube is still functional. [4].

From previous investigations [5], it was found that between 57% and 69% of the CFLs are discarded prematurely. Considering only the lamps delivered by PRONUREE, there have been discarded between 16.8 and 20.3 million of CFLs. This represents between 84 and 102 kg of mercury dumped into the environment unnecessarily.

Methodology

Electronic ballast topology

The electronic ballast can be separated into two distinct parts: a autoresonant series inverter and an uncontrolled rectifier.

Figure 2 shows the autoresonant inverter circuit that is used in the great majority of CFLs.

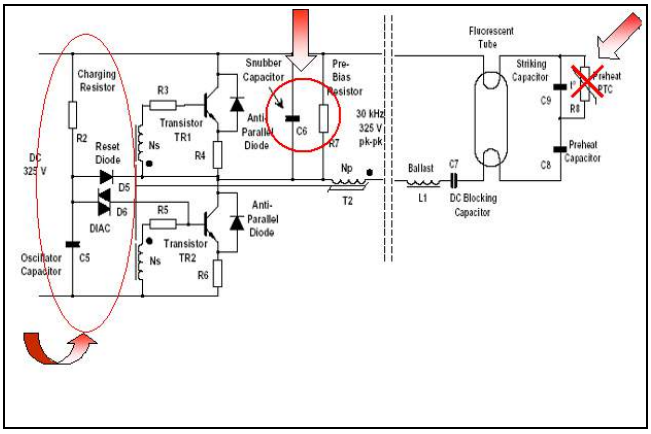

Figure 2. Complete topology of an electronic ballast for fluorescent lamps (Lux América 2010).

It can be seen that the compact fluorescent lamp is part of the series resonant circuit, connected by their filaments. In many cases, in order to cut costs, companies sacrifice the installation of some components (indicated by an arrow). Even though these are not essential in the LFC, they are necessary to improve its functionality and stability.

Figure 3 shows the uncontrolled rectifier which is responsible for passing the current to the previous circuit.

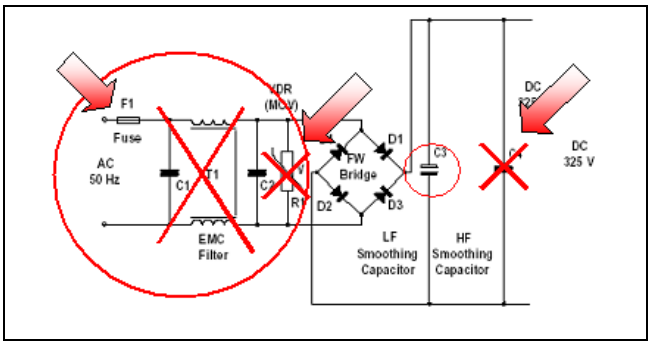

Figure 3. Entrance circuit for an electronic ballast without correction in the power factor (Lux America 2010).

Also, as in the investor, most manufacturers do not install the components indicated. But in this case, not installing one of these components does not affect the quality and stability of the lamp itself, but it generates electromagnetic pollution which affects other devices installed in the same power grid [6].

Typical faults detected.

From previous work [7], a variety of faults that generate premature discard of the lamps were detected. These are detailed in Table I.

Table I. Faults that generate premature discard and the percentage of incidence on discarded lamps.

Cut filament	**20%**
Transistor	**14%**
Electrolytic capacitor	**13%**
High temperature	**8%**
Humidity	**5%**

Welding	**4%**
Insects	**1%**
Faultless	**5%**

It should be noted that the last item (faultless) were lamps discarded by users that were still operational. This may be due to poor contact in the E27.

Looking at these data, 51% of faults correspond to cut filament, transistor, electrolytic capacitor and welding. Temperature failures often lead to failures in transistors, welding problems, among others, but if the lamp is repaired the fault will continue to exist.

Respect to relieved faults they can be projected to different countries given similar conditions on the quality of electrical service. In countries where electrical distribution systems are continuously audited it is expected a lower number of global failures. However, lamps purchased from other countries show as electronic ballast topology with the same construction deficiencies in regard to the safety elements indicated in Figure 3.

Security conditions and instruments for evaluating CFLs.

To evaluate and test energy-saving lamps, we must apply the voltage across its terminals respective supply (in Argentina this corresponds to 220 VAC). In order to do this, the use of isolation transformers is not advisable because if the operator accidentally touched two power cables, there would be no rescue device to help him. Instead, using a test box is recommended. The test box consists of a differential switch, a bipolar switch, E27 socket and a light indicator that shows when there is tension in the E27. In Figure 4, the diagram is described in detail.

In order to develop a correct detection and evaluation of CFLs, the following elements are recommended:

- Voltmeters and ampere meters for AC and DC.
- Meter diodes and transistors.
- Capacity meter.
- Ohmmeter.
- various test resistance: small values are used (from 1 to 100 ohms).
- Several compact fluorescent tubes of various powers
- Ballasts Several test of various powers.
- Transistors and electrolytic capacitors used in CFLs.

All measuring instruments can be replaced by a single tester.

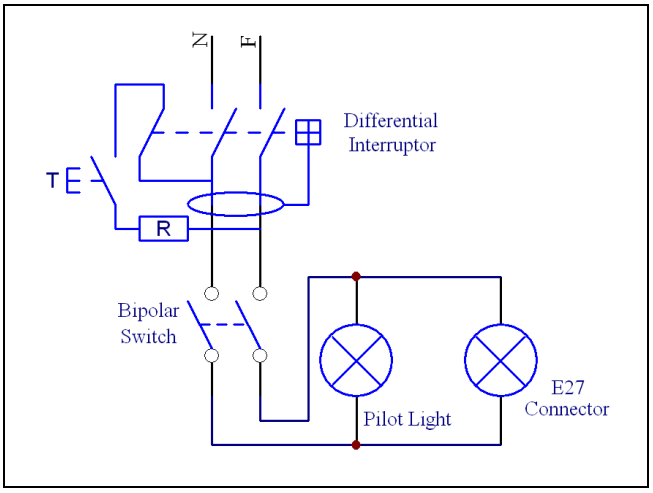

Figure 4. Electric Schema of evaluation and test for E27 equipment.

Protocol for fault detection and CFL evaluation oriented at premature discard detection and repair ballast.

The following evaluation protocol seeks to separate the problems of the lamp and the ballast.

Lamps with broken glass are separated from the ones with non-broken class. An evaluation of the proper functioning of the ballast only will be made to the former.

Lamps with non-broken glasses are connected to the test box and energized. If they turn on, they will have a simple cycling test done (they are turned on for15 minutes which is the time it takes for the light to enter steady state). If, after this, the lamp is stable (i.e. it does not turn off and turn on or it generates a blink), then it is left for final evaluation. If the lamp has an abnormality in its illumination, it is considered that the tube is dead. In this case, the ballast is recovered for later evaluation.

If the lamp does not turn on, then it is disassembled and the filaments are measured. If one of them is cut, then a resistor is connected in parallel with it to close the circuit autoresonant and try again. If this turn on, then it will have the cycling test done. If, after this, the lamp is stable, then it is left for final evaluation. If the lamp has an abnormality, then the filament was cut due to exhaustion. In this case, the lamp is discarded and the ballast is stored for later evaluation.

If the filaments are well, then the lamp is disassembled and evaluated with test ballast. If the lamp turns on, it will have the cycling test done. If, after this, the lamp is stable, measurements of voltage and current are performed. If they are within the acceptable parameters for the specified power, working ballast is installed and it is left for final evaluation. The original ballast is passed to the instance of evaluation.

Before starting the evaluation of ballast, it must be observed that there is no cold welding. If there, another evaluation is needed to see if the fault can be solved. If some fused track or input fuse (if the lamp has it) is observed to be open, then it must be verified that the transistors and electrolytic capacitor are not causing a short circuit.

To evaluate the correct functioning, a test lamp with the corresponding power is connected and the cycling test is performed. If after this period there are no abnormalities in the lamp and the

temperature is normal, then the ballast is labeled as useful and stored for reuse.

If the lamp does not turn on, then the correct operation of the transistors has to be measured. If these are in short circuit and open, then they must be replaced and retested as a whole. If it doesn't turn on, the ballast is discarded.

If the transistors are well, then the value of the electrolytic capacitor has to be verified. If devalued, it must be replaced and the cycling test remade. If this is accomplished without abnormalities, then the ballast can be reused. Otherwise, the ballast is discarded.

Protocol for final evaluation of repaired lamps.

To consider a lamp to be good, a pilot cycling, and electrical and lighting measurements should be made.

The cycling, suggested a pilot, is turning on the lamp, letting it run for 15 minutes, turning it off and waiting for it to cool. This process should be repeated at least 5 times. Then, if there are no anomalies in cycling, power consumption measurements of the LFC and light intensity are performed. If these values are within the acceptable, the lamp can be considered to be good. Otherwise, it must return to the evaluation instance.

Discussion

Although there is a possibility of remanufacturing CFLs, it still remains difficult to carry out because each trade mark has different models of cabinets that are incompatible with each other. In the particular case of PRONUREE program, they have been used three different suppliers have been used but with the same lamp power. So this decision could facilitate the remanufacturing.

In addition, when the lamp is disassembled their cabinets are damaged because most of them are stuck and they have to be broken to separate the ballast from the lamp. A proposal for improvement would be to separate the fluorescent lamp from the electronic ballast, through a connector. This would help the final user to reuse the electronic ballast when the tube is dead.

Conclusions

CFLs are efficient lighting equipment, regarding the incandescent lamps, but these have failures because, in their manufacture, obsolete settings are used [8].

Current lighting technology is orienting to the use of LEDs. With this increased reliability and stability of the equipment is obtained, but they are still expensive and with similar and even lower levels of efficiency than CFLs [5].

Despite new technologies, CFLs are still used massively and are obligatory in some countries. Thus, the proposal of remanufacturing is presented as a viable alternative for reducing dump pollutants into the atmosphere, such as mercury and lead. Furthermore, remanufacturing involves a reduction in costs and an extension of the useful life of these devices, resulting in a more viable economic equation for those countries that are importers.

All the remanufacturing process presented here, from the evaluation stage of the failure to reinsericón can be applied in different countries in which the economic equation and the environmental impact permit. Largely, these two parameters depend on the number of lamps used annually and specific standar of processing and final disposal of dangerous waste.

References

[1] Secretaría de Energía, PROGRAMA NACIONAL DE USO RACIONAL Y EFICIENTE DE LA ENERGIA, Decreto 140/2007. Ministerio de Planificación, Presidencia de la Nación, 21 de diciembre del 2007, http://infoleg.mecon.gov.ar/infolegInternet/anexos/135000-139999/136078/norma.htm

[2] El Gobierno ya entregó 29,5 millones de lámparas bajo consumo. Télam, sección Economía, Energía, 3 de Marzo de 2014, http://www.jornadaonline.com/Econom%C3%ADa/110051-El-Gobierno-ya-entreg%C3%B3-295-millones-de-l%C3%A1mparas-bajo-consumo

[3] Preocupación por el mercurio de las bombillas de bajo consumo. Terra, Ecología Práctica , 20 de Enero del 2012, http://www.terra.org/categorias/articulos/preocupacion-por-el-mercurio-de-las-bombillas-de-bajo-consumo

[4] Vincitorio, F., Brutti, C., González, A., Ronchi, F., Romano, C., ESTUDIO DE FALLAS EN LÁMPARAS DE BAJO CONSUMO, DETERMINACIÓN DE LA INCIDENCIA DEL DESCARTE PREMATURO. LuxAmérica 2008 – Actas de congreso. Nov., 2008.

[5] Vincitorio, F., Frund, J. L., Balducci, D. N., Rispoli, L. D., Fabre, J. CICLADO DE LFC COMO MÉTODO DE DETERMINACIÓN DE LA CONFIABILIDAD Y EL DESCARTE PREMATURO. XI Congreso Iberoamericano de Iluminación, Lux América 2012, Memorias, Oct. 2012, pp. 256-261.

[6] Frund, J. L., Vincitorio, F., Balducci, D. M. N., Freyre C. E., Chort, A., Favre, J. High Frequencies in AC Distribution Lines: a New Technical Challenge. VII Simposio Internacional sobre la Calidad de la Energía Eléctrica - SICEL 2013, Memorias, Nov. 2013, pp. 1-4.

[7] Vincitorio, F., Brutti, C., Frund, J. L., LA ELECTRÓNICA DE LAS LÁMPARAS DE BAJO CONSUMO VENTAJAS, DESVENTAJAS Y PROBLEMAS. X Congreso Iberoamericano de Iluminación, Lux América 2010, Memorias, Oct. 2010, pp. 365-372.

[8] Grunwaldt G.- "Electronic Ballast" US Patent 3084283. Apr. 1963.

Construction of Three Phase Linear Induction Motor

Construcción de Motor Lineal Trifásico de Inducción

Sebastián Ocampo Gutiérrez[1], Roberto Largo Taborda[2], Nicolás Toro García[3], Fredy E. Hoyos Velasco[4]

ABSTRACT

This paper explores the construction process of a linear induction motor (LIM), the basic concepts behind key aspects of linear induction machines construction and the testing process of a working prototype. Making use of three phase systems, fundamental devices are used to produce a machine governed by means of electromechanical forces, based on varying magnetic fields and energy propagation all generated by three phased systems. The prototype developed is characterized in its mechanical configuration and subsequent tests are performed to address energy usage efficiency in different coil arrangements, varying key parameters which rule the movement generated by it, equivalent circuit analysis are employed. Automation circuits are implemented, rudimentary solving problems of directional movement, enabling the LIM to perform changes in direction.

Keywords: Three Phase Systems, Linear Induction Motor, Electromagnetic Devices, per-phase equivalent circuit.

RESUMEN

Este artículo explora el proceso de construcción de un motor lineal de inducción (LIM), los conceptos básicos tras los aspectos más importantes en la construcción de máquinas de inducción linear, y el proceso de pruebas, diseño y desarrollo de un prototipo funcional de un motor lineal. Haciendo uso de sistemas trifásicos se produce una máquina gobernada por procesos electromecánicos basados en inducción, a partir de los cuales se genera una respuesta mecánica que se traduce en desplazamiento. Se caracteriza mecánicamente el dispositivo desarrollado y se realizan pruebas para verificar fenómenos de uso de energía en diferentes configuraciones posibles de sus componentes, variando parámetros fundamentales que controlan el movimiento generado. Se exploran circuitos equivalente. Sistemas básicos de automatización son usados para permitir el cambio de dirección del motor generando finalmente una plataforma para pruebas de sistemas más complejos directamente relacionados con el análisis de señales y sistemas.

Palabras clave: Sistemas Trifásicos, Motor Lineal de Inducción, Dispositivos Electromagnéticos, Circuito Equivalente por Fase.

[1] Engineering Physics Student, Department of Physics, Universidad Nacional de Colombia, Medellín, Colombia., socampo@unal.edu.co

[2] Engineering Physics Student, Department of Physics, Universidad Nacional de Colombia, Medellín, Colombia. rlargot@unal.edu.co

[3] Ph. D. Engineering Industrial Automation, Department of Electrical, Electronics and Computer Engineering, Grupo de Investigación en Recursos Energéticos (GIRE), Universidad Nacional de Colombia, Manizales, *Bloque Q, Campus La Nubia, Manizales, 170003, Colombia*. ntoroga@unal.edu.co

[4] Ph. D. Engineering Industrial Automation, Scientific and Industrial Instrumentation Research Group, Universidad Nacional de Colombia, Medellín, Calle 59 A N 63-20, Medellín, 050034, Colombia.. fehoyosve@unal.edu.co

Introduction

A motor can be defined as a device that transform electric energy into mechanical energy. A traditional motor usually transform this energy intake into a rotatory movement (it generates torque) even if that is changed afterward into other forms of movement [1].

A linear motor works under the same principles as a rotary motor, given only a different characteristics form its designed conception, making it more task-specific right from its core fundamentals: A LIM is tailored to generate force, generate linear momentum instead of angular momentum [2].

For virtually every rotary electric machine, there is a linear motion counterpart. So is also the case with induction machines, they are called linear induction machines (LIMs), which directly develop an electromagnetic force, called thrust, along the direction of the travelling field motion in the air gap [3].

From a comparison view, a LIM operates as its rotary counterpart does, changing concepts and functions like thrust instead of torque and linear speed instead of angular speed, based on principle of travelling field in the air gap, described by de physics distribution of constitutive elements [3].

Induction motors are widely used as actuators in industrial applications because of the simplicity in construction, lack of maintenance and low cost. Using LIMs for industrial applications which require linear motion suppress the need for gears and other motion conversion mechanisms, hence fast acceleration and deceleration is feasible, they are also capable of working in hostile environments facilitating thrust and speed control. Furthermore, size is diminished, as more common motion mechanisms tends to use a bigger volume for its operation; put pulleys and chain systems in contrast to induction machines.

Even though a LIM presents an interesting dynamics not always considered for designing devices [4].

A comparison to the LIM counterpart is in order to understand the working principle of the devices:

- The main differences between the natures of this devices lies in the rotary nature and linear nature of them. Which is vastly self-explanatory.
- Both work under an induction principle, which can be described as the generation of an electromotive force whenever a conductor in subjected to a varying magnetic field.
- This devices use three phase AC input to generate its varying magnetic field, running through coils.

Linear induction machines are being actively investigated for use in high-speed ground transportation. Other applications including liquid metal pumps, magnetohydrodynamic power generation, conveyors, cranes, baggage handling systems, as well as a variety of consumer applications that have contributed to an upsurge in interest in linear induction machines.

Unfortunately, analysis of a linear induction machine is complicated by the so-called "end effect". In a conventional round-rotor induction motor the behavior of the machine need to be calculated only over one pole pitch. The solution for the remaining pole-pitches can then be simply obtained by symmetry.

However, the symmetry argument cannot be used for a linear induction machine since the electrical conditions change at the entrance and exit, be it the edge borders or mover ends in the LIM [5].

All the differences between linear and rotary IMs suggest the main merits and demerits of LIMs, which are summarized in table [3].

MERITS	DEMERITS
Direct electromagnetic thrust propulsion; no mechanical transmission or wheel adhesion limitation for propulsion	Due to large air gap to pole pitch (g/τ) ratios–g/τ > 1/250 the power factor and efficiency tend to be lower than with rotary IMs.
Ruggedness; very low maintenance costs	The efficiency is to be compared with the combined efficiency of rotary motor + mechanical transmission counterpart
All advanced drive technologies for rotary IMs may be applied without notable changes to LIMs	Efficiency and power factor are further reduced by Longitudinal end effects.
Precision linear positioning (no play (backlash) as with any mechanical transmission)	Additional noise and Vibration due to Uncompensated normal force, unless the latter is put to use to suspend the mover (partially or totally) by adequate close loop control.
Easy topological adaptation to direct linear motion applications	

This work presents and experimental assembly of a three phased LIM with a nominal voltage of $208V_{line\text{-}line.}$ The developed platform work as a basis for further study, applying fundamental concepts in the area of signal analysis and manipulation. First section places a mathematical basis given to further understand the LIM behavior, analyzing the per-phase equivalent circuit, Eddy Currents diagram and Automation Systems developed and implemented.

In the second section a comprehensive prototyping summary is treated, listing the design processes and problems encountered while development.

Linear Induction Motor Modeling.

In a conventional round-rotor induction motor the behavior of the machine is only needed to be calculated over one pole pitch. The solution for the remaining pole-pitches can then be obtained by symmetry.

However, the symmetry argument cannot be used for a linear machine since the electrical conditions change at the entrance and exit.

The imaginary process of cutting and unrolling the rotary machine to obtain the linear induction motor (LIM) is by now classic (Figure 1.1 [3]).

The primary may now be shorter or larger than the secondary. The shorter component will be the moving part, hence the longer will stay stationary. A LIM can either be Single-Sided (Figure 1.1.e) or Double-Sided (Figure 1.1.d)

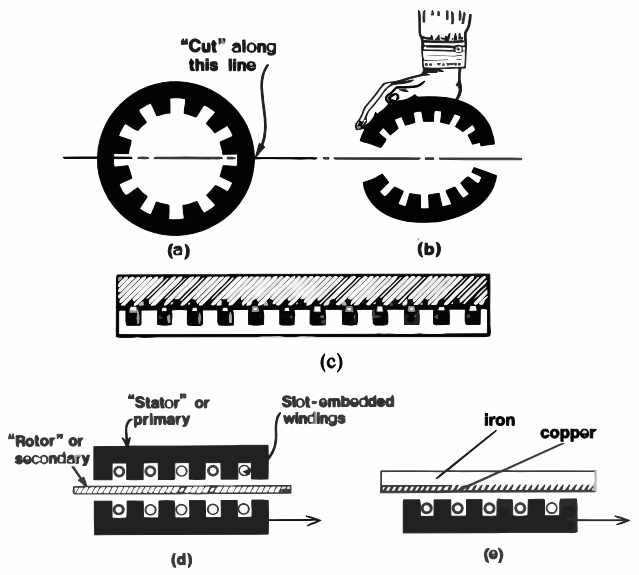

Figure 1.1. Unrolling process from RIM to LIM [3]

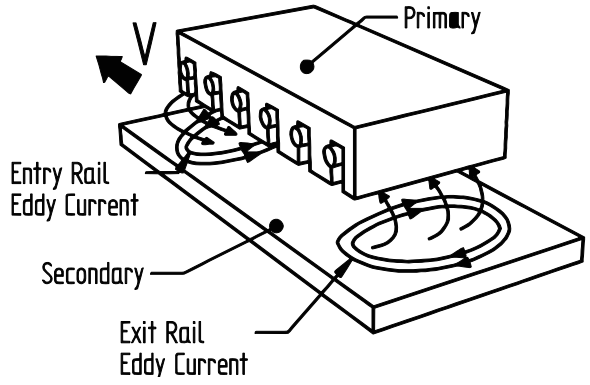

Figure 1.2. Eddy current generation at the entry and exit of the air gap when the primary coil moves with velocity V.

As stated, in a linear machine electrical conditions change at the entrance and exit level [6], as shown in Figure1.2, where eddy currents form along the primary, inducing the static element.

Equivalent Circuit for LIM.

When working with induction machines, it is always a good strategy to take it apart in chunks by mathematical means to develop models that take into account more details in the designing process. As shown in figures 2.1 and 2.2, a basic per-phase circuit can easily be expanded to span the full phases working principle of a LIM, enabling handling of mathematical model in a more compact way.

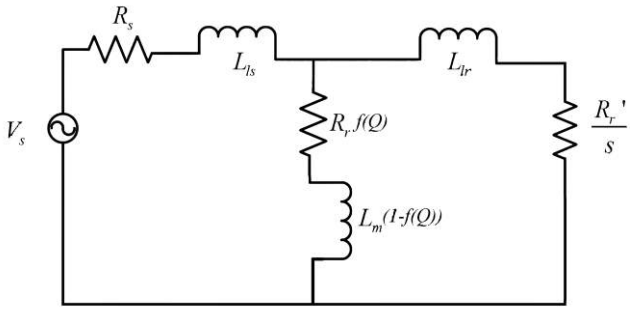

Figure 2.1. per-phase equivalent circuit of a three-phase LIM

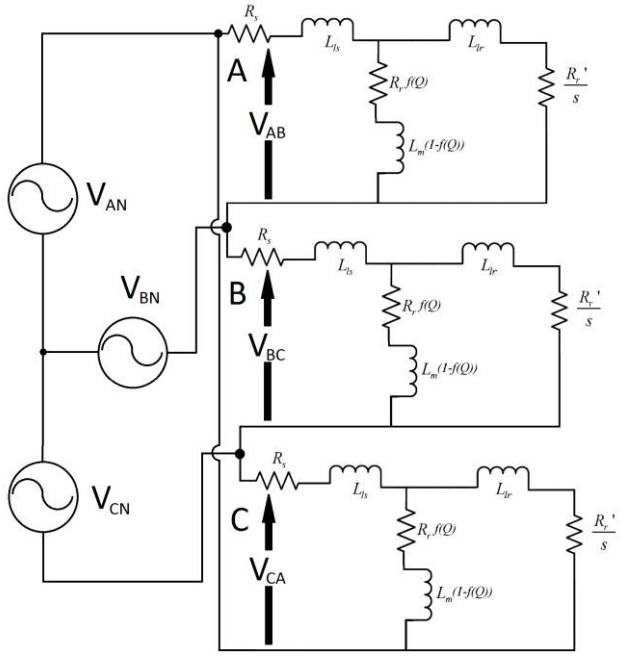

Figure 2.2. LIM three phase equivalent circuit

Automation Control

As a need to ease the behavior of the prototype, and expanding its capabilities, a conveyor belt design was implemented. However, a longitudinal distance displacement in one direction must be automatically and autonomously inverted for longer operating time.

For this purpose, a rather rudimentary, yet effective system was implemented, making use of basic electrical devices, such as relays and contactors.

The control circuit design is presented in figure 2.3 and represents a limit switch control interface, actioned by the LIM itself after completing a full extend travel to either side of the conveyor belt.

Some thought when into unravelling a problem encountered with pushbuttons enabling both contactor during direction change status, solved al shown in the Control Circuit diagram on figure 2.1

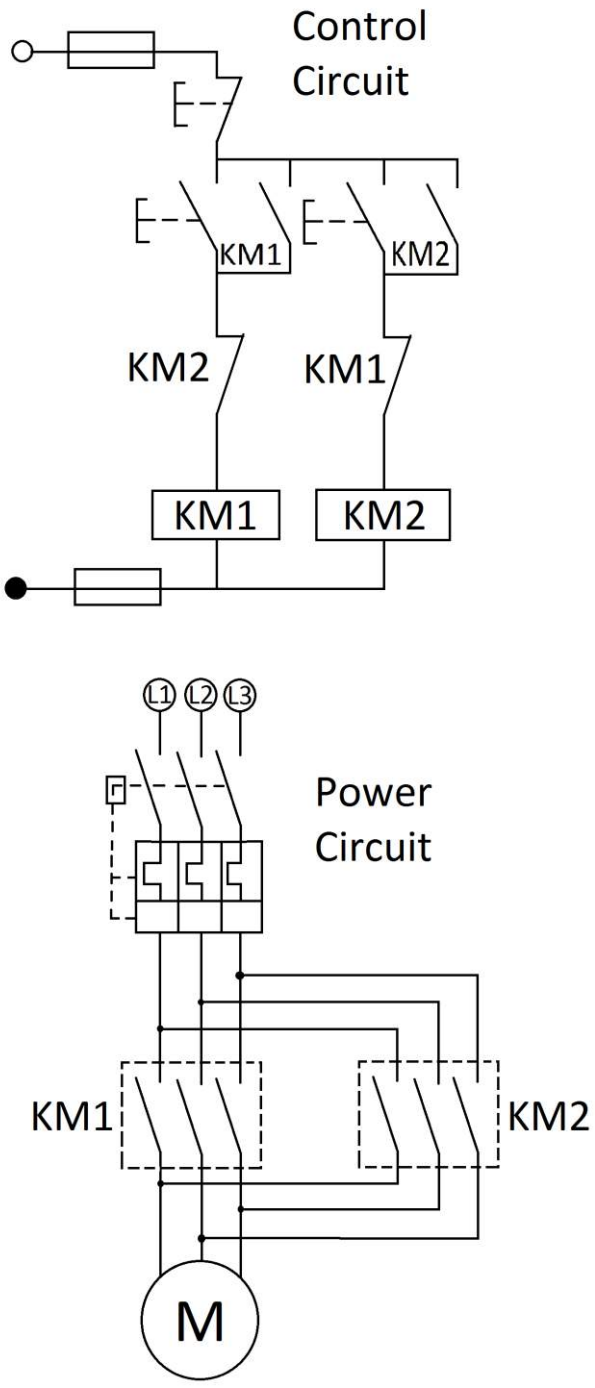

Figure 2.3. Automation drive circuit for LIM three phase

Prototyping.

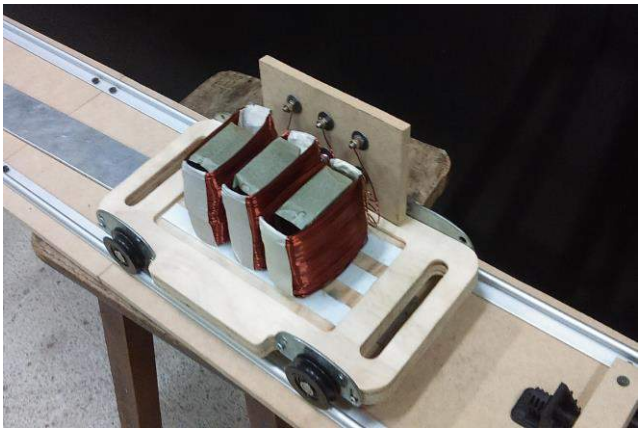

Figure 3.1. Second Iteration Prototype

After taking in consideration the design objectives and the mathematical background, prototyping is the next step. The available three phase connection provided 110V RMS, having ~208V phase to phase.

The first designed LIM was made by putting 9 coils, each one had 50 turns of 18:5 gage copper wire, in line over a core made out of silicon steel 40mm*240mm*0.5mm stripes layered to avoid eddy currents on the coils cores. In this first arrangement of coils they were permanently connected in Y configuration, where the first, forth, and seventh coil were connected to the first phase, the second, fifth, and eighth coil were connected to the second phase, and the third, sixth, and ninth coil were connected to the third phase.

As it is a Y configuration all three coil series systems were connected finally to a neutral line, this neutral line doesn't need to be connected since in Y configuration with the same load in every line the neuter has 0A current. This first design worked properly but generated little, and barely noticeable, force.

Table 1. Preliminary Design Especifications

Preliminary Design		
	Material	**Dimensions**
Coils	**Copper**	**50 turns 18.5 AWG**
Core	**Laminated Silicon Steel 0.5 thickness**	**40mm*70mm*12mm**

An automation solution is given in the connection present in Figure 2.3 for the lead a, b, and c, allowing it to change direction by limit switching instead of manually switching lines.

Here KM1 and KM2 are contactors, each one having three Normally Open (NO) switches and one Normally Closed (NC). The NC switch from the contactor is connected in series with the opposite contactor coil, avoiding short disabling one contactor when the other is active.

There are three limit switches, one connected in series at the beginning of the Control Circuit, being a NC limit switch: pushing on it de-energizes all the circuit.

The other two present limit switches are NO, pressing them energizes the motor in either direction, alternating them.

The second design was formed by only three (3) coils also made of 18,5 gauge copper wire, but with a massive difference: each one of these new tree coils has 250 turns. This second design of LIM was mounted into a little wagon and rails to allow it to move, and onto the wagon were also mounted some banana female connectors for each coil terminal to allow changing between Δ and Y configuration easily.

Table 1. Final Design Especifications

Final Design		
	Material	**Dimensions**
Coils	**Copper**	**250 turns 18.5 AWG**
Core	**Laminated Silicon Steel 0.5 thickness**	**40mm*70mm*12mm**

Having all this into account, this working prototype specifications are:

- Adjustable air gap to a maximum of 15mm.
- Usable railing length of 1.0 meters.
- Maximum voltage of $120V_{line.}$
- Maximun current 1,5A.
- 250 turns per coil.
- Power 0,1kW

Conclusions

A linear induction motor was designed and constructed. Two attempts were made and tested using Y and Δ configurations. The first design worked properly but generated little, and barely noticeable, force. A better performance under Δ configuration was obtained in the Single-Sided LIM prototype.

An Automation drive circuit for LIM three phase was given allowing to change direction by swapping two of the three feeding lines, using a limit switching instead of manually switching lines.

Flexibility for experiments allowing different configurations for behavioral studies is one of the most important features of the LIM proto-type In addition an easy method for LIM construction, permits to obtain a very cheap prototype for labs in technical schools.

Acknowledgements

This work was supported by the Universidad Nacional de Colombia Sede Manizales with the research group on energy resources (GIRE- COL0144229) and The Universidad Nacional de Colombia Sede Medellín (Instrumentación Científica e Industrial-COL0037917) with research project HERMES 30115.

References

[1] A. Fitzgerald, S. Umans and C. Kingley, Electric Machinery, McGraw-Hill Education, 2013.

[2] P. C. Sen, Principles of Electric Machines and Power Electronics, John Wiley & Sons Inc, 2013.

[3] I. Boldea and S. A. Nasar, The Induction Machine Handbook, CRC Press LLC, 2002.

[4] N. T. García, Dynamical Analysis of Three–phase Systems Controlled by ZAD-FPIC Techniques, Manizalez: Universidad Nacional de Colombia, 2012.

[5] T. A. Lipo and T. A. Nondahl, "Pole-by-pole d-q model of a linear inductuion machine," *IEEE Transactions on Power Apparatus and Systems,* Vols. PAS-98, no. 2, p. 629, 1979.

[6] J. Liu, F. Lin, Z. Yang and T. Q. Zheng, "Fiel oriented control of linear induction motor considering attraction force and end-effects," in *International Power Electronics and Motion*, 2006.

Effect of fault-clearing time on the sizing of the ground mesh in a 220kV station according IEEE-80 Standard and its profitability

Efectos del tiempo de despeje de falla sobre el dimensionamiento de la Malla de Tierra en una Estación de 220kV, conforme Norma IEEE-80 y su rentabilidad

Mitjans Felipe: engineer, Universidad Nacional de Asunción, Paraguay; Master of Science, Universidad Politécnica de Cataluña, España
Pulfer Jean-Claude: engineer, Swiss Federal Institute of Technology Lausanne, Switzerland; Master of Science, Swiss Federal Institute of Technology Zurich, Switzerland

ABSTRACT
The present article aims to analyze and demonstrate that it is technically and economically feasible to optimize the design of the ground mesh in an electric station, considering as a parameter the fault-clearing time, according to the IEEE-80 standard, field experience and scientific literature, regardless if the event is internal or external. In this case the fault-clearing time is reduced from 0.5 seconds to shorter times, so that no fibrillation occurs in the human body and the values of the permissible touch and step voltages of the 220 kV station's ground mesh won't be compromised. For this purpose are considered the surface dimensions of a conventional 220 kV station according to the technical specifications of the national company ANDE. The rules listed in the IEEE-80 Standard and the introduction to the mathematical method for calculating the distribution of the potential gradient is the focus of this research. For the economic evaluation are analyzed the material and installation savings and the measurements of a ground mesh system using copper conductors.

Keywords: step voltage, touch voltage, fence voltage, ground mesh, short circuit

RESUMEN
El presente artículo tiene por objeto analizar y demostrar que es técnica y económicamente viable optimizar el dimensionamiento de la malla de tierra de una estación eléctrica, tomando como parámetro la variable del tiempo de despeje de falla, conforme a la Norma IEEE-80, experiencias de campo y literatura científica, independientemente si el evento es interno o externo. Para el efecto se reduce el tiempo de despeje de falla de 0,5s a tiempos menores, de tal manera que no ocurra fibrilación en el cuerpo humano y que no se vean comprometidos los valores de tensión de toque y tensión de paso admisibles de la malla de tierra de la estación de 220 kV. Para tal efecto se toman las dimensiones superficiales de una estación convencional de 220 kV establecidas por la empresa estatal ANDE conforme a sus especificaciones técnicas. Las reglas enumeradas en la Norma IEEE-80 y la introducción al método matemático sustentado para el cálculo de la distribución del gradiente de potencial de volagees son el centro del análisis de este trabajo de investigación. En lo que respecta a la evaluación económica se analiza el ahorro que se obtiene en material, montaje y las mediciones de un sistema de malla de tierra utilizando como conductor cobre.

Palabras clave: Tensión de paso, tensión de toque, tensión de cerca, malla de tierra, cortocircuito

Received: June 20th 2015
Accepted: Oct 15th 2015

Introduction

The design of Grounding Systems, specifically concerning the sizing of the ground mesh, is part of the activities related to the design of all electric stations, regardless of their voltage level. It is an essential activity in both project engineering and the safety of people.

This article bases its methodology on the mathematical development stated in the ANSI / IEEE 80 Standard "Guide for Safety in AC Substation Grounding" and mathematical models extracted from scientific literature to be applied to practical cases, so that design engineers of electric stations and electrical and electromechanical engineering students know the standards to be able to solve practical problems they will face during their professional lives. The calculations begin with the assessment of the values of short-circuit currents for the different types of scenarios of events that may occur within a standard 220kV station. Then a fixed value of apparent soil resistivity, usually calculated by the Werner method, is adopted. Follows the calculation of the pa-

rameters obtained by the mathematical model under the IEEE 80 Standard, in which are applied options in the variation of the fault-clearing time. In all cases the size of the ground mesh perimeter is rectangular, but it's also possible to choose a square shape.

Regarding the calculation of allowable stress values of touch and step voltage it is adopted as fault-clearing time interval 0.5 s to 0.12 s, considering that the human body has a permissible current fibrillation of up to 3 s (Kindermann, 1991). The step, touch and fence volages of the project will be calculated on a rectangular mesh for a person weighing 70kg. As the inertial reference frame are taken rectangular coordinates (x, y) at one end of the mesh. Then, the behavior of the project voltages along the rectangular axes is assessed to be compared with the allowable values. The sizing of the conductor is part of this article, according to those available on the market, made of tinned copper. The earth electrodes are of the copperweld and the connectors of the compression type (ANSI/IEEE 80, 2000; ANDE, 2008; ANDE, 2013).

The mathematical model described by Kindermann (1991) is used to calculate the fence voltage near the endpoints of the station. This value is compared with the permissible touch voltage. Then, the optimum location of the earth electrodes inside the station is evaluated, taking into account the variation of the volage gradient. Comparative tables are drawn up for each of the proposed cases to find out the most optimal cases to be presented.

The concepts developed here will allow to the designer of grounding systems of electric stations, in particular regarding the sizing of the ground mesh, to have available a fairly practical methodology, starting with obtaining the field data, continuing with the design itself and finishing with the resistance measurement of the already built grounding system.

Evaluation of the short circuit current for a 220 kV station

Table 1 shows the values of the effective short-circuit current (kA) for the different scenarios based on studies made by ANDE for a standard station with voltage levels 220/23 kV. The single-phase short circuit current on the 23kV side of the bar has the highest phase-to-ground amperage (I_{CC} = 9.60 kA). For the sizing of the ground mesh is considered only 70% of this maximum current (ANSI/IEEE-80-2000 Standard).

Table 1: Values of short-circuit currents for different failure scenarios in kA. Source: ANDE, 2013

Voltage level	kV	220	23
Single-phase	F	5.76	9.60
	N	5.72	15.51
Three-phase	Ia	4.939	6.494
Phase-ground	Ia	5.35	9.154
Phase-phase	Ib = Ic	4.278	5.624
Phase-phase-ground	Ib	4.442	9.556
	Ic	5.761	9.602
	In	5.72	15.51

Resistance of the grounding mesh and soil resistivity

To calculate the resistance of the grounding mesh is required the soil resistivity as an input. As a reference for the apparent soil resistivity is employed a value of 200 Ohm-m, given that the methodology of calculating soil resistivity is not part of the present article (ANDE, 2013). Furthermore, to evaluate the allowable volage in the mesh is required the resistivity of the surface layer of the station covered by crushed stone, whose resistivity is 3000 Ohm-m (ANSI/IEEE-80-2000 Standard).

Maximum permissible voltages

The permissible maximum volages are defined as indicated in the ANSI / IEEE 80 Standard. Step and maximum allowable touch voltages depend on soil resistivity. In the station you have 2 layers, the ground and crushed stone. Therefore should evaluate the reduction due to reflection (Kindermann, 1991). The reflection factor is given by equation (1), where ρ is the resistivity of the crushed stone and ρ_s the apparent resistivity of the soil.

$$k = \frac{\rho - \rho_s}{\rho + \rho_s} \qquad (1)$$

$$C_s = \frac{1}{0.96}\left[1 + 2\sum_{j=1}^{1000}\frac{k^j}{\sqrt{1+\left(2j\frac{h_s}{0.08}\right)^2}}\right] \qquad (2)$$

With this value and a thickness of the crushed stone layer of 0.10 m equation (2) is used to calculate the reduction coefficient of the surface layer C_s used to calculate the effective resistance of a person's foot in presence of surface material of finite thickness (Ramírez, 2010).

Duration of short circuits

To determine the permissible touch and step volages is considered that the duration of the short circuit will be in seconds. The durations of failure t_f and of shock t_s are typically assumed as equal, unless the duration of failure is the sum of successive impacts as those produced by the automatic reclosing of the SF6 type switches of 220 kV, which have an opening time of 0.06 s and a closing time 0.16 s (IEC N° 62271-100 Standard). The selection of failure duration t_f, may reflect times of rapid clearance of the transmission station and slow clearance times for distribution and industrial substations. The selection of t_f and t_s can result in the most pessimistic combination of factors of decreased fault currents and allowed currents by the human body (Ramírez, 2010).

Typical values for t_f and t_s are in the range 0.25 to 1 s (Ramírez, 2010). According to Kindermann (1991) 99.5% of people weighing 50 kg or more can endure without an occurrence of ventricular fibrillation within a range of 0.03 to 3 s. This time interval

is a permissible and acceptable limit, so that no fibrillation will occur during the time the person is under touch or step volage. The crash time is limited by the performance of the protection systems, according to the curve of the relay (Kindermann, 2005). Thus, for a greater fault current in the system passing through the grounding, the relay curve provides the time for action of the protection systems, bearing in mind that the general principle of the protection systems is to eliminate the quickest possible fault, so to have the smallest number of customers without power. For digital relays there is no need to have time curves printed on paper, because it operates associating the curve to a function that reproduces the normalized curve (IEEE Standard C37.112-1996). For a deeper and more realistic technical analysis as set out in the preceding paragraphs we shall take as reference of the fault clearing time of the switch the value of t_s = 0.12 s (ANDE, 2013).

Maximum permissible voltages

The safety of a person depends on the amount of energy that it can be absorb during a certain period of time, which in this case is the duration of the fault. Consequently, the maximum allowable volages depend on the weight of the person and on the duration of the short circuit. According to the ANSI / IEEE 80 Standard can be considered people weighing 50 kg and 70 kg respectively. For a more realistic analysis is applied the mathematical model of the maximum permissible step and touch volages to achieve security for the personnel weighing 70 kg, as shown in equations (3) and (4) obtained from Kindermann (1991).

$$V_{p_{70}} = (1000 + 6C_s\rho_s)\frac{0.157}{\sqrt{t_s}} \quad (3)$$

$$V_{t_{70}} = (1000 + 1.5C_s\rho_s)\frac{0.157}{\sqrt{t_s}} \quad (4)$$

Sizing of ground mesh conductor

Table (II) shows the constants of different types of conductors used for the selection and sizing of grounding systems of stations. For a more simplified technical analysis are considered the constants of tinned bare soft type copper wire with 100% conductivity (ANSI/IEEE 80-2000 Standard).

The thermal limit of the conductors is determined by the used splice. In this case is considered the compression type having the following values:

Operating temperature of the conductor: T_a = 40°C

Maximum temperature inside the conductor (with compression splicing): T_m = 250°C

Thermal coefficient of resistivity (reference temperature: 20°C): α_r = 0.00393 1/°C

Inverse of the thermal coefficient of resistivity at 0°C: K_0 = 234°C

Resistivity of the conductor of the mesh (reference temperature: 20°C): ρ_r = 1.7241 μΩ cm

Thermal Capacity Factor: T_{CAP} = 3.422 J/(cm³ °C)

Table II: Material constants of conductors for ground mesh. Source: ANSI/IEEE 80-2000 Standard

Description	Material conductivity (%)	α_r factor at 20 °C (1/°C)	K_0 at 0 °C (0 °C)	Fusing[a] temperature T_m (°C)	ρ_r 20 °C (μΩ-cm)	TCAP thermal capacity [J/(cm³·°C)]
Copper, annealed soft-drawn	100.0	0.003 93	234	1083	1.72	3.42
Copper, commercial hard-drawn	97.0	0.003 81	242	1084	1.78	3.42
Copper-clad steel wire	40.0	0.003 78	245	1084	4.40	3.85
Copper-clad steel wire	30.0	0.003 78	245	1084	5.86	3.85
Copper-clad steel rod[b]	20.0	0.003 78	245	1084	8.62	3.85
Aluminum, EC grade	61.0	0.004 03	228	657	2.86	2.56
Aluminum, 5005 alloy	53.5	0.003 53	263	652	3.22	2.60
Aluminum, 6201 alloy	52.5	0.003 47	268	654	3.28	2.60
Aluminum-clad steel wire	20.3	0.003 60	258	657	8.48	3.58
Steel, 1020	10.8	0.001 60	605	1510	15.90	3.28
Stainless-clad steel rod[c]	9.8	0.001 60	605	1400	17.50	4.44
Zinc-coated steel rod	8.6	0.003 20	293	419	20.10	3.93
Stainless steel, 304	2.4	0.001 30	749	1400	72.00	4.03

[a]From ASTM standards.
[b]Copper-clad steel rods based on 0.254 mm (0.010 in) copper thickness.
[c]Stainless-clad steel rod based on 0.508 mm (0.020 in) No. 304 stainless steel thickness over No. 1020 steel core.

The minimum conductor section in mm2 is expressed by equation (5) proposed by Kindermann (1991).

$$A = I_{cc}\sqrt{t_c\alpha_r\rho_r\frac{10^4}{T_{CAP}Ln\left(1+\frac{T_m-T_a}{K_0+T_a}\right)}} \quad (5)$$

Using the above constants in this equation the minimum section is: A = 20 mm².

However, the smallest size of tinned copper conductor commonly used for grounding in electrical stations is AWG code 2/0 (= 67.46 mm²), which has an area equivalent to 133.1 MCM and a diameter d = 0.01 m. This oversizing allows future expansions and a better safety of persons (ANSI/IEEE 80-2000 Standard).

Earth mesh geometry

The ground mesh, which is the subject of the technical and economic analysis in the present article, is located in a 100 m long and 100 m wide plot at a depth h = 0.6 m from the surface. It will be designed to maintain the safety of a person with a minimum weight of 70 kg (ANDE, 2008). As the potential is a vector quantity, is taken as inertial reference frame one of the corners of the mesh, considering that the potential gradient distribution exhibits higher values in the corners.

Table (III) shows 5 cases of clearing time t_s with its respective mesh geometry and conductor cost for the mesh considering a specific cost of US$25/m (ANDE, 2015). For all 5 cases the length of the conductors in the rectangular axes (L_x; L_y) will remain constant. The mesh is divided into squares with a variable separation (D_x; D_y) generating a variable number of parallel conductors (n_x; n_y).

Table III: Correlation between geometry of earth mesh and fault clearing time. Source: ANDE, 2015

t_s (s)	L_x (m)	L_y (m)	D_x (m)	D_y (m)	n_x (un)	n_y (un)	L_t (m)	Cost (US$)	Relat. cost (%)
0.12	95	85	10	10	10	9	1768	44,200	100
0.2	95	85	7	7	14	13	2488	62,200	141
0.3	95	85	5	5	20	18	3473	86,825	196
0.4	95	85	4.5	4.5	22	20	3833	95,825	217
0.5	95	85	4	4	25	22	4278	106,950	242

The total conductor length is given by Lt increased by 63 m due to the total length of the 21 earth electrodes having each a length of 3 m, so to help to reduce the resistance of ground mesh. The earth electrodes with a diameter of ¾ " are of the Cooperweld type. They will be distributed on the mesh in places of greater sensitivity concerning failure events, such as the star center of the power transformer, transmission line arresters and perimeter fence, so to reduce touch and step volages of the planned ground mesh (ANDE, 2013).

Table III shows clearly that the selection of the fault clearing time has a significant impact on the cost of the ground mesh. For longer durations the costs are much higher, due to a larger quantity of copper conductors used for the mesh. For instance, a time of 0.5 s generate 242% higher costs compared to a duration of 0.12 s.

Ground mesh parameters

Ground resistance

To calculate the resistance of the ground mesh R_g the following formula given by equation (6) is used (Kindermann, 1991).

$$R_g = \rho\left[\frac{1}{L_t}+\frac{1}{\sqrt{20A}}\left(1+\frac{1}{1+h\sqrt{\frac{20}{A}}}\right)\right] \quad (6)$$

Constants for project volage calculations

Prior to the calculation of the project mesh potential, have to be determined the constants K_m (geometric factor), K_i (current dispersion factor) and K_s (geometric factor for step voltage) on both axes (x; y). For each of these constants is used the highest value to calculate the project volages (ANSI/IEEE-80-2000 Standard).

The K_i constant helps to correct the effect of the distribution non-uniformity of the current to the ground. The highest current dispersion is verified on the periphery of the mesh and mainly in its vertices. K_i is calculated by equation (7) proposed by Kindermann (1991).

$$K_i = 0.656 + 0.172n \quad (7)$$

K_m is calculated by equation (8) below (Kindermann, 1991).

$$K_m = \frac{1}{2\pi}\left[\ln\left(\frac{D^2}{16hd}+\frac{(D+2h)^2}{8Dd}-\frac{h}{4d}\right)+\frac{1}{\sqrt{1+h}}\ln\frac{8}{\pi(2n-1)}\right] \quad (8)$$

The constant K_s is given by equation (9) indicated below. This factor introduces to the calculation the effect of depth of the mesh, as well as the separation and the number of conductors (Kindermann, 1991).

$$K_s = \frac{1}{\pi}\left[\frac{1}{2h}+\frac{1}{D+h}+\frac{1}{D}\left(1-0.5^{(n-2)}\right)\right] \quad (9)$$

Touch and step voltages of the project

For the calculation of both the touch and the step volages of the project short circuit current I_{cc} can be reduced by 70%. They are function of soil resistivity, the current through the mesh and the lengths of the used cables L_t and electrodes L_j. Touch voltage is given by equation (10) and step voltage by equation (11) (Kindermann, 1991).

$$V_t = \rho I_{cc}\left(\frac{K_m K_i}{L_t + 1.15L_j}\right)10^3 \quad (10)$$

$$V_p = \rho I_{cc}\left(\frac{K_s K_i}{L_t + 1.15L_j}\right)10^3 \quad (11)$$

Fence voltage of the project

Depending on the degree of risk, the location of the plot and the characteristics of the mesh it has to be decided how to fence the area properly. Usually, it is used a metallic fence for being economic, but also conductive. It is subject to native voltage currents shorts station that the physical principle of magnetic induction energized metal fences. So, any person in contact with the metallic fence will be subject to a potential difference.

It has to be verified that the value of the fence potential V_c is below the limit of the allowable touch potential. The parameter K_c is a coefficient, which relates all the parameters of the mesh with the position of the person, who is in contact with the metallic fence. Its value is given by equation (12) proposed by Kindermann (1991). The parameter x represents the distance between a person weighing 70 kg touching the fence and the fence itself. K_c has to be calculated for both cases, x being 0 and 1 m. It has to be stressed, that the verification of the fence voltage is critical for the sizing of the ground mesh, considering that potential gradients are highest at the borders of the station.

$$K_c = \frac{1}{2\pi}\left\{\ln\left[\frac{\left(h^2+x^2\right)\left[h^2+(D+x)^2\right]}{hd\left(h^2+D^2\right)}\right]+2\ln\left\{\left[\frac{2D+x}{2D}\right]\left[\frac{3D+x}{3D}\right]\left[\frac{(n-1)D+x}{(n-1)D}\right]\right\}\right\} \quad (12)$$

The fence potential V_c is given by equation (13) proposed by Kindermann (1991).

$$V_c = \rho I_{cc}\left(\frac{K_c K_i}{L_t + 1.15L_j}\right)10^3 \quad (13)$$

Table IV. Parameters and earth potential of the projected mesh, source: ANSI/IEEE-80-2000 Standard, Kindermann (1991).

t_s(s)	K_i	K_s	K_m	K_c	V_p (V)	V_t (V)	V_c (V)	$V_{p'}$ (V)	V_r(V)	R_g (Ohm)
0.12	2.37	0.32	0.88	0.27	562	1514	463	5000	1600	1.09
0.2	3.00	0.35	0.73	0.29	569	1186	468	3921	1244	1.06
0.3	4.09	0.38	0.59	0.32	611	944	507	3302	1015	1.04
0.4	4.44	0.39	0.55	0.34	620	865	529	2773	879	1.03
0.5	4.78	0.41	0.51	0.35	622	772	545	2480	787	1.03

* admissible values.

The results in Table IV show clearly how the selection of the fault clearing time t_s affects the elaboration of a ground mesh project, concerning the parameters, as well as the touch, step and fence voltages and their distribution inside the mesh. Considering that the duration of failure or clearance has an inverse behavior to the allowable values of the potential gradient, with a minimum duration of 0.12 s there will be a clearance of a 100% of allowable volage values, without being exceeded compared to the project voltages to maintain the security of the people for the analyzed scenario. Another point to take into account is that the allowable step voltage values are limited to 5000 V for the minimum value of failure time, considering that safety boots are made for this allowable value (ANDE, 2013).

Conclusions

It can be concluded, that the projected ground mesh for a 220/23kV station with the proposed fault time interval reaches levels of touch, step and fence voltages, which are within safe limits required by the IEEE 80 Standard. Also the value of the ground mesh resistance is within the allowable value of this same standard.

The mathematical model and the methodology proposed in the present article was designed for a rectangular mesh, however is also valid for a square mesh without committing the allowable values of the potentials. Regarding the economic evaluation it can be observed, that the reduction of the time of failure will lower considerably the investment costs. Besides, it would be advisable to reengineer the protection settings, specifically concerning the protection scheme and their synchronization in case of events, considering that it's a key factor in the power system scheme of any electrical station. As a final point it has to be stressed, that the calculation of the fence voltage represents a new concept for the sizing of ground meshes. However, this calculation is very important to guarantee safety of any person being inside the station plot or touching the fence.

References

ANDE: Especificaciones Técnicas Nº 03.02.07.22 de Conectores de Sistemas de Puesta a Tierra, 2008

ANDE: Licitación Pública Internacional Ande Nº 262-2008, Especificaciones Técnicas, Construcción de la Estación Villarrica 220kV, 2008

ANDE: Plan Maestro de la Administración Nacional de Electricidad, 2013-2023

ANDE: Dpto. de Operación de Sistema, 2013

ANDE: Dpto. de Planificación, 2013

ANDE: Especificaciones Técnicas Nº 03.04.06.83, Suministro de jabalinas de puesta a tierra, 2013

ANDE: Oficina de Higiene y Seguridad Industrial, 2013

ANDE: Consulta realizada al Departamento de Proyectos Electromecánicos en fecha 16/01, 2015.

ANSI/IEEE Standard 80-2000, "Guide for Safety in AC Substation Grounding". Revision of IEEE Standard 80-86

ANSI/IEEE Standard 80-2000, "Guide for Safety in AC Substation Grounding", 2000

IEC Standard Nº 62271-100, 220kV breakers

IEEE Standard C37.112-1996: Inverse Time Characteristic Equations for Overcurrent Relays, 1996

Kindermann, Geraldo: Corto Circuito, 1990

Kindermann, Geraldo: Aterramento Eléctrico, 1991

Kindermann, Geraldo: Protecao de sistemas eléctricos de potencia, 2005

Ramírez, José y Cano Eduardo: Sistema de Puesta a Tierra: Diseñado con IEEE-80 y evaluado con MEF, 2010

Impact Analysis of Asymmetric Conditions on an Oil-Filled Distribution Transformer Performance

Análisis del impacto de condiciones de asimetría en el desepeño de un trasnformador de distribución sumergido en líquido aislante.

Harold Francisco Mazo Mantilla[1], Michael Andrés Salcedo Merchán[2], Andrés Pavas[3], Iván Camilo Durán[4]

ABSTRACT

This paper shows the results obtained from the simulation of a study case about the impact of asymmetric operational conditions on oil-filled distribution transformer useful life. The results depend on the supplied energy level through three different demand profiles (unbalance) mixed with two asymmetric conditions (no asymmetric condition and two additional cases with different asymmetric conditions). The disturbance analysis is realized through the FBD and symmetrical components theories, in order to obtain an equivalent factor to the I_{pu}, which will be used to characterize the transformer loss of life from the temperature rise in the transformer (oil). Finally, it is realized a discussion about the results obtained and the possible analysis field for future studies of this topic (asymmetric conditions).

Key words: Aging factor, demand profile, hot spot, load unbalance, loss of life, phase displacement, thermal-electrical model**.**

RESUMEN

El presente documento muestra los resultados obtenidos a partir de la simulación de un estudio de cado acerca del impacto de las condiciones asimétricas de operación en la vida útil de transformadores de distribución sumergidos en líquido aislante. Los resultados dependen del nivel de energía entregado a través de tres diferentes perfiles de demanda (desbalanceados) combinados con dos condiciones de asimetría (sin condición de asimetrías y dos casos adicionales diferentes de condiciones de asimetría). El análisis de las perturbaciones es realizado a través de las teorías FBD y de componentes simétricas, con el fin de obtener un factor equivalente a I_{pu}, el cual se empleará para caracterizar la pérdida de vida útil acelerada del transformador a partir de los aumentos de temperatura en él. Finalmente, se realiza una discusión acerca de los resultados obtenidos y del los posibles campos de análisis para futuros estudios realizados en este tema (condiciones operacionales de asimetría).

Palabras clave: Desbalance de carga, desplazamiento de fase, factor de envejecimiento, modelo termoeléctrico, pérdida de vida, perfil de demanda.

Received: January __th 2011
Accepted: February __th 2012

INTRODUCTION

The current loads used from the users produce many harmful effects on the transformer operation, due to the non-linear loads connected to the distribution system. As part of the distribution system, the transformers receives all the disturbances from the user loads, which damages the transformer insulation (paper and insulating oil). The insulation degradation generates an accelerated loss of life on the transformer, affecting the distribution system performance due to more frequently changing of the system elements, i.e., a higher monetary inversion.

Furthermore, a significant part of the current studies are focused on waveform distortion (harmonic), setting aside the asymmetric condition analysis, which promotes the analysis method development for the asymmetric conditions on distribution transformers (<300 kVA), from the current elements to analyze the transformer loss of life.

1. MODELLING OF UNBALANCE EFFECT ON OIL-FILLED DISTRIBUTION TRANSFORMERS.

The characterization of the damage level of the oil-filled transformer insulation due to the asymmetric conditions is carried out through a thermal-electrical evaluation model, which permits an analysis of the degradation level of the insulations and the transformer useful life.

The electrical model for a transformer operating under asymmetric conditions is based on the power losses presented during its operation, i.e., the effects generated such us a low power factor (phase displacement) or an over fluxing in the core (unbalance).

Those effects are characterized through a power separating method, which permits to analyze the disturbances effects (non-active power) independently from the normal transformer operation (active power) using the FBD theory 0, in

[1] Electrical Engineer of the National University of Colombia. hfmazom@unal.edu.co
[2] Electrical Engineer of the National University of Colombia.masalcedom@unal.edu.co
[3] Electrical Engineer, Magister and PhD of the National University of Colombia. Professor of the National University of Colombia, Colombia. fapavasm@unal.edu.co
[4] Electrical Engineer, Magister and PhD candidate in Electrical Engineering of the National University of Colombia. icdurantl@unal.edu.co
A. Pavas, and I. Duran are with the Program of Acquisition and Analysis of Electromagnetic Signals (PAAS-UN) of the National University of Colombia.

order to obtain a factor that permits the active and non-active effects grouping.

Once the effects on the transformer are characterized by their grouping, the obtained factor permits to characterize the temperature variations and the transformer thermal characteristics due to the asymmetric conditions by the implementation of a loss of life model. The estimation realized with this model is carried out from the Arrhenius equation, which is an accepted quantification method of transformer loss of life related to temperature changes.

1.1. Electrical modelling.

For an operational asymmetric condition on the transformer, the electrical performance is evaluated through the next steps 0:

- The transformer power losses are determined under the operational asymmetric conditions.
- Active (non-disturbance and symmetric) and non-active power is described, in order to organize the power losses.

The common used model for the transformer analysis (pi-model) is not very useful in order to evaluate the performance of a three-leg transformer under asymmetric conditions; because of this, it must be involved a model that permits to include each phase current contribution to the core net flux (figure 1).

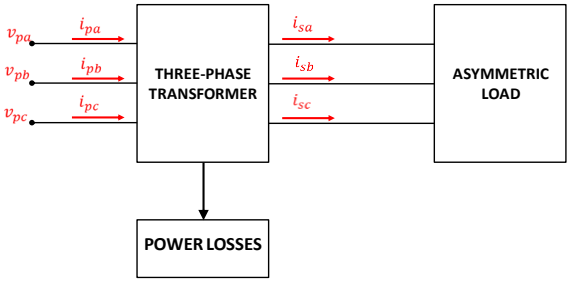

Fig. 1 Model used to describe the core net flux. (*Source: The authors)*

This model lets to analyze the magnetic flux of a one-core three-leg transformer, in which the primary and secondary windings (per phase) are in the same leg; it permits that the magnetic flux be distributed as it is shown in the figure 2.

This transformer distribution allows the magnetic flux analysis depending on the hysteresis cycle (non-saturation considered for this exercise, transformer lineal performance); the magnetic flux on figure 2 is be modelled through a magnetic circuit, as shown in figure 3.

From the magnetic circuit is obtained the expression: (1)

$$\Im_k = N_p i_{pek} + N_s i_{sk}, k = a,b,c \qquad (1)$$

Where:

$\Re_k$: Reluctance for each transformer leg ($k = a,b,c$).

$\Re_0$: Dispersion reluctance.

$\Im_k$: Magnetomotive Force (fmm).

N_p , N_s : *Primary and secondary winding turns.*

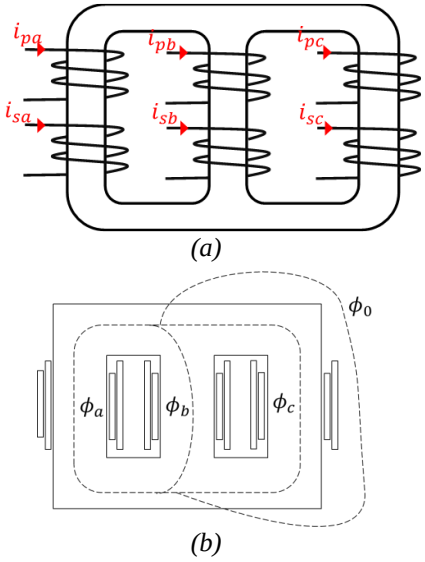

Fig. 2 Electromagnetic element distribution on the three-leg transformer: (a) currents distribution; (b) magnetic flux. (*Source: The authors)*

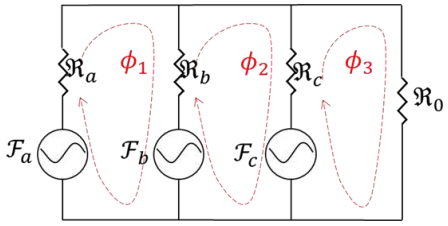

Fig. 3 Transformer magnetic circuit. (*Source: The authors)*

Once the unbalance magnetic effect on transformer is determined, the asymmetric effect magnitude on the transformer must be characterized. It is realized through the transformer active and non-active power delivered by the transformer, applying to the FBD theory.

This theory permits a power analysis by means of a current decomposition for poly-phase systems, i.e., a current separation between active and non-active currents as is shown in (2):

$$I_e^2 = I_a^2 + I_x^2 \; ; \quad I_x^2 = I_{au}^2 + I_{Qu}^2 + I_{Qd}^2 + I_h^2 \qquad (2)$$

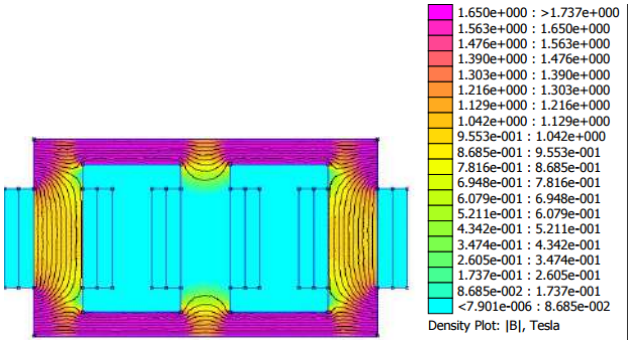

Fig. 4. Example of magnetic flux distribution for an unbalance condition. (*Source: The authors)*

Where I is the transformer current, I_e is the effective current, I_a is the active current (active consumed power), I_x is the non-active current, I_{au} is the active unbalance current, I_{Qu} is the reactive unbalance current, I_{Qd} is the reactive displaced current and I_h is the harmonic current.

For this case, the harmonics effects are despised, then this topic is already analysed in other papers. With this current decomposition, it is possible to describe the asymmetric grouped effects, in order to obtain a factor called "$\tilde{I}_{pu}$" (per unit current), which will permit the transformer thermal behaviour for its loss of life, through the expression (3):

$$\tilde{I}_{pu} = \sqrt{I_a^2 + I_x^2} = \sqrt{I_a^2\left(1 + \frac{I_x^2}{I_a^2}\right)} \qquad (3)$$

Once the asymmetric condition is characterized, the transformer unbalance condition must be determined by means of its derating. According to other papers, the transformer derating consists in five steps:

<u>*Step 1*</u>: Transformer load losses calculation under balance and sinusoidal condition:

$$P_T = P_{NL} + P_{LL} \;;\; P_{LL} = P_{I^2R} + P_{EC} + P_{OSL} \qquad (4)$$

<u>*Step 2*</u>: Addition of an unbalanced condition (load or voltage), maintaining the fundamental load currant and output voltage at rated values:

$$I_S{}^1 = V_S{}^1 = 1pu \qquad (5)$$

Step 3: If the output voltage is modified by a reactive power demand, compensate it by adjusting the fundamental input voltage.

Step 4: Re-calculate the total power losses under asymmetric conditions to determine the additional losses:

$$\Delta Losses\% = \frac{P_{Loss-new} - P_{Loss-rated}}{P_{Loss-rated}} \times 100\% \qquad (6)$$

Step 5: Using a simulation support software, decrease the load magnitude to equal the total losses and the rated losses, using an randomly valued resistance in series with the load, to adjust its value:

$$P_{loss} \mid_{I_S{}^1 = I_{derrated}} = P_{Loss,rated} \qquad (7)$$

Step 6: The derated apparent power is calculated as:

$$kVA_{derated} = kVA_{rated} \times I_{derated} \qquad (8)$$

$$Derating = (1 - I_{derated}) \times 100\% \qquad (9)$$

Nevertheless, it is important to describe the asymmetric load effects with a more recognized method, i.e., the "symmetrical components". The applying of the symmetrical ingredients permits to determine an asymmetric level in voltage or current of three-phase systems.

First, must be calculated the symmetrical components from the three-phase quantities, as the Fontescue theorem is shown in (10):

$$\begin{bmatrix} I_0 \\ I_1 \\ I_2 \end{bmatrix} = \frac{1}{\sqrt{3}} \begin{bmatrix} 1 & 1 & 1 \\ 1 & \alpha & \alpha^2 \\ 1 & \alpha^2 & \alpha \end{bmatrix} \begin{bmatrix} I_a \\ I_b \\ I_c \end{bmatrix} \quad \begin{bmatrix} V_0 \\ V_1 \\ V_2 \end{bmatrix} = \frac{1}{\sqrt{3}} \begin{bmatrix} 1 & 1 & 1 \\ 1 & \alpha & \alpha^2 \\ 1 & \alpha^2 & \alpha \end{bmatrix} \begin{bmatrix} V_a \\ V_b \\ V_c \end{bmatrix} \qquad (10)$$

Once the symmetrical components are defined, must be defined the voltage and current unbalance factor (VUF and CUF), as follows:

$$VUF = \frac{V_2}{V_1} = \sqrt{\frac{1 - \sqrt{(3 - 6\beta)}}{1 + \sqrt{(3 - 6\beta)}}} \qquad (11)$$

$$\beta = \frac{V_{ab}{}^4 + V_{bc}{}^4 + V_{ca}{}^4}{(V_{ab}{}^4 + V_{bc}{}^4 + V_{ca}{}^4)^2} \qquad (12)$$

Where V_{ab}, V_{bc} and V_{ca} are the rms values of fundamental frequency voltage fasors of the three-phase system, Z_1 and Z_2 are the positive and negative impedance components of the transformer. The Factors CUF and VUF permit to describe the unbalance level for the transformer current and voltage.

1.2. Thermal modelling

Once the factor $\tilde{I}_{pu}$ is obtained, can be determined the heat transference on the oil-filled distribution transformer due to grouping effect of the asymmetric condition, the power losses and the load. The very complex interaction of the transformer with its natural and electrical environment (heat flux through the transformer oil to and from the environment) is known, generating a thermal-dynamical interaction between them (transformer and environment).

The current thermal model proposed in the IEEE C57.91 evaluates two important temperatures for the useful life-aging factor of the transformer: the hot spot (Θ_H) and the top

oil (Θ_{Oil}) temperatures, through a triple interaction with the ambient temperature (Θ_A).

The top oil temperature variation due to its interaction with the ambient temperature is calculated as described in (13):

$$\frac{I_{pu}^{\sim 2}\beta+1}{\beta+1}\left[\Delta\Theta_{Oil-R}\right]^{\frac{1}{n}} = \tau_{Oil}\frac{d\Theta_{Oil}}{dt}\left[\Theta_{Oil}-\Theta_A\right]^{\frac{1}{n}} \quad (13)$$

Where: $I_{pu}^{\sim}$ is the load current per unit; β is the ratio of load to no-load losses; τ_{oil} is the top oil time constant in min; $\Delta\Theta_{oil\text{-}R}$ is the rated top oil rise over ambient in °C; n is the exponent who depends of the cooling method (empiric) IEEE C57.91.

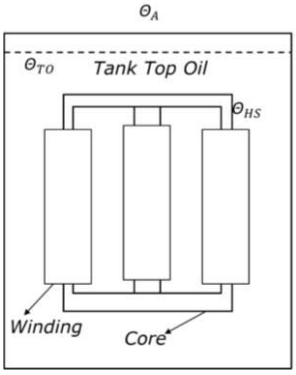

Fig. 5 Transformer thermal interaction. (*Source: The authors)*

Once the top oil temperature rise is determined, the hot-spot temperature is calculated through (14):

$$\frac{I_{pu}^{\sim 2}\left[1+P_{EC-Rated(pu)}\right]}{1+P_{EC-Rated(pu)}}\left[\Delta\Theta_{H-R}\right]^{\frac{1}{m}} = \tau_H\frac{d\Theta_H}{dt}\left[\Theta_H-\Theta_{Oil}\right]^{\frac{1}{m}} \quad (14)$$

Where: $I_{pu}^{\sim}$ is the load current per unit; Θ_H is the hot-spot temperature in °C; τ_{oil} is the top oil time constant in min; $\Delta\Theta_{H\text{-}R}$ is the rated hot spot rise over ambient in °C; m is the Empirical exponent (depending on the cooling method).

Once both temperature models (hot-spot and top oil) are determined, the transformer thermal model is complete. The final model graphic is displayed on fig.
The implementation of (14) and (15) determines the transformer aging acceleration through the transformer hottest spot behavior. The transformer aging factor is characterized resorting to the Arrhenius equation 0, applied to the oil-filled transformers aging.

Once the transformer hottest spot temperature is characterized, the aging factor for the transformer is at first obtained from the modified Arrhenius equation in (15), as described in IEEE C57.91:

$$F_{AA} = e^{\left[\frac{B}{383}-\frac{B}{\theta_H+273}\right]} \quad (15)$$

Where B is a constant depending on the reference temperature. In this case, the reference temperature is 110 °C, so from IEEE C57.91, so the constant value is B = *15000*. Finally, the Per Unit loss of life (L_F) of the transformer is obtained according to (16):

$$L_F = \frac{\int F_{AA}dt}{\int dt} \quad (16)$$

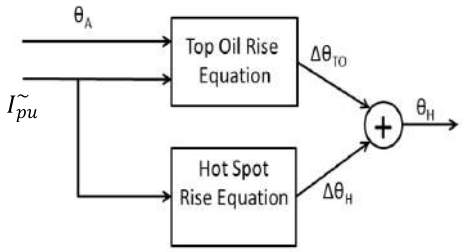

Fig. 6 Transformer mathematical thermal model. (*Source: The authors)*

2. STUDY CASES

As study cases were developed three asymmetric conditions: the first refers to a symmetric condition (non-unbalance, non-phase displacement); the second refers to an unbalanced current case without phase displacement; the third case refers to an asymmetric current condition (unbalanced load and phase displacement). The transformer conditions and characteristics are shown in table I; the load values used on the three cases to generate the asymmetric conditions are shown in table II.

Table I. Transformer Description (*Source: IEEE C57.91)*

Characteristic	Magnitude / Characteristic
Rated Power (kVA)	75
Voltage (V)	11400/214
Connection group	Δ-Y
DC Resistance (primary winding, Ω)	2,023
DC Resistance (secundary winding, Ω)	0,0083
No load losses (P_{NL}, VA)	687,7
Rated total stray losses ($P_{TSL\text{-}Rated}$, kVA)	1,43
Rated top oil rise over ambient ($\Delta\theta_{TO}$, °C)	38,3
Rated hot spot rise over top oil ($\Delta\theta_H$, °C)	22
Ambient temperature (θ_A, °C)	25
Reference hottest spot temperature (°C)	110
Ratio of load loss (rated) to no load loss	5,48
Top oil time constant (hrs)	3,5
Hot spot time constant (hrs)	0,167
Exponent *m*	0,8
Exponent *n*	0,8
Expected useful life (years)	22,5

The analyzed cases do not consider the core saturation, whose impact is expected to accelerate the transformer degradation due to the addition of harmonics effect, which have been already evaluated.

The oil-filled transformer and its characteristics are ideally determined using Standards values, i.e., the transformers values were taking from 0. The evaluated transformer is an ONAN transformer type (Oil Natural Air Natural), so the empirically determined constants *m* and *n* are taken from the IEEE Standard **¡Error! No se encuentra el origen de la referencia.**.

Table II. Used load description for each case *(Source: The authors)*

	Resistance [Ohm]	Current [pu]	Angle [Grade]
Case 1			
Phase A	1+j0	0.97	-1
Phase B	1+j0	0.97	-121
Phase C	1+j0	0.97	119
Case 2			
Phase A	0.81+j0	1.21	-1.21
Phase B	1.02+j0	0.97	-121
Phase C	1.23+j0	0.8129	119.16
Caso 3			
Phase A	0.81+j0	1.36	72.95
Phase B	0.72+j0.81	1.17	-149.93
Phase C	0.76+j0.82	0.88	-1.4

Table IV. Symmetrical components values for each case. *(Source: The authors)*

	$\%i_0$	$\%i_2$	Ix/Ia (%)
Caso 1	0	0	0
Caso 2	11.67	11.62	26.19
Caso 3	20.64	35.12	69.3

The first case indicates a reference case in which the transformer load is about the 100% of its rated power, being this case near to the real charge of a distribution transformer, although the power quality disturbance level is ideal (in operation, there is more effect with larger magnitude and impact on transformer performance).

The second and the third case refer cases in which there is an asymmetrical condition around the transformer nominal current (1pu): the second case only includes load unbalance ant the third case includes load unbalance and phase displacement. In the table III are shown the obtained values for the effective, active and non active currents (including its components) in each case.

Once were obtained the current orthogonal components for each case, were calculated the symmetrical components from the values of the table II and the asymmetric characterization from (3), being shown these results in the table 4.

Table III. Obtained values for each component on the orthogonal decomposition. *(Source: The authors)*

	Case I	Case II	Case III
$\mathbf{I_e}$	245.23	209.09	245.23
$\mathbf{I_a}$	245.23	202.27	201.47
$\mathbf{I_x}$	0	52.98	139.82
$\mathbf{I_{au}}$	0	40.10	70.22
$\mathbf{I_{Qd}}$	0	0.58	77.85
$\mathbf{I_{Qu}}$	0	33.99	133.54

In the figure 7 are shown the final loss of life results for a 20.55 years time evaluation, which is recommended from the IEEE C57.91. It is shown that the most reference case (case 1) is the least harmful scenario for the transformer (less loss of life). It is so due to the non-presence of PQ disturbances.

The results for the case 2 indicates that the selected unbalance value between the phases generate a considerable loss of life, due to the presence of this PQ disturbance, which is generated from the occurrence of a displacement due to the unbalanced magnetic flux in the core (depreciation of harmonic effects).

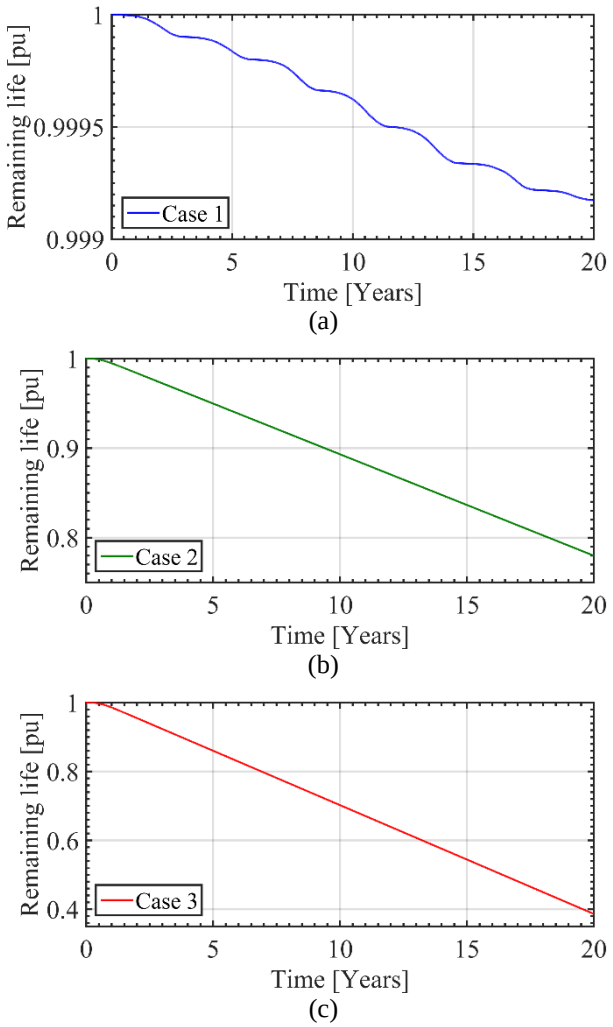

Fig. 7. Obtained loss of life for each case: (a) Case 1; (b) case 2; (c) case 3. (Source: The authors)

As the case 3 included unbalance and phase displacement, it results on the most detrimental case for the transformer loss of life. The conjoined effects of load unbalance and phase

displacement generates the largest loss of life for the transformer, due to the added effects of the PQ disturbances and the rated power in transformer (hot spot temperature rise).

The remaining life limits for table V are characterized by three zones: three green zone is for the remaining life values between 0,95 to 1 pu; the yellow zone is for the remaining life between 0,70 to 0,95 pu; and the red zone is for the remaining life between 0 to 0,70 pu.

Table V. Remaining life for each asymmetric case.

	Year 5	Year 10	Year 15	Year 20
Case 1	**0.9998**	**0.9996**	**0.9993**	**0.9992**
Case 2	**0.9498**	**0.8931**	**0.8365**	**0.7798**
Case 3	**0.8602**	**0.7022**	**0.5442**	**0.3863**

3. DISCUSSION

As it was shown, the asymmetric condition effects generate a low impact on the transformer loss of life, due to the low provision to the increase of the total delivered power by the transformer, i.e., in relation with the load charge magnitude.

It provides a new question about the transformer operation under these conditions: ¿what will be the impact on transformer loss of life, when the asymmetric condition implicates an overloading on the transformer?

It is important to be the next step on the asymmetric conditions on distributions transformers operation, because the core saturation characterized from the hysteresis cycle was not contemplated in this paper.

Additionally, a load that exceeds the transformer rated power allows a rising on the hot spot temperature, accelerating the transformer loss of life, being this effect (core saturation and hot-spot temperature) an interesting, harmful and more realistic state for the distribution transformers with rated power under 300 kVA.

4. CONCLUSIONS

Although the use of non-linear charges is extended, the effect that they generate on the distribution system due to unbalanced load and phase displacement is not so larger as the generated by the harmonics.

Even though the unbalance load and the phase displacement generates a higher acceleration on transformer loss of life, the impact of unbalance on transformer loss of life is larger than the impact of phase displacement.

The impact of PQ disturbances on the loss of life acceleration for oil-filled transformers depends on the load magnitude, i.e., the larger load the larger PQ disturbance effects.

References

Aragon, J. “Experimental investigations on the dissolved gas analysis method through simulation of electrical and thermal faults in transformer oil” Duisburg, Germany. p. [89-94]. 2014.

Duran, I.,Duarte, O.,Pavas, A. "Insulation temperature increase in power transformers due to stationary disturbances: comparision of methods". Conference: Power Electronics and power Quality Applications - PEPQA 2013, Bogotá, Colombia. July, 2013.

IEEE Standards Association. "IEEE C57.91-2011 Guide for loading mineral oil-immersed transformers and step-voltage regulators". New York, United States. p [14-21]. March the 7th, 2012.

Masoum, M.,Moses, P.,Masoum, A.. "Derating of Asymmetric Three-Phase Transfromers Serving Unbalanced Nonlinear Loads". Curtin University of Technology. Perth, Australia. 2008.

Mazo, H.,Salcedo, M.,Pavas, A.,Duran, I.. “Modeling of a Distribution Transformer Performance Operating under Harmonic Polluted Conditions”. PEPQA, Universidad de los Andes. June the 2th -4th, 2015. Bogotá, Colombia.

Meyer, J.; Bollen, M.; Amaris, H.; Blanco, A.M.; Gil de Castro, A.; Desmet, J.; Klatt, M.; Kocewiak, Ł.; Rönnberg, S.; Kai Yang, "Future work on harmonics - some expert opinions Part II - supraharmonics, standards and measurements," Harmonics and Quality of Power (ICHQP), 2014 IEEE 16th International Conference on , vol., no., pp.909,913, 25-28 May 2014.

Njafi, A., Iskender, I., Genc, N. „Evaluating and Derating of Three-Phase Distribution Trnasformer Under Unbalanced Load Using Finite Element Method”. Gazi University. March the 24th-25th 2014. Malaysia.

Pavas, A. Blanco, A., Parra, E. Applying FBD-power theory to analysing effective lighting devices impact on power quality and electric grid efficiency.

Pedra, J.,Sainz, L.,Córcoles, F., R. Lopez, M. Salichs. "PSPICE Computer Model of a Nonlinear Three Phase Three-Legged Transformer". Universidad Politécnica de Cataluña. Barcelona, España. 2004.

Pop, G., Chindris, M., Bindiu, R. "Determination of power losses in transformers working in unbalanced and harmonic polluted networks". Technical University of Cluj. Cluj, Rumania. 2009.

Study of Partial Discharge Based on Time-Frequency Analysis Using Local Polynomial Fourier Transform

Estudio de Descargas Parciales Basado en un Análisis Tiempo-Frecuencia Usando la Transformación Local Polinomial

María C. Forero[1], Herbert E. Rojas[2]

ABSTRACT

In recent years, for partial discharge (PD) analysis, signal processing techniques have been applied in the time-frequency domain such as Short Time Fourier Transform (STFT), Wavelet Transform (WT) and Wigner Distribution (WD), among others. Local Polynomial Fourier Transform (LPFT) is a linear time-frequency representation which is a generalization of STFT. This paper present a study of partial discharge based on time-frequency analysis using Local Polynomial Fourier Transform. The analyzed PD signals were simulated using two mathematical models: PD single-pulse model and PD pulse sequence model. As part of the study, the waveform of PD signals selected were characterize in the time domain and the Fast Fourier Transform (FFT) was used in the analysis at frequency domain. Finally, to demonstrate the versatility of the proposed signal processing technique (based on LPFT) and its application on PD signals, the results obtained with the LPFT of polinomial order m=2 and m=3 were compared with those obtained applying STFT. The results show that the LPFT is able to reveal low and medium frequency components which are due to the secondary peaks and oscillations of the PD pulses, which are not detected when the STFT is used.

Keywords: instantaneous frequency (IF), local polynomial Fourier transform (LPFT), partial discharges (PD), time-frequency analysis,

RESUMEN

Durante los últimos años, para el análisis de descargas parciales (DP) se han venido usando técnicas para el procesamiento de señales en el dominio tiempo-frecuencia como la transformación de corto tiempo de Fourier (STFT), la transformación de Wavelet (WT) y la distribución Wigner (WD), entre otras. La transformación local polinomial de Fourier (LPFT) es una representación tiempo-frecuencia lineal que generaliza la STFT. Este trabajo presenta un estudio relacionado con la aplicación de la LPFT para el análisis y caracterización de señales generadas por DP. Las señales de DP analizadas son generadas a partir de simulaciones que aplican un modelo matemático para producir pulsos sencillos y secuencias de pulsos. Como parte del estudio, sobre las señales de DP seleccionadas se realizó un análisis en el dominio del tiempo para caracterizar las formas de onda y se usó la transformada rápida de Fourier (FFT) para hacer un análisis en el dominio de la frecuencia. Finalmente, para demostrar la versatilidad de la técnica de procesamiento propuesta (basada en la LPFT) y su aplicación en señales de DP, se comparan los resultados obtenidos usando LPFT de orden polinomial m=2, m=3 y una técnica convencional como es la STFT. Los resultados muestran que la LPFT es capaz de revelar componentes de baja y media frecuencia que se relacionan con los picos secundarios y las oscilaciones de los pulsos de DP, los cuales no son detectados cuando se usa la STFT.

Palabras clave: análisis tiempo-frecuencia, descargas parciales (PD), frecuencia instantánea (IF), transformación local polinomial de Fourier (LPFT)

Received: July 17th 2015
Accepted: Oct 15th 2015

Introduction

Traditionally, the analysis methods for signal processing of discharge (PD) are based on the time or frequency domain. In the case of the time domain, some features of the signal, such as time intervals, amplitude levels are easily extracted for visual inspection but are susceptive to noise (Sejdić, Djurović, & Jiang, 2009). Otherwise, in the frequency domain techniques as the Fourier transform (FT) can get the amplitude spectrum and the power spectrum of signals, however it cannot get the information in time-frequency plane. Further, the FT assumes the stationarity of the signal (Katkovnik, 1995), which in the analysis of PD is not satisfied because they are non-periodic signals and the fast transient features in the PD signals can be ignored o cannot be revealed efficiently Ma, Zhou, & Kemp, 2002). For these reasons, the FT has serious limitations as analysis method of PD.

In last decades, several researchers have used time-frequency (TF) analysis methods to study the electromagnetic disturbances, which are non-stationary signals as the PD. Some examples of

[1] María C. Forero. Electrical Engineering Student, Universidad Distrital Francisco José de Caldas, Colombia. Electromagnetic Compatibility and Interference Group GCEM, Colombia. Correspondence author, E-mail: mcforerom@udistrital.edu.co. Tel: +57-1-7051800 Ext: 2128

[2] Herbert E. Rojas. Electrical Engineer, M.Sc. in Electrical Engineering and candidate to Ph.D. from Universidad Nacional de Colombia, Colombia. Assistant Professor in Electrical Engineering Department, Universidad Distrital Francisco José de Caldas Colombia. Electromagnetic Compatibility and Interference Group GCEM. E-mail: herojasc@udistrital.edu.co

these signal-processing techniques are the short-time Fourier transform (STFT), the Wigner-Ville distribution (WVD), the Wavelet transform (WT), the fractional Fourier transform (FRFT) and the local polynomial Fourier transform (LPFT). These techniques provides information of amplitude levels in TF bands and the energy concentration of the signal, i.e they provides time and frequency characteristics at the same time (Li, Bi, Stankovic, & Zoubir, 2011).

With respect to the study of PD, the STFT has been used to identification of PD from acoustic emission signals (Chai, Md Thayoob, Ghosh, Sha'ameri, & Talib, 2006), In (Lu & Boxue, 2008)(Lu & Boxue, 2008) to study PD in transformers a pattern recognition method using filtering in time-frequency domain is presented. Other signal processing techniques used in the analysis of PD are the Wavelet Transform (WT) and Wigner Distribution (WD). (Ma, Zhou, & Kemp, 2002; Phukan & Karmakar, 2000) and (Caironi et al., 2002) some example of PD study use WT and WD.

The LPFT is a generalization of the STFT which provides better energy concentration and higher resolution using a polynomial in its complex exponent (Sejdić et al., 2009). Additionally, the LPFT can be used to estimate the instantaneous frequency (IF) of a signal and its derivatives (Li et al., 2011). These elements allow the LPFT to determine approximately the time-frequency variations of a signal.

LPFT has been used in several applications such as signal processing of varying signals, singularity detection, radar imaging (Popović, Djurović, Stanković, Thayaparan, & Daković, 2010); (Sun, Wang, Fang, Yang, & Song, 2015), (Thayaparan, Djurovic, & Stankovic, 2006), interference suppression in communications (Stanković & Djukanović, 2005) sonar and the IF estimation (Katkovnik, 1995). However, LPFT has not been used to analysis of electromagnetic interference as the PD. This paper presents an analysis of PD signals using the LPFT. These signals were simulated applying the mathematical model proposed by (Mortazavi & Shahrtash, 2008)-

The rest of this paper is organized as follows: the mathematical structure of STFT and LPFT is described in Section 2. The parameters and model of PD pulses used in simulations are presented in Section 3. In Section 4, the analysis in time domain and frequency domain of PD signals is presented. The time-frequency analysis of PD single-pulse and PD pulse-train using LPFT is described in Section 5. Finally, conclusions are drawn in Section 6.

Theory of time–frequency analysis

Short–time Fourier Transform (STFT)

The STFT is evaluated by applying a suitable windowing function to the original signal and evaluating the conventional Fourier transform (FT) of the resulting length sequence (Katkovnik, 1995). The STFT of the signal $y(t)$ is expressed as follows:

$$Y_h(\omega,t)=\int_{-\infty}^{\infty}\rho_h(u)y(t+u)e^{-j(\omega u)}du \qquad (1)$$

Where ρ_h is a windowing function and h is a length of the window. The spectral content at the point t, defined as periodogram, can be given by:

$$I_h(\omega,t)=|Y_h(\omega,t)|^2 \qquad (2)$$

STFT is simple to implement but it provides low resolution for time-varying signals (Li et al., 2011).

Local polynomial Fourier Transform (LPFT)

LPFT is a generalized form of the STFT and it is a linear time-frequency representation (L-TFR), which is defined as (Katkovnic, 1995):

$$Y_h(\bar{\omega},t)=\int_{-\infty}^{\infty}\rho_h(u)y(t+u)e^{-j\theta(u,\bar{\omega})}du \qquad (3)$$

To calculate the LPFT computationally, it is better to use the following definition:

$$Y_h(\bar{\omega},t)=\sum_{n=-\infty}^{\infty}\rho_h(nT_s)y(t+nT_s)e^{-j\theta(u,\bar{\omega})} \qquad (4)$$

Where y is the signal, T_s is the sampling time of the signal. The function $\rho_h(nT_s)$ is windowing function of length of the window h that formalizes the location of fitting with respect to the center point nT_s. The function ρ_h is a finite support function and must satisfy the following properties used in non-parametric estimation, in particular:

$$\begin{aligned}&\rho_h(u)\geq 0,\quad \rho(0)=\max_u\rho_h(u)\\ &\rho_h(u)\to 0\ \text{ as }\ |u|\to\infty\quad;\quad \int_{-\infty}^{\infty}\rho_h(u)du=1\end{aligned} \qquad (5)$$

Where $u=nT_s$. In (4) the exponential term $\exp[-j\theta(u,\bar{\omega})]$ is the LPFT kernel function defined as:

$$\theta(u,\bar{\omega})=\omega_1 u+\omega_2\frac{u^2}{2}+\cdots+\omega_m\frac{u^m}{m!} \qquad (6)$$

The set of LPFT estimators for IF (first-order) and higher orders is defined as $\bar{\omega}(t)=\big(\omega_1(t),\omega_2(t),\omega_3(t),\dots,\omega_m(t)\big)$, where $\bar{\omega}\in R^m$ and m is the LPFT polynomial order. From the definition shown in (3), it can be concluded that $Y_h(\bar{\omega},t)$ is a periodic function of $\bar{\omega}\in R^m$, with periods equal to $2\pi\, s!/T^s$ with $s=1,2,\dots,m$.

Similarly, to the STFT periodogram (2), which is defined as an energy distribution in the conventional time-frequency plane $t-\omega(t)$, the Local polynomial periodogram (LPP) is defined as an energy distribution in the $t-\bar{\omega}(t)$ space, as follows:

$$I_h(\bar{\omega},t)=|Y_h(\bar{\omega},t)|^2 \qquad (7)$$

The LPP allows to determine the energy concentration distribution and estimate the IF of a signal (Katkovnik, 1997; Li & Bi, 2009). When, $m=1$ the LPFT $Y_h(\bar{\omega},t)$ in (4) becomes to the STFT defined in (1) and $I_h(\bar{\omega},t)$ in (7) becomes to the conventional periodogram presented in (2). However, when m increases, the complexity of the polynomial exponent in (6) also increase. Therefore, the LPFT could be interpreted as an L-TFR that shows an energy distribution in $t-\bar{\omega}(t)$ space with the highest level of detail.

To determine the values of $\bar{\omega}(t)$ at each time, the LPA looks for the highest energy concentration points in the LPP defined in (8), by the following optimization problem (Katkovnik, 1997):

$$\bar{\omega}(t,h)=\underset{\bar{\omega}\,\epsilon\, Q\,\subset\, R^m}{arg\max} I_h(\bar{\omega},t) \qquad (8)$$

The adequate location of the estimators from the LPA is insured through the window function ρ_h. This function only considers the observations in the neighborhood of a "center" point t. There are different ways to solve the optimization problem described in (8).

Simulation parameters

PD single-pulse model

For study and computation of PD signals, single-pulses were mathematically defined for the analysis in time and frequency domain. In this case, the model used in the simulation of PD pulses was a damping oscillatory exponential function defined as follows (Mortazavi & Shahrtash, 2008):

$$x(t) = \begin{cases} Ae^{-(t-t_0)/\tau}\cos(2\pi f_0(t-t_0)) & t \geq t_0 \\ 0 & t < t_0 \end{cases} \quad (9)$$

Where, A is the amplitude of the pulse, t_0 is the time of pulse occurrence, τ is the damping factor and f_0 is the frequency of oscillation. An example of a PD single-pulse signal is shown in Figure 1.

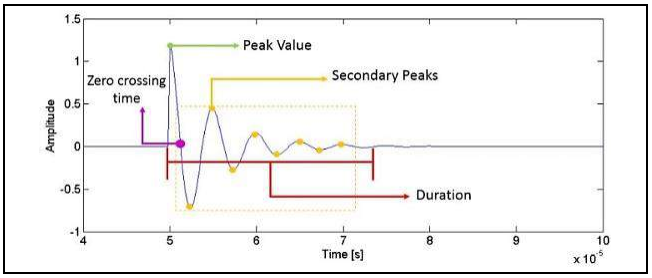

Figure 1. PD single-pulse signal
Source: authors

The characteristics of the PD pulse waveform are defined as:

- Peak value: maximum value of the PD pulse
- Secondary peaks: quantity of positive or negative peaks with amplitudes between the peak value and above 2% of the peak value
- Duration: time period when PD pulse occurs
- Zero crossing time: first point where the signal changes from positive to negative (or vice versa) and the signal value is zero

PD pulse sequence model

Experimental applications provide measurements of sequential PD with different characteristics. In this paper, the pulse sequence (PS) is defined as a pulse train signal consisted by three successive PD single-pulses. This model is given by:

$$x(t) = \begin{cases} A_0 e^{-\frac{t-t_0}{\tau}}\cos(2\pi f_0(t-t_0)) & t \geq t_0 \\ 0 & t < t_0 \\ A_1 e^{-\frac{t-t_1}{\tau_1}}\cos(2\pi f_1(t-t_1)) & t \geq t_1 \\ 0 & t < t_1 \\ A_2 e^{-\frac{t-t_2}{\tau}}\cos(2\pi f_2(t-t_2)) & t \geq t_2 \\ 0 & t < t_2 \end{cases} \quad (10)$$

Where, A_i is the amplitude, t_i is the occurrence time, τ_i is the damping factor and f_i is the oscillation frequency of each single-pulse i that composes the PD sequence pulse. The characteristics of the PD waveform with three pulses is like as the model of one pulse. In this paper, three signals are selected as case studies: two PD single-pulse (PD1 and PD2) and one PD pulse train (PD3). Table 1 shows the variables used in simulations to obtain the PD pulses using (9) and (10). In addition, Figure 2 shows the waveform of PD1, PD2 and PD3 signals.

Table 1 Variables of simulate PD

Variable / Signal	*PD1*	*PD2*	*PD3*
$A\ [p.u.]$	0.8	1.2	$A_1 = 0.8; A_2 = 1.0; A_3 = 1.2$
$t\ [\mu s]$	50	150	$t_1 = 50; t_2 = 150; t_3 = 275$
$\tau\ [\mu s]$	3	7	$\tau_1 = 3; \tau_2 = 3; \tau_3 = 3$
$f\ [KHz]$	300	300	$f_1 = 150; f_2 = 300; f_3 = 260$

Source: authors

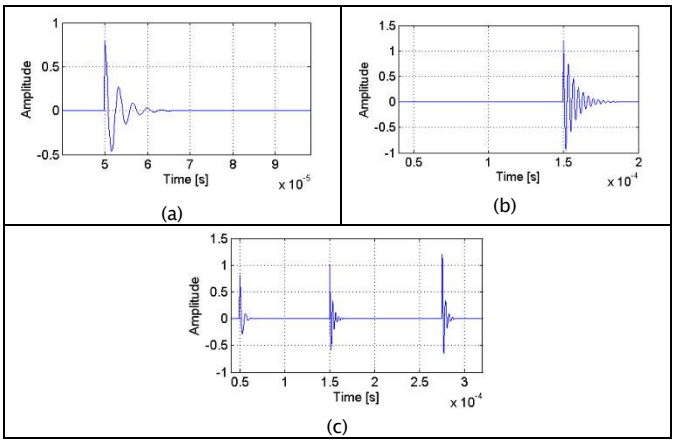

Figure 2. Waveform signals (a) PD1, (b) PD2, (c) PD3
Source: authors

In this work, the PD single-pulse and PD pulse sequence were simulated with a sampling period of $T_s = 0.2\ [\mu s]$. The initial time of PD1 and PD3 is $49.8\ [\mu s]$ and for PD2 is $149.8\ [\mu s]$. The end time of each signal changes. Thus, for PD1 the end time was 99.8 $[\mu s]$, for PD2 was 199.8 $[\mu s]$ and for PD3 was 319.8 $[\mu s]$.

Analysis in time and frequency domain

Analysis in time-domain

In order to obtain the features of PD signals in time-domain a routine in MATLAB © was implemented. This application estimate the peak value (PV), secondary peaks (SP), duration (T) and zero crossing time (ZC) of the PD signals. Table 2 shows the characteristics of PD1 and PD2 single-pulse signals. Comparing the characteristics of PD1 with PD2 it can be observed that both signals have the same frequency (300 kHz) and the zero crossing time is $1 \times 10^{-6}\ [s]$. However, PD1 has fewer secondary peaks than PD2 because the damping factor (τ) of PD1 is also less.

Table 2 Characteristics of PD1 and PD2 signals

Characteristics / Signal	*PD1*	*PD2*
Peak value [p.u.]	0.8	1.2
Peak value time $[\mu s]$	50	150
Zero crossing time $[\mu s]$	50.8	150.8
Secondary peaks	7	12
Duration of signal $[\mu s]$	13	21.2

Source: authors

Characteristics for each pulse that composes the pulse-train PD3 are shown in the Table 3. In this signal, t is constant and the oscillation frequency changes for each pulse (see Table 1). It can be observed that when the frequency of the pulse-train increases the duration and secondary peaks increase too, whereas the zero crossing time decrease.

Table 3 Characteristics of PD3 signal

Characteristics	*Pulse PD3-1*	*Pulse PD3-2*	*Pulse PD3-3*
Frequency (kHz)	150	300	260
Peak value [p.u]	0.8	1	1.2
Peak value time [μs]	50	150	275
Zero crossing time [μs]	51.6	150.8	276
Secondary peaks	2	5	4
Duration [μs]	8,8	9,6	9

Source: authors

Analysis in frequency-domain

The traditional method to analyze signals in frequency domain is the Fourier transform (FT). Figure 3 shows the amplitude of spectrograms for PD1 and PD2. These spectral components are obtained using the Fast Fourier Transformation (FFT), function included in MATLAB©. Analyzing the spectral components of PD single-pulses, the frequency range in which the spectrogram is above 50% of its peak value is from 215 kHz to 410 kHz for PD1 signal and 259 kHz-347 kHz for PD2 signal. However, for both DP signals the peak value of spectrogram is presented at 300 kHz.

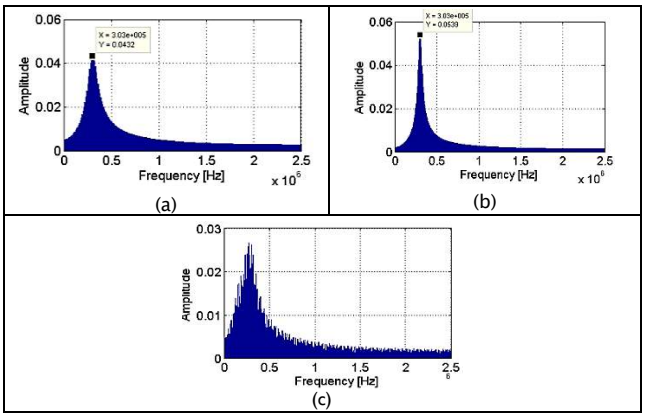

Figure 3. Spectrogram for (a) PD1, (b) PD2, (c) PD3
Source: authors

Figure 3 (c) shows the spectrogram for PD3 signal. It is possible to observe that part of the sequence-pulse frequency is distributed between 130 kHz and 600 kHz, but the frequency of each pulse cannot be identified. For this reason, the spectrogram of each single-pulse is shown in Figure 4.

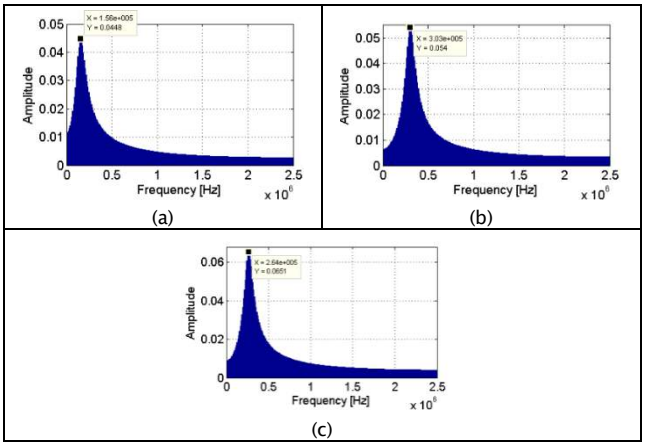

Figure 4. Individual spectrogram for each pulse on PD3 signal (a) pulse PD3-1, (b) pulse PD3-2, (c) pulse PD3-3
Source: authors

It can be observed that peak value of spectrogram for pulse PD3-1, pulse PD3-2 and pulse PD3-3 are presented near to 150 kHz, 300 kHz and 260 KHz, respectively.

Analysis in time-frequency domain

Time-frequency analysis using STFT

In this section the frequency spectra in the time-frequency plane of PD1, PD2 and PD3 are presented. All spectrograms are obtained using a computational application developed by authors. In the first case, STFT was calculated using the LPFT and LPP definitions presented in (4) and (7) with $m = 1$. In all cases, a Gaussian windowing function is used with a bandwidth $h = 250$ samples (duration a 50 μs).

Figure 5 and Figure 6 show the normalized periodogram in two dimensions (2D) for PD1 and PD2 signals, respectively. The predominant energy of PD1 is presented between 240 kHz and 400 kHz at 48 μs-65 μs. On the other hand, for PD2 the frequency is distributed mainly in a range of 230-400 kHz with a time interval of 149.8 μs-160 μs. In both cases the peak value of the periodogram is presented in 300 kHz.

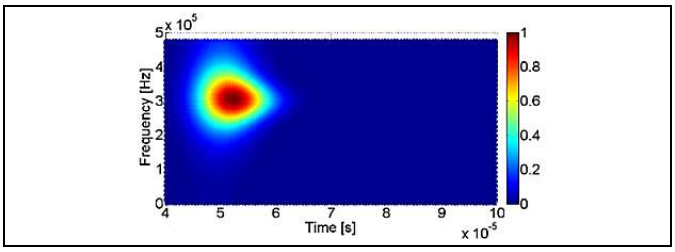

Figure 5. STFT spectrum of PD1 with $\boldsymbol{h = 250}$
Source: authors

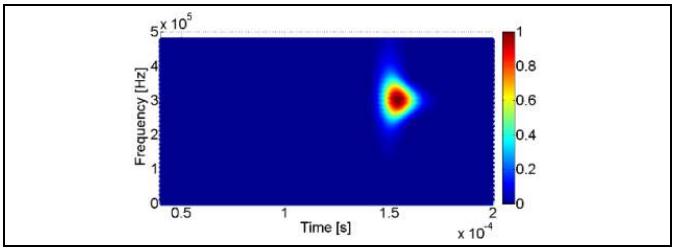

Figure 6. STFT spectrum of PD2 with $\boldsymbol{h = 250}$
Source: authors

Figure 7 shows the spectrum of the PD3 pulse-sequence signal. For PD3-1 pulse the frequency range is between 100 kHz and 200 kHz with a duration of 23 μs (between 40 μs and 63 μs). The periodogram of PD3-2 pulse presents a frequency range of 230-410 kHz in a time interval of 149.8 μs-163 μs. In addition, for the third pulse, the periodogram is located between 274 μs and 288 μs with a frequency range of 180 kHz-400 kHz and a peak value of 260 kHz. Finally, the maximum energy concentration of PD3 sequence-pulse signal is presented in PD3-3, which is the single-pulse that has the highest amplitude of the pulse sequence.

From this time-frequency analysis, it can be concluded that STFT allows to know the relation between time-frequency. However, it not possible to observe low frequency components and the

frequency behavior of signal due to oscillations and ripples related to damping factor. For this reason, this work proposes a time-frequency analysis using LPFT.

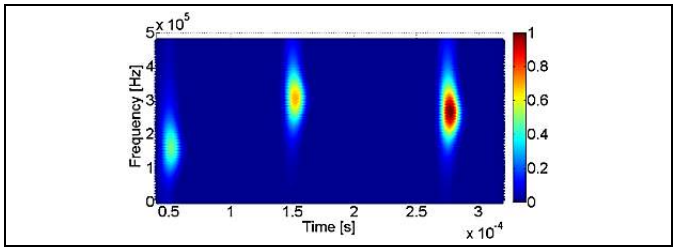

Figure 7. STFT spectrum of PD3 with $\boldsymbol{h = 250}$
Source: authors

Time–frequency analysis using LPFT

In order to promote the advantages and versatility of LPFT, this section presents the analysis of the PD signals using this technique. To estimate LPFT and LPP, definitions in (4) and (7) are applied. However, in this case the polynomial orders were $m = 2$ and $m = 3$. These polynomial orders were selected to reduce the computational complexity, because when m increases the number of operations also increase (Li et al., 2011)

Figure 8 shows the normalized LPP (LPPn) of DP1 signal in 2D. For this PD pulse the LPPn reveals an energy concentration from low frequencies up to 500 kHz. Using both polynomial orders, the peak value of normalized LPP was observed in 300 kHz and located between 51 μs and 56 μs. In addition, LPP shows some lines from low frequency to 250 kHz between 51 and 60 μs. These lines represent the frequency components of the seven secondary peaks (positive and negative) which compose the signal.

It is important to highlight that the energy concentration of the components of low and medium frequency is reduced when signal amplitude decreases. However, when $m = 3$ it is possible to observe that the energy concentration of secondary peaks is increased with respect to the LPP obtained with $m = 2$. In this case, when polynomial order is higher the energy of the signal presents better resolution between 50 and 60 μs.

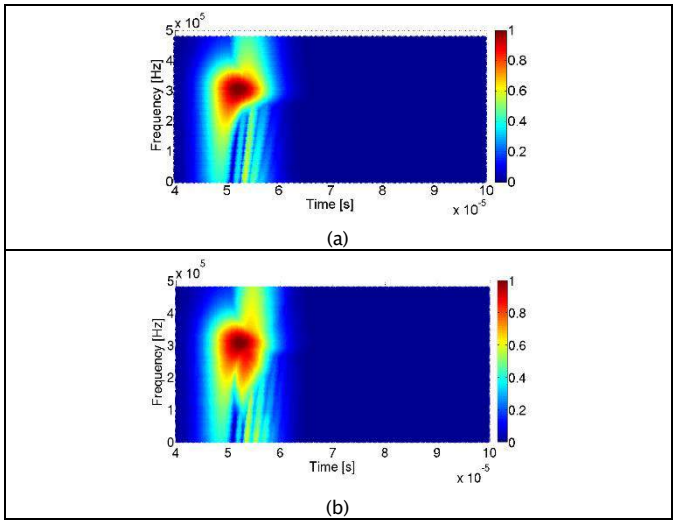

Figure 8. LPP of PD1 with $\boldsymbol{h = 250}$ (a) for $\boldsymbol{m = 2}$ (b) for $\boldsymbol{m = 3}$
Source: authors

The LPPn for PD2 signal is shown in Figure 9. It can be observed that the maximum value of LPP is in 300 kHz at 151[μs]. The energy concentration of DP2 increase from low frequency regions to the maximum value and then decrease. As in PD1 single-pulse, the LPP of PD2 signal shows several lines from low frequency to 300 kHz between 151 μs and 160 μs. These lines are closer to each other due to PD2 pulse varies much faster in time than PD1 signal. Using a polynomial order $m = 3$, the LPP presents a better energy concentration. Furthermore, the frequency spectrum of PD2 signal obtained with a third order LPFT presents components of low and medium frequency (vertical lines between 151 μs-160 μs) with higher energy than those observed in the LPP when $m = 2$.

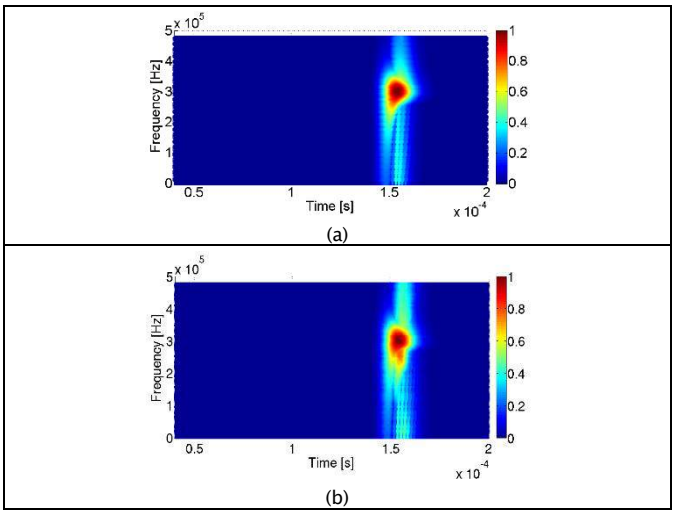

Figure 9. LPP of PD2 with $\boldsymbol{h = 250}$ (a) for $\boldsymbol{m = 2}$ (b) for $\boldsymbol{m = 3}$
Source: authors

Figure 10 shows the LPPn of PD3 pulse-sequence signal. For the three pulses PD3-1, PD3-2 and PD3-3 the LPPn reveals an energy concentration from low frequencies up to 150 kHz, 300 kHz and 260 kHz, respectively. In the case of PD3-1, the frequency range of highest energy concentration is between 120 kHz and 180 kHz with duration of 20 μs (between 40 μs and 60 μs). For PD3-2 the highest energy concentration presents a frequency range of 250-350 kHz in a time interval of 149.8 μs-158 μs. Finally, for third pulse, the highest energy concentration of LPP is located between 264 μs and 280 μs with a frequency range of 200 kHz-300 kHz and a peak value of 260 kHz.

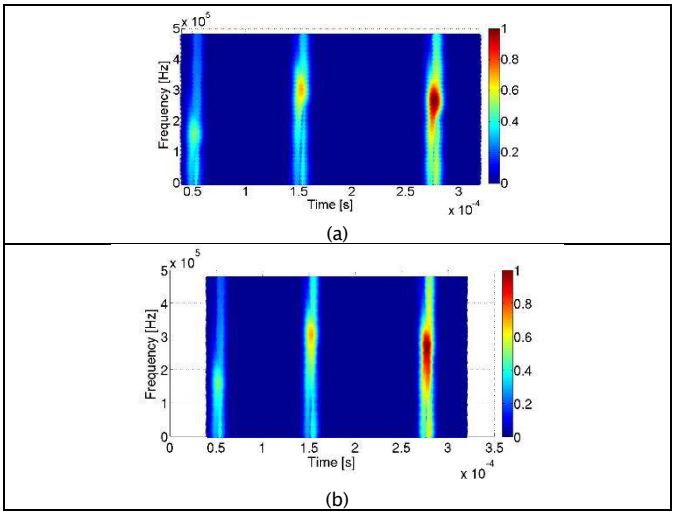

Figure 10. LPP of PD3 with $\boldsymbol{h = 250}$ (a) for $\boldsymbol{m = 2}$ (b) for $\boldsymbol{m = 3}$
Source: authors

Manner similar to the spectrum obtained for single-pulse signals, Figure 10 shows some lines related with low and medium frequency components. These components have frequencies from 200 Hz to the frequency where the LPP is maximum (for three pulses). These lines represent the frequency components of secondary peaks and fluctuations, which compose each pulse. When secondary peaks increase, these components increase too. The energy concentration of these additional components depend on the peak value. Finally, the maximum energy concentration of PD3 signal is presented in PD3-3, which is the single-pulse that has the highest amplitude of the pulse sequence.

Conclusions

In this paper, the process to use local polynomial Fourier transform (LPFT) for analysis of partial discharge pulses was described. This signal processing technique is presented as an effective method in the time-frequency domain to study electrical transient signals. For PD signals this analysis took into account their amplitude, duration, secondary peaks, frequency components and energy concentration.

Main frequency components of the PD pulses in the time-frequency plane can be correctly obtained by STFT and LPFT. However, the LPP provided by the LPFT allows to observe low and medium frequency components (from 200 Hz to maximum frequency of signal) related with the secondary peaks and fluctuations of the DP pulses, which are not detected when the STFT is used. In addition, the LPFT provides the highest energy concentration of PD sequence-pulses.

Finally, simulations show that the LPP of the analyzed PD signals presents a better resolution (in time and frequency) when the polynomial order is $m = 3$. Using this polynomial order the energy concentration of the secondary peaks is increased and the frequency components of the damping oscillatory portion of the PD signal are easier to identify.

References

Caironi, C., Brie, D., Durantay, L., Rezzoug, A., Champigneulles, R., Nancy, U. H. P., … Vandoeuvre, L. (2002). Interest & utility of time frequency and time scale transforms in the partial discharges analysis. In *IEEE International Symposium on Electrical Insulation* (pp. 516–522).

Chai, M. L., Md Thayoob, Y. H., Ghosh, P. S., Sha'ameri, A. Z., & Talib, M. A. (2006). Identification of different types of partial discharge sources from acoustic emission signals in the time-frequency representation. In *Proceedings First International Power and Energy Conference (PECon 2006),* (pp. 580–585).

Katkovnik, V. (1995). A new form of the Fourier transform for time-varying frequency estimation. *Signal Processing*, *47*, 187–200.

Katkovnik, V. (1997). Nonparametric Estimation of Instantaneous brequency, *Statistics & Probability Letters*. *43*(1), 183–189.

Li, X., & Bi, G. (2009). The reassigned local polynomial periodogram and its properties. *Signal Processing*, *89*(2), 206–217.

Li, X., Bi, G., Stankovic, S., & Zoubir, A. M. (2011). Local polynomial Fourier transform: A review on recent developments and applications. *Signal Processing*, *91*(6), 1370–1393.

Lu, Y., & Boxue, D. (2008). Eperimental Study on Pattern Identification of Transformer Partial Discharge by Filtering Method Matching Time and Frequency. *ELECTRIC POWER*, *41*, 16–19.

Ma, X., Zhou, C., & Kemp, I. J. (2002). Interpretation of wavelet analysis and its application in partial discharge detection. *IEEE Transactions on Dielectrics and Electrical Insulation*, *9*, 446–457.

Mortazavi, S. H., & Shahrtash, S. M. (2008). Comparing denoising performance of DWT,WPT, SWT and DT-CWT for Partial Discharge signals. In *2008 43rd International Universities Power Engineering Conference* (pp. 1–6). IEEE.

Phukan, R., & Karmakar, S. (2000). Acoustic Partial Discharge Signal Analysis using Digital Signal Processing Techniques. In *IEE Indian Conference (INDICON)* (pp. 1–6).

Popović, V., Djurović, I., Stanković, Lj., Thayaparan, T., & Daković, M. (2010). Autofocusing of SAR images based on parameters estimated from the PHAF. *Signal Processing*, *90*, 1382–1391.

Sejdić, E., Djurović, I., & Jiang, J. (2009). Time–frequency feature representation using energy concentration: An overview of recent advances. *Digital Signal Processing*, *19*(1), 153–183.

Stanković, Lj., & Djukanović, S. (2005). Order adaptive local polynomial FT based interference rejection in spread spectrum communication systems. *IEEE Transactions on Instrumentation and Measurement*, *54*(6), 2156–2162.

Sun, C., Wang, B., Fang, Y., Yang, K., & Song, Z. (2015). High-resolution ISAR imaging of maneuvering targets based on sparse reconstruction. *Signal Processing*, *108*, 535–548.

Thayaparan, T., Djurovic, I., & Stankovic, L. (2006). Focusing distorted ISAR images using Adaptive Local Polynomial Fourier Transform. *2006 International Radar Symposium*, *1*(2), 2–5.

An Integrated & unified model base approach from design to operation & optimization of power system

Metodología Unificada e Integrada desde Diseño a Operación y Optimización de Sistemas de Potencia Eléctrica

Shaikh Sahid Hossain, *Member, IEEE & Tanuj Khandelwal, Senior Member, IEEE*

Abstract-- With the growth of power system and the maturity of the utility and movement towards smarter grid gives the birth of lots of innovative technologies and applications. Verities of solutions, systems etc. and their respective humungous amount of data, multiple operating system and different data base etc. creates the non-uniformity of usage and differences in data sharing within utility groups hence the challenge in integrated system approach. Traditionally the operational system uses electrical models/data base that differs considerably in detail & structure from the models used during the design and planning stage. Linkage between different models, mapping applications, operational systems etc. are typically not being maintained. Hence the incompatible and different data formats in turn creating the differences in design, engineering, planning, operation & maintenance group and cost in millions of dollars for every upgrade, addition of network, maintaining the system and improving the system for optimization and smarter grid.

Thus there is need of unified approach. This paper describes and examines the complete cycle of power system implementation (from design, planning, GIS, operation, maintenance, optimization, CIS etc.) with unified electrical model & data base approach. The major objective is to have the similar technologies involved at this stage with the one network model sharing approach from power system off line analysis to real time environment for SCADA, Smart Grid, DMS applications by interfacing with GIS & other mapping tools. This will also make the availability of electrical asset at all level. Use of the unified model base approach for the smart grid with real time power analytics solution in DER environment empowers the engineers and operators for taking the right supervisory decision and optimization of electrical system.

Keywords: Power Management, E-SCADA, Model, Smart Grid, DMS, Power Analytics

Palabras Clave: Gerenciamiento de Sistemas de Potencia, SCADA Eléctrico, Redes Inteligentes, DMS, Análisis de Sistemas de Potencia.

I. Introduction

With the ambitious efforts of deployment of the smart grid across the globe with the conventional grid and integrating the newly developed renewable sources and elements like microgrid, a zero-net energy commercial building, Plug-in (Hybrid) Electric Vehicles (PHEV), a wind farm or solar panels etc. puts questions on the data interpretability and ease in integration to realize the objective of a smarter grid. This creates a vulnerable availability of various newer technologies, solutions, platform, interfaces, standards, operating systems, SCADA, DMS, EMS, SAS, Real Time Analytics, decision making tools, M2m, MDAS, GIS etc. with the chaos of mix and match the designer, contractor, engineer, planner, protection, operator, maintenance, asset management etc. falls under the trap of multi-product mix within the utility/industrial Power system.

This aim of this paper is to introduce the unified and integrated model based enterprise solution which provides unified model across different process and stake holders for ease in design to maintain the power system. Also this paper describes and examines the complete cycle of power system implementation (from design, planning, GIS, operation, maintenance, optimization, CIS etc.) with unified electrical model & data base approach. The major objective is to have the similar technologies involved at this stage with the one network model sharing approach from power system off line analysis to real time environment for SCADA, Smart Grid, DMS applications by interfacing with GIS & other mapping tools. This will also make the availability of electrical asset at all level. Use of the unified model base approach for the smart grid with real time power analytics solution in DER environment empowers the engineers and operators for taking the right supervisory decision and optimization of electrical system.

- Emphasis on Power system modelling on design environment
- Integration of Model with GIS for Geospatial view and analytics
- Graduating the as-built model with GIS from Design to Operation
- Operating on top of the electrical GIS model for supervisory control
- Maintenance support & Electrical Asset Information
- Optimization with Power Analytics

II. The Challenge & Deficiencies in Current Practice

The below are the daily challenges and deficiencies seen in the operating conditions:

- Traditionally, Real-Time systems such as SCADA, PMS & DMS use power system models that differ considerably in detail and structure from the models used for offline studies, Analysis and planning

Shaikh Sahid Hossain is with ETAP Automation FZ-LLC (ETAP) DIC-1, Suite 207, Dubai, UAE (e-mail: Hossain.shaikh@etap.com).
Tanuj Khandelwal is with ETAP/OTI, 17 Good Year, Irvine, CA, USA (e-mail: Tanuj@etap.com)

- Linkages between the different models at various stages of projects are typically not maintained, and the different models often have incompatible data formats
- Power system models for real-time systems are typically much simpler than the corresponding representations for offline power flow and dynamics studies
- State estimation is required in order to predict missing measurements.
- Systems that use model calibration methods are ineffective for majority of practical power networks since limited measurements are available
- Identification & automatic filtering of errors in source of measurements
- Different stake holders in the project cycle have spate tools for modelling, engineering, analysis, operation & maintenance hence the chaos of data base incompatibility

In summary there is no fundamental approach for interoperability in single system which can provide the conception to the inception of production. Hence this paper approaches on linking the tools and tackles used at different stages of the project for a unified and integrated model based approach.

Successful power systems engineering projects start at the design stage. Because of the opportunity afforded by "model-based" power system analysis, the choice of a modeling and analysis platform is now a strategic decision with substantial long-term implications. In the model-based world, the one-line model – and all of the intelligent devices within in – functions as a synergistic "ecosystem" of shared data and resources.

III. Description of Electrical Model

Electrical model is a user-friendly intelligent single line diagram interface for creating and managing the network database used for schematic network visualization. The purpose of the model is to supply in concise from the significant information about the system. Traditionally, the importance of different features in a single line diagram (SLD) varies with the problem under considerations, and the amount of information included in the SLD, depends on the purpose which the diagram is intended. For instance, the location of circuit breakers and relays are unimportant in doing a load study. Similarly showing the CT/PT, line, cable, node etc. are unimportant in a SCADA/PMS/DMS system. This is the birth of various model used for many application like planning, study to operation & maintenance.

However the aim of this paper to define the structure where the users can interactively create, analyze, monitor, operate and manage the electrical network as well as execute simulation scenarios, analytics and analyze their results in a simple and intuitive manner in one unified model and database.

IV. Explanation on Project Cycle

Project Cycle	Development Environment
Design	• Intelligent Modeling Environment • Integrated Analysis Tools • Rule-Based Driven Design • Geo-Spatial Data base
Construction	• Engineering & Schematics • Equipment (Load, Cable, etc.) Management • Revisions & Version Control
Commission	• Information Management • Work Flow & Permits • Records Management
Operation	• PMS/EMS/SCADA - Real-Time • Simulation & "What If" Analysis • Automated Optimal Control • DMS & Smart Grid
Maintenance	• Asset Management • Power Management Workflow • Emergency Recovery

In the different project cycle various responsible stake holders get involved from consultant, FEED engineering contractors, EPC contractors, Switch Gear Manufactures, Power Automation Solution provider, then operator & maintenance team. Among the different stake holders, various teams will further engage on execution of the project such as planning, engineering, designing, constructions etc. With the various people involvement it's merely possible to manage the common data base and one single electrical model from start to end. Unless a process and unified solution is being proposed which not only full-fills the unified and integrated model approach but also have rich suite of operational applications and design algorithms.

V. Application Mapping at Each Cycle of Project

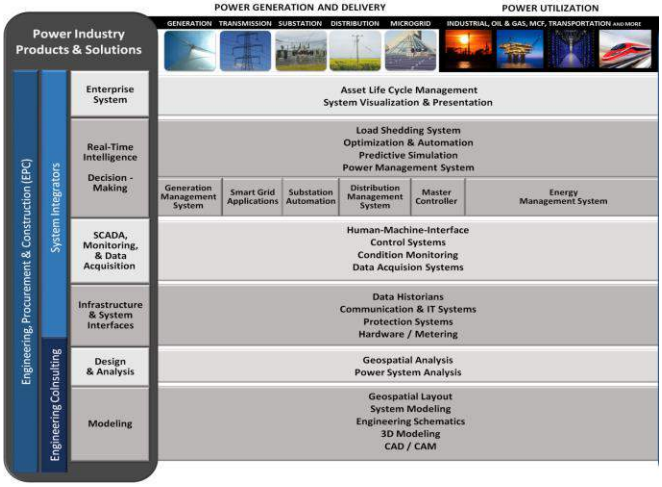

At each cycle the various applications are required as per the above mapping. Thus it's creates multi data base and multi-layer of information. This also complicates the data and model management by all the parties involved in the project.

Thus the need is to have the unified model for ease in design, engineering, analysis and operation.

VI. Approach to Have a Verified and Validated Model

The first thing towards providing an integrated and unified electrical model from design to operation needs a verified and validated model.

- Planning and operating decisions are based on the results of power system simulations & analysis
- Optimistic models can result in under-investment or unsafe operating conditions
- Pessimistic models can also lead to unnecessary capital investment, thereby increasing the cost of electric power
- Realistic & validated models are needed for ensuring reliable and economic power system operation. Hence it is a very crucial phase
- Validate the network model with real-time and/or archived data in order to prepare a benchmarked model used for:
  - Designing, analysis & expansion
  - State estimation & load distribution
  - Monitoring & Control
  - Predictive simulation "what-if"
  - Forensic analysis
  - Global Optimization
  - Proactive contingency analysis & Remedial Actions
  - Embedded Real Time & Historical Power Analytics
  - Model based Automated operation
    - PMS
    - SCADA
    - DMS
    - EMS
    - Smart Grid
    - EMCS
    - SAC
    - SCMS etc.
  - Integrated Asset Information
  - Maintenance Management
  - Used for future planning & expansion
- Observe, Measure, Analyze actual behavior to understand system behavior
- Engineering judgment and generally accepted practices applied to:
  - Measuring or testing components or systems
  - Selecting component models
  - Determining component model constants
  - Tuning the overall system

Validation means confirming that the simulated response (whether for a component or the overall power system) to a disturbance (steady-state or transient) reasonably matches the measured response to a similar disturbance

VII. Migration Journey from Design to Operation with Unified Model

With the approach of ETAP enterprise solution which provides the fundamental applications into the control, protection and management of future power systems with unified approach. Figure 1 provides major strategies through Electrical Transient and Analysis Program (ETAP) enterprise software to graduate from design to operation in a verified and validated model used from design to operation.

The above picture shows ETAP one model approach from intelligent modelling to power system network analysis to protection coordination, transient and finally graduate to operational environment for EMS, PMS, DMS, SCADA etc.

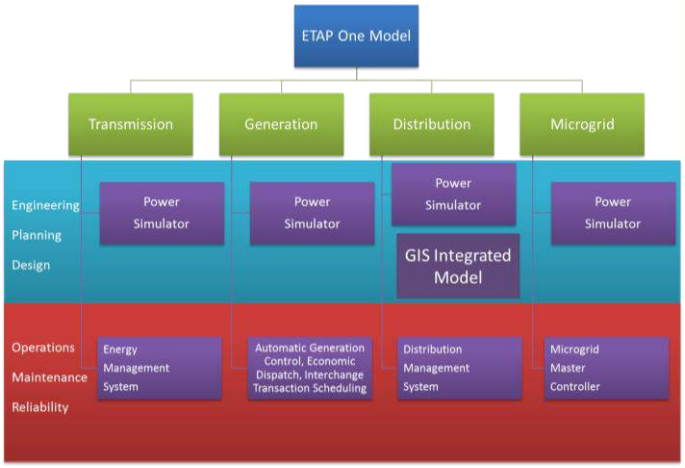

The approach shows the conventional off line power system studies model graduating to the real time operational model by connecting to the existing automation infrastructure or directly with the filed devices to realize the state of art of operational application.

VIII. Step by Step Approach on the Migration

The below figure shows the process flow and conversion of design model to operator and maintenance model with integrated system. The model keeps on updating at each level.

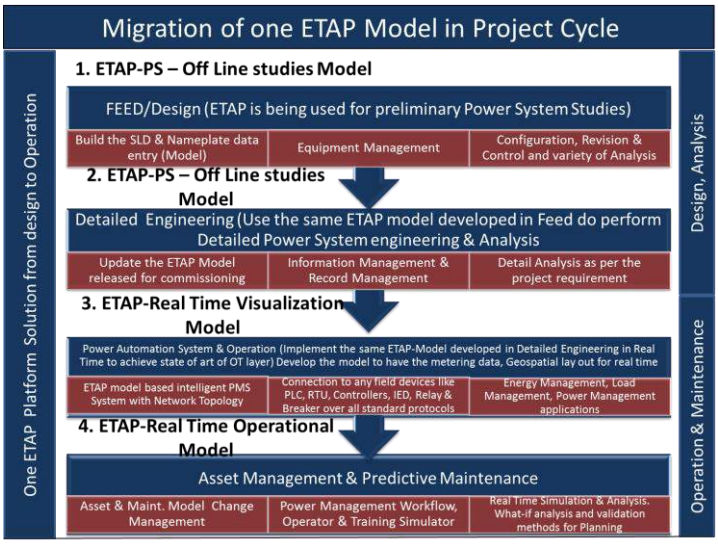

Some of the crucial steps are defined below with the methodology:

1) Model gets generated with inception of the project
2) Same gets updated at detailed engineering level after all studies being completed
3) Model gets created per the industry either as SLD format, equivalent circuit model or geo-spatial diagram
4) The same model gets updated with all the field communicable devices such as breaker, relay, meter, CT, Pt, bus, transformer, sensor etc.
5) The updated model with field devices gets mapped to the actual device for real time data monitoring over various communication protocols
6) Simplified operator views will be created per the project requirement on the same model
7) With the sophisticated operational algorithms the power automation objectives are run on the model to achieve the functional requirements
8) Along with the components characteristics the system also analyzes the reliability and maintenance requirement

Thus by the above explained steps one model gets into various phases by various department to achieve the project objective while maintaining the integrated and unified model approach with high engineering accuracy with less efforts.

IX. Application Mapping in One Model Approach

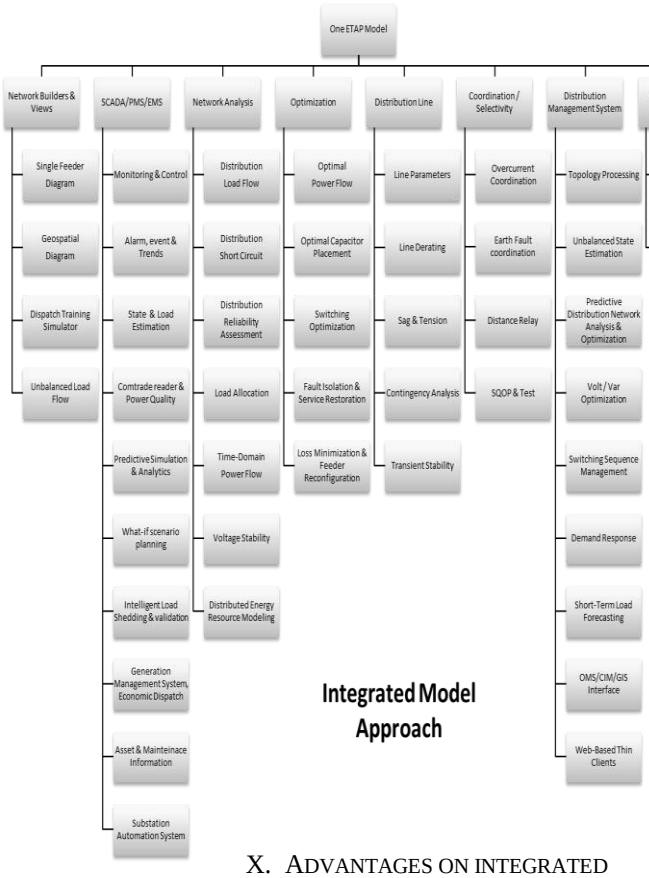

X. Advantages on Integrated Model Based Approach

With the integrated model approach the below advantages could be realized by an engineering construction, consulting & operating company:

- Avoid duplication of data
  - Data is in one location
  - Eliminates man-hours spent synchronizing multiple databases
- Common Graphical Interface
  - Engineers and Operators can become familiar with each other's requirements
  - Eliminates duplicate graphics - CAD, SCADA, Analysis Tools
  - GIS, underground cables, protection, dynamic controls, substation grounding, renewables, distributed generation, logical single line diagram, AC & DC networks
- Connectivity with Real-Time and Built-in Real-Time Applications
  - Complete network predictive simulation can be performed at any combination of system voltage levels
- Reducing IT Burden
  - Managing multiple licenses and software's
  - Integration or Data Adapter maintenance

- Improved operations by close integration of Operational tool with Power Analytics
- Increased operator efficiency with one system, eliminating the need to go to multiple systems with potentially different data
- Integrated security analysis for substation and circuit operations to check for tags in one area affecting operations in the other
- Streamlined login and authority management within one system
- Simplified data engineering via coordination of SCADA point and GIS data changes

Furthermore the below advantages will be realized:

- Bring your designed offline model and integrate with Automation infra for PMS functions with less effort and have the up to date model
- Perform Predictive analysis viz. Load Flow, Short Circuit, Relay Co-Ordination, Transient Stability with online data from the field
- Monitor power system performance & assets for stable operations
- Get to the root cause of process interruptions with historical data with the flexibility to see them in a digital play back mode
- Predict & prevent events before they occur
- Reduce the engineering Man Hour for developing the accurate models and networks as those are readily available from design.
- Support to the operation and maintenance team with switching procedures, work order management, energizing & de-energizing the components/feeders
- Conduct "what-if" analysis for better operation and optimization in cost
- Captive generation at plant then you can conduct the Automatic Generation Control to calculate the demand supply gap and tune your governor and exciter accordingly
- Future expansion power system study will be seamless
- You would have the entire plant's electrical asset information available with their physical and real time attributes
- This will help to achieve the uniformity of operation within your organization from design, engineering, operation, maintenance till finance etc.
- You could always update the advisory mode to Supervisory mode for control operations and achieve the functionalities like: ILS, control, AGC etc.
- Achieve the maintenance information
  - Empower operator with validation tools
  - Operator & Training simulations
  - Decision based on the power analytics
  - Validation of action peace of mind
- SCADA, DMS, Smart Grid & Microgrid operations with the domain knowledge based on model
- Always having updated electrical network information of the plant/facility
- INTEGRATION OF DEPARTMENTS

XI. CONCLUSION

With the approach of integrated and unified model based system from design to operation the biggest benefit is the peace-of-mind of knowing that operational unprecedented predictive analytics and simulation capabilities are at work around-the-clock, protecting you from power problems, even issues that are far in the future.

With one suite of design & operational tool that offers a fully integrated enterprise solution. Through design, analysis, continuous monitoring, simulation, and optimization of electrical, process, manufacturing, and management systems that are in place, this unified model approach with system software can maximize the entire production process, reduce losses, and increase profits.

Using a model based design & Power automation software allows the users to extend the traditional data acquisition systems to an intelligent power software solution for operators, dispatchers, engineers, and decision makers. The robust and proven analysis algorithms combined with portable and flexible foundation provides a highly available Power Automation system, comprehensive modeling environment, operator-friendly user interface, and state-of-the-art power & energy management applications.

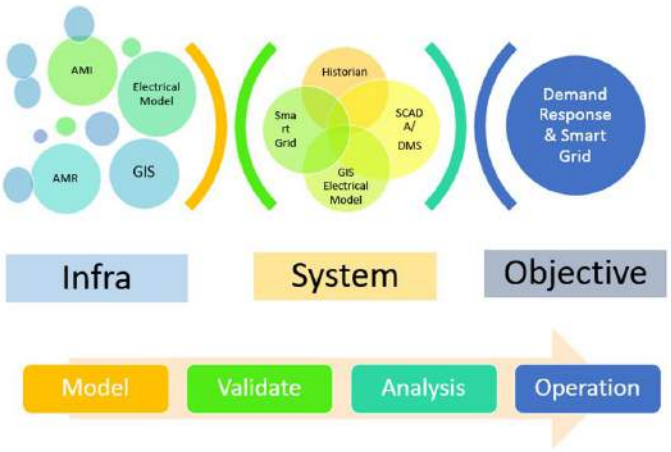

A standard operational system evaluates collected data in a non-electrical system environment without recognizing the

interdependencies of equipment. Extending the power monitoring system by equipping it with an appropriate electrical system model, simulation Modules, and playback routines will provide the system operator and engineer with a powerful new set of approach to a project. Using these tools, the user can accurately design, analyze, and predict the behavior of the electrical system in response to a variety of changes.

Finally, the unified and integrated model approach from design to operation gives the flexibility from thinking, designing, analyzing, implementing, operating, maintaining the electrical system in one environment which is ease in use and sharing and transferring with minimum engineering effort and maximum return.

XII. REFERENCES

[1] Power System Design Basis, Pabla
[2] NERC White Paper

XIII. BIOGRAPHIES

Shaikh Sahid Hossain received his Bachelor's degree in Electronics and Instrumentation Engineering from B.P.U.T, Orissa in 2004 and his Master's degree in Business Administration from Preston University, USA in 2008 followed by Post Graduate Program in General Management from Indian Institute of Ahmedabad in 2009. Before joining ETAP, he worked as a Development consultant at Larsen & Toubro. His projects involved implementation for Power Management System, Process Automation. He was also involved in the establishing the power automation business in MENA & SAARC region. Mr. Hossain has been working as Vice President for MENA & SAARC for the Engineering Consulting Services, Power Automation Solutions and Power System Design department at ETAP since 2010 at Dubai office. His duties involve product architecture design, creating the new process for development of automation solutions, training and pre-sales application engineering for ETAP family of products. He has been a member of IEEE-Smart Grid for over three years and is a working group member of the PCIC-ME.

Tanuj Khandelwal received his Bachelor's degree in Electronics and Telecommunications Engineering from University of Bombay in 1999 and his Master's degree in Electrical Engineering from California State University, Long Beach in 2001. Before joining OTI, he worked as an Associate Engineer at PricewaterhouseCoopers. His projects involved application development for Power Derivatives in a deregulated market. He was also involved in the Operating Procedures Audit of CAISO in 2001 and worked on streamlining power contracts for Nevada Power. Mr. Khandelwal has been working as an Electrical Engineer for the Engineering Consulting Services department at OTI since 2001. His duties involve algorithm design, testing, engineering and software support, training and application engineering for ETAP family of products. He has been a member of IEEE for over five years and is a working group member of the IEEE Std. 739 (Bronze Book), IEEE Std. 551 (Brown Book) as well as a member of the IEEE Rail Transit Vehicle Interface Standards Committee.

Analysis of technical and economic feasibility for the implementation of a power generation system using wind energy in the Paraguayan Chaco

Análisis de prefactibilidad técnica y económica para la implementación de un sistema de generación de energía eléctrica utilizando energía eólica en el Chaco paraguayo

Mitjans Felipe: engineer, Universidad Nacional de Asunción, Paraguay; Master of Science, Universidad Politécnica de Cataluña, España

Pulfer Jean-Claude: engineer, Swiss Federal Institute of Technology Lausanne, Switzerland; Master of Science, Swiss Federal Institute of Technology Zurich, Switzerland

ABSTRACT

This article aims to present a new and sustainable approach focused on power generation from wind in Paraguay, specifically in the Western Region. In this context is presented an analysis of technical and economic feasibility, whose results are based on a study of the wind resource available in the region, using for this purpose a weather station mounted in the location *La Patria*. The wind data measured at a height of 10 m above the ground were then extrapolated to a height of 80 m using mathematical models available in literature. Finally, these data were correlated with those from the weather station of the location *15 de Agosto* obtained by Baez (2011), considering a frequency of 30 min. between the measurements. The results of the assessment have demonstrated the feasibility of installing a system of wind generators able to produce an electric output of 46 MW, operating with a capacity factor of 25%. The results have been consistent with studies that support the future wind farm of 49 MW projected in the Department of Tarija (Bolivia), located at the same geographic latitude as *La Patria*, even considering that the wind resource in the last location has been measured only during a four months period (November 2012 to February 2013), which corresponds to a period of year with relatively low wind speeds. In order to conduct a more comprehensive analysis of technical and economic feasibility, this paper presents a technical study using the computer simulation tool MatLab/Simulink and the RETScreen software. The analysis by simulations considered a realistic scenario assuming that the wind generator system is connected to the national grid (SIN), after the construction of a 220 kV transmission line from the place of generation to the transformer station of *Loma Plata*. For the economic analyses have been taken into account the benefits and incentives associated to such generation projects regarding to carbon credits for CDM projects (Clean Development Mechanism). As an alternative has also been discussed the negotiation of Certified Emission Reductions CER and finally has been considered the possibility of a governmental contribution for implementing this kind of projects.

Keywords: *Wind power generation- renewable energy - MatLab/Simulink - RETScreen.*

RESUMEN

El presente artículo tiene como objetivo presentar una propuesta novedosa y sustentable enfocada en la generación de energía eléctrica a partir del recurso eólico existente en el Paraguay, específicamente en la Región Occidental. En este contexto se presenta un análisis de prefactibilidad técnica y económica, cuyos resultados han sido sustentados en base al estudio del recurso eólico disponible en la región utilizando para el efecto una estación meteorológica montada en la localidad *La Patria*. Los datos medidos a una altura de 10 m sobre el nivel del suelo han sido extrapolados a 80 m utilizando modelos matemáticos disponibles en la literatura. Finalmente fueron correlacionados con los datos de la estación meteorológica de la localidad *15 de Agosto* obtenidos por Báez (2011), considerando una frecuencia de 30 min. entre las mediciones. Los resultados del análisis han demostrado la factibilidad para la instalación de un sistema de generación eólica capaz de producir una potencia eléctrica de 46 MW, operando con un factor de planta de 25%. Los resultados son coherentes con los estudios que sustentan el futuro parque eólico de 49 MW proyectado en el Departamento de Tarija (Bolivia), situado en la misma latitud geográfica que *La Patria*, aun considerando que el recurso eólico en esa última localidad ha sido medido por un periodo de solo cuatro meses (Noviembre de 2012 a Febrero de 2013), los cuales corresponden a una época del año con velocidades de viento relativamente bajas. A fin de realizar un análisis de prefactibilidad técnica y económica más abarcante, este artículo presenta un estudio técnico utilizando la herramienta de simulación computacional MatLab/Simulink y el software RETScreen. El análisis mediante simulaciones considera un escenario realista asumiendo que el sistema eólico se encuentra conectado al Sistema Interconectado Nacional (SIN), previa construcción de una línea de transmisión de 220 kV desde el punto de generación hasta la estación eléctrica de *Loma Plata*. Para el análisis económico se han tenido en cuenta los beneficios e incentivos asociados a este tipo de proyectos de generación, en lo que respecta a los bonos de carbono para proyectos del tipo MDL (Mecanismo de Desarrollo Limpio). Además, ha sido analizado como alternativa la negociación de Certificados de Emisiones Reducidas CER y finalmente ha sido considerada la posibilidad de un aporte estatal para la implementación de este tipo de proyecto.

Palabras clave: *Generación de energía eólica – Energías renovables –MatLab/Simulink – RETScreen.*

Received: Juny 19th 2015
Accepted: Oct 15th 2015

1. Introduction

We are observing growing global climate problems due to the excess of emitted greenhouse gases to the atmosphere and the lack of commitment by the developed countries to comply with the Kyoto Protocol. Therefore, the search for energy alternatives, like the renewable energies, can help to mitigate these problems. Countries like China, the USA and some European countries are currently developing the use of technologies based on renewable energy resources. Currently, only 13.5% of primary energy supply worldwide and 22.2% of electricity generation is from renewable sources (IEA, 2014).

In South America Brazil stands out as one of the countries with the greatest innovation in technologies associated with renewable energy, followed by Argentina and Uruguay. Latin America invested in renewable energy in 2013 US$ 15.5 billion, a small amount compared to the USA, China and Europe which invested US$ 35.8, 56.3 and 48.4 billion respectively. Paraguay's energy matrix is characterized by a high primary supply of renewable and local sources, particularly hydropower and biomass. According to the national energy balance of 2014, 57% of the energy offer corresponded to hydro, 27% to biomass and the remaining 16% to hydrocarbons, which are 100% imported (VMME, 2015). Recent prefeasibility studies have shown that the energy matrix of Paraguay could be diversified with other methods of generating electricity. Even decentralized and distributed generation could be viable getting a decrease of losses in the transmission lines, as generation would be closer to load demand. One of these viable alternatives is wind power. The zones of the highest wind potential in Paraguay are the north of the Chaco, as well as the northeast, center-west and southeast of the oriental region. However, there is still no reliable evaluation of this potential, such as a wind map based on quality measurements. National authorities are currently promoting projects for studies in this area. On the other hand in Paraguay there are considerable limitations for the installation of large-scale wind power systems with high profitability due to a lack of energy policies that would strengthen the act No. 3009/06 about "Independent Production and Transport of Electric Power", especially regarding differentiated tariffs for generated electricity. In order to remedy this situation was recently submitted to Congress a bill on renewable energy, which should create favorable legal and economic conditions for the development of all types of renewable energies in Paraguay. Between a possible strength that raise this paper it exists a new macro-energetic scenario, which inserts innovation to the current energy matrix, promoting decentralization of the load demand, improving the quality of life of the population of the Department of Boquerón, the area that has been considered for the feasibility study of the integration of wind technology. Taking into account the natural growth of the area of the Mennonite colonies in the Central Chaco, future implementation of wind power systems proposed in this paper would generate a positive impact to the Paraguayan Power System through a considerable power relief in the Northern Transmission Line System.

2. Wind Potential in Paraguay

Paraguay winds are characterized by three main phenomena, namely:
1. The flow from high pressure centers on the western edge is controlled by the South Pacific anticyclone and the eastern part is controlled by the South Atlantic anticyclone.
2. The Andes and the Altiplano are acting as a barrier, suppressing winds from the west throughout the country.
3. The generated wind is depending on the intensity of the quasi-stationary low-pressure center in the Chaco (Brizuela et al., 1997).

As a result of the convergence of the phenomena mentioned above there are generally low wind speeds throughout the year mainly in the eastern part of Paraguay, belonging to the high pressure zone. On the Paraguayan and Argentinian Chaco and the Pampa lands is located an almost stationary low pressure system. In winter, when the low pressure zone is located on the Paraguayan Chaco, winds are blowing from the eastern sector rotating to northeast in the center of Paraguay, as can be seen in Fig.1.

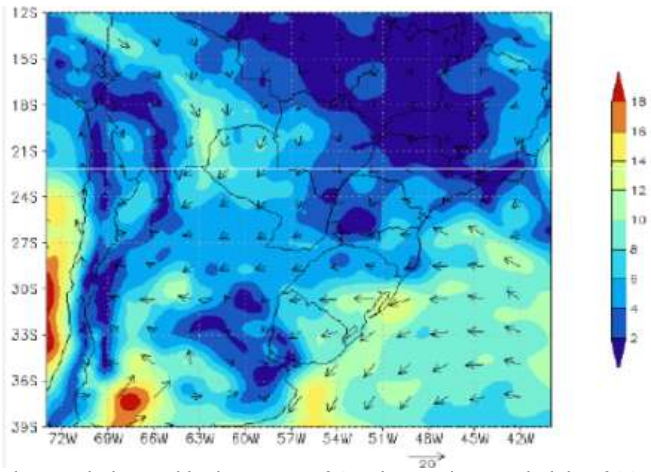

Fig. 1: Wind speed in the center of South America at a height of 30 m above the ground in m/s, Source: DINAC, 2013.

Fig. 2: Location of the main weather stations in the measurement area, Source: Google Earth and own.

In summer, the southernmost location of the depression centered over the mountainous Pampa area produces northern and northeastern winds in the Paraguayan Chaco. There is a huge seasonal variation of the wind in this area. Peaks are expected during the months of August to December due to the rapid heating of the area (Brizuela et al., 1997).

2.1. Weather Station of *La Patria*

The weather station of *La Patria* was installed in November 2012. It is located in the western region, specifically in the Department of Boquerón at a distance of approximately 130 km northwest of the city of *Mariscal Estigarribia* and about 500 km northwest of the capital Asuncion (see Fig. 2) .The instruments have been provided by the Center for Appropriate Technology (CTA) of the Catholic University of Asuncion (UCA).

Both the anemometer and the wind vane were calibrated and synchronized for a measurement range of an average speed and an average wind direction with measuring frequency of 30 min. Both instruments have been installed by the staff of the National Direction of Civil Aeronautics (DINAC) on a mast 10 m above ground. Data have been stored in a data logger and then processed in a computer.

The wind speed data have been transmitted per GPRS to a central database (FECOPROD, 2012). To get the values of wind speed at a height of 80 m the measured values were extrapolated using Equation (1) taken from Villarrubia, 2014.

$$v_{80} = v_{10} \frac{ln(^{80}/_{z_0})}{ln(^{10}/_{z_0})} \qquad (1)$$

v_{80} and v_{10} represent the wind speed at a height of 80 m and 10 m above ground respectively (in m/s), and z_0 the roughness length downwind considering in this case a value of 0.28 m (Villarrubia, 2014).

Fig. 3 shows the wind rose of the *La Patria* weather station during the measurement period. It can be seen that the prevailing winds are blowing from the northeastern sector (NE) to east- northeast (ENE), which occurred in daytime with a weight of 21 and 25% respectively for The total of all measurements processed during the four months measured. In the schedule nocturne los prevailing winds are from the west (W) south-southwest (SSW) with a weight ranging between 5% and 7%. This abrupt change in wind direction is due to pressure changes atmospheric entre day and night generated by temperature changes. During the day the room temperature is increasing together with an increase in wind speed. At night the reverse process occurs.

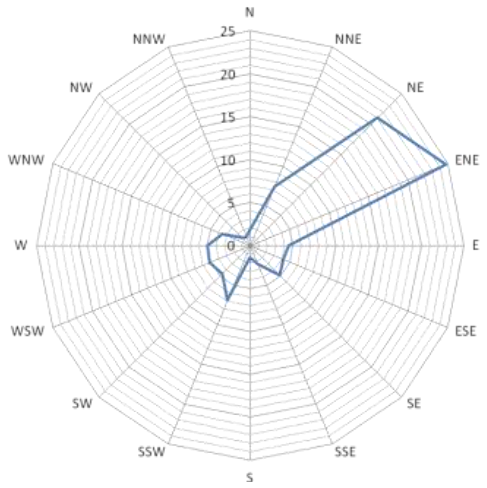

Fig. 3: Wind rose of La Patria. Source: Mitjans, 2013

Fig. 4 shows that the average hourly wind speed during the measurement period increases during the day from 7 a.m. reaching its maximum value of 16 m/s at around 4 p.m. and decreasing sharply overnight reaching minimum of 7 m/s. The average speed for the four months of measurement extrapolated to a height of 80 m was 11.2 m/s. However, it is worthy to mention that the measurements were performed during the year period with the lowest wind speeds. The annual average would then be higher than the mentioned value.

Comparing the results of the *15 de Agosto* weather station made by Baez (2011) (see Fig. 5) with the ones of *La Patria*, it can clearly be seen that the average wind speed in *La Patria* is higher than in *15 de Agosto* throughout the whole measurement period. This confirms that there is a higher wind potential in the northwestern Chaco than in its central part making it very likely the feasibility to install a large scale wind generation system.

Fig. 4: Average hourly wind speed between November 16th, 2012 and February 16th, 2013 in *La Patria*. Source: Mitjans, 2013

However, there is some uncertainty as wind speed data along a one year period are not available for none of the weather stations of the studied area. So, mathematical models had to be used to be able to get a clearer view. In Bolivia, specifically in the Department of Tarija, located on the same latitude as *La Patria*, after the recently concluded yearlong wind measurement campaign at a height of 80 m, it is planned to install a 49.5 MW wind farm, what reinforces the hypothesis of the trend, that wind speed increases in the area of the Department of Boquerón from east to west (Evwind, 2013).

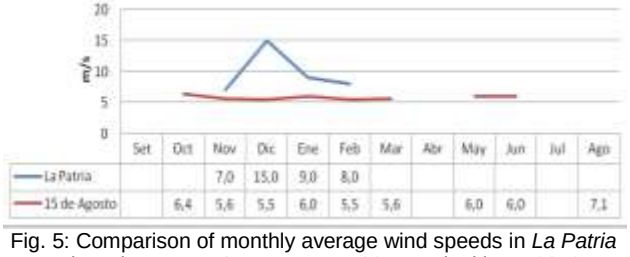

	Set	Oct	Nov	Dic	Ene	Feb	Mar	Abr	May	Jun	Jul	Ago
La Patria			7,0	15,0	9,0	8,0						
15 de Agosto		6,4	5,6	5,5	6,0	5,5	5,6		6,0	6,0		7,1

Fig. 5: Comparison of monthly average wind speeds in *La Patria* and *15 de Agosto*. Source: Baez, 2011 and Mitjans, 2013.

In order to develop a mathematical model to estimate the nonlinear behavior of the average wind speed between the two stations, have been processed separately the monthly data of the *La Patria* weather station measured between November 16th, 2012 and February 16th, 2013 and of the *15 de Agosto* weather station measured between December 10th, 2008 and October 24th, 2010. Data are missing for several months to complete one year due to faulty measuring equipment (see Fig. 5). However, the results obtained by mathematical and statistical models help to confirm, that the minimum annual average wind speed at a height of 80 m above the ground is about 7 m/s, representing an annual average power of 325 W/m^2.

The correlation rate between the two stations is 77% with a standard deviation of 5.13% and a variance of 26.36%.The sudden change of wind speeds due to the change of atmospheric pressure and temperature between day and night forms ridges in the frequency distribution of wind speeds, a behavior that is outside the Weibull distribution (see Fig. 6).

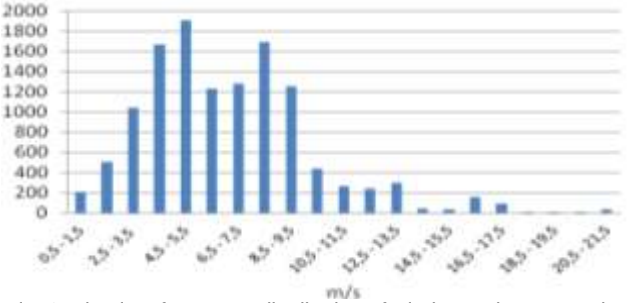

Fig. 6: Absolute frequency distribution of wind speed at *La Patria*. Source: Mitjans, 2013

The asymmetry factor k of the Weibull function is obtained by the empirical equation (2), where v is the annual average wind speed:

$$k = 0.73\, v^{0.5} \qquad (2)$$

The scale factor c of this function is obtained by equation (3):

$$c = \frac{v}{\Gamma\left(1+\frac{1}{k}\right)} \qquad (3)$$

Fig. 7 shows the Weibull distribution density p(v) from equation (4) for different typical asymmetry factors k comparing them with the distribution of the processed measured values of *La Patria*.

$$p(v) = \frac{k}{c}\left(\frac{v}{c}\right)^{k-1} e^{\left(-\frac{v}{c}\right)^{k}} \qquad (4)$$

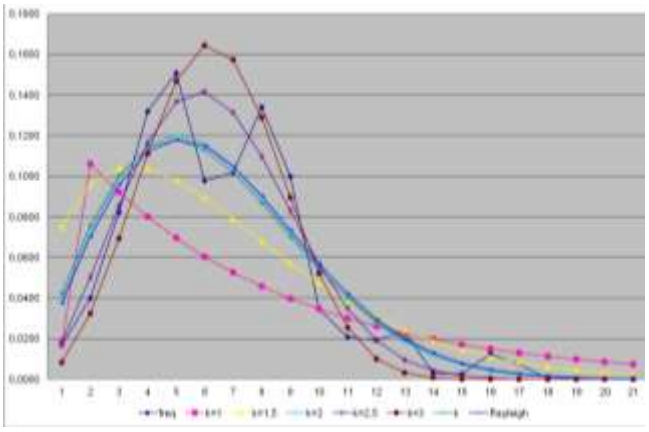

Fig. 7: Weibull distribution for different k factors and the wind speeds distribution measured in *La Patria*. Source: Mitjans, 2013

Based on the analysis performed with the RETScreen software has been selected a three-bladed variable pitch wind generator with a power rating of 2.3 MWe, a cut-in speed wind of 3 m/s and a rated wind speed of 9 m/s. These data are consistent with the wind profile measured by the different meteorological stations used as a starting point for the development of the present study. The wind farm will have an installed capacity of around 46 MW composed of 20 turbines mounted on 80 m high towers. It would have a capacity factor of 25% and an annual generation capacity of 100.5 GWh. Inside each wind turbine the voltage level is lifted from 0,69 to 30 kV. When operating off the national grid, they will be connected by autrotransformers to a 30/23 kV station to be installed at a 30 km distance from the point of generation. When operating connected to the national grid (SIN), the voltage levels of the single-phase transformers would be 30/220 kV. In this case a 130 km long overhead transmission line of 220 kV single circuit will be necessary from the site of the wind farm to the existing transformer station of *Mariscal Estigarribia*, which will have to be modified to operate at a voltage level of 220 kV (Ande, 2013 and Mitjans, 2013).

3. Western System of the Paraguayan Grid

Noting the extensive length between the points of generation and consumption of energy, specifically in the Western Region, this paper aims to propose a new macro-energy scenario with regard to the implementation of emerging technologies for power systems. By this mean could be solved partially the problems that might arise in a not too distant future, considering the rate of annual growth and the imminent use of all available energy from the 2 binational hydropower plants by 2030 (GIZ, 2013) .

Fig. 8 shows the projections of the energy demand of the Western System in a medium term (2013-2022), seen from the *Loma Plata* 220 kV station, which supplies the whole Central Chaco area, with the cities of *Loma Plata, Filadelfia, Neuland* and *Mariscal Estigarribia* having actually a load factor close to 70% and an annual growth rate of 10% (Ande, 2013). This projection demonstrates the limits to cover the estimated demand, considering that the amount of energy to be generated by the wind farm represents 67% of the amount of energy needed to cover the entire energy demand in 2013 (see Fig. 8).

Based on this premise this paper raises two possible scenarios. The first is based on the operation of the wind farm as a generation system isolated from the distribution grid. The second presents an wind power system connected to the national grid (SIN), given that the construction of a second 220 kV overhead transmission line to the *Loma Plata* station is planned only for 2021, after terminating of two overhead 500 kV transmission lines to the *Villa Hayes* station, one from Yacyreta and another from Itaipu (Ande, 2013).

.

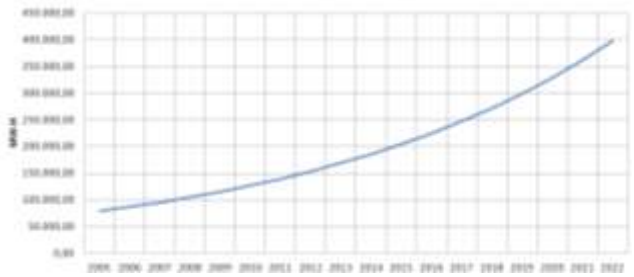

Fig. 8: annual energy demand of the Western System. Source: Ande, 2013 and Mitjans, 2013.

The main advantage associated to the implementation of such emerging technologies for power systems is, that the power transformer at the 220 kV *Loma Plata* station will operate with less load. This will benefit the voltage profile at the bars of the Northern System and will reduce the technical energy losses of the 220 kV transmission line between *Vallemí* and *Loma Plata*, given the extensive length of 200 km between both stations and the high impedance on this line (Ande, 2013).

4. Analysis by simulations

Using data obtained by the analysis performed with the RETScreen software has been developed an analysis by simulation using the Matlab/Simulink software tool. In this simulation environment results are obtained using a variable-step simulation considering the integration method based on implicit Runge-Kutta formula (ode23tb). The block diagram represents the wind farm interconnected to the national grid (see Fig. 9 (a)). To simplify the analysis by simulations were considered the installation of three groups of wind turbines of 15 MW each providing a total power source close to the 46 MW calculated with the RETScreen software. These are connected to a 30 kV output bar to make possible the power export on a 220 kV line of 130 km from the wind farm installed in *La Patria* to the *Mariscal Estigarribia* station.

The wind turbines use squirrel cage induction generators and the reactive power absorbed by each induction generator is compensated by a capacitor bank (400 kvar by each group of 15 MW) connected to a low voltage bar (B690) (see Fig. 9 (b)). The generator stator is connected directly to the mains of 50 Hz. The generator rotor is coupled to the variable speed wind turbine. A Proportional-Integral (PI) controller is used to control the pitch angle of the blades of the wind turbines to limit the power output at the rated mechanical power. The block diagram of the PI controller is shown at the bottom of Fig. 9 (a).

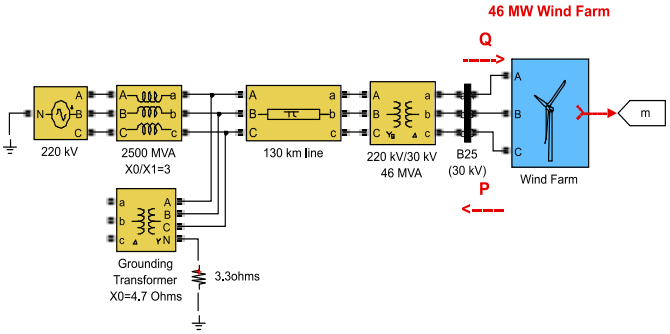

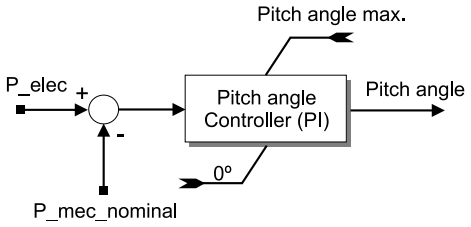

(a) Above: General scheme.
Below: Diagram of the blades' pitch angle control

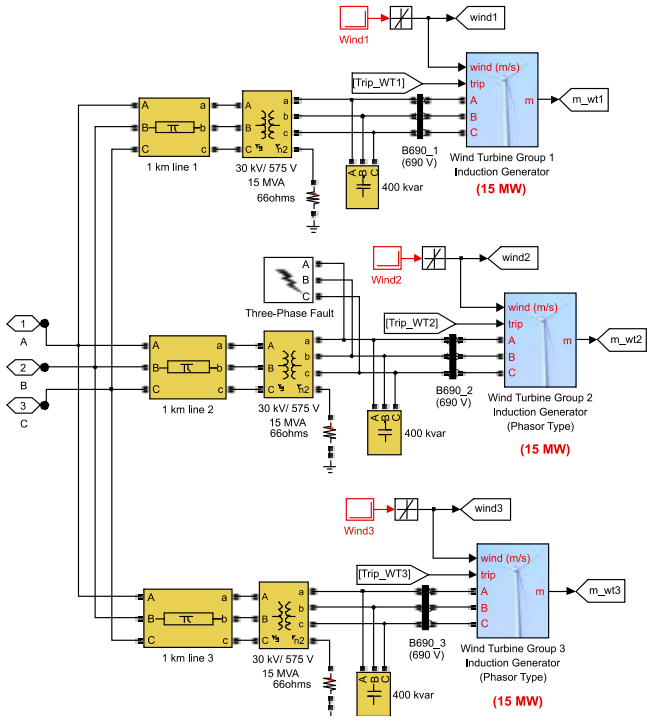

(b) Wind turbines grouped into three groups of 15 MW.

Fig. 9: Block diagram of wind farm interconnected to the national grid (SIN). Source: own elaboration

The characteristic curves describing the variation of the mechanical power as a function of turbine speed for wind speeds within a range of 4 to 10 m/s is shown in Fig. 10(a). It shows, that the wind speed to obtain the nominal mechanical power (1 pu = 15 MW) is 9 m/s.

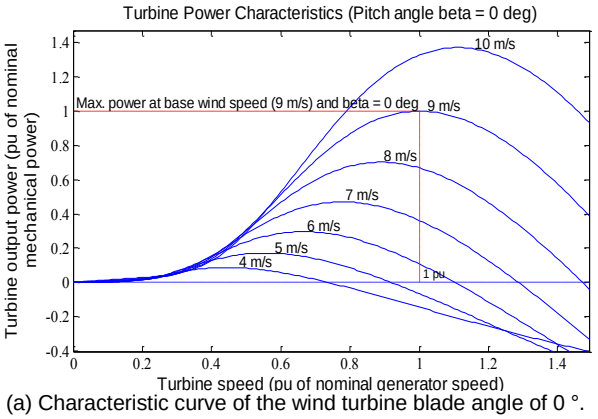

(a) Characteristic curve of the wind turbine blade angle of 0 °.

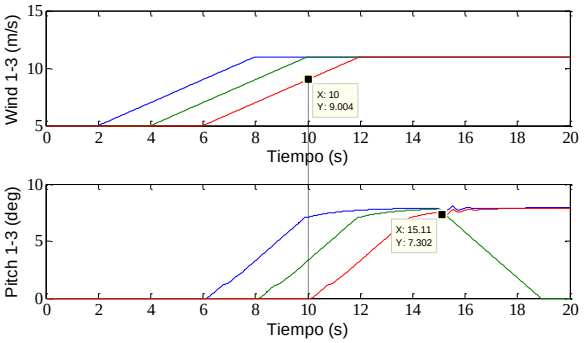

(b) Changes in wind speed and their effect on the pitch angle of the blades.

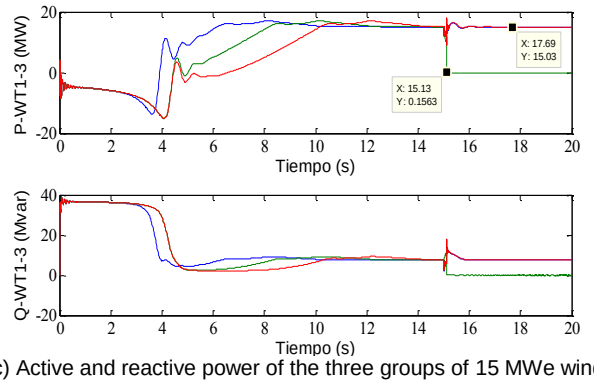

(c) Active and reactive power of the three groups of 15 MWe wind turbines.

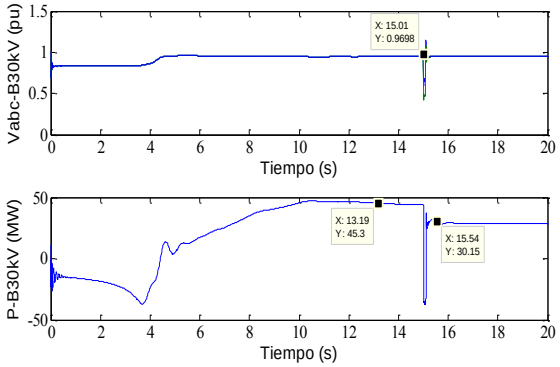

(d) Voltage and active power variations at the 30 kV bar.

Fig. 10: Analysis of the proposed scheme by simulations interconnected to the SIN. Source: own elaboration

In order to verify the results when considering a realistic scenario of variable wind speeds fluctuating around the average speed measured in *La Patria* (equivalent to 7 m/s), was simulated the response of the wind power system by checking the stresses on the 30 kV bar under variable wind conditions. Initially, the wind speed applied to each group of turbines was fixed to 5 m/s. Then, from a time equal to 2 s (for the particular case of group 1) the wind speed was increased from 5 m/s to 11 m/s in a time interval of 3 s. The same wind gust is applied to the wind turbines of group 2 and 3 with a delay of 2 and 4 s respectively (see Fig. 10(b)). In this figure can also be seen that the blades are held constant at an angle of zero degrees, when the electrical power output is far below its nominal value. When the output power is increased above its nominal value as a result of an increase in wind speed, the PI controller acts on the control variable (angle of the blades of the turbines) in order to compensate the increased power maintaining the output power controlled on its nominal value (15 MW by group, see Fig.10(c)).

To verify the effect that introduces a temporary malfunction of one group of turbines, it has also been simulated the effect of a fault on the low voltage terminals of turbine group 2 (see Fig. 10(b) block Three-Phase Fault), applied to a time of 15 s. It can be seen in Fig. 10(c), that under these operating conditions the group 2 automatically protects itself leaving to provide active and reactive power to the 30 kV bar. Finally, Fig. 10(d) shows the voltage changes in the on the 30 kV bar, where can be seen that under normal operating conditions the bus voltage is close to 0.97 pu. The evolution of the total power of the 30 kV bar can also be observed, which reaches the maximum value (close to 46 MW) after 10 s and that when registering the temporary power failure is reduced to approximately 30 MW by effect of the protection of the wind turbines, that make up the group 2.

5. ECONOMIC CONSIDERATIONS

Assuming the considerations that have been brought out in this paper, with respect to the installed power of 46 MW and the amount of 20 2.3 MW wind turbines, a total investment of about US$ 110,000,000 is estimated. Considering an own contribution by ANDE of about US$ 20,000,000, an external financing of about US$ 90,000,000 would be required. In the amount of the investments mentioned above, have been considered the benefits provided by Law Nº: 60/90 on the promotion of investments. For this type of projects based on renewable energies and energy efficiency there are available funds with very low interest rates and flexible repayment periods. For the profitability calculations an interest rate of 1% per annum and a grace period of 2 years was considered.

The economic analysis shows, that the investment required for the commissioning of the 46 MW wind farm would be repaid by an energy sales selling price of 200 US$/MWh, the equivalent of US$ 21,000,000 annually. On the other hand, being a renewable energy project it could benefit from the Clean Development Mechanism (CDM). However, since it is currently paralyzed by the countries which signed the Kyoto treaty, until the agreements of DOHA 2012 will be ratified, it will not be possible to issue and sale of Certified Emission Reductions CER (Mitjans, 2013). Taking this point as background, the economic viability could be supported by the Voluntary Carbon Market, which has actually a value of 3 US$/ tCO_2 (EU.ETS Carbon Price, 2013). Considering as baseline a natural gas power station with the same power using 75% of the generated energy to be equivalent to the amount of carbon dioxide not emitted into the atmosphere, it could be generated an additional annual income of about US$ 235,000 (Olade, 2003).

Additionally, in the international market for this kind of projects are considered governmental subsidies of around 15 US$/MWh, what represents an additional income, that could eventually repay the investment within a reasonable period, reaching thus a total annual income of US$ 23,000,000. For a plant factor of 25% investments could be amortized within 10 years resulting in an IRR of 8.23% and a NPV of US$ 89,000,000. Taking the same criteria mentioned above with a plant factor of 50% a total annual income of US$ 44,000,000 would be generated and investments could be amortized over a period of 4 years resulting in an IRR of 26.08% and a NPV of US$ 396,000,000. This analysis demonstrates the feasibility of the project.

6. CONCLUSIONS AND RECOMMENDATIONS

Despite the incomplete data on wind speed at the site of measurement in *La Patria* it was found by the present study that the installation of a 46 MW wind farm is technically and economically viable. To prove it in a more forceful way, it would be necessary the realization of a full year lasting measurement campaign, preferably at 80 m height. Besides, the enactment of the law of renewable energy currently under consideration in Congress would create a legal framework and favorable economic conditions for this endeavor.

References:

IEA: Key World Energy Statistics, 2014

A. Brizuela, J. Benítez y M.E Castell: El recurso eólico en Paraguay, Fondo Argentino de Cooperación Horizontal, Instituto Nacional de Tecnología, Normalización y Metrología (INTN), Dirección Nacional de Aeronáutica Civil (DINAC), 1997.

M. Villarrubia: Energía Eólica, Ediciones CEAC, 2004.

Dirección Nacional de Aeronáutica Civil (DINAC), 2013.

www.evwind.com/2013/04/22/eolica-en-bolivia-primera-torre-de-medicion-para-impantar-parque-eolico-en-tarija.

Administración Nacional de Electricidad (ANDE): Plan Maestro 2013-2023.

GIZ: Situación de las Energías Renovables en Paraguay, 2011.

EU. ETS Carbon price. Thompson Reuters Point Carbon, 2013.

Renewable Energy Policy Network for the 21st Century: Renewable 2014, Global Status Report.

F. Mitjans: Generación hibrida Eólica-Solar para el fortalecimiento del Chaco Paraguayo, Tesis de Maestría en Energía para el desarrollo Sostenible, Universidad Católica de Asunción, Octubre 2013.

Viceministerio de Minas y Energía: Balance Energético Nacional 2014.

Organización Latinoamericana de Energía (OLADE), 2003.

Apuntes de la Maestría en Energía para Desarrollo Sostenible, Modulo 6, Energía Eólica, Universidad Politécnica de Cataluña (España), 2010.

www.fecoprod.com.py/lapatria, 2012.

J. Báez: Evaluación del potencial de energía eólica en el Chaco paraguayo, Tesis de Maestría en Energía para el Desarrollo Sostenible, Universidad Católica de Asunción, 2011.

Comparative Study of the performance of a hybrid PVT panel with water as coolant under two different weather conditions

Estudio comparativo del rendimiento de un panel PVT con agua como refrigerante bajo dos diferentes condiciones climáticas.

Hugo Arias[1], Javier Cabrera[2], Johann Hernández[3]

ABSTRACT

This paper describes the performance comparison of a Photovoltaic-Thermal (PVT) solar collector in thermosyphon closed loop mode under two different weather conditions, fully cloudy and partially cloudy scenarios. The PVT electrical and thermal performance were evaluated and compared with a same unmodified factory Photovoltaic (PV) panel for both scenarios. The PVT performance was evaluated by electrical, thermal and primary energy savings efficiencies. It was found that the PVT total efficiency increased 7.28 % under the partially cloudy scenario, due mainly to the thermal energy gain. At the fully cloudy scenario this improvement was 2.12 %, which indicates that for places where present mostly cloudy conditions, the PVT enhancement will not be so significant.

Keywords: Hybrid photovoltaic thermal solar collector PVT, thermosyphon, electrical yield, thermal energy, primary energy savings.

RESUMEN

Este documento describe la comparación del rendimiento de un colector solar Fotovoltaico-Térmico (FVT) en modo termosifón de lazo cerrado bajo dos diferentes condiciones climáticas, totalmente nublado y parcialmente nublado. El rendimiento eléctrico y térmico del panel FVT fue evaluado y comparado con un mismo panel Fotovoltaico (FV) sin modificaciones de fábrica para los dos escenarios. El rendimiento del panel FVT fue evaluado por su eficiencia eléctrica, térmica y el ahorro de energía primaria. Se encontró que la eficiencia total del panel FVT incrementó 7.28 % para el escenario parcialmente nublado, debido principalmente a la ganancia en energía térmica. En el escenario totalmente nublado la mejora fue de 2.12 %, lo cual indica que para lugares que presenten condiciones climáticas mayormente nubladas, la mejora en el rendimiento del sistema FVT no es tan significativa.

Palabras clave: Colector solar fotovoltaico-térmico PVT hibrido, termosifón, eficiencia eléctrica, energía térmica, ahorro de energía primaria.

Received: July 10th 2015
Accepted: Oct 15th 2015

Introduction

In the recent decades the development of renewable nature electricity sources has been one of the world main priorities. The development and deployment of non-conventional energy sources (NCES) has as main objectives the reduction of environmental pollution and diversify the energy matrix to reduce the climate change vulnerability. Even though the conventional sources (fossil fuels) continues providing more than 70 % of the global electricity production [1] and will keep most of this percentage, it is necessary to raise the NCES participation given that the increase of electrical energy demand caused by the industrial and population growth makes the world current energetic model unsustainable.

Photovoltaics are the source of energy that has the biggest growth in the last lustrum, around 55 %; reaching an installed capacity of 139 GW until 2013 according to the global status report (GSR) of REN21. Also solar thermal energy has added 55.4 GWth in solar heating, which sum a total of 326 GWth of world installed capacity. Photovoltaic thermal (PVT) systems which integrate these two renewable sources have been developed since 1970´s focused on PVT collectors with the primary aim of increasing PV efficiency [2]. Solar PV and solar thermal applications are regarded as potential solutions for the current energetic model.

The R&D in solar cells has encouraged innovative cell manufacturing techniques, in [3] - [4] a review of them is described. The efficiency of average commercial wafer-based silicon modules increased from about 12 % to 16 % in the last decade [5]. The relation between solar PV and solar thermal system is evident, because the non-harvestable energy by the PV system could be used as thermal potential by the solar collector, which is considered as energy cogeneration [6]. Furthermore the PV and solar thermal integration allows exploit more efficiently the energetic potential by the heat evacuation to a thermal system which can

[1] Hugo Arias: Electrical engineering student, Universidad distrital Francisco José de Caldas, Colombia. LIFAE. E-mail: hugo.arias.forero@gmail.com.
[2] Javier Cabrera: Electrical engineering student, Universidad distrital Francisco José de Caldas, Colombia. LIFAE. E-mail: javierhcabrera88@gmail.com.
[3] Johann Hernandez: Phd, Engineering, Universidad Nacional, Colombia. Director LIFAE. E-mail: johann.hernandez@gmail.com.

be subsequently used, and enable higher energy density per unit area.

To improve the PV performance, much research effort has been spent on the development of hybrid photovoltaic-thermal (PVT) collector technology using water as the coolant [2], [7] mostly flat plate solar collector (FPSC) have been used in PVT. Many types of FPSC have already been developed [2], [7], and [8]. They may be classified depending on the heat transfer fluid, the number of glass covers, the absorber design, etc.

Many researches have been made on PVT solar collector with forced circulation [2], [7] which needs an electrical supply for pumping. This electric energy is not considered in the primary energy savings and the energy balance. Natural circulation systems not require a power supply, meaning that the energy savings calculations are more accurate.

This paper focus on the performance comparison of single glaze FPSC under two different weather scenarios, which use water as coolant due to its higher heat capacity compared with air, allowing have a more effective cooling medium. A passive heat transfer system (thermosyphon) was designed and constructed with unexpensive materials without neglecting a good thermal performance.

Experimental Rig Description

In order to test electrical and thermal performance of the PVT solar collector, an open flow system operating in thermosyphon mode was constructed. The system consist of 3 major components, the PVT and PV module, the thermal circuit which includes the heat transfer system and the water tank, and finally the data acquisition and monitoring system.

The PVT collector was installed and tested under outdoor field conditions in Bogotá, Colombia (latitude 4°39' N, longitude 74°3' W). The PV and PVT collectors were mounted on an E-W oriented structure, and tilted 4° towards south. To compare the electrical and thermal performance between the PV and the PVT solar collector, the experimental test were carried out simultaneously. The experimental rig is shown in Figure 1.

PT100 thermistors were selected as temperature sensors due to its accuracy, repeatability and stability; also the relatively linear relation between temperature and resistance [9]. This relation was fitting by linear regression according to the load circuit electrical parameters.

The irradiance was measured by a Kipp & Zonen CMP3 pyranometer located in a weather monitoring station near the PVT structure and its output voltage was recorded with a Rigol DM3068 precision multimeter connected to the data acquisition system (DAS). In this study the output power, inlet fluid temperature, outlet fluid temperature, the PV and PVT backside temperature and mass flow rate were measured and recorded.

Data was collected and stored every minute using a data acquisition system (DAS) according to the IEC 61724/1998 standard [10]. It was implemented with low cost combination devices, an Arduino UNO as hardware and LabVIEW VI as data logger and monitoring software. These data was subsequently used to estimate the electrical and thermal efficiency and the primary energy savings.

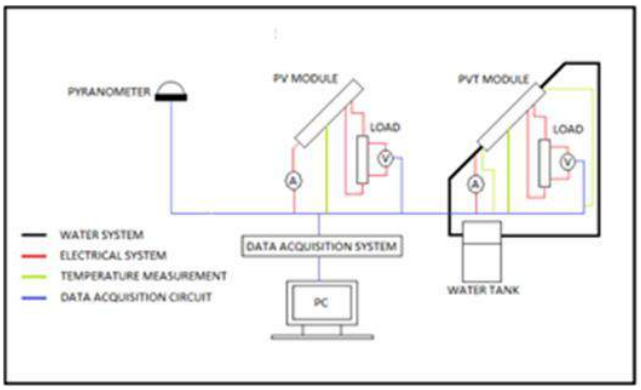

Figure1. Experimental rig diagram

Theoretical Basis

The PVT collector allows enhancing the PV performance through the PV module heat evacuation. The PVT performance could be evaluated by a combination of efficiency expressions [11], the PVT overall performance (ηT) and the primary energy savings (ηf) indicators defined in (1) and (2) respectively.

$$\eta T = \eta PV + \eta th \qquad (1)$$

$$\eta f = \eta PV/\eta P + \eta th \qquad (2)$$

Where (ηP) is the electric-power generation efficiency of a conventional power plant; its value can be taken as 38% [7]. The evaluation indicator of the primary energy saving efficiency also considers the quantity of the energy that the PVT system converts into usable energy [2]. The thermal and electrical performance of the PVT panel was evaluated based in the daily average widely-known efficiency equations. The electrical efficiency on the PV and PVT units was calculated from (3) where (Qe) is the output electric power, (Ac) is the collector area and (G) is the irradiance on the panel.

$$\eta PV = Qe\ /\ (Ac\ G) = (Im\ Vm)\ /\ (Ac\ G) \qquad (3)$$

The thermal efficiency of a conventional (FPSC) is the ratio between the useful thermal energy and the incident solar radiation (4). This thermal energy is expressed in terms of the inlet-outlet fluid temperature gradient (ΔT), the mass flow rate ($\dot{m}$) and the heat capacity of the heat transfer fluid (Cp). It is an effective method to evaluate the PVT thermal performance under several weather conditions.

$$\eta PV = {Q_{th}}/{A_c G} = {\dot{m} C_p (T_{out} - T_{in})}/{(AcG)} \qquad (4)$$

Results and Discussion

The PVT solar collector was tested under uncontrolled environmental conditions, to secure compliance on the measurement methodology both panels were tested under the same weather and electrical conditions during the same period. For the performance evaluation of both panels (PV and PVT) was determined evaluate two different weather conditions, the most common climate conditions in Bogotá. The first scenario was partially cloudy (January 2015), scenario under which the best weather condition was presented, i.e. high irradiance under long time periods, although cloudy periods was presented too. The second scenario was fully cloudy (may 2015), in this scenario low irradiance weather conditions were predominating – less than 400 W/m^2 – and high cloudiness.

In this paper, January 30 was used as example to analyze the PVT panel performance at the partially cloudy scenario, during which the solar irradiance on the panels had the longest period with highest irradiance intensity (greater than 600 W/m^2), and for the fully cloudy scenario, May 30 was used as evaluation period.

Partially cloudy scenario

In this scenario was presented the high irradiances - higher than 800 W/m^2 - longest time period, which last 40 minutes between 1:14 and 1:53 pm. The highest irradiance of all measurements was 1283.21 W/m^2 and occurred at 1:15 pm. Under this scenario the highest PV and PVT operation temperatures were achieved, 73.03 and 43.29 °C respectively. Should be noted that the panels maximum temperatures not presented simultaneously, because the thermal inertia of both panels is different due to their constructive characteristics. It is observe that PV panel temperature responds faster against the change of irradiance as it's shown in Figure 2, while the PVT temperature responds slowly due to its thermal inertia, but once the thermal energy of the storage tank has risen, this inertia allows the PVT panel temperature to be steadier than the PV temperature.

The PVT higher thermal inertia allowed the PVT temperature to be momentarily higher than the PV at the end of the higher irradiation period, between 1:44 and 1:49 pm, however, the posterior decrease of irradiance returned the PVT temperature to lower values of the PV operation temperature. This could indicate that the mass flow rate is not enough faster to evacuate the panel thermal energy to the storage tank, which means a temperature increase on the PVT panel.

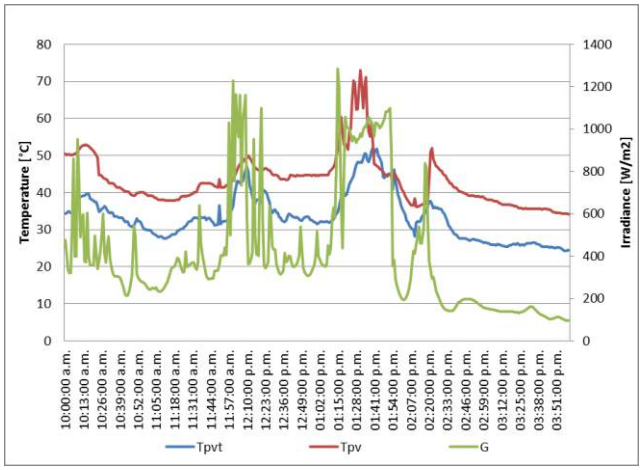

Figure2. PV and PVT temperature variations at the partially cloudy scenario

Regarding the heat transfer fluid temperatures (water), it was observed that the water inlet temperature always was smaller than the outlet water temperature, as it is shown in Figure 3, the mean gradient temperature was 9.75 °C; nevertheless at the end of the measurement period, between 3:28 to 4:00 pm, the inlet fluid temperature was slightly higher than the outlet fluid temperature, this may be due to the thermal energy stored in the thermal tank, which represents a considerable decrease in the thermal efficiency when there is a low irradiation and the storage tank has enough thermal energy stored during the day.

It was confirmed that the PV electrical efficiency is inversely proportional to the irradiance that impacts it. Both for the PV panel to the PVT panel the electrical efficiency behavior is in counter phase with the solar energy available. The PVT electrical efficiency was superior to the PV electrical efficiency at every time as Figure 4 shows. The higher PVT yield gain against the PV one was 0.56 % and the mean gain was 0.26 %, achieving a maximum value of 9.87 %. Although it was not a huge enhancement, it represents and improvement in the PV efficiency.

The PVT mean and maximum electric power were increased a 0.58 and 0.62 % respectively, in a power base of 50 W at standard technical conditions STC. For the daily mean irradiance (410 W/m^2) and a power base of 20 W, the PVT mean and maximum electric power were increased a 1.45 and 1.56 %.

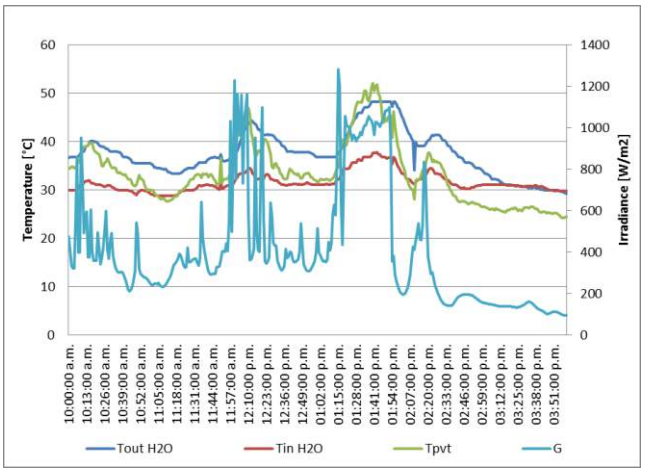

Figure3. Inlet and outlet HTF temperatures and rear surface PVT temperature under partially cloudy scenario

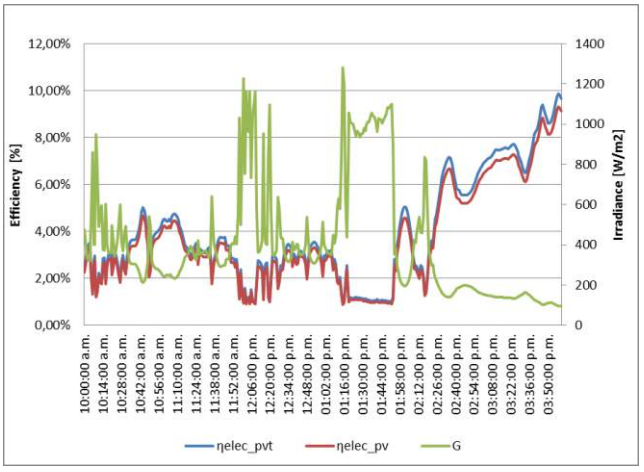

Figure4. PVT and PV electrical efficiencies at partially cloudy scenario

The PVT global performance was far superior that the PV performance, because not just the mean electrical efficiency was enhanced 0.26 %, but it also managed to have thermal energy available. The PVT total efficiency reached a maximum value of 16.58 %, which represents an improvement of 6.72 % regarding the maximum PV total efficiency.

The PVT panel achieved a maximum and mean thermal power of 22 and 10.7 Wth respectively, whereby was achieved to heat 20 liters of water at 31.6 °C. This fact shows a clear advantage of the PVT panel due this panel provides a higher energy density per unit area, i.e. a higher exploitation of the space available.

Regarding the primary energy savings indicator, the PVT panel showed an important enhancement of its total efficiency which achieved a maximum primary energy savings of 28.14 %, while

the PV panel got a 9.30 %, i.e. the PVT panel took advantage of the solar resource an 18.83 % more than the PV panel, as Figure 5 shows.

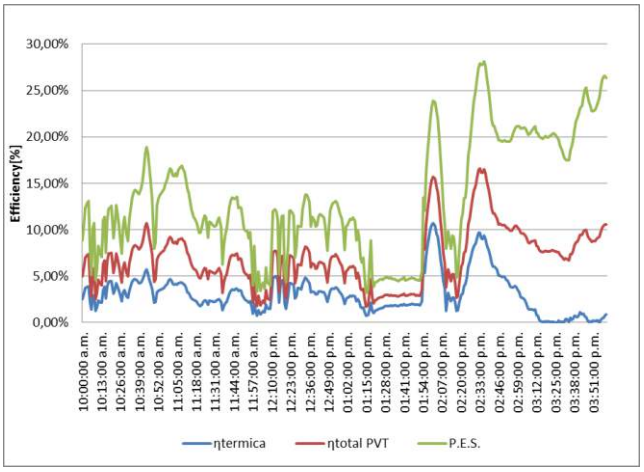

Figure5. Thermal, total and primary energy savings PVT efficiencies at partially cloudy scenario

Fully cloudy scenario

This scenario was predominantly cloudy, just few high irradiance peaks of short duration were presented, i.e. a time period greater than 20 minutes with higher irradiance than 600 W/m^2 never happened. The mean irradiance was 373.38 W/m^2. As in the partially cloudy scenario the highest PV and PVT temperatures (48.25 y 39.09 °C respectively) were in the highest irradiance time, which took place at 1:03 pm and was 1134.79 W/m^2. The panel's temperatures did not increase instantaneously due to their thermic inertia. It was observed that the PV temperature responds faster to irradiance change, and was higher than the PVT temperature every time as it is shown in Figure 6. The mean thermal gradient between both panels was 3.92 °C suggesting that for fully cloudy conditions the decrease in PV operation temperature, with flat plate cooler system in thermosyphon mode is not meaningful.

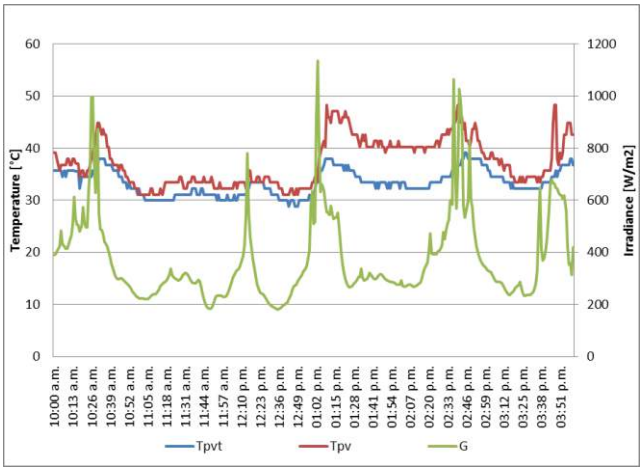

Figure6. PV and PVT temperature variations at fully cloudy scenario

As Figure 7 shows, the inlet and outlet fluid temperatures present a lot of fluctuations for this scenario; in the first measurement hour the outlet fluid temperature was higher than the inlet temperature, and thereafter the inlet temperature was greater than the outlet until an irradiance peak increased again the outlet temperature over the inlet temperature values. From this behavior could be seen that for a fully cloudy condition the thermal efficiency is too low due to the temperature fluctuation and the low thermal gradient (0.39 °C). This also indicates that the mass flow rate is much lower than the partially cloudy scenario and scenarios with higher irradiance levels, i.e. there is not an appropriate evacuation of the residual heat in the PVT panel.

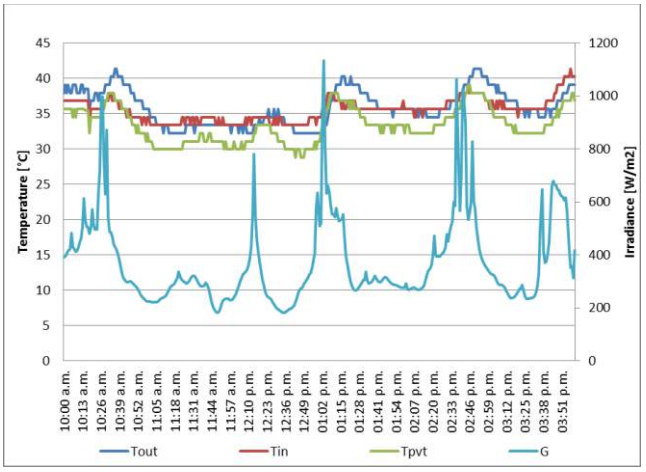

Figure7. Inlet fluid, outlet fluid and back surface PVT temperatures at fully cloudy scenario

Just like the partially cloudy scenario, it was confirmed that the PV electrical efficiency is higher for low irradiance levels, no matters the time of the year as Figure 8 shows; however for this fully cloudy scenario, the electrical efficiency of both panels was much lower than the partially cloudy condition, the PV and PVT was 4.15 and 4.37 % smaller than the partially cloudy efficiencies. So under high cloudiness conditions the PVT electrical efficiency was 0.35 % greater than the PV panel, in contrast with the larger irradiance condition, where the maximum difference was 0.56 %, i.e. it diminished a 0.21 % the mean PVT electrical performance.

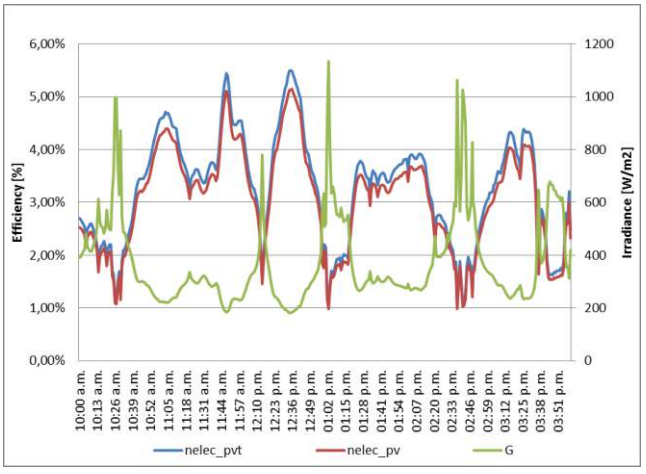

Figure8. PV and PVT electrical efficiencies at fully cloudy scenario

As Figure 9 shows, the PVT panel global efficiency was superior to the PV panel efficiency, quantitatively the PVT panel had a maximum total yield of 7.27 %, while the PV panel got a 5.15 %, and namely the last one was 2.12 % less efficient. Besides the PVT panel generated a maximum thermal power of 8.22 Wth and a mean thermal power of 0.71 Wth, i.e. a daily thermal energy of 4.22 WthH-day. In contrast with the partially cloudy scenario, the thermal efficiency was 7.97 % lower, indicating that

under high cloudiness conditions there are not large energy benefits in the PVT system.

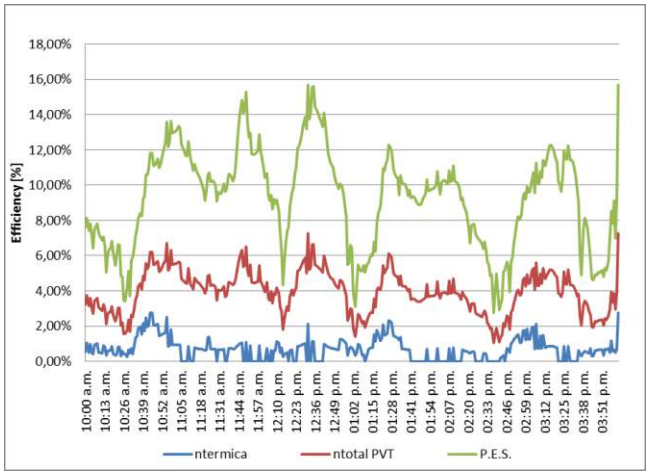

Figure9. PVT thermal, total and primary energy savings efficiencies at fully cloudy scenario

According to the results of the test carried out on both panels under fully cloudy and partially cloudy scenarios, a comparative chart was created (see Table1), where the main characteristics and energy benefits provided by two devices (PV and PVT) are shown.

Table1. PV and PVT energy benefits comparative chart

FULLY CLOUDY SCENARIO			PARTIALLY CLOUDY SCENARIO		
PARAMETERS	**PV**	**PVT**	**PARAMETERS**	**PV**	**PVT**
Pmax [W]	**4.468**	**4.716**	**Pmax [W]**	**4.545**	**4.858**
Pmean [W]	**3.893**	**4.149**	**Pprom [W]**	**3.978**	**4.269**
Pthermal [Wth]	**-**	**8.228**	**Pthermal [Wth]**	**-**	**22.047**
u_electrical [WH-día]	**26.80**	**28.296**	**u_electrical [WH-día]**	**27.27**	**29.147**
u_thermal [WthH-día]	**-**	**4.221**	**u_thermal [WthH-día]**	**-**	**64.380**
Tpanel [°C]	**48.25**	**39.097**	**Tpanel [°C]**	**73.03**	**52.069**
Tinlet [°C]	**-**	**35.508**	**Tinlet [°C]**	**-**	**37.742**
Toutlet [°C]	**-**	**41.386**	**Toutlet [°C]**	**-**	**48.330**
ηelect %	**5.15**	**5.50**	**ηelect %**	**9.30**	**9.87**
ηtérmica %	**-**	**2.76**	**ηtérmica %**	**-**	**10.73**
ηtotal %	**5.15**	**7.27**	**ηtotal %**	**9.30**	**16.58**
P.E.S.%	**5.15**	**15.68**	**P.E.S.%**	**9.30**	**28.14**

Conclusions

The PVT panel offers greater energy benefits than the PV panel, not just improving the electric power available and the electrical efficiency, but also generating thermal energy which were not preciously available.

The natural circulation water (thermosyphon) cooling system reduces significantly the panel operation temperature, which allows the panel to supply higher electrical outlet power and this way enhance its performance.

The PVT total efficiency increased 7.28 % under the partially cloudy scenario, due mainly to the thermal energy gain. At the fully cloudy scenario this improvement was 2.12 %, which indicates that for places where presents mostly cloudy conditions, the PVT enhancement will not be so significant.

The results reveal an enhance in the solar resource exploitation, important argument for possible expansions in solar parks and residential facilities, taking advantage of the PVT thermal potential in water preheaters, domestic hot water systems or an endless number of applications where heat is used.

Acknowledgement

The authors would like to thank to the LIFAE laboratories for providing the infrastructure, laboratories facilities and technical support.

References

[1]REN 21, "Renewables 2014 Global Status Report," REN 21 Secretariat, Paris, Francia, 2013.

[2]E. a. A. Fudholi., "Performance analysis of photovoltaic thermal (PVT) water collectors," *Energy Convention and Managment,* pp. 641-651, 2013.

[3]E. a. B. Parida, "A review of solar photovoltaic technologies," Renewable and Sustainable Energy Reviews, vol. 15, p. 1625–1636, 2011.

[4]FRAUNHOFER INSTITUTE, "Photovoltaics Report," Fraunhofer ISE, Freiburg, 2014.

[5]SOLAR ENERGY GROUP, School Of Physics, "Spectral Beam Splitting Technology For Increased Conversion Efficiency In Solar Concentrating Systems: A Review," 2004.

[6]A. M. A. Banupriya Balasubramanian, "Current State-of-the-Art Solar Photovoltaic (PV) Technologies," *Australian Journal of Basic and Applied Sciences,* vol. 8, no. 6, pp. 455-468, 2014.

[7]J. Z. L. M. Y. L. Ruobing Liang, "PerformanceEvaluation of new type hybrid photovoltaic/thermal solar collector by experimental study," *Applied Thermal Engineering,* no. ISSN 1359-4311, pp. 1-25, 2014.

[8]P. B. A. K. Uzma Qureshi, "Effect of operating parameters on the performance of the hybrid solar PVT collector under different weather condition," *Environment and Technology,* vol. 3, no. ISSN 2278-3687, pp. 1563-1570, 2014.

[9]ARIAN CONTROL & INSTRUMENTACIÓN, "Pt100, Su Operación, Instalación y Tablas.," Santiago, 2011.

[10]IEC 61724 :1998, "Photovoltaic System Performance Monitoring -Guidelines for Measurement, Data exchange and Analysis".

[11] Wei. H, Yang, Z, Jie. J, "Comparative experiment study on photovoltaic and thermal solar system under natural circulation of water", Applied Thermal Engineering, no. ISSN 1359-4311, pp 3369-3376, 2011.

Dynamic Model of Operational Information Flow on Electric Power Distribution Systems

Modelo dinámico de flujo de información operacional en sistemas de distribución de energía

Francisco Arias[1], German Zapata[2], Rodolfo García[3]

ABSTRACT

In many cases, when considered to automate an operational process, methods allowing to guide such automation in a scaled way, are not taken into account. The main objective of this article is to present a dynamic methodology of operational information flow allowing to guide the decision making related to operational process automation, thus, shortening uncertainty. The application of the operational information flow methodology is presented as a study case in order to improve the current restoration process within the electric power distribution system of CODENSA.

Keywords: Operational Information Flow, Business Process Management, Process Automation and Electric Power distribution Systems.

RESUMEN

En muchos casos, cuando se desea automatizar un proceso operacional no se tienen en cuenta métodos que permitan guiar dicha automatización de forma escalada. El objetivo principal de este artículo es presentar una metodología dinámica de flujo de información operacional que permite guiar la toma de decisiones relacionadas con la automatización de procesos operacionales reduciendo la incertidumbre. Como caso de estudio se presenta la aplicación de la metodología de flujo de información operacional para mejorar el proceso actual de restablecimiento en el sistema de distribución de energía de CODENSA.

Palabras clave: Flujo de Información Operacional, Gestión de Procesos de Negocio, Automatización de Procesos y Sistemas de Distribución de Energía.

Received: 23 June 2015
Accepted: 23 August 2015

Introduction

Ahead of carrying out the automation of a manual process, it is necessary to perform a deep study allowing to picture the benefits of such automation as well as to identify its potential risks.

It is intended through this article to bring forward a guided-by-stages methodology enabling to objectively choose one or several automation options, thus, shortening the risks of such automation. The main stages of this methodology are listed below:

Modeling, Feasibility, Engineering and Development.

The operational information flow methodology will be presented as a study case to improve the current restoration process within the electric power distribution system of CODENSA.

The article content is organized as follows. The section 2 introduces the theoretical concepts being related to the addressed issue. The section 3 presents a dynamic methodology to generally set up the operational information flows. Finally, the section 5 puts forward some conclusions as well as the future work.

Theoretical Framework

This section introduces the theoretical concepts being related to the addressed issue.

Information Flow Models.

The information flow models represent how the information flows through the processes as well as how it turns into as it tours via a system. The system receives different inputs transformed by hardware elements, software elements or humans to lead an output [Pressman, 2002].

The information flow models are embedded in a business process. "[…]; when we peer under the top layer of that model, what is exposed is the model for how both information and control are propagated through the business application." [Loshin, 2003].

Business Process Models

A business process "a collection of activities whose final aim is the production of a specific output that is of value to the customer. A business process has a goal and is affected by events occurring in the external world or in other processes" [Aldin, 2009].

[1] Francisco Arias: Systems Engineering, National University, Colombia. Master in Systems Engineering, National University, Colombia. Technical Coordinator Group T&T, National University, Colombia. E-mail: fjariass@gmail.com
[2] German Zapata: Electrical Engineer, National University, Colombia. Applied Science Doctor, Andes University, Venezuela. Associate Professor, National University, Colombia. E-mail: gdzapata@unal.edu.co
[3] Rodolfo Garcia: Electrical Engineer, National University, Colombia. Master in Economy, National University, Colombia. Construction division high voltage works, CODENSA, Colombia. E-mail: rgarcia@endesacolombia.com.co

A business process model is an abstract rendering of the organization processes allowing to identify the agents involved within the business and how they perform the organization activities. Within this model, each of the process tasks can be represented as well as only those being essential to render the offered service or product.

Processes Automation

The processes automation is the replacement of traditionally manual tasks by automatic tasks (machines, robots, or any other kind of automatism).

The processes costs, service and quality are improved through automation [Jiménez, 2003]. The work is done faster and does not require of operators that were previously needed.

Electric Power Distribution Systems

Different departments are involved within an electric power distribution system. Each of these departments have tasks aimed to a specific contribution [Turan Gönen, 2014].

The distribution companies specialized the tasks through four departments to the restoration process in order to optimize the process itself.

Control Center: the control center is responsible for supervising, operating and controlling the electrical system at high-tension and medium-tension in real time.

Telecontrol Center: the telecontrol center is responsible for maintaining, operating and improving the telecommunications system allowing the proper functioning of the control center operational processes, such as the communication with the equipment.

Low-tension Control Center: it is in charge of supervising, controlling and operating the low-tension electrical system that includes the lines connecting the transformers on the transmission towers to the users' electric power meters. As the alarms and operations are not automatized at low-tension, the user is the one in charge of identifying and warning of the failures by calling to the customer service line.

Information Management: this department is responsible for the distribution system technical information management, keeping the system information updated online. Thus, the control center can make choices without falling into mistakes due to not updating the system. When the control center or the low-tension control center restore the service, they must report on the repaired failure to the information management department.

Dynamic Methodology to set up the Operational Information Flow

This methodology allows to make choices related to operational processes' automation. Such methodology includes 4 stages. Fig. 1.

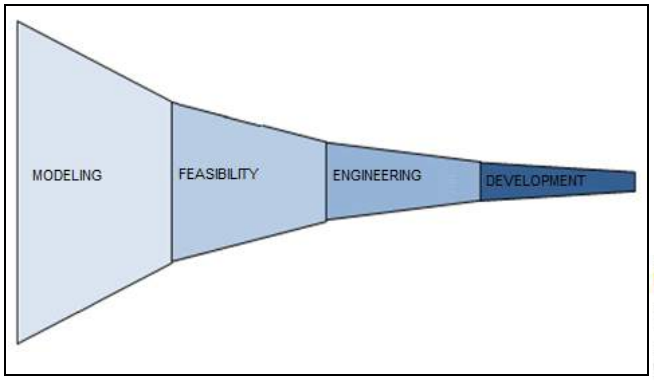

Figure 1. Information dynamic model stages.

Modeling Stage

The sub-processes and the existing dynamic of a specific issue or area are identified in this stage. Detailed information of each sub-process as well as the damage level are obtained in this stage that is divided into 3 phases:

Processes' Setting-up Phase: the main goal of this phase is to identify the macro-processes involved in the issue (issue general idea).

Current Process Modeling Phase: modeling each of the macro-processes previously identified, is intended in this phase. The activities, logic gates and events existing in each macro-process have to be bore in mind within such modeling (issue specific details).

Current Process Simulation Phase: The tasks' length, the logic gates' likelihood and the times related to the events, are identified in this phase. Finally, a simulation is set up in order to identify the issue dynamic.

Feasibility Stage

The main purpose is to study the feasibility of automating some of the identified sub-processes within the modeling stage.

It is recommended to identify different assessment criteria to carry out such feasibility study (along with the expert personnel on the issue) and afterwards, to assess each sub-process.

Engineering Stage

The engineering studies required are made to automate the sub-processes selected in the feasibility stage, in addition, the software engineering models related to the automation are developed.

As a result of this stage, the technical specifications are brought out in order to execute the automation plan or, at worst, to reject the automation.

Development Stage

The network automation plan is executed. Such plan includes two main activities: field equipment installation and the software platform development.

Study Case

The dynamic model of the operational information flow presented herein, was implemented at CODENSA Company in order to improve the current restoration process within the electric power distribution system.

Modeling Stage Results

Six macro-processes were identified regarding the information setting-up stage: failure detecting, failure locating, failure isolating, searching for temporary supplies, failure repairing, and network resetting Fig. 2.

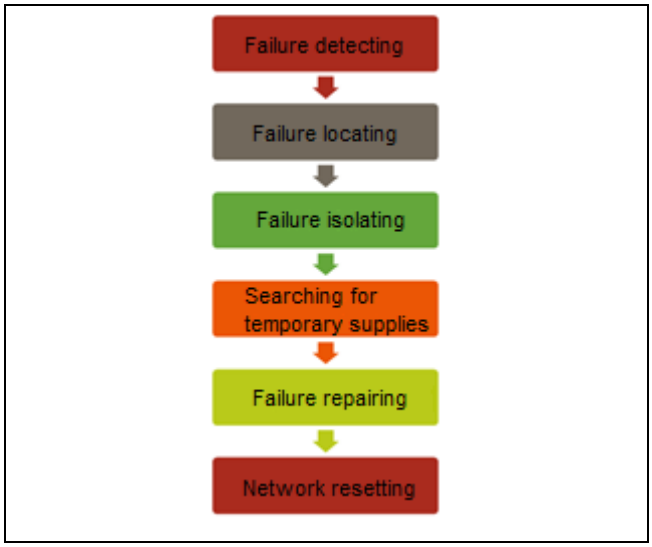

Figure 2. Macro-processes related to the restoration.

The modeling of each macro-process within the current process modeling stage was made through the tool Oracle BPM suite. The activities, logic gates and events existing in each macro-process as well as those described by the CODENSA personnel, were bore in mind within such modeling. Refer to figure 3 to see the detail model of the "Search Substitutions" macro-process.

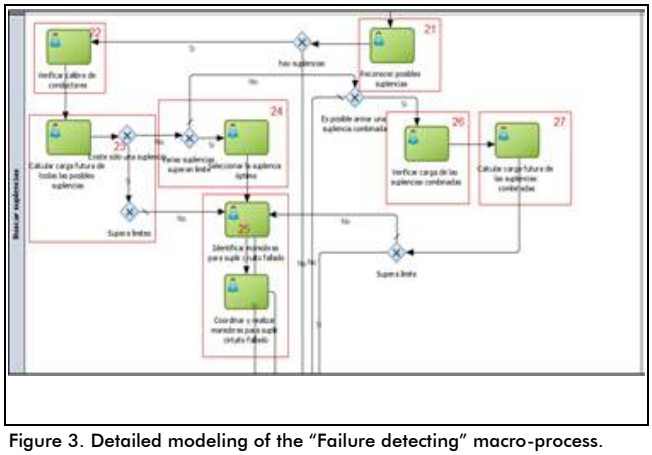

Figure 3. Detailed modeling of the "Failure detecting" macro-process.

The length of the tasks, the logic gates likelihood and the time related to the events were set up for the simulation. It should be pointed out that the information used for the simulation set-up was obtained from the control center personnel interviews so as from the monthly reports from the Average Handle Time (AHT).

After the simulation set-up was performed, different tests were executed by altering the times (1 month, 3 months and 12 months) as well as altering the set-up parameters related to the tasks, gates and events.

The simulations showed up the damage level of each sub-process within the general process of restoration (refer Fig. 4)

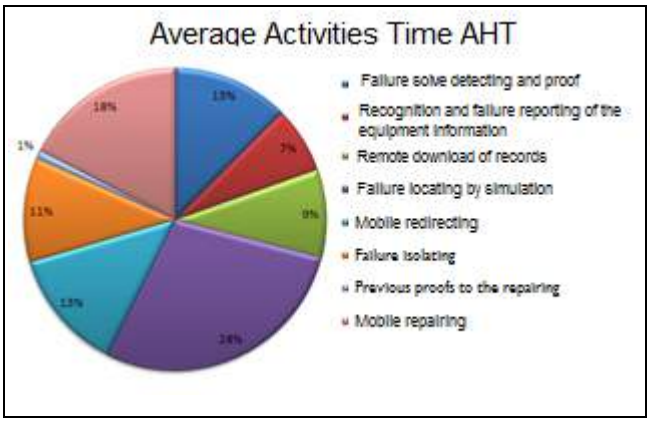

Figure 4. Damage level of each sub-process.

Modeling Stage Results

As a result of the modeling stage, 5 sub-processes affecting to a greater extent the restoration process were identified (refer table 1).

Table 1. Damage per sub-process

Sub-process	Level	General description
Failure locating	28%	Sub-process allowing to identify the circuit area where the failure is located and, therefore, to where the mobile must be directed.
Mobile's redirecting	13%	Sub-process allowing to execute field maneuvers whether to identify the failure exact location, isolating the failure, repairing the failure or restoring the circuit. Such maneuvers are coordinated by the control center personnel.
Failure solve detecting and proof	13%	Sub-process allowing to identify the event occurrence from the SCADA alarms as well as to proof if the failure was solved by the field equipment (e.g. reconnectors).
Failure isolating	11%	Sub-process allowing to isolate the failure location to go ahead with the repairing. If the failure repairing requires long times, it is necessary to resort to temporary supplies in the circuit.
Remote download of records	9%	Sub-process allowing to manage the monitoring and safe equipment information. This information is used within the failure locating sub-process, as well as to search for temporary supplies and to proof the circuit general status.

4 feasibility criteria were analyzed for each sub-process: current automation level, if field maneuvers are required, if there are existing equipment in the market allowing to automate the sub-process, and if there are existing software in the market allowing to automate the sub-process.

The feasibility criteria results for each sub-process are presented in table 2.

Table 2. Feasibility criteria assessment

Sub-process	Current automation level	Requires field equipment maneuvers.	There are equipment in the market.	There are software in the market
Failure locating	Low	No	Yes	Yes
Mobile's redirecting	Low	Yes	No	No
Failure solve detecting and proof	High	No	Yes	Yes
Failure isolating	Low	Yes	No	Yes
Remote download of records	Medium	No	Yes	Yes

The following statements can be concluded from the feasibility criteria assessment:

The automation of the "mobile's redirecting" and "failure isolating" sub-processes is discarded due to the fact that both processes require field interventions that must be performed on-site.

The automation of the "failure solve detecting and proof" sub-process is discarded due to the fact that nowadays this sub-process is automated in a greater extent.

It is possible to carry out the automation of the "failure locating" and "remote download of records" sub-processes.

Automating the "failure locating" sub-process would represent a restoration time improvement of 28% higher than automating the "remote download of records" sub-process representing a 9% improvement.

According to the previous statements, it was decided to automate the "failure locating" sub-process.

Software Engineering and Modeling Stage Results

The engineering study to automate the failure locating was made in 4 phases: criteria definition to the equipment integration on a failure locating system, equipment selection according to the specified criteria, selection and characterization of the circuit to intervene, and equipment location within the circuit.

The failure locating platform modeling is accomplished after the engineering studies.

Criteria Definition Phase Results: the main goal of this phase is to identify the criteria required for any equipment intended to be integrated to a failure locating system. The criteria were classified into design criteria (refer table 3) technical criteria (refer table 4), communication criteria (refer table 5) and operation criteria (refer table 6).

Table 3. Design criteria.

Design Criteria
4 hours minimum autonomy (battery)
Outdoor working equipment.
Modular design of its components
Portable equipment
Easy installation

Table 4. Technical criteria

Technical Criteria
The equipment must allow ground connection
Lightning resistance
Failure current measurement and detection
Setting-up option of shutdown limits

Table 5. Communication criteria

Communication Criteria
Current communications' infrastructure compatibility
ENDESA profile, protocol 104
GPRS communication
Equipment status reporting
Integration likelihood to the SCADA

Table 6. Operation Criteria

Operation Criteria
Reading times < 5 ms
Data releasing times < 10 s

Equipment Selection Phase Results: The search of equipment fulfilling such criteria is accomplished after the criteria definition to the equipment integration on the failure locating system. From this equipment search 2 technologies were identify.

Unit to automate the failure indicator communication: this unit allows to automate the communication of the failure indicators currently installed at CODENSA (refer Fig. 5)

DISCOS equipment: the DISCOS System has been mainly designed to provide current and voltage measures within the medium-tension and low-tension electric power networks whether during usual functioning conditions or failures (refer Fig. 6).

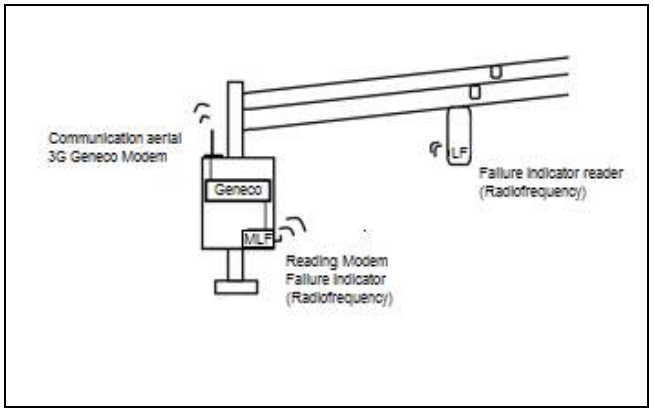

Figure 5. Unit to automate the failure indicator communication.

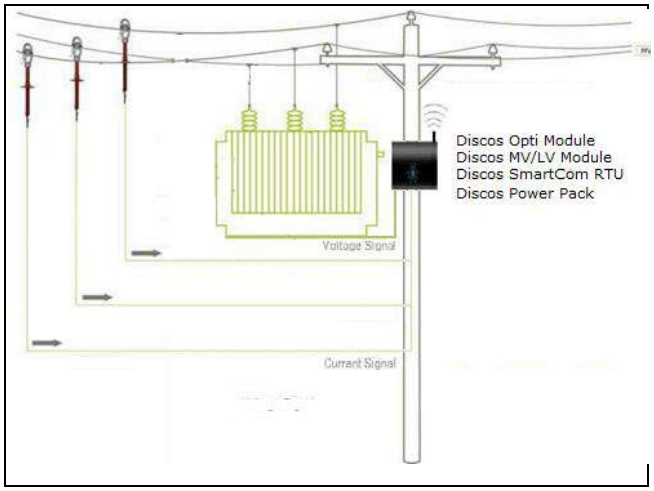

Figure 6. DISCOS system set-up on an electric power network.

Results from the phase of Selection and Characterization of the Circuits to intervene: after an analysis of different selection criteria was made, 13 potential circuits were identified to carry out the automation (refer table 7)

Table 7. Potential circuits to carry out the automation.

Circuit	Ind. Cal.	C1	Topology	C2	Dist. (km)	C3	CT	#
Minero	4,5	0,20	7,0	0,37	80	0,14	0,71	5
Tibacuy	3,5	0,16	5,5	0,29	87	0,13	0,57	10
Yacopi	3,5	0,16	5,5	0,29	150	0,00	0,45	13
Cabrera	3,5	0,16	5,5	0,29	95	0,11	0,56	11
Hacienda	3,5	0,16	6,0	0,32	134	0,03	0,50	12
Espigas	3,5	0,16	6,5	0,34	63	0,17	0,67	7
El_pomar	3,5	0,16	6,0	0,32	39	0,22	0,69	6
Urbiza	3,5	0,16	8,0	0,42	11	0,28	0,85	2
Plastihoga	3,5	0,16	8,0	0,42	23	0,25	0,83	3
Urbanizac	3,5	0,16	8,0	0,42	23	0,25	0,83	3
Malterias	3,5	0,16	5,0	0,26	47	0,21	0,62	8
Termales	**3,5**	**0,16**	**9,5**	**0,50**	**45**	**0,21**	**0,87**	**1**
Naranjal	4,0	0,18	6,0	0,32	91	0,12	0,61	9

The **Termales** circuit from the **Tabio** substation was chosen according to the results in table 7.

A scale representation of the **Termales** circuit from the **Tabio** Substation is presented in figure 7.

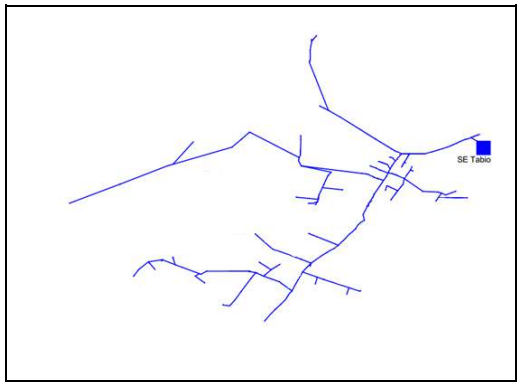

Figure 7. Termales circuit from Tabio

Equipment Locating Phase Results: 8 are the available failure indicators sets which are distributed along the circuit according to installed load criteria, cut and maneuver elements proximity (switches) and accessibility to the installation location.

Firstly, each equipment set is intended to be placed near a cut and maneuver element in order to section the circuit during a failure event. In addition, it was attempted to evenly distribute the installed load on the circuit for each of the sections. Finally, the access routes to the installation location were bore in mind to have an accessibility picture.

The figure 8 shows the final location proposal for the failure indicators and the figure 9 presents each of the sections the circuit was divided into.

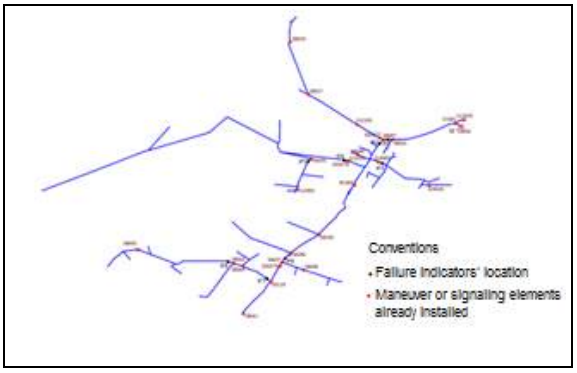

Figure 8. Location of the 8 failure indicators sets.

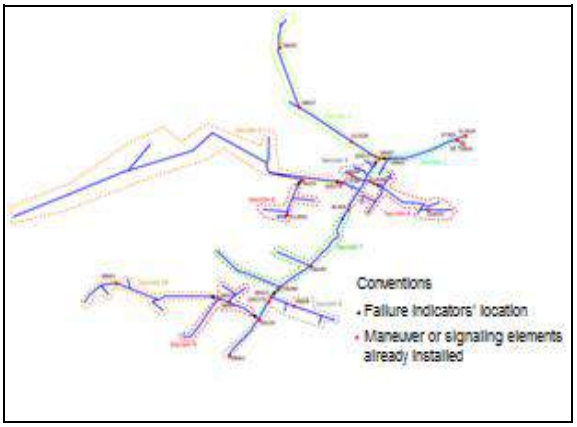

Figure 9. Circuit sectioning regarding the failure indicators' location.

Software modeling: such model is mainly compound by field equipment, failure locating system and user interface.

Field Equipment: refers to the failure indicators, DISCOS equipment and safe equipment. These equipment are in charge of broadcasting the circuit information at all times (steady status or failure status).

Failure Locating System: application in charge of processing the information in order to locate the failures.

User Interface: web application used to visualize the information provided by the failure locating system.

Users: anyone wanting to watch the failures within the Termales circuit from Tabio (must have required permissions)

All the integrated elements of the failure locating system can be observed in figure 10.

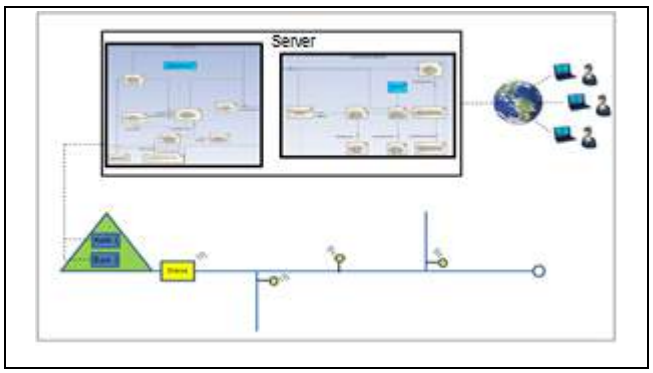

Figure 10. Integrated elements of the failure locating system.

Development Stage Results

The network automation plan is executed in this stage. Such plan includes 2 main activities: on-field equipment installation and software platform development.

The equipment installations were accomplished in 4 days. The first day, the DISCOS equipment was installed. The second day, 4 indicators' sets were installed. The third day, the ground connections were installed as well as 4 indicators' sets. The fourth day, equipment tests were performed.

Two pictures corresponding to the installation on the circuit can be seen in figures 11 and 12.

Figure 11. DISCOS equipment installation.

Figure 12. Indicators' set installed.

The software platform was developed as a web system allowing to have remote access to the failure locating system.

The main system interface can be seen in figure 13. It is compound of four units:

Global Positioning Unit (1): through this unit, both the unit and its equipment's geographic location can be seen. In addition, it presents the failing section according to the results provided by the failure locating system by indicators as well as from the results provided by the failure locating system by simulation. It should be pointed out, that this unit admits graphic information from supports so as from the substation.

Identified Failures by Indicators Unit (2): this unit presents a historical summary of the circuit failures as well as if such failures have been identified by the user.

Circuit Status and Failure Locating by Simulation Unit (3): this unit presents the current information that the DISCOS equipment identifies at the circuit's head as so if its current values report whether a usual or a failure status. In addition, it simulates the simulated failure location based on the current datum identified by the DISCOS equipment.

Historical Information Unit (4): through this unit the circuit historical information can be checked, either the punctual value of the failure indicators or the failure current values identified by the DISCOS equipment.

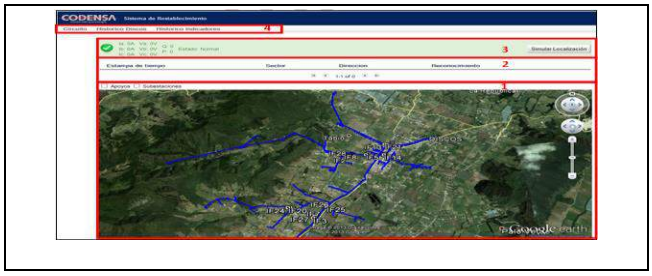

Figure 13. Developed software platform.

Conclusions

A dynamic model of operational information flow was presented. This model allows to guide the decision making related to the operational process automation.

The model application of the operational information flow was presented as a study case in order to improve the current restoration process on the electric power distribution system of CODENSA

As a future work, it is expected to have the proposed model formalized to be applied on different automation processes within CODENSA or any other company.

Acknowledgments

This paper presents results of the research project "Model of Operational Information Flow for CODENSA Distribution System", implemented by the National University of Colombia - Medellín and financed by COLCIENCIAS and CODENSA, entities which are given a special recognition.

References

[Loshin, 2003] Loshin, David. Business Models and Information flow. En: Business Intelligence: The Savvy Manager's Guide, Getting Onboard with Emerging IT. San Francisco: ElSevier Science, 2003, p. 66.

[Aldin, 2009] Aldin, Laden and DE CESARE, Sergio. A comparative analysis of business process modeling techniques. OxfordShire: U.K. Academy for Information Systems (UKAIS), 2009, 17p.

[Pressman, 2002] Pressman S., Roger. Modelado del análisis. En: Ingeniería del Software – Un enfoque práctico. Quinta edición. Nueva York: McGraw-Hill, 2002, p. 199-218.

[Jiménez, 2003] Emilio Jiménez. Técnicas de automatización avanzadas en procesos industriales / Advanced Automation Techniques on Industrial Process. Universidad de La Rioja, ISBN: 84-689-0360-4.

[Turan Gönen, 2014] Turan Gönen. Electric Power Distribution Engineering. Third Edition. ISBN 9781482207002.

Electromechanical Transients Study in an Unbalanced Active Distribution System: A Colombian Study Case

Estudio de Transitorios Electromecánicos en un Sistema Activo de Distribución Desbalanceado: Un Estudio de Caso Colombiano

Juan Carlos López Cardona[1], Juan David Marín Jiménez[2], Sandra Ximena Carvajal Quintero[3], Camilo Younes Velosa[4]

ABSTRACT

In this article the analysis of the impact of electromechanical transients caused by the aperture of a line in an unbalanced Active Distribution System using the methodology of modeling and simulation in PowerFactory DIgSILENT software is presented. The results allow to determine the voltage limits coupled to the electrical system and the considerations to be taken into account for the settlement of the event. The paper is organized in the following way, presents an introduction to the topic of electromechanical transient and Active Distribution System, followed by the description of the case study and simulations, then the analysis and interpretation of the results are presented and finally the conclusions and recommendations.

Keywords: Active Distribution System, electromechanical transients, dynamic stability, Small Hydro Power Plants.

RESUMEN

En el presente artículo se presenta el análisis del impacto que tienen los transitorios electromecánicos causados por la apertura de una línea en una Sistema Activo de Distribución desbalanceado empleando la metodología de modelado y simulación en el software DIgSILENT PowerFactory. Los resultados obtenidos permiten determinar los límites de tensión acoplados al sistema eléctrico y las consideraciones que se deben tener en cuenta para la solución del evento. El artículo se encuentra organizado de la siguiente manera, se presenta una introducción al tema de los transitorios electromecánicos y a los Sistemas Activos de Distribución, seguido la descripción del estudio de caso y simulaciones, seguidamente se presenta el análisis e interpretación de los resultados obtenidos y finalmente las conclusiones y recomendaciones.

Palabras clave: Sistema activo de distribución, transitorios electromecánicos, estabilidad dinámica, Pequeñas Centrales Hidroeléctricas.

Received: July 24th 2015
Accepted: Oct 15th 2015

INTRODUCTION

In the last years, the electric distribution networks have suffered the technology development penetration that gives origin a change in the paradigm of the planning and operation of these networks (Dias, 2014). Commonly, the distribution systems had a very defined and know characteristics: A grid connected to transmission system that satisfies with give to the final users a quality, reliable and safe service. Nevertheless, different acts like the non-conventional generation inclusion, changes in the demand behavior, energy and information flows since generators until the loads and the other way around, the rise of new necessities like the energy storage, and others that have gone taking important part in the distribution grids, have done that its composition is not simple like the last described, however it becomes in a more complex set as in construction as operation (Sioshansi, 2012).

[1] Electrical Engineer, Electronic Engineer, Magister Candidate in Electrical Engineering, Universidad Nacional de Colombia, Manizales, Colombia. Member investigation group Environmental, Energy and Education Policy (E3P) Universidad Nacional de Colombia, e-mail: jclopezcar@unal.edu.co
[2] Master in Electrical Engineering, Ph.D Candidate, Universidad Nacional de Colombia. Member investigation group E3P, Universidad Nacional De Colombia, Manizales branch, e-mail: jdmarinj@unal.edu.co
[3] Full Professor, Electrical and Electronic Department Universidad Nacional de Colombia, Manizales Branch. Ph.D in Engineering Automatic Line, Universidad Nacional de Colombia. Researcher Group Enviromental, Energy and Education Policy (E3P), Universidad Nacional de Colombia, e-mail: sxcarvajalq@unal.edu.co
[4] Full Professor, Electrical and Electronic Department Universidad Nacional de Colombia, Manizales Branch. Ph.D in High Voltage, Universidad Nacional de Colombia. Researcher Group Enviromental, Energy and Education Policy (E3P), Universidad Nacional de Colombia,
e-mail: cyounesv@unal.edu.co.

Currently the electric energy generation was centralized and it was far away of the consumption centers, that is to say, big generation plants, hydric or thermals (for says the most used in the world), connect them to the distribution network through extensive lines laying belong to transmission system. However, the distributed generation appearance, has allowed that the electric energy is generated a little bit more close of the final user, is a lot more controllable and start to change the network settings (Boillot, 2014).

Since the demand side had been changes related with its behavior. Now is not the passive user, that was connected in the network for satisfied its necessities for becomes an active participant in the supply process (Sioshansi, 2012). End-user are implementing generation through non-conventional resources, creating a bi-directional electrical flow and bi-directional information, these concepts is known as Producer-consumer or *"Prosumer"* (Chowdhury and Crossley, 2009).

Viewing the distribution system since its two sides (generation and demand) it can imagine a few portion of it with its own generation and its specific characteristics demand operating in particular mode in coordination with other factors intrinsic in the same network like storage device, correct protection systems and demand management programs in pro of rational energy use, giving origin a new paradigm called "*active distribution networks*" *(*Chowdhury and Crossley, 2009*)*.

Due of the growing complex in the distribution network, this cannot analyze of the same way that did some years ago, where for example, the stability of voltage analysis just were in the transmission network . Now is necessary of realize in the distribution network due to distributed generation (Carvajal, 2011).

As mentioned above the complexity of the distribution network is giving, as in its planning as in its operation and in this ideas order the vulnerability to disconnections had been latent (Calderón-Guizar, 2010). The most frequent events in the electric power systems and cause the greater amount of operative difficulties in the electric distribution networks are the monophasic and three-phasic faults, which trigger transient events, which should analyze for to know its consequences and solve methods (IEEE, 2014).

Colombia is a country socially convulsed and geography diverse, presents a high vulnerability to faults in its electric system. For a side, the terrorist attempts against the electrical infrastructure and the other the nature events like lightings, fall of trees in transmission lines, and others, do the stability in the networks and continuity in the service is a permanent challenge.

In addition, in May 2014 it has been implemented in Colombia, a regulation that encourages investment in distributed generation and currently, the capacity of DG is limited rigidly by distribution network operator (DNO) to avoid the negative effects of high level penetration. Active distribution networks, is a researcher proposal based major in implementation of local and coordinated control of voltage, flows and fault levels. For control distribution networks is necessary first understand the behavior of distributed grid when occur any faults. In this paper, an analysis of electromechanical transients caused by faults in a distribution networks with small hydroelectric power plants is proposed. Considering the high embedded of this type of distributed generation in Colombia.

ACTIVE DISTRIBUTION SYSTEMS

An active distributions system is defined as an electric system that has the ability of operate connected to the transmission system and assume time can disconnecting of him and operate in islanding mode with all guarantees in the supply of service and the quality of the same (Romero, 2015). This disconnection of the transmission system can gives accidentally because of inspected event like are the faults, they can be due natural phenomenon (for example the lightings, fall of trees in lines, animals in some bay in the substation, and others) or for human faults (mistakes in electrical operations or maneuvers of grid operator). (Boillot, 2014).

Inside of the active distribution system concept, is very important to know the definition of mini-grid, being that, like can to see more forward, one of the possible consequences of the appearance of a fault in an active distribution system is the building of a mini-grid.

A mini-grid can be defined like an electric distribution network which is operating typically in values under 11 kV (DANIDA and UNEP, 2012). The electric energy that powers the mini-grid comes of different small local sources, generally implementing renewable energies. Is important to say that in a mini-grid can existing or not, storage devices (Hazelton, 2013).

In the same way, the active distribution systems different to the conventional distributions network, have a high penetration of distributed energy resources, which those are basically three: distributed generation, storage systems and participative demand (Chaulan, 2014). The central zone of the country, is rich in hydric resources and for this reason the hydraulic generation is the most used in the region and in this kind of generation the rotary machines playing a vital role for becomes the necessity of analyze events inside of them like is the case of the electromechanical transients. The hydric wealth in this zone of the country has accommodated to building of small plants of minor capacity compared to the big generators and are called *"small hydroelectric power plants SHP"*, which are those that have a capacity installed minor or equal to 20MW and in turn can be subdivided according to its power in pico-centrals (0.5-5 kW), micro-centrals (5-50 kW), mini-centrals (50-500 kW) and small centrals (500-5000 kW) (INEA, 1997). The SHP have been means of generation that have entered to a very important place in the planning of the active distribution systems.

In an unbalanced active distribution system, which have distributed generation through SHP, passive demand and addition to is operating in islanding mode, going to realize a study for determine the impact that the electromechanical transients can cause on that system when it have a single phase to ground fault.

TRANSIENT EVENTS

A transient is defined as an electric power system parameters disturbing that can presents like consequence of a high contingency like a fault in the system (Kundur, 1994). Given a transient event, the system response is called *"transient regime"* that have like main characteristic a progressive extinction in time, and this time is that the system use for recover the normal values. The last differs of the *"permanent regime"* that is the system response without disturbances (Vénikov, 1985).

Different authors have classified the disturbances that can happens in an electric power system according to various criteria. One of those criteria classification is according to the duration in

time of the disturbance event. The short-term transients are called electromagnetics. The transients of median term are called electromechanicals and finally the transients that considers the long term which preserve the name of transients though some authors have been defined like thermo-energetics transients (Vénikov, 1985).

Electromagnetic Transients

An electromagnetic transient is the instantaneous response of an electric system to sudden changes of its initial state to different state, caused for maneuvers inside the same system, for faults in the network or lightings (Vénikov, 1985).

Electromechanical Transients

The electromechanical transients are those that interact between the mechanic energy storage in the rotary machine and the electric energy storage in the electric system. Is considered inside this group those events happened in t=5s and its duration can reach to presents for a few minutes (Vénikov, 1985). The study of this kind of transients, can means to future, established boundary conditions of dynamic stability of the parameters of the different machines coupled to the electric power system like are the motors in the plants and along the network (Kuiva, 2008).

The simulations that will show in this article were made implementing this last kind of transients.

STUDY CASE

The simulations made in the present study case, were made above a real model of the electric distribution system in a town called Salamina.

Salamina is a town in the north zone in the Caldas department which is in the center of west of the Andean Region of Colombia, like is shown in the Figure 1.

Figure 1. Location of Salamina – Caldas – Colombia [Source: www.salamina-caldas.gov.co]

There, in the Salamina substation that has a transformer 33/13.2 kV with a capacity of 4MW. The line of 33 kV that reach to Salamina substation, comes of the Interconnected National System (SIN). Of the bus bar of 13.2 kV left three powers of lines that distributed for the town (SLM12L12, SLM12L13, and SLM23L15).

"La Frisolera" is the name of the SHP that have planned put on service in the town of Salamina - Caldas and inside of its three alternatives of connection required by CREG ("*Comisión Reguladora Energía y Gas)* in the resolution CREG 025-95 (Networks code) and CREG 106-06. The alternative studied in this paper is the connection of *"La Frisolera"* in the feeder SLM23L12. In the Figure 2 can observe the single-line diagram of the network.

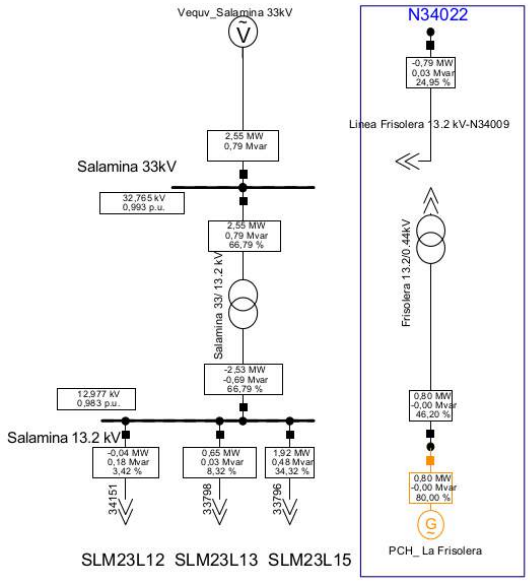

Figure 2. Single line diagram network of study

The Table 1 shows a summary of the distribution system in that will realize the simulations.

Table 1. System distribution parameters

Parameters	Values
Transformer capacity	4MW
Power size	2/0 ACSR
SHP capacity	1 MW
Generation capacity	0.8MW

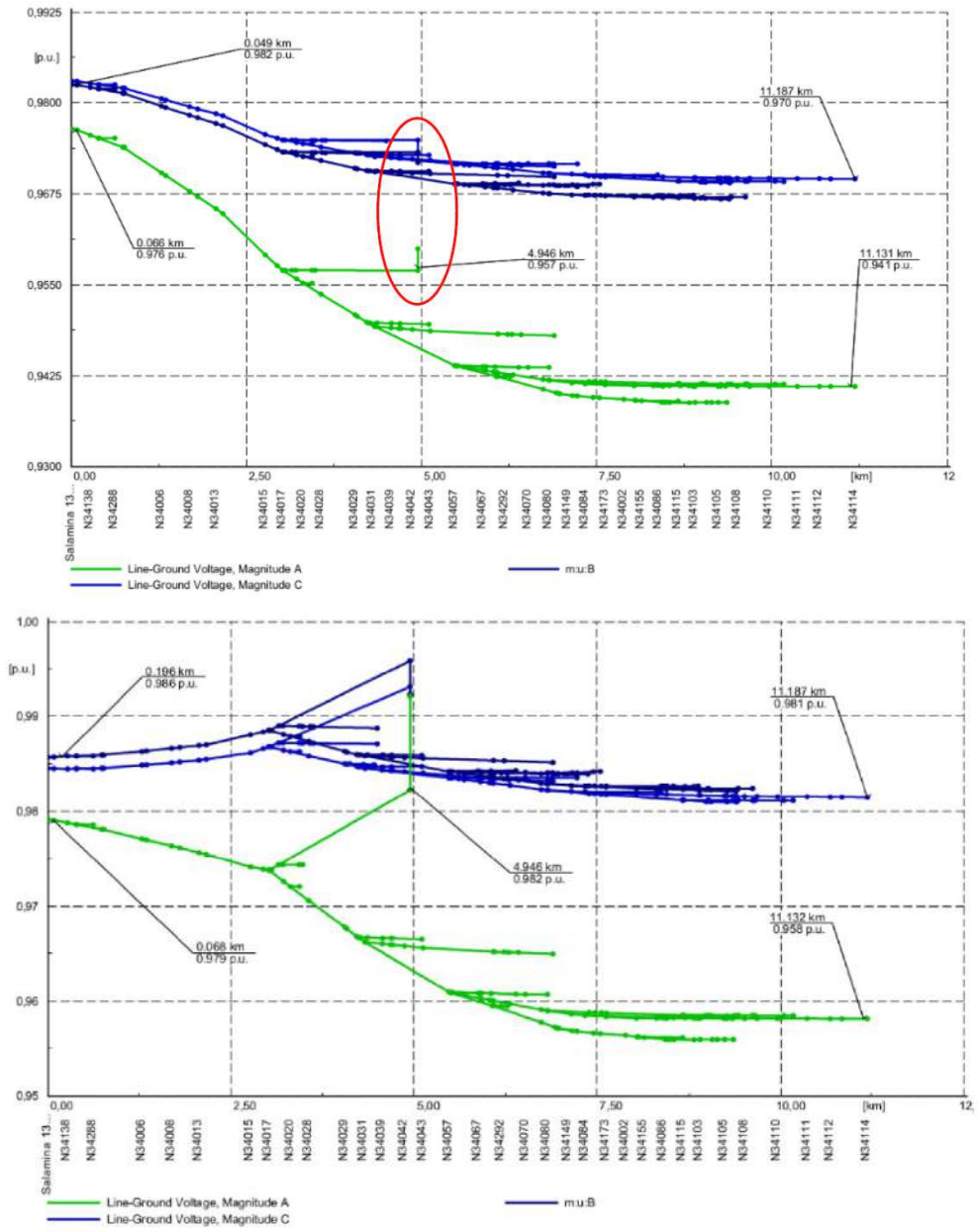

Figure 3. Unbalanced active distribution system and improve voltage profile after connection of SHP "*La Frisolera*"

The SHP "*La Frisolera"* is equipped with a synchronous machine with a capacity of 0.8 MW and the distribution network to study. The active distribution system is unbalanced; the chargeability of the three phases is different. This event can be seen in the Figure 3. This figure shows the unbalance before and after the connection of SHP *"La Frisolera"* thus allowing for the improvement in voltage profile due to the connection of the SHP.

The demand, in this case does not have self-generation, cogeneration and demand management programs, for these reason is a passive demand.

This demand is absolutely residential which it involves a behavior following the characteristic curve of electric energy consume in the residential sector in Colombia and assumes that along of the distribution line does not exist special loads such as those are commonly use in the industrial sector.

When happen a fault in the bus bar Salamina 13.2 kV, the overcurrent protection (relay 50/51) operate and the switch in the low side of the transformer Salamina 33/13.2 kV is open, and the town is disconnected of the SIN. Afterward of occurred the fault and is not clear yet, the switches of the lines SLM23L12 and the protection of transformer are open (see Figure 4) and is possible implement the operation by islands.

The SLM23L12 line, has connected in some place of its path, the SHP *"La Frisolera"* with capacity of 0.8 MW for be dispatched and both (line and generator) form and island outside of the transmission system. In the beginning the system reference machine was the voltage of the transmission system, but after the event the new reference machine is the SHP.

SIMULATIONS AND RESULTS

The simulation consists in a single phase to ground fault that occurs on feeder SLM23L12 after the island has formed. *T*he

objective is to analyze the impact on active distribution system or mini-*grid* unbalanced after a single-phase fault occurs.

Simulation cases

Case 1: After two seconds the island or mini-grid in the SLM23L12 circuit is formed. Simulating a single-phase fault on phase A (phase lower voltage level) at five seconds is performed, then 100 ms (typical time set by a recloser) after the fault it is clear and the mini-grid continues its normal operation.

Figure 4 shows that during the first two seconds the feeder has a stable voltage between 13126 V and 13014 V, after two seconds the island is formed, appearing an electromagnetic transient voltage variation which is within the recommended limits +/-10% [IEEE 1547]. Once the voltage begins the process of stabilization, a failure within 5 seconds and 100 ms after it is cleared simulated, appearing a voltage drop on Phase A of 12758 V and finally the voltage establish with a value of 13824 V.

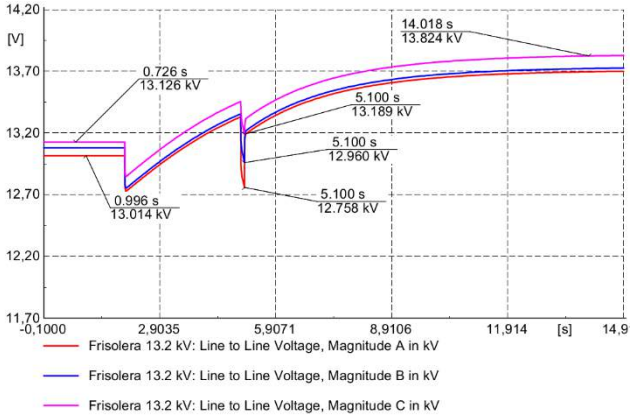

Figure 4. Case1: Answer of voltage in the substation of SHP "La Frisolera" to the single-phase fault on phase A

Case 2: After two seconds the island or mini-grid in the SLM23L12 circuit is formed. Simulating a single-phase fault on phase C (phase with higher voltage) at five seconds is performed, then 100 ms after (typical time set by a recloser) the fault it is clear and the mini-grid continues its normal operation.

Figure 5 shows that during the first two seconds the feeder has a stable voltage between 13126 V and 13014 V (values similar to Case 1), after two seconds the island is formed, appearing an electromagnetic transient voltage variation which is within the recommended limits +/-10% *[IEEE 1547]*. Once the voltage begins the process of stabilization, a failure within 5 seconds and 100 ms after it is cleared simulated, appearing a voltage drop on Phase C of 12012 V and finally the voltage *establish* with a value of 13810 V.

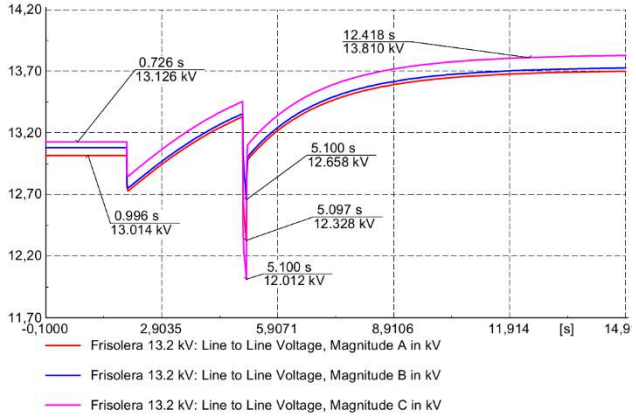

Figure 5. Case 2: Answer of voltage in the substation of SHP "La Frisolera" to the single-phase fault on phase C

After performing the simulation of the formation of the island and the simulation of single-phase fault on different phases of the circuit SLM12L12, the Mini-grid presents operating in isolation, which will have the condition until the moment the service is restored STN. In Figure 6, the final condition of the mini-grid is show.

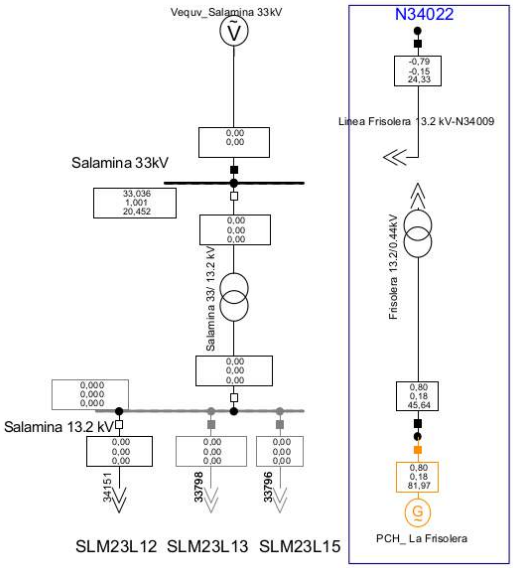

Figure 6. Single line diagram network of study after the fault

CONCLUSIONS

The probability of a single-phase fault occurrence distribution systems is around 70% (compared to other types of failure), unbalanced systems such failures can cause tripping generator protection relays, substations and bars. In this paper it is shown that the response of an active unbalanced distribution system before a disconnection event, the limits are in appropriate ranges. However, when the Active Distribution System operates in isolated mode (Mini grid forming) the system becomes more vulnerable to events of single-phase faults.

Due it is not possible to determine the place where a failure occurred, the simulation is performed in the major and minor

phases loaded. The simulation shows that an active unbalanced distribution system, failures occurred on the most loaded phases may cause the protections (relay 81) of the machines operate and not allow operation by islands.

Therefore, to have a proper operation mini-grids is necessary to know the percentage of imbalance of Active Distribution System and adjust the protections against over current (relays 50/51) and against overvoltages (relay 81) in generators and substations.

REFERENCES

Vénikov, V. Procesos transitorios electromecánicos en los sistemas eléctricos de potencia. MIR, Rusia. 1985

IEEE. Handbook of electrical power system dynamic. WILEY, USA & Canadá. 2013

Kundur, P. Power system stability and control. McGraw-Hill, USA. 1994

Sioshansi, F. Smart grid. Integrating renewable, distributed and efficient energy. AP, USA & GB. 2012

Boillot, M. Advanced smart grids for distribution system operators. WILEY, USA & GB. 2014

Choudhury, S., Choudhury, S.P., Crossley, P. Microgrids and active distribution and control. The Institution of Engineering and Technology, GB. 2009

IEEE. Microgrids architectures and control. WILEY, GB. 2014

García, C., Iturbe, R. Análisis de los transitorios electromecánicos en una planta de generación. España. 2014

Pecas, J., Hatziargyriou, N., Mutale, J., Djapic, P., Jenkins, N. Integrating distributed generation into electric power systems: A review of drivers, challenges and opportunities. Electric Power System Research. Vol.52, pp. 1189–1203. 2007

Carvajal, S., Marín, J. Impacto de la generación distribuida en el sistema eléctrico de potencia Colombiano: Un enfoque dinámico, Tecnura. Vol. 17 p.p. 77-89. 2013

Carvajal, S., Marín, J. Arango, S. Feasibility of intentional islanding operation whit small hydropower plants. In transmission and distribution: Sixth IEEE PES pag 1-6. 2012

Tabares, H., Hernadez, J. Typical demand curves of electric power for the residential, commercial and industrial sector of Medellin, using artificial neural networks and algorithms of interpolation, Fac. Ing. Univ. Antioquia. Vol. 46, p.p 110-118. 2008

Energy Losses Minimization in Smart Microgrid

Minimización de Pérdidas de Energía en Microrredes Inteligentes

A. J. Ustariz-Farfan[1], C. Younes-Velosa[2], C. Arango-Lemoine[3] and E. A. Cano-Plata[4]

ABSTRACT

In this paper, energy losses minimization in smart microgrids using capacitors banks and energy storage systems. An optimization methodology based on heuristic search is presented. The proposed methodology approach was developed as a management system based on losses control. This management system works centrally in order to improve the voltage profile and to reduce energy losses to its minimum values. The 33-bus test system (modified) was used to evaluate the performance of the proposed method.

Keywords: Energy losses, smart microgrid, heuristic search, optimization.

RESUMEN

En este artículo, se investiga la minimización de pérdidas de energía en las microrredes inteligentes utilizando bancos de condensadores y sistemas de almacenamiento de energía. Una metodología de optimización basada en búsqueda heurística ha sido presentada. El enfoque metodológico propuesto, es concebido como un sistema de gestión del control de pérdidas. Este sistema de gestión, actúa de forma centralizada para mejorar el perfil de tensión y reducir al mínimo las pérdidas de energía. El sistema de prueba de 33-barras (modificado) fue utilizado para evaluar el desempeño del método propuesto.

Palabras clave: Pérdidas de energía, microrred inteligente, búsqueda heurística, optimización.

Received: July 30th 2015
Accepted: Oct 15th 2015

Introduction

Traditional schemes of generation, transmission and distribution of electric energy still not fit correctly to nowadays necessities and behavior of the market, because today's networks were designed and constructed in order to achieve necessities of last century. Thus, there is an urgent necessity of introduce new research fields of electric engineering that include new technological concepts, such as microgrids (Lasseter and Paigi, 2004) and smart grids (Díaz, and Hernández, 2011), in order to decentralize decisions, to automatize facilities, to systematize and continuous monitoring of networks and installed equipment (Wakefield, 2011).

In the electric networks of the future, information availability and new technologies of communication will allow a better management of the existing resources. In consequence, new infrastructure will allow control and monitoring not only of energy generation systems but final users that consume such energy, increasing the energy efficiency (El-hawary, 2014). Additionally, simulation tools of a dynamic system, such as a smart grid, will allow us to validate new concepts and approaches of resources optimization.

Due to the scenarios described before, an important modernization of electric networks has been developed recently. This modernization implies a more complex operation of the distribution network, because such network is not longer consider as a radiated one where electric power flow starts on the head of the system and ends at the end of the feeder. On the other hand, modern distribution networks show a different behavior, because micro generators (small hydropower units, photovoltaic systems, small wind farms and other removable energies) located all around the distributed system connect and disconnect without any kind of control by the network operator (Pathirikkat et al. 2014).

Microgenerator connection and disconnection and their variability and location on the lowest hierarchical scheme generates new technical and regulatory problems such as power and energy losses minimization or improving voltage level of the network. This issues are the challenges of the scientific community for the future. Thus, optimal defining and location of microgenerators to be installed, as well as optimal specification of size and location of capacitive banks, location of voltage regulator and sizing of ener-

[1] Armando Jaime Ustariz Farfan: Electrical Engineer, Universidad Industrial de Santander, Colombia. PhD in Engineer, Universidad Nacional de Colombia, Colombia. Associate Professor, Universidad Nacional de Colombia-Sede Manizales, Colombia. E-mail: ajustarizf@unal.edu.co

[2] Camilo Younes Velosa: Electrical Engineer, Universidad Nacional de Colombia, Colombia. PhD in Engineer, Universidad Nacional de Colombia, Colombia. Titular Professor, Universidad Nacional de Colombia-Sede Manizales, Colombia. E-mail: cyounesv@unal.edu.co

[3] Cesar Arango Lemoine: Electrical Engineer, Universidad Nacional de Colombia, Colombia. MSc in Electrical Engineer, Universidad Nacional de Colombia, Colombia. Titular Professor, Universidad Nacional de Colombia-Sede Manizales, Colombia. E-mail: carangol@unal.edu.co

[4] Eduardo Antonio Cano Plata: Electrical Engineer, Universiada Nacional de Colombia, Colombia. PhD in Engineer, Universidad de Buenos Aires, Argentina. Titular Professor, Universidad Nacional de Colombia-Sede Manizales, Colombia. E-mail: eacanop@unal.edu.co

How to cite: Journal Space xxxxxxxxxxxxxxxxxxx
xxxxxxxxxxxxxxxxxxxxxxxxxxxxxxxxxxxxxxxxxxxxxxxxxxxxxxxxxxxxxxxxxxx

gy storage systems in modern distribution networks will be the problems to be solve.

This paper gives an approach of discussions that nowadays are present about smart girds in the frame of micro grids concepts. The main focus of the work are the new challenges imposed by this novel concept of power losses minimization methods and improvement of voltage levels in distributed systems.

Electric networks evolution

At the beginning, the electric systems were based on the generation of continuous current close to the consumption site. Then, due to the increase of demand caused by demographic issues, the system became in a centralized one, because the generation facilities were located in the geographic center of consumption, while the users of the service of electric energy were growing up around this place. (Amann, 2013).

Over time, electric generation was established as it is known today, that is to say, based on alternating current, that allows to take the current from the generation center to any place far away. In this structure, planning, management, coordination and operation of electric network is establish as a centralized one.

In a centralized energy system, it can be observed five basic components, such as: (a) generation plants, (b) reducing or elevating voltage transformers stations, (c) high voltage transmission lines, (d) medium and low voltage distribution lines, and (e) control centers where the network is managed, coordinated and operated. This components, are interconnected and allow to transport energy form the generation center to the final consumers.

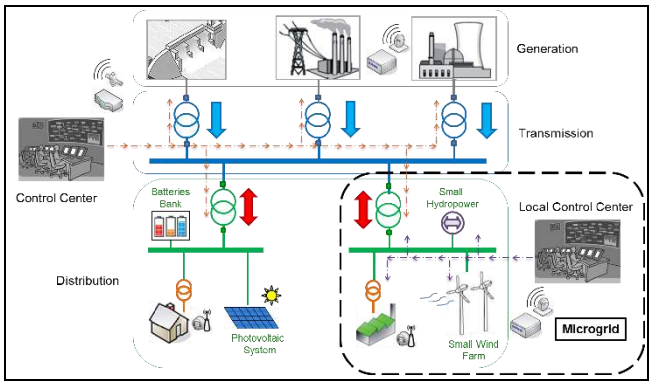

Figure 1. Electric supply system of the future

In the 70s oil crisis, climate change and high rate of demand of electric energy around the world, generated the necessity of alternative technologies to on one hand ensure and on the other hand to save and use efficiently natural resources. One of this alternatives is to generate the energy as close as possible to the consumption place (Peças et al, 2007). This kind of system is known as distributed generation.

In the last years, an alternative solution to obtain a better utilization of distributed resources is to conceive the set of microgenerators and the loads as a subsystem or microgrid (Qiang et al, 2012).

During last years, en alternative solution to obtain a better utilization of generation distributed resources is to observe all the microgenerator set and its loads as a subsystem or migrogrid (Qiang et al, 2012). This solution could be complemented with a new concept of electric networks I which two issues converges: (a) the electric power flow and (b) the information flow. This new thought of electric networks, named smart grid (Fig. 1), tries to find that electricity and information flow together in real time, allowing a better and more efficient management of the power systems, energy distributed sources and microgrids (Zeng et al, 2013).

Smart microgrids characterization

Energy losses control study is important to know characteristics and behavior of electric components that compound an electric smart microgrid. The following characterization and models are carried out in fundamental frequency.

Electric loads models

In this work, the electric loads are characterized and modeled as the complex power consumed by a specific bus.

$$S_k^{load} = P_k^{load} + jQ_k^{load} \quad (1)$$

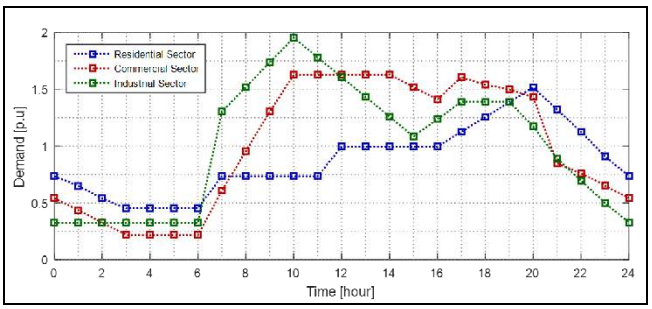

Figure 2. Electric energy consumption (dairy demand).

Fig. 2 shows the typical consumption of electric energy for residential, commercial and industrial sectors in a 24 hour period.

Distributed generation models

A distributed generator (renewable energy source) can be represented, in a basic model, as an ideal voltage source. Such source behaves as a generator that injects active or reactive power with a specific value.

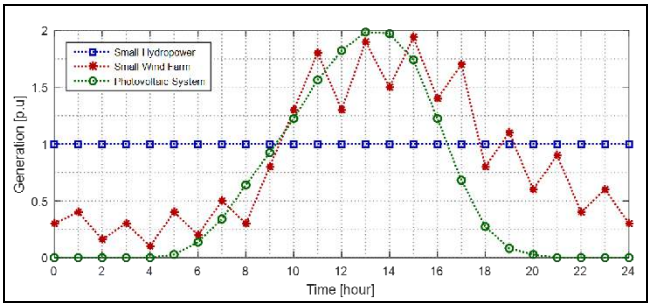

Figure 3. Electric energy injection (dairy generation).

Fig. 3 shows the curves of electric energy injection for each distributed generator in a 24 hour period.

Active and reactive power generated exclusively depends on the kind of distributed generation to be modeled, it means,

small hydropower inject active and reactive power,

$$S_k^{SHP} = P_k^{SHP} + jQ_k^{SHP} \quad (2)$$

small wind farm inject active power and consume reactive pow-

er,

$$S_k^{SWF} = P_k^{SWF} - jQ_k^{SWF} \quad (3)$$

and photovoltaic system inject only active power,

$$S_k^{PVS} = P_k^{PVS} \quad (4)$$

Energy storage system models

With the aim of using renewable energy in the best way without any kind of problems related with variability, energy intermittence or electric grid instability, the storage system must be designed and constructed as a robust system that allows to local power system interact with renewable energy sources of different characteristics. Storage system implemented in this study has been represented as an ideal battery. Such battery only injects or consume active power, it means, the energy storage system is a constant power model.

$$S_k^{BAT} = \pm P_k^{BAT}; \quad (+): \text{observed}; \ (-): \text{delivered} \quad (5)$$

Energy losses reduction

Location of capacitive banks, voltage regulators and network reconfiguration are the main methods to reduce losses in distribution systems (Aman et al, 2014; Dolli and Jangamshetti, 2012; Ababei and Kavasseri, 2011). Nevertheless, distributed generating units and storage systems also can be used in order to reduce losses (Gopiya et al, 2012; Karanki et al, 2013). The challenges of those technologies are location, size and adequate operating strategies. Even if location is fixed, an incorrect size can increase losses in microgrids.

Proposed methodology

The goal is to find the optimal location of capacitors banks and batteries banks inside the smart microgrid, in order to minimize active power losses and improve voltage profile.

Problem definition: It is necessary to know the effectiveness of the capacitors banks and batteries banks as compensative elements, as well as their behavior when they are interacting with other elements of the system. The problem is established as an optimization case with discrete and non-lineal characteristics.

It is necessary to minimize the objective function:

$$P_{loss} = \sum_{j=1}^{N-1} \left(I_j^{line}\right)^2 R_j^{line} \quad (6)$$

The restriction of power flow equations are

$$U_{\min} \le U \le U_{\max}$$
$$\sum Q_{\text{capacitor}} \le \sum Q_{load} \quad (7)$$

The standard size of the capacitors banks,

$$Q_{\text{capacitor}} = [Q_{C1};\ Q_{C2};\ Q_{C3}\ \ldots\ Q_{CN}] \quad (8)$$

and the standard size of the batteries banks,

$$P_{BAT} = [P_{B1};\ P_{B2};\ P_{B3}\ \cdots P_{BM}] \quad (9)$$

Heuristic search based algorithm: The correct way to select optimally the size of capacitors banks and batteries banks to be placed in any of the buses of the microgrid, consist in check each one of the possibilities and take the one with the lower level of losses. For this reason, the method consist on evaluating the configurations that are created by unitary changes developed in previously defined configurations. This process establish an organized search of the optimal, following the rule "first the best". The pseudo-code of the algorithm based on a heuristic search is described as follow:

Step 1 - to define a base configuration. Generally, this base configuration is chosen as the option when capacitors banks and batteries banks are unconnected.

Step 2 - to develop a local search. In this step, configurations that has only one change respect to the base configuration must be validated and the objective function must be calculated as many times as possibilities of unitary combinations classifying the configurations from the best to the worst.

Step 3 - to carry out a global search. In order to do this step, it is necessary to take some decisions that allow organize the search with the aim of improve the objective function using the results obtained from the local search as follow: (a) In depth *"Selecting the best change obtained in the local search, establishing the taken decision and repeating the process"* and (b) In width *"Taking the established decision in depth, taking the opposite decision and establishing now this one in order to keep searching the optimal depth"*

Set 4 - to define truncating criteria, which must reduce the searching space without affecting the algorithm capacity to find the optimal.

Among the most important characteristics of the algorithm can be remarked: (a) The algorithm always works better when the depth search is carried out, (b) in most of the cases there are a reduction of the options to find an optimal when a width search is carried out and (c) the search can be represented in a tree form.

Test system

The proposed methodology has been applied to a radial distribution system with variable conditions of load and generation. This test system is a modification of the 33-bus radial distribution system presented by (Kashem et al, 2000), where a small hydropower of 1,6 MW/0,9 MVAr in the bus # 3, a small wind farm of 1,5 MW/-0,7 MVAr in the bus # 9 and a photovoltaic system of 1,2 MW in the bus # 27 have been included. Single-line diagram and electric data of the smart mirogrid are shown in Fig. 4 and Table 1 respectively.

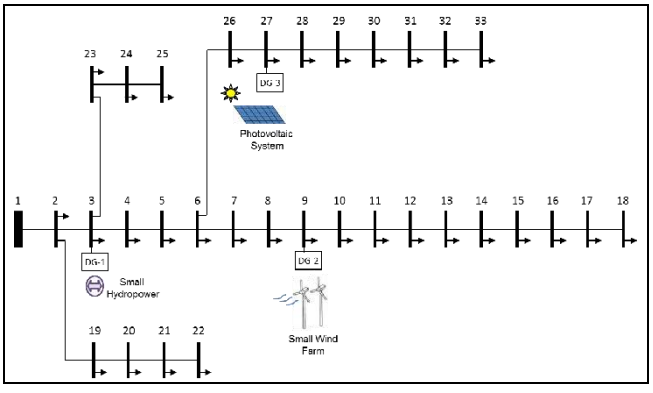

Figure 4. Single-line diagram for 33-bus smart microgrid

Table 1. Data for 33-bus smart microgrid

BUS	LINE	LOAD IN BUS - K

J – K	R (ohm)	X (ohm)	Load Type	P (MW)	Q (MVAr)
1-2	0,0922	0,0470	Commercial	0,100	0,060
2-3	0,4930	0,2512	Commercial	0,090	0,040
3-4	0,3661	0,1864	Commercial	0,120	0,080
4-5	0,3811	0,1941	Commercial	0,060	0,030
5-6	0,8190	0,7070	Commercial	0,060	0,020
6-7	0,1872	0,6188	Commercial	0,200	0,100
7-8	0,7115	0,2351	Commercial	0,200	0,100
8-9	1,0299	0,7400	Residential	0,060	0,020
9-10	1,0440	0,7400	Residential	0,060	0,020
10-11	0,1967	0,0651	Residential	0,045	0,030
11-12	0,3744	0,1298	Residential	0,060	0,035
12-13	1,4680	1,1549	Residential	0,060	0,035
13-14	0,5416	0,7129	Residential	0,120	0,080
14-15	0,5909	0,5260	Residential	0,060	0,010
15-16	0,7462	0,5449	Residential	0,060	0,020
16-17	1,2889	1,7210	Residential	0,060	0,020
17-18	0,7320	0,5739	Residential	0,090	0,040
2-19	0,1640	0,1565	Commercial	0,090	0,040
19-20	1,5042	1,3555	Commercial	0,090	0,040
20-21	0,4095	0,4784	Commercial	0,090	0,040
21-22	0,7089	0,9373	Commercial	0,090	0,040
3-23	0,4512	0,3084	Industrial	0,090	0,050
23-24	0,8980	0,7091	Industrial	0,420	0,200
24-25	0,8959	0,7071	Industrial	0,420	0,200
6-26	0,2031	0,1034	Industrial	0,060	0,025
26-27	0,2842	0,1447	Industrial	0,060	0,025
27-28	1,0589	0,9338	Industrial	0,060	0,020
28-29	0,8043	0,7006	Industrial	0,120	0,070
29-30	0,5074	0,2585	Industrial	0,200	0,600
30-31	0,9745	0,9629	Industrial	0,150	0,070
31-32	0,3105	0,3619	Industrial	0,210	0,100
32-33	0,3411	0,5302	Industrial	0,060	0,040

Simulation results

All simulations have been carried out using software developed in Matlab®. The following are the restrictions used in the cases studied in this work. (a) the lower an upper limits of voltage are fixed in 0.95 p.u. and 1.05 p.u., (b) the slack bus is always located at the bus # 1, (c) the base voltage is 13,2 kV and (d) the base power is 100 MWA.

Additionally, in order to test the optimization algorithm propose, some aspects must be defined (a) the 16:00 hour of operation in the production and demand curves are defined as the mean operation condition, (b) the standard size of the capacitors banks are [300; 600; 900] kVAr, (c) the standard size of the batteries banks are [250 500 750 1000] kW, (d) several capacitors banks can be placed and (e) only one batteries bank can be placed.

Table 2 shows the optimized compensation results for the test system. Results includes location and optimal size of the capacitors banks and the batteries bank.

Table 2. Optimized compensation results with heuristic search

BUS	CAPACITOR [kVAr]	BATTERY [kW]
8	600	-
10	900	-
25	300	-
30	900	-
11	-	750

Fig. 5 shows the voltage profile of the 33-bus electric microgrid. It can be observed the results for the base configuration (uncompensated) and the case when the compensative equipment are located, connected and optimally dimensioned (compensated).

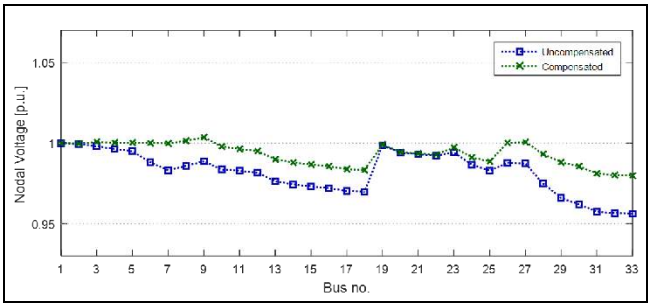

Figure 5. Comparison of voltage profile for 33-bus smart microgrid

Table 3 shows the load flow results of the 33-bus smart microgrid before and after the optimal compensation. It can be observed that a reduction of 74,2% for active power losses and 72,8% for reactive power losses when 4 capacitive banks and one storage system are installed.

Table 3. Load flow results of 33-bus smart microgrid

CASE	NODAL VOLTAGE				LOSSE POWER	
	Max.		Min.			
	Bus	p.u.	Bus	p.u.	kW	kVAr
Uncompensated	1	1,0000	33	0.9562	214,40	153,11
Compensated	3	1,0036	33	0.9799	55,38	41,61

After all simulations carried out in this section it can be concluded that the methodology for optimal locating and dimensioning of capacitive banks and storage systems presented is adequate to be implemented in a management system of energy losses control in electric smart microgrids.

Losses Control Management

In general, the voltage and reactive power control management applied to a smart microgrid must be an advanced system running periodically in response to request of the network operator in the control center (Rahimi et al, 2012). This process uses the ability of remote control that compensative equipment have, in order to optimizing the management of the smart microgrid in real time.

For this reason, the control variables in management systems are the control adjusts of the commutable capacitive banks and the storage power or injected by the battery banks.

Automation system integration

For operating and maintenance of electric networks some system monitoring and management tools are necessary. Traditionally, Supervisory, Control and Data Acquisition System (SCADA), Order Management System (OMS) and Distribution Management System (DMS) have been designed to offer this kind of support. Nevertheless, those systems only acquire information in real time up to the distribution feeder heads and are not able to process big volume of data.

On the other hand, during last years it has been a growth of automated substations, automated feeders and Advanced Measurement Infrastructure (AMI). This issues have presented a new approach of centralized control (Keping et al, 2014). All this automated possibilities have deliver adequate sensors, actuators and bidirectional communications between installed equipment and the control center of the smart microgrid under design.

Proposed management system

Implemented strategy: The implemented strategy look forward reducing power losses in 33-bus electric microgrid, using the heuristic search algorithm automatically. In this case, the computational procedure has been carried out for each level of load and generation in a 24 hours period as a base scale (see Fig. 2 and Fig. 3). The smart management system characteristic implemented is that microgrids studied operate under optimal criteria of minimization of losses and centrally controlled.

Circuital scheme: Losses control management in smart microgrids and distributed optimization are an open field for future research of electric systems. Fig. 6 shows the automated control system implemented. The arrows interconnecting each compensation equipment with the control center represent the adopted communication system. This two ways communication system allows to control each SVC and the storage system.

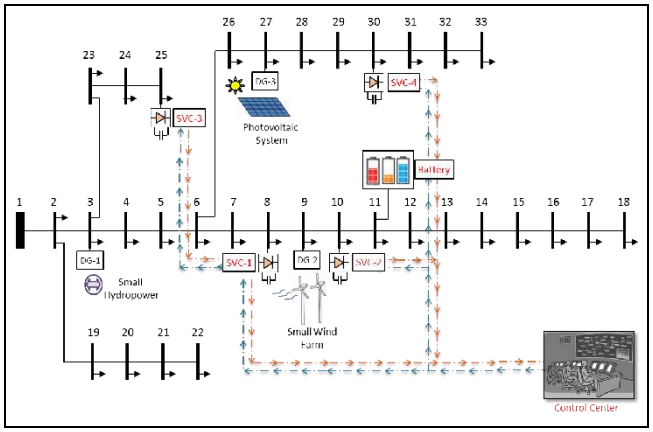

Figure 6. Circuital scheme of the proposed management system

Simulation results

In order to test the proposed management system, it has been assumed that the capacitive banks are replaced by Static VAR Compensators (SVC). These devices commute in steps of 10 kVAr in the Rank of (0 - 900) kVAr.

Moreover, the energy storage system presents three operation options: (a) storage at 750 kW/h, (b) injects at -750kW/h or (c) it disconnected.

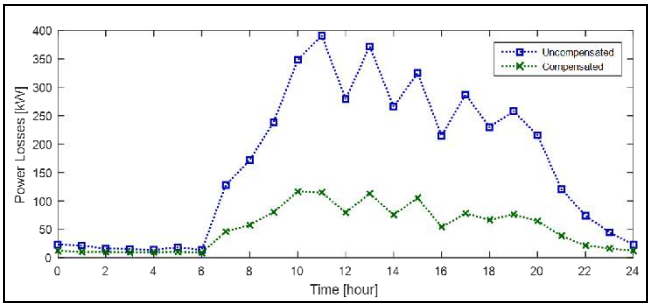

Figure 7. Comparison of power losses for 33-bus smart microgrid

Fig. 7 shows the behavior of the power losses evolution before and after the compensation of the 33-bus Smart microgrid. Here, energy total losses can be calculated in the 24 hours scale of time. In the uncompensated case, this losses are 4,1 MWh/day and in the compensated case 1,3 MWh/day, for a losses total reduction of 68,7%.

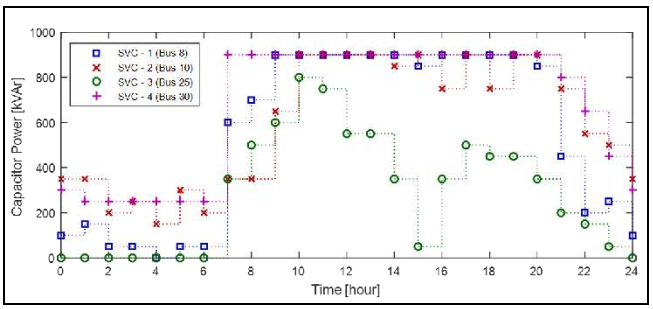

Figure 8. Optimal capacitor power injected

Fig. 8 shows the optimal reactive power injected by each one of the SVC in each hour of the day. It can be observed how few injection of reactive power is presented during valley time in the demand curves and a high injection in peak hours, helping the voltage profile control. On the other hand, the SVC located in the bus # 25 presents a different behavior in relation with the others, even with a disconnected period between 0:00 to 6:00 time.

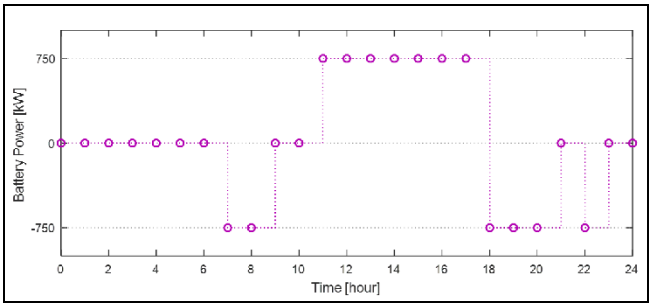

Figure 9. Optimal battery power stored/delivered

Fig. 9 shows the optimal active power stored/delivered by the storage system in each hour of the day. It can be observed that the hours when solar energy or wind energy generates the most, the batteries bank storages and during the hours when the demand requires this energy, it is injected again into the mirogrid.

Consequently, the methodology implemented shows an adequate control of reactive power injected and active power stored/delivered, thus an important reduction of energy losses is obtained.

Conclusion

An optimization algorithm based on a heuristic search for improve the voltage profile and minimize the power losses is presented. The algorithm is adapted for determine le location and sizing of reactive power of capacitive banks (commutable or SVC) and the injection/storage of active power in energy storage systems. The methodology implemented had shown very good results, guaranteeing an efficient and reliable process to be adopted into the nowadays concept of smart microgirds. From the results, it can be remarked the following observations: (a) an optimal location of storage system and capacitive banks for smart microgrids is a very important issue during planning and operation of the future distribution networks and (b) a system of management and control centralized is one of the most desirables and important functions of smart microgrids in order to improve the voltage profile and minimize the energy losses.

Acknowledgements

The authors gratefully acknowledge the financial support for this research provided by Universidad Nacional de Colombia-Sede Manizales, Colombia.

References

Ababei, C., Kavasseri R., Efficient Network Reconfiguration Using Minimum Cost Maximum Flow-Based Branch Exchanges and Random Walks-Based Loss Estimations., IEEE Transactions on Power Apparatus and Systems, Vol. 26, No. 1, 2011, pp. 30-37.

Aman M. M., Jasmon G. B., Bakar A.H.A., Mokhlis H., Karimi M., Optimum shunt capacitor placement in distribution system - A review and comparative study., Renewable and Sustainable Energy Reviews, Vol. 30, No., 2014, pp.429–439.

Amann G., La Evolución de la Red Eléctrica desde el paradigma del siglo XX hasta las Redes Inteligentes., II Congreso de generación distribuida, Madrid, 2013.

Díaz C., Hernández J., Smart Grid: Las TICs y la modernización de las redes de energía eléctrica-Estado del Arte., Revista Sistemas y Telemática, Vol. 9, No. 18, 2011, pp.53-81.

Dolli S.A., Jangamshetti S.H., Modeling and Optimal Placement of Voltage Regulator for a Radial System., International Conference on Power, Signals, Controls and Computation (EPSCICON), 2012, pp.1-6.

El-hawary M. E. The Smart Grid – State-of-the-art and Future Trends., Electric Power Components and Systems, Vol. 42, No. 3-4, 2014, pp. 239-250.

Gopiya N. S., Khatod D. K., Sharma M. P., Optimal allocation of distributed generation in distribution system for loss reduction., International conference on product development and renewable energy resources (ICPDRE 2012), India, 2012, pp. 42-46.

Karanki S.B., Xu D., Venkatesh B., Singh B.N., Optimal location of battery energy storage systems in power distribution network for integrating renewable energy sources, IEEE Energy Conversion Congress and Exposition, 2013, pp.4553-4558

Kashem, M. A., Ganapathy, V., Jasmon, G. B., Buhari, M. I., A novel method for loss minimization in distribution networks., International Conference on Electric Utility Deregulation and Restructuring and Power Technologies Proceedings, 2000, pp.251, 256.

Keping Y., Li Z., Zheng W., Mohammad A., Zhenyu Z., Sato T., CCN-AMI: Performance evaluation of content-centric networking approach for advanced metering infrastructure in smart grid., IEEE International Workshop on Applied Measurements for Power Systems Proceedings, 2014, pp.1-6.

Lasseter R.H., Paigi P., Microgrid: a conceptual solution., 35th Annual IEEE Power Electronics Specialists Conference, Germany 2004, pp.4285-4290.

Pathirikkat, G., Reddy, M. J. B., Mohanta, D., Stability concerns in smart grid with emerging renewable energy technologies., Elect. Power Compon. Syst., Vol. 42, No. 3–4, 2014, pp. 418–425.

Peças J. A., Hatziargyriou N., Mutale J., Djapic P., Jenkins N. Integrating distributed generation into electric power systems: A review of drivers, challenges and opportunities., Electric Power Systems Research, Vol. 77, No. 9, 2007, Pages 1189-1203, 2007.

Qiang L., Lin Z., Ke G., Review on the dynamic characteristics of micro-grid system., 7th IEEE Conference on Industrial Electronics and Applications, 2012, pp.2069-2074.

Rahimi S., Marinelli M., Silvestro F., Evaluation of requirements for Volt/Var control and optimization function in distribution management systems., IEEE International Energy Conference and Exhibition, 2012, pp.331-336.

Wakefield M.P., Smart distribution system research in EPRI's smart grid demonstration initiative., IEEE Power and Energy Society General Meeting, San Diego, CA, 2011.

Zeng Z., Zhao R., Yang H., Micro-sources design of an intelligent building integrated with micro-grid., Energy and Buildings, Vol. 57, No., 2013, pp 261-267.

Hybrid linear/non-linear adaptive controller for battery charger/discharger in renewable power systems

Controlador hibrido lineal/no-lineal adaptativo para un sistema de carga/descarga de una batería en sistemas de energía renovable

C. A. Ramos-Paja[1], D. González[1], S. I. Serna-Garcés[2]

ABSTRACT

This paper presents the control of an Energy Management System (EMS) for renewable DC sources connected to the load and a battery. The EMS is aimed at improving the performance of electric systems such as electrical vehicles and stand-alone applications. This work considers a Boost converter controlled by a Maximum Power Point Tracking algorithm (MPPT) to maximize the power generation of a renewable DC source. Moreover, a battery charger/discharger, based on a bidirectional dc/dc converter, is used to control the energy flows between the generator, the battery and the load. This paper proposes a sliding-mode current controller to guarantee the global stability of the bidirectional converter, i.e. of the EMS. In addition, a digital adaptive controller is proposed to regulate the voltage of the EMS DC bus, which enables to provide a stable load voltage. Detailed simulation results validate the proposed controller.

Keywords: EMS, adaptative controller, bidirectional dc/dc converter, sliding-mode controller, renewable power systems.

RESUMEN

Este artículo presenta un sistema de administración de energía (EMS – Energy Management System) para fuentes de energía renovable DC conectada a una carga y una batería. El EMS tiene como objetivo mejorar el desempeño del sistema eléctrico en vehículos eléctricos o aplicaciones autónomas. Este trabajo considera un convertidor Boost controlado por un algoritmo para el rastreo del punto de máxima potencia con el fin de maximizar la generación de potencia DC de la fuente de energía no renovable. Por otra parte, un sistema de carga/descarga de batería basado en un convertidor DC/DC bidireccional, es utilizado para controlar el flujo de energía entre la fuente, la batería y la carga. Este artículo propone un control de corriente por modos deslizantes con el fin de garantizar la estabilidad global del convertidor bidireccional. Adicionalmente, un control digital adaptativo es propuesto para regular el voltaje del bus DC del EMS, cuyo objetivo es proveer un voltaje estable a la carga. Resultados de simulaciones validan el controlador propuesto.

Palabras clave: Sistema de administración de energía, controlador adaptativo, convertidor DC/DC bidireccional, control por modos deslizantes, energía renovable.

Introduction

Renewable energy systems are a suitable alternative for developing micro-grids for stand-alone applications. In particular, the use of fuel cells (FC) and photovoltaic (PV) modules as power sources has significantly increased due to its pollution free operation, which is a major concern nowadays (Romero-Cadaval, et al., Sept 2013). The selection of a FC or PV source depends on the application: FC systems provide uninterrupted power production when fuel is provided (Ramos-Paja, et al., June 2010), which is a major characteristic of the classical combustion engines. However, FC can operate with clean fuels such as hydrogen to avoid environmental pollution. Moreover, FC are not constrained to the Carnot limit (Ramos-Paja, et al., June 2010), hence they are much more efficient in comparison with combustion engines. In contrast, PV systems only provide energy when the sun light (irradiance) is present. Therefore, an auxiliary power source is required to support the load during nights or in step-up transients (Sun, Zhang, Xing, & Guerrero, Oct 2011) (Ramos-Paja, Bordons, Romero, Giral, & Martínez-Salamero, March 2009). However, PV systems do not require fuel storage, which is a major advantage in terms of cost. In such a way, FC systems are mainly used for critical applications such as buck-up power sources for hospitals or telecommunications and automobiles (Ramos-Paja, Bordons, Romero, Giral, & Martínez-Salamero, March 2009) (Chen, May 2014), while PV systems are used for non-critical applications such as stand-alone sources and street lights (Romero-Cadaval, et al., Sept 2013). Moreover, FC and PV generators have been combined to support critical loads with low fuel consumption (Bizon, Oproescu, & Raceanu, Jan 2015): the PV source produces the power achievable with the sun light, while the FC system produces the power in excess required by the load; hence if the PV source produces enough power the FC does not operate.

Renewable generators also require an optimization system to guarantee an efficient operation named Maximum Power Point Tracker (MPPT). In the case of PV systems the MPPT defines the operation voltage that maximizes the power produced (Romero-Cadaval, et al., Sept 2013); otherwise, despite being exposed to high sun irradiance, the PV module could produce almost no energy. A clear description of such a problem is given in (Femia,

[1] Departamento de Energía Eléctrica y Automática, Facultad de Minas, Universidad Nacional de Colombia, Medellín, CO. E-mail: {caramosp, dgonzalezm}@unal.edu.co

[2] Departamento de Electrónica y Telecomunicaciones, Facultad de Ingenierías, Instituto Tecnológico Metropolitano, Medellín, CO.
E-mail: danielgonzalez, sergioserna}@itm.edu.co

Petrone, Spagnuolo, & Vitelli, July 2005). In the case of FC systems, the requested electrical power could be produced at different current/voltage values as explained in (Ramos-Paja, Spagnuolo, Petrone, & Mamarelis, April 2014): since the hydrogen consumption is proportional to the FC current (Ramos-Paja, Bordons, Romero, Giral, & Martínez-Salamero, March 2009), then the optimal operation condition is achieved when the load power is supplied at the minimum FC current. In both FC and PV cases, the implementation of the MPPT requires two devices: a digital processor to execute the MPPT algorithm, and an unidirectional dc/dc converter to define the source voltage or current. In addition, the operation of the MPPT generates a bandwidth limitation since the transition from one optimal condition to another one is not instantaneous (Femia, Petrone, Spagnuolo, & Vitelli, July 2005) (Ramos-Paja, Spagnuolo, Petrone, & Mamarelis, April 2014), or even not possible if the sun irradiance or fuel are constrained. Moreover, since the associated dc/dc converter is controller to track the optimal operation condition, i.e. by the MPPT, such a dc/dc converter is regulated as follows: in PV systems the converter input voltage is controlled (Bianconi, et al., March 2013), while in FC systems the converter input current is regulated (Ramos-Paja, Spagnuolo, Petrone, & Mamarelis, April 2014). Therefore, the output voltage of the dc/dc converter is not regulated. Such a condition makes impossible to provide a stable operation voltage to the load.

The previous limitations have been addressed by adding a battery as depicted in **Figure 1**: in load transients the battery provides or absorbs the power difference between the generator and load profiles. Such a condition enable the system to supply any load profile, and at the same time, to store energy when the load is not consuming, or even to recover energy produced by the load, e.g. regenerative break in electrical vehicles. In addition, a bidirectional dc/dc converter (named charger/discharger) is added to interface the battery and the load with two main objectives: first, the charger/discharger is regulated to provide a stable voltage to the load; and second, the charger/discharger isolates the battery and load voltages, it making possible to use any battery for any load voltage requirement. The main problem in this kind of power systems concerns the design and control of the Energy Management System (EMS) required to regulate the power exchanged between the battery, the generator and the load. This paper proposed an EMS based on a hybrid linear/non-linear adaptive controller regulating the charger/discharger. In such a way, the charger/discharger is controlled to provide the required operation voltage to the load, and at the same time, to manage the battery power flow in agreement with the generator production and load requirement. The main challenge in such a solution is to guarantee the voltage stability in any operation condition. Moreover, since the bidirectional dc/dc converter must to manage both positive (discharge) and negative (charge) power flows, a single controller is difficult to design for both tasks. Therefore, this proposed solution combines a nonlinear controller to guarantee global stability, and an adaptive controller to ensure a consistent performance in any condition.

The paper is organized a follows: Section II presents the EMS topology and the charger/discharger circuit, Section III presents the non-linear controller designed to guarantee stability and Section IV presents the adaptive controller designed to provide an stable load voltage. Section V verifies the control system performance by means of simulation results and Section VI presents the paper conclusions.

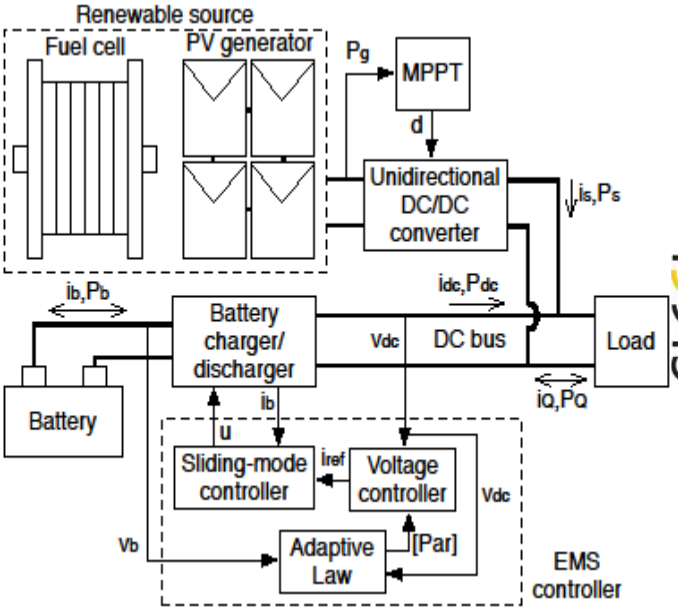

Figure 1: Hybrid fuel cell/photovoltaic power system.

Energy Management System

Figure 1presents a widely adopted structure for power systems based on renewable generators (Bizon, Oproescu, & Raceanu, Jan 2015): a generator managed by a dc/dc converter, which in turns is controlled by an MPPT controller to ensure optimal operation; and a battery interfaced with a charger/discharger, i.e. a bidirectional dc/dc converter. The outputs of both dc/dc converters are connected to form a bidirectional dc bus. Since the loads are connected to such a dc bus, then the dc/dc converters must to provide a stable voltage to the bus in any operation condition. Since the dc/dc converter associated to the renewable generator is controller to ensure an MPPT operation, the output voltage of such a dc/dc converter is not controlled. Therefore, that unidirectional dc/dc converter behaves as a power source providing the profile P_s with non-regulated current i_s. In consequence, the charger/discharger must be controlled to provide a regulated voltage v_{dc} to the dc bus. This condition implies that such a bidirectional dc/dc converter must to behave as a voltage source with a power profile equal to the difference (positive or negative) between the load and generator powers, i.e. $P_{dc} = P_Q - P_s$ and $i_{dc} = i_Q - i_s$ since v_{dc} is controlled.

The bidirectional dc/dc converter, i.e. charger/discharger, must be implemented with synchronous structures (Jang & Agelidis, May 2011) to enable both positive and negative current flows from/to the battery. A classical structure used for such an application is the bidirectional topology presented in Figure 2, which interfaces common low-voltage batteries v_b with high-voltage dc buses v_{dc}, i.e.$v_b < v_{dc}$. In such an electrical scheme the battery is modeled by a voltage source v_b with current i_b, while the dc bus is modeled by a capacitor C_{dc} and a current source i_{dc}. Such a model makes possible to account for step load transients, both positive or negative. Moreover, the Mosfets of the dc/dc converter are complementary controlled with the signal u: when $u = 1$ the vertical Mosfet is turned ON and the horizontal Mosfet is turned OFF, when $u = 0$ the vertical Mosfet is turned OFF and the horizontal Mosfet is turned ON.

As previously described, the main challenge in this system concerns to guarantee the voltage stability: the non-linear nature of the dc/dc converter makes impossible to guarantee global stability using a classical lineal controller; in addition, a single controller must be designed to control the converter in both positive and negative power flows, which is not a trivial task. Several authors have recognized such a drawback of the linear controllers, using non-linear controllers to guarantee global stability on dc/dc converters, e.g. (Bianconi, et al., March 2013), (Zhao, Qiao, & Ha, March 2014), (Inthamoussou, Pegueroles-Queralt, & Bianchi, Sept 2013).

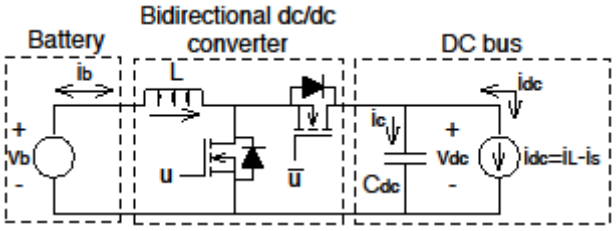

Figure 2: Charger/discharger electrical scheme.

The following sections propose a new control solution based on combining an analog non-linear controller with a digital adaptive controller to ensure a consistent performance in any condition.

Sliding-Mode Current Controller

The first challenge is to design a non-linear controller to ensure global stability of the charger/discharger in any operation condition. This paper proposes to design a Sliding-Mode Controller (SMC) due to its robustness and low sensitivity to parameters variations (Zhao, Qiao, & Ha, March 2014), (Tan, Lai, & Tse, March 2008) and (Sira-Ramírez, Aug 1987). Such characteristics allow to disregard parasitic losses without impacting significantly the validity of the sliding-mode analyses as illustrated in (Bianconi, et al., March 2013), (Zhao, Qiao, & Ha, March 2014) and (Inthamoussou, Pegueroles-Queralt, & Bianchi, Sept 2013).

The bidirectional condition of the charger/discharge of Figure 2 implies that such a circuit must be analyzed for both positive and negative current flows. From the definition of the converter' output power $P_{dc} = P_L - P_s$, positive battery currents i_b stand for the battery providing power, i.e. boost condition since $v_b < v_{dc}$, while negative battery currents i_b stand for the battery absorbing power, i.e. buck condition.

Boost condition (discharge)

In this condition the battery current i_b flows from the battery to the dc bus. Figure 3 shows the simplified electrical scheme of such an operation condition. The switched differential equations (1) and (2) describe the circuit behavior, where u is the binary control signal of the Mosfets, L represents the inductor value and C_{dc} represents the capacitor value.

$$\frac{di_b}{dt} = \frac{v_b - v_{dc}\cdot(1-u)}{L} \qquad (1)$$

$$\frac{dv_{dc}}{dt} = \frac{i_b\cdot(1-u) - i_{dc}}{C_{dc}} \qquad (2)$$

Then, the inductor current must be controlled to ensure the system stability. Such a controller is designed as an SMC based on the switching function $\Psi_d = i_b - i_{ref}$ and sliding surface $\Phi_d = \{\Psi_d = 0\}$. In such a surface i_{ref} represents the reference value imposed to the inductor current, which in turns ensure an stable behavior. However, to guarantee the correct behavior of the SMC, three conditions must be granted (Sira-Ramírez, Aug 1987) (Tan, Lai, & Tse, March 2008): transversality, reachability and equivalent control.

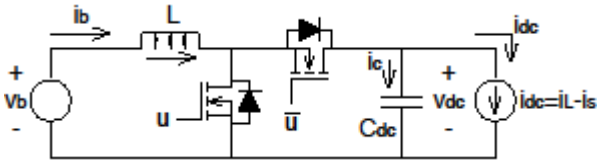

Figure 3: Boost (discharge) condition the charger/discharger.

The transversality condition analyzes the ability of the SMC to affect the system dynamics. This condition is granted if $\frac{d}{du}\left(\frac{d\Psi_d}{dt}\right) \neq 0$ (Sira-Ramírez, Aug 1987). For the boost system (1)-(2) under the control of Φ_d, the time derivative of the switching function is given by (3), and replacing (1) into (3) leads to (4), which confirms the transversality condition.

$$\frac{d\Psi_d}{dt} = \frac{di_b}{dt} \qquad (3)$$

$$\frac{d}{du}\left(\frac{d\Psi_d}{dt}\right) = \frac{v_{dc}}{L} > 0 \qquad (4)$$

The reachability conditions analyze the ability of the SMC to reach the surface. i.e. the desired condition, which in this case is $i_b - i_{ref} = 0$. The reachability conditions depend on the sign of the transversality condition (Sira-Ramírez, Aug 1987), which in this case is positive. Therefore, the reachability conditions to fulfill are:

$$\lim_{\Psi_d \to 0^-} \left.\frac{d\Psi_d}{dt}\right|_{u=1} = \frac{v_b}{L} > 0 \qquad (5)$$

$$\lim_{\Psi_d \to 0^+} \left.\frac{d\Psi_d}{dt}\right|_{u=0} = \frac{v_b - v_{dc}}{L} < 0 \qquad (6)$$

Relations (5) and (6) verify the reachability conditions. Finally, the equivalent control condition establishes that the average value of the binary control signal must be within the signal limits (Sira-Ramírez, Aug 1987). The analysis of the equivalent control is performed within the sliding surface, hence $\Psi_d = 0$ and $\frac{d\Psi_d}{dt} = 0$. Moreover, in dc/dc converters the binary control signal could be $u = 1$ or $u = 0$, hence the equivalent control value u_{eq} must be constrained within $0 < u_{eq} < 1$. Then, replacing u by u_{eq} in (1) and taking into account condition (3), $u_{eq} = 1 - \frac{v_b}{v_{dc}}$. Such an expression leads to relation (7), which verifies the equivalent control condition.

$$0 < u_{eq} < 1 \;\rightarrow\; v_b < v_{dc} < v_{dc} + v_b \qquad (7)$$

In conclusion, since transversality, reachability and equivalent control conditions are fulfilled, the SMC designed with $\Psi_d = i_b - i_{ref} = 0$ is stable. Therefore, under the action of such an SMC, $i_b = i_{ref}$ in any operation condition. An additional analysis required for designing the SMC concerns the implementation law (Tan, Lai, & Tse, March 2008): from the reachability conditions (5) and (6) it is noted that $\Psi_d < 0$ (or $\Psi_d \to 0^-$) requires $u = 1$, while $\Psi_d > 0$ (or $\Psi_d \to 0^+$) requires $u = 0$. Such information will be used afterwards to synthesize the implementation circuit for the SMC.

Buck condition (charge)

In this condition the battery current i_b flows from the dc bus to the battery. Figure 4 shows the simplified electrical scheme with the new current conventions, where the following switched differential equations describe the circuit behavior:

$$\frac{di_b}{dt} = \frac{v_{dc}\cdot(1-u)-v_b}{L} \quad (8)$$

$$\frac{dv_{dc}}{dt} = \frac{i_{dc}-i_b\cdot(1-u)}{C_{dc}} \quad (9)$$

Similar to the boost case, the inductor current must be controlled to ensure system stability. Again, such a controller is designed as an SMC based on the switching function $\Psi_c = i_b - i_{ref}$ and sliding surface $\Phi_c = \{\Psi_c = 0\}$. In this case i_{ref} follows the convention of Figure 4. It must be pointed out that such a current will be negative in the convention of Figure 3. The transversality condition is analyzed from (8)-(9) and (10), which leads to relation (11). Such an expression confirms the transversality condition.

$$\frac{d\Psi_c}{dt} = \frac{di_b}{dt} \quad (10)$$

$$\frac{d}{du}\left(\frac{d\Psi_c}{dt}\right) = -\frac{v_{dc}}{L} < 0 \quad (11)$$

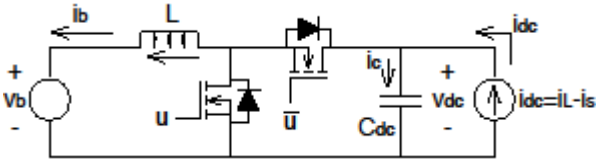

Figure 4: Buck (charge) condition the charger/discharger.

The reachability conditions for $\Psi_c = 0$, defined by the negative value of the transversality condition, are verified in (12) and (13).

$$\lim_{\Psi_c\to 0^-} \frac{d\Psi_c}{dt}\Big|_{u=1} = -\frac{v_b}{L} < 0 \quad (12)$$

$$\lim_{\Psi_c\to 0^+} \frac{d\Psi_c}{dt}\Big|_{u=0} = \frac{v_{dc}-v_b}{L} > 0 \quad (13)$$

Finally, the equivalent control is analyzed for $\Psi_c = 0$ and $\frac{d\Psi_c}{dt} = 0$. Then, replacing u by u_{eq} in (8), (9) and (10), u_{eq} is obtained as in (14), which verifies the equivalent control.

$$0 < u_{eq} = 1 - \frac{v_b}{v_{dc}} < 1 \;\rightarrow\; v_b < v_{dc} < v_{dc} + v_b \quad (14)$$

Again, the SMC designed with $\Psi_c = i_b - i_{ref} = 0$ is stable and it ensures $i_b = i_{ref}$ in any operation condition. From the reachability conditions (12) and (13) it is noted that $\Psi_c < 0$ (or $\Psi_c \to 0^-$) requires $u = 1$, while $\Psi_c > 0$ (or $\Psi_c \to 0^+$) requires $u = 0$. Such conditions are the same ones obtained in the boost condition, which will be used for the design SMC implementation circuit.

SMC implementation

Taking into account that both switching laws of boost and buck cases are the same ($u = 1$ if $\Psi_{c,d} < 0$ and $u = 0$ if $\Psi_{c,d} > 0$), a single unified SMC circuit can be designed to control both cases. To implement both SMC the current conventions in Figure 3 are used: the sliding surface of the buck condition $\Psi_c = i_b - i_{ref} = 0$ is rewritten as $-i_b = -i_{ref}$ while the sliding surface of the boost condition is expressed as $i_b = i_{ref}$. With such an unified convention, positive values of i_{ref} will impose positive battery currents, i.e. discharge the battery, while negative values of i_{ref} will impose negative battery currents, i.e. charge the battery.

In addition, to avoid infinite (and impractical) switching frequencies for the SMC circuit, an hysteresis band $2H$ is added to the surface as explained in (Tan, Lai, & Tse, March 2008). In such a way, the practical switching law becomes:

$$u = 1 \quad \text{if} \quad \Psi_{c,d} \le -H \quad (15)$$

$$u = 0 \quad \text{if} \quad \Psi_{c,d} \ge H \quad (16)$$

With the previous switching law the battery current will be constrained within $i_{ref} - H \le i_b \le i_{ref} + H$ for any operation condition. The hysteresis band $2H$ is defined following physical constraints: limit the switching frequency, limit the inductor current ripple, among others (Tan, Lai, & Tse, March 2008). The switching laws (15) and (16) are implemented in the hybrid analog/digital circuit of Figure 5. The circuit at the left implements exactly such inequalities: if $\Psi_{c,d} \le -H$ the Set input of the Flip-Flop is triggered, which sets the Flip-Flop output $Q = u = 1$; while if $\Psi_{c,d} \ge H$ the Reset input of the Flip-Flop is triggered to reset the Flip-Flop output $Q = u = 0$. A more practical circuit is presented at the right side of the figure, in which the switching law is rewritten as (17) and (18).

$$u = 1 \quad \text{if} \quad i_b \le i_{ref} - H \quad (17)$$

$$u = 0 \quad \text{if} \quad i_b \ge i_{ref} + H \quad (18)$$

Then, the implementation circuit of the right side of Figure 5 measures the battery current and hysteresis band limits to produce the Mosfet activation signals u and $\bar{u}$.

Finally, the previously designed SMC guarantees the system stability in any operation condition by ensuring the condition $i_b = i_{ref}$. The following section presents the design of an adaptive controller to define i_{ref}.

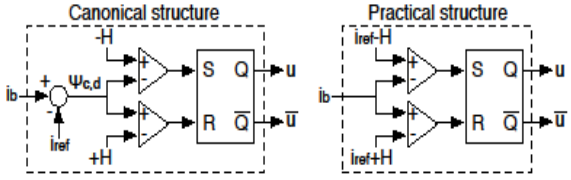

Figure 5: Implementation circuits for the SMC.

EMS Voltage Controller

Taking into account the inductor current control performed by the SMC, the circuital scheme of the charger/discharger can be modeled as in Figure 6, where the inductor and Mosfets are represented by a current source. Such a model is accurate since the inductor current is controlled, hence it behaves as a current source with $i_b = i_{ref}$. The main discrepancy concerns the effect of the horizontal Mosfet operation on the current delivered to the dc bus. Therefore, the current source receives the command i_{ref} but delivers the horizontal Mosfet current i_{MosH}. Since the horizontal Mosfet is active for $u = 0$ (or $\bar{u} = 1$), the average current of such a Mosfet is given by (19), where $d = 1 - \frac{v_b}{v_{dc}}$ represents the converter duty cycle and $d' = 1 - d$ represents the complementary duty cycle. Therefore, the current source model includes a variable gain equal to d'.

$$i_{MosH} = d' \cdot i_b = d' \cdot i_{ref} \quad (19)$$

The mathematical model describing the behavior of dc bus voltage, obtained from Kirchhoff laws and Laplace transform, is given in (20); while the transfer function between such a voltage and the reference current of the SMC is given in (21).

$$V_{dc}(s) = \frac{1}{C_{dc}\cdot s}\cdot\left(d'\cdot I_{ref}(s) - I_{dc}(s)\right) \quad (20)$$

$$Gv_{/i}(s) = \frac{V_{dc}(s)}{I_{ref}(s)} = \frac{d'}{C_{dc}\cdot s} \quad (21)$$

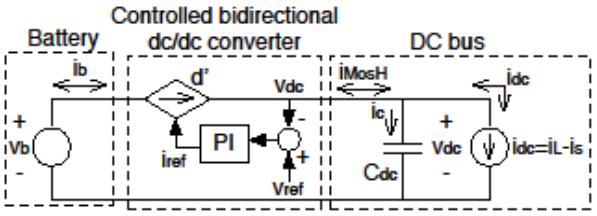

Figure 6: Charger/discharger model including the SMC and voltage controller.

An additional voltage controller is required to regulate the bus voltage, i.e. to provide a stable voltage v_{ref} to the load. This paper considers the design of a PI controller, given in (22), but any other structure could be adopted. Then, the closed loop transfer function between the bus voltage and the desired reference voltage is given by (23).

$$PI(s) = k_p + \frac{k_i}{s} \qquad (22)$$

$$\frac{V_{dc}(s)}{V_{ref}(s)} = \frac{\left(\frac{d'}{C_{dc}}\right)\cdot(k_p\cdot s+k_i)}{s^2+\left(\frac{d'}{C_{dc}}\right)\cdot k_p\cdot s+\left(\frac{d'}{C_{dc}}\right)\cdot k_i} \qquad (23)$$

From the denominator analysis of (23), and from the classical dynamic behavior of second order systems (Ramos-Paja, González, & Saavedra-Montes, Accurate calculation of settling time in second order systems: A photovoltaic application, March 2013), the expressions given in (24) are obtained. In such expression t_s, ρ and ω_n represent the settling-time, damping ration and natural frequency of the dc voltage, respectively.

$$t_s = \frac{3.9}{\rho\cdot\omega_n}, \qquad \rho\cdot\omega_n = \frac{d'\cdot k_p}{2\cdot C_{dc}}, \qquad \omega_n^2 = \frac{d'\cdot k_i}{C_{dc}} \qquad (24)$$

Then, k_p and k_i are calculated from (24) to guarantee the desired dynamic behavior of the bus voltage, i.e. t_s and ρ:

$$k_p = \frac{7.8\cdot C_{dc}}{d'\cdot t_s}, \qquad k_i = \frac{d'\cdot k_p^2}{4\cdot C_{dc}\cdot\rho^2} \qquad (25)$$

Since the complementary duty cycle d' changes with the operation conditions, i.e. bus and battery voltages, such k_p and k_i parameters must to be adapted. Therefore, the adaptive PI controller must to measure the battery and bus voltages to modify k_p and k_i, i.e. vector [Par] in Figure 1, according to the adaptive law imposed by (25). The implementation of the voltage controller is performed using a digital processor to simplify the adaptive law calculation. In such a way, Figure 7 presents the proposed block diagram: the bus and battery voltages are acquired using Analog-to-Digital Converters (ADC), which are available in many Digital Signal Controllers (DSC), such data is processed by the adaptive law to tune the PI parameters. Such a PI controller is a discretized version of (22) based on the bilinear transformation. Finally, the limits of the hysteresis band are calculated and imposed to the SMC circuit (Figure 5) using two Digital-to-Analog Converters (DAC).

Control System Performance

The scheme of Figure 1 was implemented in the power electronics simulator PSIM, which is a standard for dc/dc converters simulation (Ramos-Paja, et al., June 2010) (Femia, Petrone, Spagnuolo, & Vitelli, July 2005) (Bianconi, et al., March 2013). The charger/discharge (Figure 2) was controlled using the hybrid linear/non-linear controller formed by the SMC circuit described in Figure 5 and the adaptive PI controller described in Figure 7. To illustrate the control system performance the following parameters were adopted: $L = 100\ \mu H$, $C_{dc} = 100\ \mu F$, $v_b = 12\ V$ and a required load voltage $v_{ref} = 48\ V$. In addition, the hysteresis band was set to $H = 1\ A$ to ensure a switching frequency around $50\ kHz$. The ADC and DAC were simulated by quantization blocks of 12 bits with a sampling time of $100\ kHz$. Moreover, the adaptive law and digital PI controller were executed using a C-block to simulate the digital processor. Finally, the performance parameters were set as $t_s = 3\ ms$ and $\rho = 0.707$.

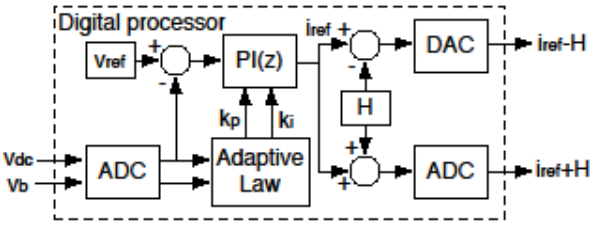

Figure 7: Block diagram of the adaptive digital controller for vdc.

The simulation considers the pulsating load profile depicted in Figure 8: the load current i_Q is $8\ A$ up to $15\ ms$, at that instant i_Q changes to $4\ A$. Moreover, the renewable generator produces a power profile (depicted in terms of the generator current is) that changes due to the environmental, fuel supply and MPPT operation. For example, up to $5\ ms$ the generator produces enough power to supply the load, but at $5\ ms$ the power production is reduced, which forces the charger/discharger to extract power from the battery (depicted in terms of the battery current i_b) to supply the load. The bus current i_{dc} is the difference between the current requested by the load and the current supplied by the source.

Similarly, at $15\ ms$ the generator produces power in excess due to an instantaneous load change, which forces the charger/discharger to store the remaining power into the battery, i.e. negative i_b current. Finally, at $26\ ms$, the battery voltage starts to oscillate to simulate an additional perturbation.

The simulations results, presented in Figure 8, show a satisfactory performance of the control system: the bus voltage v_{dc} is accurately regulated under all the perturbations for both charge and discharge conditions. Moreover, the satisfactory performance of the SMC is also verified, i.e. $i_b = i_{ref}$, even under a strong perturbation on v_b. Finally, Figure 8 also reports the evolution of k_p and k_i, which put in evidence the requirement of the adaptive law to guarantee the desired dynamic performance, i.e. $t_s = 3\ ms$ and $\rho = 0.707$.

Finally, it must be point out that any other dc/dc converter parameters, or performance parameters values, could be defined since the adaptive law will adjust the PI controller.

Conclusions

The paper has presented a EMS for an electric system composed by a renewable DC source, a battery and a load bus. This system was based on a battery charger/discharger controlled to regulate the DC bus voltage. The proposed solution was based on two cascade controllers for the charger/discharger: an adaptive controller designed to regulate the voltage of the DC bus accounting for changes of the model parameters, and a non-linear controller designed to regulate the battery current. This non-linear controller is based on the sliding-mode theory to guarantee the system stability in any operation condition.

Finally, a future improvement of this work consist in including the voltage regulation into the sliding surface to perform a more precise design of the converter dynamics, accounting for the

battery charge/discharge profile, and including the battery state of charge (SOC) regulation.

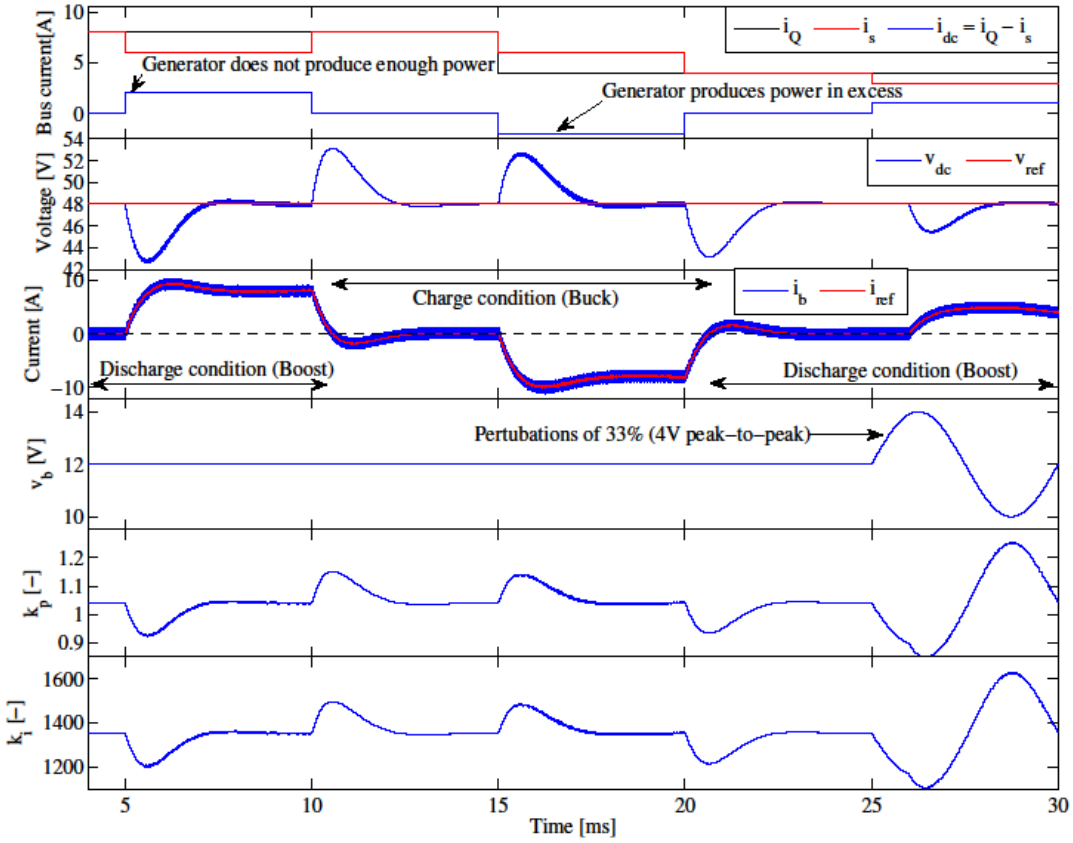

Figure 8: Simulation of the EMS under load and battery perturbations.

Acknowledgment

This paper was supported by Universidad Nacional de Colombia, Instituto Tecnológico Metropolitano and COLCIENCIAS under the projects FC-121056236765, RECONFOP- 21386 (Jóvenes Investigadores-2013), P14215 and P14220, and the doctoral scholarship 012-567.

Bibliografía

Bianconi, E., Calvente, J., Giral, R., Mamarelis, E., Petrone, G., Ramos-Paja, C., . . . Vitelli, M. (March 2013). A fast current-based mppt technique employing sliding mode control. *IEEE Transactions on Industrial Electronics, 60*, 1168-1178.

Bizon, N., Oproescu, M., & Raceanu, M. (Jan 2015). Efficient energy control strategies for a standalone renewable/fuel cell hybrid power source. *Energy Conversion and Management, 90*, 93-110.

Chen, H. S. (May 2014). A study on green consumer intention of portable hydrogen fuel cells. *Energy Education Science and Technology Part A: Energy Science and Research, 32*, 2027-2036.

Femia, N., Petrone, G., Spagnuolo, G., & Vitelli, M. (July 2005). Optimization of perturb and observe maximum power point tracking method. *IEEE Transactions on Power Electronics, 20*, 963-973.

Inthamoussou, F. A., Pegueroles-Queralt, J., & Bianchi, F. D. (Sept 2013). Control of a supercapacitor energy storage system for microgrid applications. *IEEE transactions on energy conversion, 28*, 690-697.

Jang, M., & Agelidis, V. (May 2011). A minimum power-processing-stage fuel-cell energy system based on a boost-inverter with a bidirectional backup battery storage. *IEEE Transactions on Power Electronics, 26*, 1568-1577.

Ramos-Paja, C., Bordons, C., Romero, A., Giral, R., & Martínez-Salamero, L. (March 2009). Minimum fuel consumption strategy for pem fuel cells. *IEEE Transactions on Industrial Electronics, 56*, 685-696.

Ramos-Paja, C., Giral, R., Martínez-Salamero, L., Romano, J., Romero, A., & Spagnuolo, G. (June 2010). A pem fuel-cell model featuring oxygen-excess-ratio estimation and power-electronics interaction. *IEEE Transactions on Industrial Electronics, 57*, 1914–1924.

Ramos-Paja, C., Spagnuolo, G., Petrone, G., & Mamarelis, E. (April 2014). A perturbation strategy for fuel consumption minimization in polymer electrolyte membrane fuel cells: Analysis, design and fpga implementation. *Applied Energy, 119*, 21-32.

Romero-Cadaval, E., Spagnuolo, G., Franquelo, L. G., Ramos-Paja, C., Suntio, T., & Xiao, W. (Sept 2013). Grid-connected photovoltaic generation plants: Components and operation. *IEEE Industrial Electronics Magazine, 7*, 6-20.

Sira-Ramírez, H. (Aug 1987). Sliding motions in bilinear switched networks. *IEEE Transactions on Circuits and Systems, 34*, 919-933.

Sun, K., Zhang, L., Xing, Y., & Guerrero, J. (Oct 2011). A distributed control strategy based on dc bus signaling for modular photovoltaic generation systems with battery energy storage. *IEEE Transactions on Power Electronics, 26*, 3032–3045.

Tan, S. C., Lai, Y., & Tse, C. (March 2008). General design issues of sliding-mode controllers in dc-dc converters. *IEEE Transactions on Industrial Electronics, 55*, 1160-1174.

Zhao, Y., Qiao, W., & Ha, D. (March 2014). A sliding-mode duty-ratio controller for dc/dc buck converters with constant power loads. *IEEE transactions on industry applications, 50*, 1448-1458.

Market Clearing Model for Microgrids with Probabilistic Security Criteria: Formulation and Implementation

Modelo de Despacho para Microrredes con Criterios de Seguridad Probabilísticos: Formulación e Implementación

Luis E. Luna[1], Horacio Torres[2], Andrés Pavas[3]

ABSTRACT

This paper proposes an energy-reserve market clearing model for microgrids considering probabilistic security criteria. The probabilistic security criteria include pre-selected scenarios associated to unreliability of generators and uncertainties caused by the stochastic behavior of loads and renewable units. In contrast to traditional deterministic reserve-constrained market clearing models, this paper determines the optimal amount of reserve as the point at which the sum of its operating costs and the expected cost of load shed reach a minimum. The proposed model is formulated as a two-stage stochastic programming problem, where the first stage represents the hour-ahead energy-reserve market, and the second stage the balancing market.

An energy management procedure is developed in order to implement the stochastic programming problem on the real microgrid ATENEA located at the installations of the National Renewable Energy Centre of Spain. The generation and reserve schedules obtained with the stochastic approach are assessed and compared with those of a purely deterministic security-constrained case.

Keywords: Market clearing, microgrids, mixed integer nonlinear programming, probabilistic security, reserve, stochastic programming.

RESUMEN

Este artículo propone un modelo de despacho de energía-reserva para microrredes considerando criterios de seguridad probabilísticos. Los criterios de seguridad probabilísticos incluyen escenarios preseleccionados asociados a la falla de generadores y a las incertidumbres causadas por el comportamiento estocástico de cargas y unidades renovables. A diferencia de los modelos de despacho tradicionales con restricciones de reserva determinísticas, este artículo determina la cantidad óptima de reserva como el punto en el que la suma de sus costos de operación y el costo esperado del deslastre de carga alcanza un mínimo. El modelo propuesto es formulado como un problema de programación estocástica de dos etapas, donde la primera etapa representa el despacho de energía-reserva de la hora siguiente, y la segunda etapa el mercado de balances.

Un procedimiento de gestión de la energía es desarrollado con el fin de implementar el problema de programación estocástica en la microrred ATENEA ubicada en las instalaciones del Centro Nacional de Energías Renovables de España. Los programas de generación y reserva obtenidos con el enfoque estocástico se evaluaron y compararon con aquellos obtenidos de un caso con restricciones de seguridad puramente determinísticas.

Palabras clave: Despacho, microrredes, programación no lineal entera mixta, seguridad probabilística, reserva, programación estocástica.

Received: January __th 2011
Accepted: February __th 2012

Nomenclature

Indices.

i	Index of dispatchable generators, from 1 to *I*.
j	Index of nondispatchable generators, from 1 to *J*.
m	Index of buses, from 1 to *M*.
t	Index of time periods, from 1 to *T*.

[1] Luis Ernesto Luna. Electrical Engineer, Escuela Colombiana de Ingeniería, Colombia. MSc in Electrical Engineering, Universidad Nacional de Colombia, Colombia. PhD Candidate in Electrical Engineering, Universidad Nacional de Colombia, Colombia. E-mail: lelunar@unal.edu.co

[2] Horacio Torres. Electrical Engineer, Universidad Nacional de Colombia, Colombia. MSc in Electrical Engineering, Universidad Nacional de Colombia, Colombia. Head of PAAS-UN Research Group, Universidad Nacional de Colombia, Colombia. E-mail: htorress@unal.edu.co

[3] Andrés Pavas. Electrical Engineer, Universidad Nacional de Colombia, Colombia. MSc in Electrical Engineering and PhD in Electrical Engineering, Universidad Nacional de Colombia, Colombia. Assitant professor, Universidad Nacional de Colombia, Colombia. E-mail: fapavasm@unal.edu.co

How to cite: Luna, L., Torres, H., Pavas, A. (2015). Market Clearing Model for Microgrids with Probabilistic Security Criteria: Formulation and Implementation, Ingeniería e Investigación, 35(Sup X), xx-xy. DOI: http://dx.doi.org/10.15446/ing.investig.v35nSx.xxxxx

x Index of net load scenarios, from 1 to *X*.

y Index of unit outage scenarios, from 1 to *Y*.

z Index of aggregated scenarios, from 1 to *Z*.

Variables.

$f_t(m,s)$ Power flow through line *(m,s)* in period *t*.

g_{it} Power output of dispatchable generator *i* in period *t*.

g_{jt} Power output forecast of nondispatchable generator *j* in period *t*.

$l_{mt}^{sh}(z)$ Involuntarily shed load at bus *m* in period *t* and aggregated scenario *z*.

r_{it}^{up} Up reserve capacity of dispatchable generator *i* in period *t*.

r_{it}^{dw} Down reserve capacity of dispatchable generator *i* in period *t*.

r_{it}^{su} Start-up reserve capacity of dispatchable generator *i* in period *t*.

r_{mt}^{up} Up reserve capacity of flexible demand at bus *m* in period *t*.

r_{mt}^{dw} Down reserve capacity of flexible demand at bus *m* in period *t*.

u_{it} Binary variable (1 if dispatchable generator *i* is online in period *t*; 0 otherwise).

$y_{it}^{up}(z)$ Up reserve deployed by dispatchable generator *i* in period *t* and aggregated scenario *z*.

$y_{it}^{dw}(z)$ Down reserve deployed by dispatchable generator *i* in period *t* and aggregated scenario *z*.

$y_{it}^{su}(z)$ Start-up reserve deployed by dispatchable generator *i* in period *t* and aggregated scenario *z*.

$y_{mt}^{up}(z)$ Up reserve deployed by flexible demand at bus *m* in period *t* and aggregated scenario *z*.

$y_{mt}^{dw}(z)$ Down reserve deployed by flexible demand at bus *m* in period *t* and aggregated scenario *z*.

Parameters.

C_{it} Offer cost of dispatchable generator *i* in period *t*.

C_{it}^{NL} No-load offer cost of dispatchable generator *i* in period *t*.

C_{it}^{SU} Start-up offer cost of dispatchable generator *i* in period *t*.

C_{jt} Offer cost of nondispatchable generator *j* in period *t*.

C_{mt} Offer benefit of flexible demand at bus *m* in period *t*.

C_{it}^{R} Offer cost of up/down reserve capacity of dispatchable generator *i* in period *t*.

C_{mt}^{R} Offer cost of up/down reserve capacity of flexible demand at bus *m* in period *t*.

C_{it}^{O} Cost due to outage of dispatchable generator *i* in period *t*.

C_{jt}^{O} Cost due to outage of nondispatchable generator *j* in period *t*.

d_{mt} Load forecast at bus *m* in period *t*.

D_{mt}^{max} Maximum power that can be consumed by flexible demand at bus *m* in period *t*.

D_{mt}^{min} Minimum power required by flexible demand at bus *m* in period *t*.

E_{m}^{hour} Minimum hourly energy consumption for flexible demand at bus *m*.

$F^{max}(m,s)$ Maximum capacity of line *(m,s)*.

G_i^{max} Capacity (maximum power output) of unit *i*.

G_i^{min} Minimum power output of unit *i*.

$p(z)$ Probability of aggregated scenario *z*.

$v_{it}(z)$ Binary parameter (0 if dispatchable generator *i* fails in period *t* and aggregated scenario *z*; 1 otherwise).

$v_{jt}(z)$ Binary parameter (0 if nondispatchable generator *i* fails in period *t* and aggregated scenario *z*; 1 otherwise).

V_{mt}^{LOL} Value of lost load at bus *m* in period *t*.

$\Delta l_{mt}(z)$ Net load forecast error at bus *m* in period *t* and aggregated scenario *z*.

φ_t Duration of time period *t*.

Sets.

Λ Set of transmission lines.

M_I Mapping of the sets of dispatchable units into the set of buses.

M_J Mapping of the sets of nondispatchable units into the set of buses.

Remark: When augmented with the argument *(z)*, the above variables and parameters represent their value given that stochastic scenario *z* has occurred in the microgrid.

Introduction

The integration of renewable sources into microgrids represents one of the biggest challenges to their operators and planners (IEEE, 2011), (Luna et al, 2011). In order to accommodate the unpredictable nature of renewable power, the generation and demand scheduled in an electricity market need to be modified during the real-time operation of the microgrid (Katiraei et al, 2008). The spinning reserve (SR) is the service traded in the market to materialize physically the required adjustments necessary to maintain a secure network operation (Gooi et al, 1999).

Increasing the SR requirement can reduce the probability and severity of involuntary load shedding. However, providing SR has a cost because additional units may be committed and other units may operate below their optimal output. Thus, determining the optimal amount of SR to be provided as a function of the system conditions represents a relevant issue to be solved. Traditional market clearing processes adopt a deterministic approach to estimate the reserve capacity needs. These processes ignore the stochastic nature of the events that call for balancing energy, and consequently, reserve requirements are estimated independent of both the probability of stochastic scenarios affecting the power system and their impact on system operation costs.

In (Kirschen, 2002) it is suggested that power system security analysis methods should evaluate the "credibility" of scenarios and their "expected" consequences by means of probabilistic methods. Various probabilistic approaches have been developed for optimizing the SR required in a power system under stochastic scenarios. Reference (Ortega & Kirschen, 2010) assumes that the reserve market is independent of the energy market, which ignores the strong coupling between the supply of energy and the provision of reserve capacity. In microgrids, the reserve cost

may become very significant due to their highly stochastic operation, therefore the use of a simultaneous energy and reserve market clearing procedure allows avoiding uneconomical out-of-merit operation, the start-up of extra units, as well as unnecessary load shedding. In (Wang & Gooi, 2011) and (Liu & Tomsovic, 2012) it is proposed an energy-reserve day-ahead scheduling model that considers probabilistic methods for estimating the SR requirement under equipment failure and uncertainties caused by load and nondispatchable units. These approaches do not clear the balancing market in advance of the realization of the scenarios involved, which is necessary to evaluate the real-time reserve deployment actions. References (Bouffard et al, 2005a), (Bouffard et al, 2005b), (Bouffard et al, 2008), (Morales et al, 2009), (Ruiz et al, 2009) and (Papavasiliou et al, 2011) formulate a day-ahead and balancing market clearing model with stochastic security. These approaches clear the electricity markets in advance of the realization of the scenarios represented generally by unreliability of units or by aggregated demand and wind uncertainty.

All these models do not consider the simultaneous occurrence of the main stochastic scenarios involved in a power system; they do not include the flexible actions of microgrids that permit to improve the security, reliability, quality and efficiency of the system; and these market clearing formulations are not implemented and analyzed on real power systems.

This paper proposes a multi-period energy-reserve market clearing procedure with unit commitment for microgrids considering probabilistic security criteria. The procedure is formulated as a two-stage stochastic programming problem (Birge and Louveaux, 1997). The contributions of this paper are:

1. Introducing the flexibility actions of microgrids associated to battery management and demand response programs into the market clearing formulation.
2. Including a reserve valuation method into the stochastic programming problem that determines the economically optimal level of reserve capacity and reserve deployment within a microgrid. This method permits to optimally manage the failure of units and the uncertainty associated to loads and renewable units.
3. Implementing and testing the market clearing problem on a real network, microgrid ATENEA (Cener, 2015).

The rest of this paper is organized as follows. Section II formulates the market clearing model as a mixed integer nonlinear programming problem. Section III describes in detail the microgrid ATENEA. Section IV presents the energy management procedure and provides results of its implementation on the real microgrid. Section V summarizes the paper with conclusions and discussion.

Market Clearing Model

Description.

A market clearing model for microgrids, that adopts a probabilistic security approach to estimate the reserve capacity needs, is formulated. This model defines the optimal amount of SR to be provided as the point at which the sum of its operating costs and the expected cost of load shed reach a minimum.

The market clearing model is a two-stage stochastic programing problem. The first stage involves the hour-ahead market, which takes place several minutes in advance and settles contracts to energy delivery for the next hour in m-min intervals. The second stage considers the balancing market that serves to competitively settle the energy adjustments required to ensure the constant balance between electricity supply and demand. The balancing market takes place a few seconds before energy delivery and constitutes the last market mechanism to balance production and consumption. This market is particularly relevant for microgrids because of scenarios associated to unreliability of units (Billinton & Allan, 1996) and uncertainties caused by the stochastic behavior of loads and renewable units (e.g., wind and solar power producers).

The coexistence of both markets is well-justified. On the one hand, the hour-ahead market is useful for those power plants that need advance planning in order to efficiently and reliably adjust their production levels. This market considers decisions associated to commitment states of units, and the scheduled energy and reserve capacity throughout the scheduling horizon. On the other hand, the balancing market constitutes a competitive mechanism to efficiently cope with the energy imbalances by allowing flexible firms to adjust their hour-ahead positions. This market considers decisions associated with the deployment of reserve, and the involuntary load shedding in each scenario.

Reserves are either of the up/down or start-up type. Generation-side up/down reserve is provided by committed generators only, while start-up reserve involves changes in the scheduling status of generators. For instance, a generator that is scheduled off can provide start-up reserve if it can be turned on to produce energy within the scenario occurrence. For a consumer, providing up-going reserve implies being ready to voluntarily decrease its level of consumption within the scenario occurrence (Parvania & Fotuhi-Firuzabad, 2010). In the case of down-going reserve, consumers providing this service would be asked to increase their consumption level.

A reasonable way to compute reserve needs using a probabilistic approach is through the expected load not served (ELNS). The ELNS is a stochastic security metric that represents the average amount of energy not supplied as a result of load shedding actions. It is presented as a weighted average energy value that accounts for the probability of uncertain factors and the damage that these factors cause to the system in the form of involuntary curtailed load. The load shedding actions are involuntary as opposed to voluntary demand reduction offered as up-reserve. Moreover, the ELNS can be expressed linearly, and hence, easily included and penalized inside the objective function.

$$ELNS_{mt} = \sum_{z \in Z} p(z) \cdot l_{mt}^{sh}(z) \qquad (1)$$

The SR requirements are determined based on the cost of its provision and the benefit derived from its availability, i.e., ELNS. This way, the amount of reserve that is scheduled matches the value it provides to system users.

Problem formulation.

The objective function aims at minimizing the expected cost, which includes both the cost related to the hour-ahead electricity dispatch and the expected cost of the anticipated balancing actions to be taken during the real-time operation of the microgrid. The optimization problem is solved using mixed integer nonlinear programming methods, and the objective function is stated in equation (2). The objective function to be minimized groups separately those terms representing the costs pertaining to the energy-reserve dispatch [from line 1 to line 4], and those

representing the expected costs needed to keep the microgrid balanced under the full set of scenarios considered [from line 5 to line 8].

$$\sum_{t=1}^{T}\varphi_t\left[\sum_{i=1}^{I}\left(C_{it}\cdot g_{it}+C_{it}^{NL}\right)+\sum_{j=1}^{J}C_{jt}\cdot g_{jt}+\sum_{i=1}^{I}C_{it}^{R}\cdot\left(r_{it}^{up}+r_{it}^{dw}+r_{it}^{su}\right)+\sum_{m=1}^{M}C_{mt}^{R}\cdot\left(r_{mt}^{up}+r_{mt}^{dw}\right)\right]+\sum_{t=1}^{T}\sum_{i=1}^{I}C_{it}^{SU}+\sum_{z\in Z}p(z)\left\{\sum_{t=1}^{T}\varphi_t\left[\sum_{i=1}^{I}C_{it}\cdot\left(y_{it}^{up}(z)-y_{it}^{dw}(z)+y_{it}^{su}(z)\right)+\sum_{m=1}^{M}C_{mt}\cdot\left(y_{mt}^{up}(z)-y_{mt}^{dw}(z)\right)-\sum_{i=1}^{I}C_{it}^{O}(z)-\sum_{j=1}^{J}C_{jt}^{O}(z)+\sum_{m=1}^{M}V_{mt}^{LOL}\cdot l_{mt}^{sh}(z)\right]\right\} \quad (2)$$

It is assumed that renewable producers are not competitive agents, and consequently, this generation is considered as a negative demand, which is equivalent to state that $C_{jt}=0$.

The objective function is subject to constraints pertaining to both hour-ahead and balancing market (Morales et al, 2014), that describe the operational rules of dispatchable units and flexible demands.

First-Stage Constraints Pertaining to the Hour-Ahead Market Operation (Not Depending on Scenario z).

Power Balance:

$$d_{mt}=\sum_{i:(i,m)\in M_I}g_{it}+\sum_{j:(j,m)\in M_J}g_{jt}-\sum_{s:(m,s)\in\Lambda}f_t(m,s),\ \forall m,\forall t. \quad (3)$$

Due to the technical and operational conditions of distribution networks, the power flow relation $f_t(m,s)$ uses the nonlinear ac load flow model.

Capacity limits:

On the one hand, the power production and reserve capacity of a dispatchable generator is ultimately conditioned by its capacity (maximum power output) and minimum power output, that is:

Up/Down Reserve:

$$g_{it}+r_{it}^{up}\le G_i^{max}\cdot u_{it},\ \forall i,\forall t. \quad (4)$$

$$g_{it}-r_{it}^{dw}\ge G_i^{min}\cdot u_{it},\ \forall i,\forall t. \quad (5)$$

Start-Up Reserve:

$$0\le r_{it}^{su}\le G_i^{max}\cdot(1-u_{it}),\ \forall i,\forall t. \quad (6)$$

On the other hand, the change in the scheduled load of flexible demand at bus *m* in period *t* is bounded above and below by its maximum and minimum load levels, which is formulated mathematically by the next constraints:

$$d_{mt}-r_{mt}^{up}\ge D_{mt}^{min},\ \forall m,\forall t. \quad (7)$$

$$d_{mt}+r_{mt}^{dw}\le D_{mt}^{max},\ \forall m,\forall t. \quad (8)$$

Second-Stage Constraints Pertaining to the Balancing Market Operation (Depending on Scenario z).

Power Balance:

The second-stage power balance constraint, described in equation (9), groups separately those terms representing the real-time power variations because of scenarios associated to unit outages and uncertainties caused by the stochastic behavior of net load forecast error (difference between the load forecast error and the power output forecast error of renewable units) [from line 1 to line 2], and those representing the power balancing actions required to counteract the mentioned variations [from line 3 to line 5].

$$\sum_{i:(i,m)\in M_I}g_{it}\cdot(1-v_{it}(z))+\sum_{j:(j,m)\in M_J}g_{jt}\cdot(1-v_{jt}(z))+\Delta l_{mt}(z)=\sum_{i:(i,m)\in M_I}(y_{it}^{up}(z)-y_{it}^{dw}(z)+y_{it}^{su}(z))+l_{mt}^{sh}(z)+y_{mt}^{up}(z)-y_{mt}^{dw}(z)+\sum_{s:(m,s)\in\Lambda}\left(f_t(m,s)-f_t(m,s)(z)\right),\ \forall m,\forall t,\forall z. \quad (9)$$

Transmission Capacity:

$$-F^{max}(m,s)\le f_t(m,s)(z)\le F^{max}(m,s),\ \forall(m,s)\in\Lambda,\forall t,\forall z. \quad (10)$$

Consumption Limits:

$$\sum_{t=1}^{T}d_{mt}(z)\cdot\varphi_t\ge E_m^{hour},\ \forall m,\forall z. \quad (11)$$

Shedding Limits:

$$l_{mt}^{sh}(z)\le d_{mt}(z),\ \forall m,\forall t,\forall z. \quad (12)$$

This part of the formulation, which involves the actual operation of the system (second-stage constraints), also include minimum up/down time of dispatchable generators and ramping constraints of both generating units and flexible demands. For the sake of

conciseness, the mathematical formulation of these constraints is omitted.

First- and Second-Stage Constraints Pertaining to the Hour-Ahead and Balancing Market Operation.

Power Decomposition:

The actual power output of dispatchable generator *i* during period *t* and under scenario *z* is defined as:

$$g_{it}(z) = g_{it} + y_{it}^{up}(z) - y_{it}^{dw}(z) + y_{it}^{su}(z), \forall i, \forall t, \forall z. \quad (13)$$

Moreover, the actual load for flexible demand at bus *m* in period *t* and scenario *z* is expressed as:

$$d_{mt}(z) = d_{mt} - y_{mt}^{up}(z) + y_{mt}^{dw}(z), \forall m, \forall t, \forall z. \quad (14)$$

Reserve Deployment Limits:

On the one hand, the reserve deployment of a dispatchable generator is conditioned by its reserve capacity. This can be written as:

Up/Down Reserve:

$$0 \le y_{it}^{up}(z) \le r_{it}^{up} \cdot v_{it}(z), \forall i, \forall t, \forall z \quad (15)$$

$$0 \le y_{it}^{dw}(z) \le r_{it}^{dw} \cdot v_{it}(z), \forall i, \forall t, \forall z. \quad (16)$$

Start-Up Reserve:

$$G_i^{min} \cdot u_{it}(z) \le y_{it}^{su}(z) \le r_{it}^{su}, \forall i, \forall t, \forall z. \quad (17)$$

On the other hand, the maximum up/down reserve deployment of flexible demand at bus *m* in period *t* is described in the next constraints:

$$0 \le y_{mt}^{up}(z) \le r_{mt}^{up}, \forall m, \forall t, \forall z \quad (18)$$

$$0 \le y_{mt}^{dw}(z) \le r_{mt}^{dw}, \forall m, \forall t, \forall z. \quad (19)$$

The stochastic programming problem was solved using DICOPT, a mixed integer nonlinear programming solver under GAMS (Rosenthal, 2015).

Case Study

The market clearing model was analyzed on the three-phase microgrid ATENEA located at the installations of the National Renewable Energy Centre of Spain (CENER) in Sangüesa, Navarre, Spain. This microgrid is a low-voltage (400/230 V) installation that can operate interconnected or isolated from the distribution network. The main elements are (Aguado et al, 2012):

- Renewable generators: A photovoltaic generator (PV) of 25.2 kWp.
- Batteries: A vanadium flow battery (VFB) capable of delivering 50 kW during 4 hours, and a lead acid battery (LAB) capable of delivering 50 kW during 2 hours.
- Conventional generators: A diesel turbine (DT) of 55 kW and a gas microturbine (GT) of 30 kW.
- Loads: A three-phase bank of programmable resistive loads of 87.63 kW that allows emulating any load profile.

The microgrid ATENEA is shown in Figure 1, where the distribution system represents the generator 1, the GT the 2, the DT the 3, the LAB the 4, the VFB the 5, and the PV is the generator 6. The five distribution lines have identical impedance values. The resistance and reactance are all 0.0547 p.u. and 0.0283 p.u. respectively, on a base of 1 MW and 0.4 kV.

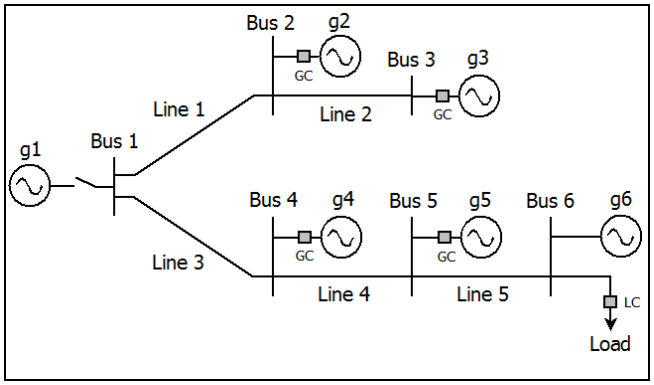

Figure 1. Microgrid ATENEA.
Source: The authors

The stochastic programming formulation analyzes the scheduling of this 6-buses microgrid over a horizon of four periods of 15 min, i.e., one hour.

The demand for the next scheduling horizon in 15-min periods is emulated using the three-phase bank of programmable resistive loads. The standard deviation of the load forecast error is assumed to be 5% of the 15-min load forecast. In addition, the loads are located at bus 6 and offer up to 10% of the demand at each period as reserve services (both up- and down-going) at the rate of 16 dollar cents per kilowatthour. It is also assumed that these loads value involuntary loss-of-load at the rate of 500 dollar cents per kilowatthour during all four periods.

The hourly irradiance forecasts are evaluated using mesoscale numerical weather prediction models operated and combined with statistical post-processing based on learning machines at CENER (Perez et al, 2013).

The stochastic behavior of net load forecast error throughout the next scheduling horizon is represented accurately by 625 possible scenarios. The size of this scenario set is too large, resulting in an optimization model that is intractable. Hence, to achieve tractability, statistical techniques (Heitsch & Römisch, 2003) are applied in order to reduce the number of scenarios while retaining the essential features of the original scenario set. The reduced scenario set obtained through this process includes 40 scenarios. Likewise, the stochastic behavior of the unit outages over the next scheduling horizon is modeled by 15625 possible scenarios. Because the size of this scenario set is too large, the number of scenarios is reduced by considering only single failures that represent the 99.99% of the unit outages probability distribution. The reduced scenario set includes 25 scenarios.

The generating unit data are found in Table 1. The fuel-consuming generators incur fixed start-up cost C_{it}^{SU} in dollar cents. Each generator offers a single block of energy ranging between its technical minimum G_i^{min} and maximum G_i^{max} at the bid composed by rate cost C_{it} in dollar cents per kilowatthour (fuel cost for fuel-consuming units and energy purchase cost for storage units) and fixed no load cost C_{it}^{NL} in dollar cents per hour (hourly payback amount for the investment). The generation-side reserve capacity services C_{it}^{R} for up-going reserve, for down-

going reserve, and for start-up reserve are offered at rates in dollar cents per kilowatthour.

Table 1. Generating unit data

	Generator *i*			
	2	3	4	5
G_i^{max} (kW)	30	48	50	50
G_i^{min} (kW)	2	2	0	0
C_{it} (¢/kWh)	19.23	25	8.53	11.44
C_{it}^{NL} (¢/h)	120.17	33.78	138.27	492.68
C_{it}^{SU} (¢)	1.60	15.28	0	0
C_{it}^{R} (¢/kWh)	0.4	0.4	0.4	0.4
λ_i (faults/years)	6	6	6	6

Source: The authors

The failure rate λ_i of both the network and the PV is 6 faults/year. The hourly price of the energy supplied from the network to the microgrid C_{it}, for February of 2015, is defined in Table 2 in dollar cents per kilowatthour.

Table 2. Energy prices from IBERDROLA on February, 2015

Hour	C_{it} (¢/kWh)	Hour	C_{it} (¢/kWh)	Hour	C_{it} (¢/kWh)
0-7	6.37	10-12	11.07	18-20	11.07
8-7	9.39	13-17	9.39	21-23	9.39

Source: The authors

The distribution network and the batteries are considered special sources, because they can sell energy to or buy energy from the microgrid. The bid offer of the network C_{it} to buy energy from the microgrid is zero, because of the actual regulatory conditions of the microgrid ATENEA do not permit to remunerate the energy supplied to the network. Likewise, the bid offer of the batteries C_{it} to buy energy from the microgrid equals the bid offer of the network to sell energy to the microgrid, assuming that the batteries are only charged with energy supplied from the network.

Energy Management Procedure

Description.

In order to implement the market clearing model on the microgrid ATENEA, an iterative energy management methodology was developed using JAVA. The methodology is described below as a four-step procedure, where the first step is executed once a day, the second every 1 hour, the third every 15 minutes, and the fourth step every 10 milliseconds.

First-step: Daily at 06:00 am, the microgrid control client receives from the weather station server the hourly irradiance forecasts of Sangüesa, Navarre, Spain for the next 24 hours. These forecasts are stored in the file called "forecast".

At 06:00 am of each day, the demand of the microgrid is forecasted for the next 24 hours with a 15-min resolution. These forecasts are stored in the "forecast" file.

The irradiance forecasts have an hourly resolution, therefore the same forecast for the four 15-min periods of the next scheduling horizon is considered. The forecasts for the next scheduling horizon are stored in a file called "input" containing the input parameters of the market clearing model developed in GAMS.

Second-step: 5 minutes before starting the next scheduling horizon, the state of charge of batteries (LAB and VFB), the power generated by fuel-consuming units (GT and DT), and the demand consumed by loads are read from the SCADA. These parameters are sent to the client control and stored in the "input" file. Moreover, the hourly bid price of the energy supplied by the distribution network for the next scheduling horizon is identified, and stored in the "input" file.

The net load scenarios that can occur during the next scheduling horizon along with their associated probability of occurrence are identified from the PV availability, the irradiance forecast and the demand forecast for the next scheduling horizon. The unit outage scenarios that can occur during the next scheduling horizon along with their probability of occurrence are identified from the failure rate of the units and the generators availability. These scenarios and probabilities are stored in the "input" file.

After completing the "input" file, the stochastic programming problem developed in GAMS for the next scheduling horizon is executed. This program generates the "output" file containing the first-state variables, evaluated before the revelation of scenarios, and the second-state variables, obtained after the revelation of the scenarios considered throughout the next scheduling horizon.

Third-step: At the beginning of the first period (at minute 0) of the scheduling horizon, the power generated by PV, the demand consumed by loads, and the units status (fault/safe) are read from the SCADA. These parameters describe the actual operation of the microgrid.

The scenario *z* that represents the actual condition of the microgrid is identified, from the pre-selected scenarios of net load and units status. Then, the optimal operations of both dispatchable units $(g_{it}(z))$ and loads $(d_{mt}(z))$ for the scenario previously identified are selected from the "output" file. The optimal operations of elements are stored in the file "setpoint", and sent as setpoints to the SCADA for their immediate execution by elements of the microgrid.

The same procedure developed for the first period (at minute 0), is performed for the second (at minute 15), the third (at minute 30) and for the fourth period (at minute 45) of the scheduling horizon.

The operation described in the third-step represents the secondary regulation of the microgrid. The response time of this regulation is up to 15 min after the occurrence of the stochastic event.

Fourth-step: Every 10 milliseconds the SCADA monitors and controls the power supplied by each of the units and the power demanded by loads, in order to ensure the continuous balance between production and consumption in the microgrid. The actions that ensure the power balance every 10 ms are performed by a unit of the microgrid called "master". The LAB is the "master" in the isolated condition of the microgrid, and the distribution network in the connected condition.

The operation explained in the fourth-step represents the primary regulation of the microgrid.

Furthermore, the SCADA monitors every 10 ms the operational configuration of the microgrid (interconnected/islanded), in order to reassign the ``master" if there is a change in the configuration.

Results and Analysis.

The energy management methodology was evaluated throughout seven consecutive scheduling horizons, i.e., seven hours. The operational configuration of the microgrid ATENEA considers this grid interconnected to the distribution network limiting the capacity of the network to 15 kW.

The load forecasts d_{mt} and the irradiance forecasts h_t over the seven scheduling horizons in 15-min periods are given in Table 3.

Table 3. Load forecast (kW) and irradiance forecast (W/m²)

Hour	d_{m1}	d_{m2}	d_{m3}	d_{m4}	h_1	h_2	h_3	h_4
10	35.0	43.5	47.5	45.0	292.2	292.2	292.2	292.2
11	50.0	54.0	52.5	44.0	455.7	455.7	455.7	455.7
12	25.0	29.0	19.0	17.0	570.7	570.7	570.7	570.7
13	5.0	3.5	6.5	6.0	628.2	628.2	628.2	628.2
14	7.5	5.0	11.0	15.0	624.8	624.8	624.8	624.8
15	35.0	40.0	43.0	37.5	561.0	561.0	561.0	561.0
16	30.0	34.0	32.5	26.0	440.9	440.9	440.9	440.9

Source: The authors

Table 4 provides a breakdown of the expected cost of the microgrid, in dollar cents, into the cost pertaining to the energy supply, the cost of hiring reserve capacity, the expected cost of the balancing actions to be taken during the real-time operation, and the expected cost of the load shedding. This table shows that the market clearing solutions during the fourth and fifth scheduling horizons (hours 13 and 14) exhibit economic benefits for the microgrid, since the PV energy output is higher that the demand throughout these time periods, and therefore, the LAB is charged.

Table 4. Breakdown of expected cost (¢)

Hour	Energy	Reserve capacity	Reserve Deployment	ELNS	TOTAL
10	606.63	6.03	13.85	5.24	631.75
11	671.22	6.95	8.65	5.35	692.17
12	122.04	5.57	-0.45	1.45	128.62
13	-99.34	12.84	8.86	0.12	-77.52
14	-57.46	10.01	2.46	0.52	-44.48
15	401.59	6.19	21.40	5.18	434.36
16	303.20	5.88	18.59	2.15	329.82
TOTAL	1947.88	53.47	73.36	20.01	2094.72

Source: The authors

The reserve capacity cost is comparatively significant mainly due to the uncertainty in the PV power forecast. In this sense, it should be taken into account that, on the one hand, PV constitutes an important source of cheap renewable energy but, on the other hand, reserves are required in order to accommodate its unpredictable variability and, thus, to maintain the security and reliability of the system.

The results presented below describe and analyze the energy management in the microgrid for the second scheduling horizon (hour 11). The remaining horizons have the same treatment.

Table 5 summarizes the key features of the optimal schedule obtained for the second horizon. This table outlines the optimal generation and reserve schedules of the dispatchable units as well as the demand reserve contributions. Generator 1, being the cheapest, supplies its maximum power capacity during all the four periods and therefore does not provide any reserve. Generators 4 and 2, being the next cheapest units, pick up the residual demand and provide up and down reserves during the periods 1 to 3 and 4, respectively. In addition, generators 3 and 5 are never turned on. The PV provides a negative demand during the four periods, depending on the irradiance forecasts. The load at bus 6 provides up and down voluntary reserves, and furthermore, as seen in the last row of Table 5, the optimum market clearing schedule calls for some involuntary load shedding during all the four periods. This table also shows that due to the high value of lost load (500¢/kWh), the ELNS at bus 6 over the scheduling horizon is relatively low.

What makes this last result particularly interesting is that in spite of its high cost, the market clearing solution still calls for some amount of load shedding. This result is unique to the stochastic market clearing approach, reflecting the fact that some scenarios have both a low probability and a low impact in light of the relative expected costs of reserve deployment and load shedding. This brings out the essence of the probabilistic security, which considers simultaneously the credibility and severity of the scenarios making up the security criteria.

Table 5. Power (kW), reserve capacity (kW), and ELNS (kWh)

	Hour 11			
	1	2	3	4
g_{1t}	15	15	15	15
r_{1t}^{up}	0	0	0	0
r_{1t}^{dw}	0	0	0	0
r_{1t}^{su}	0	0	0	0
g_{2t}	0	0	0	17.52
r_{2t}^{up}	0	0	0	9.97
r_{2t}^{dw}	0	0	0	5.57
r_{2t}^{su}	0	0	0	0
g_{3t}	0	0	0	0
r_{3t}^{up}	0	0	0	0
r_{3t}^{dw}	0	0	0	0
r_{3t}^{su}	0	0	0	0
g_{4t}	23.52	27.52	26.02	0
r_{4t}^{up}	4.99	4.58	5.09	0
r_{4t}^{dw}	1.29	1.37	1.34	0
r_{4t}^{su}	0	0	0	0
g_{5t}	0	0	0	0
r_{5t}^{up}	0	0	0	0
r_{5t}^{dw}	0	0	0	0
r_{5t}^{su}	0	0	0	0
g_{1t}^{PV}	11.48	11.48	11.48	11.48
d_{1t}	50.00	54.00	52.50	44.00
r_{1t}^{up}	4.61	5.40	5.25	4.40
r_{1t}^{dw}	5.00	5.40	5.25	0
$ELNS_{1t}$	1.24×10^{-3}	2.69×10^{-3}	3.80×10^{-3}	2.96×10^{-3}

Source: The authors

At the beginning of the each period for the second scheduling horizon, the power generated by PV, the demand consumed by loads, and the units status were read from the SCADA. Next, it is analyzed in detail how reserve is deployed and how load is shed during each time period of the scheduling horizon, because of the actual condition of the microgrid.

On the one hand, the SCADA reported that all the generators included in the market clearing are in safe condition for each of the four periods, therefore, the actual units status is represented by the pre-selected unit outage scenario *y=1*. On the other hand, the SCADA reports let to analyze that the net load forecast errors for the first, second, third and fourth periods are -0.99 kW, 4.31 kW, -1.14 kW and -0.63 kW, respectively. Thus, the actual operation is represented by the pre-selected net load scenario *x=4*. The power balancing actions required to counteract the scenarios *y=1* and *x=4* for each of the periods are presented in the Table 6.

Table 6. Reserve deployed (kW), and load shed (kW)

	Hour 11			
	1	2	3	4
y_{1t}^{up}	0	0	0	0
y_{1t}^{dw}	0	0	0	0
y_{1t}^{su}	0	0	0	0
y_{2t}^{up}	0	0	0	0
y_{2t}^{dw}	0	0	0	5.03
y_{2t}^{su}	0	0	0	0
y_{3t}^{up}	0	0	0	0
y_{3t}^{dw}	0	0	0	0
y_{3t}^{su}	0	0	0	0
y_{4t}^{up}	4.01	4.58	4.11	0
y_{4t}^{dw}	0	0	0	0
y_{4t}^{su}	0	0	0	0
y_{5t}^{up}	0	0	0	0
y_{5t}^{dw}	0	0	0	0
y_{5t}^{su}	0	0	0	0
l_{1t}^{sh}	0	0	0	0
y_{1t}^{up}	0	0	0	4.40
y_{1t}^{dw}	5.00	0.27	5.25	0

Source: The authors

The optimal operations of units and loads in period *t* and aggregated scenario *z* for the second scheduling horizon are sent as setpoints to the SCADA for their immediate execution by elements of the microgrid.

Stochastic Versus Deterministic Market Clearing Models.

The objective function of the deterministic security-constrained market clearing problem only includes those terms in equation (2) representing the costs pertaining to the energy-reserve dispatch [from line 1 to line 4]. Furthermore, this function is subject to the first-stage constraints pertaining to the hour-ahead market, and a fixed amount of reserve capacity is scheduled by including reserve constraints in the optimization procedure (Luna et al, 2015).

The deterministic market clearing model specifies the upward reserve capacity as the PV power forecast, and the downward reserve is represented as half this power for each period of the scheduling horizon. This is, because the reserve capacity optimized by the stochastic programming problem on the microgrid ATENEA mainly varies with the PV power output, however, this solution does not necessarily hold in other systems.

It is of interest to compare the results obtained with the stochastic approach to those of a purely deterministic security-constrained schedule. The deterministic and stochastic total costs cannot be readily compared because they are obtained through completely different objective functions. Nonetheless, Table 7 lets to make a comparison of energy and reserve capacity costs between the two models throughout the seven scheduling horizons.

Table 7. Breakdown of cost (¢)–Stochastic versus Deterministic

Hour	Stochastic		Deterministic	
	Energy	Reserve capacity	Energy	Reserve capacity
10	606.63	6.03	606.63	4.42
11	671.22	6.95	671.22	6.89
12	122.04	5.57	138.93	8.63
13	-99.34	12.84	-99.34	9.50
14	-57.46	10.01	-57.46	9.45
15	401.59	6.19	401.59	8.48
16	303.20	5.88	303.20	6.67
TOTAL	1947.88	53.47	1964.77	54.03

Source: The authors

This comparison permits to demonstrate that the energy and the reserve capacity costs of the stochastic schedule are lower than those associated with the deterministic schedule. The efficiency gain of the stochastic programming solution versus that of the deterministic solution equals 16.89¢ + 0.56¢ = 17.45¢. This result illustrates that when one considers the probability of stochastic scenarios affecting the microgrid and their impact on system operation costs, it is possible to pre-position the microgrid more economically, while still achieving a high level of security on the average.

Figure 2 compares the reserve capacity obtained from the stochastic and the deterministic market clearing model throughout the seven scheduling horizons.

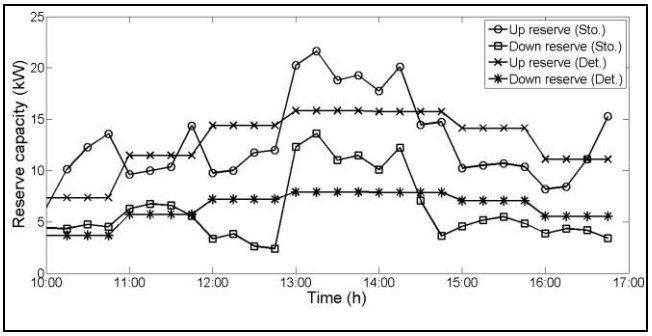

Figure 2. Comparison of reserve capacity–Deterministic versus Stochastic.

Source: The authors

This figure shows that the up and down reserves scheduled by the deterministic model are insufficient during some periods with respect to the reserves optimized by the stochastic problem. Whereas, during others, they exceed what is economically justifiable.

Conclusions

This paper proposes a market clearing model for microgrids adopting a probabilistic approach to estimate the reserve capacity needs. This model is a flexible and novel formulation that co-optimizes the hour-ahead and the balancing markets, in order to manage optimally the operation of grids with high levels of uncertainty.

An energy management methodology was developed for implementing the stochastic programming problem on the real microgrid ATENEA, located at the installations of CENER. The expected costs, the energy-reserve scheduling and the balancing actions to maintain the microgrid security were optimized and evaluated for seven consecutive scheduling horizons. These results have underlined that the stochastic methods should be considered in the operation planning of microgrids, since they offer many advantages and there are no major technical impediments in their implementation.

The scheduling results of the proposed stochastic formulation were compared with those obtained with a purely deterministic formulation. The preventive security control solution was found to be sub-optimal in the deterministic market clearing model, because this case does not consider neither the stochastic nature of a microgrid operation nor its economics. These studies have highlighted the potential economic benefits of a stochastic market clearing model.

Acknowledgment

The authors would like to thank the SILICE group for their support and suggestions. The authors would also like to thank the Renewable Energy Grid Integration Department (IRE) of CENER for their invaluable assistance in the market clearing model implementation on the microgrid ATENEA. This work was supported by the Administrative Department of Science, Technology and Innovation of Colombia (COLCIENCIAS) under the doctoral scholarship 511 of 2010.

References

Aguado, M., Garde, R., & Rivas, D. (2012). *El papel del almacenamiento de energía en la microrred de CENER*. Proceedings of the 1st Smart Grids Conference, Madrid, Spain.

Billinton, R., & Allan, R. N. (1996). *Reliability Evaluation of Power Systems*. 2nd ed. New York, NY, USA. Plenum.

Birge J. R., & Louveaux, F. (1997). *Introduction to Stochastic Programming*. New York. Springer-Verlag.

Bouffard, F., Galiana, F. D., & Conejo, A. J. (2005a). *Market-clearing with stochastic security-part I: Formulation*. IEEE Transactions on Power Systems. vol. 20, no. 4, pp. 1818-1826. DOI: http://dx.doi.org/10.1109/tpwrs.2005.857015

Bouffard, F., Galiana, F. D., & Conejo, A. J. (2005b). *Market-clearing with stochastic security-part II: Case studies*. IEEE Trans. Power Syst. vol. 20, no. 4, pp. 1827-1835. DOI: http://dx.doi.org/10.1109/tpwrs.2005.857016

Bouffard, F. & Galiana, F. D. (2008). *Stochastic security for operations planning with significant wind power generation*. IEEE Transactions on Power Systems. vol. 23, no. 2, pp. 306-316. DOI: http://dx.doi.org/10.1109/tpwrs.2008.919318

Cener. (2015). Microgrid ATENEA. Retrieved from http://www.cener.com/es/integracion-red-energias-renovables/microrred.asp.

Gooi, H. B., Mendes, D. P., Bell, K. R. W., & Kirschen, D. S. (1999). *Optimal scheduling of spinning reserve*. IEEE Trans. Power Syst., vol. 14, no. 4, pp. 1485-1490. DOI: http://dx.doi.org/10.1109/59.801936

Heitsch H., & Römisch, W. (2003). Scenario reduction algorithms in stochastic programming. Comput. Optim. Appl. vol. 24, pp. 187-206. DOI: http://dx.doi.org/10.1023/a:1021805924152

Institute of Electrical and Electronics Engineers [IEEE]. (2011). *Standard Guide for Design, Operation, and Integration of Distributed Resource Island Systems with Electric Power Systems*, (Std. 1547.4). Retrieved from IEEE Online.

Katiraei, F., Iravani, R., Hatziargyriou, N., & Dimeas, A. (2008). *Microgrids management*. IEEE Power Energy Mag. vol. 6, no. 3, pp. 54-65. DOI: http://dx.doi.org/10.1109/MPE.2008.918702

Kirschen, D. S. (2002). *Power system security*. Power Eng. J., vol. 16, pp. 241-248. http://dx.doi.org/10.1049/pe:20020502

Liu, G., & Tomsovic, K. (2012). *Quantifying spinning reserve in systems with significant wind power penetration*. IEEE Transactions on Power Systems. vol. 27, no. 4, pp. 2385-2393. DOI: http://dx.doi.org/10.1109/tpwrs.2012.2207465

Luna, L. E., & Parra, E. (2011). *Methodology for assessing the impacts of distributed generation interconnection*. Journal Ingeniería e Investigación, vol. 31, no. 2, pp. 36-44.

Luna, L. E., Torres, H., & Pavas, A. (2015). *Spinning reserve analysis in a microgrid*. Journal DYNA, vol. 82, no. 192, pp. 85-93. DOI: http://dx.doi.org/10.15446/dyna.v82n192.48580

Morales, J. M., Conejo, A. J., & Perez-Ruiz, J. (2009). *Economic valuation of reserves in power systems with high penetration of wind power*. IEEE Trans. Power Syst. vol. 24, no. 2, pp. 900-910. DOI: http://dx.doi.org/10.1109/tpwrs.2009.2016598

Morales, J. M., Conejo, A. J., Madsen, H., Pinson, P., & Zugno, M. (2014). *Integrating Renewables in Electricity Markets, Operational Problems*. New York. Springer, 2014.

Ortega-Vazquez, M. A., & Kirschen, D. S. (2010). *Assessing the impact of wind power generation on operating costs*. IEEE Transactions on Smart Grid, vol. 1, no. 3, pp. 295-301. DOI: http://dx.doi.org/10.1109/tsg.2010.2081386

Papavasiliou, A., Oren, S. S., & O'Neill, R. P. (2011). *Reserve requirements for wind power integration: A scenario-based stochastic programming framework*. IEEE Trans. Power Syst. vol. 26, no. 4, pp. 2197-2206. DOI: http://dx.doi.org/10.1109/tpwrs.2011.2121095

Parvania M., & Fotuhi-Firuzabad, M. (2010). *Demand response scheduling by stochastic SCUC*. IEEE Transactions on Smart Grid, vol. 1, no. 1, pp. 89-98. DOI: http://dx.doi.org/10.1109/tsg.2010.2046430

Perez, R., Lorenz, E., Pelland, S., Beauharnois, M., Van Knowe, G., Hemker Jr., K., Heinemann, D., Remund, J., Müller, S. C., Traunmüllerf, W., Steinmauer, G., Pozo, D., Ruiz-Arias, J. A., Lara-Fanego, V., Ramirez-Santigosa, L., Gaston-Romero, M., & Pomares, L. M. (2013). *Comparison of numerical weather prediction solar irradiance forecasts in the US, Canada and Europe*. Solar Energy, vol. 94, pp. 305-326. DOI: http://dx.doi.org/10.1016/j.solener.2013.05.005

Rosenthal, R. E. (2015). GAMS: A User's Guide. Washington, DC. GAMS Development Corp.

Ruiz, P. A., Philbrick, C. R., Zak, E., Cheung, K. W., & Sauer, P. W. (2009). *Uncertainty management in the unit commitment problem*. IEEE Trans. Power Syst. vol. 24, no. 2, pp. 642-651. DOI: http://dx.doi.org/10.1109/tpwrs.2008.2012180

Wang, M. Q., & Gooi, H. B. (2011). *Spinning reserve estimation in microgrids.* IEEE Transactions on Power Systems, vol. 26, no. 3,pp. 1164-1174. DOI: http://dx.doi.org/10.1109/tpwrs.2010.2100414

Modeling and parameter identification of photovoltaic modules

Modelado e identificación de parámetros de módulos fotovoltaicos

Jhon Alexander Cabrera[1], Andrés Mauricio Jácome[2], Juan Manuel Rey[3], Javier Solano[4]

ABSTRACT

This paper proposes and validates an algorithm to determine photovoltaic (PV) modules model parameters using the information provided by the PV module suppliers. The effect of temperature and solar irradiation variations on the parameters are analyzed for three PV models discussed on the literature. Advantages and drawbacks of the models are compared to determine the best adapted to be used in simulation of PV modules for sizing and energy management. The retained model and parameter identification algorithm is validated with the specifications of two different PV modules.

Keywords: Modeling and simulation, photovoltaic modules, parameter identification.

RESUMEN

Este trabajo propone y valida un algoritmo para determinar los parámetros del modelado de módulos fotovoltaicos usando las especificaciones entregadas por los fabricantes. El efecto de la temperatura y de la irradiación es analizado en tres modelos usados en la literatura. Las ventajas y desventajas de cada uno son comparadas para determinar la mejor solución para simular paneles fotovoltaicos para aplicaciones de dimensionado y gestión de energía. El modelo considerado y el algoritmo de identificación de parámetros son validados con las especificaciones de dos diferentes módulos fotovoltaicos.

Palabras clave: Modelado y simulación, módulos fotovoltaicos, identificación de parámetros.

Received: July 24th 2015
Accepted: Oct 15th 2015

Nomenclature

STC	Standard test conditions
PV	Photovoltaic
I_{pv}	Photocurrent (A)
$I_{pv,n}$	Photocurrent at STC (A)
$I_{sc,n}$	Short circuit current at STC (A)
I_0	Diode saturation current (A)
V_t	Diode thermal voltage (V)
a	Diode ideality factor (-)
R_s	Series resistance (Ω)
q	Absolute charge on an electron ($1.602\mathbf{x10^{-19}}$C)
V_{oc}	Open circuit voltage (V)
$V_{oc,n}$	Open circuit voltage at STC (V)
G	Solar irradiance (W/m^2)
Gn	Solar irradiance at STC (1000 W/m^2)
T	Cell temperature (K)
Tn	Temperature at STC (25 °C)
K	Boltzmann's constant ($-1.381\text{x}10^{-23}$ J/K)
K_I	Temperature coefficient of short cicuit current(A/K)
K_V	Temperature coefficient of open circuit voltage(V/K)
N_S	Number of cells in series (-)
R_P	Shunt resistance (Ω)
P	Constant (-)

Introduction

Solar PV power systems have been widely commercialized as a renewable and clean energy source with multiple potential benefits. PV modules are typically represented by equivalent electrical circuits, which can vary their topology and number of elements according to the modeling requirements [1]–[3]. The element's parameters are calculated by experiment measurements [4]–[6], especially with the *I-V* characteristic curve, which, in general, are determined by manufactures under Standard Test Conditions (STC). Modeling and parameter identification of photovoltaic models allow improving the simulations and design of PV systems prior to installation

Performance of most type of panels (i.e. multi-crystalline, mono-crystalline, thin-film) is strongly affected by variations of cell temperature and solar irradiation [7]. For this reason, modeling the panel without considering these variations could result inaccurate even for design stages which require simple and low computational-cost models, as energy management and PV systems sizing.

This paper is organized as follows: Section II presents three PV models. Section III proposes and validates an algorithm to identify the parameters of the PV models. Section IV selects one PV model and Section V presents the conclusions of the research.

[1] Electrical Engineering Student, Universidad Industrial de Santander, Colombia
[2] Electrical Engineering Student, Universidad Industrial de Santander, Colombia
[3] Assistant Professor, Universidad Industrial de Santander, Bucaramanga, Colombia
[4] Assistant Professor, Universidad Industrial de Santander, Bucaramanga, Colombia

Photovoltaic modules modeling

Three widely used models are considered in this section.

One-diode model considering Rs (4-p model)

Figure 1 illustrates the series resistance PV model. In this model, the series resistance represents the internal losses due to current flow and connecting wires [1][2]. Due to its simplicity, this model is widely used to estimate the non-linear *I-V* characteristic curve. This model is also known as four-parameter (4-p) model, these parameters are I_{pv1}, I_0, a and R_s. The following set of equations describes the PV model. Eq. (1) represents the output current and the other equations are used to identify I_{pv1} and I_0:

$$I=I_{pv1}-I_d=I_{pv1}-I_0\left(\exp\left(\frac{V+IR_s}{a*V_t}\right)-1\right) \quad (1)$$

$$I_0=I_{pv1}\left(\exp\left(-\frac{V_{oc}}{a*V_t}\right)\right) \quad (2)$$

$$I_{pv1}=I_{sc,\,n}\left(\frac{G}{G_n}\right)+K_I(T-T_n) \quad (3)$$

$$V_{oc}=V_{oc,n}+V_t\mathrm{Ln}\left(\frac{G}{G_n}\right)+K_V(T-T_n) \quad (4)$$

$$V_t=\frac{N_S KT}{q} \quad (5)$$

One-diode model considering Rs and Rp (5-p model)

The one-diode PV model considering R_s and R_P is shown in Figure 2. In this model, the shunt resistance is considered in order to improve the accuracy of the modeling. This resistance represents the leakage current of the p-n junction [1] [5]. In literature, this model is the so-called five-parameter (5-p) model as the model requires the determination of five parameters values, i.e. a, R_s, R_P, I_{pv2} and I_0. The 5-p model is characterized by its Eq.(6) and the other ones to find I_{pv} and I_0 :

$$I=I_{pv2}-I_d-I_p=I_{pv2}-I_0*\left(\exp\left(\frac{V+R_sI}{V_t*a}\right)-1\right)-\frac{V+R_sI}{R_P} \quad (6)$$

$$I_{pv2}=(I_{pv2,n}+K_I*\Delta_T)\frac{G}{G_n} \quad (7)$$

$$I_{pv2,n}=\left(\frac{R_s+R_P}{R_P}\right)*I_{sc,n} \quad (8)$$

$$\Delta_T=T-T_n \quad (9)$$

$$I_0=\frac{I_{sc,n}+K_I*\Delta_T}{\exp(V_{oc,n}+K_V*\Delta_T/V_t*a)-1} \quad (10)$$

Two-diode model

In a real solar cell, the recombination losses in the diode depletion region are significant, especially at low voltage levels [4], for this reason, this model adds another diode to the equivalent circuit, as is shown in Figure 3. This allows improving the non-linear *I-V* curve characteristics as it is fitted to the specifications. This model is more accurate for polycrystalline cells [6]. The following set of equations represents the *I-V* relationship of the PV panel:

$$I=I_{pv2}-I_{d1}-I_{d2}-I_p=I_{pv2}-I_{01}*\left(\exp\left(\frac{V+R_s*I}{V_t*a1}\right)-1\right)-I_{02}*\left(\exp\left(\frac{V+R_s*I}{V_t*a2}\right)-1\right)-\frac{V+R_s*I}{R_P} \quad (11)$$

$$I_{01}=I_{02}=I_2=\frac{I_{sc,n}+K_I*\Delta_T}{\exp(V_{oc,n}+K_V*\Delta_T/V_t*(a1+a2/p))-1} \quad (12)$$

I_{01} and I_{02} represent reverse saturation currents for each diode, while $a1$ and $a2$ represent ideality factors. Equation (11) can be simplified considering the expression $(a1+a2)/p=1$, where $a1=1$ and the variable p can be chosen to be ≥ 2.2 [4]. According to this, Equation (11) can be rewritten as Equation (13).

$$I=I_{pv2}-I_2*\left(\exp\left(\frac{V+R_s*I}{V_t}\right)+\exp\left(\frac{V+R_s*I}{V_t*(P-1)}\right)-2\right)-\frac{V+R_s*I}{R_P} \quad (13)$$

Model parameters determination and validation

PV modules specifications or datasheets does not provide model parameters; nevertheless these specifications provide *I-V* curves. Those curves are generally presented for different irradiances at constant temperatures and for different temperatures at constant irradiances. The aim of this section is to propose and validate a procedure to determine PV model parameters (e.g. R_s , R_P or a) using the information provided by the PV module supplier.

The algorithm illustrated in Figure 4 is proposed to determine the set of parameters which minimizes the difference between the data provided by the supplier and simulation results. In this paper the algorithm is implemented in Matlab using the Fmincon function (Find minimum of constrained nonlinear multivariable function), however the algorithm could be implemented using techniques such as genetic algorithms or simulated annealing.

The iterative algorithm requires defining a set of initialization parameters which define the convergence of the algorithm. Considering typical values found on literature, the following initialization values are considered: the series resistance range is defined as $0.3 < R_s < 1$, the shunt resistance is defined as $R_p > 10$ and the diode ideality factor range is defined $1 < a < 1.6$.

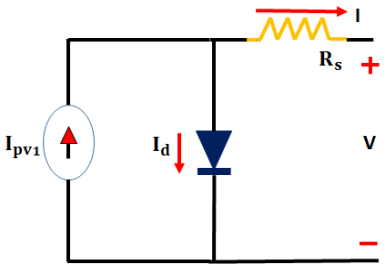

Figure 1. One-diode model considering Rs (4-p model).

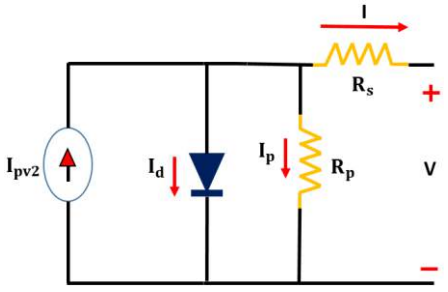

Figure 2. One-diode model considering Rs and Rp (5-p model).

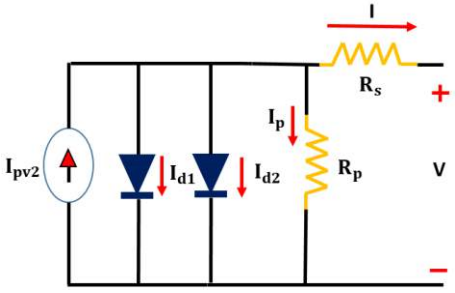

Figure 3. Two-diode model.

The proposed algorithm is used to determine the model parameters using the information provided in the specifications of the Shell SM55 Photovoltaic Solar Module and to determine set of parameters for the three PV models presented in this paper.

One-diode model considering series resistance (4-p model)

This model requires defining a set of two parameters, the series resistance *Rs* and the diode ideality factor *a*. The algorithm can be used to simultaneously determine both parameters, however as simplicity is preferred, the algorithm is implemented to find one of the parameters while the second is fixed.

The *I-V* curve with constant temperature is used to determine the value of R_s and a in 5 values of irradiance. Figure 5 illustrates the obtained relationship between R_s and G, for a fixed value of the ideality factor a. Figure 6 presents the relationship between a and G, for a fixed value of the series resistance.

The *I-V* curve with constant irradiance is used to determine the value of R_s and *a* in 5 values of temperature. Figures 7 and 8 show the obtained relationship between *a, Rs* with *T,* respectively. The results show that the value of R_s is not dependent of the PV temperature. Similar results are found for the dependence of *a* and *T*. This result is useful as it facilitates the implementation of the model.

This subsection verified that the R_s model provides accurate simulation results for operation at irradiances and temperatures provided by the supplier. It can be noted that R_s and *a* are monotonic decreasing functions with the irradiance. This is useful because the relationships can be represented by exponential or linear functions. This is presented on next Section.

One-diode model considering series and shunt resistance (5-p model)

This model requires defining a set of three parameters, the series resistance R_s , the shunt resistance R_p and the diode ideality factor *a*. The algorithm can be used to simultaneously determine all the parameters, to determine two parameters when the third is let constant (3 possibilities) or to determine only one parameter with two constant (3 possibilities).

The algorithm is performed to define the parameters in the different possibilities but results are only presented when the algorithm is used to simultaneously determine all the parameters. Figures 9, 10 and 11 illustrate the results of the algorithm to determine the relationship between *a*, R_s, R_p with *G*. Figures 12, 13 and 14 illustrate the results of the algorithm to determine the relationship between R_s, R_p and *a* with T.

The results obtained in this subsection show that the R_s and R_p model provides accurate simulation results for operation at irradiances and temperature provided by the supplier. However, it is difficult to identify monotonic relationships between the model parameters (R_s ,R_p and a) with the model inputs (G and T).

Two-diode model

As in the two resistances model, this model requires three parameters, the series resistance R_s, the shunt resistance R_p and the diode ideality factor a. The algorithm is performed to define the parameters in the different possibilities but results are only presented when the algorithm is used to simultaneously determine R_s and R_p with the ideality factor is set constant. Figures 15 and 16 illustrate the results of the algorithm to determine the relationship between R_s, R_p and a with *G*. Figures 17 and 18 show the relationship between R_s, R_p and a with *T*.

The results obtained in this subsection show that the two diodes model provides accurate simulation results for operation at irradiances and temperature provided by the supplier. However, it is difficult to identify monotonic relationships between the model parameters (R_s, R_p and a) with the model inputs (G and T). Table 1 shows a summary of features of the identified PV models.

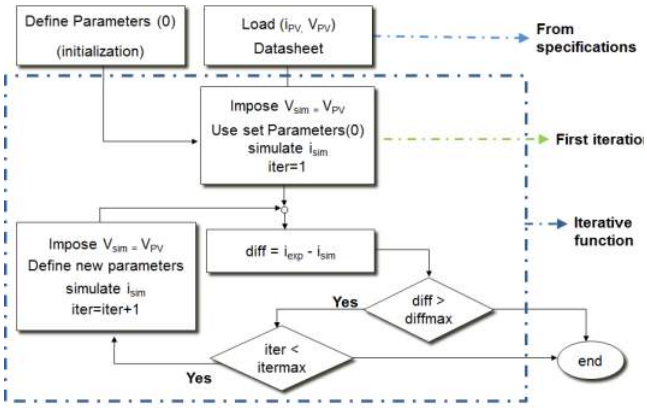

Figure 4. PV module parameter identification flowchart.

Table 1. Features of the identified PVP models.

Features	4-p model	5-p model	Two-diode model
Provides accurate simulations at irradiances and temperatures provided by the PV module supplier.	✓	✓	✓
Parameters are easy to identify.	✓	✓	✓
The relationships between parameters and irradiance can be modeled by monotonic functions.	✓	✗	✗
Parameters do not depend of the PV temperature.	✓	✗	✗

Table 2. Algorithm results between parameters and irradiance for the three identified PV models.

4-p model	5-p model	Two-diode model
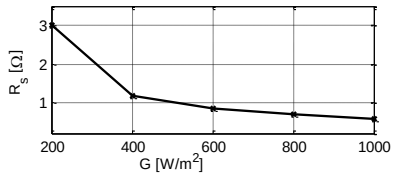 Figure 5. SM55 PV module - Rs Vs G. a=1; T=25°C.	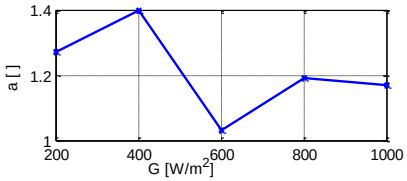 Figure 9. SM55 PV module- a Vs G T=25 °C.	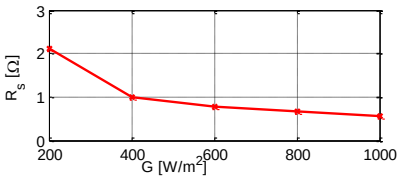 Figure 15. SM55 PV module- Rs Vs G: a1=1; a2=1.3; p=2.3; T=25 °C.
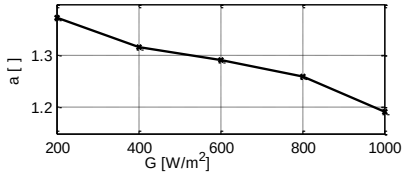 Figure 6.SM55 PV module a Vs G. Rs=0.5 [Ω]; T=25°C.	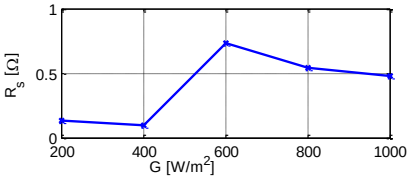 Figure 10. SM55 PV module - Rs Vs G ; T=25 °C.	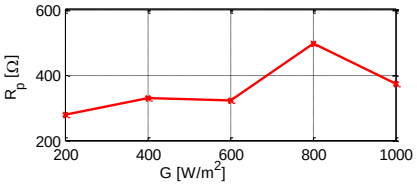 Figure 16. SM55 PV module-Rp Vs G: a1=1; a2=1.3; p=2.3; T=25 °C.
	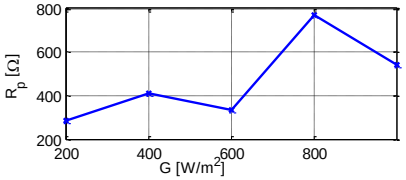 Figure 11. SM55 PV module- Rp Vs G ; T=25 °C.	

Table 3. Algorithm results between parameters and temperature for the three identified PV models.

4-p model	5-p model	Two-diode model
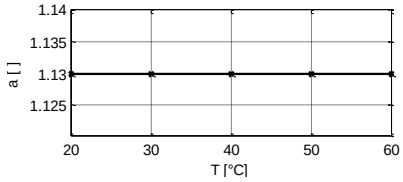 Figure 7 SM55 PV module - a Vs T. Rs=0.5 [Ω]; G=1000 W/m^2.	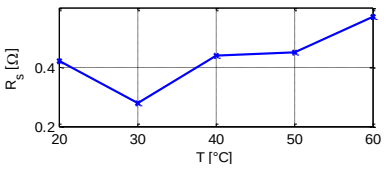 Figure 12. SM55 PV module - Rs Vs T ; G=1000 W/m^2.	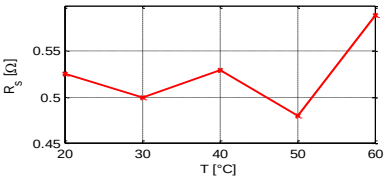 Figure 17. SM55 PV module- Rs Vs T: a1=1; a2=1.3; p=2.3; G=1000 W/m^2.
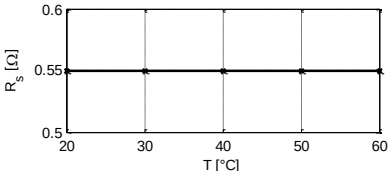 Figure 8 SM55 PV module - Rs Vs T. a=1; G=1000 W/m^2.	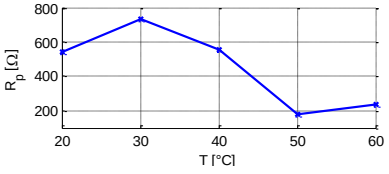 Figure 13. SM55 PV module - Rp Vs T ; G=1000 W/m^2.	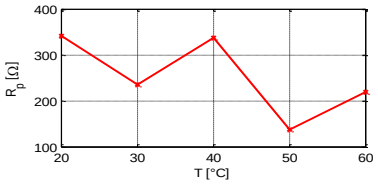 Figure 18. SM55 PV module- Rp Vs T: a1=1; a2=1.3; p=2.3; G=1000 W/m^2.
	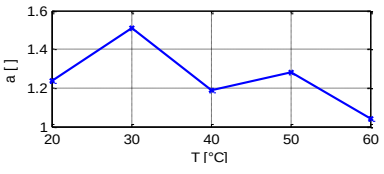 Figure 14. SM55 PV module - a Vs T; G=1000 W/m^2.	

To validate the algorithm results, simulations are performed to determine the *I-V* curves using the relationships between parameters and irradiance, temperature from Table 2 and 3 respectively. The three models considered can be used to model PV modules behavior, all of them provide accurate simulation results for operation at irradiances and temperatures values provided by the supplier. Figures 19 and 20 present *I-V* curves using one-diode model considering Rs and Rp.

For a comprehensive comparison, the errors between simulation results from each PVP model considered and the specifications of PV module are calculated. The absolute error is defined as the absolute difference between the datasheet and simulation current values of the *I-V* curves for a given voltage point. These are carried out for the five points of irradiance and temperature as shown in Table 4 and Table 5, respectively. In general, the three PVP models identified exhibit low errors for all environmental conditions (*G* and *T*).

Model selection

Last section showed that PV modules can be accurately modeled with all the considered models. It can be seen that the one-diode one resistance model's parameters are the simplest to calculate. Also, these are not dependent on the temperature and their dependence with the input (G) can be modeled with monotonic functions. For the reasons expressed above, the one-diode one resistance model seems to be the more practical to model PV modules in order to simulate them.

In this section fit functions are used to model the dependence of R_s and a with G. This can be useful to interpolate *I-V* values for values of irradiance when no information is given by the supplier. Figures 21 and 22 respectively illustrate the obtained relationship between R_s and G, and a and G obtained with the parameter identification algorithm and the fit function. R_s Vs *G* is fitted using an inverse curve and the ideality diode factor is fitted by a linear curve. The results obtained with constant series resistance and variable ideality factor is shown in Figure 23. Similar results are obtained by using the inverse fit function.

The parameter identification algorithm is applied to determine the model parameters for a Shell ST40 photovoltaic solar module and the results are presented below. Figure 24 illustrates the relationship between the series resistance and the irradiance. Figure 25 presents the relationship *a* Vs *G*. Figure 26 shows the results obtained by using the parameters interpolated in the fit linear function. Similar results are found by using the fit inverse function.

Table 4. Absolute percentage errors for different irradiation levels.

Irradiation (W/m²)	4-p model	5-p model	Two-diode model
200	2.859	0.3248	0.2688
400	1.1645	0.2236	0.1479
600	0.7494	0.09829	0.0982
800	0.2806	0.1385	0.2111
1000	0.1828	0.2036	0.2613

Table 5. Absolute percentage errors for different temperature levels.

T(°C)	4-p model	5-p model	Two-diode model
20	0.3628	0.1168	0.1028
30	0.7612	0.7211	0.7101
40	0.3632	0.1835	0.1315
50	1.3196	0.5258	0.3288
60	0.3609	0.2054	0.1014

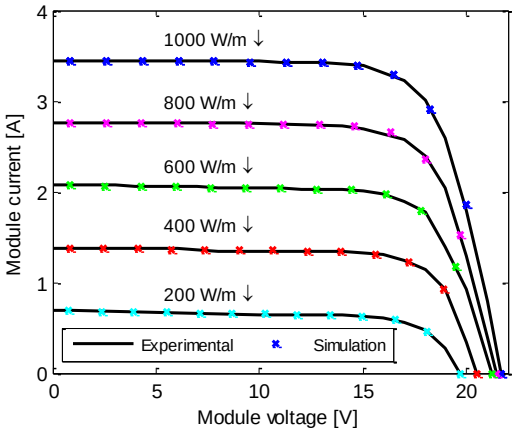

. Figure 19. SM55 PV module- I VS V; T=25 °C.

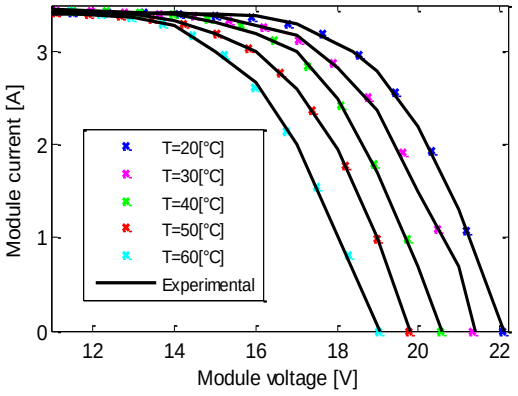

. Figure 20. SM55 PV module -I VS V; G=1000 W/m^2.

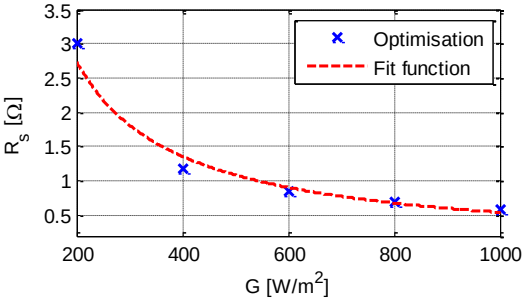

Figure 21. SM55 PV module- Rs VS G; a=1; T=25 °C.
Fit function: Rs=562.37G^ (-1.005). R^2=0.9778.

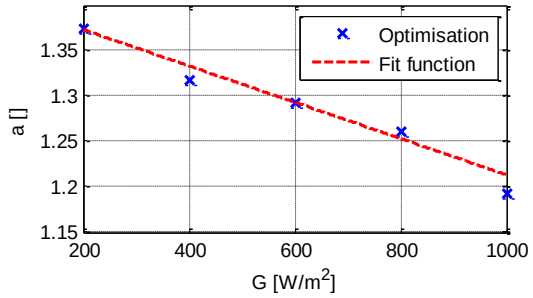

Figure 22. SM55 PV module- a VS G; Rs=0.5 [Ω]; T=25 °C;
Fit function: a=-0.0002G+1.4135. R^2=0.9733.

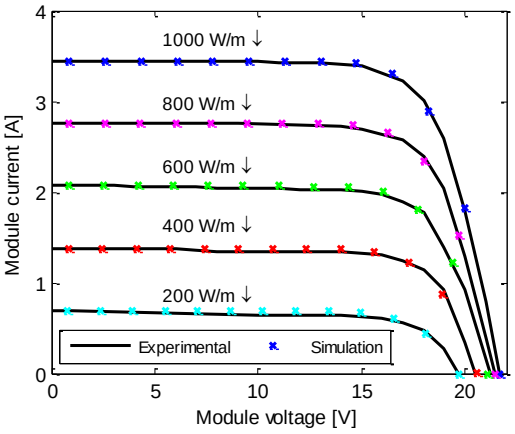

Figure 23. SM55 PV module - I VS V; Rs=0.5[Ω]; T=25 °C.

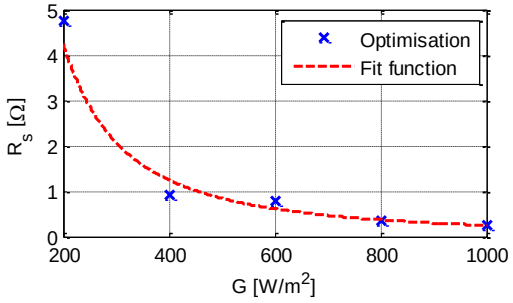

Figure 24. ST40 PV module -Rs VS G; a=1; T=25 °C
Fit function: Rs=48777G^ (-1.764). R^2=0.9644.

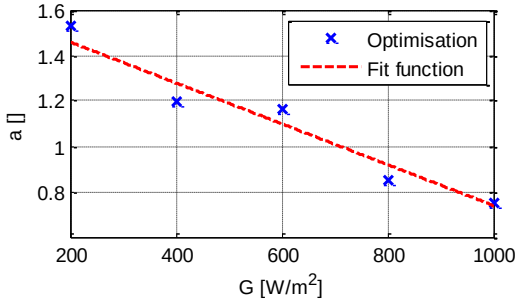

Figure 25. ST40 PV module -a VS G; Rs=0.5[Ω]; T=25 °C
Fit function: a=-0.00096G+1.6399. R^2=0.9488.

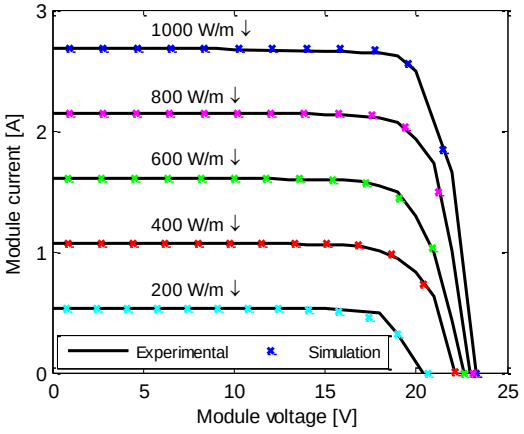

Figure 26. ST40 PV module -I VS V; Rs=0.5[Ω]; T=25 °C.

Conclusions

This paper proposes and validates an algorithm to determine photovoltaic (PV) modules model parameters using the information provided by the PV module suppliers. The effect of temperature and solar irradiation variations on the parameters are analyzed for three PV models on the literature. The retained model and parameter identification algorithm is validated with the specifications of two different PV modules.

The paper showed that PV modules can be modeled with accuracy with all of the considered models at least in the conditions presented in the supplier specifications. The one-diode one resistance model seems to be the more adapted to model PV modules in order to simulate them.

References

[1] Ma T, Yang H, Lu L. Solar photovoltaic system modeling and performance prediction. Renew Energy 2014; 36:304-315.

[2] Khezzar R, Zereg M, Khezzar M. Modelling improvement of the four parameter model for photovoltaic modules. Sol Energy 2014; 110:452-462.

[3] Nishioka K, Sakitani N, Uraoka Y, Fuyuki T. Analysis of multicrystalline silicon solar cells by modified 3-diode equivalent circuit model taking leakage current through periphery into consideration. Sol Energy Mater Sol cells 2007; 91:1222-7.

[4] Ishaque K, Salam Z, Taheri H. Accurate MATLAB Simulink PV System Simulator Based on a Two-Diode Model. Journal of Power Electronics 2011.

[5] Villalva, M.G., Gazoli, J.R., et al., 2009. Comprehensive approach to modeling and simulation of photovoltaic arrays. IEEE Transactions on Power Electronics 24 (5), 1198–1208.

[6] Etienne Saloux, Alberto Teyssedou, Mikhaïl Sorin, Explicit model of photovoltaic panels to determine voltages and currents at the maximum power point. Solar Energy, 85(5), 713-722.

[7] C. Carrero, J. Amador, S. Arnaltes. A single procedure for helping PV designers to select silicon PV modules and evaluate the loss resistances. Renewable Energy, 32(15), 2579-2589.

[8] Shell, Shell solar product information sheet. <http://www.solarcellsales.com/techinfo/technical_docs.cfm>

Power Injection To Public Network, From A Permanent Magnet Axial Generator Coupled To An Exercise Bike

Inyección De Energía Eléctrica a La Red Pública, Obtenida De Un Generador Axial De Imanes Permanentes Acoplado A Una Bicicleta Estática

Daniel E. Cañon[1], Emmanuel Sandoval[2], Johann A. Hernández [3], Miguel C. Garcia[4]

ABSTRACT

This paper presents the design and implementation of a device capable to manage power delivered by a permanent magnet axial generator, coupled to an exercise bike, in order to inject the generated energy to a residential point of public voltage electrical network, for this purpose an electric and electronic circuit is was developed to generate, manage the store and inject energy. Also, an application based on a microcontroller PIC16F877A was implemented, which manage and regulate the proper operation of all the components implemented. As result of this project, an stand-alone device was created, capable to inject to the public power network an average of 190 Watts (W), 78 Wh of energy with process efficiency of 85.85%, with open possibility to be applied for systems with higher generation capacity.

Keywords: Power Generation, Power Management, Power Batteries, Axial Generator, Power Injection To Grid, Charge Controller, Microcontroller.

RESUMEN

Este articulo presenta el diseño e implementación de un equipo que gestiona la energía eléctrica entregada por un generador axial de imanes permanente acoplado a una bicicleta estática, con el fin de inyectar la energía a un punto de la red pública de baja tensión, para esto se desarrolla un circuito eléctrico que genera, almacena e inyecta la energía eléctrica, también se desarrolla un circuito electrónico de control basado en un microcontrolador PIC16F877A el cual está encargado del funcionamiento de todos los dispositivos implementados.

Como resultado de este proyecto se obtiene el prototipo de un equipo automático que inyecta a la red eléctrica publica una potencia promedio de 170 w, una energía de 78 Wh y una eficiencia en el proceso de 85,1%, Además el diseño implementado es aplicable para sistemas de mayor potencia.

Palabras clave: Generación de electricidad, Gestión energética, baterías eléctricas, Generador Axial, Inyección de Energía Eléctrica a la red, controlador de carga, Microcontrolador.

Received: July 29th 2015
Accepted: Oct 25th 2015

Introduction

According to the Interamerican Development Bank (IDB), the energy demand for the next few years in Latin America will increase, making necessary to explore alternative sources of power supply to be responsible for this consumption and serve as support for the distribution network [1].

Distributed generation is an applicative solution which power is produced near to consumption centers, with the purpose of self-sufficiency and sometimes sell surplus energy to the grid [2]. Starting from that definition, this paper presents the design and implementation of a prototype whose function is control the charge of 3 batteries (Lead Acid), getting energy from an axial permanent magnet generator coupled to a stationary bike, later this energy will be injected to the distribution network at end user single-phase of low voltage node.

The system is controlled by a PIC16F877A microcontroller, which programing uses two processes, first is a buck converter to control the current of the battery charge (constant-voltage constant current method) and second is an automatic relay configuration to connect the batteries to the inverter who is connected to the public grid for power delivery. To design this prototype some tests were performed for injection machine modeling and methodology that defined both components as the operation mode.

Finally the results of the machine obtain a power of 78Wh injected and a prototype that works automatically.

Autor 1: Electrical engineer, FJC university district, Colombia. LIFAE, decanond@correo.udistrital.edu.co
Autor 2: Electrical engineer, FJC university district, Colombia. LIFAE, esandoval@correo.udistrital.edu.co
Author 3: Electrical Ing. MsC. PhD . National university of Colombia, , Colombia, LIFAE, Jahernandezm@udistrital.edu.co
Autor 4: Electronic Engineer, FJC university district, Colombia , jagarcialo@unal.edu.co

How to cite: Journal Space xxxxxxxxxxxxxxxxxxxx
xxxxxxxxxxxxxxxxxxxxxxxxxxxxxxxxxxxxxxxxxxxxxxxxxxxxxxxxxxxxxxxxxxxxxxx

Development Methodology

As result of previous research in laboratory for alternative sources of energy, of the University Francisco José de Caldas in Bogota, an axial permanent magnet generator was implemented, this machine was coupled to a stationary bike and play the role within the prototype as power supply to be stored and later fed into the grid of final user, this generator is constituted for 3 stators, 27 coils and 2 rotors with 36 neodymium iron boron magnets and delivers a sinusoidal signal [3], with the following characteristics equivalent model:

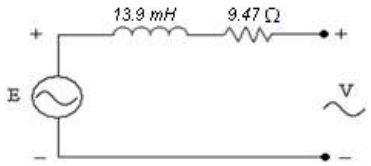

Figure 1 Model equivalent axial permanent magnet generator AC
voltage, output terminal: 0–73 V peak
Power frequency: 0–80 Hz
Connection: single phase
Z: 9.47+ (0,087*f)i [Ω]

Since this data, they develop stages for the design and construction of injector device:

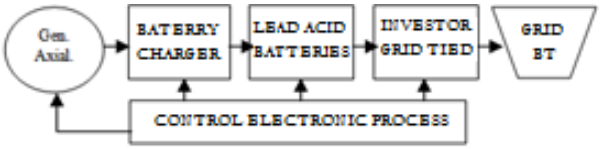

Figure 2. Block diagram of the prototype grid feeding.

Stage signal conditioning

This type of generator have a particular characteristic, voltage and frequency are dependent of rotational speed which gives the user when pedal the bike coupled to the generator, having a potential variability in the mode of pedaling. Aiming to adapt the electrical signal for better control of it, a stage of full-wave rectification is implemented with capacitive filters [4], obtaining a variable DC signal amplitude with ripple of 3%, with the following output characteristics:

DC voltage output terminal empty: 0-53 Vdc
DC output terminal voltage under load: 0-37 Vdc
Maximum output current 1.3 A

Energy storage

Generator tests, found a maximum power of 48W, given the variability of the speed applied for average pedaling routine, the optimal way to store energy is established using lead acid batteries of 12 VDC @ 7.5 Ah sealed.

Battery charger

A battery charger was implemented using the method of "constant current constant-voltage" suitable to the voltage and current levels of generator described to charge a lead acid battery efficiently.

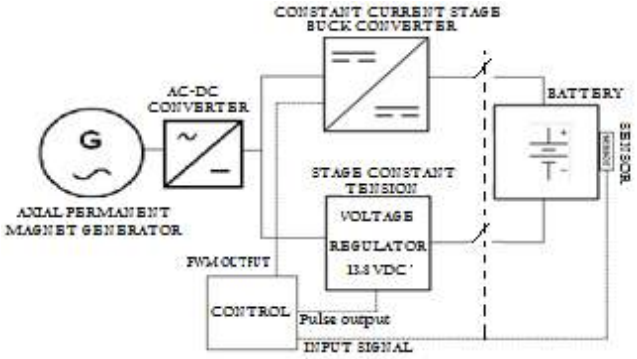

Figure 3. Electrical connection diagram battery charger

A battery charging circuit is designed and implemented using a cycle of constant current from DC-DC Buck converter [5], which it is governed by a standard PWM, generated and controlled by PIC16F877A. For constant voltage stage is used a regulator electronic circuit for13.8 VDC.

Figure 4 shows the superposed chart of current and voltage applied to each battery controlled by the charger.

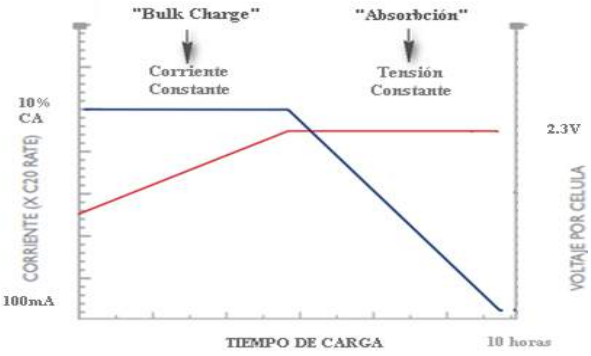

Figure 4. Stages for battery charge

Injection to the network:

For the conversion DC-AC an inverter with factor of 0.9, with average power injection to the network of 150 Watts, is chosen for Grid Tied inverter DC-AC AEP WPI-36V150W120, equipped with synchronization tools. Common inverters on the market have DC input power levels greater than 24VDC, for this reason was necessary that the voltage level supplied for storage devices, in this case, lead-acid batteries, reach a level of 36 VDC, in the first instance, was considered to use a type DC-DC converter Boost [5], which allow to raise a 12VDC battery to the required level. However, coupling problems with the other devices, reflected in substantial efficiency losses, for this reason, was decided to perform an array of contacts automated and controlled by a microcontroller to connect in series three 12-volt batteries.

Additionally, for this implementation, was necessary to consider low levels of voltage, current and power, delivered by generator, this is why the battery charger is only able to deliver energy to one battery at the time, to solve this, a switching mechanism was developed allowing to perform functions of battery connection and charger control for each cell. An automated way governed by the programmable control device.

The prototype developed has he following two functions:

- Load control of 3 lead acid sealed batteries, 7.5Ah 12VDC. Battery charger implemented switches each battery autonomously, once load level is reached, move to the next. The same control device coupled to the A/D converter determines that loading point remains constant current or constant voltage complying with the charging requirements specified by the manufacturer. In Figure 5 upper part, the connection diagram shows the contacts used.

- Discharge lead-acid batteries and injecting energy into the inverter. This process is performed by another group of contacts set to connect in series the three storage systems commanded by an external signal that also connect it to Grid Tied inverter, with its output connected to the low voltage network at end user node. In Figure 5 bottom, the connection diagram for this stage.

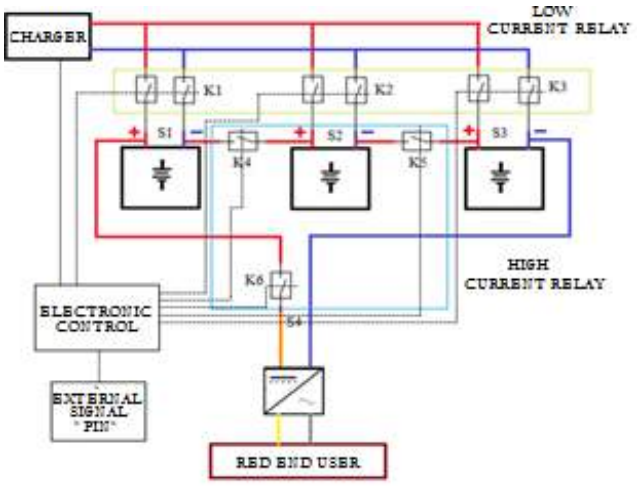

Figure 5. Relay connection for automatic switching of battery charging and connection to the Grid Tie Inverter.

Power injection period to LV network

The time of energy injection process is determined theoretically by the ability of batteries to deliver continuous power; this value is set from the discharge curve determined by the manufacturer [4], with reference to the rate of discharge of the battery which in this case is 0.66. The ICA value shows a time range of battery discharge of 30 to 60 minutes [6].

Process Control and Peripherals

A control system is implemented based on a PIC16F877A [7] microcontroller, which its PWM feature is used, also A/D converter and ports, to perform routines that govern the different devices, sensors and monitor signals necessary to implement various processes, such as:

- Charging and discharging of batteries
- Injection of energy to the grid
- Turning the controller equipment
- Audible and visual informative signals about battery status and use of the machine to the user
- Control of idle operation of the prototype

Also support devices and peripherals as implementation informative display of voltage and current of battery, front control for bicycle user, auxiliary system Li-ion battery as power source for electronic devices equipped with external charger and a charge indicator incorporated.

Experimental Results

Of the construction of the machine (Figure 6), tests were performed to determine the proper operation of devices for power injection to the network, this consist in:

Figure 6. Main parts of the prototype machine storage and injection of electricity network.

Testing the battery charger

Those tests verify that Buck converter makes the change of magnitude maintaining constant current in each battery charge, also, PWM normal operation of the electronic components and, check the actions taken to control different situation for machine use, ensuring proper operation of the PIC software.

Battery charge – Time test

According to test with control the obtained time an average time of 12.25 hours.

Grid feeding test

Injection of energy stored in the batteries was done, this download is deep, and the power curve defined the injection that can deliver the inverter.

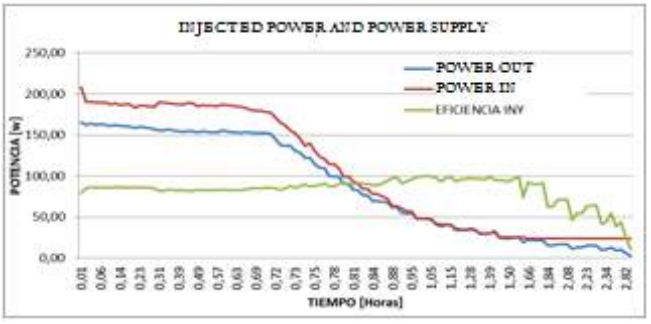

Figure 7. Power fed into the grid

For the description of this curve is divided into 4 parts, resulting in the following function:

$$f(x) = \begin{cases} 17{,}77x^2 - 29{,}474x + 164{,}54 & 0 < t \leq 0{,}71\ h \\ 2656{,}7x^2 - 4731{,}3x + 2173{,}3 & 0{,}71 < t \leq 0{,}84\ h \\ 151{,}23x^2 - 407{,}36x + 305{,}18 & 0{,}84 < t \leq 1{,}42\ h \\ 3{,}3289x^2 - 27{,}569x + 58{,}054 & 1{,}42 < t \leq 3{,}64\ h \end{cases}$$

Equation 1. Characterization Curve injection to the grid

This function determined the injected energy value at 78 Wh, the total energy that is able to inject the prototype is 190 Wh and the instantaneous maximum power that was injected was 192 W.

Energy Balance

The energy balance is based on a consumption which requires the prototype for a charge cycle versus injection and energy supplied to the grid.

Energy consumed by the prototype: The prototype have a lithium ion battery (Li-ion) [8], which feeds the control electronics and switching on the loading and feeding operation; this supplies energy to auxiliary services as prototype battery charger and power injector to the network.

Energy injected into the network: The network delivery investor an energy of 78 Wh.

Ending Balance: The power resulting from this process is:

$$78\ \text{Wh} - 10.248\ \text{Wh} = 67.752\ \text{Wh}$$

This represents an efficiency of 86.86%, in each cycle.

Conclusions

• A design and implementation methodology was for very low power generators.

• According to electrical performance tests, was found that permanent magnet axial generator used is a machine that delivers a very low power, pushing to use an energy storage processes by battery pack for long charging time of each cell.

• The charging method for lead acid batteries was the MSRP, but was necessary to limit the initial charging current of the battery at 0.1C capacity storage device, since the generator has to deliver higher current limiting to 1.3 A.

• For optimum operation of the inverter was necessary to present alternatives to increase the DC input voltage, evidencing that serial interconnection of batteries was the optimal arrangement. Alternative of Boost converter is presented but was discarded due to the inefficient operation at this implementation.

• Using a battery pack was viable, since its control does not demand a significant power in the energy balance of the prototype.

• The device is capable of deliver up to 45 minutes of constant energy at a high level, but this value should be restricted because of the ability to deep discharge, in order to avoid premature damage of batteries.

• Injection tests network shown no variations or peaks, due change of the equivalent impedance which is reflected in the injection site, because the variation of load required on site.

• Control for power delivered was designed for specific variables of generator, but this charger can be used to deliver up to 2 amps of load and certain modifications can be applied to processes of higher currents and voltages.

• Charge controllers with low power batteries are not commercial but are required to build the design with all component sizing, Special attention must be taken with the design of it, because oversized devices makes arise inefficiency.

• This project could be implemented in a fitness center or gym with high number of rotary motion machines, in order to implement the same type generators over different machines equipped with any electronic system similar. It will benefit to add the power generated by users to charge batteries in a controlled quick and efficiently way.

References

[1] i.-a. D. B. Bid, «Rethinking Our Energy Future, Bogota, Junio 2013.,» Bogota, 2013.

[2] c. M. S. Botero, ««análisis del instrumento regulatorio "Medición Neta "(Net Metering) Y Su Potencial Aplicación Al Caso Colombiano,» Energetica Universidad Distrital, pp. 53-65, 2008.

[3] j. C. González gereda y d. L. Silva, Generación De Energía Eléctrica Por Medio De Una Maquina De Trabajo Físico Con Movimiento Rotativo E Implementando Un Modelo De Motor Magnético, Bogota: Universidad Distrital Francisco Jose De Caldas, 2012

[4] GTE, Conversores DC-DC, España: Grupo De Tecnologia Electronica, 2014

[5] D. W. Hart, Electronica De Potencia, Madrid- España: Prentice Hall, 2001

[6] Fulibatery, Ficha Tecnica Valve Regulated Lead-Acid Rechargeable Battery Fl1275, China: Fulibatery, 2014.

[7] Microchip, «Descripcion general del pic16f877a,» 2014. [en línea]. available:www.bairesrobotics.com.ar/data/pic16f877guia%20detallada%20parte2.pdf.

[8]S. SDI, Specification Of Product For Lithium-Ion Rechargeable Cell Model : icr18650-22p, seoul, korea: samsung battery business division , 2014.

Real-Time Hybrid Simulator of the Distribution Network for Smart Grid Applications

Simulador Híbrido en Tiempo Real de la Red de Distribución para Aplicaciones de Redes Inteligentes

Morales, D.X.[1], Medina, R.D [2]

ABSTRACT

Free power markets and strong integration of distributed generation change the operation and control of distribution grids significantly. Traditional networks must evolve to the concept of "Smart Grid". These new grids can manage new services in a clever manner, keeping power quality, safety edges and optimal costs. In order to probe new smart grids concepts is necessary to model the system, its characteristics, stability and different topologies. This paper presents a methodology for the purpose of modeling low voltage networks in a Matlab-Simulink® environment, using a Real Time Simulator. Additionally, authors use real information to validate the showed methodology.

Keywords: Smart Grids, Real Time simulations, PHIL, LV modeling.

RESUMEN

Los mercados liberalizados y la fuerte integración de generación distribuida cambian significativamente la operación y control de las redes de distribución. Las Redes tradicionales deben evolucionar al concepto de "Smart Grid". Estas nuevas redes pueden gestionar nuevos servicios de forma inteligente, manteniendo la calidad de energía, los márgenes de seguridad y costos óptimos. Con el fin de investigar los nuevos conceptos de redes inteligentes es necesario modelar el sistema, sus características, la estabilidad y diferentes topologías. Este trabajo presenta una metodología con el propósito de modelar redes de baja tensión en un entorno Matlab-Simulink, utilizando un simulador de Tiempo Real. Además, los autores utilizan datos reales para validar la metodología.

Palabras clave: Redes Inteligentes, Simulaciones en Tiempo Real, PHIL, Modelado en Baja tensión

Received: July 27th 2015
Accepted: Sep 15th 2015

1. Introduction

Transformation of traditional power grids in to smart grids, take place initially in distribution networks; since distributed generation, equipment with control and coordination ability is connected in low voltage networks.

In order to understand and manage these challenges Utilities Companies (UC) adopts two possible approaches: *i)* traditional one, which is to strengthen the power grid, build substations and increase generation and transport capacity, and, *ii)* implement a smart grid (SM).

Historically end users has been passive with patterns unpredictable and non-scheduled consumption, with the arrival of the SM, these users could manage their consumption based on hourly rates interacting with UC through smart metering and selling excess energy from electric vehicles, storage and distributed generation; users will now prosumer (producer + consumer)[1].

Denmark is pioneer in the development of smart grids; in its report "Smart Grids in Denmark" [2], it concludes that an Smart Grid is the most effective strategy to manage electric system evolution and prepare it to deal future challenges.

A smart grid can be defined as: "….an electricity network that can intelligently integrate the actions of all users connected to it - generators, consumers and those that do both functions to efficiently deliver sustainable, economic and safe power supply" [3].

Smart grid includes users (most of them connected at low voltage) it is necessary to undertake the modeling of the low voltage network, in order to have a model in which to test the smart grid concepts.

2. Modeling of electric network

According [4] the first step involves modelling the different elements of the grid such as lines, wires, transformers, loads and unconventional elements like photovoltaic panels, smart buildings, electric vehicles and domestic wind turbines. Also, parameters and blocks used into Matlab-Simulink are described in [4]. Once the network is modelled, it is possible to analyse it in order to test new strategies and to assess the network impact considering new services.

2.1. Modelled network description

Proposed network modelling in medium and low voltage is contemplated in "Ecuador Smart Grids Project", driven by the Ecuadorian Ministry of Energy; which seeks to having the detailed electrical network in order to implement Smart Grid applications and evaluate the impact of new technologies; Table I shows details.

[1] D.X. Morales is with INP at Universidad Politécnica Salesiana (e-mail: Diego.Morales-Jadan@ense3.grenoble-inp.fr).
2 R. D. Medina, is with DAAD at Universidad Politécnica Salesiana, (e-mail: rmedinav@ups.edu.ec).

TABLE I
DESCRIPTION OF ONE SUBSTATION WITH ITS TRANSFORMER

Substation	Trafo	Power (KVA)	Customers
SE1	Tr1	100	90
SE2	Tr2	100	110
SE3	Tr3	75	55
SE4	Tr4	50	40

Low voltage network is on 220V phase-phase, 3F4C configuration, the whole project include three feeders in four cities. Substation were chosen due: *i)* its strong relation between them (there are possibility of reconfiguration), *ii)* large number of feeders in low voltage and, *iv)* high concentration of distributed generation and smart meters.

2.2. Scenarios

Main advantage of real time simulations is the possibility to perform scenarios reducing computation effort [5]. For testing the real time simulator, seven scenarios were defined:

Scenario S1
Unbalanced network topology, where the main load is concentrated on the phase C with no reactive power,

Scenario S2 y S3
These scenarios have the same chargeability that S1 but have the highest consumption in phases A and B respectively

Scenario S4
Chargeability is only 16% and load is located in phase A

Scenario S5
Chargeability is 32% and load is also located in phase A

Scenario S6
It has 100% use of the transformer; moreover, network is balanced

Scenario S7
It considers loads with reactive power in order to evaluate the model's accuracy.

S1, S2 and S3 cases allows to validate mutual line parameters, S6 and S7 could be useful to evaluate the best phase connection for DGs [6] and the other ones let to evaluate the model in real and different situations that could happen in a distribution network. With the intention to compare results, authors use an algorithm developed in General Algebraic Modeling System (GAMS) by [7], which is ideal for modeling linear, nonlinear and mixed integer optimization problems. It is useful with large and complex problems. Therefore, GAMS could be tailored easily to optimize load flow, where restrictions are the equations of power flow and the objective function is to maintain voltage levels within acceptable limits

3. Real time simulator

Several realistic online simulations are necessary to build a common understanding of functions of a SG [8]. These real-time simulations should include all participants playing reliability roles as coordinators, transmission and distribution network operators, power plants operators, aggregators and substations operators. These simulations seek to identify the impact on the grid of a high penetration level of distributed generation [9] and electric vehicles. In addition, they serve to test control strategies, which will be implemented in real life. A hybrid simulator has two parts[3]: a digital part, where the whole network in medium and low voltage is modelled, also the SCADA communication, and an analogic one with the interface to communicate field devices (charging stations for electric vehicles, inverters, and so on).

3.1 HIL and PHIL

Hybrid simulators usually are divided into 2 groups: *i)* Hardware in the Loop (HIL) and *ii)* Power Hardware in the Loop [4]. PHIL Simulator unlike HIL integrates a power amplifier between analogic and digital part, whereas HIL exchanged with digital part only control and monitoring signals. As presented in Fig. 1.

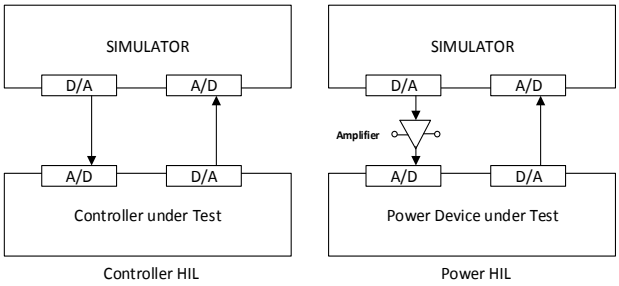

Figure 1. Hybrid HIL simulators and PHIL [10]

RT-LAB is a Simulink fully integrated software; it was selected inasmuch as allows incorporating real time measures into simulations using OPAL RT cards for analogic and digital inputs/outputs.

3.2 Real Time feature

Flexibility and scalability of RT-LAB allows us any simulation for control applications in order to test advanced distribution functions (reconfiguration, cut / off, peak shift, etc.) on the network. Those simulations can integrate distributed generators and new services connecting real devices in order to assess their impact on the real grid or even micro grids.[11]. Main advantages of RT-LAB are:

- ✓ Possibility to include real devices in simulations
- ✓ Real time simulations
- ✓ Low cost
- ✓ Increased functionality for testing parameters or impacts
- ✓ Automatic scripts to run 24h / 7d simulations

A key point in real time simulations is to sampling time setting "Ts", which is constant during simulation, real-time status is lost if: *i)* Ts is small enough, *ii)* input signals are not read, *iii)* model calculations are not computed, and, *iv)* model outputs are not updated. Fig. 2 presents an error on Ts assignment.

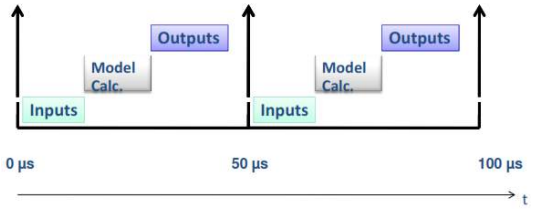

[3] OPAL RT (2013) Module 1: Real-Time System Fundamentals

a)

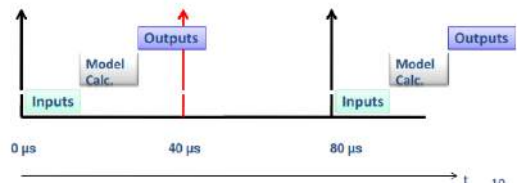

b)

Figure 2 Sampling time "Ts" a) properly selected 50us, b) selected wrongly 40us

4. Results

Figure 3 shows a section of low-voltage network modelled, "Three Phase Dynamic Load" blocks are fed with real demand curves following a random approach [12] for their selection from the available database.

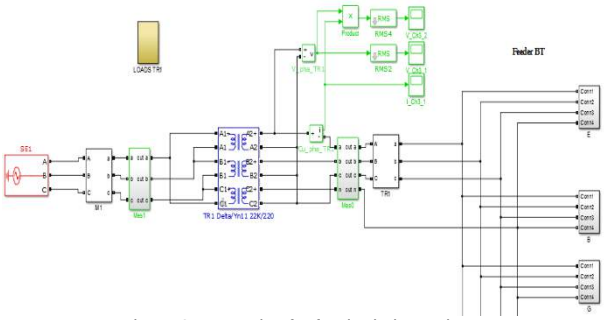

Figure 3. Example of a feeder in low voltage

A summary of the comparative analysis of results between the two models, Current and GAMS is presented in the table 2 and 3.

TABLE 2
IMBALANCE IN THE FARTHEST NODE (%)

	GAMS	*Current Model*
Scenario 1	*0.4757*	*0.4793*
Scenario 2	*0.4725*	*0.4793*
Scenario 3	*0.4725*	*0.4793*
Scenario 4	*1.5041*	*1.5421*
Scenario 5	*3.2459*	*3.2881*
Scenario 6	*0.0000*	*0.0010*
Scenario 7	*0.0000*	*0.0000*

Table 2 shows that imbalance percentage in farthest node is almost the same. While table 3 shows that active power values are very similar, there is little difference in reactive power results; this difference arises because Current model considers capacitance of the lines, but GAMS model does not. Voltages and currents were compared node-by-node with difference lower than 1%. Results of scenario 1, 4 and 7, wherein G is GAMS and C is Current model.

TABLE 3
RESULTS OF THE MAIN SCENARIOS

	Scenario 1		***Scenario 2***		***Scenario 3***	
	G	*C*	*G*	*C*	*G*	*C*
P (kW)	*492.8*	*494.4*	*168*	*169.5*	*492.7*	*494.4*
Q (kVAr)	*15.7*	*16.5*	*6.3*	*6.5*	*113.3*	*114.4*
S (KVA)	*493.1*	*494.6*	*168.1*	*169.6*	*505.6*	*507.4*

Once validated both models, real curves for active and reactive power with 144 points (sampling every 10 min) are assigned. Customers per phase and per node were allocated. A random curves assignment was use. Table 4 shows curves distribution.

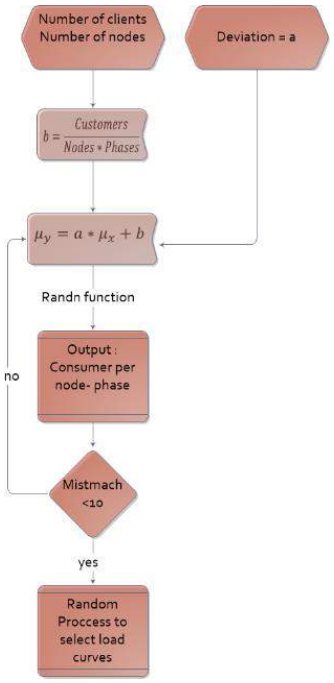

Figure 4. Random Approach Methodology [4]

Fig. 4 shows random load profile assignment methodology, it was proposed in [4]. As inputs, we need client and node number. Then the script performs calculations to select curves and client number in order to assign it automatically.

Multiple simulations were performed in order to evaluate: *i)* transformers load, *ii)* relative lines load, *iii)* voltage profiles in nodes. Figure 5a presents a daily load curve in the transformer; it is close to measured curves. Figure 5b shows a more detailed analysis of the same transformer where imbalance generated by variability of end users per node is considered

TABLE 4
RESULTS OF RANDOM APPROACH FOR CLIENT NUMBER AND DEMAND CURVES SELECTION.

Node	Phase	Consumer Number	Curve Names
10	A	1	1,19,12,60
	B	3	18,11
	C	4	15,5

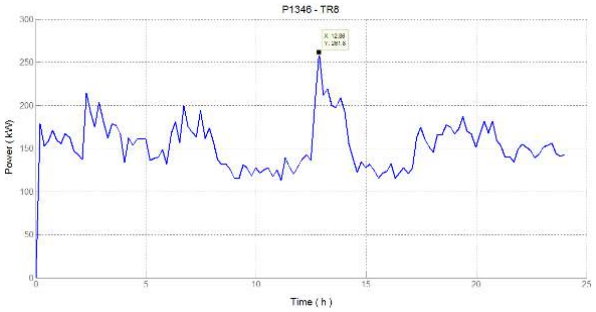

a)

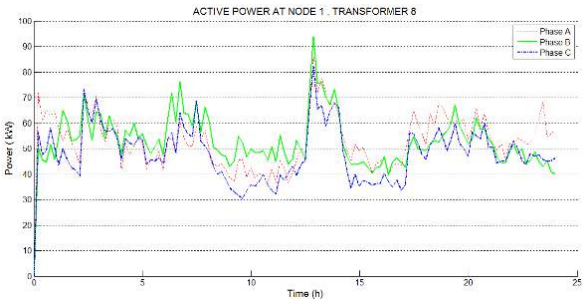

b)

Figure 5. a) Power in the transformer b) imbalance between phases in the transformer [13]

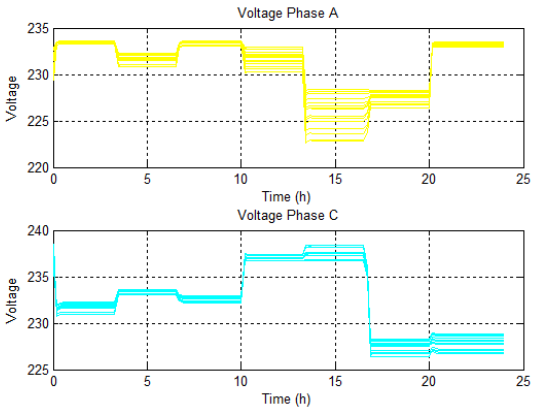

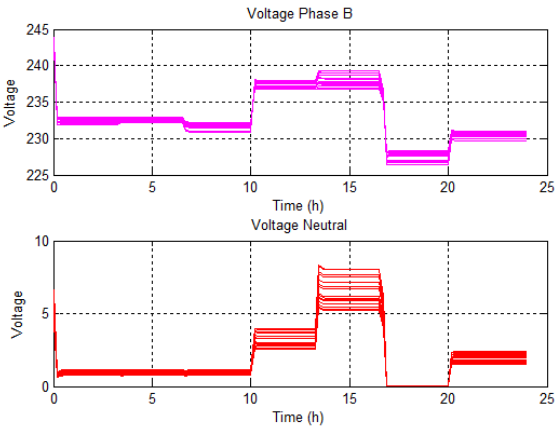

Figure 6. Voltage at all the nodes

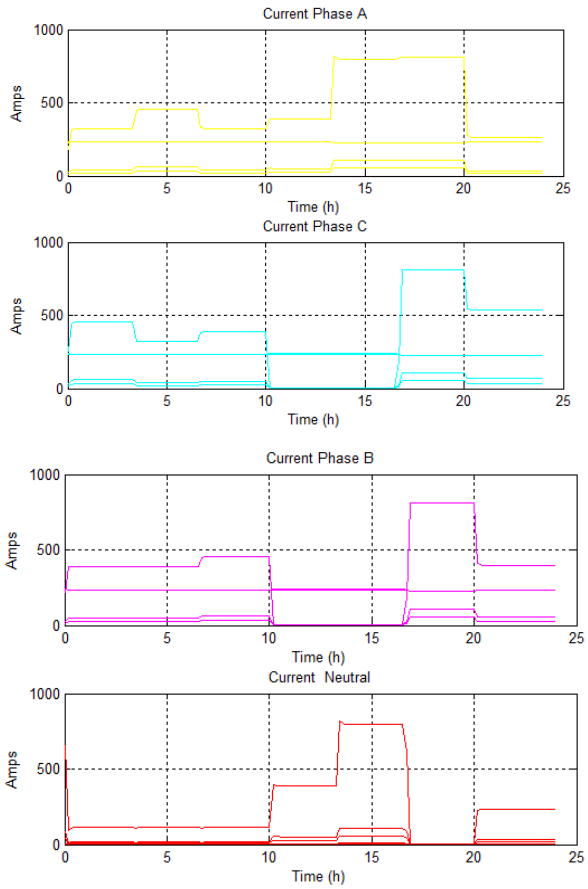

Figure 7. Current at all the nodes

Conclusions

Real-time simulations with PHIL simulators allow analyzing various scenarios with reduced optimizing costs time and effort; also offer the possibility of connecting real devices in the simulation. Different models in low voltage have been implemented in different environments like Simulink and GAMS and as results are similar, they show that this methodology is reliable. Random approach for selection of curve is adequate in order to recreate the particularity of electrical networks. Modelling methodology of low voltage networks modelling applies innovative concepts and provides proce-

dures for obtaining reliable, contrasted and very useful results for a future application of advanced functions in distribution. When simulation results are compared with measured values, they show a difference of less than 2%.

Using real time simulation is possible to get accurate information such as voltage profiles, line current, and power in peak hours, phase imbalance, end user profile, and current in the power transformer and so on. All this information is necessary to understand the network state in both present and future scenarios.

Hence, the simulations help us to build a new vision based in smart grids which consider new services and effective strategies to face the challenges ahead for the distribution networks.

Once modelled and tested effectively the network, it possible to add communication to smart meters using IEC61850, as well as to implement a direct communication with a Virtual Power Plant in order to receive set point for DGs.

References

[1] A. J. D. Rathnayaka, V. M. Potdar, T. Dillon, O. Hussain, and S. Kuruppu, "Analysis of energy behaviour profiles of prosumers," in *Industrial Informatics (INDIN), 2012 10th IEEE International Conference on*, 2012, pp. 236-241.

[2] Energinet.dk, "Smart Grid in Denmark," http://www.danishenergyassociation.com/Theme/SmartGrid2.aspx, 2011.

[3] E. s. g. t. Platform, "What is a Smart Grid," http://www.smartgrids.eu/ETPSmartGrids, 2014.

[4] D. X. Morales and R. D. Medina, "Proposal and Requirements for a Real-Time Hybrid Simulator of the Distribution Network " *IEEE CHILECON2015* 2015.

[5] M. Kezunovic, "Teaching the smart grid fundamentals using modeling, simulation, and hands-on laboratory experiments," in *Power and Energy Society General Meeting, 2010 IEEE*, 2010, pp. 1-6.

[6] A. Mercier, C. Benoit, and Y. Besanger, "Best phase connection for DGs using individual smart meter data," in *PES General Meeting | Conference & Exposition, 2014 IEEE*, 2014, pp. 1-5.

[7] C. Benoit, "Ecriture LF Cplex " Master, Institut Polytechnique de Grenoble, France, 2013.

[8] G. Feng, L. Herrera, R. Murawski, E. Inoa, W. Chih-Lun, P. Beauchamp, *et al.*, "Comprehensive Real-Time Simulation of the Smart Grid," *Industry Applications, IEEE Transactions on*, vol. 49, pp. 899-908, 2013.

[9] P. Kotsampopoulos, V. Kleftakis, G. Messinis, and N. Hatziargyriou, "Design, development and operation of a PHIL environment for Distributed Energy Resources," in *IECON 2012 - 38th Annual Conference on IEEE Industrial Electronics Society*, 2012, pp. 4765-4770.

[10] A. Mercier, "Etude de l'insertion massive de production décentralisée et des charges non conventionnelles dans les réseaux urbains dans le contexte Smart Grid," Master, Institut Polytechnique de Grenoble, France, 2013.

[11] W. Jing, S. Yulun, L. Wendong, G. Ji, and A. Monti, "Development of a Universal Platform for Hardware In-the-Loop Testing of Microgrids," *Industrial Informatics, IEEE Transactions on*, vol. 10, pp. 2154-2165, 2014.

[12] M. Gilvanejad, H. Askarian Abyaneh, and K. Mazlumi, "Estimation of the overload-related outages in distribution networks considering the random nature of the electrical loads," *Generation, Transmission & Distribution, IET*, vol. 7, pp. 855-865, 2013.

[13] D. Morales, "Modeling of distribution networks in a Real-time simulator for 'smart grids' Applications," Master, Institut Polytechnique de Grenoble, France, 2014.

Mechanism Design for Demand Management with Stratified Population Overview

Diseño de mecanismos aplicado a la gestión de la demanda con aproximación para población estratificada

Mateo Alejandro Cortés Guzmán[1], Eduardo Alirio Mojica-Nava[2]

ABSTRACT

This paper briefly reviews different approaches to the electricity demand management problem, including economic mechanism design. A particular mechanism reviewed proposes some incentives able to achieve, after a variable period, a Pareto optimal of the system depending on population dynamics and consumption preferences. A modification is proposed so the mechanism takes into consideration basic strata information as a variation in consumption preferences that affects population dynamics to the convergence of an equilibrium consumption level. Further research may lead to propose and validate a particular and detailed mechanism that emphasizes particularities of the Colombian electricity system, especially strata implications in consumption preferences of users.

Keywords: Mechanism design, demand management, game theory, incentives, stratified population.

RESUMEN

En este artículo se revisan diversas aproximaciones al problema de gestión de la demanda de electricidad, incluyendo la rama de diseño de mecanismos, tomada de la economía. El mecanismo base revisado contempla incentivos que permiten lograr, después de un periodo variable, un óptimo de Pareto del sistema dependiendo de la dinámica de la población y las preferencias de consumo. Se propone una modificación del mecanismo analizado, de tal manera que tiene en cuenta información de estratificación como una variación en las preferencias de consumo que afecta la respuesta dinámica de la población y su convergencia a un nivel de equilibrio del consumo. Trabajo futuro en el tema permitirá proponer y validar un mecanismo completo que haga énfasis en las particularidades del sistema eléctrico colombiano, específicamente respecto a las implicaciones de la estratificación social de la población en las preferencias de consumo.

Palabras clave: Diseño de mecanismos, gestión de la demanda, teoría de juegos, incentivos, población estratificada.

Received: July 24th 2015
Accepted: August 20th 2015

Introduction

Social continuous development and quick technological changes often make our lifestyle rely greatly on electricity as main energy source for daily tasks and activities. However, the misuse of the resource brings with it the consumption of more energy than what is actually needed to be generated, transmitted and distributed. This non-optimal energy use impacts both ecosystems according to the generation method and utilities cost because of the additional infrastructure and complexity of the power system, form substations to distribution circuits reaching every user.

Regarding optimal use and final energy consumption, some works have been done with variable mathematical formalism and intensive use of empirical data (Baharlouei, Hashemi, Narimani, & Mohsenian-Rad, 2013; Barreto, Mojica-Nava, & Quijano, 2014; Mhanna, Verbič, & Chapman, 2014). Narrowing the scope to Colombian case, characterizations and descriptions of industrial electric load have been performed and some incentive-driven methods for demand management of specific loads have been proposed as well, without employing mechanism design and other game-theoretic approaches. In economics, *mechanism design* refers to the mathematical structure which models the way economic activity is driven, guided, and developed (Hurwicz & Reiter, 2006). Mechanism design foundations can be applied to any process modeled as a game with private or incomplete information, like auctions or, in the present case, *demand management.*

The main objective of this paper is to lay the foundations and set the first stages of a *mechanism* designed to meet the particularities of Colombia's power grid. The mechanism is intended to state rules and conditions needed to achieve a more efficient use of electricity, also considering various types of incentives, restrictions, and strata information. The mechanism should be refined and validated using historical data from electricity suppliers in Colombia.

[1] Mateo is an Electronics Engineer and Electrical Engineer, Universidad Nacional de Colombia, Colombia. M.S. student in Electrical Engineering, Universidad Nacional de Colombia, Colombia. E-mail: macortesgu@unal.edu.co

[2] Eduardo is an Electronics Engineer, Universidad Industrial de Santander, Colombia. M.S. in Electronics Engineering, Universidad de los Andes, Colombia. Ph.D. in Automatique et Informatique Industrielle, Ecole des mines de Nantes, France. Associate Professor with the Department of Electrical and Electronics Engineering, Universidad Nacional de Colombia, Colombia. E-mail: eamojican@unal.edu.co

How to cite: Journal Space xxxxxxxxxxxxxxxxxxxx
xxxxxxxxxxxxxxxxxxxxxxxxxxxxxxxxxxxxxxxxxxxxxxxxxxxxxxxxxxxxxxxxxxxxx

Rationale and State of the art

Development and society growth entail a proportional increase in electricity demand, which may be satisfied either by using a combination of electricity generation methods employing the resources available locally, or in the worst of the scenarios, importing it from another country.

In Colombia, nearly two-thirds of the total energy is produced by means of hydraulic generation (Unidad de Planeación Minero Energética, 2013), which is usually considered in literature as a clean and renewable technology. However, when dams are used as in most of hydroelectric centrals in Colombia, the place where the dam was built cannot be reused for agriculture or cattle raising (Killingtveit, 2014). This has negative impacts on ecosystems and biodiversity. Greenhouse gases effects on hydrogeneration are often negligible (Killingtveit, 2014), except when the amount of decaying organic matter flooded in the dam is high enough to noticeably increase gases level.

On the other hand, in dry weather seasons thermal generation becomes more important, employing coal or natural gas as fuel, and comprising about 30% of the total installed capacity of the Colombian power system (Unidad de Planeación Minero Energética, 2013). Thermal generation represents a detrimental effect on environment since such production method brings about great amounts of greenhouse gases emissions (Killingtveit, 2014). The consideration of both environmental impact and additional economic cost of new power-generation projects and its integration to the grid, makes desirable an optimal use of electric energy and installed electrical capacity.

Traditionally, electricity demand is modeled in an aggregated form as a load curve showing load peaks in specific hours and a minor consumption the rest of the time; its use has been widespread since more than two decades ago (Andersson, Jansson, & Klevâs, 1989). Consumption peaks in a load curve imply the need of an installed maximum generation capacity, whose power would not be totally consumed the whole time.

Demand management implies the possibility of modifying users' consumption profiles either individually or as part of a variable group by means of economic or performance incentives. Such management can be modeled in various ways and by deploying several approaches, each one trying to gather and reflect upon the main technical and economical features and behaviors of the users (Bompard et al., 2005; Yang, Zhang, & Tong, 2006).

In the Colombian case some methods for industrial sector demand management using pricing initiatives and direct load control have been put forward. The study by Espitia Silva & Ramos Acevedo (2014) makes emphasis on the possible impact of the load curve of specific facilities. Also, Rivera (2013) analyzes the effect of a differential fee for non-regulated users of the industrial sector aiming to lower the load curve peaks charging the users a higher kWh price in peak hours; his study concludes that the feasibility of the load curve shifting from industrial customers greatly depends on the type of industry and the specific needs; it also points that in most cases the consumption does not have important variations during the day, differently from the behavior of the residential sector electricity demand.

Because of the natural complexity of the problem, some assumptions limiting the scope of the theoretical model used to predict the behavior of the users are usually made, without accurately analyzing the individual consumption of each one. This entails deviations from actual users' energy demand and behavior, and errors that affect technical, commercial and management decisions aimed at satisfying demand (Baharlouei et al., 2013; Gelazanskas & Gamage, 2014; Samadi, Mohsenian-Rad, Schober, & Wong, 2012; Yang et al., 2006).

Various authors have treated the demand management problem with different approaches and mechanism propositions seeking for an optimal distribution of the demanded energy of a group of users using adequate incentives (Marden, Arslan, & Shamma, 2009; Mhanna et al., 2014). It is worth noticing that, in most cases, the validation has been only partially covered by simulations with moderately detailed models, without reaching a comparison with empirical or historical data, which would allow to draw conclusions about the usefulness of applying proposed mechanisms to a real system or part of it.

Recently Barreto *et al.* have proven the inefficiency of the electricity system comparing the users' behavior regarding to electricity consumption with the *tragedy of the commons*, (Barreto, Mojica-Nava, & Quijano, 2013; Barreto et al., 2014).[3] In this research it is proposed a mechanism of indirect revelation that compares the convergence and incentives of some traditional population dynamics to achieve the efficiency of the system at certain cost (net positive incentives must be provided) depending on the users' particular preferences and the dynamic evolution of the system. Population dynamics expresses the evolution of the state of the society, as described by Sandholm in (Sandholm, 2010). The authors conclude that the mechanism requires subsidies of external origin at least during the transition period of the system to the optimal.

The equations stated for each dynamic, for a given population game are as follows:

> Let $F: X \to \boldsymbol{R}^n$ be a population game with a set of pure strategies named $(S^1, \dots, S^p)$ with population masses $m_p \in \boldsymbol{Z}^+$ and X the state space. Each population $p \in P$ is large but finite and has Nm_p members, where $N \in \boldsymbol{Z}^+$ is called *population size*. The set of possible social states $\boldsymbol{X^N} = \{x \in X: Nx \in \boldsymbol{Z}^n\}$ is a discrete grid in the state space X (Sandholm, 2010).
>
> $F_i^p: X \to \boldsymbol{R}$ denotes the payoff function of the population p playing the strategy $i \in S^p$.
>
> $\overline{F}^p(x)$ is the average payoff for the population p, i.e.,
>
> $$\overline{F}^p(x) = \frac{1}{m^p} \sum_{i \in S^p} x_i^p \, F_i^p(x) \qquad (1)$$
>
> x_i^p is the social state of the population p playing the strategy i.
>
> $\hat{F}_i^p$ is the excess payoff to strategy $i \in S^p$,
>
> $$\hat{F}_i^p(x) = F_i^p(x) - \overline{F}^p(x) \qquad (2)$$

1. *Replicator dynamic:*

[3] The tragedy of the commons refers to a dilemma presented by Garrett Hardin in 1958. In the original case, several individuals sharing a common resource act in a selfish and rational way contrary to the best interests of the whole group by depleting the resource. The term may be used for describing a variety of behaviors in the society including exploitation of natural resources, and in the particular case, for the generation of electricity.

$$\dot{x}_i^p = x_i^p \hat{F}_i^p(x) \tag{3}$$

2. *Brown-Von Newmann-Nash dynamic:*

$$\dot{x}_i^p = \left[\hat{F}_i^p(x)\right]_+ - x_i^p \sum_{k \in S^p} \left[\hat{F}_k^p(x)\right]_+ \tag{4}$$

$[.]_+$ means the expression enclosed in brackets is positive.

3. *Smith dynamic:*

$$\dot{x}_i^p = \sum_{j \in S^p} x_j^p \left[F_i^p(x) - F_j^p(x)\right]_+ - x_i^p \sum_{j \in S^p} \left[F_j^p(x) - F_i^p(x)\right]_+ \tag{5}$$

4. *Logit dynamic:*

With noise level $\eta > 0$;

$$\dot{x}_i^p = \frac{\exp\left(\eta^{-1} F_i^p(x)\right)}{\sum_{k \in S^p} \exp\left(\eta^{-1} F_k^p(x)\right)} - x_i \tag{6}$$

Implementation

From the mechanism presented by Barreto *et al.* (2013, 2014) it is analyzed the effect of variable energy cost in the final consumption profile of a group of users with similar preferences. This is the starting point for the proposal of a modification in the fitness function for addressing the behavioral changes associated to a stratified population, by decreasing in a fixed percent the utility of the users with higher energy use profiles.

Demand Management Game Theory Model

Demand management problem can be characterized as a game with a number of single or grouped users with specific preferences, a utility function related to a fitness function, and a population dynamics model which defines the set of differential equations that predict the system evolution. For the sake of simplicity, in the modifications made to the mechanism proposed by Barreto *et al.*, it is used a set of Matlab software called PDtoolbox[4] (Barreto, 2014) available under the BSD license.

The mechanism proposed by Barreto et al., (2014) considers that the load is analyzed in hourly time lapses, and for each agent i there is a profit function $U_i(\mathbf{q})$:

$$U_i(\mathbf{q}) = v_i(\mathbf{q}_i) - \sum_{t=1}^{T} q_i^t \, r(\| \mathbf{q}^t \|_1), \tag{7}$$

Where $q_i^t \geq 0$ is the amount of energy consumed by the user i in the t^{th} time interval (from a 24 h period); $\mathbf{q}_i = \left[q_i^1, \dots, q_i^T\right] \in \boldsymbol{R}_{\geq 0}^T$ is the daily consumption profile of user i; $\boldsymbol{q}$ is the electricity consumption of the population; r the unitary price function and $\| . \|_1$is the l-norm.

$v_i(\mathbf{q}_i) = v(\mathbf{q}^k, \alpha_i^k)$ is the *valuation function*, *i.e.* the economic value given by the i^{th} user to his daily energy consumption, such that:

$$v(\mathbf{q}^k, \alpha_i^k) = v_i^k(q_i^k) = \alpha_i^k \log(1 + q_i^k) \tag{8}$$

Being $\alpha_i^k \geq 0$ a parameter that characterizes the valuation (of i^{th} agent at k^{th} time) of $q \geq 0$ power units, so that the valuation is increasing as α_i^k increases.

Incentives proposed are expressed as:

$$I_i(\mathbf{q}) = \|\mathbf{q}_{-i}\|_1 \left(h_i(\mathbf{q}_{-i}) - r\left(\|\mathbf{q}\|_1\right)\right) \tag{9}$$

Where $h_i(\mathbf{q}_{-i})$ estimates the electricity price when the i^{th} user does not take part in the electricity system and $\mathbf{q}_{-i}$ is a vector that represents the consumption of the population except for the i^{th} agent.

Adding incentives $I_i(\mathbf{q})$ to the profit function $U_i(\mathbf{q})$ for the i^{th} agent it is obtained the function in eq. (10):

$$W_i(q_i, \mathbf{q}_{-i}) = v_i(q_i) - q_i r\left(\|\mathbf{q}\|_1\right) + I_i(\mathbf{q}). \tag{10}$$

Then, the idea is to maximize customers benefit:

$$\begin{aligned} \underset{\mathbf{q_i}}{\text{maximize}} \quad & W_i(q_i, \mathbf{q}_{-i}) \\ \text{subject to} \quad & \sum_{t=1}^{T} q_i^t \leq Q_i. \end{aligned} \tag{11}$$

Where $N \in \boldsymbol{N}$ are the customers and $q_i^t \geq 0, i = \{1, \dots, N\}, t = \{1, \dots, T\}$

Resolving the optimization problem, the fitness function T_i^k that maximizes benefit of eq. (11) is:

$$T_i^k(\mathbf{q}^k) = \frac{\alpha_i^k}{1 + q_i^k} - 2\beta \left(\sum_{j=1}^{N} q_j^k\right) \tag{12}$$

With $\beta \geq 1$ a parameter related to the generation cost of electricity. According to (Barreto et al., 2014), this fitness function gets a Nash equilibrium state of the system after a transition period.

Base Simulation Results

Running the game for a 24h-daily- period with $P = 6$ populations, $Q_i = 50\ kWh$ and uniform initial conditions, α_i^k is chosen with an increased value for greater i assuming that users have different load profiles. The load profile shape for the test case is based on XM predictions for November 2014, in Fontibón's substation in Bogota, Colombia[5]. Incentives are introduced from 2 to 5 time units in a 30 time units simulation.

In figures 1 and 2 can be seen that varying β parameter, associated with the production cost of energy, users will tend to lower their power expenses, and will have less utility, related to the higher cost they will pay for energy. Also the convergence of the population is faster for most dynamics, as users will try to save costs.

[4] Population Dynamics Toolbox

[5] Information available online on http://www.xm.com.co/Pages/PronosticoOficialdeDemanda.aspx

In fig. 3 and 4 each line represents a group of users with similar preferences. It can be observed that users with lower valuation profiles will extra limit their consumption, according to the increased prices. It is not straightforward to select a dynamic over another among traditional ones, and should be convenient to establish some particular dynamics which best fit the population under analysis, which is still an open problem for the case of Bogotá population.

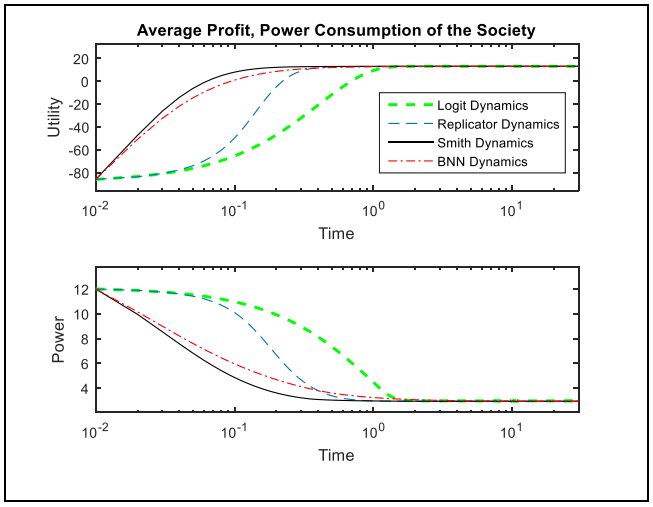

Figure 1. Average Utility and power evolution for various dynamics, with $\beta = 1$.

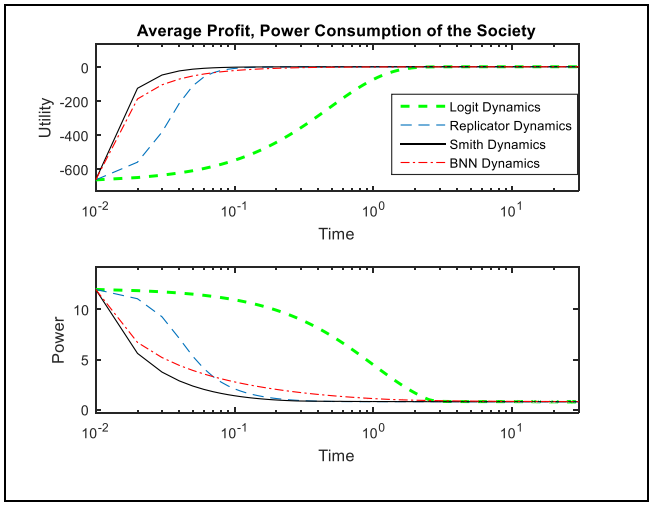

Figure 2. Average Utility and power evolution for various dynamics, with $\beta = 5$.

Mechanism Variation including Strata Consideration

Now, let introduce a variation in the fitness function associated to an added cost c_a proportional to the users valuation profile α_i^k, in order to make a basic implementation of socioeconomic strata, assuming that users in higher strata will have a higher consumption profile that it is desirable to have regulated, so that eq. (12) becomes:

$$F_i^k(\mathbf{q}^k) = \frac{\alpha_i^k}{1+q_i^k} - (1 + c_a * \alpha_i^k)2\beta\left(\sum_{j=1}^{N} q_j^k\right) \qquad (13)$$

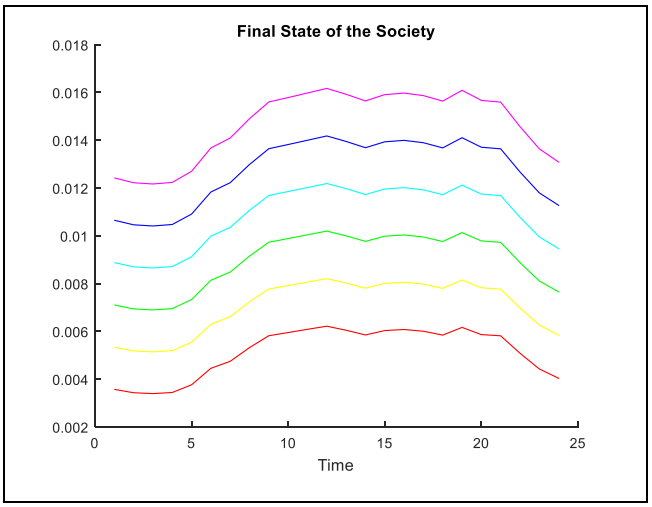

Figure 3. Final state of users, with $\beta = 1$.

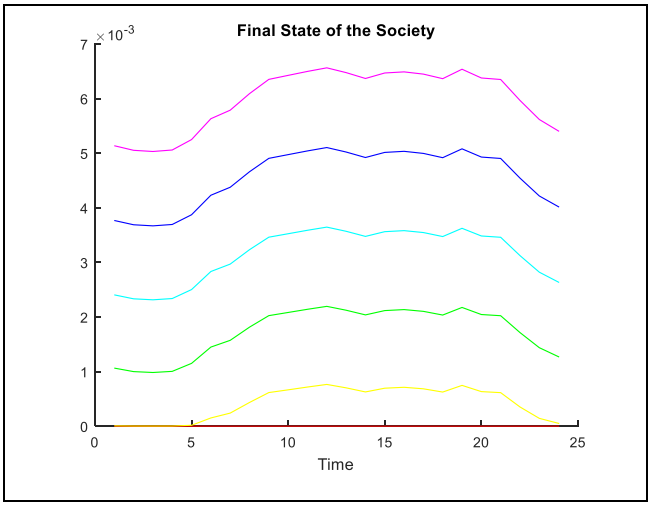

Figure 4. Final state of users, with $\beta = 5$.

The game was run mantaining all the conditions except for the *added cost* c_a, which was supposed as 10% and 30%. Hence, in figs. 5 to 8 the implications of the modification in the mechanism can be seen, for the game with every other condition kept the same. The total incentives for the population will increase or decrease depending on the population dynamics. It shows an important variation specially for Smith dynamic, where incentives' peak near the ending of the transition period gets lower as the *added cost* increases, getting overall lower incentives as well; Replicator dynamic has great variation too, extending the period where high incentives are demanded during the transition period when the *added cost* is greater.

As shown in fig. 5 and 6, the chosen dynamics greatly affects the amount of incentives used for the population in the transition to equilibrium process. This turns in a sensitive stage the selection of the population dynamics which best fit Bogotá's stratified population preferences and evolution in time.

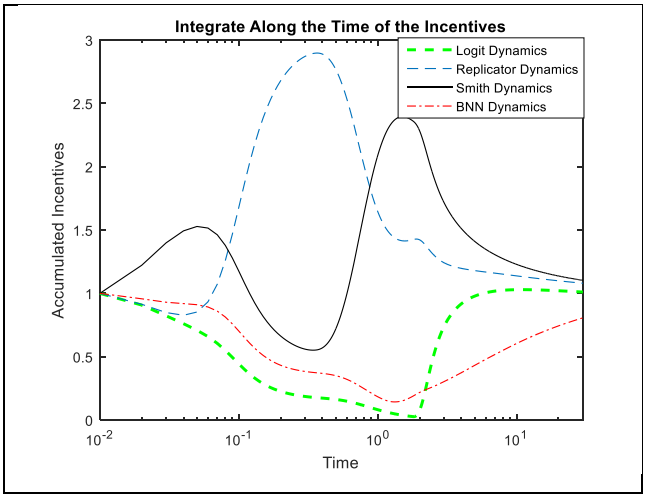

Figure 5. Cumulative incentives for the modified mechanism case, with added cost of 10%

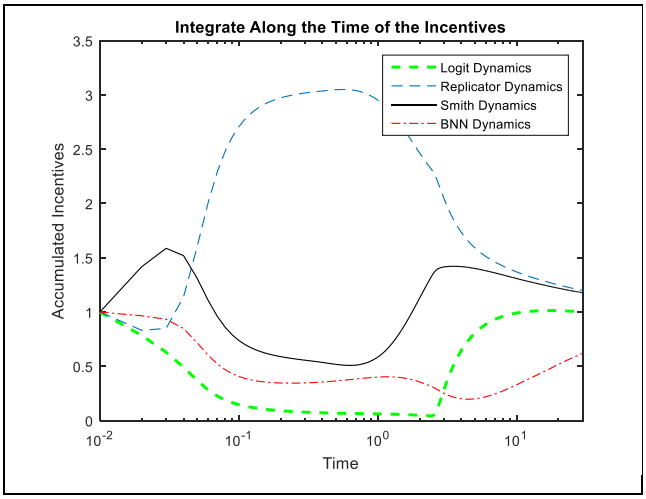

Figure 6. Cumulative incentives for the modified mechanism case, with added cost of 30%

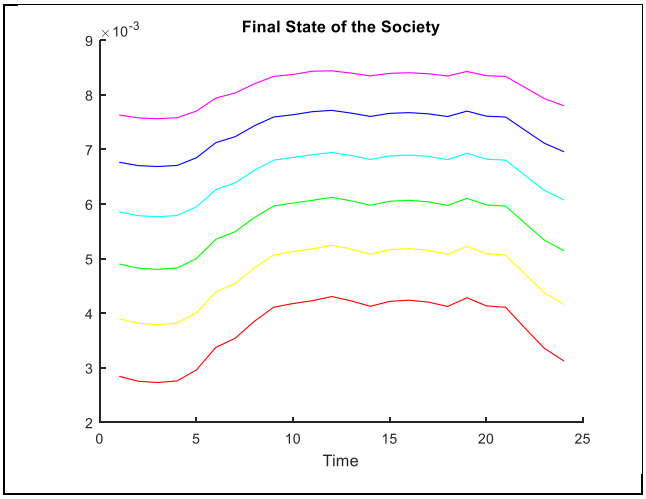

Figure 7. Final state of users, with β=1 and modified fitness function, with added cost of 10%

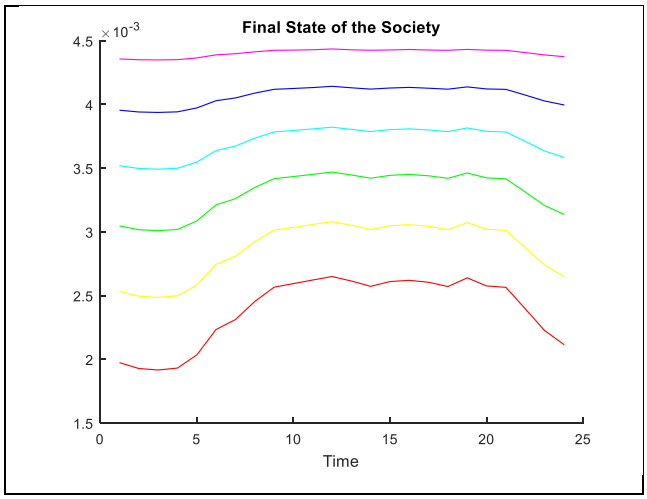

Figure 8. Final state of users, with β=1 and modified fitness function, with added cost of 30%

Equilibrium states of the society are shown in figures 7 and 8, where each line represents a group of users with the same consumption preferences, *i.e.* ranked in the same socioeconomic stratum. It is observed that all strata are affected by lowering their original consumption profile peaks shown in figure 3, having a flatter profile. The effect is specially marked for the users with greater valuation profiles which will become more homogeneous.

Conclusions

It has been reviewed the mechanism proposed by Barreto, Mojica-Nava, and Quijano (Barreto et al., 2013, 2014), analyzing variations of electricity generation cost as an introduction to the modification in the fitness function of the mechanism presented immediately after. The fitness function in the mechanism is associated to the maximum utility of the population, which may vary if the existence of users' economic strata is considered, as in the Colombian power system case.

The proposed modification of the mechanism leads to changes in incentives requirements during transition time before equilibrium state is reached, and also makes users with higher demand curve profiles to flatten their demand during the transition; thus obtaining a better energy distribution and use according to a central resource allocator entity. This variation of the mechanism sets the first stage of a much bigger project, and future work and research will be focused on addressing the particularization needed for the Colombian case including more variations and complexity for the incentives. Also, best fit population dynamics must still be derived for the actual behavior of Colombian users, as a whole or grouped in classes (strata).

Besides the best fit model and population dynamics which has to be proposed, it has to be taken into account comprehensive experimental data inclusion to the mechanism design for accurate characterization of real-world population. The experimental data may be historical records of consumption of just a part of the system, like Bogota, and shall be used for refinement and validation of the particularized mechanism.

The completed mechanism would state with sufficiency the rules and conditions needed to achieve a more efficient use of electricity, considering the necessary incentives, restrictions, and strata information of the users.

It would be interesting also take a complimentary approach considering the problem as a cooperative control game, as proposed by (Marden et al., 2009; Mojica-Nava, Barreto, & Quijano, 2015), associating a desired power usage for active agents with a consensus value, handling users stratification and comparing feasibility of implementation in a real world population.

References

Andersson, A., Jansson, A., & Klevâs, J. (1989). Model for load simulations by means of load pattern curves. In 10th International Conference on Electricity Distribution, CIRED (Vol. 6, pp. 545–549). Brighton: IEEE. Retrieved from http://ieeexplore.ieee.org/articleDetails.jsp?arnumber=206140

Baharlouei, Z., Hashemi, M., Narimani, H., & Mohsenian-Rad, H. (2013). Achieving Optimality and Fairness in Autonomous Demand Response: Benchmarks and Billing Mechanisms. IEEE Transactions on Smart Grid, 4(2), 968–975. Retrieved from http://ieeexplore.ieee.org/lpdocs/epic03/wrapper.htm?arnumber=6476052

Barreto, C. (2014). Population Dynamics Toolbox. Retrieved from https://github.com/carlobar/PDToolbox_matlab

Barreto, C., Mojica-Nava, E., & Quijano, N. (2013). Design of mechanisms for demand response programs. In 52nd IEEE Conference on Decision and Control (pp. 1828–1833). IEEE. Retrieved from http://ieeexplore.ieee.org/articleDetails.jsp?arnumber=6760148

Barreto, C., Mojica-Nava, E., & Quijano, N. (2014, August 22). Incentives-Based Mechanism for Efficient Demand Response Programs. Cornell University Library. Retrieved from http://arxiv.org/abs/1408.5366

Bompard, E., Carpaneto, E., Ciwei, G., Napoli, R., Benini, M., Gallanti, M., & Migliavacca, G. (2005). A game theory simulator for assessing the performances of competitive electricity markets. In 2005 IEEE Russia Power Tech (pp. 1–9). IEEE. http://doi.org/10.1109/PTC.2005.4524524

Espitia Silva, E. S., & Ramos Acevedo, D. A. (2014). Identificación de oportunidades para la gestión de la demanda en el sector industrial colombiano. Universidad Nacional de Colombia, Facultad de Ingenieria Eléctrica Y Electrónica. Trabajo de Grado Pregrado En Ingeniería Eléctrica. Bogotá.

Gelazanskas, L., & Gamage, K. A. A. (2014). Demand side management in smart grid: A review and proposals for future direction. Sustainable Cities and Society, 11, 22–30. http://doi.org/10.1016/j.scs.2013.11.001

Hurwicz, L., & Reiter, S. (2006). Designing Economic Mechanisms. Cambridge University Press.

Killingtveit, Å. (2014). Future Energy. Future Energy. Elsevier. http://doi.org/10.1016/B978-0-08-099424-6.00021-1

Marden, J. R., Arslan, G., & Shamma, J. S. (2009). Cooperative control and potential games. IEEE Transactions on Systems, Man, and Cybernetics. Part B, Cybernetics : A Publication of the IEEE Systems, Man, and Cybernetics Society, 39(6), 1393–1407.

Mhanna, S., Verbič, G., & Chapman, A. C. (2014). Towards A Realistic Implementation Of Mechanism Design In Demand Response Aggregation. In 18th Power Systems Computation Conference. Wroclaw, Poland.

Mojica-Nava, E., Barreto, C., & Quijano, N. (2015). Population Games Methods for Distributed Control of Microgrids. IEEE Transactions on Smart Grid, PP(99), 1–1. Retrieved from http://ieeexplore.ieee.org/lpdocs/epic03/wrapper.htm?arnumber=7145472

Rivera, B. (2013). Impacto de los precios de bolsa en los usuarios del servicio de energía eléctrica en el sector industrial. Universidad Nacional de Colombia, Departamento de Ingeniería Eléctrica Y Electrónica. Trabajo de Grado Pregrado En Ingeniería Eléctrica. Bogotá.

Samadi, P., Mohsenian-Rad, H., Schober, R., & Wong, V. W. S. (2012). Advanced demand side management for the future smart grid using mechanism design. IEEE Transactions on Smart Grid, 3(3), 1170–1180.

Sandholm, W. H. (2010). Population Games and Evolutionary Dynamics. MIT Press. Retrieved from http://books.google.com.co/books/about/Population_Games_and_Evolutionary_Dynami.html?id=pZH6AQAAQBAJ&pgis=1

Unidad de Planeación Minero Energética. (2013). Plan de Expansión de Referencia Generación – Transmisión 2013 – 2027 UPME. Bogotá. Retrieved from http://www1.upme.gov.co/sala-de-prensa/fotonoticias/plan-de-expansion-de-referencia-generacion-transmision-2013-2027

Yang, H., Zhang, Y., & Tong, X. (2006). System Dynamics Model for Demand Side Management. In 2006 3rd International Conference on Electrical and Electronics Engineering (pp. 1–4). IEEE. Retrieved from http://ieeexplore.ieee.org/lpdocs/epic03/wrapper.htm?arnumber=4017939

Contribution of the All Data Methodologies for Design of Demand Management Programs in the Industrial Sector

Contribución de las Metodologías All Data para el Diseño de Programas de Gestión de Demanda en el Sector Industrial

Daniela Valencia Lopez[1], Sandra Ximena Carvajal Quintero[2], Jairo Pineda Agudelo[3]

ABSTRACT

Big Data concept is a global trend, creating endless possibilities for the use of data generated by dynamic networks. The challenge is the transformation of this large volume of data into useful information for the electrical system. An example of this is the application of demand management programs (DMP) for the optimization of power system management in real time. This paper presents approach for DMP in Colombia, especially in industrial sector and uses an integrated average value autoregressive model (SARIMA) to create a model in order to propose a PGD according to characteristics of electricity consumption of an industrial user.

Keywords: All Data; Demand Management Programs (DMP); Industrial demand; Energy Efficiency; Time Series Analysis.

RESUMEN

Big Data es concepto con tendencia mundial, que permite un sinfín de posibilidades para el uso de los datos generados por las redes dinámicas. El desafío es la transformación de este gran volumen de datos en información útil para el sistema eléctrico. Un ejemplo de esto, es la aplicación de los Programas de Gestión de la Demanda (PGD) para la optimización de la gestión del sistema de energía en tiempo real. En este trabajo se explica el concepto de PGD en Colombia, especialmente en el sector industrial y utiliza un modelo autorregresivo de valor medio integrado (SARIMA) para crear un modelo que permita proponer un PGD aplicable a las características de consumo de electricidad de un usuario industrial.

Palabras clave: All Data; Programas de Gestión de Demanda (PGD); Demanda Industrial; Eficiencia Energética; Análisis de Series de Tiempo.

Received: July 24th 2015
Accepted: Sep 15th 2015

Introduction

According to International Energy Agency statistics, industrial sector is one of the main electricity consumers, it represents 42.3% of world electricity consumption in the world in 2012 (IEA, 2014). For this reason, PGD implementation at the industrial sector is necessary to balance supply and demand ratios electrical networks and to reduce the cost of electricity for industrial consumers.

In Colombia, regulated demand management programs are not well developed yet, but there is the Law 1715, 2014 that encourages efficient use of electrical energy by means of the implementation of energetic savings strategies and the usage of non-conventional energy, mainly those that are renewable, promotion, stimulus and encouragement to the development of efficient activities are declared public utility and social interest affairs and national convenience.

Article 31 of the current law proposes to establishment of regulatory mechanisms to encourage the demand response, by shifting peak hour's consumption and this way achieving a flattening of the demand curve, responding to reliability requirements (Dyer et al., 2008).

The main motivators to achieve an efficient use of energy at the industrial sector are economic, environmental, political and social, to mention some of them. To improve these aspects, demand control strategies must be implemented, as a result of the accelerated growth of the world`s industry and electrical consumption.

In Colombia, electrical energy demand grew in January 2013 4.5% compared with January 2012 (2.4%). This growth is caused mainly by an increase of regulated demand (residential and small business consumption), result of the high temperatures in the country. Table I shows the growth percentage of electrical energy demand in different regions.

[1] Author Description: Candidate Magister, Universidad Nacional de Colombia, Manizales Branch. Integrant investigation group Environmental, Energy and Education Policy (E3P) Universidad Nacional de Colombia. E-mail: davalencialo@unal.edu.co

[2] Full Professor, Universidad Nacional de Colombia, Ph.D in Engineering Automatic Line, Universidad Nacional de Colombia. Researcher Group E3P, Universidad Nacional de Colombia. E-mail: sxcarvajalq@unal.edu.co

[3] Associate Professor Universidad Nacional de Colombia, Manizales Branch, Statistical, Social Universidad Católica de La Salle, Colombia. Magister in Regional Development and Territory Planning, Universidad Autónoma de Manizales, Colombia. Investigation Group E3P, Universidad Nacional de Colombia.E-mail: jpinedaa@unal.edu.co

Table 1. Performance of regional energy demand GWh–January 2013

REGION	JANUARY 2013	GROWTH
Centro	1256.5	0.0%
Antioquia	716.6	3.7%
Costa Atlántica	1037.4	7.6%
Valle	558.5	7.2%
Oriente	515.1	6.8%
CQR (Caldas, Quindío y Risaralda)	199.5	0.2%
THC (Tolima, Huila y Caquetá)	199.0	4.2%
Sur (Cauca y Nariño)	142.8	0.0%
Chocó	17.0	8.3%
Guaviare	3.9	4.3%

Ref. Behavior in demand for electricity in Colombia 02/25/2013 XM. Market experts

In a similar way, energy demand in the non-regulated market showed a 4.5% increase in January 2013, this growth can be observed in Table 2.

Table 2. Performance of the demand for regulated and unregulated energy for economic activities GWh SIN – National Interconnected

User type	January 2012	January 2013	Growth
REGULATED	3,172.0	3,333.6	5.1%
UNREGULATED	1,595.3	1,666.6	4.5%
Manufacturing Industry	642.3	647.4	0.8%
Mining and Quarrying	347.2	379.4	9.3%
Social, community and personal services	217.9	213.6	-2.0%
Trade, Repair, Restaurants and hotels	134.9	150.4	11.5%
Electricity, Gas and Water Town	120.8	123.8	2.5%
Transport, Storage and Communication	53.0	57.1	7.7%
Agriculture, Forestry, Hunting and Fishing	40.6	47.9	18.1%
Financial establishments, Insurance and Real Estate	35.7	43.6	22.1%
Construction	2.8	3.4	20.3%

Ref. Behavior in demand for electricity in Colombia 02/25/2013 XM. Market experts

With these growth percentages of electrical energy demand in the country it appears a need to perform demand management actions to achieve an important effect on efficient energy consumption, as indicated by law 1715, 2014. Taking into account that industrial facilities demand consumes big amounts of electricity, a strategy for efficient use of energy will be to implement DMP to improve electrical networks reliability (Ding and Hong, 2013). Through strategies possessing the DMP against reduction of load, as well as growth control thereof providing greater flexibility of the electric energy system (Gellings and Smith, 1989).

In figure I, it can be observed the electrical energy demand growth in Colombia during the last 10 years.

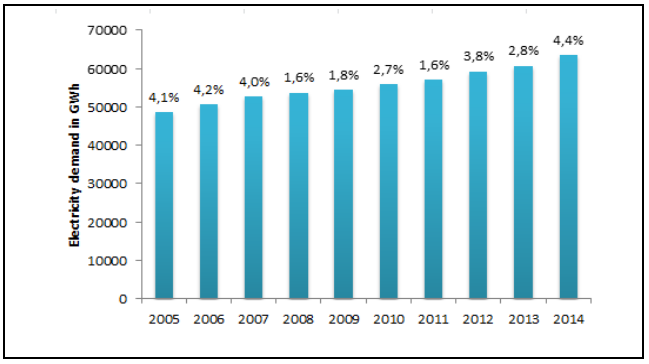

Figure 1. Behavior of energy demand in Colombia for the past 10 years

The first three years, electrical energy demand in Colombia underwent an accelerated growth, becoming less for the following four years and finally it has a more important growth in year 2014 as compared with the immediately previous year.

It is necessary to keep in mind that the main involved in DMP implementation at the industrial sector is the non-regulated user, the success of the execution of such strategies is mainly related to the users participation in such programs, where they gain benefits and no major changes are required, this makes necessary to know the consumption profile of each user.

Data on energy measurement become raw material for analysis, one step to follow is to take advantage of data to transform it into useful knowledge in order to provide answers to operational matters and solve problems with more speed and precision (Potter, 2014).

As study case there are measurement data of a non-regulated user in the manufacturing industry (coffee threshing) (DANE 2015), this is one of the main activities of the CQR region that comprises Caldas, Quindío and Risaralda departments. As noted previously, this activity has shown a 0.8% electrical energy consumption increase in the time between years 2012 and 2013. Compared with the other activities of the manufacturing industry it doesn't contribute with a high percentage. The objective is to implement strategies to reduce the growth of the electrical energy demand in the country or in another way, strategies that allow having more efficient electrical energy consumption.

The approach of this research is focused in proposing a DMP implementation strategy to the Colombian industrial sector, taking into account the different features shown by these users, as well as the variety of factors that may affect their consumption, as weather and the raw materials level changes according to the harvesting conditions, to mention some of them.

The article is organized as follows: Section II describes DMP and their main features. In Section III a general view of All Data methodologies and time series currently used for data analysis are provided. Section IV describes the electrical series demand of an industrial user whose main activity is coffee threshing. In Section V results are analyzed and conclusions close the article.

DMP Overview.

Demand Management is a portfolio of strategies to improve the electrical energy system from a consumption standpoint. It goes from improving energetic efficiency by means of the use of better materials, smart energy fees with stimulus for certain consumption patterns to a sophisticated real time control of distributed

energetic resources (Palensky and Dietrich, 2011). This can be clearly observed in Figure 2.

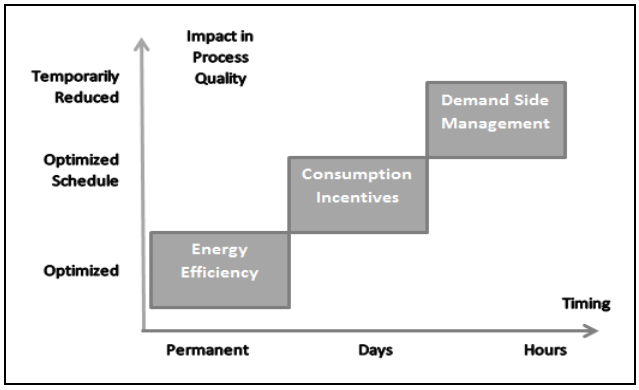

Figure 2. Definition of Demand Side Management

DMP are oriented to the regulation of the electrical energy market, these can design a specific model for each hour of the day, perform a balance and participate in an active way in the market (Martinez and Rudnick, 2012). In addition, they are directed to the reduction of the electricity cost; solve transmission lines congestion because it can delay inversions in transmission networks and increase reliability indexes in electrical systems.

DMP have been implemented to achieve a best participation of demand facing the cost or the needs to improve reliability levels of the electrical system, searching to mitigate power restrictions in an electrical system or to get a more efficient handling of this resource, obtaining also economic benefits for trading companies as well as for the end user (Baratto, 2010).

The need to have balanced and coordinated systems brings an interest to the network operators to participate in DMP. A bidirectional market allows buyers and sellers to find and negotiate the type of market in which they want to participate enjoying mutual benefits (Aalami et al., 2008).

Basically DMP are divided in two main categories, called time based programs and stimuli based programs. Time based programs are: use times programs (Aalami et al., 2008), critical peaks prices and real time prices. Stimuli based programs are: demand response programs in emergency times, load direct control, interruptions/reductions programs, market capacity, demand offer programs and random services programs, as can be seen in Figure 3.

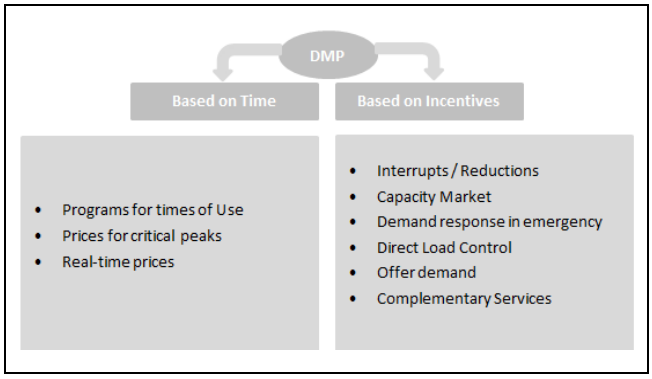

Figure 3. Distribution of DMP

Time based programs feature is that prices change during different periods according to the cost to provide electricity, for example:

- High prices on peak times
- Moderate prices on out of peak periods
- Low prices on low load periods

These types of programs don't receive stimuli or penalties.

Stimuli-based programs can be voluntary or mandatory.

Consumer's demand depends on the elasticity of electricity costs as well as on the stimuli and the penalty costs determined by DMP (Aalami et al., 2008).

DMP were created to obtain utilities treating reductions of maxim demand peaks as an alternative for the capacity from a perspective of the integrated planning of resources. Since the 80's, DMP have evolved to incorporate efficiency as well as load management (Spees and Lave, 2007).

The load side management plans, implements and monitors the activities that influencing consumer in the electricity use so that they can produce desired changes in forms of load, as well as in the time patterns and magnitude of the same (Gellings, 1985). The active management of load transforms the demand curves, driving to stability or providing programed peak and valley, so that the power system it can effectively plan and control the generation and the expansion of both systems transmission and distribution. Also it contribute at the decongestion of system, emergency support and backing when the users they have active participation and they possess elements of cogeneration and autogeneration (UPME, 2014).

Demand management is divided mainly in two parts, passive demand management and active management. Passive demand management includes educational material, auditing for the customers amidst other passive forms where the end user is trained about the value of performing an efficient use of the energy, as well as the consumers' knowledge of the benefits they could obtain participating on a DMP. Active demand management is the inclusion of more important changes in the typical demand behaviour, for example, change or implementation of a new technology or the active participation of an user into a DMP where the consumer in a voluntary or obligatory way makes the pertinent consumption reductions and receives stimuli for his participation.

Electricity reductions, according to a recent study of the Economic Board for Latin America and Caribbean, estimates that the savings potential is important, establishing that 25% of the electrical energy consumption can be avoided with the active demand participation (Merril, 2014).

Overview Methodologies All Data in Data Analysis.

The volume and complexity of the available information overwhelm human and computer resources. Different approaches, technologies and tools are dealing with different data types as for example mining, learning and management of existing information which is growing more and more. From small data understanding (Small Data), academy and industry recently embraced big data (Big Data), linked data (Linked Data) and open data (Open Data). Each one of these concepts has specific foundations, algorithms and techniques and is appropriate and successful for different application types. While every concept is approached from a

standpoint that allows a better understanding (and potential optimization), there is no application or service that can be developed without taking into account all the data types mentioned above, which are grouped in All Data (Pineda et al., 2015) as it can be seen in Figure 4.

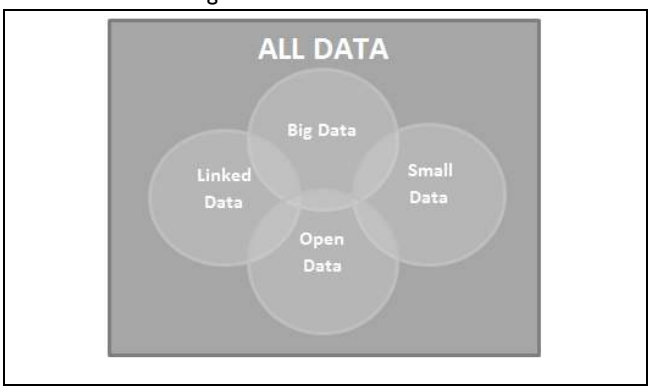

Figure 4. Grouping methodologies All Data

Next, different data types are described in a more specific way:

Big Data: Refers to big data volumes, where all the information is collected and it is associated with the immediacy to apply over advanced analytics technics (Joyanes, 2013) (McAfee and Brynjolfsson, 2012) (Piatetsky, 2014).

Small Data: It refers to the use of small data to make inferences obtained from polls; these are not closely related to immediacy in the statistic answers.

Open Data: It is understood as the opening of digital data, there is also place for physical data. Data opening is requested more and more to complement analytic studies. Access promotion is then linked to the process transparency.

Linked Data: It refers to data obtained through internet, on this approach there is a close relationship with the internet of things (IOT), it collects the information produced by all types of electronic devices communicated through internet, as for example electronic measurement devices, domotics, etc. They can easily become a Big Data.

Management of this type of tools to analyse big amounts of data requires identifying, mixing and managing multiple data sources, as well as the capacity to build advanced analytics models to predict and optimize results. Taking into account that the most critical component is related to the capacity to transform the passive contribution of energy demanders to an active contribution and in real time to achieve the DMP purposes of the industrial users, then a strategy for the DMP would be the design of a LOBS's model as it can be seen in Figure 5.

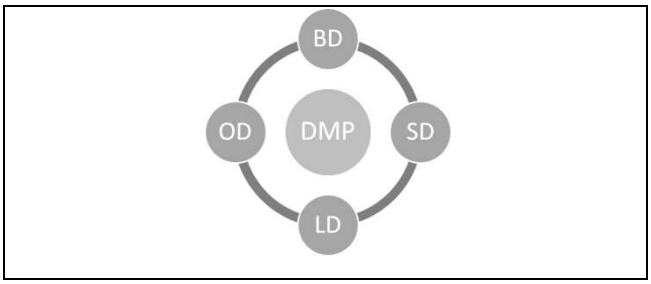

Figure 5. Grouping methodologies All Data

This model links All Data to improve the reliability of the information you have and then migrate to scenarios with big amounts of information to offer alternative schedules to industrial users according to scales stablished for an electrical energy consumption classification and subsequently identify the specific DMP.

The design and implementation of DMP efficient required in first term of the recognition of complex phenomenon as it is the energy market and its multiple impacts in a world amply interdependent and articulate.

It is therefore of assume a theoretical position that recognize inherent multidimensionality at a DMP and hence it is not just a problem of technical character that pretend modify the consumption habits, and, in the actual condition of Colombia voluntary decrease and considerably, the energy demand.

The sustainability of programs of this magnitude a demand consider aspects that go from environmentally to the political, including economic issues and social. That implies in ultimately an ethical dimension.

However, the strategy of associated information with a DMP queries this dimensionality and offers its answers considering the various possible sources. In the case of the experience currently it develops in the industrial sector of Manizales it has with a first source of supplies automatic data through smart meters capable of making telemetering (Article 3, Resolution CREG 131/1998) (linked data) which bring volumes increasing of data (big data) about the periodic consumption of energy. This should be collated with the information on the industrial characteristics of production regarding at activities each of the process where it presents an energetic expenditure as the type of engines, refrigerators, illumination, among others, as well as know volumes and variety of production, size, among others externalities that affect directly the processes of production. The latter usually come from the application of polls and studies inside of industry in question (small data) and contextualized with information of the biggest database that offered the government entities which provide rates of variation in the production, classification of different industries as well reports on capacity of the industrial sector for practice to energy efficiency (ISO 50001, 2011) (DANE, 2015) (UPME, 2015) (open data).

La integración de estas cuatro fuentes, junto con una analítica apropiada es la Conduce a una propuesta de todos los datos promovidas por la primera conferencia en Barcelona, con el interés de calificar la decisión procesa anuncio en particular los relacionados con la energía (ALLDATA, 2015).

The technic that will be used refers to the study of the Time Series originated in the periodic data collection on electrical energy consumption, this is the foundation to build the demand curve, to build consumption models and to predict demand, and the technic will be explained in more detail next.

Time Series Analysis

The analysis of experimental data that have been observed for different time points leads to new problems in statistic modeling. Correlation by time-adjacent points sampling may be restricted by the applicability of some traditional statistic methods, depending that this adjacent observations are independent and distributed identically. The approach answers mathematical and statistical questions posed by such time correlations that commonly referred as time series analysis (Shumway and Stoffer, 2010).

(Box and Jenkins 1976) (Box 1994) develop a systemic models class called Autoregressive integrated moving average ARIMA to handle a modeling of correlated time and prediction, this model includes a prediction for the processing of more than one series

entry at a time through the multivariate ARIMA or through the transfer function model.

Series of electricity demand of an industrial user (coffee processing)

The series of electricity demand of the industrial user consists of hourly time series of the electricity consumption of the coffee threshing specialized facility located in Manizales city; this is one of the main agricultural activities in the city. A collection of the electrical energy consumption in MWh was collected in the time between September 2014 and January 2015, all the data were used to estimate the parameters.

In Figure 6 it can be seen a graph of the time series that covers the time from September 1, 2014 to January 30, 2015; days are identified by 24 hours periods.

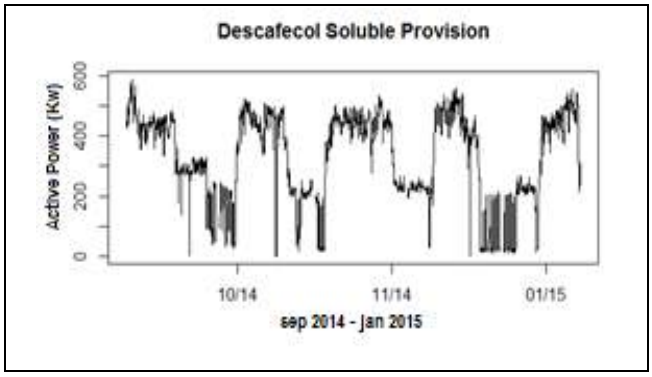

Figure 6. Active power consumption of the Industrial Company

It is clear that the first days of the month show similar demand patterns, while the last days of the month have the lowest peaks of electricity demand and then show different demand patterns, this is caused by the variation of the agricultural production because there are different factors that affect the production and then the threshing variates in time.

It can be observed that there is an important variation as sampling time goes, in Figure 7 the first sampling week consumption can be observed.

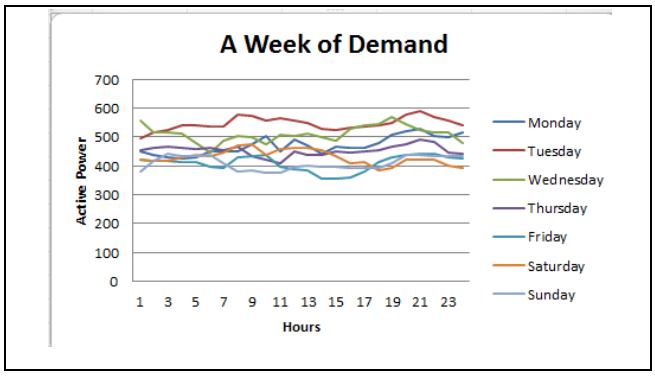

Figure 7. Active power consumption of the Industrial Company

It can be seen that consumption every day has a different behaviour, being higher starting the week, by the end of the week, electrical energy demand decreases. Consumption in an industrial user doesn't have a typical curve as the home user.

Model Applied

The Seasonal Autoregressive integrated moving average - SARIMA model is introduced by (Box and Jenkins, 1976) to analyze the pattern of the individual time series. The SARIMA model is noted as ARIMA $(p,d,q)(P,D,Q)s$, where p and P express the orders of the autoregressive terms non-seasonal and seasonal respectively; d and D are the orders of the differentiation non-seasonal and seasonal respectively; while q and Q are the orders non-seasonal and seasonal of the mobile average component and s is the seasonal period.

SARIMA can be expressed as:

$$\emptyset_p(B)\Phi_P(B^s)\nabla^d\nabla_s^D y_t = \theta_q(B)\Theta_Q(B^s)\,\varepsilon_t, \qquad (1)$$

Where ∇^d and $\nabla_s^D$are the non-seasonal and seasonal differentiation operators respectively; B is the backwards displacement operator; ε_t is a White noise process with zero mean and constant variance; $\emptyset_p(B)$ and $\Phi_P(B^s)$, are the p y P order polynomials, they represent the non-seasonal and seasonal autoregressive components respectively; $\theta_q(B)$ and $\Theta_Q(B^s)$ are the q y Q order polynomials, they represent the mobile average non-seasonal and seasonal respectively.

If the data series of the industrial user is non-stationary differences and/or transformations must be done to make it stationary (Ismail et al., 2015).

Results

Different SARIMA models are used to predict or Project the electricity demand of an industrial user. Results have been obtained using R software (Chambers, 2015). They indicate a 2 order polynomial in the non-seasonal component and 1 order in the seasonal component that has a 24 hours period; it is necessary to make a difference in the non-seasonal component and it is not necessary to difference in the seasonal component and finally there is a 2 order polynomial in the mobile average component, for the non-seasonal as well as for the seasonal part.

SARIMA (2, 1, 2) (1, 0, 2) [24]

The output with the results provided by the R software is shown next.

```
ARIMA (2, 1, 2) (1, 0, 2) [24] with drift

Coefficients:
          ar1      ar2      ma1      ma2    sar1    sma1    sma2    drift
      0.9665  -0.0795  -0.8117  -0.1286  0.8976  -0.7432  0.0042  -0.0730
s.e.  0.1056   0.1080   0.1057   0.1093  0.0158   0.0240  0.0200   0.5179

sigma^2 estimated as 559.7:  log likelihood=-15708.69
AIC=31435.38   AICc=31435.43   BIC=31490.9
```

The coefficients of each one of the SARIMA method variables can be observed with its corresponding standard deviation, where `ar1` corresponds to $\emptyset_1$, `ar2` corresponds to $\emptyset_2$, `ma1` corresponds to θ_1, `ma2` corresponds to θ_2, `sar1` corresponds toΦ_1, `sma1` corresponds to Θ_1, `sma2` corresponds to Θ_2, and finally the term `drift` refers to the ε_t constant.

The terms `AIC=31435.38` `AICc=31435.43` `BIC=31490.9` are AIC the Akaike's information criterion, AICc is the AIC with deviation corrected and BIC is the Bayesian information criterion, these terms are defined in (Shumway and Stoffer, 2010), they refer to the criteria to choose the best model, being the best model the one that has the lowest AIC.

The steps to follow are the model refining that will allow predicting the electricity consumption based on a series of data to identify how convenient is the model.

Then build on the basis of the depurated model the scenarios of DMP that can be applied according to the behavior of the con-

sumption curves, also, with new data information, modify the model to make it more precise.

Also find in other All Data methodologies useful information that allow to identify new models that will enrich the investigation, as for example small polls to industrial users and national polls that provide useful open data to influence electricity consumption inter alia.

Finally it is proposed to the local network operator the possibility to perform an individualized information treatment to predict the behavior of industrial customers, given that the electricity consumption varies depending on multiple factors according to the economic activity accomplished, which brings complexity by the diversity of DMP implementation strategies to industrial users.

Acknowledgments

The authors would like to express their gratitude to Direction of Investigation Manizales DIMA of the University National of Colombia and M.S. Jaime Leon Hincapie Daza for their valuable help, collaboration and support provided.

Conclusions

SARIMA model was investigated in this work for electricity demand prediction of an industrial user from Caldas specialized in coffee threshing, that through a time series, a prediction of the electricity consumption behavior can be realized and will be presented to the user immediately after that will allow to reduce the decision making time and then reduce the times to apply appropriate DMP strategies.

This work has raised concerns about the behavior of the industrial user because this one doesn't present a typical behavior day after day, this is reflected thanks to the change in raw material levels according to the changing conditions presented by the coffee harvest, among other factors that can affect directly the consumption as the weather, time of the year, demand of the elaborated product, etc.

As it can be seen in Figure 7, the electricity consumption curve for this specific type of industrial user doesn't show critical peaks during the day and then it can be inferred that the success of DMP application to this type of users focuses mainly on stimuli based programs.

References

IEA, 2014. Key World Energy STATISTICS 2014, International Energy Agency, 2014. www.iea.org/statistics/mgds

Law 1715, 2014. By regulating the integration of renewable energies non-conventional of energy to the system national, May 13, 2014, Gobierno Nacional de la Republica de Colombia, Bogota, http://wsp.presidencia.gov.co/Normativa/Leyes/Documents/LEY%201715%20DEL%2013%20DE%20MAYO%20DE%202014.pdf.

C. H. Dyer, G. P. Hammond, C. I. Jones, R. C. McKenna, Enabling technologies for industrial energy demand management, Department of Mechanical Engineering, University of Bath, Bath, UK, Energy Police, Oct 2008.

Y. Ding and S. Ho Hong, A Model of Demand Response Energy Management System in Industrial Facilities, Department of Electronics and System Engineering Hanyang University, Ansan, Korea, IEEE SmartGridComm 2013 Symposium - Demand Side Management, Demand Response, Dynamic Pricing.

C. W. Gellings and W. M. Smith. Integrating Demand-Side Management into Utility Planning. PROCEEDINGS OF THE IEEE, VOL. 77, NO. 6, JUNE 1989.

J. Potter, 2014. Analytics at SMUD evolve with the smart grid, Nov 04.

DANE 2015, Clasificación Industrial Internacional Uniforme de todas las actividades económicas Revisión 3.1 Adaptada para Colombia. Trilla de café, http://formularios.dane.gov.co/senApp/nomModule/aym_index.php?url_pag=clasificaciones&alr=&cla_id=2&sec_id=4&div_id=15&gru_id=26&cla_ide=193&url_sub_pag=_05&alr=&

P. Palensky and D. Dietrich, Demand Side Management: Demand Response, Intelligent Energy Systems, and Smart Loads, IEEE TRANSACTIONS ON INDUSTRIAL INFORMATICS, VOL. 7, NO. 3, AUGUST 2011

Martinez, V.J. and Rudnick, H., Design of demand response programs in emerging countries, Power System Technology (POWERCON), 2012 IEEE International Conference on doi: 10.1109/PowerCon.2012.6401387, November 2012, Santiago de Chile, Chile.

P. Baratto, 2010. Implementation of a program of demand response in electricity market unregulated customers in Colombia, Rev. maest. Derecho econ. Bogotá (Colombia) Vol 6. N° 6: 259-292, dic 2010.

H.A. Aalami, M. Parsa Moghaddam, G.R. Yousefi, Demand response modeling considering Interruptible/Curtailable loads and capacity market programs, Department of Electrical Engineering, Tarbiat Modares University (TMU), Tehran, Iran, Applied Energy, Jul 2009.

K. Spees and L. B. Lave, "Demand Response and Electricity Market Efficiency", Published by Elsevier Inc., doi:/10.1016/j.tej.2007.01.006, April 2007, Vol. 20.

C. W. Gellings, "The Concept of Demand-Side Management for Electric Utilities", PROCEEDINGS OF THE IEEE, VOL. 73, NO. 10, OCTOBER 1985.

UPME 2014, INSTALLED CAPACITY OF SELF-GENERATION AND COGENERATION IN SECTOR OF INDUSTRY, OIL, PUBLIC TRADE COUNTRY, Final Report Version 1.1, May 2014.

D. Merrill, 2014., Careful with easy answers of Big Data. HBR, August 5.

J. Pineda, S. Carvajal, D. Valencia, "Big Data for Demand Management Programs Designing for Colombia's Industrial Sector", ALLDATA 2015 : The First International Conference on Big Data, Small Data, Linked Data and Open Data, Copyright (c) IARIA, 2015. ISBN: 978-1-61208-445-9, Barcelona 2015.

L. Joyanes, 2013., "Big Data Analysis of large volumes of data in organizations", Alfaomega Marcombo Ediciones Técnicas.

A. McAfee and E. Brynjolfsson, Big Data: The Management Revolution October, 2012, https://hbr.org/2012/10/bigdatathemanagementrevolution/ar,

G. Piatetsky, 2014., Big Data Winter ahead - unless we change course, warns Michael Jordan, Oct 30, 2014., http://www.kdnuggets.com/2014/10/big-data-winter-ahead-unless-we-change-course.html

Article 3, Resolution CREG 131/1998 http://apolo.creg.gov.co/Publicac.nsf/1aed427ff7829119652567 51001e9e55/c2d01cc1ae3da04a0525785a007a5fa5/$FILE/Cr131-98.pdf.

ISO 50001, Systems Power Management, 2011, http://www.iso.org/iso/iso_50001_energy-es.pdf

UPME, Mining and Energy Planning Unit, 2015, http://www1.upme.gov.co/

ALLDATA 2015, The First International Conference on Big Data, Small Data, Linked Data and Open Data ALLDATA 2015 April 19 - 24, 2015 Barcelona, Spainh ttp://www.iaria.org/conferences2015/ALLDATA15.html

R. H. Shumway and D. S. Stoffer, Time Series Analysis and Its Applications, With R Examples, Springer Text in Statistics, ISSN 1431-875X, ISBN 978-1-4614-2759-9, DOI 10.1007/978-1-4419-7968-3, 3rd Edition 2010, pp 1-39

G. E. P. Box and G. M. Jenkins, Time Series Analysis: Forecasting and Control. Revised edition, San Francisco: Holden-day, 1976

M. A. Ismail, A. R. Zahran, E. M. Abd, El-Metaal. Forecasting Hourly Electricity Demand in Egypt. Using Double Seasonal Autoregressive Integrated Moving Average Model. Statistics department. Faculty of economics and political science, Cairo University. Giza, Egypt. IARIA, 2015. ISBN: 978-1-61208-445-9

J. Chambers, 2015. R is a language and environment for statistical computing and graphics. It is a GNU project which is similar to the S language and environment which was developed at Bell Laboratories (formerly AT&T, now Lucent Technologies) by. R can be considered as a different implementation of S. http://www.r-project.org/about.html

Dynamic Manager for Electrical Energy Efficiency in Buildings

Gestor Dinámico Inteligente para la Eficiencia Energética en Edificaciones

Christian G. Quintero M. [1], Jamer R. Jimenez Mares[2]

ABSTRACT

This paper studies a management model for electrical energy efficiency that allows the integration of several alternatives energy generation sources such as wind, photovoltaic and fuel cell power in order to minimize the power consumption in a building. An intelligent approach is presented to manage the power consumption of appliances. This approach takes into account variables such as temperature, luminance and presence. The integration of several Demand Side Management (DSM) criteria are carried out through dynamic and intelligent selections according to variable performance, customer´s preferences and operation based on comfort or consumption. Likewise, a diagnosis analysis through energy audit is carried out to evaluate electrical appliances proficiency and customer habits. Finally, the design of a fuzzy logic-based manager is presented to select which electrical source and what proportion of energy is needed to satisfy power consumption. According to our experimental results obtained from about 120 several case studies, each of which consists in setting an energy usage during 24 hours with several behavior, energy savings between 27% and 33% can be achieved with the proposed dynamic manager, and is about 5% saver than an individual management criterion.

Keywords: Demand Side Management (DSM), energy audit (EA), energy efficiency, management criteria for electrical energy and alternative energy.

RESUMEN

Este articulo estudia el diseño de un modelo de gestión para la eficiencia de energía eléctrica que permite la integración de diversas fuentes de generación de energía eléctrica como la eólica, fotovoltaica y celda de combustible con el fin de minimizar el consumo de energía eléctrica en una edificación. Se presenta una metodología inteligente para gestionar el consumo de energía eléctrica de los dispositivos eléctricos. Esta propuesta toma en cuenta las siguientes variables exogenas: temperatura, luminarias y presencia. La integración de múltiples criterios de gestión de la demanda de energía (DSM) es llevada a cabo a través de selecciones dinámicas e inteligentes de acuerdo a las preferencias del usuario y la operación basada en confort o consumo. De igual manera, se realiza un diagnóstico a través de un proceso de auditoría energética con el objetivo de evaluar la eficiencia de los dispositivos eléctricos y hábitos de consumo. Finalmente, se presenta el diseño de un gestor basado en lógica difusa para seleccionar la fuente de energía eléctrica y la proporción de la misma requerida para satisfacer la demanda de energía eléctrica. De acuerdo con los resultados experimentales obtenidos en 120 casos de estudio, cada uno de los cuales consistió en establecer un uso de la energía durante 24 horas con diferentes comportamientos, es posible alcanzar ahorros de energía entre 27% y 33% a través del gestor dinámico inteligente, el cual es 5% más ahorrador que un criterio de gestión individual.

Palabras clave: Gestión de la demanda, auditoria energética, eficiencia energética, criterio de gestión para la energía eléctrica y energía alternativa.

Received: July 24th 2015
Accepted: August 23th 2015

Introduction

In industrialized countries the 40% of the energy is consumed by buildings, where 68% is in the form of electricity (Frank & Goswami, 2007; Huang, 2006; Lior, 2010; Tascikaraoglu, Boynuegri, & Uzunoglu, 2014). Recent research shows that 20%–30% of this energy consumption can be saved through optimized operation and management without changing the structure and hardware configuration of the building energy supply system (A. Di Giorgio, 2012; D. Zhang, N. Shah, 2013; Guan, Xu, & Jia, 2010; N. Gudi, L. Wang, 2012). Likewise, the possibility to achieve higher generation levels without the environmental impact that comes with conventional generation systems has motivated the use of these technologies with renewable sources (Craddock, 2008; M. Sechilariu, B. Wang, 2013; S. Kahrobaee, R.A. Rajabzadeh, S. Leen-Kiat, 2013). However, despite these efforts the world power consumption still growth year in year out (EIA, 2014).

Challenges related to large variability in efficiency strategies based on integration of several criteria as audit energy, demand side management and alternatives energy source remain little explored. Integrating different management approaches offers the possibility of exploiting strengths and compensating their weaknesses when they are used all together. However, this approach requires a model able to operate according to basics

[1] Christian G. Quintero M. is with the Department of Electrical and Electronics Engineering at Universidad del Norte, Colombia. Km 5 Vía Puerto Colombia. Tel.: (+57 5) 3509509 ext.: 3263.

[2] Jamer R. Jimenez Mares is with the Department of Electrical and Electronics Engineering at Universidad del Norte, Colombia. Km 5 Vía Puerto Colombia. Tel.: (+57 5) 3509509 ext.: 3263.

How to cite: Journal Space xxxxxxxxxxxxxxxxxxxx
xxxxxxxxxxxxxxxxxxxxxxxxxxxxxxxxxxxxxxxxxxxxxxxxxxxxxxxxxxxxxxxxxxxxx

principles of efficiency from generation and consumption.
In order to overcome related limitations for the management of electrical energy, it is possible combining those activities that involves identification, implementation and verification of improvement plans where the main goal is reducing the consumption of electricity without impacting customer´s comfort (Ravibabu, Praveen, Ch, P, & M, 2009). Therefore, it is important for the adequate management of energy efficiency to include three functional stages: energy audit, efficient management of the electrical appliances and renewable sources. (1) Energy audit provides opportunities for electrical energy saving through identification of bad consumption habits and appliances whose operation and technology cause an excessive level of power consumption (Gomes, Coelho, & Valdez, 2011; Wang & Huang, 2009). (2) Electric energy management allows setting suitable operation points according to exogenous variables (e.g., temperature, luminance, presence, among others) and customer´s preferences adjustment to efficiency policies. (3) The use of alternatives energy sources integrated with a stage of demand management has two advantages: first, the integration of such technologies allows coordinating the operation of individual systems in order to provide suitable energy conditions for all appliances connected to the power grid. Second, the implementation of a management stage provides the possibility to operate the appliance efficiently depending on the need. The management stage involves basic integration knowledge according to principles of efficiency.
Several authors have worked on power consumption saving without impacting the customer's comfort (Frank & Goswami, 2007)(Salehfar, 1999)(Ravibabu et al., 2009). The application of *Demand Side Management* (*DSM*) techniques like *Load Priority* provides suitable management according to customer´s variables. In other cases, those appliances with more consumption during peak demand are identified. Management criteria using computational intelligent techniques provide a reduction of power consumption around 10 to 30 % (Goel, Wu, & Wang, 2010; Matallanas et al., 2012; Ravibabu et al., 2009; Salehfar, 1999).
In this paper, we introduce a framework which it carries out the integration of energy audit, multiple criteria of electrical energy management and alternatives energy sources. A neural network-based criterion has been developed taking into account policies of efficiency and exogenous variables as temperature, presence, luminance, use profile (e.g. computer) and type of activity. Additionally, a fuzzy logic based criterion inspired on differential tariff has been developed. The design of a hybrid manager using several *DSM* and intelligent criteria is proposed, using selection preferences based on priority, comfort or consumption. The selection of each criterion depends on the curve proposed by the dynamic manager (*DM*), which is determined according to the adjustment of efficiency policies in each appliance. Finally, a fuzzy manager for an alternative power station has been designed. This station is composed of three types of energy sources (wind, photovoltaic and fuel cells). These three energy sources are integrated in order to increase system reliability in terms of compliance with the electrical energy demand (S. Kahrobaee, R.A. Rajabzadeh, S. Leen-Kiat, 2013). The meteorological variables provide information to the models used by the *Supply Manager* (*SM*) to establish the amount of power that can be generated by the wind generation (*EGS*), photovoltaic generation (*PGS*) and cell fuel generation systems (*CGS*).

Methodology

Figure 1 presents a scheme of the proposed management model.

Dynamic Manager

This module shows the recommendations according to the selected management criterion. The *DM* has the possibility of establishing recommendations according to management criterion that fit better to the environment conditions. Energy audit is the basis to estimate power consumption savings. The systematic execution of the audit with the user's role provides an opportunity to identify those appliances that present inefficient operation.

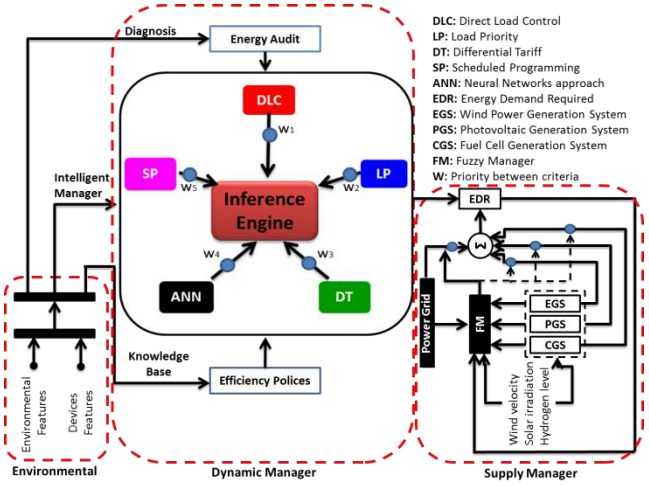

Figure 1. Management Model for Energy Efficiency.

As noticed in Figure 1, the dynamic manager has five management criteria: Direct Load Control (*DLC*), Load Priority (*LP*), Scheduled Programming (*SP*), Differential Tariff (*DT*) and Artificial Neural Networks approach (*ANN*). The main objective of the dynamic manager is to propose functional states or a power consumption curve that provides proper operation of the appliance according to the needs of comfort and consumption of electricity (power savings). To achieve this goal, a fuzzy inference engine was implemented for the case of computers, luminaries and televisions. For the air conditioner case, genetic algorithms were used to minimize the proportionality constant (K_U) that indicates the cooling or heating quantity. In computers, lights and televisions the membership functions were designed according to the efficiency guidelines showed in (Gracia, Delgado, Usón, Bribián, & Scarpellini, 2006); for the air conditioner, genetic algorithms were required because it is important to minimize the cooling level without impacting the comfort of the customer. However, due to the appliance operation constraints (e.g., available functional states) it is necessary to select those states that have greater similarity with the proposed *DM*. The states proposed by the *DM* depend on priority and preferences customer selection (individual, priority, comfort or consumption).

An efficient management of air conditioner must guarantee comfortable temperature with less power consumption. The opportunities of savings are related to isolation of the environment and efficiency of the appliance in operation and technology. In this case, only considerations related to operation are used for the design of dynamic manager. The proposed approach seeks modeling the temperature profile in building during 24 hours in function of external temperature ($M(t)$), heat generated within the building ($H(t)$), e.g., luminaries, people and machines and heater or air conditioner ($U(t)$), in order to

establish suitable cooling level (K_U) that allows maintaining stable the indoor temperature within the comfort requirements. Equations (1) to (9) are used in the proposed approach (Nagle, Saff, & Snider, 2005).

$$\frac{dT(t)}{dt} = K[M(t) - T(t)] + H(t) + K_U[T_D - T(t)] \quad (1)$$

$$U(t) = K_U[T_D - T(t)] \quad (1)$$

$$Tp(t) = B_2 - B_1F_1(t) + Ce^{(-K_1t)} \quad (2)$$

$$F_1(t) = \frac{\cos(wt)+\left(\frac{w}{K_1}\right)\text{sen}(wt)}{1+\left(\frac{w}{K_1}\right)^2} \quad (3)$$

$$w := \frac{2\pi}{24} \quad (4)$$

$$K_1 := K + K_U \quad (5)$$

$$B_1 := \frac{BK}{K_1} \quad (6)$$

$$B_2 = \frac{K_UT_D+KM_0+H_0}{K_1} \quad (8)$$

$$C = T_0 - B_2 + B_1F_1(0) \quad (7)$$

Where,

$M(t)$: Outdoor temperature

$H(t)$: Cooling (heater) rate

$T(t)$: Indoor temperature

K_U: Cooling level

w: Angular frequency of variation.

$\frac{1}{K_1}$: Constant of time with heating and air conditioner.

B_2: Mean temperature in building (daily) without considering the exponential term.

$B_1F_1(t)$: Sinusoidal variation of temperature in building corresponding of outdoor temperature variation.

K: Positive constant, that depends on physical properties of building as amount of doors and windows and type of isolation. For a typical heating and air conditioning, K_U is a little less than 2; for a common building, the constant K is between ½ and ¼ (Nagle et al., 2005).

Equation (3) is the solution of differential equation (1). Function (1) describes the relation between $T(t)$ and K_U. The main idea is optimizing function (10) according to constraints presented in (11 – 13). Function (10) allows evaluating the cooling point required to maintain the indoor temperature within the comfort zone, while function (11) is useful to measure the level of comfort.

$$P_{AC} = f(K_U) \quad (10)$$

$$22ºC \leq T(t) \leq 26ºC \quad (11)$$

$$1.4 \leq K_U \leq 1.48 \quad (12)$$

$$0 \leq P_{AC} \leq P_{ACmax} \quad (13)$$

Furthermore, the proposal seeks to avoid an excessive number of on/off operations on the air conditioning appliance; hence optimization technique is implemented in order to established optimal points of cooling level (K_U) according to temperature deviation of comfort zone. A proportional control is integrated to the thermal model presented in (Nagle et al., 2005) to perform progressive adjustment to the cooling level and thus prevent the appliance from always operating at cooling peaks.

The integration of fuzzy inference engine (for the case of PC, TV and luminaries) and genetic algorithm (for the case of air conditioner) provide operation curves adjusted to the energy efficiency policies. However, the selection of each management criterion depends on customer preferences, e.g., priority list, consumption-based or comfort-based. Hence, the main idea is that *DM* selects the suitable management criterion at each instant time according to these preferences.

Load Priority (LP) (Ravibabu et al., 2009): For this case of study, the air conditioning system was considered as vital[3]. Figure 2 shows an example of application of the load priority criterion for a case study. The results show a reduction in consumption during peak demand.

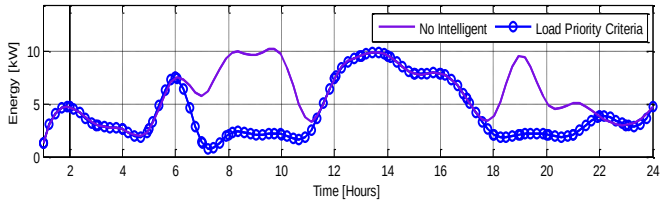

Figure 2. Load priority criteria results

Direct Load Control (DLC) (Goel et al., 2010): The main objective of this proposal is to determine the disconnection time required for saving energy without affecting comfort levels. A detailed analysis of each membership functions is carried out in (Salehfar, 1999).

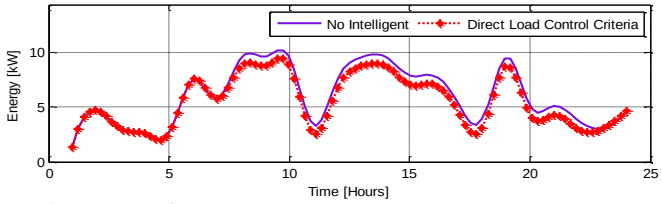

Figure 3. Direct Load Control results

Figure 3 shows an example of application of direct load control criterion for a case study. The results show a reduction in consumption of electricity due to the direct management of the air conditioner.

Differential Tariff (DT): The implementation of this approach were showed in (Christian G. Quintero M.;Jamer R. Jimenez Mares, 2012).

In Figure 4 the power consumption is shown before and after the implementation of the fuzzy system based on the differential tariff criterion.

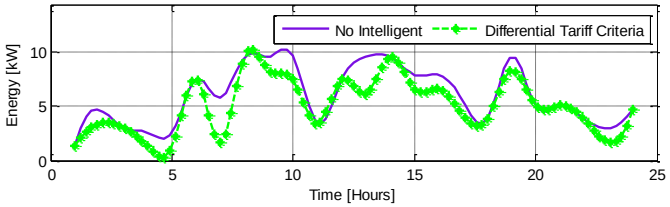

Figure 4. Differential tariff results

Scheduled Programing (SP): This criterion seeks to achieve energy savings based scheduling on and off device at certain instants of the day.

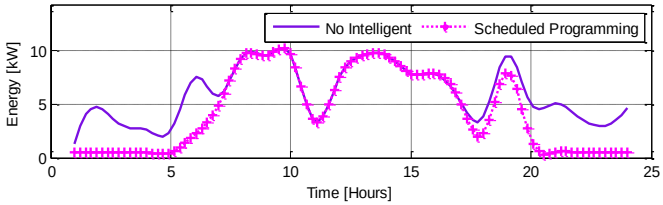

Figure 5. Scheduled programming results

The inputs used for this criterion were presented in (Christian G. Quintero M.;Jamer R. Jimenez Mares, 2012). Figure 5 shows an example of application of scheduled programming in a case of study.

Neural Networks (ANN): The implementation of this approach

[3] They are those appliances selected as relevant by customer.

were showed in (Christian G. Quintero M.;Jamer R. Jimenez Mares, 2012). The proposed architecture has an ANN for each device, given that it can handle independently the loads. The representation of possible situations for each device to control was carried out. For example, PC unoccupied, the system will compare the PC use profile with presence level to determinate if it is necessary carry out any task or not. The obtained data was used to train the neural networks, to obtain a good performance with feed-forward back-propagation network architecture. One hidden layer and sigmoid tangential transfer function were implemented for four ANNs. In this paper, the selection and determination of the number of layers and neurons was adjusted using an iterative algorithm.

Figure 6 shows an example of application of the proposed approach based on neural networks for a case of study. In this case computers, televisions, air conditioner and luminaries have been selected as devices to manage.

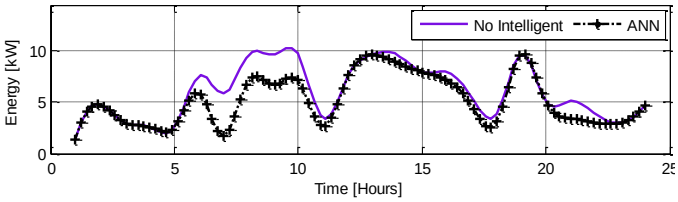

Figure 6. Results of implementation using neural networks

DM based on priority (PMF): It is a non-intelligent approach that seeks to select each criterion according to the priority (w_i) established by the user. However, a threshold was applied in order to consider a possibility of switch to other criterion (immediately lower priority) when the criterion with higher priority does not exceed the threshold set by the user saving.

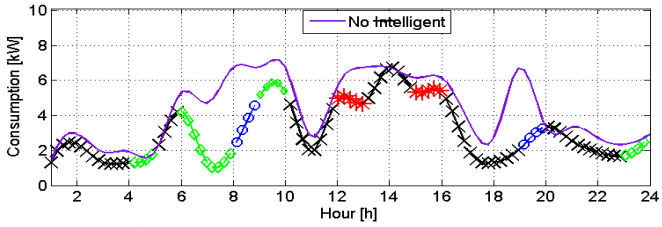

Figure 7. Results of DM based on priority list

Figure 7 shows a case of study where demand management criterion of electric energy using neural networks was selected as the first in priority list followed by differential tariff, load priority, direct load control and scheduled programming, respectively. The criterion colors/markers correspond to the showed in Figure I.

DM based on consumption (DMC): It is an intelligent approach that allows selecting the criterion with greater similarity to the power consumption proposed by dynamic manager. The design of the inference engine of the dynamic manager was performed using genetic algorithms (air conditioner) and fuzzy logic (luminaries, television and computer).

- *Air conditioner:* The genetic algorithm implemented in air conditioner case establishes the cooling factor required to maintain the temperature within the comfort zone. In this proposal the thermal model showed in the methodology was used to evaluate the thermal effect in the environment. The cooling factor was adjusted by genetic algorithm in each instant of time according to variables presented in the methodology. The cooling factor selected by *DM* sets the indoor temperature in comfort zone.
- *Computer:* In this case a fuzzy inference engine was used to present recommendations about efficient operation of computer. The proposed design has four inputs and one output, this considered scheduled activity as new variable.
  - *Inputs*: scheduled activity, presence, PC use profile, time to evaluate the workload.
  - *Output*: *proposed states*.
- *Luminaries*: The efficient operation of luminaries is associated to some variables presented in (Energía, 2011). Likewise, a fuzzy inference engine was used in the computer case.
  - *Inputs*: *type of activity*, *presence* and *illuminance level*.
  - *Output*: *illuminance level required*.

The efficient operation of television is evaluated only considering the presence level within the environment.

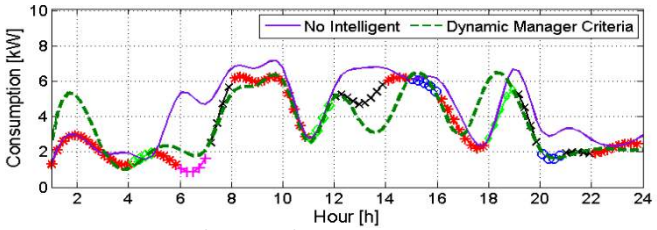

Figure 8. Results of *DM* based on consumption

Figure 8 shows three charts corresponding to power consumption before (solid/purple line) and after (color/marker according to the selected criterion) of application of proposal and, power consumption curve proposed by dynamic manager (red/dotted line).

DM Based on Comfort (DMCF): It is an intelligent approach that allows selecting the criterion with greater similarity to the functional states proposed by dynamic manager. The other characteristics are similar to the presented in the design of *DM* based on consumption.

Figure 9 shows the proposed curve by *DM* based on comfort. In this case, the criterion based on *ANN* were selected more than the others criteria due to consider the environmental characteristics.

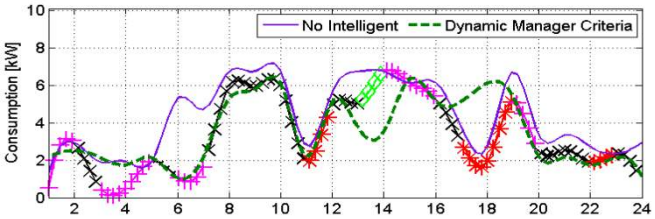

Figure 9. Results of *DM* based on comfort

Supply Manager

This block provides the proper weighting of the energy available in each of the systems of power generation (wind, photovoltaic and fuel cells) (N.C. Batista, R. Melício, J.C.O. Matias, 2013; Z. Guo, W. Zhao, H. Lu, 2012). The energy requirement depends on the input variables related to weather conditions, electricity demand and management criterion selected. The selection of alternative energy sources to be used in integration to an intelligent management system is considered from the development, cost and future of this technology. According to this, it was opted for the selection of power generation from wind speed (wind), solar radiation (photovoltaic) (Romero, 2010) and level of hydrogen (fuel cell) (Colclaser, 1999; Hashem, 2009). The mathematical models were analyzed in (Christian G. Quintero M.;, Ledesma.;, & Mares., 2013).

The inference engine (*SM*) works according to rules "if then" based on expert knowledge gathered from the operation of the proposed generation systems. With the implementation of these rules, the goals are: 1) To fulfill with EDR recommendations, 2) To determine the power required for each subsystem of the alternative power plant based on management scenario selected

and, 3) To allow the power grid supply only in cases where the hybrid alternative energy system cannot meet the *EDR*.

Design of Fuzzy Controller

The implementation of this approach were presented in (Christian G. Quintero M.;Jamer R. Jimenez Mares, 2012).

Experimental Results

In order to reach independence in the experiments, different profiles has been set for power consumption obtained from the functional states of the appliance, which ones have been randomly generated for each experiment. Furthermore, to evaluate the degree of uniformity in the performance of each one of the criteria, an analysis was performed by varying the type of appliance to be managed. Finally, a comparison of distribution of consumption for each one of the management criteria of electric energy demand used in this work was performed.

All appliances that turn off during 10 hours were scheduled. *Load priority* (*LP*) is performed with a fuzzy controller that controls PC, TVs and luminaries without affecting the air conditioning performance. The *LP* management is reached during peak hour. *DLC* is set to control only the air conditioning.

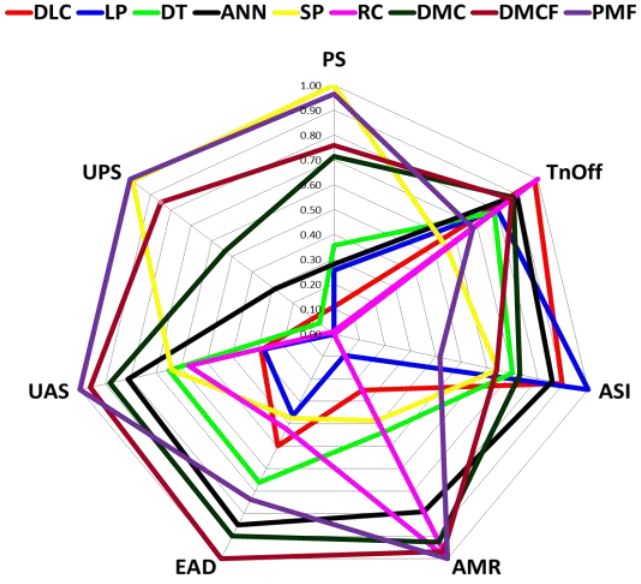

Figure 10. Radar chart to evaluate the management criteria of energy electric demand with the response variables.

The energy supply system of this customer consists of distribution power grid, wind generation system (capacity of 1109 kW), photovoltaic generation system (capacity of 1100 kW) and fuel cells energy (capacity of 940 kW). The test is performed for a typical summer season, a day at the beginning of week (Mallo, 2000), meteorological as wind velocity data and daily solar irradiation from (Craddock, 2008).

Response variable:

Power consumption savings (PS), Time no off (TnOff), Appliance states invariability (ASI), Appliance management regularity (AMR), Environment adaptability (EAD), User adjusted suitability (UAS) and Uniformity (UPS).

Demand Management Evaluation

Figure 10 shows the performance of each one criterion considerate in this proposal. This chart allows easy identification and assessment of each criterion according to the scopes and constraints presented.

The energy audit process is a good complement for the selection of each criterion because it allows reaching power savings near to 33%. In this case was modified the model and characteristics of the appliances to evaluate the response of audit process in terms of power consumption.

Evaluation and Verification SM Operation

In the TableV are shown the studies cases used to evaluate the performance of fuzzy manager for alternatives energy sources.

TABLE V. Studies Cases for the SM

CS	Date	Criteria	WS [km/h]	OT [°C]	FL [%]	WC
Case 1	April 1st, 2014 5:00	Profitability	14.8	25	30	Clear
Case 2	April 1st, 2014 9:00	Reliability	5.6	27	100	Clear
Case 3	April 1st, 2014 9:00	Priority	5.6	27	100	Clear
Case 4	April 1st, 2014 24:00	Percentage	31.5	26	5	Night Clear

CS: Case of study, WS: Wind Speed, OT: Outdoor Temperature, FL: Fuel Level, WC: Weather Conditions

The results of the evaluation of *SM* in the three management scenarios available (cost, reliability and priority of the *EE*, *PE* and *FC*) are carried out. The comparison is performed in a single case and one hour (5, 9, 9 and 24 hours, respectively), under the same environmental conditions, resulting in a level of satisfaction of the identical *EDR*. Table VI presents the satisfaction percentages of active sources according to the conditions hourly weather variables showed in case of study 1.

TABLE VI. Results of Studies Cases for the SM

	Case of study 1		Case of study 2		Case of study 3		Case of study 4	
	% SS	% S	% SS	% S	% SS	% S	% SS	% S
Wind	59.0	59.0	17.3	0.0	17.3	17.3	100.0	50.0
Photovoltaic	26.2	26.2	100.0	100.0	100.0	82.7	28.0	28.0
Fuel Cell	4.6	4.6	100.0	0.0	100.0	0.0	0.8	0.8
Power Grid	100.0	10.2	100.0	0.0	100.0	0.0	100.0	21.2

SS: Satisfaction and S: Supply

This scenario seeks to fulfill with the demand using the most economic subsystem. Currently wind power generation systems are between cost efficiency and more cost effective than *PV* and these than the fuel cell. During profitability management the *EE* is taken as first choice.

In scenario showed in Table VI the manager provides priority to the subsystem that is generating the most power for a specific *EDR*. In this case the *PE* is taken as first choice.

Table VI shows as the power order of each subsystem is indicated by the operator under his own criteria. While in the scenario showed in Table VI, the maximum percentages of operation of each subsystem are assigned by the user. The subsystems set of the plant can supply from 0 to 100% of the power required by the *EDR*.

Conclusions

The results and analysis carried out during this proposal has allowed highlighting the characteristics of each criterion taking into account the response variables discussed in the section of experimental results. However, the main goal in this proposal is reaching power consumption savings without impacting customer´s comfort; hence it's necessary considering the performance of all proposed approach. According to the concept of energy efficiency, this proposal is suitable because

allows to reach power saving levels without impacting the comfort of user (e.g., temperature and illuminance).

DM based on priority allows to reach power saving and uniformity level similar to the scheduled program but improving some characteristics as environment adaptability, appliance management regularity, user adjusted suitability and Non off time. *DM* based on consumption presents a suitable behavior in comparison to others criteria proposed by state of art; however, in comparison to the other two proposals (*DM* based on comfort and *DM* based on priority), presents a performance that is less in uniformity, suitability and power saving. *DM* based on comfort provides opportunities of power savings even without the necessity of shut off completely the appliance in a long period of time. Furthermore, some characteristics relevant for the management as environment adaptability, user adjusted suitability and uniformity to diversity appliance are suitable in comparison to other criteria.

Energy sources management scenarios on profitability and reliability show similar results when the goal is guarantee that the most cost effective is also the most reliable. In the reliability case *CGS* was more suitable than *EGS* and *PGS*, while in profitability case the *EGS* was more selected by fuzzy manager due to the low cost of this energy type.

References

A. Di Giorgio, L. P. (2012). An event driven smart home controller enabling consumer economic saving and automated demand side management. *Applied Energy*, 92–103.

Christian G. Quintero M.;, Ledesma.;, J., & Mares., J. R. J. (2013). Intelligent Management of Alternative Energy Sources Based on Fuzzy Logic. *Renewable Energy & Power Quality Journal (RE&PQJ)*, (11).

Christian G. Quintero M.;Jamer R. Jimenez Mares. (2012). Towards an Intelligent Management Approach for Power Consumption in Buildings Case Study. In *Informatica (CLEI), 2012 XXXVIII Conferencia Latinoamericana* (pp. 1–10). IEEE. http://doi.org/10.1109/CLEI.2012.6427182

Colclaser, D. J. H. and R. G. (1999). Transient modeling and simulation of tubular solid oxide fuel cells. In *Energy Conversion, IEEE transactions on* (pp. 749–753).

Craddock, D. (2008). *Renewable energy made easy: free energy from solar, wind, hydropower, and other alternative energy sources*. *Atlantic publishing*. Atlantic Publishing Company.

D. Zhang, N. Shah, L. G. P. (2013). Efficient energy consumption and oper-ation management in a smart building with microgrid. *Energy Conversion and Management*, 209–222.

EIA, U. S. E. I. A.-. (2014). International Energy Statistics. Retrieved from http://www.eia.gov/

Energía, M. de M. y. Reglamento Técnico de Iluminación y Alumbrado Público (2011). Retrieved from http://www.minminas.gov.co/minminas/downloads/UserFiles/File/ENERGIA/RETILAP/Resolucion180540ConAnexoGeneral.pdf

Frank, K., & Goswami, Y. (2007). *Energy Efficiency and Renewable Energy*. (F. and T. Group, Ed.). Francis and Taylor Group.

Goel, L., Wu, Q., & Wang, P. (2010). Fuzzy logic-based direct load control of air conditioning loads considering nodal reliability characteristics in restructured power systems. *Electric Power Systems Research*, *80*(1), 98–107. http://doi.org/10.1016/j.epsr.2009.08.009

Gomes, J., Coelho, D., & Valdez, M. (2011). Energy Audit in a School Building Technology , Professional and Artistic School of. In *In Energetics (IYCE), Proceedings of the 2011 3rd International Youth Conference on . IEEE* (pp. 1–6). Retrieved from http://ieeexplore.ieee.org/stamp/stamp.jsp?tp=&arnumber=6028314&isnumber=6028112

Gracia, A. M., Delgado, A. V., Usón, A. A., Bribián, I. Z., & Scarpellini, S. (2006). *Disminución de Costes Energéticos en la Empresa*. (F. Editorial, Ed.).

Guan, X., Xu, Z., & Jia, Q.-S. (2010). Energy-Efficient Buildings Facilitated by Microgrid. *IEEE Transactions on Smart Grid*, *1*(3), 243–252. http://doi.org/10.1109/TSG. 2010.2083705

Hashem, M. (2009). Modeling and control of fuel cells: distributed generation applications. *IEEE Press. Canada*.

Huang, Y. J. (2006). The impact of climate change on the energy use of the US residential and commercial building sector. *Lawrence Berkeley National Laboratory*, *Report No.*

Lior, N. (2010). Sustainable energy development: the present (2009) situation and possible paths to the future. *Energy*, 3976–3994.

M. Sechilariu, B. Wang, F. L. (2013). Building-integrated microgrid: advanced local energy management for forthcoming smart power grid communication. *Energy and Buildings*, 236–243.

Mallo, C. (2000). Predicción de la demanda eléctrica horaria mediante redes neuronales artificiales. *Departamento de Economía Cuantitativa, Universidad de Oviedo, España.*

Matallanas, E., Castillo-Cagigal, M., Gutiérrez, a., Monasterio-Huelin, F., Caamaño-Martín, E., Masa, D., & Jiménez-Leube, J. (2012). Neural network controller for Active Demand-Side Management with PV energy in the residential sector. *Applied Energy*, *91*(1), 90–97. http://doi.org/10.1016/j.apenergy.2011.09.004

N. Gudi, L. Wang, V. D. (2012). A demand side management based sim-ulation platform incorporating heuristic optimization for management of household appliances. *International Journal of Electrical Power & Energy Sys-Tems*, 185–193.

N.C. Batista, R. Melício, J.C.O. Matias, J. P. S. C. (2013). Catalão, Photovoltaic and wind energy systems monitoring and building/home energy management using Zig-Bee devices within a smart grid. *Energy*, 306–315.

Nagle, R. K., Saff, E. B., & Snider, A. D. (2005). *Ecuaciones diferenciales y problemas con valores en la frontera*. Pearson Eduación.

Ravibabu, P., Praveen, A., Ch, V. C., P, R. R., & M, K. R. T. (2009). An approach of DSM Techniques for Domestic Load Management using Fuzzy Logic, 1303–1307. http://doi.org/10.1109/FUZZY.2009.5277401

Romero, M. (2010). Energía Solar Fotovoltaica. *Editorial CEAC*.

S. Kahrobaee, R.A. Rajabzadeh, S. Leen-Kiat, S. A. (2013). A multiagent mod-eling and investigation of smart homes with power generation, storage, and trading features. *IEEE Transactions on Smart Grid*, 659–668.

Salehfar, H. (1999). Fuzzy Logic-Based Direct Load Control of Residential Electric Water Heaters and Air Conditioners Recognizing Customer Preferences In a Deregulated Environment, 1055–1060.

Tascikaraoglu, A., Boynuegri, A. R., & Uzunoglu, M. (2014). A demand side management strategy based on forecasting of residential renewable sources: A smart home system in Turkey. *Energy and Buildings*, *80*, 309–320. http://doi.org/10.1016/j.enbuild.2014.05.042

Wang, X., & Huang, C. (2009). Energy Audit of Building : A Case Study of A Commercial Building in Shanghai, (50478113), 2005–2008.

Z. Guo, W. Zhao, H. Lu, J. W. (2012). Multi-step forecasting for wind speed using a modified EMD-based artificial neural network model. *Renewable Energy*, 241–249.

Impact of the integration of electric vehicles in low voltage residential electrical networks

Impacto de la integración de los vehículos eléctricos en las redes eléctricas de baja tensión residencial

Dubán Pedraza[1], Javier Niño[2], Manuel Ortiz[3], Gabriel Ordóñez[4], Javier Solano[5]

ABSTRACT

This paper assess the impact of the inclusion of electric vehicles on existing residential networks in Santander, a region in Colombia. The study is based on consumer profiles supplied by the network operator. It takes in account the national electrical code and charging profiles of commercial electric vehicles. The paper aims to determine whether an electrical vehicle can be plugged in the existing electrical low voltage network.

Keywords: Residential electrical networks, charging infrastructure, electric vehicles.

RESUMEN

En este trabajo se evalúa el impacto de la inclusión de los vehículos eléctricos en las redes residenciales existentes en Santander, una región en Colombia. El estudio se basa en perfiles de consumidores suministrados por el operador de red y toma en cuenta las especificaciones y normas que regulan el diseño y construcción de redes eléctricas residenciales, así como los perfiles de carga de vehículos eléctricos comerciales. El trabajo tiene como objetivo determinar si un vehículo eléctrico puede ser conectado en la red de baja tensión eléctrica existente.

Palabras clave: Redes eléctricas residenciales, infraestructura de carga, vehículos eléctricos.

Introduction

Residential low voltage electric networks in Colombia design respects technical specifications determined by a national electrical code [2]. Plugging electrical vehicles (EV) in these networks increases not only the power delivered but also the power losses and voltage drops [1-5].

This paper focuses on determine the impact of plugging EV on the existing electrical infrastructure for residential users in Santander, a region of Colombia. The national electrical code specifies the minimum wire sections for the feeders, then it indirectly specifies the minimal nominal power for residential units. The national code specifies for each socioeconomic strata the section of the conductors and the quantity of circuits are determined by the constructed area.

This work aims to determine whether is possible to connect an EV as extra electrical load to the existing infrastructure in residential centers. It is based on the information provided by the network operator, the national electrical code for residential networks and the charging profiles for EV commercially available in the market.

As the EV becomes a reality, not only on developed countries, this research aims to be a contribution to the implementation of policies that determine technical specifications to design new low voltage residential networks where EV can be safely connected in Santander.

There are different scenarios for the study of integration of electric vehicles in low voltage residential electrical networks. The first considers single-family residence units (houses) and the second considers multi-family residence units (buildings). In the former the feeder, the metering point and the EV charger are relatively close; in the latter the metering is close to the point of recharge, but far from the feeder. This paper focuses on the first scenario.

CHARGE OF EV IN A LOW VOLTAGE RESIDENTIAL ELECTRICAL NETWORK.

Safely charging EVs using the existing electrical infrastructure depends on the residential unit load profile, on the wire section and also on the type of charger used in the vehicle.

Stratification in Colombia.

Socioeconomic stratification in Colombia is a geographical classification of residential areas based on the average income of the residents in the sector. This allows differentially charging public services: the high strata pay more and the lower strata pay less. As the energy consumption increases with the household income,

[1] D. Pedraza, Electronic Engineer from the Universidad Industrial de Santander, Colombia. E-mail: duban.pedraza@correo.uis.edu.co

[2] J. Niño, Electronic Engineer from the Universidad Industrial de Santander, Colombia. E-mail: javieert20@hotmail.com

[3] M. Ortiz is a Professor at the Universidad Industrial de Santander, Bucaramanga, Colombia. E-mail: majortiz@gmail.com

[4] G. Ordóñez is a Professor at the Universidad Industrial de Santander, Bucaramanga, Colombia. E-mail: gaby@uis.edu.co

[5] J. Solano is a Professor at the Universidad Industrial de Santander, Bucaramanga, Colombia. E-mail: jesolano@uis.edu.co

stratification is used to determine technical specifications to design residential electrical networks. For this reason, electrical networks in high strata are designed with higher nominal power than networks in low strata.

Average consumption profiles.

Figures 1 and 2 show profiles of consumption determined by the regional network operator in Santander. Depending on the socio-economic strata, the average consumption in Santander is 4.04, 3.67, 5.13, 5.99, 6.94 and 7.88 kW/day, respectively for strata 1 to 6.

Low-voltage residential electrical networks.

Residential electrical circuits for residential units in Colombia can be 120V single-phase, 208V bi-phase or 208V three-phase. The minimum gauge cable in all topologies is the AWG #8. Depending on the topology the minimum rated powers in residential units are 4.56, 7.9 and 13, 69 kW.

EV chargers.

This work scope to study existing residential low voltage networks. Taking account of the rated powers on the national electrical code, it can be concluded that semi-fast and fast chargers cannot be considered, at least with the current normativity. The inclusion of these chargers would require updating the national electrical code for low voltage networks. As only slow chargers could be connected to existing residential networks, in order to simplify the study, only the peak power of the EV chargers is considered.

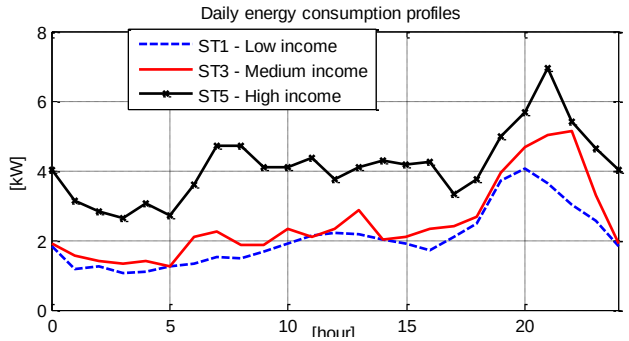

Figure 1. Consumption profiles in residential areas strata 1, 3 and 5.

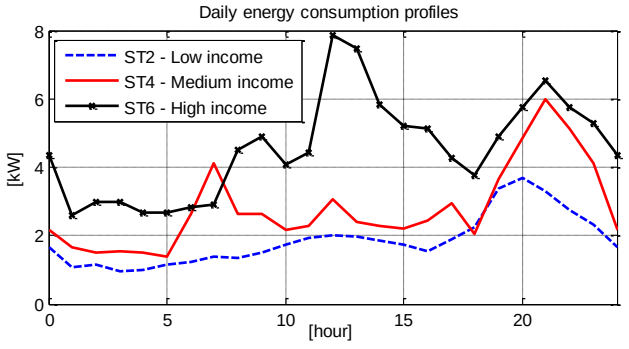

Figure 2. Consumption profiles in residential areas strata 2, 4 and 6.

Simulation results.

Simulations are presented for the lower and the higher strata as representative for this study. Two different scenarios are considered. In the worst case scenario the EV is charged simultaneously with the peak consumption. This is a likely scenario considering that network operators in Colombia do not applies differential charges in peak hours. A second scenario considers the hypothetical inclusion of differential electricity charges and the charge of the EV is performed in valley hours. This is the ideal scenario to the user because the lower cost of the energy and for the operator which can have flatters demand curves. For simulation the 3.3kW Nissan Leaf charger is considered.

Figures 3 and 4 present simulation results for the lower (ST1) and the higher (ST6) strata respectively. Two different cases are considered: single phase and bi-phase circuits. Simulations results show that in low strata residential units with single-phase circuits the considered EV cannot be charged using the existent electrical infrastructure, nevertheless, in bi-phase and then in three phase circuits it is possible to safely charge EVs at least using slow chargers. This is mainly due the relatively low power consumptions profiles compared with the minimum rated powers in the national electrical code.

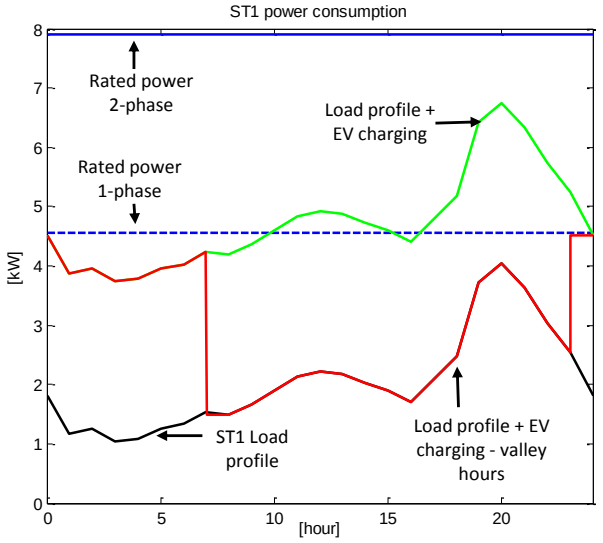

Figure 3. Power profile - Charge of EV in ST1.

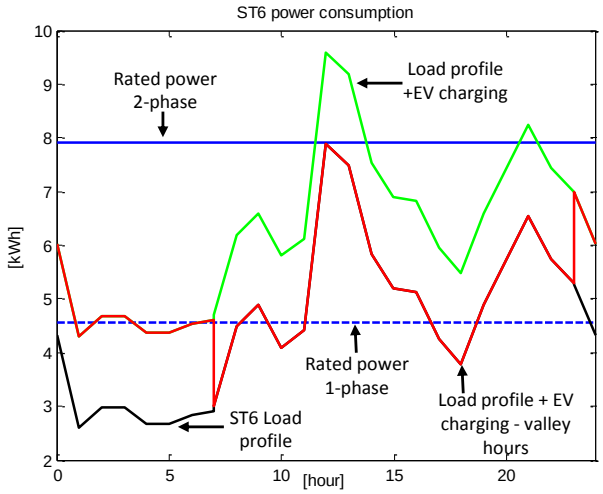

Figure 3. Power profile - Charge of EV in ST1.

Simulation results shows that in higher income strata neither in single-phase nor in bi phase circuits EV can be safely charged. Nevertheless, in three phase circuits with a rated power of 13.69kW the considered EV charger can be plugged to the existent electrical infrastructure

Conclusions and outlooks.

During the next years it is not expected to have EV connected to the grid in low income residential sectors; however it seems that existing EV can be connected in bi phase and three phase circuits in residential networks in single-family resident units. On the other hand, in high income residential sectors where the penetration of EV is expected to be fast increasing, it could be more complicated to connect EV due to the fact that the power consumption is high and the networks are then operating close to the nominal power. Only in three phase circuits EVs could be safely charged.

According to the results obtained on this research, it seems that with the existent normativity, electrical vehicles cannot be connected to the low voltage networks in Santander, Colombia.

For this reason it could be necessary to either update the national electrical code to consider deploying new electrical infrastructure to enable charging EV in safety.

References

[1] Clement-Nyns, K., Haesen, E., Driesen, J. The impact of charging plug-in hybrid electric vehicles on a residential distribution grid. Power Systems, IEEE Transactions on, 25(1), 2010 371-380.

[2] Departamento Nacional de Planeación. Unidad de Planeación Minero Energética. Reglamento técnico de instalaciones eléctricas RETIE. (2006).

[3] Lopes, João A. Peças, Soares, Filipe Joel, et Almeida, Pedro Miguel Rocha. Integration of electric vehicles in the electric power system. Proceedings of the IEEE, 2011, vol. 99, no 1, p. 168-183.

[4] Peas Lopes, J. A., Soares, F. J., & Almeida, P. R. Identifying management procedures to deal with connection of electric vehicles in the grid. In Powertech, 2009 IEEE bucharest (pp. 1-8). IEEE.

[5] Pieltain Fernández, L., Roman, T. G. S., Cossent, R., Domingo, C. M., Frias, P. (2011). Assessment of the impact of plug-in electric vehicles on distribution networks. Power Systems, IEEE Transactions on, 26(1), 206-213.

Retraining Air Lines 220kV Transmission in the Paraguayan Power System using High Temperature Conductors and Low Sag (HTLS) and their feasibility

Recapacitación de Líneas de Transmisión Aérea de 220kV en el Sistema Eléctrico Paraguayo, utilizando Conductores de Alta Temperatura y baja flecha (HTLS) y su factibilidad

Mitjans Felipe: engineer, Universidad Nacional de Asunción, Paraguay; Master of Science, Universidad Politécnica de Cataluña, España
Pulfer Jean-Claude: engineer, Swiss Federal Institute of Technology Lausanne, Switzerland; Master of Science, Swiss Federal Institute of Technology Zurich, Switzerland

ABSTRACT
In the present study was assessed the technical and economic feasibility to change in high voltage aerial transmission lines conventional ACSR conductors by High Temperature and Low Sag (HTLS) conductors of similar diameter and weight with the aim to increase the transmission capacity of these lines without the need to change the towers made of galvanized steel. It could be shown comparing the energy losses and the respective investment cost of 4 different types of HTLS conductors, that the GTACSR type conductors offer the highest economic advantage under the considered scenario.

Keywords: High Temperature and Low Sag conductor – ACSR - Grosbeak conductor – repowering.

RESUMEN
En el presente estudio se evaluó la viabilidad técnica y económica de la sustitución de conductores convencionales del tipo ACSR en líneas aéreas de transmisión en alta tensión por conductores de Alta Temperatura y Baja Flecha (HTLS) de similar diámetro y peso con el objetivo de incrementar la capacidad de transmisión de estas líneas, sin necesidad de cambiar las torres hechas de acero galvanizado. Se pudo demostrar mediante la comparación de las pérdidas eléctricas y el respectivo costo de inversión para 4 distintos tipos de conductores HTLS que los del tipo GTACSR ofrecen la mayor ventaja económica bajo el escenario considerado.

Palabras clave: conductor de alta temperatura y baja flecha (HTLS) - ACSR - conductor Grosbeak - recapacitación

Received: June 16th 2015
Accepted: Oct 15th 2015

Introduction

We are observing globally climatic changes due to the excess of greenhouse gas emissions (mainly CO_2) and the lack of commitment of most of the industrialized countries to reduce their emissions according to the goals of the Kyoto Protocol. Only the implementation of new energy alternatives like the renewable energies and the implementation of energy efficiency measures on a huge scale would help to reduce these greenhouse gas emissions. Countries like China, Japan and the USA, as well as most of the European countries are incentivizing through subsidies, feed-in tariffs and other economic mechanisms the development of renewable energies, like solar, wind and biomass energy. In South America mainly Brazil, followed by Argentina and Uruguay are committed with the development of renewable energy technologies (Mitjans, 2013).

One of the main goals of this study is to present a better alternative to the construction of thermal power plants near the centers of electricity demand to balance the capacity lack of the 220 kV transmission lines coming from the existing hydraulic power plants by analyzing different technical alternatives to increase their transmission capacity. Such a thermal power plant exists actually for example in Salto del Guairá, located at the northern end of the Itaipú lake. These alternatives shouldn't involve the change of the existing isolators, neither the variation of the mechanical loads received by the towers using conductors with a similar diameter and weight as the existing conductors, which have to support actually during most of the time higher loads than their nominal capacity of the lines until the new 500 kV transmission line Itaipú-Villa Hayes will be fully charged (ANDE, 2013).

In the present article is considered a current of 800 Amps to make a technical and economic comparison between four different High Temperature and Low Sag (HTLS) conductor technologies considering that none of them are reaching the knee point.

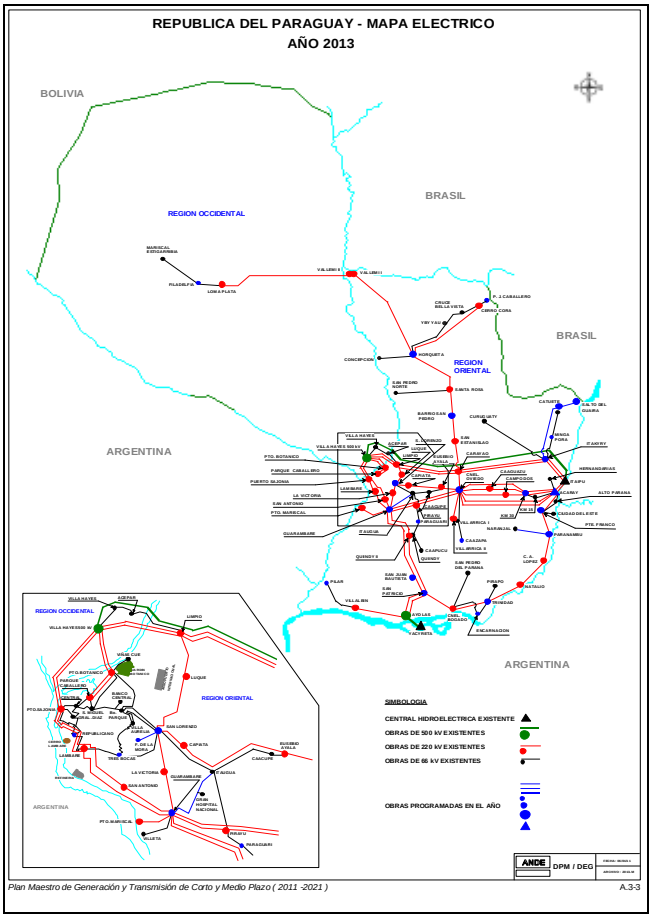

Fig. 1: Master Plan of the Paraguayan Electric System (2013 – 2023). Source: ANDE, 2013

Besides, the value of the ohmic resistance has a quasi-lineal behavior, what allows assessing their thermal and mechanic performance for the required conditions (CEMIG, 2010).

For technical analysis one stage with each of the technologies existing wires in the international market and high temperature low sag (HTLS) using criteria of International Standards and Technical Specifications of the state company ANDE was raised. It was verified that the conditions of maximum mechanical stress are not overcome by changing driver conventional ACSR 636 MCM, "Grosbeak" Code by one of high temperature and Low Sag (HTLS), the same diameter and weight type without changing the required insulators in the existing transmission line. For this purpose a pilot overhead transmission line of 100 km in length, an ampacity in normal operation 550Amperios, but operating with a load of 800 Amperios in 220kV voltage level was considered.

The comparison of electrical losses between each of the technologies mentioned above line length was evaluated. Among the economic variables an interest rate of 10% anual over a period of 20 years, the cost of Itaipu Binacional rate of 22.60 US $ / kW-month and a load factor for the transmission line 50 is considered % (ANDE, 2013).

Actual situation of the Paraguayan electric system

Due to the recent commissioning of the 500 kV aerial transmission line Itaipú-Villa Hayes there is a need to increase the transmission capacity as well as in the Northern System Carayaó-Horqueta 1x220 kV, as in the Southern System with the commissioning of the autotransformers 2 x 375 MVA 500/220 kV at the Yacyretá bar, what generated the unfailing need to potentiate with HTLS conductors the aerial transmission line Ayolas-San Patricio 2 x 220 kV (see fig. 1).

This way could be accompanied the economic and social development of the Southern Region of Paraguay considering the installation of many industrial plants provoking practically a doubling of the actual energy consumption. Besides, it should be taken into account that the commissioning of the 500 kV line Itaipú-Villa Hayes, making possible the injection of an additional power of 2000 MW, provoking a reorientation of the power fluxes in the Paraguayan electric system, mainly in the Northern and Southern Systems, generating a new electric gravitation center. In case of an out of service of this 500 kV line the main 220 kV lines should be able to contain this power (ANDE, 2013).

The conventional AL 1350 conductors (Aluminum Conductor Steel Reinforced ACSR) are the conductors traditionally used in Paraguay for transmission lines of the 220 and 66 kV levels. Their maximum projected operation temperature is 90°C under the most adverse climatic conditions (40°C ambient temperature during daytime and 35°C during nighttime). When the conductor surpasses 100°C during more than 3000 accumulated hours, starts an annealing process in the filaments of the conductor and then the decay of its mechanic properties (NEXANS, 2010). The nonconventional conductors of the HTLS type allow to increase the transmission capacity up to 300% of the nominal power compared to conventional ACSR type conductors with the same weight, diameter and slag. This makes this technology a very attractive alternative in most of the cases without the need of adaptation of the supporting towers made of reticulated galvanized steel representing important savings in investment costs (CEMIG, 2010).

Conductors with HTLS technology

HTLS conductors with thermal resistant technology (T-ACSR)

This type of conductors has a similar thermal expansion coefficient as an ACSR type conductor, reason why the mechanic behavior of the T-ACSR type conductor is like a conventional conductor. For this reason it's a much cheaper than any HTLS conductor. But the T-ACSR cable has a much higher breaking strain than a normal ACSR 636 MCM cable. This can be verified through the polynomial data of this conductor corresponding to the values of a conductor with steel core. This means that the complete cable (core and crown) is submitted to a much higher tensile stress, in the way that it is possible to install a cable with a similar diameter as the ACSR 636 MCM Grosbeak code cable. Besides, it can be obtained a much smaller slag during load injection considering the most adverse climatic conditions (ANDE, 2010).

It is important to mention that the traction to which is submitted the conductor generates a geometrical deformation of the threads of the aluminum crown usually of the heat-resistant type. This in turn leads to a distortion of the electric field of the cable and to losses of active power, as well as facilitates the formation

of a hot spot or the crown effect. The temperature in this kind of cables oscillates between 80°C during normal operation conditions and 90°C during an emergency regime. This proves that the T-ACSR cable has practically a similar behavior as a conventional ACSR cable of the same size and the same code (ANDE, 2006).

The installation mode of this cable is similar to the conventional steel core cable tolerating splicing in the middle of the span, but it generates a lot of electric losses due to the steel core, which is a semiconductor, leading to a considerable heating of the conductor compared to other technologies with the same ampacity and environmental conditions. There is no need for special lockwashers during mounting.

HTLS conductors with composite core technology (ACCC and ACCR)

These conductors are of the compound core type (see fig. 2). It could be defined as a material obtained by agglutination of two or more elements exercising matrix and reinforcement functions. The matrix confers the structure of the compound aluminum while the reinforcing materials improve the mechanical, electromagnetic and chemical properties.

Within this category of conductors with compound core exist the ACCR (Aluminum Conductor Composite Reinforced) and the ACCC (Aluminum Conductor Composite Core) conductors. The core of the ACCR conductors is made of aluminum oxide (Al_2O_3) on an aluminum matrix, while in the ACCC conductors it is made of carbon fibers covered by an insulating layer of epoxy resin. A similar function exercises the zinc oxide recovering in the conductors with steel core preventing galvanic corrosion (ASTM N° B232).

Fig.2: ACSR and ACCC conductor, Source: CEMIG, 2010

The compound cores have a thermal expansion coefficient up to three times lower, what reduces considerably the slag of these conductors. The conducting layers of ACCR are composed of an aluminum zirconium alloy permitting continuous operation temperatures of up to 210°C. This kind of conductors has lower technical losses than the thermal resistant conductors, have a lower weight than conventional conductors with steel core ACSR, but need special lockwashers during their mounting. They tolerate splicing in the middle of the span. Also, the components of the core have different expansion coefficients, what could provoke internal cracks, what requires a special attention during mounting and commissioning (CEMIG, 2010). These cracks provoke losses of the crown effect. These conductors require special mounting equipment and the replacement of the existing ironworks and terminals, due to the fact that they are operating at only 90°C under extreme conditions (ANDE, 2009).

HTLS conductors with Gap Type technology (GTACSR)

The Gap Type ACSR conductors (GTACSR) have a layer of synthetic material between the steel core and the aluminum conducting crown, what reduces considerably the slag of these conductors (see fig. 3). This synthetic material in fact is a high temperature grease permitting an independent movement between the steel core and the thermal resistant crown, resulting in a thermal expansion coefficient almost two times lower than in a conventional ASCR conductor (CEMIG, 2010).

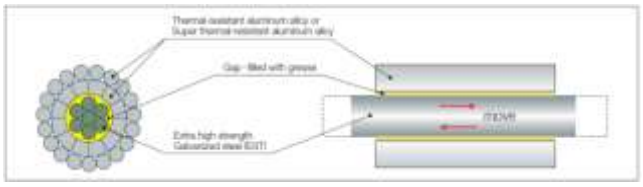

Fig. 3: GTASCR conductor. Source: CEMIG, 2010

This conductor supports a temperature of up to 240°C. Its installation is somehow difficult, because it doesn't allow splicing in the middle of the span. For this reason it has to be done at the towers converting the suspending towers into anchoring ones. So, those will have 3 anchoring chains with its corresponding insulators without mattering that those are of tempered glass or polymeric silicon rubber. Therefore, it's necessary to install small triangle shaped profiles in the brackets occasioning in the towers a surge of up to 20% of the Everyday Strench in the original line (CEMIG, 2010).

Another point to take into account is the need to study the load tree of the towers, independently if their foundation are of the self-supporting or the fettered type. In the second case this study has to be more detailed. To this has to be added a loss of around 30% of the conductor length due to the splicing at the suspending structures and not in the middle of the span. In fact, these losses differ for each transmission line repowering project with this kind of conductor, what makes necessary to do a detailed study concerning these losses with the aim to reduce them to the minimum.

As well it has to be considered, that in the points of splicing the conductor loses its diameter homogeneity causing a distortion of the electric field and as a consequence of this a huge crown effect and active power losses. For the elaboration of the laying and tightening table it has to be considered that it has to be done each span separately after having converted the suspending structures to anchoring structures and not as it is usually done by the PLS-CADD software. Besides, have to be changed the existing ironworks and terminals due to the fact that they are suited to a temperature of only 90°C under extreme conditions. This technology is actually installed and operating in the aerial transmission lines Coronel Oviedo-Guarambaré (2 x 220 kV) and Coronel Oviedo-San Lorenzo (1 x 220 kV). 1100 km of this kind of conductor have already been installed in the frame of the "Summer 2014 Program". With this conductor operating the transmission capacity reached 340 MVA in each one of these three circuits (ANDE, 2013; ANDE, 2010; ANDE, 2011).

Technical considerations on conductors with HTLS technology

As benchmark parameters for the comparison of the different HTLS type have been considered the diameter (similar or slightly smaller than the ACSR 636 MCM Grosbeak code cable) to pre-

vent the crown effect, and the specific weight of the conductor to make unnecessary the reinforcement of the towers and its foundations (see table 1).

Table 1: Comparison of different HTLS technologies (diameter, weight, resistance).

Technology	Diameter (mm)	Weight (kg/km)	Resistance* (Ohm/km)
ACSR 636M CM	25.16	1302	
GTACSR	24.4	1301	0.0943
ACCC	25.15	1245	0.0791
T-ACSR	25.16	1302	0.1154
ACCR	24.25	1227	0.1167

* 800 Amps, 25°C ambient temperature

It's important to stress, that for each one of the proposed conductors the tension for the final condition at creep (20% of the breaking tension of the conductor) and at maximum wind speed (40% of the breaking tension of the conductor) haven't been surpassed considering a maximum wind speed of 145 km/h. Besides, for all the proposed technologies the emergency condition at final condition (17% of the breaking tension of the conductor). The standard span used for the simulation and the corresponding economic study of the conductors is 400 m, which are common for 220 kV aerial transmission lines. Besides, for flat land the sag for any of the conductor types should not exceed 14 m for the maximum load and the most adverse climatic conditions (ANDE, 2006; FURNAS, 2008).

Table 2: Comparison of different HTLS technologies (temperature, traction, sag).

Technology	Conductor temperature (°C)	Traction EDS (%)	Traction maximum wind (%)	Sag (m)
GTACSR	87	20	39	14
ACCC	82	19	40	11
T-ACSR	97	20	38	13
ACCR	91	19	40	12

For the analysis realized with the above mentioned criteria has been considered the load tree of a reticulated type tower made of galvanized steel. The security distance between the cable and the ground for the most adverse climatic conditions (40°C) and the maximum load is 8 m. The span conditions for wind are not modified, but those for weight depending on the weight of the conductor and its breaking tension (NBR N°5422).

For the above established conditions and looking at the obtained results (see table 2) it can be observed, that none of the selected technologies can be rejected to substitute the ACSR 636 MCM Grosbeak code cable of the technical point of view, mainly concerning the sag and the geometric characteristics of the cable such as its diameter and its weight.

Computational results

As the computations were performed simulations with the Anaredes Software to compare the same size, weight and diameter between conventional wire and conductor HTLS type, (see table 3), the electrical behavior that would have a overhead transmission line (ANDE, 2013).

Table 3: Electrical parameter of the overhead Transmition Line.

Parameter Line			
	Resistance	Reactance	Capacitance
	Ohm/km	Ohm/km	Micro siemens/km
Old Wire ACSR 300MCM Code, Ostrich.	0,21418	0,39994	2,8546
New Wire HTLS ACCC 160MCM, Code Helsinki.	0,17937	0,40927	2,8107

As shown, although the line resistances to be slightly lower, the values of inductive reactance and capacitance are not affected, since the inductance and capacitance of the line are mainly determined by the geometrical arrangement of the conductors. With the change of wire, it would have a higher thermal capacity, but power transmission limitations caused by the high level of reactance are removed.

Assessment of the electric and magnetic fields in conductors with HTLS technology

According to the results obtained with the PLS-CADD software we can observe the behavior of the electric and the magnetic fields in a cross section of a 220 kV aerial transmission line applying each of the HTLS technologies (see fig. 4). The values are all within the admissible limits inside the security lane, which in our case has a width of 50 m (Ley N°976/82).

The maximum values of the electric and the magnetic fields reach on the axis of the line 0.7 kV/m and 6.5 μT respectively. These values are in line with the international standards. So, there are no reasons against the HTLS technologies to substitute the conventional conductors with the same weight and diameter considering a current of 800 Amps (Díaz, 2008).

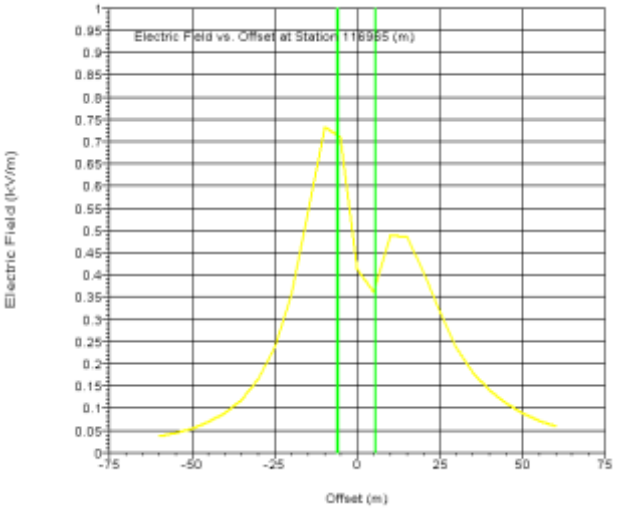

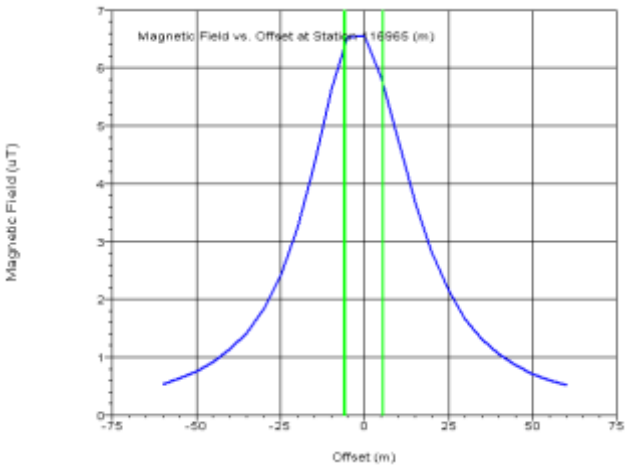

Fig. 4: Results of the electric and magnetic field on the width of the servitude strip of a 220kV transmission line with HTLS technology conductors

Economic considerations on conductors with HTLS technology

For the economic considerations have been taken into account the reference costs of the respective conductors, energy losses for a 220 kV simple circuit (R,S,T) transmission line with a length of 100 km, a load of 800 Amps and the reference cost for the mounting of the conductors. Within the economic variables have been considered an annual interest rate of 10% for a period of 20 years, the electricity fee at Itaipu with 22.6 US$/kW-month, a load factor of the transmission line of 50% and a present value for the technical losses of 2540 US$/kW, which was used to analyze and the electric losses for each one of the HTLS technologies (Itaipu, 2010).

Table 4: Cost and energy lost comparison of HTLS conductor technologies for a 100 km long three phase transmission line. Source: (ANDE, 2010; Itaipu, 2010)

Technology	Materials (US$)	Mounting (US$)	Energy loss (US$)	Total cost (US$)	%
GTACSR	2,400,000	4,000,0000	11,497,056	17,897,056	100
ACCC	4,200,000	6,000,000	9,643,872	19,843,872	111
T-ACSR	2,100,000	4,000,0000	14,069,568	20,169,568	112
ACCR	7,500,000	6,000,000	13,399,008	26,899,008	150

Table 4 shows for each HTLS technology the cost for repowering a conventional line considering the respective cost for materials, mounting and energy losses. The lowest total cost is obtained using GTACSR conductors. ACCC and T-ACSR cables are 11 and 12% more expensive. ACCR cables are even 50% more costly. Compared to a new 220 kV aerial transmission line with conventional ACSR 636 MCM Grosbeak code cable having a specific cost of 160,000 US$/km, considering a 40 years life span, but not the energy losses, the GTACSR cable is just 12% more expensive, but it has a 45% higher ampacity limit (ANDE, 2010).

Outlook

Each one of the above presented technologies of HTLS conductors could be used for the repowering of existing aerial transmission lines independently of the tension level in which the load increase is planned. It has to be stressed that the present technical and economic study only considers a load repowering but not the increase of the tension. This should also be analyzed to get a more complete situation of the viable possibilities.

For this purpose could be analyzed for example a 60 km long 66 kV aerial transmission line to be repowered to 132 kV. For the repowering would be used HTLS conductors with diameter and weight equivalent to those of ACSR 300 MCM Ostrich code cables, commonly used in the Paraguayan grid system for this tension level, as well as tempered glass insulators. This way could be modified the energized line and assessed the crown effect, which could exist due to the increase of the quantity of insulators. The study would conclude with computer simulations to find the optimum length of a 66/132 kV line using HTLS conductors and increasing the quantity of the existing glass insulators without changing the diameter and the weight of the conductors checking whether the tension drop will not surpass 0.9 pu (ANDE, 2013).

Conclusions

According to the comparing technical and economic analysis in the present study none of the proposed HTLS technologies can be rejected, as all of them are according to the technical standards regarding energy transmission. Observing the economic aspects we see that the GTACSR has a clear advantage compared to the other options considering the proposed scenario. But on the other hand it presents higher difficulties for its mounting.

In the case of T-ACSR conductors, despite of its lower material cost, it doesn´t have a lower total cost due to the higher costs of the energy losses. But it's precisely this point which is fundamental to take into account for the decision making between one or another technology. Nevertheless, for short transmission lines this aspect will not have this misbalancing effect. Another point to mention is that these cable technologies cannot be used only for transmission lines, but also inside stations, specifically for the bars, taking into account that the load to which they can be subjected in case of a failure at the bars concerning their short circuit level.

It has to be stressed that independently of the chosen HTLS technology there is no need to change the insulators, neither the ones of tempered glass nor the polymeric ones made of silicon rubber or the line post type rigid ones, because in this case the repowering is for load and not for tension level. Dissipation of the additional heat due to the load increase is done in the ironworks, which necessarily have to be changed, because those for conventional conductors are designed to operate at only 90°C (ANDE, 2009).

As a final point has to be mentioned that the manufactures of HTLS conductors compared to a conventional ACSR 636 MCM Grosbeak code cable of the same diameter and weight guarantee a 300% higher ampacity, without modifying the sag. But in most of the cases this is not possible, because this load increase is referred only to the thermal capacity of the conductor due to their low ohmic resistance, but it doesn't take into account the electric capacity, for which variables such as capacitancy and

inductancy for long transmission lines present admissible values and are limiting the electric capacity and by consequence its thermal capacity, due to the similarity of these variables with the conventional conductors with steel core.

References

ANDE, Especificaciones Técnicas N° 03.02.01.45: Suministro de conductor de aluminio con alma de acero ACSR, Licitación Pública Internacional LPI N°162, 2006.

ANDE, Especificaciones Técnicas N° 03.06.02.11: Conjunto de aisladores y herrajes para conductor y cable de guardia, Suministro de conductor de aluminio con alma de acero ACSR, 2009.

ANDE, Especificaciones Técnicas: Suministro de conductores de Alta Temperatura y Baja Flecha, HTLS. Licitación Pública Internacional LPI N° 613, 2010.

ANDE, Especificaciones Técnicas N° 04.01.11: Cambio de conductor con bypass, Licitación Pública Internacional ANDE LPI N° 606, 2011.

ANDE, Plan Maestro de la Administración Nacional de Electricidad (2013-2023), 2013.

ASTM N° B232: Standard Specification for Concentric-Lay-Stranded Aluminum Conductors, Coated-Steel Reinforced (ACSR)

CEMIG, Estudio de Superconductores, CIGRE- Workshop Internacional, 2010.

Díaz R., Los campos electromagnéticos de frecuencia industrial y los riesgos para la salud, Investigación y Desarrollo, pág. 5., 2008.

FURNAS - CENTRAIS ELECTRICAS S.A., Apuntes del Curso de Especialización en Construcción de Líneas de Transmisión, realizado en Rio de Janeiro, Brasil, 2008.

Itaipú Binacional, Costo referencial de tarifa mensual US$/kW-mes, 2010.

Ley N° 976/82 art.1 de la Administración Nacional de Electricidad, que amplía la Ley N° 966/64, 1982.

Mitjans F., Generación Eléctrica Hibrida Eólica Solar para el fortalecimiento del Chaco Paraguayo, Maestría en Energía para el desarrollo sostenible, Universidad Católica de Asunción, 2013.

NEXANS Brasil, consulta realizada en 2010.

NBR N° 5422: Construcao da Línha da Transmicao.

.

Optimal under voltage load shedding based on voltage stability index

Esquema óptimo de deslastre de carga por baja tensión basado en índice de estabilidad de tensión

Karol Daniela Lopez-Rodríguez[1], Sandra Milena Pérez-Londoño[2], Luis Fernando Rodríguez-García[3]

ABSTRACT

This paper presents a methodology for under voltage load shedding using a metaheuristic optimization technique and a stability criterion. In this paper, two strategies are proposed to find the minimal size and location of load to shed for the recovery of normal operation conditions. The first one is based on a classical criterion for the under voltage load shedding, identifying the load to disconnect considering bus voltage level; the second includes a simplified voltage stability index SVSI, which identifies critical buses in the system. The proposed methodology is implemented in an IEEE 14 bus test system, considering a heavy loading condition with and without contingency to validate its efficiency.

Keywords: Load shedding, voltage stability, particle swarm optimization.

RESUMEN

En este artículo se presenta una metodología para realizar el deslastre de carga por baja tensión utilizando una técnica de optimización metaheuristica y criterios de estabilidad. Se proponen dos estrategias para encontrar tanto la cantidad mínima de carga a deslastrar como su localización en el sistema, para recuperar las condiciones normales de operación. El primero está basado en el criterio clásico del deslastre de carga por baja tensión, donde se identifica la carga a desconectar considerando los niveles de tensión en las barras del sistema; el segundo incluye el índice simplficado de estabilidad de tensión SVSI, el cual identifica las barras críticas en el sistema. La propuesta se valida en el sistema de prueba IEEE de 14 barras cuando es sometido a varias perturbaciones.

Palabras clave: Deslastre de carga, estabilidad de tensión, optimización por enjambre de particulas

Received: July 24th 2015
Accepted: Oct 15th 2015

Introduction

As power generation and load demand grow in an ever-increasing tendency, it has been widely reported that power systems are currently being operated closer of the operation limits because of the lack of expansion of transmission networks as the loads grow, due mainly to environmental and economic constraints. This situation has conduces to more-sensitive power systems, which are prone to voltage instabilities or collapses. This effect has been observed and reported in several power systems worldwide (IEA, 2005)(Kundur, 1994). For those power systems, which reach the stability limits, strategies for guaranteeing the generation-demand balance are required to avoid collapses, minimizing non-supplied energy and optimizing energy efficiency.

Alternatives during an impending voltage collapse include Under Voltage Load Shedding (UVLS) schemes, which are applied when the operation of control and compensation devices, such as FACTS (Nguyen and Wagh, 2009) (Greene, Dobson and Alvarado, 1997), turbine governors, automatic voltage regulators (Lerm and Silva, 2004), among others, are inefficient to reach a stable operating state after a disturbance or a contingency. UVLS is based in the possibility to disconnect some loads (or percentages of load) after a severe disturbance, in order to relocate the operating point far from the critical voltage value (Kessel and Glavitsch, 1986) (Quoe et al., 1994). The immediate problem related to UVLS is the development of a strategy to define the amount of load to shed and its location, in order to save the system from a complete blackout.

According to the literature review, several schemes for the determination of load to shed by UVLS have been proposed, due to classical strategies that shed a constant percentage of load when voltage is out of range can be inadequate for a particular or complex system (Laghari, Mokhlis, Bakar and Mohamad, 2013). These classical methods include homogeneous load shedding, centralized and decentralized load shedding (Pahwa, Scoglio, Das and Schulz, 2013) (Mollah, Bahadornejad, Nair and Ancell, 2012) (Niar, et al., 1999) (Klaric, Kuzle and Tomisa, 2005). Mathematical techniques such as linear programming (LP), nonlinear programming and the interior point method were for this purpose; however, these algorithms require approximations of the power system model to reduce the calculation time (Shen and Laughton,

[1] Karol Daniela Lopez Rodriguez, Electrical engineer, Universidad Tecnológica de Pereira, Colombia. Affiliation: Researcher at ICE3, Universidad Tecnológica de Pereira, Colombia. E-mail: kdlopez@utp.edu.co
[2] Sandra Milena Pérez Londoño: Electrical engineer, M.Sc. Universidad Tecnológica de Pereira, Colombia. Ph.D., Universidad Nacional de Colombia. Affiliation: Associated professor at Universidad Tecnológica de Pereira, Pereira, Colombia. E-mail: saperez@utp.edu.co
[3] Luis Fernando Rodriguez, Electrical engineer, M.Sc. Universidad Tecnológica de Pereira, Colombia. Affiliation: Researcher at ICE3, Universidad Tecnológica de Pereira, Colombia. E-mail: luferodriguez@utp.edu.co

1970). Metaheuristic computational techniques and their application in electric power systems are well known and have been used as an optimization tools in different applications, including fault recognition, oscillation control, planning, design and operation, among others. One of these techniques is Particle Swarm Optimization (PSO) (Zomaya and Olariu, 2006) (Kennedy and Eberhart, 1995), which were applied to improve load shedding automation. In (Amraee, Ranjbar, Mozafari and Sadati, 2007), an optimal load-shedding algorithm was developed for ULVS using two heuristic methods such as PSO and Genetic Algorithm. A new method based on sequential use of LP and PSO were used to minimize the load shedding in contingency conditions in (Tarafdar and Galvani, 2011).

Methods for UVLS only consider bus voltage magnitude to define the location and amount of load to shed. However, even if voltages reach a safe operating value, it is well known that bus voltage magnitude is not an adequate indicator of the security of power system operating conditions, especially in modern power systems (Mozina, 2007). Therefore, these UVLS strategies do not guarantee that the operating point after shedding is adequate in terms of voltage stability. A paper related with this is presented in (Kanimozhi et al., 2014), where the minimization of the total load shed and the sum of a "New Voltage Stability Index (NVSI)" were considered as objectives to restore the power flow solvability. The same index also was integrated in a load shedding scheme (Sonar & Mehta, 2015), based on swarm intelligence-Based Optimization Techniques.

In this paper, a methodology for UVLS is proposed, where UVLS is modeled as an optimization problem and solved using PSO. The objective function of the optimization problem includes a voltage stability criterion to guide the evolution process of the algorithm towards the determination of the amounts of load to shed and the improvement of the power system voltage stability. This finally leads to a reduction of the non-supplied energy and costs associated to load disconnection.

The structure of the paper is organized as follows. Section II presents the theoretical background related with voltage stability criteria and PSO algorithm. Later in Section III the methodology is exposed. Based on that, the simulation results are shown when the methodology is tested on IEEE 14 bus system subject to a several disturbances in Section IV. Finally, in Section V are presented the main conclusions of our tests and future work.

Theoretical Background

Voltage stability indices

Voltage stability indices are mathematical tools to determine the proximity of a power system to an impeding voltage collapse. These are usually formulated to indicate proximity to voltage collapse when its value is close to one and secure operating points when its value is close to zero. In order to determine an indicator of risk of voltage instability on load buses, one index proposed in literature is Simplified Voltage Stability Index (SVSI) (Pérez, Rodriguez and Olivar, 2014). This index is based on the concept of relative electrical distance (RED), which is used to select the nearest generator to a specific load bus and also the association of electrical variables to improve its performance.

For a given system, the relation between the complex current (I) and voltage vectors (V) at the generator buses (G) and load buses (L) is represented by the admittance matrix, as is given in (1):

$$\begin{bmatrix} IG \\ IL \end{bmatrix} = \begin{bmatrix} YGG & YGL \\ YLG & YLL \end{bmatrix} \begin{bmatrix} VG \\ VL \end{bmatrix} \quad (1)$$

Rearranging (1), (2) is obtained:

$$\begin{bmatrix} VL \\ IG \end{bmatrix} = \begin{bmatrix} ZLL & FLG \\ KGL & YGG \end{bmatrix} \begin{bmatrix} IL \\ VG \end{bmatrix} \quad (2)$$

where $FLG = -|YLL|^{-1}|YLG|$ is a complex matrix that gives the relation between load and source bus voltages. The REDs (i.e. the relative locations of load buses with respect to the generator buses) are obtained from the FLG matrix and given in (3) (Yesuratnam & Thukaram, 2007):

$$RLG = [A] - abs[FLG] = [A] - abs(|YLL|^{-1}|YLG|) \quad (3)$$

where [A] is the matrix with size (n - g) x g, n is the total number of buses of the network, and g is the number of generator buses. All of the elements of matrix [A] are equal to unity. The information given by the matrix RLG can be used instead of path algorithms to obtain the electrical distances between load and generator buses (Pérez, Rodriguez and Olivar, 2014).

Once the nearest generator to a specified load bus is found with the RLG matrix, the voltage drop on the Thevenin impedance ΔV_i is estimated using (4):

$$\Delta V_i = \sum_{b=1}^{nj-1} |V_b - V_{b+1}| \cong |V_g - V_i| \quad (4)$$

Where V_g and V_i are the voltage phasors at the nearest generator and the analyzed load bus respectively.

Due to simplifications in the development of this index, it is necessary the inclusion of a correction factor to avoid loss of sensitivity to the critical point of the system. This factor, denoted as β, is calculated according to (5):

$$\beta = 1 - (max\,(|V_m| - |V_l|))^2 \quad (5)$$

The correction factor is associated with the highest differences of voltage magnitudes between two buses (m and l), that can be obtained directly from PMU measurements in the analyzed power system under specific operating conditions. Considering the previous, SVSI is given in (6):

$$SVSI_i = \frac{\Delta Vi}{\beta * Vi} \quad (6)$$

The value of SVSI must be less than 1.00 in all load buses to maintain a secure system, according to the formulation based on the maximum power transfer theory (Pérez, Rodriguez and Olivar, 2014).

Particle Swarm Optimization

Similar to other stochastic searching techniques, PSO is initialized by generating a population of random solutions, which is called a swarm. Each individual is referred as a particle and represents a candidate solution to the optimization problem. A particle in PSO, like any living object, has a memory that retains the best experience, which is gained during the exploration of the solution area. In this technique, a velocity vector is associated to

How to cite: Journal Space xxxxxxxxxxxxxxxxxxxx
xxxxxxxxxxxxxxxxxxxxxxxxxxxxxxxxxxxxxxxxxxxxxxxxxxxxxxxxxxxxxxxxxxxxxx

each candidate solution. The velocity vector is adjusted during every iteration of the algorithm according to the corresponding particle experience and to the experiences of the swarm. Accordingly, in the PSO algorithm, the best experiences of the group are always shared with all particles, and hence it is expected that the particles move toward better solution areas (Kennedy and Eberhart, 1995).

The main features of PSO algorithm are the following:

a) In PSO the particles exchange information. This modified its direction in function of the previous experience of the neighborhood particles.
b) PSO stores its experience or history of each agent. The particle decides your new direction based on the best position for which went previously.
c) Usually, it has a rapid convergence to good solutions.
d) The population of the algorithm starts randomly and evolves iteration after iteration.
e) The search always pursues the best possible solution, based solely on the values of the objective function.
f) It is a stochastic technique referred in phase (initialization and transformation)
g) PSO does not create new particles during execution, they are always the same initial particles modified throughout the process.

The movement of a particle into a swarm according to the best experience of the group can be illustrated in the Figure 1.

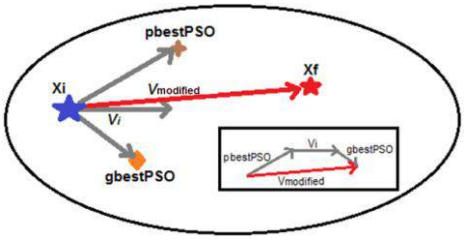

Figure 1. Movement concept of a particle into a swarm

In a n-dimensional search space, the particle position and velocity can be represented as vectors $x_i = (x_i1, x_i2 \ldots . x_in)$ and $v_i = (v_i1, v_i2, \ldots . v_in)$ respectively. The best previous experience of a *i*-th particle is saved as $pbest_i = (pbest_i1, pbest_i2, \ldots . pbest_in)$, and the best previous experience of a group is defined as $pbest_g$.
The particle position and velocity are modified in each iteration through (7-8):

$$v_{id}^{(t+1)} = \omega v_{id}^{(t)} + c_1 rand_1(0)\left(pbest_i - x_{id}^{(t)}\right) + c_2 rand_2(0)\left(pbest_g - x_{id}^{(t)}\right) \quad (7)$$

$$x_{id}^{(t+1)} = x_{id}^{(t)} + v_{id}^{(t+1)} \quad (8)$$

In (7-8), i=1,2,3,…,m is the particle index and t is the iterations number, the constants c_1 and c_2 are weights that control cognitive and social components; ω is the inertia factor in each iteration, its value decreases according to equation (9):

$$\omega^{(t+1)} = \omega_{max} - \frac{\omega_{max} - \omega_{min}}{t_{max}}\, t \quad (9)$$

Formulation of load shedding optimization problem

The best load shedding location and the minimum load shedding amount during severe contingencies are solved in this paper as an optimization problem. The objective function contains a sensitivity factor to guide the optimization problem, and the problem is subject to constraints associated to power flow restrictions and element capabilities.

Objective functions

To obtain the load percentage corresponding to each busbar according with its voltage collapse sensitivity, two schemes for load shedding are developed. These schemes are a function of the load to be shed at each bus, denoted as ΔP_i, and include a different sensitivity criterion for the objective function. The first one is related with the ULVS classical criterion based on the voltage level in the busbar and the second includes the simplified voltage stability index SVSI, which identifies critical buses in the system. The purpose is to determine the optimal quantities of active power to shed (ΔP_i are decision variables for this problem), according to the established sensitivity criterion. These schemes are explained below.

Scheme 1: Under voltage load shedding using voltage level in each bus.

Bus voltage level has a straightforward relation to buses with considerable changes in its operational state after a disturbance. This is the main concept applied for classical load shedding schemes. The objective function in this case is defined by (10):

$$min\left(\sum_{i=1}^{NL} V_i * \Delta\, PD_i\right) \quad (10)$$

where ΔPD_i corresponds to load to be shed at bus *i*, V_i is the voltage level in the bus *i* and *NL* is the total PQ busbar of the system. In this sheme, the lower voltage level of a busbar is, the most susceptible of shedding.

Scheme 2. Under voltage load shedding using simplified voltage stability index (SVSI).

This stability index is included in the load shedding scheme in order to guide the algorithm in the load shedding distribution between the buses of the system, according its contribution to voltage collapse. Therefore, the buses with higher value of SVSI, will be better candidates for shedding.
The objective function to perform load shedding using SVSI is defined in (11):

$$min\left(\sum_{i=1}^{NL} \frac{\Delta\, PD_i}{SVSI_i}\right) \quad (11)$$

where ΔPD_i, corresponds to load shed, $SVSI_i$ the voltage stability indicator of bus *i* and *NL* the total PQ busbar of the system.

Constraints of the problem

The load shedding algorithm is formulated in terms of both active and reactive power parameters (P and Q respectively). Therefore, it is necessary consider power flow constraints (12 - 13).

$$P_{Gi}^0 - P_{Di}^0 + \Delta P_{Di} = \sum_{j=1}^{N} |V_i||V_j||Y_{ij}| \cos(\delta_{ij} + \delta_j - \delta_i) \quad (12)$$

$$Q_{Gi}^0 - Q_{Di}^0 + \Delta Q_{Di} = -\sum_{j=1}^{N} |V_i||V_j||Y_{ij}| \sin(\delta_{ij} + \delta_j - \delta_i) \quad (13)$$

where the subscript "G" and "D" are related to generation and consumption at bus i, respectively. Superscript "0" indicates initial state.

In order to ensure a sufficient distance to voltage collapse, a loading margin λmin is established in according to (14-15):

$$(1+\lambda_{min})(P_{Gi}^0 - P_{Di}^0 + \Delta P_{Di}) = \sum_{j=1}^{N} |V_i^c||V_j^c||Y_{ij}| \cos(\delta_{ij} + \delta_j^c - \delta_i^c) \quad (14)$$

$$Q_{Gi}^0 - (1+\lambda_{min})(Q_{Di}^0 - \Delta Q_{Di}) = -\sum_{j=1}^{N} |V_i^c||V_j^c||Y_{ij}| \sin(\delta_{ij} + \delta_j^c - \delta_i^c) \quad (15)$$

where the superscript "c" is related to the post-contingency state. The loading margin is explained in figure 2. There, it is shown the power system behavior before (blue line) and after a contingency (green line). When a contingency occurs (for instance, a line fault in the system), the point operation defined by point {1} moves to point {2}, which it is very close to the critical point (nose curve). To enhance power system security, load shedding must guarantee a loading margin λmin, which is the distance between the new operational point after UVLS is applied {3} and the collapse point.

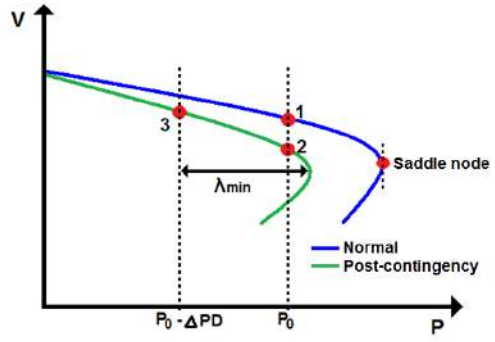

Figure 2. Loading margin into the load shedding scheme

Other model constraints are associated to the voltage levels boundaries for both initial and stressed conditions, load shedding limits and fixed power factor, presented in (16)-(19).

$$V_i^{min} \le V_i \le V_i^{max}, i \in N_L \quad (16)$$

$$V_i^{cmin} \le V_i^c \le V_i^{cmax}, i \in N_L \quad (17)$$

$$\Delta PD_i^{min} \le \Delta PD_i \le \Delta PD_i^{max}, i \in N_D \quad (18)$$

$$\frac{\Delta PD_i}{P_{Di}^0} = \frac{\Delta QD_i}{Q_{Di}^0}, \text{ fixed power factor} \quad (19)$$

Methodology

According to previous information, both load shedding schemes proposed are initialized if the voltage level at any bus of the system is under voltage threshold predefined by the user (in this paper was established in 0.9 p.u). The ULVS scheme is carried out following the flow chart shown in the figure 3.

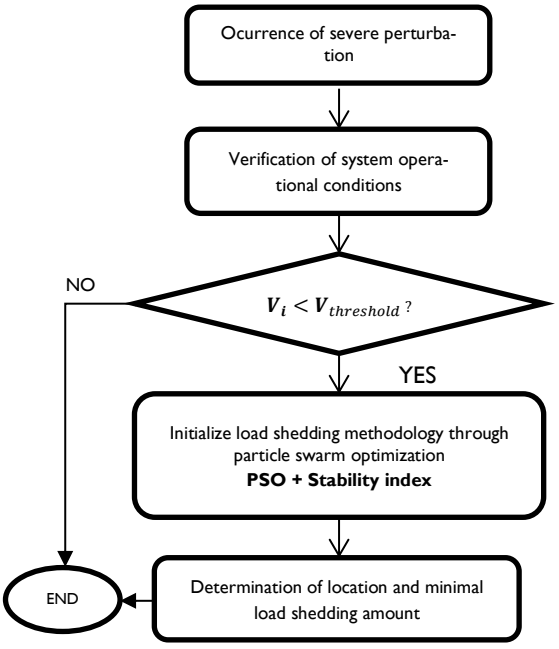

Figure 3. Flow chart of under voltage load shedding schemes

Operational conditions are determined after power flow calculations. If any bus voltage is less than a defined threshold $V_{threshold}$, the optimization process is executed to calculate the minimum amount of load to shed and its location. The required voltage stability indices are also calculated for the formulation of the objective function of the optimization problem.

Considerations related to PSO algorithm

Each particle for PSO algorithm is represented by a vector of *N* components, where *N* is the number of available loads to be shed: $[\Delta P_1 \quad \Delta P_2 \quad \dots \quad \Delta P_i \quad \dots \quad \Delta P_N]$. The initial population is generated randomly, assigning a random number between zero and the 40% of the total active power connected to the bus to each component of the particles.

If a particle reaches an infeasible solution, i.e., when one of the components is lower than zero or greater than the maximum active power shedding limit, a penalty factor is added to the objective function. Finally, as stopping criterion, each PSO execution is stopped when a fixed number of iterations is reached.

Results and discussion

Test description

The methodology previously presented is tested using the IEEE 14 bus test system (PSTCA, 2015), and PSAT as simulation tool. The test system is shown in the figure 4.

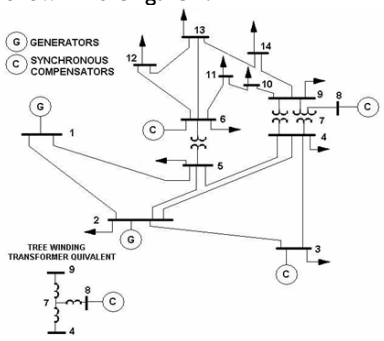

Figure 4. IEEE 14 bus test system

In order to test the effectiveness of the proposed methodology this paper presents a study for the following operating conditions:

- Heavy loading at bus 14 without contingency
- Heavy loading with contingency (single line outage 3-2)

For each case, load shedding is triggered if voltage at any bus is lower than 0.9 pu. The optimization problem sheds load until all buses have a voltage not lower than 0.95 pu. The maximum amount of load to shed at each bus is the 40% of the connected load at the bus at the moment when load shedding is triggered.

PSO parameters

PSO parameters for this application were obtained through exhaustive testing, choosing a set that led to the best results, and are summarized in Table 1.

Table 1. Parameters for PSO algorithm

Number of particles	10
Maximum particle speed	0.002
Minimum particle speed	-0.002
Cognitive coefficient c_1	1.7
Social coefficient c_2	1.7
Maximum inertia $\omega_{\max}$	0.9
Minimum inertia $\omega_{\min}$	0.4

For each loading factor, PSO algorithm executed for 20 times. Each execution is stopped after the algorithm has reached 100 iterations. A penalty factor $\alpha = 10^{10}$ is added to the objective function when an infeasible solution is reached. Each PSO execution is completed in two minutes.

Heavy loading at bus 14 without contingency

In this case, the loading at bus 14 is increased gradually until 4.3 times its nominal load. In this condition, the level voltage at that bus corresponds to 0.9 pu and therefore, the load shedding schemes are executed. Figure 5 shows the minimum load shedding amount for each loading margin (from 0.01 to 0.1 p.u).

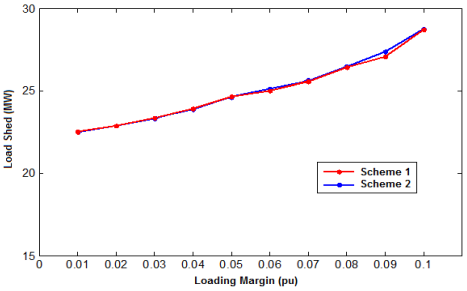

Figure 5. Load shed vs. Loading margin for heavy loading without contingency

According to figure 5, if a higher loading margin is required, a greater load amount must be disconnected. In figure 6, voltage magnitude at each bus considering a load margin of 0.1 are shown. Once load shedding procedures are applied all voltage magnitudes are above the specified threshold of 0.95 pu.

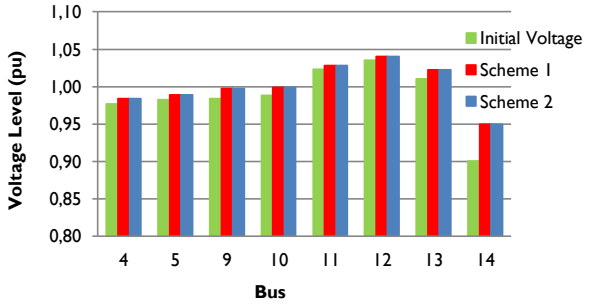

Figure 6. Voltage level at each bus for λmin 0.1

In order to verify the power system stability after the execution of the proposed methodologies, a voltage stability analysis using SVSI is performed. The obtained results are shown in the Figure 7. It is clear that the proposed solution by scheme 2 leads to a better operating state, in terms of voltage stability.

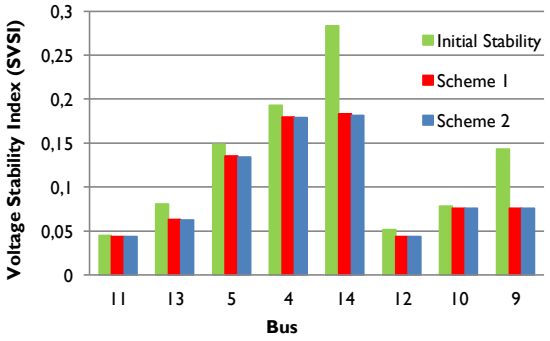

Figure 7. Voltage stability index SVSI for each bus for λmin 0.1

Heavy loading with contingency (single line outage 3-2)

In order to show the effectiveness of the proposed schemes to severe disturbances, a test was performed. The line 3-2 was disconnected and the power system loading is increased to 1.5 times its nominal value.
The minimum load shedding amount for each loading margin according to the proposed schemes is shown in the figure 8.

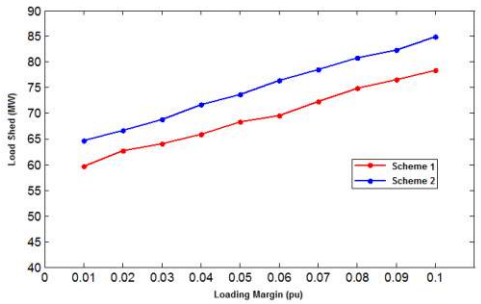

Figure 8. Load shed vs. Loading margin for heavy loading with contingency

In this case, scheme 1 sheds a less amount of load compared to scheme 2. However, both schemes follow the same tendency. Figure 9 shows the load shed corresponding at each bus for a λmin 0.1.

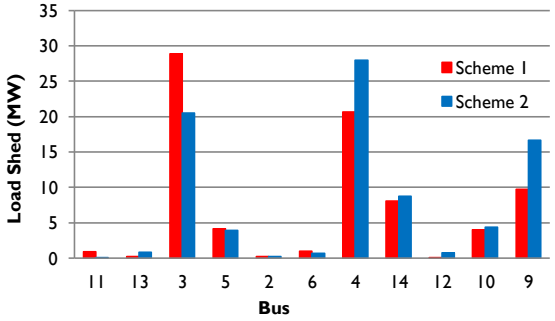

Figure 9. Load shedding amout for each bus for λmin 0.1

The voltage level before and after the implementation of load shedding schemes are shown in the figure 10.

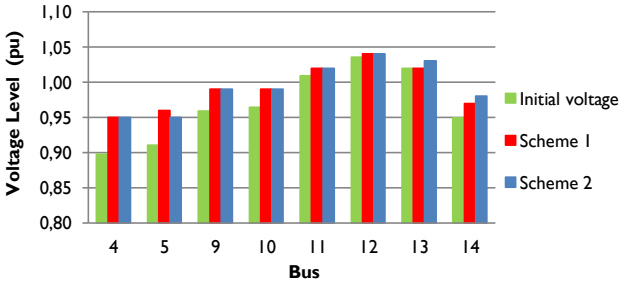

Figure 10. Voltage level for each bus for λmin 0.1

The results show that voltage levels at all buses of the power system are improved after shedding, over the expected voltage level 0.95 pu. With the final purpose to analyze the voltage stability before and after the implementation of load shedding schemes, a voltage stability study is performed using SVSI and the results are shown in the figure 11.

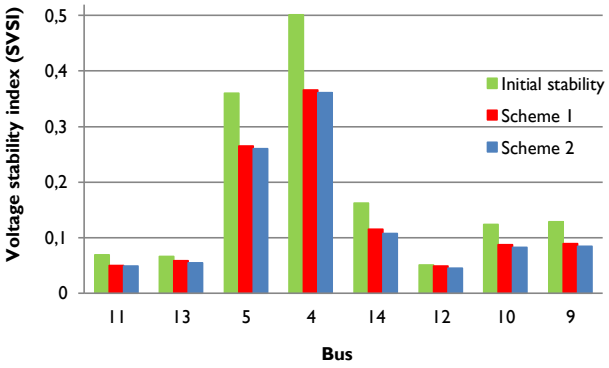

Figure 11. Voltage stability index SVSI for each bus for λmin 0.1

According to the figures 10 and 11, even if the voltage level is the same after the implementation of both load shedding schemes, there are differences in the results of voltage stability levels according to SVSI index (scheme 2). The previous information allows to conclude that load shedding considering the voltage level may not be always an effective criterion, because this does not guarantee generally the major voltage-stable condition of the system after its execution (lower index more stable operating condition).

Conclusions

This paper approaches aspects related to load shedding in power systems, as an emergency strategy for avoiding voltage collapse. Due to the necessity of the determination of the minimal amount of load to shed, two methodologies for optimal under voltage load shedding considering particle swarm optimization are proposed; one of these including stability criteria in order to guide the optimization process to a solution where shed load is minimal and voltage stability is also improved.

According to obtained results, both schemes of under voltage load shedding are efficient to increase the voltage level in every busbar of system after its execution. However, after a voltage stability analysis of the results of each scheme, it is possible to conclude that load shedding considering the voltage level is no warranty of an adequate voltage stability condition. Then, it is demonstrated the relevance of including scheme voltage stability index as SVSI into a load shedding, due to this consideration leads to a better solution in terms of voltage stability. As this methodology establishes a criterion for load shedding based on voltage stability indices, further work is focused on an online implementation, applying machine-learning techniques to reduce the computational effort associated to PSO calculations.

References

Amraee, T., Ranjbar, A.M., Mozafari, B and Sadati, N. "An enhanced under-voltage load shedding schem to provide voltage stability, Electr. Pow. Syst. Res. 77, 2007, pp. 1038-1046.

Greene, S., Dobson, I., and Alvarado, F. L. " Sensitivity of the loading margin to voltage collapse with respect to arbitrary parameters," IEEE Transactions on Power Systems, Vol. 12, No. 1, Feb. 1997, pp. 262 – 272.

IEA, International Energy Agency. "Learning from the blackouts. Transmission System Security Electricity Markets", 2005.

Kanimozhi, R., Selvi, K., and Balaji, K.M. "Multi-objective approach for load shedding based on voltage stability index consideration", Alexandria Engineering Journal, 53(4), 2014, pp. 817-825.

Kennedy, J and Eberhart, R. " Particle Swarm Optimization," Proceedings of IEEE International Conference on Neural Networks, Vol. IV, Perth, Australia, 1995, pp. 1942-1948.

Kessel, P and Glavitsch, H. "Estimating the voltage stability of a power system, IEEE Trans. Power Deliv., vol. 1, no. 3, 1986, pp. 346-354.

Klaric, M., Kuzle, I., Tomisa, T. "Simulation of undervoltage load shedding to prevent voltage collapse", IEEE Power Tech, St. Petersburg, June 27-30, 2005, pp. 1-6.

Kundur, P. "Power System Stability and Control," Toronto, McGraw-Hill, Inc, 623 – 626, 1994, pp.27-32.

Laghari, J. A., Mokhlis, H., Bakar, A.H.A., and Mohamad, H. "Application of computational intelligence techniques for load shedding in power systems: a review, Energy Convers. Manage, No. 75, 2013, pp. 130-140.

Lerm A., and Silva, A. S. "Avoiding hopf bifurcations in power systems via set-points tuning", IEEE Transactions on Power Systems, Vol. 19, No. 2, May 2004.

Mollah, K., Bahadornejad, M., Nair N.-K.C., and Ancell, G. "Automatic under-voltage load shedding: a systematic review" IEEE Power and Energy Society General Meeting. July 22-26, 2012, pp. 1-7.

Mozina, C. J. Undervoltage load shedding. 60th Annual Conf on Protective Realy Engimeers, March 2007, pp. 16-34.

Nguyen, T.T. and Wagh, S. R. "Model Predictive Control of FACTS Devices for Power System Transient Stability". Transmission & Distribution Conference & Exposition: Asia and Pacific, Seoul, Oct. 26 – 30, 2009, pp. 1- 4.

Niar, S., Abbas, A., Chifong, Y., Seabrook, J., Pereira, L., Kreipe, M., Mavis, S., and Green, T. "Undervoltage load shedding guidelines", Western System Coordinating Council, July 1999.

Pahwa, S., Scoglio, C., Das, S. and Schulz. "Load-shedding strategies for preventing cascading failures in power grid," Taylor & Francis, Electric Power Components and Systems, Vol. 41, No.9, May 2013, pp. 879-895.

Pérez, S., Rodríguez, L.F and Olivar, G. "A Simplified Voltage Stability Index (SVSI)", Elsevier Science, Electrical Power & Energy Systems, Vol. 63, 2014, pp. 806 – 813.

PSTCA, Power Systems Test Case Archive Retrieved 2015, http://www.ee.washington.edu/research/pstca/.

Quoe, T., Fandino, N., Hadjsaid, N., Sabonnadiere, J.C and VU, H. "Emergency load shedding to avoid rises of voltage instability using indicators, IEEE Trans. Power Syst. 9 (1) (1994), pp. 341-351

Shen, C.M., and Laughton, M.A. "Power system load scheduling with security constraints using dual linear programming", Proceedings of IEEE, Vol. 117, pp. 2117-2127, 1970

Sonar, V. V., & Mehta, H. D. "Load Shedding Optimization in Power System Using Swarm Intelligence-Based Optimization Techniques. Optimization", International Journal of Advance Research in Engineering, Science & Technology(IJAREST), Vol. 2, No. 5, May- 2015

Tarafdar, M., and Galvani, S. "Minimization of load shedding by sequential use of linear programming and particle swarm optimization", Turk J Elec Eng & Comp Sci, Vol.19, No.4, 2011, pp. 551- 562.

Yesuratnam, G., and Thukaram, D. "Congestion management in open access based on relative electrical distances using voltage stability criteria", Electric Power System Res. 2007;77:1608–18.

Zomaya, Y., and Olariu, S. Handbook of Bioinspired Algorithms and Applications. Taylor & Francis Group. 2006.

Is electricity regulation in Colombia prepared for to incentive modernization of distribution networks? : Challenges and proposal

¿Está la regulación eléctrica colombiana preparada para incentivar la modernización de las redes de distribución?: desafíos y propuestas

D. López-García[1], A. Arango-Manrique[2], S.X. Carvajal[3], C. Arango-Lemoine[4]

ABSTRACT

The evolution towards active distribution networks implies new challenges in the operation of electric power system, specially related to minigrids operation. Integration of distributed generation, modernization of distribution network and demand response programs require energy policies that impulse the operators investment in new technologies. This paper present review of aspects associate to an evolution towards active distribution network considers technical, economic and regulatory issues, presents the actual Colombian regulatory framework related to modernization of distribution networks (devices and programs) and show the main challenges in the operation of minigrids in Colombia.

Keywords: Active distribution systems, energy policy, minigrids, islanding operation.

RESUMEN

La evolución hacia las redes activas de distribución implica nuevos desafíos en la operación del sistema de potencia especialmente relacionados con la operación por minirredes. La integración de generación distribuida, la modernización de la red de distribución y los programas de gestión de demanda requieren políticas energéticas que impulsen la inversión de los operadores en las nuevas tecnologías. Este paper presenta un análisis los aspectos considerados en la evolución hacia las redes activas de distribución considerando temas técnicos y regulatorios, presenta el marco regulatorio colombiano relacionado con la modernización de las redes de distribución (dispositivos y programas) y muestra los principales retos en la operación de las minirredes.

Palabras clave: Minirredes, Sistemas de distribución activos, Operación por isla, políticas regulatorias.

Received: July 24th 2011
Accepted: August 20th 2012

Introduction

The evolution towards active distribution networks with distributed generation (DG), users respond to market signals, new communication devices, an integrated control system and the islanding capability when a failure occur in the Electric Power System (EPS), is a challenge in the operation of minigrids (Berry, Platt and Cornforth, 2010).

The operation of a minigrid with the islanding capability have a similar operation to a traditional EPS (Sioshansi, 2011), it implies that most operational problems encountered in the EPS appear in minigrids (Barnes, 2007). Therefore, the operation of a minigrid requires planning to a successful operation (IEEE, 2011), and to have ancillary services that allows a reliable and secure of supply (Dobakhshari, Azizi and Ranjbar, 2011).

It is necessary to define a smart planning of distribution system in order to make it and active and flexible system, taking into account new technical constraints, uncertainties associated with energy demand, the behavior of primary resources and geographic location of the minigrid (Borges and Martins, 2011).

Regulatory policies are fundamental pillar that ensure the development of minigrids. In Colombia, the future is conditioned to modify regulatory policies that allow investments in the modernization of distribution networks, in order to encourage network operators and demand to integrate to the operation of minigrid (Sioshansi, 2011).

With the publication of Law 1715 of 2014 (Gobierno de Colombia, 2014), Colombia opens up the possibility of integrate renewable resources with storage systems to the distribution network, which together with traditional DG by Small Hydro Power (SHP) or

[1] D. López-García: Member of Reserch Group E3P at Universidad Nacional de Colombia. Author is student of Electrical Engineering, Universidad Nacional de Colombia. Manizales Branch, Colombia Email: dahlopezgar@unal.edu.co

[2] A. Arango-Manrique: Master's in Industrial Automation, Electric Engineer, Member of Reserarch Group on E3P at Univrsidad Nacional de Colombia, Manizales Branch. Author is student of Doctorate in Engineering, Universidad Nacional de Colombia, Manizales Branch, Colombia Email: aarangoma@unal.edu.co

[3] S.X. Carvajal: Full Professor, Electrical and Electronic Department, Universidad Nacional de Colombia, Manizales Branch. Ph.D in Engineering Automatic Line, Universidad Nacional de Colombia. Researcher Group Enviromental, Energy and Education Policy (E3P), Universidad Nacional de Colombia, e-mail: sxcarvajalq@unal.edu.co

[4] C. Arango: Full Professor, Electrical and Electronic Department, Universidad Nacional de Colombia, Manizales Branch. Magister in Electrical Engineering, Universidad Nacional de Colombia. Researcher Group in Distribution and Electrical Power Grid (GREDyP), Universidad Nacional de Colombia, e-mail: carangol@unal.edu.co

diesel plants diversifying the energy matrix and allows to give a dynamic to distribution networks.
In this paper we analyze the features involved in the evolution towards active distribution networks and minigrid operation. Finally we analyze the current regulation in Colombia facing to operate with active distribution system, including the possible connection of new generation sources, the automation and the participation in the energy market.

Evolution towards active distribution networks.

Nowadays, the integration of new resources and technologies to the distribution networks is transforming the operation of the current electrical power system. This leads to a modernization of the passive networks with unidirectional flow and centralized generation, to active distribution networks in which distributed generation, bidirectional communication and automated distribution networks are incorporated (Chowdhury and Crossley, 2009, Hatziargyriou, 2014). To accomplish this transition, it is necessary to develop a sustainable electric infrastructure with flexible and intelligent measure and control, in addition to the integration of new technologies, leading to the operation of smart grids and minigrids (Sioshansi, 2011; Chowdhury and Crossley, 2009).The main changes that must be performed in the distribution system are shown in Figure 1. Currently, a control center coordinates the operation of the entire EPS in order to maintain a balance between generation and demand, ordering maneuvers to the operator of the local control center which supervises and controls the operation of the distribution system. However, the evolution towards active distribution networks requires automated substations and the possibility of independence of the local control center to maintain a continuous communication with distributed generation, demand and the main network in order to ensure a reliable and security of supply.

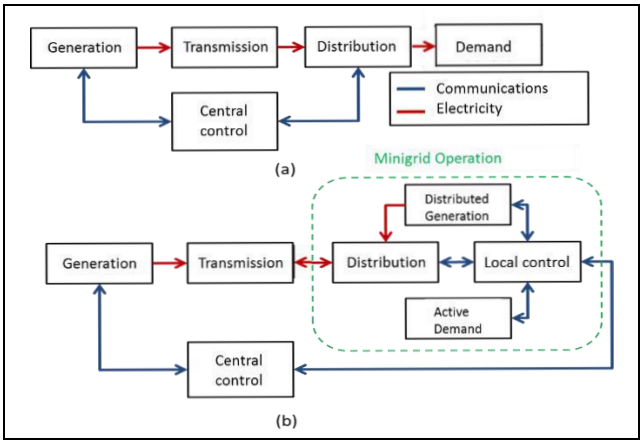

Figure 1. Operation structure (a) Current network (b) Active network. Source: Own

Minigrids operation

Minigrids operation allows to maximize small-scale integration of generation assets, automated distribution networks and demand response in order to create electrical power subsystems, which would be independent of the central interconnected system. Islanded operation of minigrid maintain the electricity supply to the connected users when a failure in the main grid causes partial or complete disconnections, therefore increasing the reliability and efficiency of the distribution network (Costa and Matos, 2005; Gharavi and Ghafurian, 2011). This disconnections would avoid expensive sanctions to transmission companies, respect of demands and penalties brought by users due to unexpected blackouts which generate economic losses (Aghamohammadi and Shahmohammadi, 2012; Carvajal and Arango, 2013). Develop islanded minigrids in order to provide reliable and security of supply, unlike the conventional operation of distribution networks, involves challenges (IEEE, 2011). Mainly, variations in generation may cause drastic changes in frequency or voltage, triggering problems in power quality, voltage collapses and abrupt changes in frequency, leading to a complete disconnection of the minigrid users (Iravani and Mehrizi-Sani, 2010).
To prevent any kind of failure in the operation by minigrids it is necessary to invest in frequency and voltage control systems in distributed plants when a failure occurs in generation (Arango-Manrique, Carvajal-Quintero and Arango-Aramburo, 2011).
As well, installing measuring and control devices across the demand to avoid disconnections when occurs power outages and in order to have an active demand response in the operation of islanded minigrids, which constitutes an additional ancillary service such as voluntary disconnection in event of faults (Vandoom, Zwaenepoel, Kooning, Meersman and Vandevelde, 2011).

Integration of new resources to the distribution system

In this section we analyze the features involved in the integration of distributed resources in the minigrid, the benefits of DG connected near to the consumption centers, and the operation of minigrids in an active distribution system.
The features required for distribution networks to operate as islanded minigrids when events occur in the EPS are defined in figure 2. The main support of minigrid operation is the regulatory policies that encourage investments of different actors in the elements required for this purpose (Ruester, Schwenen, Batlle and Pérez-Arriaga, 2014). This elements include, among others, a communication and control system that allows interoperability among the operator, minigrid sources and the users. Besides including new technologies in terms of generation, especially renewable, and meters that enable the demand to know market dynamic in order to actively participate in it. The benefits and contributions are the foundation for the efficient management of energy resources that support the EPS operation and allow the operation by islanded minigrids.

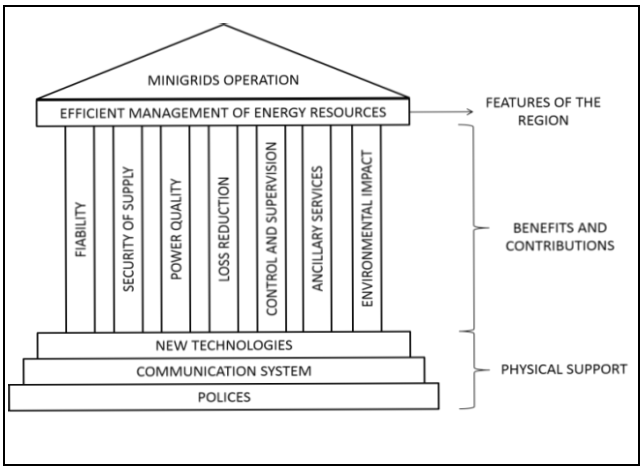

Figure 2. Synthesis of minigrids operation. Source: own

Distributed generation resources

Generation used in minigrids is small-scale generation commonly known as DG because it is connected to voltage levels of distribution networks (Belmans, Pepermans, D'haeseleer, Driesen and Haeseldonckx, 2005).

For the islanded minigrid operation, the frequency and voltage control is fundamental in order to maintain stability, because it no longer has the high inertia that is formed by interconnected generators. The converters guarantee the controllability of DER that are immersed in the minigrid (Mohamad, Mokhlis, Halim, Bakar and Wooi, 2011; Vásquez, Guerrero, Miret, Castilla and Garcia, 2010).

It is necessary to automate electrical substations in terms of communication and control according to the international standard IEC 61850 (IEC 61850, 2011) with the intention of ensure that the minigrid operate under different scenarios such as islanding detection, operation connected to the network, operation in island mode and reconnection to the network (IEEE, 2004).

The advantages of integrating DER in the distributed system are, among others, reduction of losses in distribution system, improvements in voltage profiles and power quality (Arango-Manrique, 2011). In economic terms changes are also presented when there are DER in distribution system because investments are delayed and losses costs are reduced (Matos et al, 2009).

When DER are integrated into the electricity market, the traditional operation changes and presents benefits in economic terms. In addition, it is easier for a distribution network have minigrids as local production units. It is possible to exploit the entire potential that minigrids offers to the distribution network (Barbosa Almada, 2010).

Colombia has a potential laboratory in terms of minigrids. Current distribution networks in Non Interconnected Area (ZNI by its Spanish initials) because it have advanced in issues associated with connecting generation near to consumption centers, centralized and controlled measure (smart metering) and minigrid remote control (IPSE, 2014), which would reduce the implementation cost and would allow the assessment of technical and economic impact of developing minigrids.

Relevant Laws to generation activity in Colombia are the laws 142 and 143 of 1994 which regulate public services and electricity service respectively, as well as Law 689 of 2001that refers to rational and efficient use of energy, and the law 1215 of 2008 corresponding to the cogeneration activity (Gobierno de Colombia, 1994; Gobierno de Colombia, 2001; Gobierno de Colombia 2008). To perform the generation process under clear rules in the market, CREG defines some resolutions that determine the operational and market process to each of them. With the Law 1715 of 2014 there is a possibility of deliver the surplus from self-generators to the network, their participation in the market would be regulated under the premise that they will be equal to the traditional generators. This means they must pay guarantees of the connection point, they need to be or have a generating agent who represent them in the market and have different boundaries to generation and consumption (Minminas, 2014).

Technically only large generators can provide ancillary services (CREG, 2008) and there is no regulation that requires or allows smaller plants provide ancillary services to the network or participate in secondary markets. This would provide adequate infrastructure for the islanding operation of the minigrids, keeping the variables within allowed ranges by the regulation when events are presented in the EPS (Lopes, Moreira and Madureira, 2006). However, in Colombia small-scale generation do not have frequency and voltage control devices, therefore it is unlikely minigrids operation at the present time.

There are gaps in Colombian regulation in terms of marginal or independent producer, in addition to the lack of regulation in DG issues and the consideration of the advantages for the distribution and transmission system in order to reduce costs and solve network congestions, increase reliability and reduce losses (Rodriguez Hernandez, 2009). For that reason, it is necessary to have resolutions that allow smaller plants provide ancillary services in emergencies or events that occur in the EPS.

Active distribution grid

Infrastructure of the current distribution system was mostly built several decades ago, this is why it need to be reconfigured and upgraded to connect new technologies, especially control and telecommunications to make it possible for minigrids to operate in island mode (Sioshansi, 2011).

Non-technical energy losses affect the EPS and users. Colombia registered 20% of losses in transmission and distribution systems compared to average losses of 17% in Latin America countries (World Bank, 2012).

In Colombia the technical regulated conditions in distribution systems are, in terms of regulation, associated with power quality, reliability and security of supply defined by CREG in resolution 070 of 1998 (CREG 070, 1998).

Nevertheless, based on modifications to the power quality regulation (CREG, 2005), the installation of power quality measurement devices and the report of registered information is required (IEEE, 2011) as the first step for registering information and with the aim of ensure the interoperability of the EPS, i.e. the installation of power quality measurement devices in the EPS with remote control and remote management.

Telecommunications are considered as one of the principal elements in minigrids operation and a new element that must be included in electrical infrastructure (IEEE, 2011), that is, Advance Metering Infrastructure (AMI) and Automatic Meter Reading (AMR) systems are required to ensure the participation of agents, and for an efficient management and control (Iravani et al, 2010).

Demand response

Advance metering initiatives in Colombia as still being developed. AMR systems in distribution companies are used for special clients (unregulated users) because of the market structure and according to CREG in resolutions 199 of 1997 and 131 of 1998 (CREG,1997; CREG, 1998) . Operators and electricity traders in Colombia use the measurements to perform the billing process and as a focus for the control of energy losses.

The number of meters installed in Colombia as a result of mandatory regulation and initiatives such as the Electricity Network Standardization Program (PRONE by its Spanish initials) is shown in Figure 3.

Developments related to the concentration of measurement are developed with the support of the national government, such as PRONE that is promoted by Article 63 of Law 812 of 2003 (Gobierno de Colombia, 2003) which was regulated by Decree No. 3735 of December 19 of 2003. With the aim of standardizing the electricity networks in subnormal neighborhoods associated with centralized measurement and with the purpose of reduce technical and non-technical losses in the system, this implies the installation or adjustment of the distribution networks, the connection to customers' homes and the energy meters in order to legalize users, optimize service and reduce non-technical losses (Minminas, 2003).

The Electricity Network Standardization Program will be financed even with the 20% of the collection of the Financial Support Fund

for the Electrification of Interconnected Rural Areas – FAER, according to Law 1117 of 2006 and with the resources provided under the Article 68 of Law 1151 of 2007 (Gobierno de Colombia, 2006; Gobierno de Colombia, 2007).

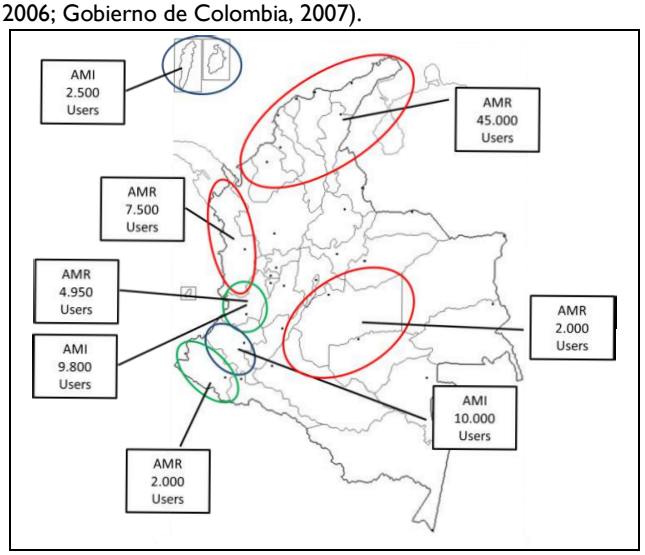

Figure 3. AMI and AMR meters installed in Colombia. Source: Own

The Electricity Network Standardization Program will be financed even with the 20% of the collection of the Financial Support Fund for the Electrification of Interconnected Rural Areas – FAER, according to Law 1117 of 2006 and with the resources provided under the Article 68 of Law 1151 of 2007 (Gobierno de Colombia, 2006; Gobierno de Colombia, 2007).

The demand response program in Colombia only appears in the reliability charge. This charge remunerates the maximum power that is able to deliver a generation plant for one year continuously in extreme drought conditions called Firm Energy Obligations (OEF by its Spanish initials)(CREG, 2006), and being a tool for generators that facilitates the compliance with the OEF. This mechanism allows generators which anticipate that their Firm Energy is not enough to meet the OEF to negotiate with users, through energy traders, voluntary reduction of energy demand (CREG, 2010). In Law 1715 of 2014 the demand participation activity is regulated, however, its implementation and its active participation in the market is unclear.

By the other side, a resolution Project define the mechanism to disconnect users when the EPS have critical conditions (CREG, 2015). However there are gaps according to the remuneration and the roll of the operators in front of the new technical conditions.

Demand is an active agent in the electricity market when a minigrid that participates in the market through disconnection schemes of non-critical users, stocks and voltage and reactive power control is implemented (NERC, 2007; Khamphanchai, Pipattanasomporn and Rahman, 2012; Torriti, Hassan and Leach, 2010); this participation promotes the reduction and the shift in demand curve, improving efficiency without interfering the quality of life of users (Ramírez Escobar, 2008).

Toward a Minigrids operation in Colombia, based in active distribution system: challenges and proposal

Although currently the development of minigrids in Colombia is just beginning, efforts must be made in order to have a regulatory scheme that enables to integrate new technologies to the distribution network. This will lead to new operational guidelines which generates additional costs to network operators, therefore it is proposed to analyze and implement regulatory policies that allow articulate ancillary services when events in the EPS or critical operating situations occur.

The resolution project CREG 179 of 2014 define the mechanism for the remuneration of the distribution networks, which gives light on automation, modernization and remuneration for increasing quality service, and for provide additional services to users (CREG, 2014).

With the implementation of a new remuneration scheme of distribution assets, the regulator expects advance toward active distribution networks. However, in the resolution project, the inclusion of DG within the operation dynamic is unclear. The benefits of connected generation near to consumption centers are neglected and only consider the surplus of the self-generators to contribute to the management of energy losses. Furthermore, benefits provided by demand to the losses management should be considered when financial compensation or payments for maintain system variables within the ranges are included.

Support capacity from the distribution system, which can be hired by users, according to the resolution project, has gaps because this could be considered as a complementary service and would increase the economic benefits for network operator.

The ideal scenario to define pilot projects that allow analyze the impacts on distribution networks without increasing risks to the interconnected power system are the ZNI. These areas operate in isolation of the main grid and as a result of PRONE, many of these areas already have centralized metering technologies that constantly monitors demand, which constitutes an important tool in minigrid operation. Nevertheless, many of the energy problems in the ZNI lies in the lack of technical information of the distribution networks conditions, the absence of studies and measurements of the energy potential of the area, and the deficient demand estimation (Pantoja, Guerrero and Fajardo, 2015). In light of the above, it is a priority obtain accurate information of the current network and of the energy potential of those areas in which the implementation is planned. Additionally, the regulation must be clear with respect to the role and the remuneration of the network operator in these new schemes of supply and respect to demand participation in the market. However, exploiting the entire potential of the ZNI as a natural laboratory for the penetration of minigrids in Colombia also depend on national efforts at research topics of energy management with the aim of articulate academic and government efforts to propose projects in active distribution networks.

Table 1 summarizes the challenges that must be faced in order to create scenarios to modernize the distribution system in Colombia, with respective proposal for how to improve interoperability, reliability, security and the use of ancillary services in distribution network.

Conclusions

Change the operation to an active distribution system involves an adjusting of existing electrical infrastructure (feeder reconfiguration and the inclusion of new measurement, control and protection devices) and include a local control to manage the resources of the minigrid.

With the perspective shown with respect to Colombian regulation, it is observed that it still requires a further development in resolutions and decrees related to the implementation of Law 1715 of 2014 in order to integrate and deploy minigrids to prevent that a monopolistic model governing the minigrids and to enable the active participation of the demand and the inclusion of independent producers.

Resolution project CREG 179 of 2014 allow progress towards the development of active distribution system, leading to modernization, automation and provision of ancillary services from medium voltage distribution networks.
In order to perform tests and analyze the behavior of minigrids, it is proposed implement pilot projects in the ZNI, because these areas have metering infrastructure and generation near to consumption centers that would allow the assessment of parameters and propose the operation of the distribution system as an isolated minigrid.
The possibility that the minigrid operation in island mode allowed to provide ancillary services when an event occur in the EPS or to postpone expansions in the distribution network is proposed. The combination of technical, regulatory and economic studies based on extensive research will guarantee a coordinate operation between the minigrid and the network operator of the distribution system to ensure an optimal operation of the minigrid and to define responsibilities among participant agents.
The offer of distributed resources, the automation and the control of the distribution system allows an efficient energy management that results in an optimization of resources and cost incurred in minigrids. Minigrids operation within a flexible distribution system changes the traditional pattern of operation giving emphasis on the DG sources installed close to centers of consumption and to the demand that actively participates in the market, turning the distribution system on an active system.
The offer of distributed resources, the automation and the control of the distribution system allows an efficient energy management that results in an optimization of resources and costs incurred in minigrids. Minigrids operation within a flexible distribution system changes the traditional pattern of operation giving emphasis on the sources of DG installed close to centers of consumption and to the demand that actively participates in the market, turning the distribution system on an active system.

Acknowledgments

The research for this paper was supported by Universidad Nacional de Colombia through the investigation department of Manizales - DIMA as part of the project, Analysis for the implementation of active distribution grid in existing distribution systems, code 23092, developed by Research Group Enviromental Energy and Education Policy – E3P.

References

Aghamohammadi, M.R., Shahmohammadi,A.: 'Intentional islanding using a new algorithm based on ant search mechanism' (2012)
Arango-Manrique, A., Carvajal-Quintero, S., Arango-Aramburo, S.: 'Contribution of Distributed Generation to Voltage Control' (2011)

Table 1. Main regulatory challenges and proposal regarding minigrids operation in Colombia.

Item	Challenge	Proposal
Distributed Generation	To implement and enforce the proposed provisions of Law 1715 of 2014 with which renewable energies with storage systems can be integrated into the distribution network, it is necessary that CREG, XM and UPME stablish the guidelines that will allow its application.	Create a framework that integrates the proposal defined by self-generators with the network operators considering the communication between the control center of the network operator and the automation of the DG.
	In order to maintain stability and improve the reliability and security of the distribution network with the addition of DG, it is essential to conduct a thorough planning that allows analyse the benefits of each connection according to the characteristics of the connection point and the geographic location (Arango-Manrique et al, 2011).	Include the DG (less than 20 MW) connected to the local distribution system in the proposals for the management of energy losses because of the benefits it has in terms of maintaining the stability and security of the electricity supply.
	The resolution project CREG 179 of 2014 stipulate that self-generators may carry out studies in order to demonstrate the benefits in reducing energy losses and can would share this benefits with the network operator (mutual agreement).	
Distribution Network	To have an evolution towards active distribution networks, in the resolution project CREG 179 of 2014, remuneration is focused on the execution of investment plans, replacement of existing assets, losses management, and improvement of service quality and introduction of new technologies.	Include in the expansion plan, programs of losses management with the implementation of new technologies associated with measurement, communication and network automation.
	Network operators must acquire new skills related to smart grids, interoperability and automated substations with the purpose of allow turning traditional distribution system on an active distribution system.	A higher remuneration is obtained by including DG in the operation of the distribution system, because it is possible to have a support system to connected users, in addition to reduce the outages number which means economic benefits to network operators.
	Take advantage of the subsidies defined by the resolution project CREG 179 of 2014 with the aim of increase the remuneration of network operators associated with maintain indexes related to service quality, expansion plans with the inclusion of new technologies to reduce energy losses and for losses management.	Propose a market of support capacity, in order to increase the investments in the distribution system.
		Implement the proposed changes to the resolution project, in order to have a distribution system with islanded capability ensuring interoperability between all assets connected to the grid (DG and demand).
Demand	To develop minigrid operation in Colombia properly, it is necessary to have an active participation of the demand focused on energy efficiency, for which it is necessary to use controllability and bidirectional measurement devices to become an active agent that may constitute an ancillary service when events occur in the EPS.	Articulate laws and resolutions to create a robust regulatory scheme that allows interoperability, the inclusion of DER to the distribution system and an active demand in order to create a scenario where it is possible to have minigrids operation in Colombia.
	Articulate through the energy market agents the Document No. 087 of 2008 which establish the conditions for participation in the mechanism of voluntary disconnection of demand which allows a generator to negotiate with electrical consumers, through energy traders, a voluntary reduction or changes in electricity consumption, when it anticipates that its energy is not sufficient to meet the Firm Energy Obligations	Implement demand management programs which enables grid operators meet with the obligations of Firm Energy framed in resolution 071 of 2006 issued by CREG, by introducing to all market agents the responsibilities and benefits of an active demand participation, stipulated by CREG in the document No. 087 which establish the conditions for participation in the mechanism of voluntary disconnection of demand.
		Take advantage of the benefits of implement smart meters in demand.

Arango-Manrique, A.: 'Caracterización de un Esquema Remunerativo para el Control de Tension en el Sistema Eléctrico Colombiano' 2011.
Barbosa Almada, J., 2010. Universidade Federal Do Ceará Análise De Impactos E Soluções Na Integração Da Geração Distribuída Ao Sistema Elétrico.
Barnes, M., Green, T., Lasseter, R., Hatziargyriou, N.: 'Real-World MicroGrids- An Overview'2007.
Belmans, R., Pepermans, G., D'haeseleer, W., Driesen, J., Haeseldonckx, D.: 'Distributed generation: definition, benefits and issues' (2005), 33, pp. 787–798
Berry, A., Platt, G., Cornforth, D.: 'Minigrids: Analysing the state-of-play'2010 Int. Power Electron. Conf. - ECCE Asia -, IPEC 2010, 2010, 2008, pp. 710–716.
Borges, C.L.T., Martins, V.F.: 'Multistage expansion planning for active distribution networks under demand and Distributed Generation uncertainties'Int. J. Electr. Power Energy Syst., 2012, 36, (1), pp. 107–116.
Carvajal, S.X., Arango, S., Larsen, E.R.: 'Evaluation of a payments proposal for blackstart services in the Colombia electricity system: A system dynamics approach' (2013)
Chowdhury, S., Chowdhury S.P., Crossley, P.: 'Microgrids and Active Distribution Networks' (2009).
Costa, P., Matos, M.: 'Reliability of distribution networks with microgrids'Power Tech, 2005 IEEE Russ., 2005, pp. 1–7.
CREG, Comisión de Regulación de Energía y Gas: 'Resolución CREG 011' (2015)
CREG, Comisión de Regulación de Energía y Gas: 'Resolución CREG 024' (2005)
CREG, Comisión de Regulación de Energía y Gas: 'Resolución CREG 063' (2010)
CREG, Comisión de Regulación de Energía y Gas: 'Resolución CREG 070' (1998)
CREG, Comisión de Regulación de Energía y Gas: 'Resolución CREG 071' (2006)
CREG, Comisión de Regulación de Energía y Gas: 'Resolución CREG 086' (1996)
CREG, Comisión de Regulación de Energía y Gas: 'Resolución CREG 107' (1998)
CREG, Comisión de Regulación de Energía y Gas: 'Resolución CREG 122' (2003)
CREG, Comisión de Regulación de Energía y Gas: 'Resolución CREG 131' (1998)
CREG, Comisión de Regulación de Energía y Gas: 'Resolución CREG 179' (2014)
CREG, Comisión de Regulación de Energía y Gas: 'Resolución CREG 199' (1997)
CREG, Comisión de Regulación de Energía y Gas:'Resolución CREG 036' (2008)
Dobakhshari, A.S., Azizi, S., Ranjbar, A.M.: 'Control of microgrids: Aspects and prospects'2011 Int. Conf. Networking, Sens. Control, 2011, pp. 38–43.
Gharavi, H., Ghafurian, R.: 'Smart Grid: The Electric Energy System of the Future [Scanning the Issue]' (2011), 99, pp. 917–921
Gobierno de Colombia: 'Ley 1117. Normas sobre normalización de redes eléctricas y de subsidios para estratos 1 y 2.' (2006)
Gobierno de Colombia: 'Ley 1151. Plan Nacional de Desarrollo 2006-2010.' (2007)
Gobierno de Colombia: 'Ley 1215. Medidas en materia de generación de energía eléctrica.' (2008)
Gobierno de Colombia: 'LEY 143 DE 1994. Régimen para la generación, interconexión, transmisión, distribución y comercialización de electricidad en el territorio nacional, se conceden unas autorizaciones y se dictan otras disposiciones en materia energética.' (1994)
Gobierno de Colombia: 'LEY 1715 DE 2014. Por medio de la cual se regula la integración de energías renovables no convencionales al sistema energético nacional.' (2014)
Gobierno de Colombia: 'Ley 689. Modifica parcialmente la Ley 142 de 1994.' (2001)
Gobierno de Colombia: 'Ley 812. Plan Nacional de Desarrollo 2003-2006.' (2003)
Hatziargyriou, N.:_'Microgrids architectures and control'. (2014)
IEC 61850 ' Communication networks and systems for power utility automation' 2011
IEEE, I. of E. and E.E.: 'IEEE 1547 Overview of Interconnection Standards'2004.
IEEE: 'IEEE 1547.4 Guide for Design, Operation, and Integration of Distributed Resource Island Systems with Electric Power Systems IEEE Standards Coordinating Committee 21 Sponsored by the' (2011)
IEEE: 'IEEE Draft Guide for Smart Grid Interoperability of Energy Technology and Information Technology Operation with the Electric Power System (EPS), and End-Use Applications and Loads' (2011)
Iravani, R., Mehrizi-Sani, A.: 'Potential-Function Based Control of a Microgrid in Islanded and Grid-Connected Modes' (2010), 25, pp. 1883–1891
J. A. P. Lopes, C. L. Moreira, and A. G. Madureira, "Defining control strategies for microgrids islanded operation," IEEE Trans. Power Syst., vol. 21, no. 2, pp. 916–924, 2006.
Khamphanchai, W., Pipattanasomporn, M., Rahman, S.: 'A Multi-Agent System for Restoration of an Electric Power Distribution Network with Local Generation', in '2012 IEEE Power and Energy Society General Meeting', (2012), pp. 1–8
Minminas, Ley 1715 de 2014, Ministerio de Minas y Energía: 'Decreto 2469' (2014)
Minminas, Ley 812 de 2003, Ministerio de Minas y Energía: 'Decreto 3735' (2003)
Matos, M., Peças, J., Rosa, M., Ferreira, R., Leite, A., Sales, W., Resende, L., Manso, L., Cabral, P., Ferreira, M., Martins, N., Artaiz, C., Soto, F., López, R., 2009. Electrical Power and Energy Systems Probabilistic evaluation of reserve requirements of generating systems with renewable power sources : The Portuguese and Spanish cases. Int. J. Electr. Power Energy Syst. 31, 562–569.
Mohamad, H., Mokhlis, H., Halim, A., Bakar, A., Wooi, H., 2011. A review on islanding operation and control for distribution network connected with small hydro power plant. Renew. Sustain. Energy Rev. 15, 3952–3962.
NERC, T.N.A.E.R.C.: 'Data Collection for Demand-Side Management for Quantifying its Influence on Reliability'2007, (December).
Pantoja, A., Guerrero K., Fajardo, D.: 'Oportunidades Energéticas con Fuentes Alternativas en el Departamento de Nariño' 2015.
Ramírez Escobar, C.A.: 'Los Precios del Mercado Mayorista de Electricidad como Expresión de la Participación Activa de la Demanda: Aplicación de la Economía Experimental'. 2008
Rodriguez Hernandez, A.: 'LA GENERACIÓN DISTRIBUIDA y SU POSIBLE INTEGRACIÓN AL SISTEMA INTERCONECTADO' (2009)
S. Ruester, S. Schwenen, C. Batlle, and I. Pérez-Arriaga, "From distribution networks to smart distribution systems: Rethinking the regulation of European electricity DSOs," Util. Policy, Apr. 2014.
Sioshansi, F.: 'Smart grid: integrating renewable, distributed & efficient energy', in 'Smart Grid Integrating Renewable, Distributed & Efficient Energy' (Elsevier Inc., 2011), pp. i–ii
Torriti, J., Hassan, M.G., Leach, M.: 'Demand response experience in Europe : Policies, programmes and implementation' Energy, 2010, 35, (4), pp. 1575–1583.
UPME, U. de P.M.E.: 'Plan de expansión de referencia: Generación- transmisión 2011-2025' (2011)
Vandoorn, T.L., Zwaenepoel, B., Kooning, J.D.M. De, Meersman, B., Vandevelde, L.: 'Smart microgrids and virtual power plants in a hierarchical control structure'2011 2nd IEEE PES Int. Conf. Exhib. Innov. Smart Grid Technol., 2011, pp. 1–7.
Vásquez J.C.; Guerrero J.M., Miret J., Castilla M y Garcia L. 2010.Hierarchical Control of Intelligent Microgrids. Industrial Electronics Magazine IEEE. Vol. 4, pp. 23-29.
World Bank: 'Electric power transmission and distribution losses (% of output)' (2012), http://datos.bancomundial.org/indicador/EG.ELC.LOSS.ZS/countries/1W-CO?display=graph
XM, 2014. Informe de Operación del Sistema y Administración del Mercado Eléctrico Colombiano. Expertos en Mercados. Operador del sistema eléctrico interconectado colombiano

Climatological Analysis in Channels of High Densities of Atmospheric Discharges Located in Paraguayan Territory in Order to Optimize Electrical Continuity Service Due to The Downfall of High Tension Towers

Análisis Climatológico en Canales de Altas Densidades de Descargas Atmosféricas Ubicadas en Territorio Paraguayo a Fin de Optimizar la Continuidad del Servicio Eléctrico Debido a Caídas de Torres de Alta Tensión

Hugo Cesar Acosta Escobar[1]

ABSTRACT
Paraguay is one of the countries with the most falls of atmospheric discharges per year but even the random and unpredictability of their fall there are regions with intense and frequent atmospheric discharges more than other regions within its territory. There are an average of 20 or more annual severe thunderstorms in the spring summer season where they can generate winds of 180-200 km h, hail and strong atmospheric discharges what they can result collapses of power lines in rural and urban areas by falling of electrical structures. The objective of this work is to correlate and demonstrate using a satellite Statistics database of Lightning (NASA), also geomagnetic map (NOAA) and geological maps about the existence of five longitudinal channels with high densities of atmospheric discharges which crosses the country. To achieve decipher their exact locations and the cause that produces it was not an easy job but hereinafter electrical utility state can plan preventive strategies to optimize the restoration of the electricity service with a shortest possible time or decrease the frequency of their occurrence.

Keywords: thunderstorms,, collapses, atmospheric discharges, electrical structures, NASA, NOAA, service continuity

RESUMEN
Paraguay es uno de los países del mundo con más caídas de descargas atmosféricas por año, pero a pesar de la aleatoriedad e imprevisibilidad de su caída, hay regiones con intensas y frecuentes descargas atmosféricas más que de otras regiones dentro de su territorio. Existe un promedio de 20 o más tormentas severas anual en la temporada de primavera verano, en donde se pueden generan vientos de 180-200 km/h, granizos y fuertes descargas atmosféricas lo que pueden ocasionar colapsos del tendido eléctrico en áreas rurales y urbana por las caídas de las estructuras eléctricas. El objetivo del trabajo es correlacionar y demostrar mediante una base de datos satelital del relámpago, mapas geomagnéticos y geológicos sobre la existencia de cinco canales o franjas longitudinales con altas densidades de descargas atmosféricas que atraviesan al país Lograr descifrar su exacta ubicación y la causa que lo produce no fue una tarea fácil; pero en lo sucesivo se podrán planificar desde la empresa estatal de servicio eléctrico, estrategias preventivas para optimizar la reposición del servicio eléctrico con un menor tiempo posible o disminuir la frecuencia de su ocurrencia.

Palabras clave: Tormentas, colapsos, descargas atmosféricas, estructuras eléctricas, NASA, NOAA, continuidad de servicio

Received: July 24th, 2015
Accepted: Oct 15th, 2015

Introduction

From the year 1982 up to date the National Electric Company (A.N.D.E) has undergone collapses in their airlines in 11 chances in lines of 220 kV 5 additional opportunities in lines of 66 kV and in lines of 23kV 32 times. The average transmission towers collapses were 3-22 structures and 10 to 30 structures in distribution lines. The average repair cost per kilometer for 220 kV lines ranging from 130,000 to 160,000 U$ in 66 kV lines ranges from 85,000 to 100,000 U$ and 23 kV lines 15,000 U$ but we must add the energy not supplied it costs between 250,000 to 600,000 U$/day (neither included the costs of industrial production). The reset time is between 36-72 hours depending on the severity of storms with atmospheric discharges and affected zone.

Cause and origin of 5 channels with higher rates of lightning discharges

The Earth's magnetic field is predominantly produced by electric currents occurring in the outer core of the earth composed of cast iron highly conductive. Physically, the magnetic field is generated to form a current line in a closed winding (Ampere's Law) a variable magnetic field generates an electric field (Faraday's

[1] Author Description: Electromechanical Engineer - Chief of Special studies of National Electricity Administration - Paraguay – Master in Management and Environmental Legislation - Professor of the Faculty of Electromechanical Engineering at the National University of Asuncion- Member of the Scientific Society of Paraguay - E-mail: hugo_acosta@ande.gov.py hugoc.acosta@gmail.com

Law) and the electric and magnetic fields exert a force on the loads that flowing in the current (the Lorentz force) which they may be represented at any point by a three-dimensional vector. On the surface of earth the magnetic field is a composite of the main magnetic field originated by an internal and external source but between of them with a temporary dependence. Geomagnetism is dominated by an axial dipole in the center of the earth very near to the rotational axis. This magnetic field changes in time in direction and amplitude due to internal and external physical processes of the earth therefore it has to be measured in regular intervals of time from the magnetic monitoring centers where they have documented historical records about these variations. The magnetic field of the terrestrial crust depends for the magnetization of the iron contained into the subsoil materials In the field of internal origin, found in these rocks they have a "memory" of the magnetic field that cross known as magnetization by two components: a) the field of crust b) Field of the core.

Magnetic field models of reference

The Earth's magnetic field is described by seven parameters. These are declination (D), inclination (I), horizontal intensity (H), vertical intensity (Z), total intensity (F) and the north (X) and east (Y) components of the horizontal intensity. By convention, declination is considered positive when measured east of north, inclination and vertical intensity positive down, X positive north, and Y positive east. The magnetic field observed on Earth is constantly changing.

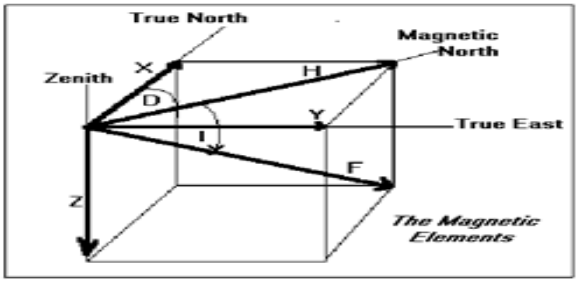

Figure1.The earth's magnetic field described by seven parameters

Magnetic field models of reference provide an easy way to calculate magnetic declination and other components. A reference field model it is a mathematical algorithm whose parameters are based on a analysis satellite magnetic surveillance whether over the world or part of the world.

Spherical harmonic analysis is the most common method used to produce global models. The World Magnetic Model (WMM) is the standard model used by the Department of Defense United States, the Ministry of Defence of the United Kingdom, the Organization of North Atlantic Treaty (NATO) and the International Hydrographic Organization (IHO), which widely used in civil navigation and is produced at intervals of five years, the present model will expire December 31st 2019 being able be found at NOAA.
website http://www.ngdc.noaa.gov/geomag/WMM/DoDWMM.shtm

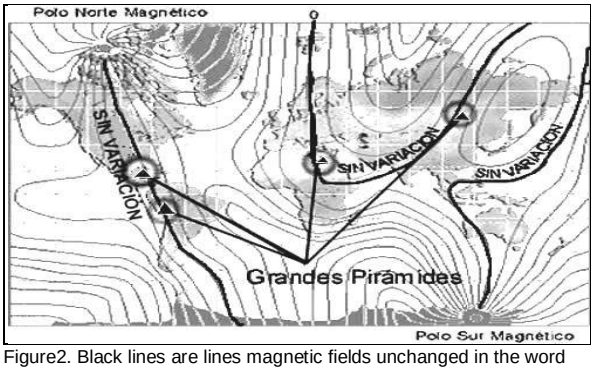

Figure2. Black lines are lines magnetic fields unchanged in the word

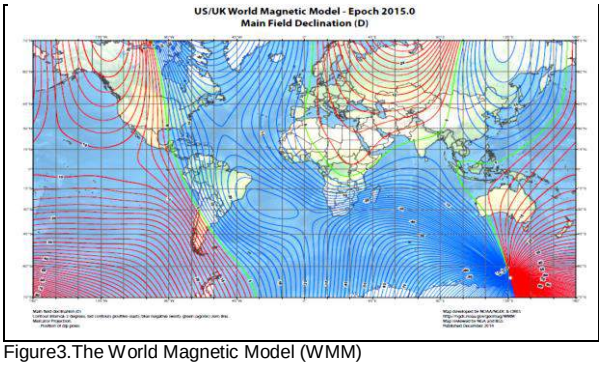

Figure3.The World Magnetic Model (WMM)

Ground magnetic anomalies

The main magnetic field is originated by the convection currents and swirls of fused materials in the core of earth while magnetized rocks of the crust are producing localized fields; these are known as magnetic anomalies. They are deviations of the main magnetic field who experiencing variations the average values in the elements of terrestrial magnetism about a particular location. Flux magnetic anomalies cover huge areas that are called regionalists, unlike local areas occupying from several square meters to thousands of square kilometers.

High atmospheric discharges events on the longitudinal sample spaces

During the development and deployment of a thunderstorm clouds they are electrostatically charged with positive and negative ions where can be generated thunderbolts and lightening of different intensities. Atmospherical discharges statistically it can be considered as a random and temporary phenomenon but however to know a little more about their activities and details in Paraguayan territory they were lowered temporary lightning samples taken from the website of the NASA (http://thunder.msfc.nasa.gov/) emitted by the LIS (Lighting Imaging Sensor) used in the satellite to detect distribution and variability of each event (lightening or rays) generated in several countries among them Paraguay. This activity is done on board the meteorological satellite TRMM (*Tropical Rainfall Measuring Mission*) http://thunder.nsstc.nasa.gov/primer/index by generating a atmospheric discharge in the earth this events are picked up through its optical sensor by means of glint and emission of an electromagnetic radiation . This events are referenced Cartographically with his latitude and longitude in almost all South American countries stored in a database of lightning with a period of 19 times per day. At the first opportunity these samples were lowered from 1998 to 2013 in annual, quarterly, and

monthly periods categorized by night and day events for relating average in Kilo-Amper of atmospheric discharges from every region of our country to utilize this information for dimensioning and design of high voltage electrical structures. The longitudinal areas of higher atmospheric discharges per square kilometer were not in our interest of this research but within the samples were detected certain areas or atmospheric discharges channels with higher intensities and frequencies that caught our attention at the LIS database but in a random manner in different times. The presumption of the existence of a longitudinal area of atmospheric discharges of greater intensity and frequency was because the phenomenon was observed repeatedly in other random samples but incompletely formed in the same places. Therefore we was assumed that there could be more than one area or several longitudinal channels of atmospheric discharges per square kilometer with similar characteristics in Paraguayan territory for this we proceeded in the LIS database to give variability in the time of random samples obtained through the mapping of atmospheric discharges in the satellite.

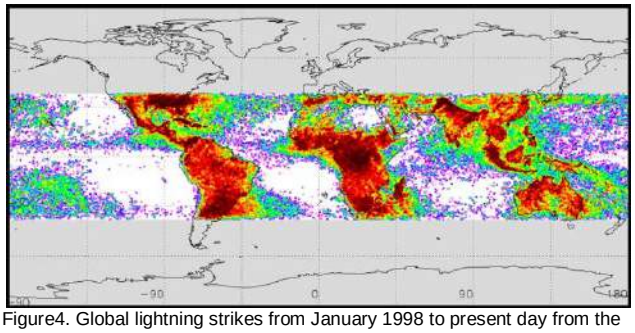

Figure4. Global lightning strikes from January 1998 to present day from the NASA/MSFC Lightning Imaging Sensor

Longitudinal areas of atmospheric discharges in Paraguayan territory

It is possible to explain the existence of areas or longitudinal channels characterized by high atmospheric discharges activities than other areas that cross the country in northwest southeast direction spaced each one in a parallel manner. These longitudinal channels or areas of high atmospheric discharges per square kilometer are not stable over time so in position and training, as it was observed in several random samples displaced by a few kilometers left and right of the longitudinal axis. It is known and reported in the magnetic monitoring centers around the world that the deviation of the main magnetic field is variable and represents 6% of the total intensity of the Earth magnetic field it produced by the movement of electrically charged particles in the atmosphere and is superimposed on the permanent magnetic field.

For explanation let's hypothetically consider a stable climate without thunderstorms and in the surface of the earth two mountains formed by igneous and metamorphic spaced from each other a few kilometers (may be 100 Km) irregularly distributed through some outcrops in the field of sparse vegetation. In this configuration we insert an imaginary cylinder containing lines anomalous magnetic fluxes that appeared thousands of years ago by induced or remnant magnetization in the rocks that were activated secondarily by the main magnetic field of the earth. In order to theoretically explain the existence of areas or longitudinal channels of high atmospheric discharges the Maxwell's equations tell us over the production and interrelationship of electric and magnetic fields.

Figure5. Location of Paraguay in South America

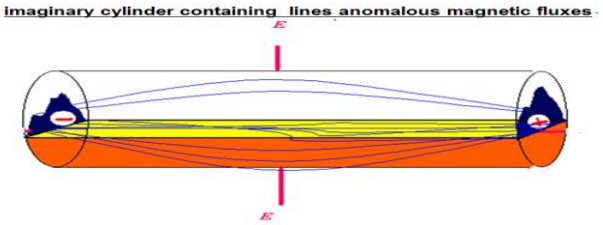

Figure6. Magnetized rocks generating anomalous magnetic fields

Let's consider this hypothetical approach spatial of a thunderstorm when crossing a magnetic anomalous flux lines moving at a certain speed within in an imaginary cylinder. The Gauss theorem relates the field divergence about this closed volume with magnetic flux lines across the surface around the volume. If nothing is lost or created within the volume, there will not be flux through its surface. The Stokes theorem relates the cross product of a vector field integrated on the surface to the line integral of the magnetic field along the curve surrounding the surface. We know that the magnetic field lines begin and end in the magnetic dipole, however, magnetic "charges" or "mono poles" do not exist.

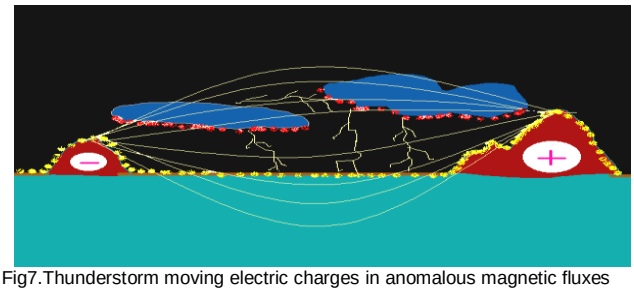

Fig7.Thunderstorm moving electric charges in anomalous magnetic fluxes

Now the flow of the secondary magnetic field is contained within the imaginary cylinder belonging to the closed surface which encloses the anomalous dipole that are generated by the two mountains magnetized secondarily by the flow of the main magnetic field of the earth. Is why all the field lines leave the surface enclosing the anomalous dipole inside the imaginary cylinder that they will return to reenter the same surface. With good condition weather there are no electric charge ions in displacement inside and outside the imaginary cylinder and there are not magnetic fluxes acting on it generated by the anomalous dipole of the two mountains but in a thunderstorm with moving electric

charges there exists a time dependence of the appearance the anomalous magnetic fluxes inducing strong electric fields when crossing the imaginary cylinder in the space formed by the two mountains. The reverse is also true: a time-dependent electric flux induces a magnetic field. Moving an electric current is also responsible for generating a magnetic field. For a surface enclosing a charge distribution (thunderstorm clouds), the flow through that surface would be related to the electric charge density contained in the volume this is a manifestation of the natural potential of the electric field. Moreover conducting a current in an electromagnetic field has been verified that a force (Lorentz). It is exerted on a load moving in an electric and magnetic field which is obeyed by all materials for which the current depends linearly on the applied potential difference. In the Magnetic anomalies the magnetic intensity has magnitude and direction that depends on the magnetic susceptibility and the remanent magnetization of the rock. The magnetic force can attract or repulse something. The magnetic effects may be caused by components little or abundance of magnetic substances in a rock. The temporal change of the magnetic field is due to the flow of material, which induces a new field, plus the temporal variation of the field when it changes by the ohmic decay. Generally the anomalous geomagnetic field, its magnitude and direction is determined by the magnetization of the magnetic rocks at superimposed on the magnitude and direction set by main geomagnetic field. As the geomagnetic field varies with time the magnitude and direction of the geomagnetic field also vary from place. Rocks can keep a remnant magnetization related to the existing geomagnetic field when these rocks were formed thousands of years ago. Structures causing magnetic anomalies are often parallel to each other as a system of parallel dikes with a high content magnetite.

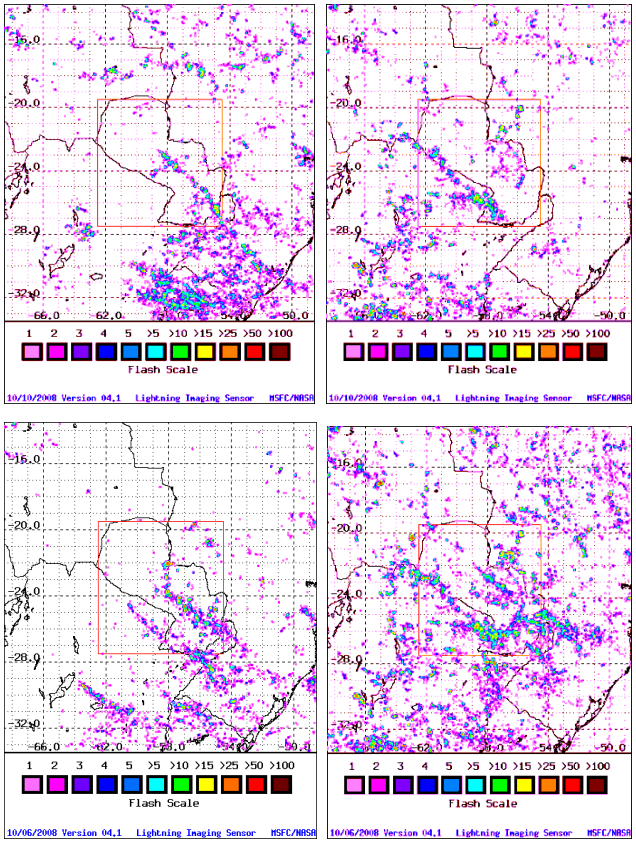

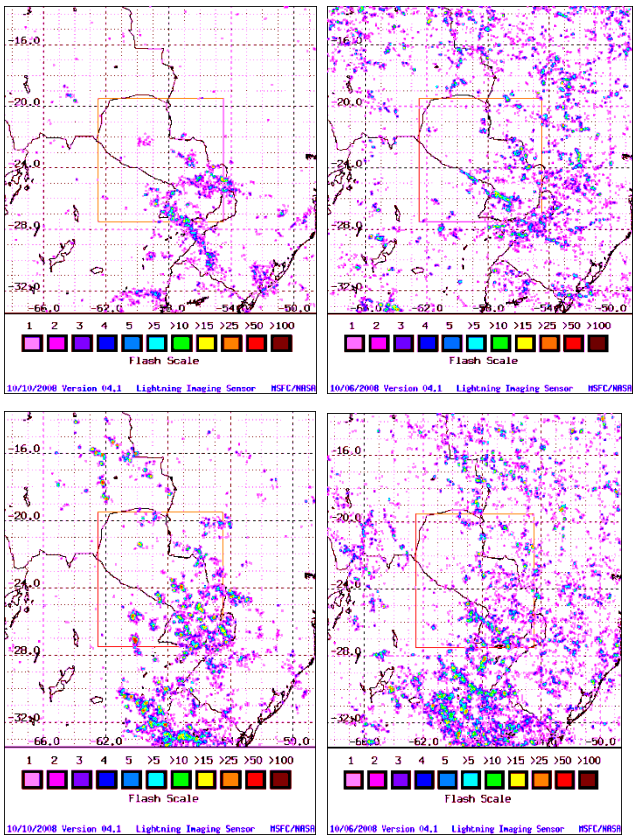

Figure8.Samples of longitudinal atmospheric discharges in Paraguay

We check later that the channels of high densities of lightning are activated longitudinally and perfectly within the magnetic anomaly profiles obtained from the World Magnetic Model (WMM) which converge with geological formations in Paraguayan territory.

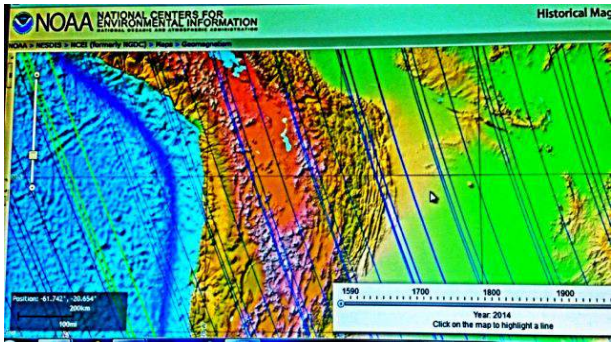

Figure9. Orografico system and Magnetic Declination 2014

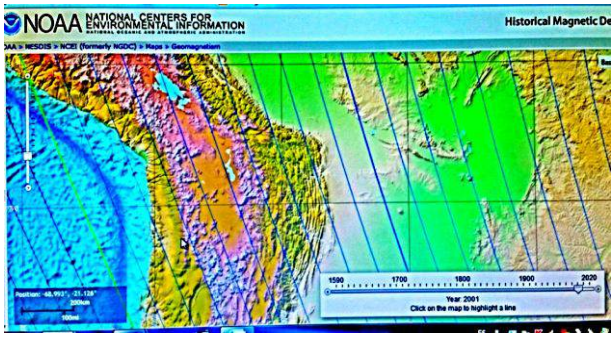

Figure10. Orografico system and Magnetic Declination 2001

We can see from the above figures that the secondary field lines are not stable like measurements (NOAA) obtained in 2014 and 2001 and more. We provide some samples of high rates of lightning by longitudinal square kilometers called PY-S1; PY-S2; PY-S3; PY-S4 investigated from the database issued by the LIS (Lighting Imaging Sensor).

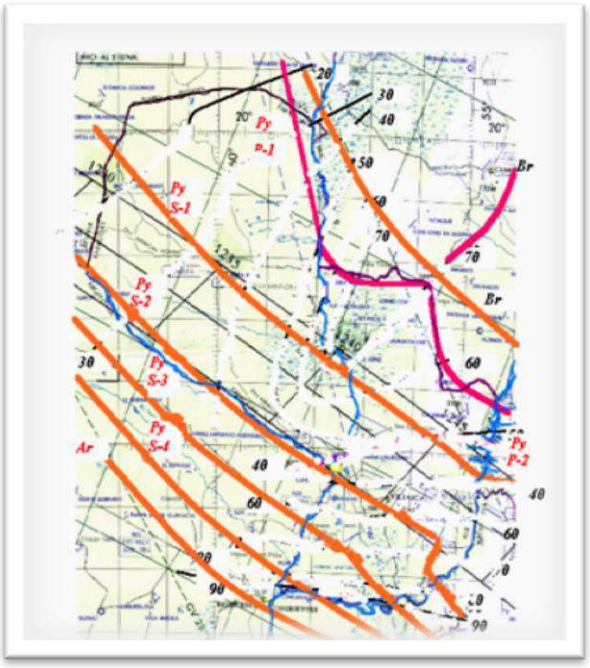

Figure11. Physical location of 5 lightning channels in Paraguay

Table1. Channel sites of falls downs of high tension towers and transformers burned situated within the longitudinal magnetic anomalies

Year	Voltage	Place	Towers falls down and transformer burned	Longitudinal channel lightning
1982	220 kV	San Jose	22 towers	Py –S1
1994	66 kV	Caapucu	1 transformer	Py-S2
1998	220 kV	San Pedro	4 towers	Py-S1
1999	220 kV	Vaqueria	3 towers	Py-S1
2003	220 kV	San Jose	8 towers	Py-S1
2004	66 kV	Paraguari	12 towers	Py-S2
2008	220 kV	CampoDos	1 transformer	Py-S1
2008	220 kV	C.A Lopez	1 transformer	Py –S1
2010	66 kV	Pilar	7 towers	Py-S4
2014	220kV	Horqueta	3 towers	Py-S2

Data from National Electricity Administration state electricity utility in Paraguay (A.N.D.E) website www.ande.gov.py

Conclution

The strategic value of the mapping of the five channels of high densities of lightning discharges and how that form in Paraguayan territory they will improve interrupt times by collapses of electrical structures this represents a management tool for making decisions both insulation and the earthing systems because may only be made below the high densities channels. Such modifications it could result in improved reliability and continuity of the electricity service due to the greater structural supportability to hazards of severe storms and may reduce the frequency of their occurrence and thereby historical collapses rates of State electric company. It can be concluded that through the interaction of satellite Lightning maps (NASA), the Orographic map of Paraguay together with the map of the World Magnetic Model (NOAA) have shown that the five channels of high densities of lightning discharges coincide with lineups in accordance with magnetized rocks occurred millions of years ago. Each channel is aligned southeast to northwest at 45 ° distancing themselves approximately 100-150 km from each other with a width between 5 to 8 km and they are not stable and oscillate about its own longitudinal axis approximately 5 to10 km. In that way, using UTM coordinates the sites were located several structures collapses occurred at the State Electric Company coinciding perpendicular crosses always under the channels of high densities of lightning. We can say in this document that there are five lightning discharges channel in Paraguayan territory. For the country, these channels represent a serious threat for the population so they can mapping the locations of major risks and warn of this fact a desire to provide efficient and effective replies by relevant agencies directed the stricken population.

References

- Lightning & Atmospheric Electricity Research *http://www.thunder.nsstc.**nasa**.gov/lis*
- The World Magnetic Model *http://www.ngdc.noaa.gov/geomag/WMM/DoDWMM.shtm*
- Boletines y datos de tormentas severas locales *http://www.meteorologia.gov.py*
- Administración Nacional de Electricidad http://www.ande.gov.py
- Caídas de torres de alta tensión *http://www.ande.gov.py*
- Caídas de torres de alta tensión
- http://www.abc.com.py
- Exploraciones mineras y método magnético http://www.geovirtual2.cl/explorac/text/0500 Universidad de Atacama SusanneGriem-Klee / sgriem@plata.uda.cl

The Impact of Peak Current Distribution on the Calculation of Backflashover Rate of Transmission Lines

El Impacto de la Distribución del Pico de la Corriente en el Cálculo de la Tasa de Backflashover de Líneas de Transmisión de Energia Eléctrica

Fernando H. Silveira[1], Silverio Visacro[2]

ABSTRACT

This work presents an investigation of the effect of cumulative peak current distribution on the calculation of the lightning performance of high voltage transmission lines in terms of backflashover rate. The evaluations considered the current distributions proposed by CIGRE, IEEE, and the one based on data measured at Morro do Cachimbo station, Brazil. The results obtained by the systematic application of the CIGRE methodology to calculate the backflashover rate of typical 138-kV transmission line indicated a large difference between the outages related to MCS distribution in comparison with those of CIGRE and IEEE distributions. In some cases, differences in the range of 45 to 80% are indicated, denoting the importance of an adequate definition of this parameter on calculations of the lightning performance of transmission lines.

Keywords: Backflashover, cumulative peak current distribution, lightning, lightning performance of transmission lines.

RESUMEN

Este trabajo presenta una investigación sobre el efecto de la distribución acumulada del pico de corriente en el cálculo de performance de líneas de transmisión de alta tensión frente a descargas atmosfericas. Las evaluaciones se consideran las distribuciones de CIGRE, IEEE, y la basada en los datos medidos en la estación Morro do Cachimbo, Brasil. Los resultados obtenidos por la aplicación sistemática de la metodología del CIGRE para calcular la tasa de backflashover de uma línea típica de transmisión de 138 kV indicaron una gran diferencia entre las tasas relacionadas con la distribución MCS en comparasion com aquellas de las distribuciones del CIGRE y IEEE. En algunos casos, difierencias de 45 a 80% se indican, que denota la importancia de una adecuada definición de este parámetro em el calculo del desempeño de líneas de transmisión frente a descargas atmosfericas.

Palabras clave: Backflashover, Distribución acumulada del pico de corriente, Descargas atmosféricas, desempeño de líneas de transmisión frente a descargas atmosfericas.

Received: July 24th 2015
Accepted: Oct 15th 2015

Introduction

The evaluation of the lightning performance of high voltage transmission lines constitutes a relevant engineering step to provide elements needed to improve the power quality delivered to the consumers.

The calculation procedure involves several previous definitions, mainly related to the modeling of the transmission line, tower-footing grounding, lightning return stroke current, method to estimate flashover occurrence, and cumulative return-stroke current distribution.

In some evaluations, differences between the real outage rate experienced by transmission lines and the one estimated by traditional methodologies are reported. Recently, some works have been investigating the possible causes of such differences [1-4].

In this context, one important aspect that deserves to be investigated concerns the effect of the cumulative return-stroke current distribution adopted to perform the calculation of the outage rate of transmission lines.

Commonly, the cumulative return-stroke current distributions presented by CIGRE and IEEE are adopted [5-6]. Both distributions are basically related to the first return stroke current data measured by K. Berger [7] in Mount San Salvatore (MSS), Switzerland. According to Berger's measure-

[1] Fernando H. Silveira is an Associate Professor of the Electrical Engineering Department of UFMG, where he is also an Associate Researcher with the Lightning Research Center (LRC), Brazil. silveira@cpdee.ufmg.br.
[2] Silverio Visacro is a Full Professor of the Electrical Engineering Department of UFMG and the Head of the Lightning Research Center (LRC), Brazil. LRC@cpdee.ufmg.br.

ments, the median peak current and front time (Td30) of first strokes are 31 kA and 3.83 us, respectively.

In spite of the widespread use of the aforementioned peak current distribution on lightning performance analysis of transmission lines, justified by the fact that Berger's data comprises the largest amount of data measured in instrumented towers, there is no consensus if these data also applies for regions of the world with different weather and relief characteristics, such as tropical regions.

Since 1985, the "Morro do Cachimbo" Station (MCS) has been operating in Southeastern Brazil with a 60-m-high instrumented tower, to establish references of lightning data for tropical regions [8-9]. Several papers about the data measured on the station have been published along the last years [10-13]. With the actual data of about 50 first return strokes, it is possible to establish the cumulative return-stroke current distribution of Morro do Cachimbo station to be used on the calculation of the lightning performance of transmission lines. The median peak current and front time (Td30) of first strokes measured at MCS are 45 kA and 4.83 us, respectively.

The purpose of this work is to present a preliminary contribution on the impact of distinct cumulative return-stroke current distribution on the calculation of the lightning performance of transmission lines in terms of backflashover occurrence, considering a typical 138 kV-line configuration as a case study.

In this work, the calculations were performed by means of CIGRE methodology described in [5]. Three return-stroke current distributions were adopted: CIGRE, IEEE, and MCS. The analyses will be presented in terms of different tower-footing grounding resistances, considering median current front times (Td30) of first strokes measured at Mount San Salvatore and Morro do Cachimbo stations.

MAIN ASPECTS OF CIGRE METHODOLOGY

Overview

The main aspects of CIGRE's methodology are presented in the CIGRE brochure 63 "Guide to procedures for estimating the lightning performance of transmission lines" that compiles the main aspects of CIGRE's methodology [5]. Since 2012, the CIGRE WG C4.23 is working on the revision of such document in order to incorporate the several recent advances presented in the literature concerning the calculation of the lightning performance of transmission lines.

The calculation of the lightning performance of high-voltage transmission lines by means of CIGRE methodology assumes analytical formulations to describe the transient behaviour of the resulting overvoltage due to direct lightning strikes to the line, including the voltage reflection on tower-footing grounding. The calculations assume linearly rising wavefront for representing the lightning return stroke current.

Based on the resulting overvoltage, the critical current able to cause backflashover is determined. The estimation of the line lightning outage rate is obtained by means of the probability of current to exceed such critical current, using a cumulative distribution function of first return stroke current.

Surge impedances are used to represent the transmission line tower and the overhead line conductors. Tower-footing grounding is modeled by a resistance whose value equals the one obtained by measurements using low frequency, low amplitude current. The soil ionization effect may be represented by means of Weck's formula [5].

CIGRE's methodology adopts the concept of a non-standard critical flashover overvoltage (CFO_{NS}) that depends on the line CFO, the nominal voltage of the line, tower-footing grounding resistance and the span length between adjacent towers. If the peak overvoltage exceeds the CFO_{NS}, a backflashover is considered.

The backflashover rate (BFR) is calculated by multiplying the probability of a current to exceed the critical current, the rate of strokes hitting the line (NL) and the 0.6 factor.

CUMULATIVE RETURN STROKE CURRENT DISTRIBUTION

CIGRE's cumulative current distribution is based on the integration of the probability density function indicated in [5]. On the other hand, the IEEE cumulative current distribution is reproduced by a simplified equation [14]. Figure 1 illustrates both current distributions. As can be noted, in the 20-60 kA range, both distributions are very similar. In the large current region and for currents below 20 kA, IEEE presents a large probability of occurrence. For the sake of comparison, the MCS current distribution is also included in this figure.

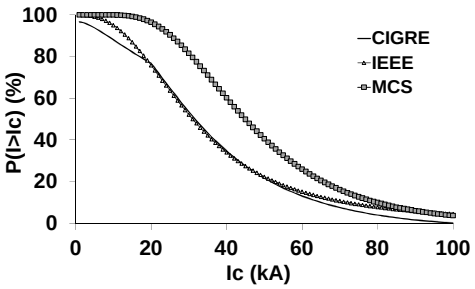

Figure 1. CIGRE, IEEE and MCS cumulative first stroke current distribution.

DEVELOPMENTS

The analyses performed in this work considered lightning striking the top of the 30-m-high 138 kV single-circuit

transmission line tower illustrated in Figure 2. The simulations assumed a 400-m long span and a 650-kV line CFO.

Two Td30 front time were assumed in simulations: 3.83 μs and 4.83 μs, corresponding to the median current parameters measured at Mount San Salvatore [15] and Morro do Cachimbo [8] stations, respectively.

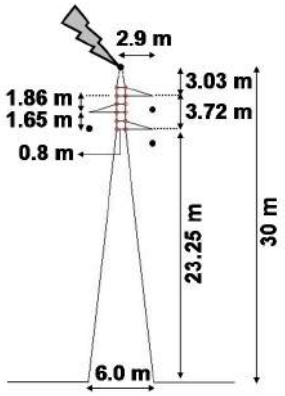

Figure 2. Geometry of the simulated 138-kV transmission line tower.

RESULTS AND ANALYSIS

The performed analyses are divided in two groups: first, results of the impact of the cumulative first stroke current distribution on the backflashover probability of occurrence are presented for 3 values of tower-footing grounding resistance Rg (10, 20, 40 Ω). Following, a case study assuming a lognormal distribution of the tower-footing resistance along the line is developed.

Tables 1 and 2 present the peak overvoltages calculated by CIGRE methodology across the lower insulator string for tower-footing grounding resistance varying from 10 to 40 Ω, for median current parameters of MSS and MCS, respectively. Previous simulations indicated this insulator string as the critical one in terms of the larger overvoltage.

Table 1. Peak overvoltages across lower insulator string. MSS median current parameters: Ip = 31 kA, Td30=3.83 μs.

Rg (Ω)	Vp (kV)	Variation (%)
10	308.9	-
20	516.5	+67.2
40	875.7	+183.5

Table 2. Peak overvoltages across lower insulator string. MCS median current parameters: Ip = 45 kA, Td30=4.83 μs.

Rg (Ω)	Vp (kV)	Variation (%)
10	423.8	-
20	718.2	+69.5
40	1213.5	+186.3

The results show the larger overvoltages related to the MCS current parameter, mainly due to its larger peak current.

Considering the cumulative distribution of first-stroke peak currents of CIGRE, IEEE, and MCS, the percentages of currents expected to overpass the value required to flashover were determined. These results are equivalent to backflashover frequency of occurrence per strike to the tower for each assumed tower-footing grounding resistance. Tables 3 and 4 show the probability of backflashover occurrence assuming current front time of 3.83 and 4.83 μs, respectively.

Table 3. Probability of backflashover occurrence. Td30=3.83 μs.

Rg (Ω)	% I > Ic			Difference MCS x CIGRE (%)	Difference MCS x IEEE (%)
	CIGRE	IEEE	MCS		
10	9.51	12.24	19.56	105.6	59.7
20	33.25	32.62	58.17	74.9	78.3
40	62.88	61.59	89.06	41.6	44.6

Table 4. Probability of backflashover occurrence. Td30=4.83 μs.

Rg (Ω)	% I > Ic			Difference MCS x CIGRE (%)	Difference MCS x IEEE (%)
	CIGRE	IEEE	MCS		
10	7.66	10.75	16.28	112.6	51.4
20	30.62	30.22	54.41	77.7	80.0
40	60.04	58.70	87.00	44.9	48.2

For the simulated current front time, the results indicate very similar probability of backflashover occurrence estimated assuming CIGRE and IEEE peak current distributions, except for the very low grounding resistance case (10 Ω). However, the comparison assuming the MCS current distribution shows large difference on the resulting probability of backflashover occurrence. In all cases, the use of the MCS current distribution leads to a larger expectation of backflashover occurrence. Moreover, such difference is even more relevant for decreasing values of tower-footing grounding resistance when comparing CIGRE and MCS current distributions.

Taking as reference the results related to the 3.83-μs current front time (MSS median current front time), for 20-Ω-tower-footing resistance, the outage rate estimated assuming MCS current distribution is about 75% and 78% larger in relation to those associated to CIGRE and IEEE distributions, respectively. Such increase would represent an estimation of 9 outages/100 km/year assuming MCS current distribution against about 5 outages for CIGRE and IEEE distributions.

The analysis considering the simulation of the 4.83-μs current front time (MCS median current front time) indicates a difference even larger in comparison to the results provided by CIGRE and IEEE current distributions. The difference varies from 78% to 45% and from 80% to 48% in the 20-to-

40-Ω-tower-footing resistance range, in relation to CIGRE and IEEE distributions, respectively.

Case study: lognormal distribution of tower-footing grounding resistance

The analysis in this section considers the tower-footing grounding resistances with median value of 20 Ω and standard deviation of 1. A number of 30 strikes to the 138-kV line per 100 km per year (N_L) was assumed. The obtained results in terms of the resulting outages for 3.83 μs and 4.83 μs current front time as function of the assumed cumulative peak current distribution are shown in Table 5.

Table 5. Outage rate as function of the cumulative peak current distribution for Td30 of 3.83 and 4.83 μs.

Front time (μs)	Outages/100 km/year		
	CIGRE	IEEE	MCS
3.83	6.5	6.7	9.7
4.83	6.1	6.3	9.2

The obtained results confirm the trend shown in Tables 3 and 4: the MCS peak current distribution is responsible for larger outage rates. For this specific case study, the resulting outage rates are about 50% and 45% larger than those associated with CIGRE and IEEE current distributions.

This difference has an important impact on the proposals of protective practices dedicated to improve the lightning performance of transmission lines.

Conclusions

This work presented a preliminary investigation of the impact of distinct peak current distributions on the calculation of the lightning performance of transmission lines in terms of backfashover rate. The evaluations considered a typical configuration of a 138-kV transmission line. Systematic simulations using the CIGRE's methodology were developed considering three cumulative peak current distributions: CIGRE, IEEE, and the one derived from the Morro do Cachimbo station (MCS) data.

The results indicated very similar outage rates calculated assuming CIGRE and IEEE current distributions. On the other hand, the use of MCS current distributions leaded to much larger expectation of backflashover occurrence. The analysis assuming a lognormal distribution of the tower-footing grounding resistance with median value of 20 Ω and standard deviation of 1 showed outage rates about 50% and 45% larger than the ones estimated assuming CIGRE and IEEE current distributions, respectively.

The obtained results show more research is needed on this topic aiming a complete definition of the causes of differences on evaluated outage rates of transmission lines. The use of more elaborated methodologies of analysis, including the realistic representation of the lightning current waveform is important in order to extent the range of application of the obtained results. Furthermore, it is important to clarify the limit of application of global data and regional data of lightning peak current distributions in evaluations of the lightning performance of transmission lines since such definition directly affects the estimated line outage rate. All these aspects are under investigation by the authors of this work.

Acknowledgment

This work was supported by The State of Minas Gerais Research Foundation (FAPEMIG), under grant TEC APQ-02141-14.

References

1. F.H. Silveira, S. Visacro, A. De Conti, "Lightning Performance of 138-kV Transmission Lines: The Relevance of Subsequent Strokes", IEEE Trans. Electromagn. Compat., v. 55, pp. 1195-1200, Dec. 2013.
2. S. Visacro, F.H.Silveira. The Impact of the Frequency Dependence of Soil Parameters on the Lightning Performance of Transmission Lines. IEEE Transactions on Electromagnetic Compat, v. 57, p. 434-441, 2015.
3. F. H. Silveira, S. Visacro, A. De Conti, F.M. Teixeira. The Influence of Lightning Stroke Current Waveform on the Calculation of the Lightning Performance of Transmission Lines. Proceedings of APL 2015 - Asia - Pacific International Conference on Lightning, 2015. p. 799-803.
4. S. Visacro, F.H.Silveira, M.H.M. Vale, Simplified representation of tower-footing electrodes for assessment of the lightning performance of transmission lines using EMTP-based platforms. Proceedings of the International Conference on Power Systems Transients (IPST2015), 2015. p. 1-5.
5. CIGRE Guide to Procedures for estimating the lightning Performance of Transmission Lines, WG 01 (Lightning), Study Committee 33, 1991.
6. IEEE Working Group on Lightning Performance of Transmission Lines, "A Simplified Method for Estimating the Lightning Performance of Transmission Lines," IEEE Trans. Power App. Syst., vol.104, no.4, pp. 919-932, Apr. 1985.
7. K. Berger, R.B. Anderson, H. Kroninger, "Parameters of lightning flashes", Electra, no.80, pp.223-237, 1975.
8. S. Visacro, M. A. O. Schroeder, A. Soares, Jr., L. C. L. Cherchiglia, and V. J. Sousa, "Statistical analysis of lightning current parameters: Measurements at Morro do Cachimbo station," J. Geophys. Res., vol. 109, no. D1, pp. D01105-1–D01105-11, 2004.
9. S. Visacro, C.R. Mesquita, A. De Conti, F.H. Silveira, Updated statistics of lightning currents measured at Morro do Cachimbo Station. Atmospheric Research, v. 117, p. 55-63, 2012.
10. M. Guimaraes, L. Araujo, C. Pereira, C. Mesquita, S. Visacro, Assessing currents of upward lightning measured in tropical regions. Atmospheric Research, v. 149, p. 324-332, 2014.
11. S. Visacro, L. Araujo, M. Guimaraes, M.H.M. Vale. M-component currents of first return strokes in natural negative cloud-to-ground lightning. Journal of Geophysical Research: Atmospheres, v. 118, p. 12,132-12,138, 2013.
12. C. R. Mesquita, R. Dias, S. Visacro. Comparison of peak currents estimated by lightning location system and ground truth references obtained in Morro do Cachimbo station. Atmospheric Research, v. 117, p. 37-44, 2012.
13. S. Visacro, M.H.M. Vale, G.M. Correa, A.M. Teixeira. The early phase of lightning currents measured in a short tower associated with direct and nearby lightning strikes. Journal of Geophysical Research, v. 15, p. D16104, 2010.

14. J. G. Anderson, "Lightning Performance of Transmission Lines". In: Transmission Line Reference Book – 345 kV and Above. 2. ed. California: Electric Power Research Institute – EPRI, 1982. pp. 545-597.

15. R. B. Anderson and A. J. Eriksson, "Lightning parameters for engineering application," Electra, vol.69, pp. 65-102, 1980.

Improved Cloud-to-Ground and Intracloud Lightning Detection with the LS7002 Advanced Total Lightning Sensor

Mejora de la nube-tierra y en la nube Detección relámpago con el LS7002 avanzada Sensor total Rayo

Nicholas L. Wilson[1], Tyler L. Buck[2], Amitabh Nag[3], and Martin J. Murphy[4]

ABSTRACT

The LS7002 detects low frequency electromagnetic signals from lightning discharges in approximately the 1-350 kHz range. The sensor builds upon the digital technology platform of its predecessor, the LS7001, by employing improved embedded software features. This digital processing enhances the sensitivity of the sensor to low-amplitude signals from lightning events. The LS7002 also uses onset corrections that reduce timing error and improve location accuracy by being able to better determine the arrival time of electromagnetic waveforms. In addition, the ability to remove noise from local sources via digital filtering allows for a better signal-to-noise ratio and more flexibility in site selection. These sensor features along with the latest central processor software (the Total Lightning Processor) allow for an enhanced cloud-to-ground flash detection efficiency of 95% and a network median location accuracy of 250 m. Additionally, with network baseline distances (distances between adjacent sensors in a network) of 300-350 km, an intracloud flash detection efficiency of about 50% can be achieved, with detection efficiency increasing for shorter baseline distances. Recently the U.S. National Lightning Detection Network (NLDN) underwent a major update, in which previous generation IMPACT and LS7001 sensors were replaced by the LS7002. As a result of the enhanced features of the LS7002 and the Total Lightning Processor, the location accuracy for cloud-to-ground lightning improved from about 300 m to as good as 200 m within the interior of the network. The detection efficiencies for cloud-to-ground and intracloud lightning flashes within the NLDN are about 95% and 50%, respectively.

Keywords: lightning detection, lightning sensors, location accuracy, detection efficiency, LS7002

RESUMEN

Se introduce el sensor LS7002 de rayo de baja frecuencia. Resultados de la validación se comparten de la Red Nacional de Detección de Relámpagos en los Estados Unidos. Ubicación precisiones han mejorado al mejor de 200 metros y en la nube de detección de rayos es cercana al 50%.

Palabras clave: detección de rayos, sensores de rayos, precisión de localización, eficiencia de detección, y LS7002

Received: July 23rd 2015
Accepted: August 24th 2015

Introduction

In 2013, Vaisala introduced the LS7002 Advanced Total Lighting sensor. By employing improved embedded software features along with the latest central processing software (the Total Lightning Processor), an LS7002 network can achieve enhanced cloud-to-ground and intracloud (IC) flash detection efficiency. Recently, a network-wide upgrade of the U.S. National Lightning Detection Network (NLDN) was completed. Prior to this upgrade, the NLDN consisted of 114 LS7001 and IMPACT-ESP (Improved Accuracy through Combined Technology - Enhanced Sensitivity and Performance) sensors, which provided both time of arrival and azimuth information. Currently, all sensors in the NLDN are upgraded to Vaisala's LS7002 technology. In addition, a new geolocation algorithm is being tested and is expected to be implemented in the NLDN central processor in mid-2014. In this paper, we discuss the enhanced features of the LS7002 and the results expected from the current network-wide upgrade on the performance characteristics of the U.S. NLDN. We also examine the peak current distributions of cloud and cloud-to-ground lightning reported by the network.

LS7002 Technology Evolution

The performance characteristics of a lightning detection network depend upon the characteristics of its sensors and the techniques used in the network's central processor to geolocate lightning.

[1] Vaisala Energy Regional Manager, Latin America: Professional Meteorology, University of Oklahoma, USA. Vaisala Inc. Boulder, Colorado, USA. E-mail: nicholas.wilson@vaisala.com
[2] Lightning Scientist: Meteorology, University of Kansas, USA. Vaisala Inc. Boulder, Colorado, USA. E-mail: tyler.buck@vaisala.com
3 Lightning Product Manager: Atmospheric Physics, University of Florida, USA. Vaisala Inc. Boulder, Colorado, USA. E-mail: amitabh.nag@vaisala.com
4 Senior Scientist: Atmospheric Physics, University of Arizona, USA. Vaisala Inc. Boulder, Colorado, USA. E-mail: martin.murphy@vaisala.com

How to cite: Wilson, et al. (2015), Improved Cloud-to-Ground and Intracloud Lightning Detection with the LS7002 Advanced Total Lightning Sensor, SICEL 2015.

The LS7002 deploys the latest in digital sensor technology. Additional improvements have been made to the algorithms used in the central processor as well.

Changes that Affect Detection Efficiency

The LS7002 employs the latest digital sensor technology along with improved embedded software with enhanced features. Digital processing improves the sensitivity of the sensor to low amplitude lightning-generated signals by a factor of about 3 as compared to the analog IMPACT-ESP sensor. The LS7002 also transmits additional waveform parameters for each measured lightning event to the central processor. Digital filtering of local noise sources allows better signal-to-noise ratio along with flexibility in site selection. Note that the LS7002, like the IMPACT-ESP and LS7001, measures both timing and angle (direction) information associated with lightning events. This allows the use of a combination of Magnetic Direction Finding and Time of Arrival techniques to geolocate lightning discharges with as few as two sensors. The combined enhancements in sensor sensitivity and embedded sensor software allow detection of low amplitude lightning events (primarily cloud pulses) and are expected to result in a cloud flash detection efficiency of around 40-50% with network baseline distances (distances between adjacent sensors in a network) of 300-350 km.

Additionally, a new lightning location algorithm (referred to herein as "burst processing") in the central processor will allow the geolocation of multiple pulses in lightning pulse bursts or trains (e.g., Rakov et al., 1996, Nag and Rakov, 2009). It is expected that multiple cloud pulses will be geolocated for each cloud flash in a large fraction of cloud flashes. This will further enhance the cloud lightning detection efficiency of the network by about 6% on average (Murphy and Nag, 2014). Finally, a new lightning classification algorithm that uses multiple waveform parameters to classify cloud and cloud-to-ground lightning with an accuracy of 80-90% has been implemented. Currently, the central processor uses waveform parameters to differentiate between cloud and cloud-to-ground lightning, but it also classifies all positive lightning events having peak currents less than 15 kA as cloud lightning. The new classification algorithm removes this hard limit for peak current for positive events and classifies lightning events solely on the basis of their waveform characteristics. These improvements to the central processor are currently under test and are expected to be deployed in mid-2014.

Changes that Affect Location Accuracy

The LS7002 sensors use waveform onset corrections, which accurately determine the arrival time of electromagnetic waveforms from lightning events at a sensor. This reduces the timing error and improves the accuracy with which lightning events can be geolocated (Honma et al., 2013). The waveform onset corrections have led to an improvement in the median location accuracy (given by the length of the semi-major axis of the 50% error ellipse) of the NLDN from about 300 m to about 200 m in the interior of the network. The location accuracy of the NLDN is evaluated using lightning strikes to towers by Cramer and Cummins (2014). The location accuracy is expected to improve further when additional factors such as propagation across uneven terrain, varying ground conductivity, and improved handling of electromagnetic wave propagation (resulting in smaller arrival time errors) are taken into account in the new central processor (to be implemented in mid-2014).

NLDN Performance Characteristics and Validation

The performance of a lightning detection network is primarily measured by its detection efficiency, location accuracy, peak current estimation accuracy, and type/polarity estimation accuracy for different kinds of lightning discharges. Figure 1 shows the current model estimated cloud-to-ground (CG) lightning flash detection efficiency for the North American Lightning Detection Network, or NALDN, which consists of the Canadian Lightning Detection Network (CLDN) and the U.S. NLDN. The flash detection efficiency is expected to be about 95% for the entire United States. Additionally, the NLDN is expected to have about 40-50% detection efficiency for cloud flashes. Figure 2 shows the current model estimated median location accuracy for the NALDN. The location accuracy is expected to be approximately 150 to 250 m over the majority of the United States, falling to the 250-500 m range toward the edges of the network.

Table 1. Summary of performance characteristics of the NLDN in 2013 evaluated using rocket-triggered lightning (Mallick et al., 2014)

Characteristic	Flashes/Return Strokes
CG Flash detection efficiency	100%
Stroke detection efficiency	76%
Median location accuracy	173 m
Misclassified return strokes	2.1%
Peak current estimation error	15%

These performance characteristics have been validated over the years using a variety of techniques such as tower studies, video camera studies, and triggered lightning studies (e.g., Jerauld et al., 2004, Biagi et al., 2005, Nag et al., 2011). Mallick et al. (2014) examined the performance characteristics of the NLDN for the 2004–2013 period using rocket-triggered lightning data acquired at Camp Blanding, Florida. Table 1 summarizes the NLDN flash and stroke detection efficiencies for 2013 in Florida. The flash and stroke detection efficiencies were 100% and 76%, respectively. The median absolute location error was 173 m, and the median absolute value of current estimation error was 15%. In 2013, 2.1% (one out of 47) of the triggered lightning return strokes (similar to subsequent strokes in natural lightning) was misclassified by the NLDN.

Evaluation of Enhanced Cloud Lightning Detection

The ratio of the number of cloud lightning pulses to the number of cloud-to-ground lightning return strokes detected by a network can serve as a measure of change in the network's cloud lightning detection efficiency from one time period to another if regional, seasonal, and storm-to-storm variations in IC-to-CG ratio are minimized. This is done by calculating the IC-to-CG ratio over the same geographical region for all time periods, taking all time periods from the same season in different years, and taking time periods long enough to contain an adequate number of thunderstorm days. Further, it is important that the network's detection efficiency for CG strokes remains relatively unchanged for the time periods under consideration.

Figure 3 shows the histogram of the hourly IC-to-CG ratio for the May 15 to June 15 period in 2010 (brown bars) and in 2013 (blue bars). Both the 2010 and 2013 datasets are from the U.S. Central Great Plains region within the latitude and longitude bounds of (31, -102) and (42, -93). Note that the upgrade of the NLDN to the new LS7002 technology was ongoing in this region in the May 15-June 15 period of 2013, and hence these results are to be treated as preliminary. The hourly IC-to-CG ratio was approximately in the range of 0.07 to 3.4 for the 2010 data with the arithmetic mean ratio being 0.84. For the 2013 data, the IC-to-CG ratio is approximately in the range of 0.22 to 21 with the arithmetic mean ratio being 4.0. This indicates roughly a factor-of-four increase in the IC-to-CG ratio after the 2013 upgrade and hence an increase in the detection efficiency of cloud lightning pulses by a factor of four under the assumption of constant CG detection efficiency. The CG stroke detection efficiency of the NLDN in 2010 was in the 75-80% range. The enhancements in NLDN sensor sensitivity in 2013 are expected to improve the CG stroke detection efficiency to about 80-85% as a result of increased detection of low-amplitude return strokes. Hence the factor-of-four increase in cloud lightning detection efficiency estimated above may be treated as a lower bound. A more rigorous analysis of the improvement in cloud lightning detection efficiency will be done in the near future using cloud lightning flashes detected by Lightning Mapping Arrays as ground truth, once NLDN data over a longer time period is available.

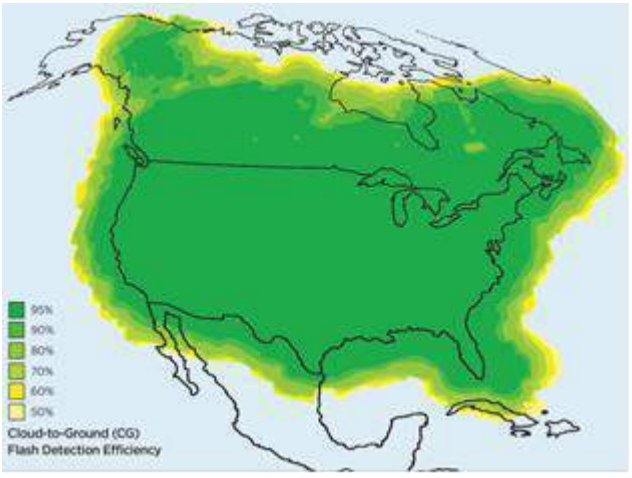

Figure 1. Map showing the model estimated cloud-to-ground flash detection efficiency of the North American Lightning Detection Network.

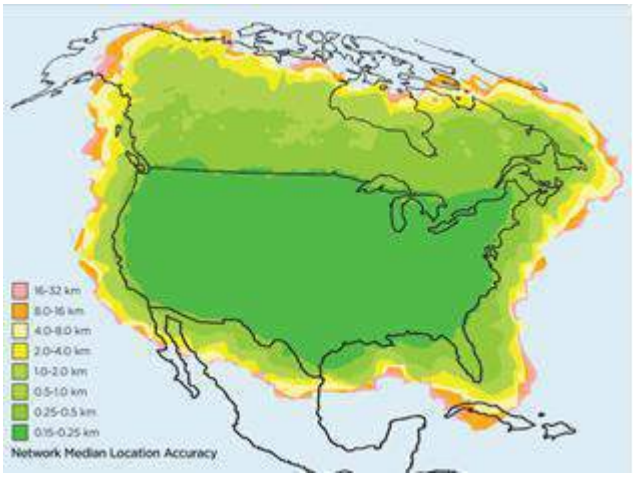

Figure 2. Map showing the model estimated median location accuracy of the North American Lightning Detection Network.

Evaluation of Enhanced Cloud Lightning Detection

The ratio of the number of cloud lightning pulses to the number of cloud-to-ground lightning return strokes detected by a network can serve as a measure of change in the network's cloud lightning detection efficiency from one time period to another if regional, seasonal, and storm-to-storm variations in IC-to-CG ratio are minimized. This is done by calculating the IC-to-CG ratio over the same geographical region for all time periods, taking all time periods from the same season in different years, and taking time periods long enough to contain an adequate number of thunderstorm days. Further, it is important that the network's detection efficiency for CG strokes remains relatively unchanged for the time periods under consideration.

Figure 3 shows the histogram of the hourly IC-to-CG ratio for the May 15 to June 15 period in 2010 (brown bars) and in 2013 (blue bars). Both the 2010 and 2013 datasets are from the U.S. Central Great Plains region within the latitude and longitude bounds of (31, -102) and (42, -93). Note that the upgrade of the NLDN to the new LS7002 technology was ongoing in this region in the May 15-June 15 period of 2013, and hence these results are to be treated as preliminary. The hourly IC-to-CG ratio was approximately in the range of 0.07 to 3.4 for the 2010 data with the arithmetic mean ratio being 0.84. For the 2013 data, the IC-to-CG ratio is approximately in the range of 0.22 to 21 with the arithmetic mean ratio being 4.0. This indicates roughly a factor-of-four increase in the IC-to-CG ratio after the 2013 upgrade and hence an increase in the detection efficiency of cloud lightning pulses by a factor of four under the assumption of constant CG detection efficiency. The CG stroke detection efficiency of the NLDN in 2010 was in the 75-80% range. The enhancements in NLDN sensor sensitivity in 2013 are expected to improve the CG stroke detection efficiency to about 80-85% as a result of increased detection of low-amplitude return strokes. Hence the factor-of-four increase in cloud lightning detection efficiency estimated above may be treated as a lower bound. A more rigorous analysis of the improvement in cloud lightning detection efficiency will be done in the near future using cloud lightning flashes detected by Lightning Mapping Arrays as ground truth, once NLDN data over a longer time period is available.

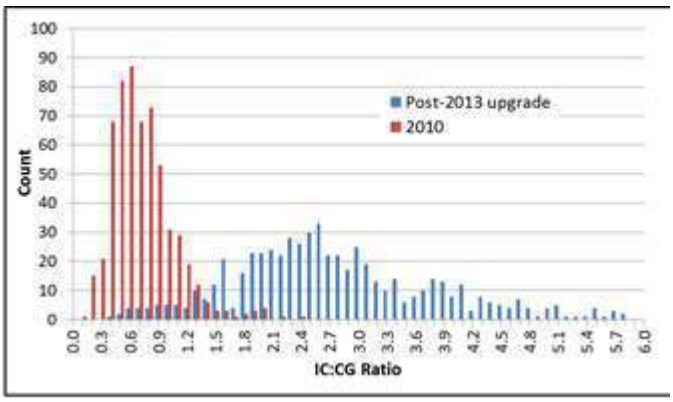

Figure 3. Histogram of the hourly ratio of the number of cloud lightning pulses to cloud-to-ground lightning return strokes detected by the NLDN in 2010 (brown bars) and 2013 (blue bars). Note that the horizontal axis is truncated at an hourly ratio of 6.0 as only 1.4% of the ratios in 2013 were above that value.

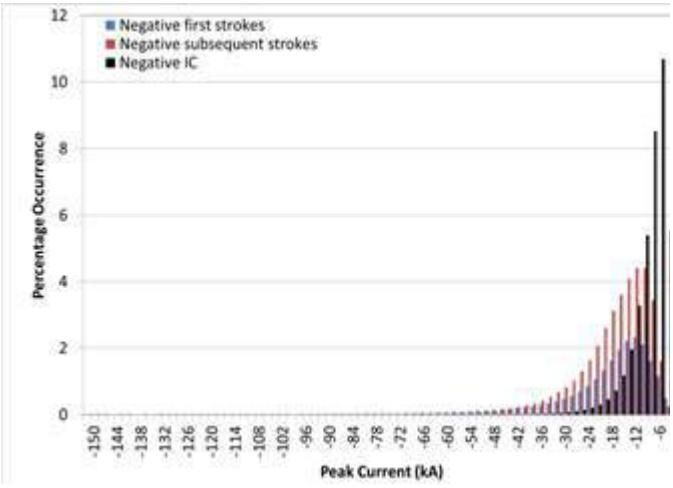

Figure 4. Histogram of NLDN-estimated peak current for negative and subsequent return strokes and cloud pulses shown in 2 kA bins. Note that the horizontal access is truncated at -150 kA as the number of events having peak currents less than that value is smaller than 0.08%.

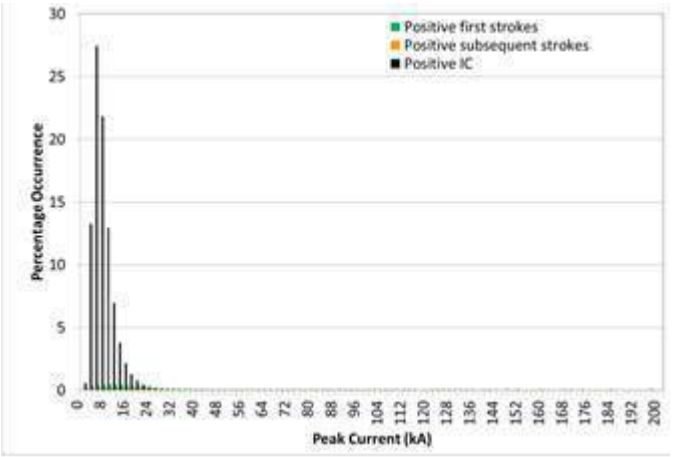

Figure 5. Histogram of NLDN-estimated peak current for positive first and subsequent return strokes and cloud pulses shown in 2 kA bins. Note that the horizontal axis is truncated at 200 kA as the number of events having peak currents greater than that value is smaller than 0.02%.

Analysis of Lightning Peak Currents

In the following analysis we examine lightning discharges reported by the NLDN in early September to late November, 2013 within the interior of the contiguous United States. About 5.5 million lightning events (CG strokes and cloud pulses) were reported by the NLDN during this period. About 63% of these were cloud pulses as classified by the NLDN. Note that this dataset was obtained by offline reprocessing of the raw data using the new geolocation algorithm (currently under test, as discussed in Section III) and hence includes the new classification technique and "burst processing". Figures 4 and 5 show the histograms of peak current for negative and positive events, respectively. Note that the horizontal axes in Figures 4 and 5 are truncated at -150 kA and 200 kA, respectively, and the number of events having peak current magnitudes beyond those limits was less than 0.08% and 0.02%, respectively. The number of NLDN-reported negative CG strokes (first and subsequent combined) was comparable to the number of reported negative cloud pulses. On the other hand, for positive events, the large majority (92%) were cloud pulses and less than 10% were first and subsequent strokes.

As noted in Section III, the NLDN peak current estimation error for cloud-to-ground subsequent strokes is 15%. The peak current is estimated using a transmission-line-equivalent model that converts the measured peak magnetic field into peak current. The same field-to-current conversion equation is used for estimating peak currents for cloud pulses as well. However, it is to be noted that the transmission line model may not be applicable for cloud lightning pulses (e.g. Nag et al., 2011), and the NLDN-estimated peak currents should be considered as a quantity proportional to the initial field peak in cloud pulses.

Cloud-to-Ground Lightning Multiplicity and Peak Currents

Of the CG flashes reported by the NLDN during this period, 81% were negative and 19% were positive. The average multiplicity (number of strokes per flash) for negative CG flashes was 2.7 and for positive CG flashes was 1.4. The NLDN flash grouping algorithm allows a maximum of 15 strokes to belong to one flash. Strokes of order greater than 15 are grouped into a separate flash. Additionally, it is possible that a small fraction of cloud pulses were misclassified by the NLDN as single stroke CG flashes and some low peak current subsequent strokes were not reported by the NLDN. Hence, the average multiplicity, especially for negative CG flashes, is likely to be slightly underestimated.

Figures 6 and 7 show the histograms of peak current for negative and positive CG strokes, respectively. The peak currents for negative first stokes ranged from -0.8 kA to -501 kA with the arithmetic mean (AM) and median peak currents being -21 kA and -15 kA, respectively. For negative subsequent strokes, the peak currents ranged from -1.1 kA to -397 kA with the AM and median being -17 kA and -15 kA, respectively. While the peak current distribution for negative first and subsequent strokes looks reasonable, it is likely that some negative leader pulses were misclassified as negative first strokes and some low peak current subsequent strokes were not reported by the NLDN or were misclassified as cloud pulses. Hence, the AM value for negative first strokes may be a slight underestimate (in absolute value) and that for negative subsequent strokes may be a slight

overestimate (in absolute value). The peak currents for positive first stokes ranged from 1.1 kA to 544 kA with the AM and median peak currents being 24 kA and 19 kA, respectively. For positive subsequent strokes, the peak currents ranged from 1.3 kA to 473 kA with the AM and median being 24 kA and 19 kA, respectively. As discussed in Section II, at present, in addition to classifying events based on waveform characteristics, the NLDN classifies all positive lightning events below 15 kA as cloud pulses. In the new algorithm, this lower limit for peak current of positive CG strokes has been removed and only a waveform-based classification is used. The removal of this lower limit can be seen in Fig. 7.

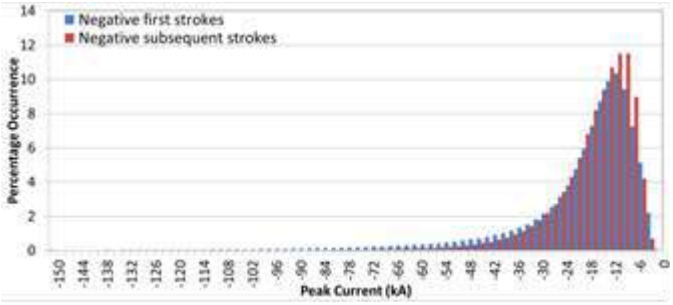

Figure 6. Histogram of NLDN-estimated peak current for negative first and subsequent return strokes shown in 2 kA bins. Note that the horizontal axis is truncated at -150 kA as only a small fraction of the return strokes have peak currents less than that value.

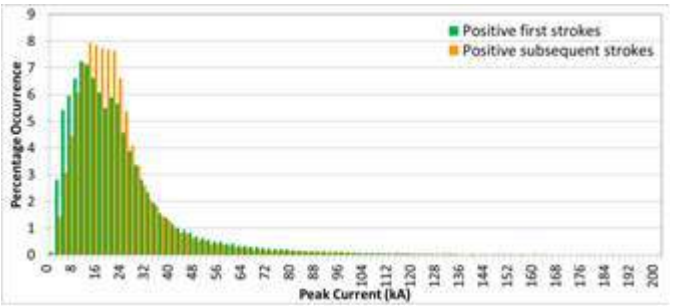

Figure 7. Histogram of NLDN-estimated peak current for positive first and subsequent return strokes shown in 2 kA bins. Note that the horizontal axis is truncated at 200 kA as only a small fraction of return strokes have peak currents greater than that value.

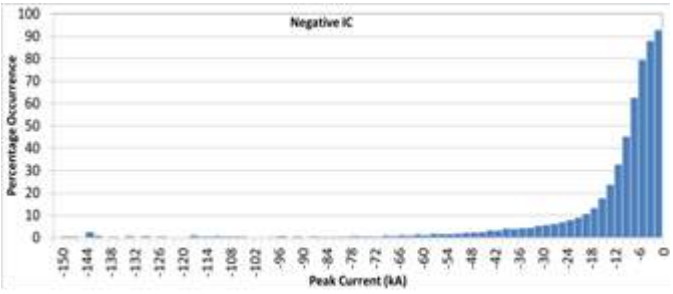

Figure 8. Percentage of NLDN-reported negative lightning events that were cloud pulses shown in 2 kA bins.

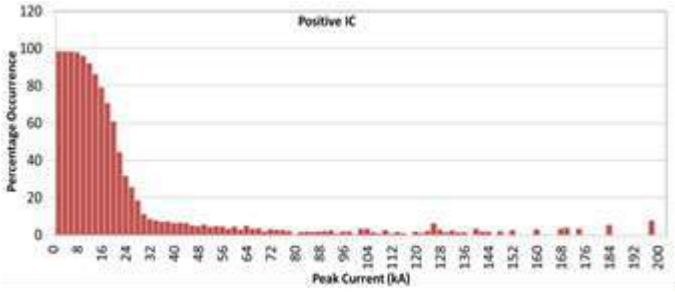

Figure 9. Percentage of NLDN-reported positive lightning events that were cloud pulses shown in 2 kA bins.

Cloud Lightning Peak Currents

In the August to November 2013 period for the area being considered in this study, the large majority (87%) of flashes reported by the NLDN were ICs. In this context, an IC "flash" was defined simply by grouping IC pulses using the same algorithm that is normally applied to CG strokes in the NLDN. Figures 8 and 9 show the percentage of negative and positive events that were cloud pulses. The majority of events with peak current magnitude less than 20 kA for positive events and less than 8 kA for negative events were cloud pulses. Interestingly, a relatively significant fraction of events in higher peak current bins are classified as cloud (e.g., in the 180-182 kA and 196-198 kA ranges in Figure 9), even though the overall number of events in those peak current ranges is small. It is possible that terrestrial gamma ray flashes that produce high-amplitude bipolar pulses are detected by the NLDN and classified as cloud discharges. However, further investigation is necessary in order to determine the nature of these events. The histogram of NLDN-estimated peak current for cloud pulses is shown in Figure 10. There were twice as many positive cloud pulses (produced due to negative charge moving upward or positive charge moving downward) than negative cloud pulses (produced due to negative charge moving downward or positive charge moving upward). The peak currents for NLDN-reported negative IC pulses ranged from -0.8 kA to -238 kA with the AM and median being -7.9 kA and -6.6 kA, respectively. For positive cloud pulses, the peak currents ranged from 0.8 kA to 370 kA with the AM and median being 7.3 kA and 6.4 kA, respectively. The shape of the positive and negative peak current distributions look similar indicating no polarity-dependent bias in the NLDN's detection efficiency. The peak of the distribution for both positive and negative cloud pulses is in the 4-6 kA absolute range. The detection threshold of the NLDN is in the 1-3 kA range depending upon location of a particular lightning event relative to the NLDN sensors, and hence, the number of events reported by the NLDN in this range is likely an underestimate and the average values for cloud pulse peak currents an overestimate.

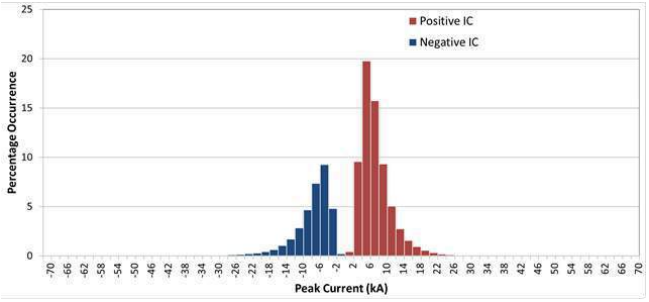

Figure 10. Histogram of NLDN-estimated peak current for positive and negative cloud pulses shown in 2 kA bins. Note that the horizontal axis is truncated at a magnitude of 70 kA at both ends as only a small fraction of cloud pulses have peak currents beyond those limits.

Conclusions

The LS7002 Advanced Total Lightning sensor employs the latest digital sensor technology, which, along with digital filtering of local noise sources, allows better signal-to-noise ratio and improves the sensitivity of the sensor to low amplitude lightning-generated signals. This provides the ability to enhance the detection efficiency for cloud and cloud-to-ground lightning. In 2013, LS7002 sensors were deployed in the U.S. National Lightning Detection Network (NLDN), replacing older generation LS7001 and IMPACT sensors. The cloud flash detection efficiency in the NLDN is expected to be about 40-50%. The hourly IC-to-CG ratio, and hence the number of cloud pulses detected the NLDN, has increased by at least a factor of four as a result of the 2013 upgrade. The location accuracy of the NLDN is expected to be about 200 m in the interior of the network. These performance characteristics continue to be validated by triggered lightning, tower strikes, network inter-comparison, and camera studies.

A new NLDN central processor is expected to be operational in mid-2014. It implements a new "burst processing" algorithm that geolocates multiple pulses in lightning pulse trains. This will further enhance the cloud lightning detection efficiency of the network by about 6% on average. A new lightning classification algorithm that uses multiple waveform parameters to classify cloud and cloud-to- ground lightning with an accuracy of 80-90% will be implemented. Additionally, the NLDN location accuracy is expected to improve further when additional factors such as propagation across uneven terrain, varying ground conductivity, and improved handling of electromagnetic wave propagation (resulting in smaller arrival-time errors) are taken into account in the new NLDN central processor.

We examined lightning discharges reported by the NLDN in early September to late November, 2013 within the interior of the contiguous United States. The majority of lightning events (63%) and flashes (87%) reported by the NLDN were ICs. This is a further indication of a significant improvement in IC detection efficiency. Of the CG flashes reported by the NLDN during this period, 81% were negative and 19% were positive. The average multiplicity for negative CG flashes was 2.7 and for positive CG flashes was 1.4. The negative and positive first stroke median peak current was -15 kA and 19 kA, respectively. The NLDN-reported CG stroke multiplicity and first stroke median peak currents may be slightly underestimated, but they are generally consistent with recent validation studies and the expected accuracy of the new cloud discharge classification algorithm.

References

Biagi, C. J., K. L. Cummins, K. E. Kehoe, and E. P. Krider (2007), National Lightning Detection Network (NLDN) performance in southern Arizona, Texas, and Oklahoma in 2003– 2004, J. Geophys. Res., 112, D05208, doi:10.1029/2006JD007341.

Cramer, J. C. and K. L. Cummins (2014), Evaluating location accuracy of lightning location networks using tall towers, 23rd International Lightning Detection Conference & 5th International Lightning Meteorology Conference, 18-21 March, Tucson, Arizona.

Cummins, K. L. and M. J. Murphy (2009), An overview of lightning locating systems: History, techniques, and data uses, with an in-depth look at the U.S. NLDN, IEEE Trans. Electromagn. Compat., 51(3), 499–518, doi:10.1109/TEMC.2009.2023450.

Cummins, K. L., M. J. Murphy, E. A. Bardo, W. L. Hiscox, R. B. Pyle, and A. E. Pifer (1998), A combined TOA/MDF technology upgrade of the U.S. National Lightning Detection Network, J. Geophys. Res., 103(D8), 9035–9044, doi:10.1029/98JD00153.

Honma, N., K. L. Cummins, M. J. Murphy, A. E. Pifer, and T. S. Rogers (2013), Improved lightning locations in the Tohoku Region of Japan using propagation and waveform onset corrections, IEEJ Trans. on Power and Energy, Vol. 133, No. 2, pp 195-202, doi: 10.1541/ieejpes.133.195.

Jerauld, J., V. A. Rakov, M. A. Uman, K. J. Rambo, D. M. Jordan, K. L. Cummins, and J. A. Cramer (2005), An evaluation of the performance characteristics of the U.S. National Lightning Detection Network in Florida using rocket-triggered lightning, J. Geophys. Res., 110, D19106, doi:10.1029/2005JD005924.

Mallick, S., V.A. Rakov, T. Ngin, W.R. Gamerota, J.T. Pilkey, J.D. Hill, M.A. Uman, D.M. Jordan, J.A. Cramer, A. Nag (2014), An update on the performance characteristics of the NLDN, 23rd International Lightning Detection Conference & 5th International Lightning Meteorology Conference, 18-21 March, Tucson, Arizona.

Murphy, M. J. and A. Nag (2014), Enhanced cloud lightning performance of the U.S. National Lightning Detection Network following the 2013 upgrade, 23rd International Lightning Detection Conference & 5th International Lightning Meteorology Conference, 18-21 March, Tucson, Arizona.

Nag, A., S. Mallick, V.A. Rakov, J. Howard, C.J. Biagi, D. Hill, M.A. Uman, D.M. Jordan, K.J. Rambo, J. Jerauld, B.A. DeCarlo, K.L. Cummins, and J.A. Cramer (2011), Evaluation of U.S. National Lightning Detection Network performance characteristics using rocket-triggered lightning data acquired in 2004–2009, Journal of Geophysical Research, 116, D02123, doi:10.1029/2010JD014929.

Nag, A., M. J. Murphy, A. E. Pifer, and J. A. Cramer (2013), Characteristic Improvements of the U.S. National Lightning Detection Network, Abstract 4.5, 6th Conference on the Meteorological Applications of Lightning Data, 93rd American Meteorological Society Annual Meeting, Performance, Austin, Texas, January 05 - 10.

Nag A., and V.A. Rakov (2009), Electric field pulse trains occurring prior to the first stroke in cloud-to-ground lightning, IEEE Transactions on EMC, 51, No. 1.

Nag, A., V.A. Rakov, and J.A. Cramer (2011), Remote measurements of currents in cloud lightning discharges, IEEE Transactions on EMC, 53, No. 2.

Rakov, V. A., M. A. Uman, G. R. Hoffman, M.W. Masters, and, M. Brook (1996), Bursts of pulses in lightning electromagnetic radiation: Observations and implications for lightning test standards, IEEE Trans. Electromagn. Compat., vol. 38, no. 2, pp. 156–164.